

**COULOMB AND INTERFERENCE EFFECTS  
IN SMALL ELECTRONIC STRUCTURES**

## II

Sponsored by:

- . CNRS(*Centre National de la Recherche Scientifique*)
- . IN2P3(*Institut National de Physique Nucléaire et de Physique des Particules*)
- . CEA(*Commissariat à l'Energie Atomique*)
- . NSF(*National Science Foundation*)

### XIVth Moriond Workshop

Villars sur Ollon, Switzerland - January 22-29, 1994

### **Coulomb And Interference Effects In Small Electronic Structures**

Series : Moriond Condensed Matter Physics

ISBN 2-86332-159-5

Copyright 1994 by Editions Frontières

*All rights reserved. This book, or parts thereof, may not be reproduced in any form or by any means, electronic or mechanical, including photocopying, recording or any information storage and retrieval system now known or to be invented, without written permission from the Publisher.*

**EDITIONS FRONTIERES**

B. P. 33

91192 Gif-sur-Yvette Cedex - France

Printed in Singapore

Proceedings of the XXIXth RENCONTRE DE MORIOND  
Series : Moriond Condensed Matter Physics  
Villars sur Ollon, Switzerland January 22 - 29, 1994

# COULOMB AND INTERFERENCE EFFECTS IN SMALL ELECTRONIC STRUCTURES

edited by

D.C. Glatli

M. Sanquer

J. Trân Thanh Vân



M 80

EDITIONS  
FRONTIERES

104

## **XIVth Moriond Workshop on : Coulomb And Interference Effects In Small Electronic Structures**

was organized by  
J. Trần Thanh Văn (*Orsay*)

with the active collaboration of :

B. L. Altshuler (*Cambridge*)  
H. Bouchiat (*Orsay*)  
G. Chardin (*Saclay*)  
Y. Gefen (*Rehovot*)  
D. C. Glatli (*Saclay*)  
C. J. P. Harmans (*Delft*)  
D. E. Khmel'nitskii (*Cambridge*)  
D. Mailly (*Bagneux*)  
B. Pannetier (*Grenoble*)  
M. Sanquer (*Saclay*)  
A. Schmid (*Karlsruhe*)  
S. Washburn (*Chapel Hill*)

## 94' RENCONTRES DE MORIOND

The XXIXth Rencontres de Moriond were held in 1994 in Villars-sur-Ollon, Switzerland, and in Méribel les Allues, Savoie, France.

The first meeting took place at Moriond in the French Alps in 1966. There, experimental as well as theoretical physicists not only shared their scientific preoccupations but also the household chores. The participants in the first meeting were mainly French physicists interested in electromagnetic interactions. In subsequent years, a session on high energy strong interactions was also added.

The main purpose of these meetings is to discuss recent developments in contemporary physics and also to promote effective collaboration between experimentalists and theorists in the field of elementary particle physics. By bringing together a relatively small number of participants, the meeting helps to develop better human relations as well as a more thorough and detailed discussion of the contributions.

This concern of research and experimentation of new channels of communication and dialogue which from the start animated the Moriond meetings, inspired us to organize a simultaneous meeting of biologists on Cell Differentiation (1970) and to create the Moriond Astrophysics Meeting (1981). In the same spirit, we have started this year a new series on Condensed Matter Physics. Common meetings between biologists, astrophysicists, condensed matter physicists and high energy physicists are organized to study the implications of the advances in one field into the others. I hope that these conferences and lively discussions may give birth to new analytical methods or new mathematical languages.

At the XXIXth Rencontres de Moriond in 1994, four physics sessions, one astrophysics session and one biology session were held :

- \* January 22-29      "Particle Astrophysics, Atomic Physics and Gravitation"  
"Coulomb and Interference Effects in small electronic structures"
- \* March 12-19      "Electroweak Interactions and Unified Theories"  
"Clusters of Galaxies"
- \* March 19-26      "QCD and High Energy Hadronic Interactions"  
" Rencontre de Biologie - Méribel "

## VI

I thank the organizers of the XXIXth Rencontres de Moriond :

- E. Adelberger, R. Ansari, A. Blanchard, F. Boehm, G. Chardin, C. Cohen-Tannoudji, T. Damour, O. Fackler, J. Faller, E. Fischbach, G. Fontaine, G. Gerbier, E. Giacobino, Y. Giraud-Héraud, G. Greene, I. Grenier, B. Guiderdoni, E. Hinds, J. Kaplan, B. Kayser, R. Pain, S. Petcov and J. Wilkerson for the session on Particle Astrophysics, Atomic Physics and Gravitation,

- H. Bouchiat, D. C. Glatli, D. Mailly and M. Sanquer for the Condensed Matter Physics session,

- P. Binetruy, A. Blondel, R. Cahn, G. Coignet, L. Fayard, P. Fayet, J.-M. Frère, L. Krauss, L. Moscoso, C. Savoy and C. Verzegnassi for the Leptonic session,

- F. Durret, A. Mazure and S. White for the Astrophysics session,

- P. Aurenche, E. Berger, A. Capella, D. Denegri, L. Montanet, B. Pietrzyck, D. Schiff, and C. Voltolini for the Hadronic session,

- A. Adoutte, M. Fellous, P. Goldstein, M. A. Gransbastien, J. C. Kader, M. Solignac, P. Sonigo, K. Trân Thanh Vân and A. Ullman for the Biology meeting,

and the conference secretaries : G. Ambonati, L. Besson, V. Chopin, S. Desbarbieux, C. Douillet, D. Josephson, A. Lecoœur, A. S. Lécuyer, F. Lefevre, D. Levêque, L. Norry, F. and N. Osswald, A. M. Perrin, J. Raguideau, R. Scattergood, V. Sobek and F. Warin.

I am also grateful to Mrs S. Müller, Ms B. Gautron, Mr C. Dallery, Ms M. Favet, Mr. P. Bernard Granger, and Mr R. Theveniot who contributed through their hospitality and cooperation to the well-being of the participants enabling them to work in a relaxed atmosphere.

These Rencontres were sponsored by the Centre National de la Recherche Scientifique (SPM and FP), the Institut National de Physique Nucléaire et de Physique des Particules (IN2P3) and by the Commissariat à l'Energie Atomique (DAPNIA). The workshop on Particle Astrophysics, Atomic Physics and Gravitation was also sponsored by the National Science Foundation. I would like to express my thanks to their encouraging support.

I sincerely wish that a fruitful exchange and an efficient collaboration between the physicists, the astrophysicists and the biologists will arise from these Rencontres as from the previous ones.

J. Trân Thanh Vân

## FOREWORD

Electrons are the simplest elementary particles that physicists can manipulate. The interaction of two electrons in the vacuum is known to a very high degree of accuracy and the basic quantum law which governs a collection of electrons was established more than sixty years ago. Condensed Matter physicists study electrons in conductors where the high density fully displays the Fermionic nature of electrons. Technological improvements in reducing the size of conductors to the micron scale and the electron temperature to the sub-Kelvin range have permitted physicists to construct conductors which are quantum mechanical objects making it necessary to go beyond semi-classical concepts in describing electronic conduction. The proceedings of the first Condensed Matter session of the “Rencontres de Moriond” on “Coulomb and Interference Effects in small electronic structures” give an instantaneous view of this field. This book brings together the contributions of physicists coming from a very broad area, i.e. physicists studying quantum transport, thermodynamics, quantum chaos or charging effects in various mesoscopic systems such as disordered metals and insulators, superconductors, 2D conductors in the Quantum Hall regime, quantum dots and metallic islands, and electron billiards.

*“Interference Effects ”:*

In a conductor, the zero point motion due to the high electronic density delocalizes the electrons despite the Coulomb interaction forming a Fermi liquid. Like free electrons, the quasi-particles which represent the excitations around the Fermi surface propagate elastically either diffusely or ballistically up to the coherence length. The quantum phase coherence of the quasi particles can be preserved over micrometers in many conductors at low temperature. On this scale, called *mesoscopic*, a conductor is a quantum mechanical object whose conduction properties reflect the wavelike nature of electrons. The appropriate theoretical description is the transmission approach pioneered by R. Landauer who

## VIII

gives here his personal view of the early history of this field. *Interference effects* are the key to understanding the microscopic mechanism of conduction *in small electronic structures*. In this book the recent experimental and theoretical advances in the transmission of electrons through disordered structures are presented (see chapter *Localisation Regime and Metal-Insulator Transition*). Elegant connections between disordered, classically chaotic and interacting systems have been discovered using random matrix approaches applied either to the transfer matrix or to the Hamiltonian (see *Energy Level Statistics*). Tunneling experiments on Quantum Dots make tangible these ideas. Semi-classical approaches emphasize the importance of shape and geometry of small systems. They demonstrate the relevance of classical chaotic and periodic trajectories in determining the quantum transmission of electron billiards, the *Thermodynamics of Mesoscopic Systems*, and the *Persistent Currents*. Experimental evidence for these tiny currents is presented. Interference Effects are also present at the interface between superconductors and mesoscopic normal conductors. Transmission formulae describe well experimental observations showing interference between correlated paths of incoming electrons and outgoing holes linked by pairs in an Andreev reflection (*Quantum Interferences in Superconducting and Normal-Superconducting Systems*).

### *“Coulomb Effects” :*

In a conductor the quantum fluctuations work against the manifestation of Coulomb repulsion. However, for a nearly isolated conductor such as a submicron metallic island or a Quantum Dot, the sharp electron number quantization reveals the discrete charge carried by an electron : an incoming or outgoing electron must pay a Coulomb energy to change the charge neutrality of the dot. Combined with superconductivity this leads to  $2e$  periodic effects in superconducting islands. In an array of superconducting islands, the vortices of the superconducting phase become quantum particles which experience Aharonov-Casher interferences induced by the electrical charge (see *Charging Effects in*

*Superconducting Microstructures*). Small electron number conducting islands, called Quantum Dots, show single particle energy level quantization just like real atoms. A combination of charge quantization and resonant tunneling helps experimentalists to make tunnel spectroscopy ( *Charging Effects and Resonant Tunneling in Quantum Dots or Normal Metal Islands*). This Coulomb effect provides a tool to study the Quantum Hall Effect in 2D systems in high magnetic fields. At a microscopic level the Coulomb interaction favors correlations which give rise to Fractional Quantum Hall states, or even more correlated states which may also be probed in experiments on mesoscopic systems. ( see *Coulomb interactions and Quantum Hall effect*).

In the quantum transport regime, in the limit of non interacting particles, the conductance provides information on the wave like properties of the electron: how these electron waves are transmitted. In contrast shot noise gives a corpuscular information : how the occupation number of transmitted waves fluctuates in a given sampling time. Recent theoretical advances in the understanding of non equilibrium noise as well as recent experimental results are presented. A complete description should work at finite frequency and include Coulomb interactions. Attempts to incorporate these effects in quantum transport theory are presented ( see: *Shot Noise and A.C. Quantum Transport*).

D.C. Glattli and M. Sanquer

## *Contents*

	<i>'94 Rencontres de Moriond</i>	V
	<i>Foreword</i>	VII
	Landauer R.            A personal view of early history.	1
	<b><i>I. CHARGING EFFECTS IN SUPERCONDUCTING MICROSTRUCTURES</i></b>	
	Joyez P. et al.            Supercurrent modulation in the superconducting single electron transistor.	25
	Hekking F.W.J.            Coulomb and interference effects in small N-S tunnel junctions.	37
	Fazio R. et al.            Proximity effect and Coulomb blockade.	49
	Elion W.J. et al.            The Aharonov-Casher effect for vortices in Josephson- junction arrays.	55
	<b><i>II. QUANTUM INTERFERENCES IN SUPERCONDUCTING AND NORMAL/SUPERCONDUCTING SYSTEMS</i></b>	
	Lenssen K.-L. H. et al.    Mesoscopic phenomena in superconductor/2DEG systems.	63
	Williams D.A. et al.      Differential resistance characteristics of superconductor- semiconductor heterostructures.	73
	Pothier H. et al.            Interference of pairs of electrons tunneling into a superconductor.	79
	Courtois H. et al.        Electron transport in a submicron metallic wire periodically in contact with superconducting Islands.	85
	Visani P. et al.            Mesoscopic effects in proximity induced superconducting cylinders of copper and silver.	91
	Gielen L. et al.            Superconducting phase boundary $T_c(H)$ of mesoscopic open and filled squares.	97
	<b><i>III. ENERGY LEVEL STATISTICS</i></b>	
	Simons B.D. et al.        Quantum chaos : energy levels as fermions.	105
	Sivan U.                    Spectral properties of disordered quantum dots.	119

Braun D. et al.	Motion of energy levels in diffusive electronic systems.	131
Altland A.	Spectral correlations in diffusive and ballistic systems.	143

*IV. THERMODYNAMICS OF MESOSCOPIC SYSTEMS  
AND PERSISTENT CURRENTS*

Benoit A. et al.	Experimental Observation of Persistent Currents.	157
von Oppen F.	Semiclassical approach to the thermodynamics of mesoscopic systems.	169
Jalabert R.A. et al.	Orbital magnetism in quantum dots: a semiclassical approach.	175
Jonson M. et al.	Macroscopic tunneling of a pinned wigner crystal-ring : anomalous temperature behaviour.	183
Leboeuf P. et al.	Tunneling and the band structure of chaotic systems.	189

*V. LOCALIZED REGIME AND METAL - INSULATOR TRANSITION*

Ovadyahu Z. et al.	Quantum coherent effects in Fermi-glasses.	197
Lerner I.V.	Spectral correlations in the vicinity of the Anderson transition.	209
Eto M.	Correlation effect on hopping conduction with spin-orbit interaction.	219
Altshuler E.L.	Persistent photoconductivity in the Coulomb glass.	225
Pichard J.L.	From chaotic scattering to localisation: A brief review of Random matrix approaches.	231

*VI. CHARGING EFFECTS AND RESONANT TUNNELING IN QUANTUM  
DOTS OR NORMAL METAL ISLANDS*

Meir Y.	Low temperature transport through a quantum dot : from the Coulomb blockade to the Kondo effect.	247
Eaves L. et al.	A Fermi-edge singularity probed by resonant tunnelling spectroscopy.	259
Raikh M.E. et al.	Two-channel resonant tunneling.	277
Kumar A. et al.	Anti-correlated oscillations in a three-lead quantum dot.	283
Presson M. et al.	Conductance spectroscopy of a Quantum dot in weak magnetic fields.	289

## XII

Lindelof P.E. et al.	Shell structure in GaAs/AlGaAs quantum dots.	295
Dubois J.G.A. et al.	Tunneling spectroscopy on the ligand stabilized metal cluster $\text{Pt}_{309}\text{Phen}_{36}\text{O}_{30}$ .	305
Sanborn B.A. et al.	Cryogenic precision capacitance bridge using a single electron tunneling electrometer.	311

### VII. COULOMB INTERACTIONS AND QUANTUM HALL EFFECT

Ashoori R.C. et al.	Atomic spectroscopy of a single quantum dot.	319
Wharam D.A. et al.	Periodic modulation of Coulomb blockade oscillations in a quantum dot at high magnetic fields.	339
Feng S. et al.	Suppression of Josephson effect and little-parks experiments in the fractional hall liquid.	349
van der Vaart N.C. et al.	Time-resolved tunneling of single electrons between confined quantum hall states.	363
Nazarov Yu.V. et al.	Wigner molecule on the top of a quantum dot.	369
Pasquier C. et al.	Threshold voltage for the transmission of low filling factor edge channels.	375

### VIII. QUANTUM WIRES

Nieuwenhuizen Th.M.	Semi-ballistic wave propagation in disordered cavities.	383
Fal'ko V. I. et al.	Quantum conductance fluctuations in 3D ballistic adiabatic wires.	389
Fasol G.	Spontaneous spin polarization in quantum wires.	395

### IX. SHOT NOISE AND A.C. QUANTUM TRANSPORT

Martin Th.	Equilibrium and shot noise in mesoscopic systems.	405
Prêtre A. et al.	Dynamic admittance of a mesoscopic capacitor.	421
de Jong M.J.M. et al.	Sub-poissonian shot noise in a diffusive conductor.	427

<i>List participants</i>		437
--------------------------	--	-----

## A PERSONAL VIEW OF EARLY HISTORY

Rolf Landauer  
IBM Thomas J. Watson Research Center  
PO Box 218, Yorktown Heights, NY 10598



### ABSTRACT

This is a personal account of two early investigations related to the theme of this workshop. The first of these analyzed the energy level structure in a one-dimensional model of a disordered solid, using the engineering model of IBM's first large scale electronic computer. The second episode dealt with the calculation of conductance from the transmissive behavior of the sample, and with the spatial variation of field and current near localized scatterers. The two cases provide an obvious contrast in the way scientific contributions find acceptance.

## 1. INTRODUCTION

This is a personal account of two early investigations related to the themes of this workshop. Personal recollections are not disciplined contributions to the history of science. Nevertheless, I believe that there is something to be learned from the differing character of the two episodes. The earlier of the two investigations dealt with computer modeling of the distribution of energy levels in a one-dimensional model of a disordered solid. The work reached its deserved state of attention, in the usual way, without difficulty. With time, as the state of understanding of the topic advanced, my contribution became obscure. That is the inevitable course for most of our publications; our colleagues cannot keep an ever increasing list of papers in mind. The other contribution to be discussed deals with the calculation of conductance from the transmissive behavior of the sample, and with the spatial variation of field and current near localized scatterers. It took decades for these notions to reach acceptance.

As the volume of scientific publications has increased, fashions have become more important. What causes one proposal to be accepted and another to be ignored matters, and deserves to be understood. We have received increased funding for science and technology, for many years. Are we using it effectively? If we publish more than we can consume, is there a purpose to the size of our fields? I hope that the contrast between the two episodes to be discussed will emphasize these questions, even if there are no simple answers.

## 2. ENERGY LEVELS IN DISORDERED ALLOYS: LOCALIZATION

The early history of this field is best summarized by a quotation from a review paper.<sup>1</sup>

Interest in disordered materials in the fifties and sixties arose from a number of sources. The need for technological assessment of amorphous semiconductor device proposals<sup>2</sup> was an important component in this. Theoretical interest in electrons in disordered

structures, however, preceded that. In the thirties disorder had been viewed as a source of scattering, acting on electrons which were presumed to be in a conduction band. This band was derived from the disordered structure by averaging out the disorder. Only in some very special ways were there attempts<sup>3,4</sup> which tried to go beyond this. By the early to middle fifties, however, it became generally clear that one could systematically ask and answer questions about the distribution of carriers in space and energy, in disordered structures. In 1953, Dyson<sup>5</sup> examined the vibrational spectrum of a disordered linear chain. The three years, 1953-1955, also saw the emergence of three papers<sup>6-8</sup> which for the first time gave a systematic investigation of the electronic structure of disordered systems. These papers anticipate, sometimes in a very primitive fashion, concepts which were rediscovered later. Thus Parmenter<sup>8</sup> provides a very clear definition of what is now called the Coherent Potential Approximation, though he does not actually employ it. All of these papers<sup>6-8</sup> discuss band edge smearing. Reference [7] alludes to the localization of electrons to neighborhoods in parts of space which are particularly favorable for that energy. If the early electronic papers<sup>6-8</sup> are to be faulted, it is for the fact that despite their heavy concentration on one dimensional models they did not recognize that all states in a disordered one dimensional structure are essentially localized. That recognition did not come until 1960.<sup>9,10</sup>

All of us, including this author, have difficulty at times, responding perceptively to the literature. This is not a tale of good guys vs. bad guys. I still have my preprint of P.W. Anderson's famous *Absence of Diffusion in Certain Lattices*<sup>11</sup> with Anderson's handwritten notation "Did I send you this?" I must have attached some significance to it, otherwise the preprint would not have survived in my files. Nevertheless, I failed to grasp what it was all about. I was interested in electrons in disordered structures, and as will become clear, in localization. I looked at Anderson's preprint and

knew that I was not particularly interested in spin diffusion. As a result, I did not take the trouble to understand Anderson's message.

I came to IBM, in the spring of 1952, some two years after receiving my Ph.D., to work in a semiconductor effort. This group was one of the precursor's of IBM's subsequent Research Division. My manager's manager inquired whether there wasn't some way we could make use of the 701, IBM's first large scale electronic computer, then in its final development stages, but in a state where the engineering model was capable of doing useful work. My proposal to calculate the energy level distribution in a one dimensional model of a disordered crystal was accepted. A collaborator, J.C. Helland, whose name appears as coauthor,<sup>7</sup> did the most burdensome part of the programming. As is common in such situations, it quickly turned out that a calculation of the energy level distribution, for a disordered potential, was not as trivial an analytical problem as I had at first assumed it would be. The procedure that I worked out was described in an IBM Technical Report, *The Use of Oscillation Theorems in the Numerical Computation of the Density of States*, dated March 8, 1954. By that time the paper by James and Ginzburg<sup>6</sup> had appeared and the description of my essentially identical method no longer seemed worth publishing. James and Ginzburg, despite awareness of the same problem, did not have a digital computer available, and could not do much with their method.

The paper by Landauer and Helland does not represent great pioneering in the use of digital computers, when contrasted, for example, to the paper by Metropolis, *et al.*, on the Monte Carlo method.<sup>12</sup> Nevertheless, it was a very early attempt to apply computers to condensed matter physics and an early utilization of computers to do experimental modeling, rather than calculating band structures or molecular wave functions. It was, in fact, an exceedingly burdensome programming chore, done at a time when higher level languages were nonexistent and subroutines almost unavailable. The primitive state of programming back then can be judged from the following. I tried to learn whether the 701 was reliable; did we need to put enough checks into the program to detect all errors? I could not get a good answer,

and decided to play it safe. Every part of the program was checked. We were, however, not sophisticated numerical analysts, and our checks were not designed sufficiently carefully, with all possible cases in mind. As a result our program stopped every few minutes, caught by a check which was too stringent. The 701 time available to us was usually at night, and I had to be there to help push the button after convincing myself that there was no real problem. Computers rarely make errors in the fifth decimal digit. An error typically causes the output to be totally unreasonable, or causes the machine to halt. But we did not know that, when we started.

We were not the only ones, in IBM, to use the engineering model of the 701 for research purposes. Nat Rochester and some of his associates, who had developed programming for the 701, were involved in an early attempt at artificial intelligence and the modeling of neurons firing at each other, on a computer. On the other hand, our work, which was less ambitious in character, may have been the first successful research use of computers within IBM. (For an alternative view of IBM's early neural network simulation see Waldrop.<sup>13</sup>)

The Landauer-Helland paper has stood up, and was correct, with one limitation. The abstract contains the phrase *localized states*, and it is clear, throughout the paper, that there is a naive and primitive attempt to come to grips with the question of localization. There is no doubt that Anderson's subsequent work<sup>11</sup> was the first serious and meaningful attempt to face the localization question, in a properly formulated way. Simpler notions about localization, however, were older and predated my own work. For a donor, say phosphorus in silicon, if the donor atom is isolated, clearly we have a localized hydrogenic state. The electron is *localized* and I believe that the word was used that way; perhaps more clearly in the case of lattice vibrations, than in the case of electrons. It was also well known in the early fifties that if one had a high density of donors, one would get an impurity conduction band. Thus, it is immediately apparent, if we view a random distribution of donors, that there will be pockets where the donor density is atypically high, and electrons will have a particularly hard time getting

away from that neighborhood. All of this was in the air when we wrote our paper.

Fig. 1, extracted from Ref. [7]; shows one of a number of numerical results. Our results also included spatial disorder, modeling liquids, as well as the compositional disorder of Fig. 1.

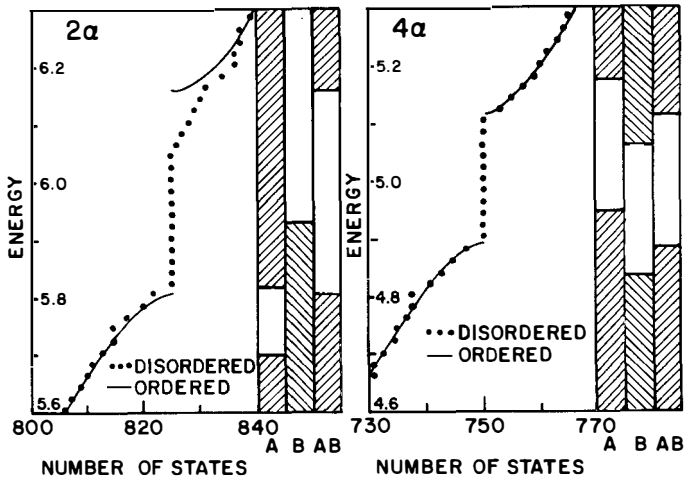


**Fig. 1.** At left is part of the results for the disordered potential  $2a$ , showing a range with no energy levels. The allowed ranges for the  $A$  crystal, the  $B$  crystal, and the ordered  $AB$  alloy are indicated by the shaded vertical regions. Note that the dots are not the locations of energy levels, but only serve to indicate the number of levels up to the energy concerned. The solid curve gives the level distribution for an infinite ordered  $AB$  chain, normalized to 75 states per band (in contrast to the slightly more irregular results obtained from a finite chain of 150 atoms). At right are similar results for a part of  $4a$ , a potential consisting of very similar  $A$  and  $B$  atoms.

The next paper to do computer calculations for disordered systems appeared four years later. It did not cite us in a way which would cause anyone to rush and look at our earlier paper. Nevertheless, our paper did not go unnoticed. It influenced Parmenter<sup>8</sup> and was cited by a number of others. In fact J. Hori<sup>14</sup> states:

As for the electronic-energy spectrum, the attempt at numerical computation was made somewhat earlier than for the vibrational one. The pioneers were Landauer and Helland (1954), who tried to calculate the band structure of the spectrum of an electron moving in a one-dimensional random array of square-well potentials.

Mott, in his review paper,<sup>15</sup> as well as in the book by Mott and Davis,<sup>16</sup> cited our work. By that time, however, the work had already started toward obscurity.

We may ask why this study found more ready acceptance than that in our next episode. First of all our community was ready for this work, demonstrated by the close proximity of Refs. [5-8]. What happens to the well known band structure, in the presence of disorder, is not a deep question. Furthermore, while Ref. [7] supplied a new tool, the computer, it was not threatening to any established efforts. The work did not question the validity of the work of others nor try to replace their viewpoint by a better alternative.

### 3. TRANSPORT AS A CONSEQUENCE OF INCIDENT CARRIER FLUX

This episode is more complex, and in contrast to the above history started with obscurity and rejection, and needed almost a quarter century to achieve some degree of recognition. Indeed, aspects of the work are still, after 30 years, struggling for acceptance. In this discussion I emphasize the early years.

In the early fifties, I developed an interest in the then prevalent way of calculating the resistance due to localized lattice defects, from their scattering cross-section. I had published a calculation of edge dislocation resistance. I had also developed an effective medium theory of the resistance of macroscopically inhomogeneous media, unintentionally reinventing an approach proposed 17 years earlier by Bruggeman. (The history of this subject is discussed in Ref. [1].) Thus, I was also very conscious of the

behavior of a macroscopic inhomogeneity or cavity, which causes the current to detour. The extra field which causes the detour, and causes the extra resistance, is a dipole field with the source charges of the field at the surface of the cavity. Note, at this point, that we have discussed the *extra field* introduced by introducing a cavity into an initially homogeneous conductor, maintaining the far away current density, or equivalently, the total current. This view, considering current introduced into a sample as the causative agent and then inquiring about the required build-up of fields, has been basic to my work. It is a natural view for those familiar with circuit theory, which has long recognized the duality between voltage sources and current sources. Solid state transport theory, however, had a narrower perspective. Fields were always taken as the cause and current flow as the response.

In the then prevalent approach, the residual resistance of elastic scatterers was calculated by averaging over an ensemble including all possible geometrical arrangements of the scatterers. After ensemble averaging the electric field and current flow are spatially uniform; spatial variations are suppressed by ensemble averaging. The fact that an actual sample was an ensemble member and not the whole ensemble, was ignored. Spatial variations were simply not a fit subject for discussion, whereas common sense would have led every elementary textbook to ask: How do current and field vary near a localized scatterer?

I did ask about spatial variations, and how the transition from a macroscopic cavity to an atomic sized defect takes place. I had hoped that an understanding of the nature of this transition might yield a tool for measuring the size of small precipitates through the temperature dependence of the resistance. I surmised, incorrectly, that the transition takes place when the inhomogeneity becomes smaller than the mean free path in the surrounding medium.

The one-dimensional case, where only a spatial field variation but no current flow variation can exist, was trivial, but did not seem important. The three dimensional case was difficult, and it took me several years to

understand how to handle it. All of this was done semiclassically. By 1956, I finally had the answer: Point defects, in a number of ways, act much more like macroscopic inhomogeneities, e.g. cavities, than the textbook discussions suggested, or I had guessed. The extra voltage needed to carry the current past the defect comes from a dipole field concentrated about the defect. The current flows around the defect in a complex spatial pattern, but one which has some resemblance to that found for a macroscopic cavity. Unfortunately all of this did not have any effect on the calculated resistance; the existing calculations gave the correct value.

Shortly after this work was completed, and before publication, I attended a meeting in Ottawa, organized by D.K.C. MacDonald on "Electron Transport in Metals and Solids". The proceedings were published in a special issue of the Canadian Journal of Physics. Fig. 2 shows the participants.<sup>17</sup> It was a remarkably impressive group. I was too young and inexperienced to try and grab a few minutes of the meeting to discuss my work. I did, however, try out a number of attendees, privately. The theoreticians scoffed, or paid no attention. I had somewhat better luck with the experimentalists, including D.K.C. MacDonald. Miland Fiske and Roland Schmitt of General Electric (Schmitt subsequently became V.P., Corporate Research and Development, of General Electric, later President of Rensselaer Polytechnic Institute and is now Chair of the Board of Governors of the American Institute of Physics) were interested, and some correspondence took place after the meeting. After submitting my work to a journal early in 1957, I got a very detailed and very negative response from the referee.

This totally negative report was my first experience of that kind. I sent the editor a detailed reply, justifying my paper, but also stating, "I do not believe that it still needs the extensive reworking that you mention, and would therefore like to withdraw my request for publication in your journal". A copy of the editor's reply follows.

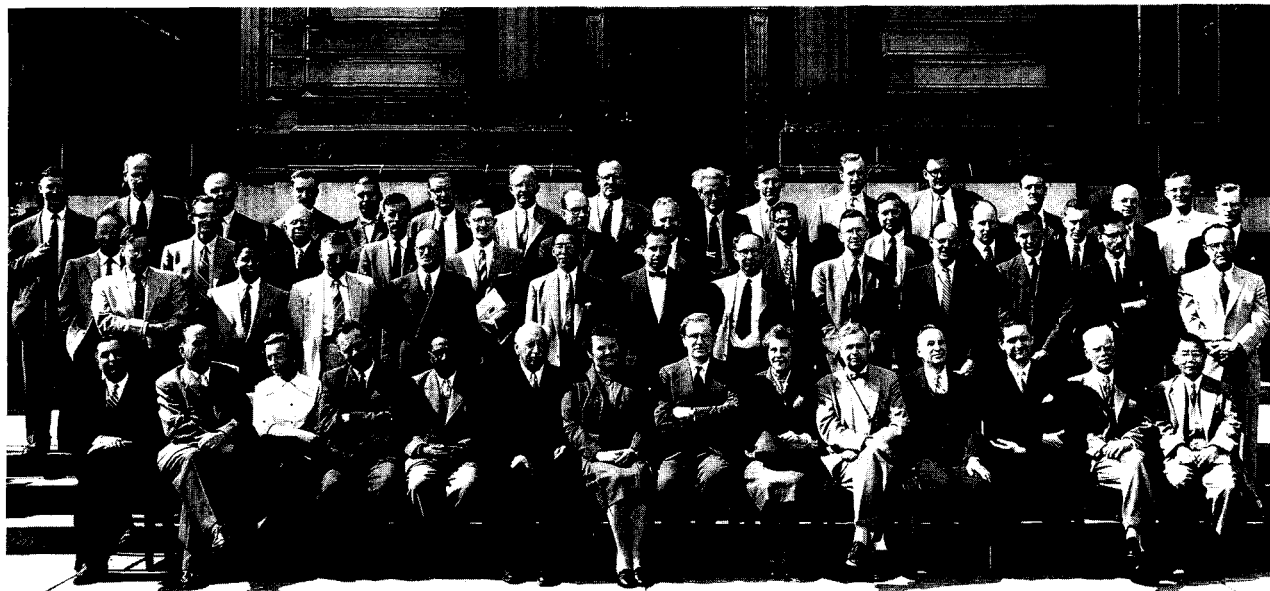


**Fig. 2.** *Conference attendees, Ottawa, Canada, 1956.*

**Back Row:** W.B. Pearson; R.B. Brode; W.J. Archibald; J. Friedel; E. Hart; D. Polder; M.D. Fiske; F.A. Kaempffer; H. Fröhlich; G.K. Horton; H.P.R. Frederikse; E. Mooser; C.F. Yost; K.A.G. Mendelssohn; R.W. Schmitt; G.K. White.

**Next Row:** M.A. Maréchal; L.G. Elliott; K.K. Darrow; J. Korringa; D.K.C. MacDonald; A. Seeger; J.S. Dugdale; A.B. Bhatia; F.R.N. Nabarro; T.H.K. Barron; R. Landauer.

**Next Row:** N. Bloembergen; R.P. Singh; A.N. Gerritsen; P.G. Klemens; R. Kubo; D. Pines; J.M. Ziman; E.H. Sondheimer; J. Bardeen; R.G. Chambers; A.C. Hollis-Hallett; C.A. Domenicali.

**Front Row:** I. Prigogine; C.J. Gorter; Miss U. Martius; J. deBoer; K.S. Krishnan; A.F. Joffé; Mrs. Joffé; N.F. Mott; Mrs. Slater; J.C. Slater; J.H. Van Vleck; P.R.R. Aigrain; G. Borelius; M. Kotani.

Not in the Photograph: E. Fawcett; F.T. Hedgcock; G. Herzberg; W.B. Lewis; P.J. Price; Ta-You Wu.

2nd April, 1957

Dear Rolf,

Thanks for your letter of March 20th. I have not yet had a chance to read your paper in the light of the comments in your letter but will try to do so and answer them in detail. In regard to your withdrawal of the paper I have assumed that you have plenty of additional copies and that, therefore, you will not need back the manuscript which you sent to me. If I am not right in this assumption please advise me immediately and I will return your manuscript by air mail.

It is possible my judgment was over-hasty and that I was unduly influenced by the report of the referee. However, the referee was one whom I had found reliable in the past and his views seem to confirm my own, admittedly superficial, impressions.

Your letter raises an issue which was not discussed in the paper and which possibly gives your results a good deal more significance than I appreciated. This is the question of the interpretation of electrolysis in alloys and the influence of the inhomogeneity of the electric field on such processes. I had forgotten about this particular problem and I would like to think about your results again in the light of this. It seems to me, however, that your paper would make a lot more sense to the general reader and not seem so "much ado about nothing" if you had related it in the introduction a little bit more closely with this problem.

I was, of course, quite aware that your method was equivalent to the ensemble averaging method. I did not mean to imply in my letter that your method was wrong but only that I thought the same conclusion could be arrived at in a simpler way. I am still not clear about the  $r/1-r$ . It would seem to me that not only the dimensions relative to a mean free path but also the spacing of the obstacles

relative to their dimensions is of significance. I still reiterate my belief that if the obstacles are inclined with respect to each other in a random way the composite resistance will not be nearly as pathological as your result although I quite agree that the simple ensemble average will not be valid in this case. As indeed shown by the work of Thornton Read on dislocations.

Very truly yours,

I do not want to be excessively critical of this particular editor. In contrast to today's editors, he was willing to get involved, and to take responsibility for his judgment. He was not just a mailing center for debates.

One point in the editor's reply is particularly worth noting. I had pointed out that the resistance of a planar barrier in a metal would be proportional to  $r/(1-r)$ , where  $r$  is the reflection probability for the barrier. In my work, at that time, this was still viewed as a result applicable to a single and highly localized obstacle. It seemed to me an obvious and sensible result. For small  $r$  it showed the expected textbook behavior; resistance was linear in  $r$ , i.e., in scattering probability. For  $r$  close to unity it *also* seemed reasonable, after all an impenetrable barrier must show an infinite resistance. Indeed this small transmission coefficient limit,  $1/(1-r)$ , was known, and had been derived by Frenkel<sup>18</sup> and by Ehrenberg and Hönl.<sup>19</sup> This is the same Ehrenberg who two decades later anticipated the Aharonov-Bohm effect.<sup>20</sup> In view of the limiting cases for  $(1-r) \ll 1$  and for  $r \ll 1$ , my result could be regarded as as a trivial interpolation. The editor, however, considered my result *pathological*.

As indicated above, I withdrew my 1957 paper from the original journal, and resubmitted it to the newly started IBM Journal of Research and Development. Its acceptance and appearance there<sup>21</sup> are probably not attributable to lower standards or to greater perceptivity on the part of that journal, but more likely to a simpler lottery effect. Sooner or later a paper

reaches a referee with the right combination of sympathy and/or laziness, who is willing to recommend acceptance.

The paper received little attention, perhaps none. At that time, the IBM Journal had more solid state physics than it carries today. The neglect of my paper, more likely, had other sources. The paper asked and answered questions which were not generally recognized. The analysis in the paper, in contrast to most of my work, was not all that simple; there was a non-trivial level of mathematical complexity. Finally, my paper did not lead to new measurable experimental results. The fact that both my laboratory and I were inexperienced in representing ourselves did not help.

I understood, at that time, that the force for motion of the defect in the presence of transport, i.e., electromigration, would be sensitive to the local field and current, and thus could serve as a probe for spatial variations. The editor's reply letter makes it clear that I had mentioned that. But I did not understand how to go about applying my new notions to electromigration theory in any detail. It took me many years, until I was able to return to the electromigration problem, and do something about that. That takes us into a separate history. I do, however, want to point out that electromigration is an important technological problem; at the same time a field in which Friedel, Nozières, and Peierls have disagreed can't be all that dull. Nevertheless, the broader transport theory community has ignored the electromigration theory debates.

In 1958 D.K.C. MacDonald organized another conference and invited me to give a paper. Conference Proceedings were prepared and distributed, and included my paper.<sup>22</sup> Unfortunately, this volume, despite the care and effort expended by its editor (Paul Marcus, at Carnegie Tech., at that time), was not quite a formal publication, and was quickly forgotten. During the meeting, MacDonald approached me, obviously uncomfortable, and asked whether in view of the shortage of time, I'd drop my paper. I had the impression, but no clear knowledge, that others had told him that he had made a mistake in inviting me. I refused, and gave my paper. The editor from the 1957 episode, whose letter I have included, was one of my more vocal

critics. Elihu Abrahams and Phil Anderson, who will reappear subsequently as heroes in this saga, were at the meeting. I doubt, however, if their subsequent return to the subject had any relationship to that. For all I know, they may have been on the tennis court, or at the bar, during my talk.

This 1958 meeting was my only opportunity to discuss the subject at a major international conference. Indeed, with the exception of one conference paper to be mentioned subsequently, it would be many years before I found any opportunity to discuss the subject, at all.

By 1960, I realized that the  $r/(1-r)$  result did not need to assume a localized barrier. The reflection probability could represent the overall behavior of an array of successive scatterers. The ease of penetration of a sample, by carriers, is measured both by the transmission probability, and by the electrical resistance. It seems obvious, therefore, that there should be a relationship, and not just in the one-dimensional case I had treated. Furthermore, the existence of such a relationship should not depend on the fine details of the theory, e.g. is it a genuinely many body theory, or not. That was clear to me. On the other hand, the analytical details of the one-dimensional case seemed totally conceptual and playful to me. It did not occur to me that films with real width and thickness might act one-dimensionally. I attempted to evaluate the ensemble average of  $r/(1-r)$ , for a set of disordered one-dimensional arrays, but had difficulties. My colleague Gordon Lasher came to the rescue, supplying the procedure which showed that the ensemble average grew exponentially, rather than linearly, with the length of the ensemble. Unfortunately, the details of Lasher's work and his interest in the problem were lost when I tried to return to the subject in 1969.

My attempts to bring this 1960 work to public attention were limited, and not very successful; I had become discouraged. I gave a paper at a conference on Statistical Mechanics and Irreversibility at Queen Mary College, in December 1960. A written version of that paper, *One Dimensional Quantum Transport Theory*<sup>9</sup> is still in existence, and bears the note: "This is an informal note, not a publication preprint". The abstract follows:

Some of the relatively sophisticated work in quantum transport theory published in recent years has obscured some of the simpler aspects of the problem by the formalism needed to meet the complexity of particular situations. The attached note considers the particularly simple problem of one dimensional diffusion past reflecting obstacles. A system of finite extent in contact with reservoirs which maintain a concentration gradient is considered, rather than a closed system. This permits analysis of a genuine steady state transport process.

The paper alludes only incidentally to Lasher's ensemble averaging technique. The discussion was oriented primarily to the exposition of the general view that transport can be considered as a consequence of fluxes incident from a reservoir.

A paper submitted, after the Queen Mary College meeting, to *Annals of Physics*, was rejected unconditionally in a letter containing only one or two sentences. This manuscript put together the contents of Ref. [22], the Queen Mary College conference paper,<sup>9</sup> and a brief allusion to the exponential rise in resistance, with length, found from Lasher's technique. An attempt to request reconsideration, by *Annals of Physics*, in 1974, was equally unsuccessful. The paper eventually appeared, with very minor updating.<sup>23</sup>

By 1969 I felt that enough was understood about localization to make my viewpoint more acceptable. Also, I was ending a period during which most of my energy had gone into management and into technology. I submitted a paper to *Philosophical Magazine*, deliberately chosen because Mott was its editor. I assumed that he would be perceptive enough to finally let my work appear. Indeed the very perceptive referee, whether Mott or not, did ask for one very valid change. The paper took less than five printed pages, with not very dense print. The paper pointed out that the ensemble, which after ensemble averaging yielded an exponential rise for the resistance, was a very dispersive one.

The  $r/(1-r)$  result was eventually rescued from permanent oblivion by the work of Anderson, Thouless, Abrahams, and Fisher.<sup>24</sup> In contrast to the prevailing and unfortunate mode of behavior, these authors went out of their way to interpret my earlier work in the most intelligent possible way, and to give me a maximum of credit. The work by Anderson, *et al.*, resulted in additional work by many others, with a particularly detailed and perceptive series of papers by Mark Azbel.

After that, the field became popular and diverse, as evidenced by this meeting. The history becomes complex, with many branches, and with inadequate elapsed time to allow the development of perspective. In our field, as elsewhere, there are poor citation practices, based on haste rather than evil intent. That makes it particularly hard to reach a reasonable perspective. I can characterize these citation practices best by a slight adaptation of a paragraph taken from Ref. [25].

There is no dearth of citations, they are thrown in liberally to appease colleagues. But they are thrown in hastily at the end, with a citation dispenser, and with little regard to the real content of the citations. I've often been tempted to invent a citation, and see if it would be copied and propagate. Eventually, however, I learned that the experiment was not needed, it already existed. Science Citation Index for 1976 carries 36 citations to two papers by a non-existent J.C. Maxwell-Garnett. Enough to qualify him for tenure at many universities! The same Science Citation Index volume also carries five citations to two papers which, remarkably enough, occur on the same journal pages; and these are by the once very real J.C.M. Garnett. Presumably the five citations come from those who actually looked at the Garnett papers, and did not just copy the author's name from earlier papers. Garnett's two papers, from 1904 and 1906, dealt with the optical properties of glasses with small metallic precipitates. At a 1977 conference I insulted many of the offending authors by displaying, via transparencies, the relevant pages from Science Citation Index. In the published proceedings<sup>1</sup> I included some bi-

ographical material about the man with this mysterious name. It had a modest effect. A decade later, in the 1986 Science Citation Index, correct and incorrect entries were about equally abundant.

I do want to allude to one more episode from 1966, when I tried to convince some of my IBM colleagues to do an experiment. I had understood and stressed all along that an array of elastic scatterers determines a transmission probability, and therefore the size of a resistance, but that the source of irreversibility came from the reservoirs. What if we eliminate the reservoirs by tying the sample onto itself, into a loop and then apply a flux? Our community then, and for a good many more years, assumed that the elastic scattering determines a resistance, and that any current flow induced by turning on the flux, would disappear with an  $L/R$  decay. I knew this was wrong, and that some relative of Josephson junction behavior should show up. I did not, however, anticipate the later conclusion,<sup>26</sup> that in the presence of flux the *ground state* of the loop would have current flow, and that no decay *at all* was to be expected. My 1966 suggestion survives in the form of two memos; the address list of one included two subsequent Nobel laureates. As IBM's Director of Physical Sciences, at that time, all the recipients were in parts of the organization reporting to me. That did not help. No one took my proposal seriously. The second of my two memos states: "I do not think too many people in the building agree with me on this, but I still think that I am right. If we can make a tunneling system out of a very good conductor, like bismuth, can't we observe some relative of Josephson tunneling?" There was a hand-written supplement: "Involving single electronic charges, of course, it would have to be a ring of bismuth interrupted by a thin tunneling layer, and driven through external flux."

The correct subsequent formulation of all of this,<sup>26</sup> written with Büttiker and Imry, had many precursors, some of them cited in that paper. A recent Ph.D. thesis by Felix von Oppen<sup>27</sup> gives a longer list. The earlier work however, emphasized in varying degrees flux quantization in samples with a large self-inductance, off-diagonal long range order, free unscattered electrons, and periodicity with applied flux (a periodic current need not be

non-vanishing). I, personally, find it very difficult, in retrospect, to look at these earlier papers and calibrate the real level of understanding by their respective investigators.

#### 4. THE FUTURE?

Some sociological questions about our way of doing science are explicit, and others are implicit, in this history. In another light, however, it is a great success story. The trail that has led to a conference like this represents a marvelous interplay between science and technology. It is, after all, the interest in small structures, arising out of the microelectronics industry, and more than that, the fabrication tools that came out of that industry, which permitted all this to happen. In 1963 my own laboratory launched its *Large Scale Integration* project; that title eventually became accepted elsewhere. I remember originating that expression, and remember my unnecessary concern at a time when racial integration in the U.S. was becoming a serious public concern, whether our title might lead to misunderstanding. From the beginning of that project we knew that electron beam photoresist exposure was a key ingredient; indeed we vastly overestimated its role. The progress in that direction was not commensurate with our vision; it was not until Alec Broers appeared a few years later that real progress took place. And while the electron beam did eventually make its way into our factories, it had a limited role there. It is no coincidence that many subsequent developments, including the realization of the two-dimensional electron gas on semiconductor surfaces, resonant tunneling structures, the scanning tunneling microscope, and some of the pioneering experimental mesoscopic studies came out of IBM's Research Division. Further history can be found in Refs. [28-31]. Of course, closely related events took place at a number of other industrial laboratories.

The trail is not at an end, but there are symptoms that the period of high excitement, when there was such a close relationship between the motion of technology and the opportunities for physics, are past. As we make de-

vices smaller and smaller they become more delicate. But as we make them smaller, we try to use more of them. That means that each device, circuit, and connection, has to become more reliable, not less. The resulting costs for development, tooling, testing and fabrication have grown explosively with each round of miniaturization. That forces a slowdown,<sup>32</sup> as explained by the Chairman of the Board of Intel.

The progress of technology will not stop, and it will continue to relate to science. But the simplest extrapolations of miniaturization will not hold; ingenuity will have to go in other directions. The cost escalation we have discussed is a result of miniaturization, not of the details of transistor physics. It would be silly to assume that a transition to new and poorly understood technologies and/or materials would make the cost problems disappear; they would get far worse. When the optimists<sup>33</sup> tell us:

When will it make economic sense to stop building \$1 billion semiconductor chip fab plants, and start figuring out how to produce molecular-scale circuits in high volume and at low cost? Chip and computer companies that neglect this issue may find themselves in the position of vacuum tube manufacturers confronting transistor technology.

it is unrealistic. I do not want to be misunderstood and say that it will be silicon CMOS circuitry, forever. Devices are likely to evolve, hereafter. But I do want to suggest that a transition to any of the many novel schemes that are casually advertised by scientists, using quantum dots, molecular behavior, single-electron tunneling, optically induced atomic transitions, etc., do not provide an easy way out. Indeed many of these proposals have problems above and beyond those posed by device control and fabrication.<sup>34</sup>

## REFERENCES

1. R. Landauer in *Electrical Transport and Optical Properties of Inhomogeneous Media*, edited by J.C. Garland and D.B. Tanner (Amer. Inst. Phys, New York, 1978) p. 2.
2. *Fundamentals of Amorphous Semiconductors* (National Academy of Science, Washington DC, 1972) Chapters VI and VII.
3. T. Muto, Sci. Papers Inst. Phys. Chem. Res. (Tokyo), **30**, 99 (1936); *ibid.* **34**, 377 (1938).
4. J.M. Luttinger, Philips Res. Rep. **6**, 303 (1951).
5. F.J. Dyson, Phys. Rev. **92**, 1331 (1953).
6. H.M. James and A.S. Ginzburg, J. Phys. Chem. **57**, 840 (1953).
7. R. Landauer and J.C. Helland, J. Chem. Phys. **22**, 1655 (1954).
8. R.H. Parmenter, Phys. Rev. **97**, 587 (1955).
9. R. Landauer, *One Dimensional Quantum Transport Theory*. Talk at the "Conf. on Statistical Mechanics and Irreversibility" (Queen Mary College, Dec. 1960), unpublished manuscript.
10. N.F. Mott and W.D. Twose, Adv. Phys. **10**, 107 (1961).
11. P.W. Anderson, Phys. Rev. **109**, 1492 (1958).
12. N. Metropolis, A.W. Rosenbluth, M.N. Rosenbluth, A.H. Teller and E. Teller, J. Chem. Phys. **21**, 1087 (1953).
13. M.M. Waldrop, *Complexity: The Emerging Science at the Edge of Order and Chaos*, (Simon & Schuster, New York, 1992), see p. 159.
14. J. Hori, *Spectral Properties of Disordered Chains and Lattices* (Pergamon, New York, 1968) p. 3.
15. N.F. Mott, Adv. Phys. **16**, 49 (1967).
16. N.F. Mott and E.A. Davis, *Electronic Processes in Non-Crystalline Materials* (Clarendon, Oxford, 1971) p. 56-57.
17. Photograph of Conference attendees from *Proc. Int. Conf. on Electron Transport in Metals and Solids*, Spec. supp. issue 12A, Can. J. Phys. **34** (1956). *Reprinted with permission of the publisher.*
18. J. Frenkel, Phys. Rev. **36**, 1604 (1930).
19. W. Ehrenberg and H. Hönl, Z. Phys. **68**, 289, (1931).
20. W. Ehrenberg and R.E. Siday, Proc. Phys. Soc. Lond. B **62**, 8 (1949).
21. R. Landauer, IBM J. Res. Dev. **1**, 223 (1957).
22. R. Landauer, in *Proc. Int. Conf. on Electronic Properties of Metals at Low Temperatures*, Aug. 25-29, 1958, (Hobart College, Geneva, NY, 1958) p. 173.
23. R. Landauer, Z. Phys. B **21**, 247 (1975).
24. P.W. Anderson, D.J. Thouless, E. Abrahams and D. Fisher, Phys. Rev. B **22**, 3519 (1980).

25. R. Landauer, in *Dynamic Patterns in Complex Systems*, edited by J.A.S. Kelso, A.J. Mandell and M.F. Shlesinger (World Scientific, Singapore, 1988) p. 388.
26. M. Büttiker, Y. Imry and R. Landauer, *Phys. Lett. A* **96**, 365 (1983).
27. F. von Oppen, Ph.D. thesis, University of Washington, 1993.
28. A.B. Fowler, *Phys. Today* **46**, 59 (Oct. 1993).
29. R.A. Webb and R.B. Laibowitz, *IBM J. Res. Dev.* **32**, 304 (1988).
30. *IBM J. Res. Dev.* **32**, 439 (1988); in particular see the section on *Nanostructure Technology*, pp. 441-522.
31. *IBM J. Res. Dev.* **37**, 287 (1993); in particular see the section on *X-ray Lithography*, pp. 291-330.
32. G. Moore, *Outlook for VLSI: Will the Balloon Burst?* in *Bull. Am. Phys. Soc.* **38**, 298 (Mar. 1993).
33. *Nanoscale Progress* **1**, 3 (Nov./Dec. 1993).
34. R. Landauer, *Physica A* **168**, 75 (1990); in *Workshop on Physics and Computation*, Edited by D. Matzke (IEEE Comp. Soc., Los Alamitos, 1993) p. 1.



**CHARGING EFFECTS IN  
SUPERCONDUCTING MICROSTRUCTURES**



## SUPERCURRENT MODULATION IN THE SUPERCONDUCTING SINGLE ELECTRON TRANSISTOR

P. Joyez, A. Filipe, D. Estève and M. H. Devoret  
Service de Physique de l'Etat Condensé, C.E. Saclay  
F-91191 Gif-sur-Yvette, France

### Introduction

The field of charging effects in normal metal and superconducting circuits was launched in the mid-eighties by the theoretical predictions of Likharev and his group<sup>1)</sup>. A couple of years later, the first conclusive experiments were conducted on normal metal circuits<sup>2)</sup>. In the following years, the theory became quite powerful at explaining in detail elaborate experiments on normal metal circuits, while even the most elementary experiments on superconducting circuits displayed several features that could not be understood. This strange situation persisted until 1992 when two papers, one theoretical by Averin and Nazarov<sup>3)</sup> and one experimental by Tuominen *et al.*<sup>4)</sup>, introduced a new idea in the subject, namely the asymmetry of a superconducting electrode with respect to an odd or even electron number. This asymmetry, while a straightforward consequence of the BCS theory<sup>5)</sup>, had not been thought observable before. Soon after, several experiments confirmed this idea<sup>6-9)</sup> and produced the first quantitative results in circuits combining superconductivity and charging effects. In 1993, another theoretical paper by Matveev *et al.*<sup>10)</sup> explored the consequences of the odd-even asymmetry on Josephson tunneling through the “superconducting single electron transistor”. This device consists of two nanoscale Josephson junctions connected in series, thereby defining an island between them. The supercurrent in the transistor results from a competition between the charging energy of a single electron on the island and the Josephson coupling energy of the junctions: the former tends to impose the number of electrons on the island whereas the latter favor quantum

fluctuations of this number. The Matveev *et al.* paper showed that the expected behavior of the supercurrent when one varies the island charge through a gate electrode could be dramatically affected by the presence of a single quasiparticle in the island: for values of the gate charge which are odd multiples of  $e$ , the predicted sharp supercurrent maximum<sup>11)</sup> is “poisoned” and becomes a supercurrent minimum. Still, this improvement of the theory did not suffice to explain why in the experiments done on this circuit<sup>12,13,4)</sup> the supercurrent was so weak and had such a complex gate voltage modulation. By incorporating normal-metal quasiparticle filters close to the island in the leads of a superconducting single electron transistor we have been able to measure for the first time a well-developed supercurrent which can reasonably be compared to a simple finite temperature extension<sup>14)</sup> of the theory of Matveev *et al.* The purpose of this paper is to explain in detail the steps of this comparison.

### Basic theoretical predictions

The basic theory of supercurrent in the transistor evaluates its “critical current”, which is defined as the maximum supercurrent that can flow through the transistor when biased by a perfect current source at  $T=0$ . Although this quantity is only indirectly related to the experimental results its calculation is still needed in a first step. The circuit we consider is the one depicted in the inset of Fig. 1. The normal metal leads act only as quasiparticle filters and have no effect on the dynamics of the circuit at low voltages. The transistor is assumed to be in the superconducting state, we assume for the moment that the voltage difference across the leads is zero. We will also assume for the moment that the electromagnetic environment has a negligible influence on the behavior of the system.

The transistor has two degrees of freedom. For example we can choose to index the state of the transistor by the numbers  $n_1$  and  $n_2$  of electrons having crossed the left and

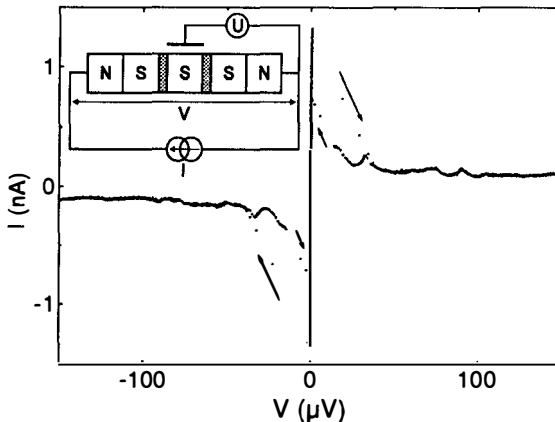


Fig. 1 Current-voltage characteristic of the superconducting single electron transistor whose lay-out is shown in upper left inset. The letters N and S refer to normal (Cu) and superconducting (Al) electrodes. The tunnel barriers are indicated by grey rectangles. The gate voltage  $U$  induces on the middle island a gate charge  $n_g$  whose value is nearly 1 for the data shown. The maximum current defines the switching current  $I_s$ .

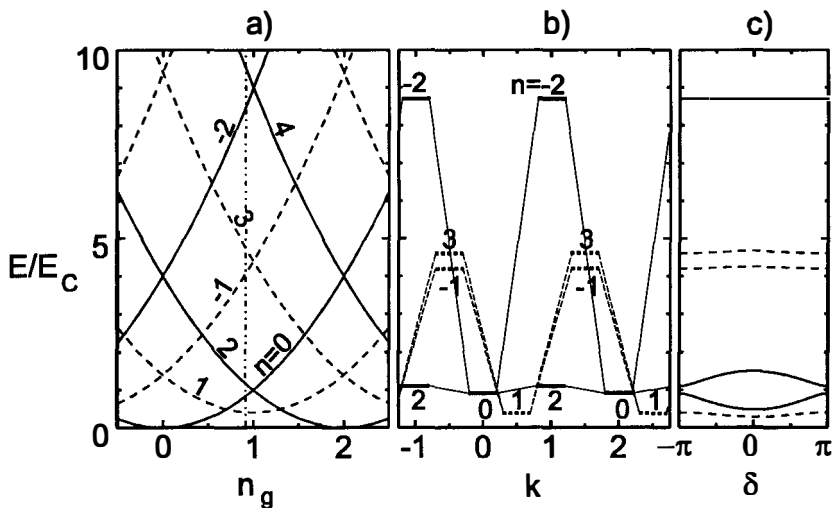


Fig. 2. a) Electrostatic plus configuration energy of the different  $n$  states as a function of  $n_g$ . Even- $n$  states are drawn using full lines. The odd- $n$  states are higher in energy than the even- $n$  states by the energy of the quasiparticles (which is at least  $\Delta$ ) and they form a continuum. The dashed lines correspond to the lowest odd- $n$  state and are plotted with an assumed value of  $\Delta=0.4 E_C$ . b) A plot of the energy states for a given value of  $n_g$ , indicated by the dotted line in panel a), showing the degeneracy of  $n$ -states with  $k$ . States of a given parity are coupled by the Josephson Hamiltonians as represented by the thin lines. c) Energy bands obtained as the result of the exact diagonalization of the total Hamiltonian with three charge states only. Full (dashed) lines correspond to eigenenergies of the Hamiltonian for the even (odd) manifold of  $n$ -states. The value of  $E_{J1}=E_{J2}=0.5E_C$  was used for this plot. We can here see how the poisoning of the supercurrent peak occurs when  $\Delta < E_C$ : in the vicinity of  $n_g=1$  a quasiparticle enters the island. The system then occupies the band formed by the  $n=\pm 1$  and  $n=3$  states. This band is very shallow compared to that of the even states at this value of  $n_g$ , resulting in a large reduction of the supercurrent.

right junction, respectively. It is also convenient to introduce the variables  $n=n_1-n_2$  and  $k=n_1+n_2$ , measuring the excess number of electrons on the island and the number of Cooper pairs having flown through the transistor, respectively. The phase difference  $\delta$  across the transistor is the conjugate variable of  $k$ . For the sake of simplicity, we will assume in the rest of this paper that the island, when neutral, has an even number of electron. The parity of the total number of electrons in the island is thus the same as the parity of  $n$ , the excess number of electrons.

The Hamiltonian of the transistor alone can be written as:

$$H=H_{el}+H_{J1}+H_{J2}+H_{qp}.$$

The first term  $H_{el}=E_C(n-n_g)^2$  is the electrostatic Hamiltonian of the circuit in which  $E_C=e^2/(2C_\Sigma)$  denotes the electrostatic energy of a single electron on the island, while

$n_g = C_g V_g / e$  is the charge (in units of  $e$ ) on the gate capacitor induced by the gate voltage  $V_g$ , which is our control “knob” over the transistor ( $C_\Sigma$  and  $C_g$  denote the total capacitance of the island and the gate capacitance, respectively). In writing  $H_{el}$  we have assumed that the gate capacitance is negligible compared with the junction capacitances. The second and third terms are the Josephson coupling Hamiltonians of the two junctions. These terms can be written:

$$H_{J1} = -\frac{E_{J1}}{2} \sum_{n,k} [ |n+2, k+1/2\rangle \langle n, k| + |n-2, k-1/2\rangle \langle n, k| ]$$

$$H_{J2} = -\frac{E_{J2}}{2} \sum_{n,k} [ |n-2, k+1/2\rangle \langle n, k| + |n+2, k-1/2\rangle \langle n, k| ]$$

Here  $E_{J1,2}$  are the Josephson coupling energies of junction 1 and 2, respectively. Since we have  $E_C \ll 2\Delta$  we will neglect the influence of charging effects on  $E_{J1,2}$ . The last term of the Hamiltonian accounts for the internal degrees of freedom of the superconductors:

$$H_{qp} = \sum_j \epsilon_j \gamma_j^\dagger \gamma_j.$$

In this expression  $\gamma_j^\dagger$  and  $\gamma_j$  are the Bogoliubov quasiparticle creation and annihilation operators and  $\epsilon_j$ , the energy of the quasiparticle. To begin with, we will assume that all the electrons in the superconductors are paired (i.e. there are no quasiparticles). In that case, at  $T=0$ ,  $H_{qp}$  can be dropped. Of course, only even- $n$  states can be considered with this hypothesis of perfect parity.

We will now find the eigenenergies of the Hamiltonian. The  $|n, k\rangle$  states are obviously eigenstates of the electrostatic Hamiltonian alone and they are all degenerate with respect to the value of  $k$ . The electrostatic energy levels are plotted as a function of  $n_g$  in Fig. 2a in full lines. The Josephson Hamiltonians  $H_{J1}$  and  $H_{J2}$  will couple all the  $|n, k\rangle$  states, lifting the  $k$ -degeneracy and forming bands. At this point it is practical to perform a change of basis, introducing the new states:

$$|n, \delta\rangle = \sum_k e^{i\delta k} |n, k\rangle$$

At  $T=0$  we are only interested in the lowest energy bands. Also, since in practice we have  $E_{J1,2} \leq E_C$ , we can neglect  $n$ -states whose electrostatic energies are above a few  $E_C$ . In the domain where  $0 \leq n_g \leq 2$  the even- $n$  states of lowest energy are  $n=0, \pm 2$ , with the  $n=\pm 2$  being degenerate at  $n_g=0$ . This degeneracy can be treated correctly in the restricted space generated by the three lowest energy states,  $| -2, \delta \rangle$ ,  $| 0, \delta \rangle$  and  $| 2, \delta \rangle$ . In this basis, the matrix of the Hamiltonian writes:

$$H = \begin{bmatrix} E_C(-2 - n_g)^2 & -\frac{1}{2}(E_{J1}e^{-i\delta/2} + E_{J2}e^{+i\delta/2}) & 0 \\ -\frac{1}{2}(E_{J1}e^{+i\delta/2} + E_{J2}e^{-i\delta/2}) & E_C(-n_g)^2 & -\frac{1}{2}(E_{J1}e^{-i\delta/2} + E_{J2}e^{+i\delta/2}) \\ 0 & -\frac{1}{2}(E_{J1}e^{+i\delta/2} + E_{J2}e^{-i\delta/2}) & E_C(2 - n_g)^2 \end{bmatrix}$$

and the secular equation takes the form of a polynomial of third degree in  $E$ :

$$(E - E_C n_g^2)(E - E_C(n_g - 2)^2)(E - E_C(n_g + 2)^2) - a(2E - E_C(8 + 2n_g^2)) = 0,$$

where

$$a = \frac{1}{4}(E_{J1}^2 + E_{J2}^2 + 2E_{J1}E_{J2}\cos\delta).$$

This equation is exactly soluble. Introducing intermediate quantities:

$$\lambda = \frac{2}{3}a + \frac{16}{3}E_C^2\left(\frac{1}{3} + n_g^2\right); \quad \mu = \frac{8}{3}aE_C + \frac{128}{3}E_C^3\left(\frac{1}{9} - n_g^2\right) \quad \text{and} \quad \theta = \text{Arccos} \frac{-\mu}{2\lambda^{3/2}},$$

the three roots are given by:

$$\xi_m(\delta, n_g) = \left(\frac{8}{3} + n_g^2\right)E_C + \sqrt{4\lambda} \cos\left(\frac{\theta + 2\pi(m+1)}{3}\right) \quad \text{with } m = 0, 1, 2.$$

These eigenenergies form bands parametrised by  $\delta$ , whose positions, shapes and amplitudes depend on the value of  $n_g$ . The treatment we have applied is valid only in the domain where  $0 \leq n_g \leq 2$  but, since the electrostatic energy diagram is periodic in  $n_g$ , the solutions to the total Hamiltonian must be periodic with  $n_g$ , with period 2, each interval of the form  $2q \leq n_g \leq 2(q+1)$  corresponding to a different set of three lowest electrostatic energy states. To extend the solution we have found, we simply duplicate it to cover the all range of  $n_g$  values. The bands are also  $2\pi$ -periodic functions of  $\delta$  (they involve  $\delta$  only through  $\cos\delta$ ).

The energy-phase relation in the ground band ( $m=0$ ) is equivalent to the  $-E_J \cos\delta$  relation of the single Josephson junction, its extrema being at  $\delta=0$  and  $\delta=\pi$ . To carry this analogy further we introduce the notation:

$$\xi_0(\delta, n_g) = E_0(n_g) f_0(n_g, \delta) \quad \text{with} \quad f_0(n_g, \pi) - f_0(n_g, 0) = 2.$$

Thus,  $E_0(n_g)$  represents the effective Josephson coupling energy of the transistor which behaves as a gate-voltage tunable Josephson junction. The strength of the effective Josephson coupling for different values of  $E_C$  at a given  $E_J = E_{J1} = E_{J2}$  is plotted in Fig. 3. The critical current of the transistor which is the maximum theoretical supercurrent that can flow through the transistor is given by the relation:

$$I_C(n_g) = \frac{2\pi}{\Phi_0} \text{Max}_\delta \left\{ \frac{\partial \xi_0(\delta, n_g)}{\partial \delta} \right\} = \frac{2\pi}{\Phi_0} E_0(n_g) \text{Max}_\delta \left\{ \frac{\partial f_0(\delta, n_g)}{\partial \delta} \right\}.$$

The maximum of the derivative of  $f_0$  does not have an analytical expression, but it turns out that its numerical value is very nearly equal to 1 for any reasonable set of parameters (1 is the value one would get with  $f_0(\delta) = -\cos\delta$ , the function of the single Josephson junction). Thus, up to an excellent approximation, the critical current is proportional to the effective Josephson coupling energy (which is just half the amplitude of the ground band), with the same proportionality factor as in the single Josephson junction, and we finally get:

$$I_C(n_g) \approx \frac{2\pi}{\Phi_0} E_0(n_g). \quad (1)$$

Therefore, Fig. 3 can also be regarded as a plot of the critical current of the transistor. We will see later how a further theoretical layer must be added on this result for an effective comparison with experiment.

### Description of the experiment

The sample was prepared using standard e-beam lithography and shadow mask evaporation techniques<sup>15</sup>). The main difference with previous experiments is the use of the 3-angle evaporation technique of Haviland *et al.*<sup>16</sup>) in order to fabricate in a single pump-down the alumina-covered Al island electrode, the two Al drain and source electrodes and the Cu (3% wt. Al) buffer electrodes (see device layout in the inset of Fig. 1). We believe that these last electrodes allow the quasiparticle population in the transistor to reach the thermal equilibrium value and prevent uncontrolled poisoning of

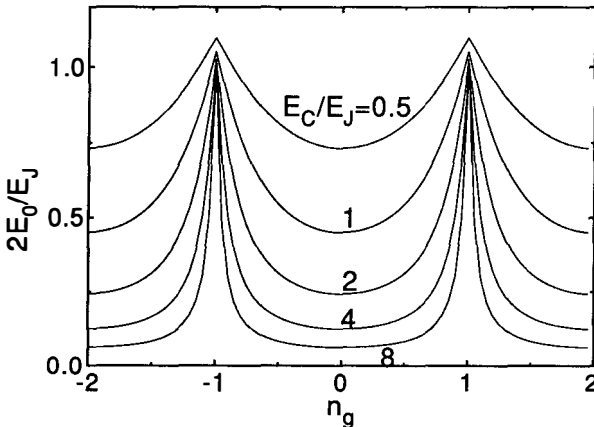


Fig. 3 Effective Josephson coupling energy of the transistor as a function of  $n_g$  for various ratios of  $E_C/E_J$ . This coupling energy is also proportional (see text) to the theoretical critical current of the transistor. The critical current peaks get narrower and the peak-to-valley ratio gets higher as  $E_J$  is reduced, but then the absolute amplitude of the peaks is reduced in proportion.

Josephson tunneling by out-of-equilibrium quasiparticles from the rest of the circuit. The electrical wiring between the sample and the measuring apparatus at room temperature was made through a series of cryogenic filters as in previous experiments<sup>6</sup>).

From the measurement of the device with the Al electrodes brought in the normal state by a magnetic field, we deduced the gate capacitance  $C_g$  and we could estimate  $E_C/k_B=1.0$  K. The normal resistance of the two junctions in series was  $R_N=49.2$  k $\Omega$ . The value  $\Delta=180$   $\mu$ eV of the gap of the superconducting aluminum was extracted from the large scale  $I$ - $V$  characteristic of the sample in zero magnetic field. Using the Ambegaokar-Baratoff relation<sup>17</sup>) we deduced from  $R_N$  and  $\Delta$  the Josephson energy  $E_J/k_B=275$  mK and critical current  $I_0=2eE_J/\hbar=11.4$  nA of each junction, supposing they are identical. In Fig. 1 we show the sub-gap current-voltage ( $I$ - $V$ ) characteristic of the transistor for  $n_g \approx 1$ . A supercurrent branch is clearly seen with nearly zero voltage like in the recent experiment by Eiles and Martinis<sup>18</sup>). Its residual slope was measured to be less than 100  $\Omega$ , our resistance resolution given the wiring of the sample to the external apparatus. This branch defines a switching current  $I_s$ , at which the device switches to a voltage set by the resistance of the current bias source, which was 12.1 M $\Omega$  for the data we present in the remainder of this paper. In Fig 4a, we show the variations of the switching current with  $n_g$  at low temperature, for different magnetic fields.

If we now compare the experimental results with the theoretical gate voltage modulation of the supercurrent using (1), we immediately notice that it can only agree qualitatively at low magnetic field and low temperature (Fig. 4a top curve vs. Fig. 3). At high magnetic field the experimental modulation pattern becomes more complicated. Moreover even at low temperature, the measured supercurrent is only a small fraction ( $\approx 1/5$ ) of the calculated critical current.

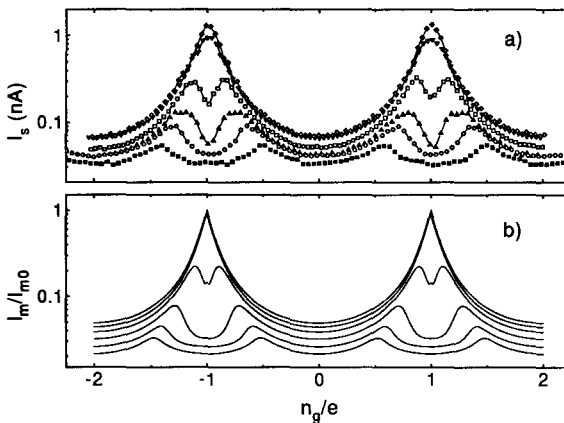


Fig. 4 a) Switching current as a function of gate charge, for several values of the magnetic field  $H$ , at  $T=65$ mK. Top to bottom:  $H=0, 0.07, 0.11, 0.14, 0.16, 0.17$  T. The dip at odd integer values of  $n_g/e$  corresponds to the poisoning of Josephson tunneling by the entrance of one quasiparticle in the island. b) Theoretical runaway current as a function of gate charge, for the same field values as in a).

### Effect of even-odd asymmetry

The change in the modulation pattern with magnetic field at zero temperature was first predicted by Matveev *et al.*<sup>10)</sup>. This arises when one takes into account the  $H_{qp}$  term of the Hamiltonian and drops the hypothesis that the number of electrons remains even at all times in the island. According to the BCS theory<sup>5)</sup>, when a single electron enters the island it cannot go into the condensate and it creates at least one excitation whose energy cost is at least  $\Delta$ , the superconducting gap in the island. This means that the ground state of the electrostatic plus configuration Hamiltonian of odd- $n$  states will be shifted by  $\Delta$  with respect to the even- $n$  states (dashed lines in Fig. 2a). Then we must consider two cases. In the first case ( $\Delta > E_C$ ), these odd- $n$  levels are so high in energy that the ground state of the system remains even at all times and then the previous derivation of the effective Josephson coupling is essentially correct. In the second case ( $\Delta < E_C$ ), in parts of the  $n_g$  domain, odd- $n$  states are the ground states of the electrostatic plus configuration Hamiltonian. This happens in the vicinity of  $n_g = 2q + 1$  (see Fig. 2a and b), where a single electron will enter the island and form odd- $n$  bands similar to the even- $n$  bands already described (the Josephson Hamiltonians only couple states of same parity). In order to distinguish the odd- and the even- $n$  bands, we introduce a superscript  $p$  in the notation for the ground band and the effective Josephson coupling, i.e.  $\xi_0^p(\delta, n_g) = E_0^p(n_g) f_0^p(\delta, n_g)$ ,  $p$  taking the value odd or even. From Fig. 2a we see that the degeneracy of the two lowest odd- $n$  states occurs at even values of  $n_g$  and we thus have  $E_0^{\text{even}}(n_g) = E_0^{\text{odd}}(n_g + 1)$ . As a consequence, when the single extra electron enters the island near  $n_g = 2q + 1$ , the effective Josephson coupling will drop from a nearly maximum value to a minimum value (see Fig. 2c): there will be a sharp, deep hole exactly at the position of the supercurrent peak. We have nicknamed this effect the “poisoning” of the supercurrent. The theory predicts also that if the gap is reduced by applying a magnetic field, the range of  $n_g$  value on which the odd state is favored extends and the “poisoning” is expected to widen up to a point where the weak remaining modulation becomes  $e$ -periodic. This corresponds qualitatively to what is observed in Fig. 4a. The hole is not as sharp and deep as predicted by the zero temperature theory of Matveev *et al.*, but this is expected from a thermal “rounding” of the effect.

### Extension of the theory at finite temperature

To go into a more detailed description of the experimental results, one must take into account i) the effect of the electromagnetic environment which affects the finite temperature dynamics of the switching of the transistor to finite voltage<sup>19,20)</sup> and ii) the effect of temperature which increases the relative probability of occupation of the odd- $n$  states with respect to the even- $n$  states, due to an entropic effect<sup>4,7)</sup>.

In the following, using the usual lumped element model, we describe the environment of the pure effective Josephson element as an admittance  $Y(\omega)$  in parallel with the current source  $I$ . We will make a classical treatment of the dynamics of the phase  $\delta(t)$  in the total circuit. Kirchoff's law writes:

$$I = \frac{2\pi}{\Phi_0} \frac{\partial \mathcal{E}_0^P(n_g, \delta)}{\partial \delta} + \int V(t - \tau) \tilde{Y}(\tau) d\tau, \quad (2)$$

where the first term is the current flowing through the Josephson element and the second term is the current in the environment, expressed as a convolution product of the voltage and the Fourier transform  $\tilde{Y}(t)$  of  $Y(\omega)$ . Assuming a short response time of the environment compared to the characteristic evolution time of the phase, one can expand the convolution product as:

$$\int V(t - \tau) \tilde{Y}(\tau) d\tau = \sum_k \frac{V^{(k)}(t)}{k!} \int (-\tau)^k \tilde{Y}(\tau) d\tau = \sum_k \frac{(-j)^k}{k!} V^{(k)}(t) Y^{(k)}(\omega = 0).$$

Replacing in (2) and using  $V = \dot{\delta} \Phi_0 / 2\pi$ , one obtains a differential equation for  $\delta$ :

$$\frac{\Phi_0}{2\pi} \left[ Y(0) \dot{\delta} - jY'(0) \ddot{\delta} - \frac{1}{2} Y''(0) \delta \ddot{\delta} + \dots \right] + \frac{2\pi E_0^P}{\Phi_0} \frac{df_0^P}{d\delta} = I.$$

The evolution of  $\delta$  is identical to that of a particle of mass  $-jY'(0)(\Phi_0/2\pi)^2$  in the tilted potential  $E_0^P f_0^P(\delta) - (\Phi_0/2\pi)\delta I$  with friction terms in  $Y(0)\dot{\delta}, Y''(0)\delta\ddot{\delta} \dots$ . This equation generalizes the equation of motion of the resistively and capacitively shunted junction (RCSJ) model<sup>21)</sup> to an effective Josephson element shunted by a general admittance.

For  $I \leq I_C(n_g)$ , this equation admits a zero-voltage solution ( $\dot{\delta} = 0$ ) corresponding to the particle sitting in a local minimum of the tilted potential. This solution is unstable against thermal fluctuations and therefore the particle will diffuse from well to well in the potential, giving rise to a departure of the supercurrent branch from the zero-voltage axis. However, for  $I_m \leq I < I_C$  this diffusive motion is itself unstable against the runaway down the potential<sup>20)</sup>, where  $I_m$  is the current for which, on the average, the energy gain due to the tilt of the potential becomes greater than energy loss due to friction. In the weak friction limit appropriate to our experiment, the losses due to each friction term can be evaluated independently using the free dynamics of the phase and one gets for the runaway current  $I_m$ :

$$I_m = \Phi_0 \left[ \alpha Y(0) \left( \frac{E_0^P}{\Phi_0^2 |Y'(0)|} \right)^{1/2} + \beta Y''(0) \left( \frac{E_0^P}{\Phi_0^2 |Y'(0)|} \right)^{3/2} + \dots \right], \quad (3)$$

where  $\alpha, \beta, \dots$  are dimensionless coefficients which are weakly dependent on  $f_0^p$ . The first term in the expansion corresponds to the well known  $4I_0/\pi RC\omega_p$  result of the RCSJ model<sup>19</sup>. Here, since we have an unshunted junction, this term arising from a fluid friction vanishes and the  $n_g$ -dependence of  $I_m$  is dominated by the second term which takes the form of a radiative-like friction.

In view of the importance of thermal fluctuations in our experiment ( $E_0^p \leq E_J/2$ ), it is certainly better to compare the  $n_g$ -dependence of the measured switching current with the theoretical  $n_g$ -dependence of  $I_m$  rather than of the critical current  $I_C$  considered by Matveev *et al.*<sup>10</sup>.

To go further, we will assume that the inverse of the transition rate between the odd- $n$  and even- $n$  states is much smaller than the characteristic time of the runaway process. These transitions involve a co-tunneling process of an electron between a normal metal lead and the island and the rate of this process can be very high due to their proximity in the sample (about  $0.25 \mu\text{m}$ )<sup>3</sup>. In the calculation of the switching current, we thus replace  $E_0^p$  by the Boltzmann average  $E_0^{av} = E_0^{odd} p_{odd} + E_0^{even} p_{even}$  where  $p_{odd}$  and  $p_{even}$  are the probabilities of being in an odd- or even- $n$  state, respectively, and which verify:

$$p_{odd/even} \propto \sum_{n \text{ odd/even}} \exp\left\{-\left[E_C(Q_g/e - n)^2 + (n \bmod 2)D(T, H)\right]/k_B T\right\},$$

where  $D(T, H)$  is the odd-even free energy difference<sup>4,6</sup> and is calculated as in Ref. 7. Note that if the inverse of the quasiparticle co-tunneling rate was longer than the time it takes for the phase to run away but still shorter than the measuring time, then one expects to see the minimum of the two switching currents defined by  $E_0^{odd}$  and  $E_0^{even}$  in Eq. (3), with sharp jumps in the modulation pattern, very much as is predicted in Ref. 10.

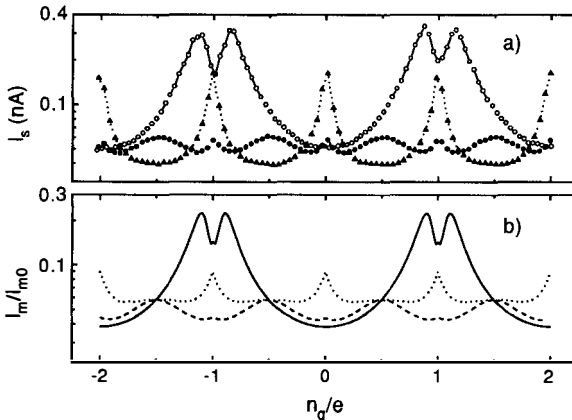


Fig. 5a) Switching current as a function of gate charge, at  $H=0.11$  T and for several values of the temperature  $T$ , showing the complex transition from  $2e$ -periodicity to  $e$ -periodicity with the increase of  $T$ . Open dots:  $T=65$  mK; solid dots:  $T=203$  mK; triangles:  $T=356$  mK. b) Theoretical runaway current as a function of gate charge, for the same temperature values as in a) (the full and dotted line correspond to the lowest and highest temperatures, respectively).

Using the preceding analysis we can calculate the function  $I_m(Q_g, H, T)$  in which enters the unknown scale parameter  $Y''(0)/Y'(0)^{3/2}$  and two adjustable parameters: i) the parameter  $\rho$  of the reduction of  $I_0$  due to penetration of magnetic field in the junctions defined by  $I_0(H) = I_0(1 - \rho H^2)$  in the low field limit of relevance here and ii) the critical field  $H_c$  such that  $D(0, H > H_c) = 0$ , which corresponds to the field at which  $I_m(Q_g)$  becomes  $e$ -periodic at  $T=0$ . In Fig. 4b, we plot  $I_m(Q_g, H, T = 65 \text{ mK}) / I_{m0}$  where  $I_{m0} = I_m(Q_g = e, H = 0, T = 65 \text{ mK})$  using the best fit values  $\rho = 18.5 \text{ T}^{-2}$  and  $H_c = 0.20 \text{ T}$  which are consistent with the junction geometry and with a previous measurement of  $D$  <sup>7)</sup>, respectively. These values are also used in Fig. 5b. A close agreement with the experimental results is obtained. The validity of our model can be checked further on the temperature dependence of the  $I_m$  versus  $n_g$  data shown in Fig. 5a taken for the intermediate field  $H = 0.11 \text{ T}$ . Experiments at higher temperatures agree less closely with theory, the relative amplitude of the peaks being greater in experiment than in theory. We believe this is due to the neglect of the influence of thermal fluctuations in the runaway process of the phase. However, the non-monotonic behavior of the  $n_g = 1$  switching current as a function of temperature is captured by our model<sup>14)</sup>.

In conclusion, we have shown that in a Josephson system where the number of quasiparticles was controlled, experimental measurements of charging effects can agree with a simple model, in contrast with preceding experiments. As Fig. 5 exemplifies, the competition between the charging energy, the Josephson energy and the odd-even free energy difference produces a complex behavior of the supercurrent as a function of gate charge, magnetic field and temperature. This intrinsic complexity, together with the absence of control over the quasiparticle population, probably explains why the data of previous experiments in the superconducting state has always been somewhat of a puzzle.

### Acknowledgements

We are grateful to John Martinis and Denis Vion for helpful comments. We also acknowledge P. F. Orfila for technical help. This work is supported in part by the Bureau National de la Métrologie under contract No. 93-2-46-0018 and by the Commission of the European Community under contract No. ERBSC1\*CT000631.

## References

- 1 K. K. Likharev and A. B. Zorin, *J. Low Temp. Phys.* **59**, 347 (1985)
- 2 T. A. Fulton and G. J. Dolan, *Phys. Rev. Lett.* **59**, 109 (1987).
- 3 D. V. Averin and Yu. V. Nazarov, *Phys. Rev. Lett.* **69**, 1993 (1992).
- 4 M. T. Tuominen, J. M. Hergenrother, T. S. Tighe and M. Tinkham, *Phys. Rev. Lett.* **69**, 1997 (1992).
- 5 J. Bardeen, L. N. Cooper and J. R. Schrieffer, *Phys. Rev.* **108**, 1175 (1957).
- 6 P. Lafarge, P. Joyez, D. Esteve, C. Urbina and M. H. Devoret, *Phys. Rev. Lett.* **70**, 994 (1993).
- 7 P. Lafarge, P. Joyez, D. Esteve, C. Urbina, and M. H. Devoret, *Nature* **365**, 422 (1993).
- 8 T. M. Eiles, J. M. Martinis and M. H. Devoret, *Phys. Rev. Lett.* **70**, 1862 (1993).
- 9 M. T. Tuominen, J. M. Hergenrother, T. S. Tighe, and M. Tinkham, *Phys. Rev. B* **47**, 11599 (1993)
- 10 K. A. Matveev, M. Gisselält, L. I. Glazman, M. Jonson and R. I. Shekhter, *Phys. Rev. Lett.* **70**, 2940, 1993.
- 11 D. V. Averin and K. K. Likharev, in *Mesoscopic Phenomena in Solids*, ed. by B. Altshuler, P. Lee, and R. Webb (Elsevier, Amsterdam, 1991), Chap. 6.
- 12 T. A. Fulton, P. L. Gammel, D. J. Bishop and L. N. Dunkleberger, *Phys. Rev. Lett.* **63**, 1307 (1989).
- 13 L. J. Geerligs, V. F. Anderegg, J. Romijn, and J. E. Mooij, *Phys. Rev. Lett.* **65**, 377 (1990).
- 14 P. Joyez, P. Lafarge, A. Filipe, D. Estève and M. H. Devoret, *Phys. Rev. Lett.* **72**, 2458 (1994)
- 15 G. J. Dolan and J. H. Dunsmuir, *Physica B* **152**, 7 (1988).
- 16 D. B. Haviland, L. S. Kuzmin, P. Delsing, K. K. Likharev, and T. Claeson, *Z. Phys. B* **85**, 339 (1991).
- 17 V. Ambegaokar and A. Baratoff, *Phys. Rev. Lett.* **10**, 486 (1963).
- 18 T. M. Eiles, and J. M. Martinis, unpublished
- 19 M. Büttiker, E. Harris, and R. Landauer, *Phys. Rev. B* **28**, 1268 (1983).
- 20 R. L. Kautz, and J. M. Martinis, *Phys. Rev. B* **42**, 9903 (1990).
- 21 W. C. Stewart, *Appl. Phys. Lett.* **12**, 277 (1968); D. E. McCumber, *J. Appl. Phys.* **39**, 3113 (1968).

# COULOMB AND INTERFERENCE EFFECTS IN SMALL N-S TUNNEL JUNCTIONS

F.W.J. Hekking

*Institut für Theoretische Festkörperphysik, Universität Karlsruhe*

*Postfach 6980, 76128 Karlsruhe, FRG*

## 1 Introduction

In the early sixties, shortly after the discovery of BCS theory, electron tunneling between a normal metal (N) and a superconductor (S) became an important tool to investigate properties of superconductors<sup>1)</sup>. With the help of single particle tunneling one could study *e.g.* the superconducting density of states or the temperature dependence of the superconducting gap. The key point is that the transport of a *single* charge through a tunnel interface between a normal metal and a superconductor (N-I-S interface) is strongly suppressed at voltages lower than  $\Delta/e$ ,  $\Delta$  being the superconducting energy gap. Indeed, energy conservation forbids the transfer of a normal electron with an energy below the gap to the superconductor, since it would have been converted into a quasiparticle with an energy larger than  $\Delta$ .

At about the same time, Andreev<sup>2)</sup> found a mechanism which allows for electron transport under subgap conditions. He considered a clean interface (without a tunnel barrier) between a normal metal and a superconductor. An electron, incident from the normal side with an energy below the superconducting gap, will be reflected at the interface as a hole. As a result, two quasiparticles are excited in the superconductor, which will eventually recombine into a Cooper pair. This process, called Andreev-reflection, will lead to an excess conductance at bias voltages smaller than  $\Delta/e$ .

In 1982, Blonder, Tinkham, and Klapwijk<sup>3)</sup> built a bridge between tunneling phenomena on the one hand, and transport through “clean” interfaces on

the other hand. Using the Bogoliubov-de Gennes equations, they studied the transport properties of an interface between a superconductor and a normal metal which is characterized by a barrier of dimensionless strength  $Z$  (normal state transmission  $T = 1/(1 + Z^2)$ ). In particular they showed how the excess current induced by Andreev-reflection is suppressed with increasing strength  $Z$ . In the limit of strong tunneling ( $Z \gg 1$ ) they found a subgap conductance proportional to  $1/Z^4$ . Since the normal state conductance in this limit, governed by single particle tunneling, is proportional to  $1/Z^2$ , one concludes that the subgap conductance is caused by two-electron tunneling: Two normal electrons tunnel through the interface and are converted into a Cooper pair.

More recently<sup>4)</sup>, the tendency towards miniaturization has led to the investigation of tunneling phenomena which occur in ultrasmall junctions, characterized by a small capacity  $C$ . The simplest example of such a system consists of a small conducting grain, coupled to two macroscopic leads by tunnel barriers. The grain is coupled capacitively to a gate electrode (capacity  $C_g$ ). This gate allows to control the number  $N$  of electrons on the grain by the gate voltage  $V_g$ . For almost any value of  $V_g$ , the ground state of the grain is non-degenerate, and variations of its charge in the course of electron tunneling increase the electrostatic energy by an amount of the order  $E_C = e^2/2C$ . This is why electron tunneling through a small grain is suppressed (Coulomb blockade). However, at certain values of  $V_g$  which form a periodic set with period  $e/C_g$ , the ground state is degenerate and the blockade is lifted. At these values of  $V_g$ , the electrostatic energies of the system with  $N$  and  $N + 1$  electrons on the grain are equal.

In case of a superconducting grain, interesting parity effects<sup>5)-8)</sup> can be observed. Since the ground state of a superconducting grain favors even numbers of electrons, its transport properties should reflect a free energy difference of the order of the superconducting gap  $\Delta$  between even and odd parity of the total number of electrons  $N$ , which participate in the ground state of the grain. If the superconducting gap  $\Delta$  exceeds the charging energy  $E_C$ , the ground state of the grain always involves an even number of electrons  $N$ . As a result, the subgap conductance is modulated with a period  $2e/C_g$  as a function of the gate voltage  $V_g$ . If  $\Delta < E_C$ ,  $N$  can be both even and odd, and the modulation pattern as a function of  $V_g$  changes: In the limit  $\Delta \rightarrow 0$  the period of the modulation  $e/C_g$  is recovered.

In addition, pronounced interference effects can occur. This is related to the fact that charge transfer through a N-I-S junction occurs via the tunneling of *two* electrons. In the diffusive transport regime (diffusion constant  $D$ ), the correlation length  $L_{cor} = \sqrt{\hbar D/\varepsilon}$  determines the length over which two

electrons with energy difference  $\varepsilon$  move phase-coherently along the same diffusion path (Cooperon propagation). The subgap conductance therefore will depend on the geometry of the tunnel junction within a length  $L_{cor}$ . Similar interference effects are known for the normal SET-transistor in the Coulomb blockade regime when higher order tunneling processes determine the transport properties<sup>9</sup>).

It is the aim of the present paper to investigate Coulomb and interference effects occurring in small N-I-S junctions. In section 2, the transport properties of a single N-I-S junction are discussed. We will focus on interference effects. In section 3, the transport properties of the N-I-S-I-N double junction are presented, with the emphasis on charging effects.

## 2 Transport properties of a single N-I-S junction

The total Hamiltonian for the N-I-S junction can be written as  $\hat{H} = \hat{H}_N + \hat{H}_S + \hat{H}_T$ . The subscripts  $N$  and  $S$  refer to the normal (left) and the superconducting (right) electrode respectively; the transfer of electrons through the tunnel interface is described by the tunnel Hamiltonian

$$\hat{H}_T = \sum_{k,p,\sigma} t_{k,p} \hat{a}_{k,\sigma}^\dagger (u_{p,\sigma} \hat{\gamma}_{p,\sigma} + v_{p,\sigma} \hat{\gamma}_{-p,-\sigma}^\dagger) + t_{k,p}^* (u_{p,\sigma} \hat{\gamma}_{p,\sigma}^\dagger + v_{p,\sigma} \hat{\gamma}_{-p,-\sigma}) \hat{a}_{k,\sigma}. \quad (1)$$

The sum is taken over momenta  $k$ ,  $p$  in the normal metal and the superconductor, respectively, and over the spin  $\sigma = \uparrow, \downarrow$ . We assume that the electron spin  $\sigma$  is conserved during tunneling. The operators  $\hat{a}^\dagger$ ,  $\hat{a}$  refer to the normal metal. For the superconductor, we introduced the quasiparticle operators  $\hat{\gamma}^\dagger$ ,  $\hat{\gamma}$  and the BCS coherence factors  $u_{p,\sigma}$ ,  $v_{p,\sigma}$ <sup>10</sup>).

Using second order perturbation theory in  $\hat{H}_T$  one can calculate the amplitude for the transfer of two electrons from the normal to the superconducting electrode:

$$A_{k\uparrow k'\downarrow} = \sum_p t_{k,p}^* t_{k',-p}^* u_p v_p \left\{ \frac{1}{\xi_k - \varepsilon_p} + \frac{1}{\xi_{k'} - \varepsilon_p} \right\}. \quad (2)$$

Here the spin dependence of the coherence factors was dropped after using the relation  $v_{p,\uparrow} = -v_{-p,\downarrow}$ . We define electron energies  $\xi_k$  and  $\zeta_p$  for the left and the right electrode respectively, and quasiparticle energies  $\varepsilon_p = \sqrt{\Delta^2 + \zeta_p^2}$ . The denominators in (2) reflect the fact that a virtual state is formed when the first electron enters the superconductor as a quasiparticle. The second electron couples to this quasiparticle, thus forming a Cooper pair. The corresponding rate  $\Gamma(V)$  for one spin direction as a function of the voltage  $eV \ll \Delta$  applied

across the junction can be found by using Fermi's Golden Rule

$$\Gamma(V) = \frac{2\pi}{\hbar} \sum_{k,k'} |A_{k\uparrow k'\downarrow}|^2 f(\xi_k) f(\xi_{k'}) \delta(\xi_k + \xi_{k'} + 2eV). \quad (3)$$

It contains the Fermi functions  $f$  for electrons with energies  $\xi_k$ ,  $\xi_{k'}$  in the normal metal. The thermal distribution for quasiparticles is approximated by a step function at sufficiently low temperatures  $k_B T \ll \Delta$ .

By introducing the function  $F(\zeta; \xi, \xi') = u(\zeta)v(\zeta)[(\xi + eV - \varepsilon)^{-1} + (\xi' + eV - \varepsilon)^{-1}]$  with  $\varepsilon \equiv \varepsilon(\zeta) = \sqrt{\Delta^2 + \zeta^2}$ , we can write (3) as

$$\Gamma(V) = \sum_{k,k',p,p'} \int d\xi d\xi' d\zeta d\zeta' \delta(\xi - \xi_k) \delta(\xi' - \xi_{k'}) \delta(\zeta - \zeta_p) \delta(\zeta' - \zeta_{p'}) \times \\ t_{k,p}^* t_{k',-p}^* t_{k,p'} t_{k',-p'} F(\zeta; \xi, \xi') F(\zeta'; \xi, \xi') f(\xi) f(\xi') \delta(\xi + \xi' + 2eV). \quad (4)$$

In coordinate representation the tunnel matrix elements can be expressed in terms of the eigenfunctions  $\psi_k(\vec{r})$  ( $\psi_p(\vec{r}')$ ) of the left (right) electrode:  $t_{k,p} = \int d^3r d^3r' \psi_k^*(\vec{r}) \psi_p(\vec{r}') t(\vec{r}, \vec{r}')$ . The amplitudes  $t(\vec{r}, \vec{r}')$  describe the tunneling from a point  $\vec{r}'$  in the right electrode to a point  $\vec{r}$  in the left electrode. They can be related to the conductance  $g(r)$  of the tunnel barrier per unit surface area (see Appendix A). We further introduce the spectral function for the left electrode:

$$K_\xi(\vec{r}_1, \vec{r}_2) \equiv \sum_k \delta(\xi - \xi_k) \psi_k(\vec{r}_1) \psi_k^*(\vec{r}_2) = \frac{1}{2\pi i} [G_\xi^A(\vec{r}_1, \vec{r}_2) - G_\xi^R(\vec{r}_1, \vec{r}_2)], \quad (5)$$

where  $G^{A(R)}$  is the usual advanced (retarded) propagator. A similar spectral function can be defined for the right electrode, by replacing energies  $\xi \rightarrow \zeta$ , and unprimed space arguments by primed ones. A last notational simplification is achieved by introducing the function

$$\Xi(\zeta, \zeta'; \xi, \xi') = \int d^3r_1 \dots d^3r_4 \int d^3r_1' \dots d^3r_4' t^*(\vec{r}_1, \vec{r}_1') t^*(\vec{r}_2, \vec{r}_2') t(\vec{r}_3, \vec{r}_3') t(\vec{r}_4, \vec{r}_4') \times \\ K_\xi(\vec{r}_1, \vec{r}_3) K_{\xi'}(\vec{r}_2, \vec{r}_4) K_\zeta(\vec{r}_2, \vec{r}_1') K_{\zeta'}(\vec{r}_4, \vec{r}_3'). \quad (6)$$

We are now in a position to express (3) as

$$\Gamma(V) = \frac{2\pi}{\hbar} \int d\xi d\xi' d\zeta d\zeta' F(\zeta; \xi, \xi') F(\zeta'; \xi, \xi') \Xi(\zeta, \zeta'; \xi, \xi') \times \\ f(\xi) f(\xi') \delta(\xi + \xi' + 2eV). \quad (7)$$

The information about the electron propagation in the left and right electrode is included in the function  $\Xi(\zeta, \zeta'; \xi, \xi')$ .

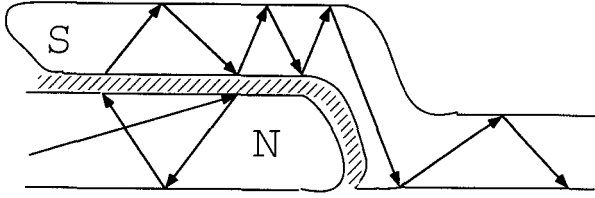


Figure 1: Ultrasmall tunnel junction.

We assume the motion to be diffusive, characterized by a diffusion constant  $D$  and elastic mean free path  $l_e$ . This is quite realistic for present-day small junction systems<sup>4</sup>). One may consider *e.g.* a junction which consists of electrodes of thin metallic and superconducting films. Typically, the thickness  $d$  of such films is about 20 nm. Tunneling occurs through a thin oxide barrier between the films (see Fig. 1). The Fermi wavelength of the films is a few Å. In this case the electronic motion is well described semi-classically in terms of diffusive boundary scattering, with  $l_e = d$ .

Our assumption means that  $\Xi$  has to be averaged in the standard way over disorder<sup>11</sup>), if the junction area  $S$  exceeds  $l_e^2$ . The phase coherence which exists between the two electrons propagating in N or S (Cooperon propagation) comes into play when the product of two spectral functions in N or S is averaged. In the normal metal this involves the well-known average

$$\langle G_{\xi}^A(\vec{r}_1, \vec{r}_2) G_{\xi'}^R(\vec{r}_1, \vec{r}_2) \rangle = \frac{\nu_N}{2\pi} P_{\xi' - \xi}(\vec{r}_1 - \vec{r}_2), \quad (8)$$

where the Cooperon  $P$  satisfies the equation

$$-\hbar D \Delta_{r_1} P_{\varepsilon} - i\varepsilon P_{\varepsilon} = \delta^3(\vec{r}_1 - \vec{r}_2). \quad (9)$$

We find  $\Xi = \Xi_N + \Xi_S$ , where (see also appendix A)

$$\Xi_N(\zeta, \zeta'; \xi, \xi') = \frac{\hbar}{32\pi^3 e^4 \nu_N} \int d^2 r_1 d^2 r_2 g(\vec{r}_1) g(\vec{r}_2) \{P_{\varepsilon}(r_1 - r_2) + P_{-\varepsilon}(r_1 - r_2)\} \quad (10)$$

involves Cooperon propagation in the normal metal. A similar expression is obtained for  $\Xi_S$  by averaging in the superconductor.

The solution of Eq. (9) will decay on a distance given by  $L_{cor} = \sqrt{\hbar D / \varepsilon}$ . For a superconductor, the relevant energy differences  $\varepsilon = \zeta' - \zeta$  contributing to Eq. (7) are of the order  $\Delta$ , whereas for the normal metal, we have  $\varepsilon \sim \max(eV, k_B T)$ . Thus, under subgap conditions the contribution from

Cooperon propagation in N is more important than the contribution from S. For the total subgap current (two spin directions) we find

$$I(V) = \frac{\hbar}{4e^3\nu_l} \int d^2r_1 d^2r_2 g(r_1) g(r_2) \times \int d\varepsilon \{f(\varepsilon/2 - eV) - f(\varepsilon/2 + eV)\} \{P_\varepsilon(r_1 - r_2) + P_{-\varepsilon}(r_1 - r_2)\}. \quad (11)$$

If the phase  $\phi$  of the superconductor varies spatially, the phase difference between the points where tunneling occurs  $\phi(r_1) - \phi(r_2)$  plays a role. This can be accounted for<sup>12)</sup> by multiplying the integrand of Eq. (11) by a phase factor  $\exp i\{\phi(r_1) - \phi(r_2)\}$ . This plays a crucial role in a recent experiment by Pothier *et al.*<sup>13)</sup>, who studied the flux dependence of two-electron tunneling for a superconducting fork, connected to a normal electrode by tunnel junctions.

We assume a constant tunnel conductance per unit surface area of the barrier:  $g = G_T/S$  where  $S$  is the junction area. The subgap conductance  $G_s = \partial I/\partial V|_{V=0}$  is given by  $G_s = R_{cor}G_T^2$ , where

$$R_{cor} = \frac{R_Q}{\pi\nu_N k_B T S} \int d^2r \int d\varepsilon \frac{e^{\varepsilon/k_B T}}{(e^{\varepsilon/k_B T} + 1)^2} \{P_\varepsilon(r) + P_{-\varepsilon}(r)\}. \quad (12)$$

Here  $R_Q = e^2/h$  is the quantum resistance.

As long as  $L_{cor} < l_e$ , we may neglect phase-coherence between the two electrons. In that case we put  $P_{\xi,-\xi}(\vec{r}_1 - \vec{r}_2) \propto \langle G_\xi^A(\vec{r}_1, \vec{r}_2) \rangle \langle G_{\xi'}^R(\vec{r}_1, \vec{r}_2) \rangle$  and find  $R_{cor} \sim R_Q/N_{eff}$ , where  $N_{eff} = k_F^2 S$  denotes the number of channels penetrating the tunnel barrier. Since  $\langle G_\xi^{R,A}(\vec{r}_1, \vec{r}_2) \rangle$  decays over a distance  $l_e$ , this contribution to the subgap conductance is smaller than the one found in the opposite limit  $L_{cor} > l_e$ . Alternatively one may say, that the phase coherence between the two electrons reduces the effective number of channels penetrating the barrier. This reduction was observed in a recent experiment<sup>8)</sup>. A numerical solution of Eq.(9) for the geometry of the junctions used in<sup>8)</sup> leads to a good quantitative estimate for  $R_{cor}$ . One thus may conclude that for  $L_{cor} > l_e$  the subgap conductance not only depends on properties of the tunnel barrier, but also on properties of the normal metal through which the two electrons move phase-coherently over a distance  $L_{cor}$ .

Several other implications of these results were discussed recently<sup>12)</sup>. Here, we will focus on the geometry depicted in Fig. 2a. It allows us to study interference effects due to two-electron tunneling by tuning the electron phases by a magnetic flux. Solving Eq. (9) for a normal ring (resistance  $R_L$ , circumference  $L$ , and aspect ratio  $\alpha$ ) at a distance  $l$  from the superconductor and threaded by a magnetic flux  $\Phi$  we find

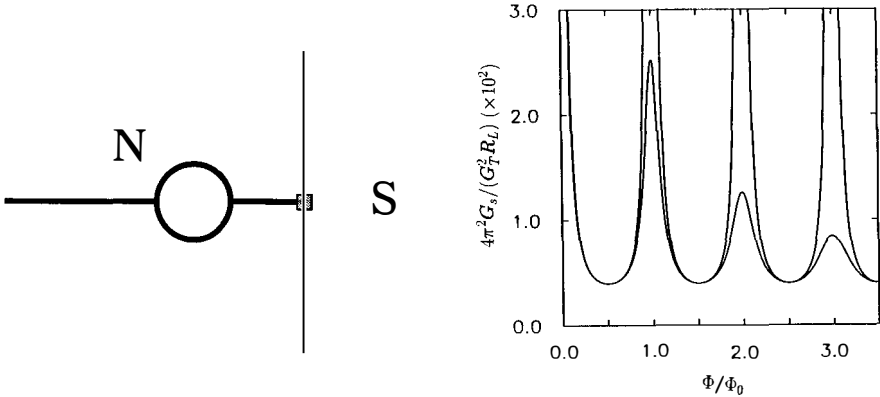


Figure 2: (a) Loop connected to superconductor. (b) Subgap conductance as a function of flux.

$$G_s = \frac{2G_T^2 R_L (1 + 2(l/L) \sin^2 \pi \Phi / \Phi_0)^2}{(\pi \alpha \Phi / 2 \Phi_0) (\cos 2\pi \Phi / \Phi_0 + 1) + (2 \sin^2 \pi \Phi / \Phi_0) (1 + 2(l/L) \sin^2 \pi \Phi / \Phi_0)}. \quad (13)$$

The result is plotted in Fig. 2b, taking  $l/L = 0.5$ ,  $\alpha = 0$  (upper curve) and  $\alpha = 0.1$  (lower curve). Divergences occur at multiples of  $\Phi_0 = h/2e$  if the aspect ratio  $\alpha = 0$ . They will be cut off *e.g.* by a finite temperature or bias voltage, which limits the result (13) to  $G_s = R_{cor} G_T^2$ , with  $R_{cor} \sim L_{cor}/e^2 \nu_N d^2 D$  the resistance of the normal wire (cross-section  $d^2$ ) per correlation length  $L_{cor}$ . The divergences also disappear when flux penetrates the arms constituting the loop, *i.e.* when  $\alpha \neq 0$ .

### 3 Coulomb blockade of two-electron tunneling

We now turn to the system depicted in Fig. 3, which consists of a superconducting grain connected to two normal electrodes by tunnel junctions. The grain is linked capacitively to the leads (capacitors  $C_l$ ,  $C_r$  in Fig. 3) as well as to a gate electrode (capacity  $C_g$ ). The latter allows to control the number  $N$  of electrons on the grain by the gate voltage  $V_g$ ; transport is achieved if a bias voltage  $V \equiv V_l - V_r$  is applied to the leads. As it was mentioned in section 1, if  $\Delta > E_C$  the grain will favor a ground state which involves an even number of electrons. We therefore expect a transport mechanism which gives a resonant contribution to the tunnel current at some particular values of the

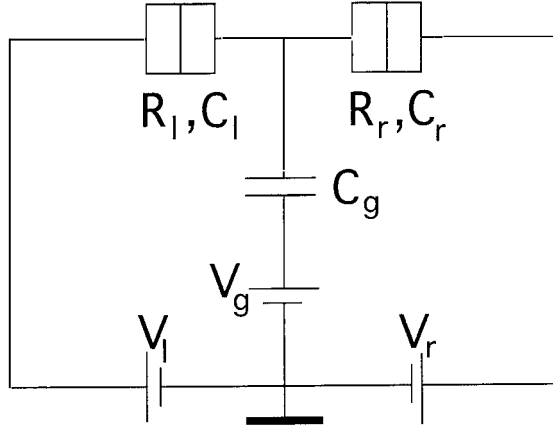


Figure 3: Schematic representation of SET-transistor.

gate voltage, when the ground state has the degeneracy  $2n \leftrightarrow 2n + 2$ . The resonances are periodic in  $V_g$  with a period  $2e/C_g$ . The origin of these resonances is similar to that for a non-superconducting system<sup>14)</sup>, but the period is twice larger than in the normal state of the grain. The period is doubled because *two* electrons are involved in the sequential transitions through the grain. Two electrons first tunnel into the grain and become a part of the superconducting condensate. Then, *another* pair of electrons tunnels from the condensate into the opposite lead, thus returning the grain to its initial state and finishing an elementary event of charge transfer. In order to describe this so-called two-electron tunneling theoretically<sup>7)</sup> we first have to adjust the results obtained for a single junction to include the charging energy. Then, we use a rate equation to connect transport through the first and the second junction.

The inclusion of the charging energy affects the results discussed in section 2. In the first step of two-electron tunneling, the grain is charged by a virtual electron, which changes the total number of electrons on the grain from  $N \rightarrow N + 1$ . This step is accompanied by a change in energy of the grain by an amount  $E_{N+1} - E_N$ , where  $E_N = (Ne)^2/(2C) + (Ne/C)(C_l V_l + C_r V_r + C_g V_g)$ . The virtual state denominators in Eq. (2) should thus be replaced:  $\xi_k - \varepsilon_p \rightarrow E_N - E_{N+1} + \xi_k - \varepsilon_p$ . Near the resonance  $N \leftrightarrow N+2$  we have  $E_N - E_{N+1} \approx E_C$ . The total energy needed to transfer two electrons onto the grain through the left junction is  $\varepsilon_l = E_{N+2} - E_N - 2eV_l$ . Energy conservation implies that we should replace  $\xi_k + \xi_{k'} + 2eV \rightarrow \xi_k + \xi_{k'} - \varepsilon_l$  in the  $\delta$ -function in Eq. (3). We

then arrive at the following expression for the rate:

$$\Gamma_i(\epsilon_i) = \frac{2\pi}{\hbar} \gamma_i \frac{\epsilon_i}{\exp(\epsilon_i/k_B T) - 1}, \quad i = l, r \quad (14)$$

with

$$\gamma_i = \frac{R_{cor}}{R_Q} \frac{G_i^2}{(\pi e^2/\hbar)^2} \frac{2\Delta^2}{\Delta^2 - E_C^2} \left\{ \arctan \sqrt{\frac{\Delta + E_C}{\Delta - E_C}} \right\}^2. \quad (15)$$

In order to find the total current through the left and the right junction, we use the fact that in the vicinity of the resonance only the states with  $N$  and  $N + 2$  electrons on the grain play a role. We define the probability  $p_N$  to find the grain in a state involving  $N$  electrons. Near the resonance we have  $p_N + p_{N+2} = 1$ . The partial currents through each junction can be expressed through  $p$ , *e.g.*  $I_{l \rightarrow g} = e\Gamma_l(\epsilon_l)p_N$ , where the subscript  $g$  refers to the grain.

At zero applied bias and low temperature  $k_B T \sim |E_N - E_{N+2}| \ll E_C$ , the partial currents to and from the grain compensate at each junction:  $I_{i \rightarrow g}^{(0)} = I_{g \rightarrow i}^{(0)}$ . From this it follows that  $p_N^{(0)} = 1 + \exp\{(E_N - E_{N+2})/k_B T\}^{-1}$ . If a small bias  $eV \ll k_B T$  is applied, a current  $I_l$  will be induced at the left junction:

$$I_l = I_{l \rightarrow g}^{(0)} V \left[ \frac{1}{\Gamma_l(\epsilon_l)} \left( \frac{\partial \Gamma_l}{\partial V} \right)_{V=0} + \frac{1}{p_N} \left( \frac{\partial p_N}{\partial V} \right)_{V=0} - \frac{1}{\Gamma_l(-\epsilon_l)} \left( \frac{\partial \Gamma_l}{\partial V} \right)_{V=0} - \frac{1}{p_{N+2}} \left( \frac{\partial p_{N+2}}{\partial V} \right)_{V=0} \right]. \quad (16)$$

Similarly, a current  $I_r$  will be induced at the right junction. Using the fact that the total current  $I = I_l = I_r$ , we obtain the differential (subgap) conductance of the N-I-S-I-N double junction:

$$G_s = \frac{4\pi e^2}{\hbar} \frac{\gamma_l \gamma_r}{\gamma_l + \gamma_r \sinh\{2eC_g(V_g - V_g^{(N)})/Ck_B T\}}. \quad (17)$$

Here  $V_g^{(N)} = -(N + 1)e/C_g$  is the gate voltage at which the resonance is reached.

At zero temperature, partial currents only flow in the direction dictated by the applied bias. Using the relation  $I = I_{l \rightarrow g} = I_{g \rightarrow r}$  we find  $I = 2e\Gamma_l(\epsilon_l)\Gamma_r(-\epsilon_r)/[\Gamma_l(\epsilon_l) + \Gamma_r(-\epsilon_r)]$ . The conductance vanishes as long as  $V_g \neq V_g^{(N)}$ , unless the bias voltage exceeds a certain threshold. We thus find current resonances as a function of  $V_g$  whenever

$$V_r - \frac{C_l}{C_g} V < V_g - V_g^{(N)} < V_l + \frac{C_r}{C_g} V.$$

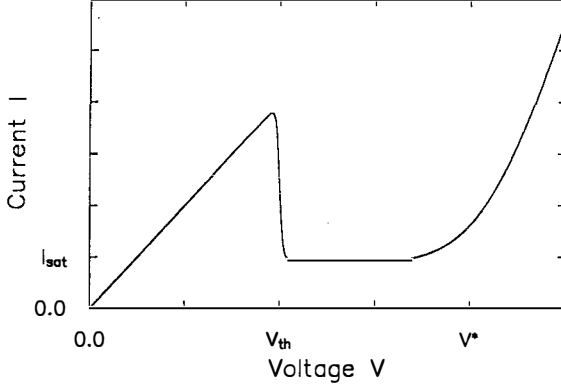


Figure 4: Overall  $I - V$ -characteristic for the double junction.

In a symmetric set-up ( $C_l = C_r$ ,  $\gamma_l = \gamma_r = \gamma$ ) with  $V_r \equiv 0$ , the current resonance has the form:

$$I(V_g) = \frac{8\pi e^2 \gamma}{\hbar V} \left[ \frac{V^2}{4} - \frac{C_g^2}{C^2} \left( V_g - V_g^{(N)} - \frac{V}{2} \right)^2 \right]. \quad (18)$$

Both the width and the height  $I_{max} = (2\pi e^2/\hbar)\gamma V$  of the peak  $I(V_g)$  depend linearly on bias voltage, which is true also a non-symmetric set-up. In this case a more general expression for  $I(V_g)$  can be derived, which is in excellent agreement with recent experimental results<sup>8)</sup>.

This proportionality holds as long as electrons can only traverse the grain in pairs. At larger bias, when quasiparticle tunneling into the grain is allowed, the transport mechanism changes abruptly. For instance, in a circuit with  $V_r = 0$  (Fig. 3), the threshold voltage at which this change occurs is  $V_{th} = (\Delta - E_C)C/(C_g + C_r)e$  (Cf. Eq. (15): the addition of a quasiparticle to the grain costs an amount of energy  $\sim \Delta - E_C$ .) At voltages above the threshold, a single electron can tunnel into the grain with a rate of the order of  $w_{qp} \sim (G_l/e)[V^2 - V_{th}^2]^{1/2}$ . The escape rate of this quasiparticle from the grain into the opposite lead ( $r$ ) is quite different. The reason is that *any* electron with an above-threshold energy in the normal lead is available for tunneling into the grain, but only *one* unpaired electron can tunnel out of the grain. The escape rate  $w_{esc}$  is determined by the tunnel width of a discrete energy level available for the “odd” electron in the grain. Although the widths fluctuate from level to level, we can estimate the typical width  $\hbar w_{esc}$  through its relation to the conductance:  $G_r \sim e^2 \nu_g w_{esc}$ . Comparison of  $w_{qp}$  with  $w_{esc}$  shows that  $w_{qp}$  is the larger one if the bias exceeds the threshold voltage by

a value  $\sim \delta_g^2/e(\Delta - E_C)$ , with  $\delta_g = 1/\nu_g$  the level spacing in the grain. At higher bias, the probability of having an odd number of electrons  $N + 1$  is the dominant one. Current through the grain is determined by the escape rate of the quasiparticle and saturates at the low level  $I_{sat} \sim G_r/(\nu_g e)$ . At even higher bias, electrons belonging to the condensate can tunnel from the grain leaving behind excitations. As a result, the usual quasiparticle transport channel opens up, and at  $eV > eV^* \equiv (\Delta + E_C)C/C_l$  current starts to grow rapidly with bias. The overall  $I$ - $V$  characteristic is sketched in Fig. 4 and compares very well to the results obtained in Ref. (6), 8). A more detailed analysis of combined single electron and two-electron tunneling is given in Ref. 15).

**Acknowledgements.** This work was done in collaboration with L.I. Glazman, K.A. Matveev, Yu.V. Nazarov, and R. Shekter. The financial support of the “Deutsche Forschungsgemeinschaft” (SFB 195) is gratefully acknowledged.

## A. Normal state conductance of a single junction

Consider a single junction between two normal metals. Using first order perturbation theory in the tunnel Hamiltonian, one can show that the rate for transferring electrons from the left ( $l$ ) to the right ( $r$ ) electrode is given by:

$$\gamma_{l \rightarrow r}(V) = \frac{2\pi}{\hbar} \sum_{k,p} |t_{k,p}|^2 \delta(\xi_k + eV - \zeta_p) f(\xi_k) [1 - f(\zeta_p)]. \quad (19)$$

The total rate  $\gamma(V)$  is found by subtracting a similar expression for  $\gamma_{r \rightarrow l}(V)$ . Arguing along the lines given in section 2, we find the total current (for two spin directions) at  $T = 0$   $I(V) = 2e\gamma(V)$ , with

$$\gamma(V) = \frac{2\pi e}{\hbar} V \int d^3 r_1 d^3 r_2 d^3 r'_1 d^3 r'_2 K_0(\vec{r}_2, \vec{r}_1) K_0(\vec{r}_1, \vec{r}_2) t(\vec{r}_1, \vec{r}_1) t(\vec{r}_2, \vec{r}_2). \quad (20)$$

The spectral function is evaluated at the Fermi surface  $\xi, \zeta = 0$ . Although we assume the electron motion to be diffusive in the metallic films on both sides of the tunnel barrier, the averaged one electron spectral function does not depend on the structure of the wave function. It decays  $\propto 1/|\vec{r}_1 - \vec{r}_2|$  for  $|\vec{r}_1 - \vec{r}_2| \gg \lambda_F$ , where  $\lambda_F$  is the Fermi wavelength. Its maximum value at  $|\vec{r}_1 - \vec{r}_2| = 0$  equals the density of states  $\nu_l$  (per spin) at the Fermi energy. We furthermore assume that tunneling occurs only between neighbouring points on the barrier  $B$  ( $\vec{r} = \vec{r} = (x, y, z = z_B)$ ):  $t(\vec{r}, \vec{r}') = t(x, y) \delta^3(\vec{r} - \vec{r}') \delta(z - z_B)$ . The normal state conductance is then given by

$$G_T = \frac{\partial I}{\partial V}|_{V=0} = A \frac{4\pi e^2 \lambda_F^2 \nu_F \nu_r}{\hbar} \int_B d^2 r t^2(\vec{r}) \equiv \int_B d^2 r g(\vec{r}), \quad (21)$$

where we introduced  $g(\vec{r})$ : the conductance of the barrier per unit surface area, and a constant  $A$  which is of order unity.

## References

- 1) For an early review, see: *Tunneling Phenomena in Solids*, edited by E. Burstein and S. Lundqvist (Plenum Press New York, 1969)
- 2) A.F. Andreev, Zh. Eksp. Teor. Fiz. **46**, 1823 (1964) [Sov. Phys. JETP **19**, 1228 (1964)]
- 3) G.E. Blonder, M. Tinkham, and T.M. Klapwijk, Phys. Rev. B **25**, 4515 (1982)
- 4) For a review see: *Single Charge Tunneling*, edited by H. Grabert and M.H. Devoret (Plenum Press, New York, 1992)
- 5) D.V. Averin and Yu.V. Nazarov, Phys. Rev. Lett. **69**, 1993 (1992); M.T. Tuominen, J.M. Hergenrother, T.S. Tighe, and M. Tinkham, Phys. Rev. Lett. **69**, 1997 (1992); K.A. Matveev, M. Gisselält, L.I. Glazman, M. Jonsson, and R.I. Shekter, Phys. Rev. Lett. **70**, 2940 (1993); R. Bauernschmitt, J. Siewert, Yu.V. Nazarov, and A.A. Odintsov, Phys. Rev. B **49**, 4076 (1994)
- 6) T. M. Eiles, J. M. Martinis, and M. H. Devoret, Phys. Rev. Lett. **70**, 1862 (1993)
- 7) F.W.J. Hekking, L.I. Glazman, K.A. Matveev, and R.I. Shekter, Phys. Rev. Lett. **70**, 4138 (1993)
- 8) J.M. Hergenrother, M.T. Tuominen, and M. Tinkham, Phys. Rev. Lett. **72**, 1742 (1994)
- 9) D.V. Averin and Yu.V. Nazarov in Ref. 4)
- 10) M. Tinkham, *Introduction to Superconductivity* (McGraw-Hill, New York, 1975)
- 11) A.A. Abrikosov, L.P. Gorkov, and I.E. Dzyaloshinski, *Methods of Quantum Field Theory in Statistical Physics* (Pergamon Press, New York, 1965)
- 12) F.W.J. Hekking and Yu.V. Nazarov, Phys. Rev. Lett. **70**, 1625 (1993); to be published in Phys. Rev. B
- 13) H. Pothier, D. Estève, and M.H. Devoret, this volume
- 14) C.W.J. Beenakker and H. van Houten in Ref. 4)
- 15) G. Schön and A. Zaikin, preprint; J. Siewert, G. Schön, and A. Zaikin, preprint

## PROXIMITY EFFECT AND COULOMB BLOCKADE

Rosario Fazio<sup>1</sup>, C. Bruder<sup>2</sup>, and Gerd Schön<sup>2</sup>

<sup>1</sup>*Istituto di Fisica, Università di Catania, viale A. Doria 6, I-95129 Catania*

<sup>2</sup>*Institut für Theoretische Festkörperphysik, Universität Karlsruhe,  
D-76128 Karlsruhe*

### 1 Introduction

Single electron charging effects influence the transport through small capacitance junction systems<sup>1</sup>). If part of the system is superconducting new phenomena have been observed<sup>2-7</sup>).

When a superconductor and a normal metal are put in contact, Cooper pairs leak to the normal region and a superconducting order parameter is induced in the metal. Since charging effects inhibit tunneling they reduce the proximity effect. Both can be modulated by gate voltages, which opens the way to modulate supercurrents. This opens the possibility to detect the effect<sup>8</sup>).

The proximity effect had been studied in macroscopic junction systems by Aslamazov, Larkin and Ovchinnikov (ALO)<sup>9</sup>. We show how charging effects in mesoscopic systems modify their results. We first study the system shown schematically in the upper inset of Fig. 1: a small normal island separated from a bulk superconductor (with gap  $\Delta$ ) by a low capacitance tunnel junction. The island is coupled capacitively to a gate voltage. In the second part of this article we consider the situation where the island is superconducting. In this case electron number parity effects can be observed in the proximity effect.

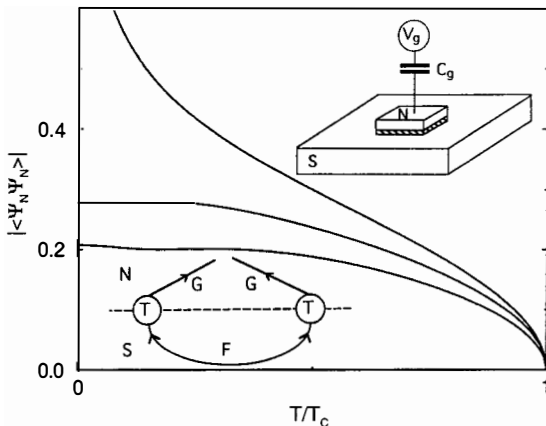


Figure 1: Temperature dependence of the induced pair amplitude (in units of  $Ge^2/hV$ ) at  $Q_g = 0$  for  $E_C/\Delta = 0$  (upper curve),  $E_C/\Delta = 0.23$  (middle curve), and  $E_C/\Delta = 0.45$  (lower curve). Upper inset: One of the setups studied. A small normal island (N) is coupled to a superconductor (S) by a tunnel junction. The gate voltage  $V_g$  applied via a capacitor  $C_g$  is used to modulate the charging effects. Lower inset: The induced pair amplitude in the normal metal (N) to second order in the tunneling in diagrammatic language. F is the Gorkov Greens function in the superconductor (S), G is the ordinary Greens function.

## 2 Model and Results

The system is described by the Hamiltonian  $H = H_0 + H_t + H_{ch}$  where  $H_0$  refers to the electrons in the normal island and the superconductor,  $H_t$  describes tunneling, and  $H_{ch}$  the capacitive Coulomb interaction. In the presence of the gate voltage source the electrostatic charging energy is  $E_{ch}(q, Q_g) = (qe - Q_g)^2/2C$ . Here  $q$  is the number of excess electrons on the island,  $C$  its total capacitance, i.e. the sum of the junction capacitance and that to the gate voltage. The gate voltage is responsible for the offset charge  $Q_g = q_g e = C_g V_g$ .

The essence of the proximity effect is a nonvanishing pair amplitude  $\langle \psi_N \psi_N \rangle$  induced in the normal metal by the coupling to the superconductor. The size of the induced energy gap  $\Delta_{ind} = \lambda \langle \psi_N \psi_N \rangle$  depends further on the effective pairing interaction  $\lambda$  in the metal. To lowest order in the tunneling matrix element  $|T|^2$ , the pair amplitude is represented by the diagram shown in the lower inset of Fig. 1. It has been analyzed by ALO<sup>9</sup>). In order to evaluate the influence of the charging energy (which is a nonperturbative effect) we formulate the problem in an effective action approach, generalizing the work of Ref. [10]. The charging energy, including the effect of the gate voltage, is

described by the action

$$S_{ch} = \int_0^\beta d\tau \left[ \frac{C}{2} \left( \frac{\hbar}{2e} \frac{\partial \phi}{\partial \tau} \right)^2 + iQ_g \frac{\hbar}{2e} \frac{\partial \phi}{\partial \tau} \right] \quad (1)$$

It is possible to write the pair amplitude as

$$\langle \psi_N \psi_N \rangle_{r_0, \tau_0} = \frac{G}{G_0} \frac{V}{N_N(0)S} \int d\tau d\tau' d^2\rho K(r_0, \rho, \tau, \tau'; \tau_0) F_S(\rho, \rho, \tau - \tau') h(\tau, \tau'; \tau_0) \quad (2)$$

Here  $G$  is the conductance of the junction and  $G_0 = 4e^2/h$  the quantum conductance. The kernel  $K$  is related to the Cooperon propagator<sup>11</sup>).

In the classical case the function  $h = 1$ , and the ALO result is recovered. The quantum fluctuations due to charging are taken into account by the phase correlator  $h(\tau, \tau'; \tau_0) = \langle \exp\{i(\phi(\tau) + \phi(\tau') - 2\phi(\tau_0))/2\} \rangle_{S_{ch}}$ . The expectation value has to be calculated using the charging action (1).

The charging effects are most important in the case of a very small island  $\hbar D/d^2 \gg \max(E_C, \Delta)$  ( $d$  is the linear dimension of the island and  $E_C = e^2/2C$ ). In this case the propagator  $p(r_1, r_2, \xi - \xi') \sim V^{-2} \delta(\xi - \xi')$  is essentially a constant; substituting this expression in eq. (2) we obtain

$$\langle \psi_N \psi_N \rangle = \frac{GV}{G_0 \beta^3} \sum_{\omega_\mu} \sum_{\omega_\nu, \omega_\eta > 0} \frac{\Delta}{(\omega_\nu + \omega_\eta) \sqrt{\omega_\mu^2 + \Delta^2}} h(\omega_\nu - \omega_\mu, \omega_\mu - \omega_\eta) e^{i\chi}. \quad (3)$$

The pair amplitude now depends on temperature and applied gate voltage. The temperature dependence is shown in Fig. 1. For  $E_C/\Delta = 0$  (upper curve) the pair amplitude diverges logarithmically for  $T \rightarrow 0$ . This is the result of ALO<sup>9</sup>). For finite values of the charging energy the proximity effect is suppressed; also the divergence at  $T = 0$  is removed. If the pairing interaction  $\lambda$  is finite, eq. 3 acquires an additional factor  $(1 + \frac{\lambda m p_F T}{\pi} \sum_{\omega_\nu > 0} \frac{1}{\omega_\nu})^{-1}$ . For repulsive  $\lambda$  this leads to a reentrant behavior at low temperatures.

The charging effects and the proximity effect can be modulated by gate voltages as shown in Fig. 2. The periodicity of the modulation is  $1e$ , reflecting the effect of single electron tunneling. Even though the rate of single electron tunneling may be low for low voltages, it still is sufficient at low sweeping rates to reset the state of the system in a setup where the island is a normal metal.

In the second arrangement, where a small superconducting island is coupled to a film of normal metal the modulation is even more pronounced. In this case a single excitation created in the superconductor does not find a partner to recombine. Hence the energy of odd electron number states lies higher by  $\Delta$  than that of the corresponding normal island. As a result a single electron

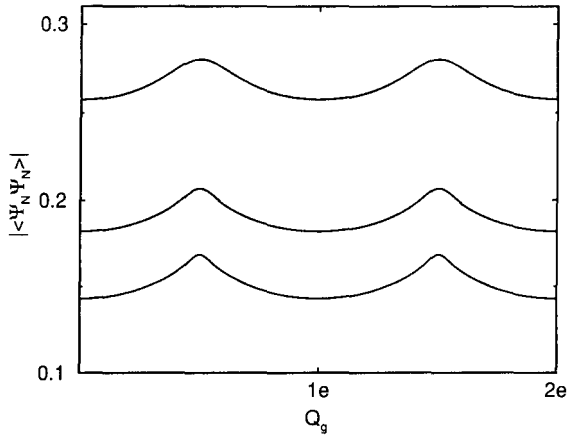


Figure 2: Dependence of the proximity effect on the induced charge  $Q_g = C_g V_g$  for  $T/T_C = 0.05$ ,  $E_C/\Delta = 0.23$  (upper curve)  $E_C/\Delta = 0.45$  (middle curve) and  $E_C/\Delta = 0.7$  (lower curve). The curves are periodic in  $Q_g$  with period  $1e$ .

tunnels at low temperatures only if the gain in charging energy exceeds the cost in excitation energy. The excitation energy can be regained when another electron enters the island<sup>4,12</sup>). This leads to the 2-e periodic long-short cyclic dependence observed in the properties of SN electron boxes<sup>3</sup>) or transistors<sup>2</sup>) and studied theoretically in Refs. [6, 7]. As long as the temperature is low we can describe the new situation by summing in the correlator only over even charges  $q = 0, \pm 2, \dots$  in the range where even electron number states have the lower energy,  $E_{ch}(\text{even}, Q_g) < E_{ch}(\text{even} \pm 1, Q_g) + \Delta$ , or only over odd charges  $q = \pm 1, \pm 3, \dots$  in the range where odd states win. The pronounced dependence of the induced pair amplitude as a function of the gate voltage is shown in Fig. 3. At low temperatures the pair amplitude diverges logarithmically at the points of degeneracy  $E_{ch}(\text{even}, Q_g) = E_{ch}(\text{even}) + \Delta$ . Only at these points the low temperature divergence of the ALO result is not removed.

In the case where  $\Delta > E_C$  quasiparticle tunneling remains suppressed for all values of the gate voltage. In this case the process which transfers charges and resets the system is Andreev reflection<sup>5,13</sup>). A 2e-periodic picture emerges with peaks in the induced pair amplitude at odd integer values of  $q_g$  (Fig. 3).

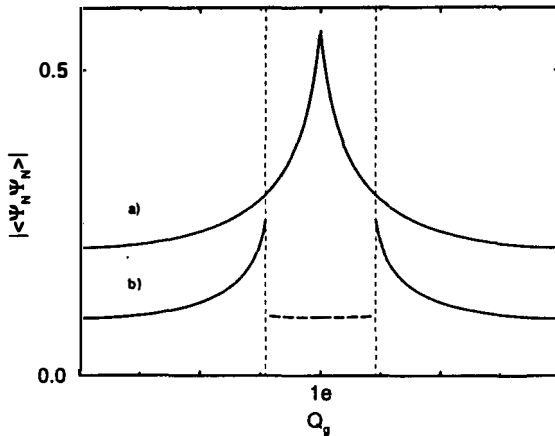


Figure 3: Dependence of the pair amplitude on  $Q_g$  in the case where the island is superconducting and parity effects reduce the regime of the odd electron number state for  $T = 0$  and (a)  $E_C/\Delta = 0.45 < 1$ , for curve (b)  $E_C/\Delta = 1.8 > 1$  (no single electron transitions). The curves have now period  $2e$ .

### 3 Conclusions

The modulation of charging effects helps to make the proximity effect visible. As an application we consider the situation where a superconducting electrode is placed on top of a normal film. If the film is thin enough a uniform pair amplitude will be induced below the electrode. A current through this normal film depends on the induced superconductivity<sup>8,14</sup>). If the electrodes have a low capacitance and are coupled to the voltage source, the current through the normal film can be modulated.

In summary we have presented an effective action description of charging effects in normal metal-superconductor tunnel junctions and shown that the Coulomb interaction in the island suppresses the proximity effect. We recover the classical results of ALO. The charging is accounted for by an extra phase correlation function modifying the classical expressions. It removes the low temperature divergences obtained in the classical limit. Several extensions can be included, e.g. relaxation processes due to the flow of Ohmic currents and the effect of a gap in the normal island induced by the proximity effect. Both regularize the divergence of the classical result.

We thank D. Esteve for stimulating discussions initiating this work, and A.I. Larkin, B. Pannetier, A. van Otterlo, F. W. J. Hekking, Yu. V. Nazarov, G. Falci, and A. D. Zaikin for many useful comments. We acknowledge the

hospitality of the ISI, Torino, and the support of the 'Sonderforschungsbereich 195' of the DFG.

## References

- [1] see for instance *Single Charge Tunneling, NATO ASI Series, Les Houches*, edited by H. Grabert and M. Devoret (Plenum, New York, 1992).
- [2] M. T. Tuominen, J. M. Hergenrother, T. S. Tighe, and M. Tinkham, *Phys. Rev. Lett.* **69**, 1997 (1992).
- [3] P. Lafarge, P. Joyez, D. Esteve, C. Urbina, and M. H. Devoret, *Phys. Rev. Lett.* **70**, 994 (1993).
- [4] D. V. Averin and Yu. V. Nazarov, *Phys. Rev. Lett.* **69**, 1993 (1992).
- [5] F. W. J. Hekking, L. I. Glazman, K. A. Matveev, and R. I. Shekter, *Phys. Rev. Lett.* **70**, 4138 (1993).
- [6] K. A. Matveev, M. Gisselält, L. I. Glazman, M. Jonson, and R. I. Shekter, *Phys. Rev. Lett.* **70**, 2940, (1993).
- [7] R. Bauernschmitt, J. Siewert, A. Odintsov, and Yu. V. Nazarov, *Phys. Rev. B* **49**, 4076 (1994).
- [8] D. Esteve, private communication
- [9] L. G. Aslamazov, A. I. Larkin, and Yu. N. Ovchinnikov, *Zh. Eksp. Teor. Fiz.* **55**, 323 (1968), [*Sov. Phys.-JETP* **28**, 171 (1969)].
- [10] U. Eckern, G. Schön, and V. Ambegaokar, *Phys. Rev. B* **30**, 6419 (1984).
- [11] P.G. de Gennes *Superconductivity of metals and alloys* W.A. Benjamin Inc. (New York - Amsterdam) (1966)
- [12] G. Schön and A. D. Zaikin, preprint
- [13] F. Guinea and G. Schön, *Physica* **B152**, 165 (1988).
- [14] H. Courtois and B. Pannetier, unpublished.

## THE AHARONOV-CASHER EFFECT FOR VORTICES IN JOSEPHSON-JUNCTION ARRAYS

W. J. Elion, J. J. Wachtters, L. L. Sohn, and J. E. Mooij  
Delft University of Technology  
Department of Applied Physics  
P.O. Box 5046, 2600 GA Delft  
The Netherlands

Vortices in superconducting networks with low-capacitance Josephson junctions can behave as macroscopic quantum particles.<sup>1</sup> The quantum mechanical properties are most prominent when the charging energy  $E_C$  of the junctions is comparable to the Josephson-coupling energy  $E_J$ . The interplay between Josephson and charging effects in this regime leads to the interesting concept of quantum interference of vortices around an induced charge. This interference is essentially the two-dimensional analogue of the familiar Aharonov-Casher effect<sup>2</sup>, where particles with magnetic flux move around an infinite line charge.

Van Wees<sup>3</sup> has studied quantum states of vortices in a ring-shaped array, bounded by superconducting banks. The charging energy of the junctions is only slightly smaller than the Josephson coupling energy. When a voltage source  $V_g$  is connected via a small capacitor  $C_g$  to the superconducting inner ring a charge  $Q=C_g V_g$  can be induced on this ring. Simultaneously, a voltage difference is induced between the inner and the outer ring that corresponds to a persistent current of vortices in the array. A charge vector potential  $A_q$  is defined that is related to the induced charge through the relation  $\oint A_q \cdot dl = Q$ . One can verify that the time derivative of this vector potential times the flux quantum  $\Phi_0$  equals the sheet current density flowing from the inner to the outer superconducting bank, which acts on the vortex as a classical force. The generalised vortex momentum becomes  $p + \Phi_0 A_q$ . In an array where vortices can cross along a doubly connected path, quantum vortices will interfere as a function of

the charge that is capacitively induced on a superconducting island enclosed by the path. The difference in the phase of the two parts of the vortex' wave function is  $(2\pi/2e)\oint A_q \cdot dl = (2\pi/2e)Q$ .

We have performed the described interference experiment<sup>4</sup>, using a specially shaped array shown in Fig. 1. Two different junction sizes are used to confine the moving vortex to the doubly connected path shown. With the gate, charge can be induced on the center island.

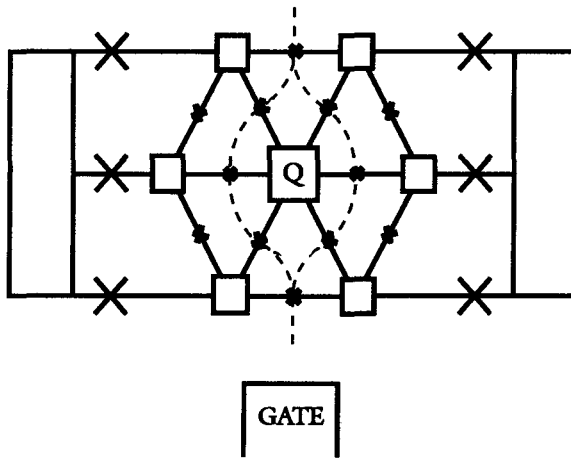


Fig. 1: Schematic layout of the sample. Rectangles are superconducting aluminum islands and crosses denote Josephson junctions. The junctions in the hexagon have a 3 times smaller junction area than the junctions that couple the array to superconducting current and voltage contacts. The dashed line pictures the possible vortex paths.

Our array consists of underdamped Al-Al<sub>2</sub>O<sub>3</sub>-Al junctions that are fabricated with a standard shadow evaporation technique.<sup>5</sup> The experiments are performed in a dilution refrigerator at temperatures down to 10 mK inside  $\mu$ -metal and lead shields. A small magnetic field can be applied by means of a Helmholtz coil. Electrical leads are filtered at the entrance of the cryostat with rfi feedthrough filters and at sample temperature with RC and microwave filters. The junctions in the hexagon have a normal state resistance  $r_n$  of 5.5 kOhm and a capacitance  $C$  of about 1 fF. The ratio of  $E_j$  over  $E_C$  is 1.5.

As a function of magnetic field, the critical current of the array exhibits sharply pronounced minima, shown in Fig. 2.

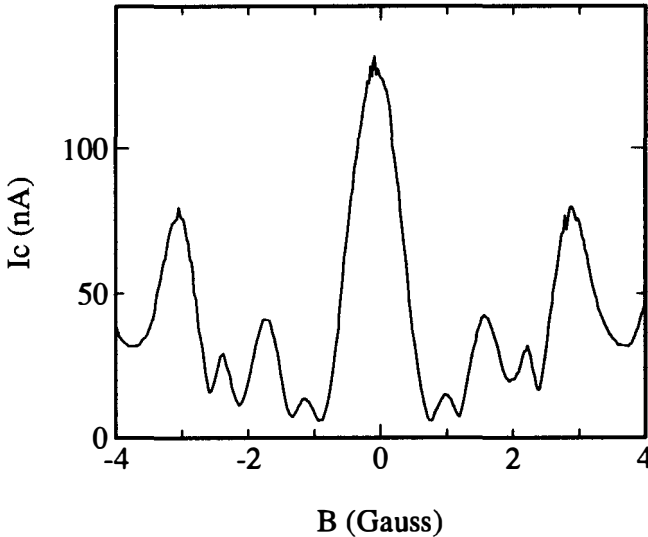


Fig. 2. The critical current as a function of magnetic field.

The dips in the critical current correspond to a value of the magnetic field where two different vortex configurations have the same energy, and the vortices can move through the array very easily. The current-voltage ( $I$ - $V$ ) characteristic of the array at a field of 1.2 Gauss is shown in Fig. 3. Above the critical current a resistive branch is visible that we will call the flux-flow regime. The BCS gap  $2\Delta/e$  is 0.4 mV for our junctions, which is beyond the scale of Fig. 3. The flux-flow branch is only observed for magnetic fields where the critical current is depressed by a factor of 4 or more. If that is not the case the array will switch to the BCS gap voltage as soon as the critical current is exceeded. Computer simulations of the array using the classical resistively and capacitively shunted junction (RCSJ) model have convinced us that the flux-flow resistance is really caused by vortices moving across the array along one of the paths shown. In contrast to the classical simulations we find that in the experiment the resistance near zero bias is not zero but about 80 Ohms, depending on the magnetic field, and that the critical current is strongly reduced. These differences are clear evidence for quantum tunneling of vortices.

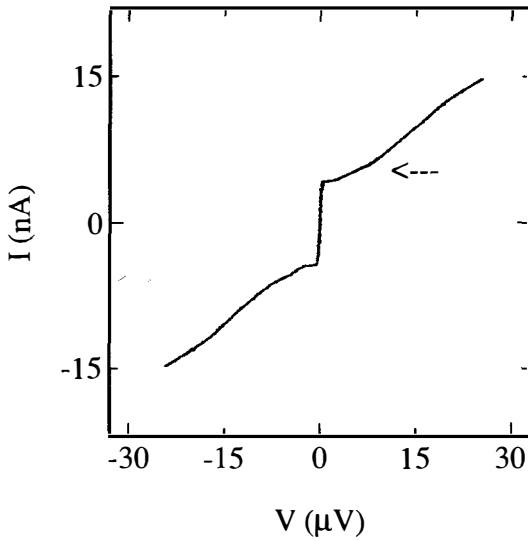


Fig. 3. Current-Voltage (IV) characteristic in a magnetic field of 1.2 Gauss. The arrow corresponds to the bias current at which the differential resistance shown in Fig. 4 was measured.

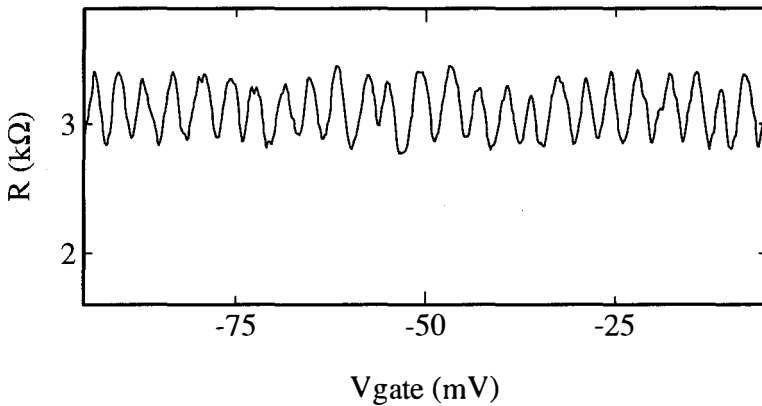


Fig. 4: Differential resistance as a function of gate voltage in a field of 1.2 Gauss. Bias current is 5 nA with 0.25 nA modulation amplitude.

With a standard lock-in technique, we current-biased our system in the flux-flow regime, and measured the differential resistance as a function of gate voltage. The result is shown in Fig. 4, corresponding to the IV characteristic of Fig. 3, at a bias current of 5 nA. With increasing gate voltage the resistance changes periodically from 2.8 to 3.3 kOhm. The period, as determined by Fourier analysis, is 3.7 mV. With increasing temperature the amplitude of the oscillation decreases and vanishes between 400 and 500 mK. For higher bias currents we generally find a smaller oscillation amplitude. A small periodic modulation of the critical current by the gate voltage is seen in the regimes where the critical current is strongly depressed by the magnetic field.

The period of the oscillations is the single electron charge  $e$ , while the Aharonov-Casher effect has a fundamental period  $2e$ . This is due to the presence of a small but finite amount of quasiparticles in our experimental system. In this case, for zero bias current, if the gate voltage is increased the potential of the centre island will rise until it exceeds the value of  $e/2C_t$ .  $C_t$  is the total capacitance of the center island, which is 6 times the junction capacitance. A quasiparticle can then tunnel onto the island and reset the potential to  $-e/2C_t$ . The induced charge is effectively limited to the range between  $-e/2$  and  $e/2$  as long as the quasiparticle tunneling times are significantly shorter than the five minute time scale on which the gate voltage is varied. The tunneling times for quasiparticles are however still about four orders of magnitude longer than those for Cooper pairs. An applied bias current therefore consists of Cooper pairs that tunnel to and from the island. Because the interference of vortices is a  $2e$  periodic effect, tunneling of Cooper pairs will not destroy the interference. We expect that as soon as quasiparticles become delocalised at the time scale of the crossing of a vortex over the array, the oscillations will disappear. This is in reasonable agreement with the temperature of 500 mK where the oscillations can no longer be detected.

Recently, several groups<sup>6</sup> have reported measurements on two superconducting junctions in series where the critical current shows periodic oscillations as a function of induced charge on the superconducting island that connects the two junctions. The question arises if there is a relation between those oscillations and the Aharonov-Casher effect for vortices in an array. In an array a moving vortex induces a phase slip across the superconducting contacts. For a single junction with  $E_j \gg E_C$  the critical current is determined by the onset of phase slips occurring across the junction. If  $E_C$  becomes comparable to  $E_j$ , these phase slips can also occur through quantum tunneling, and the critical current is reduced. For a double junction in the classical limit a phase slip will, with highest probability, occur over one of the two junctions at

a time. In the quantum mechanical limit the onset of phase slips, the critical current, will be determined by a superposition of both possibilities. The induced charge might influence the interference between these paths. In view of the relation between our array and a double junction system it is also interesting to compare the treatment of the persistent vortex current by van Wees with the persistent voltage across a single junction as described by Büttiker<sup>7</sup>.

The flux-flow branch observed in our experiment is the most important feature that discriminates the array from a double junction. This resistive branch signifies that vortices can move across the array in a controlled fashion along a well defined path, which greatly enhances the intuitive feeling for a vortex as a particle with a mass. Another difference is that in our experiment on a Josephson junction array, we did not find any influence of the gate voltage on the critical current in zero field. Oscillations are only visible when vortices are induced by the magnetic field. This is possibly related to the fact that the  $E_J/E_C$  ratio of our junctions is higher than the  $E_J/E_C$  ratio of the junctions used in ref. 6.

To conclude: we have observed quantum-mechanical interference of vortices around an induced charge. This effect is a result of the subtle interplay between Josephson and charging effects and a manifestation of the generalised Aharonov-Casher effect.

We want to acknowledge fruitful collaboration with L. J. Geerligs, U. Geigenmuller, M. Matters, Y. Nazarov and T. J. Oosterkamp. Samples were made at the Delft Institute for Microelectronics and Submicron Technology (DIMES).

---

<sup>1</sup>H. S. J. van der Zant, F. C. Fritschy, W. J. Elion, L. J. Geerligs, and J. E. Mooij, Phys. Rev. Lett. **69**, 2971 (1992) and references therein, R. Fazio, U. Geigenmuller, and G. Schön, in Proceedings of the Adriatico Research conference on Quantum Fluctuations in Mesoscopic and Macroscopic Systems, July 1990 (World Scientific)

<sup>2</sup>Y. Aharonov and A. Casher, Phys. Rev. Lett. **53**, 319 (1984)

<sup>3</sup>B. J. van Wees, Phys. Rev. Lett. **65**, 255 (1990)

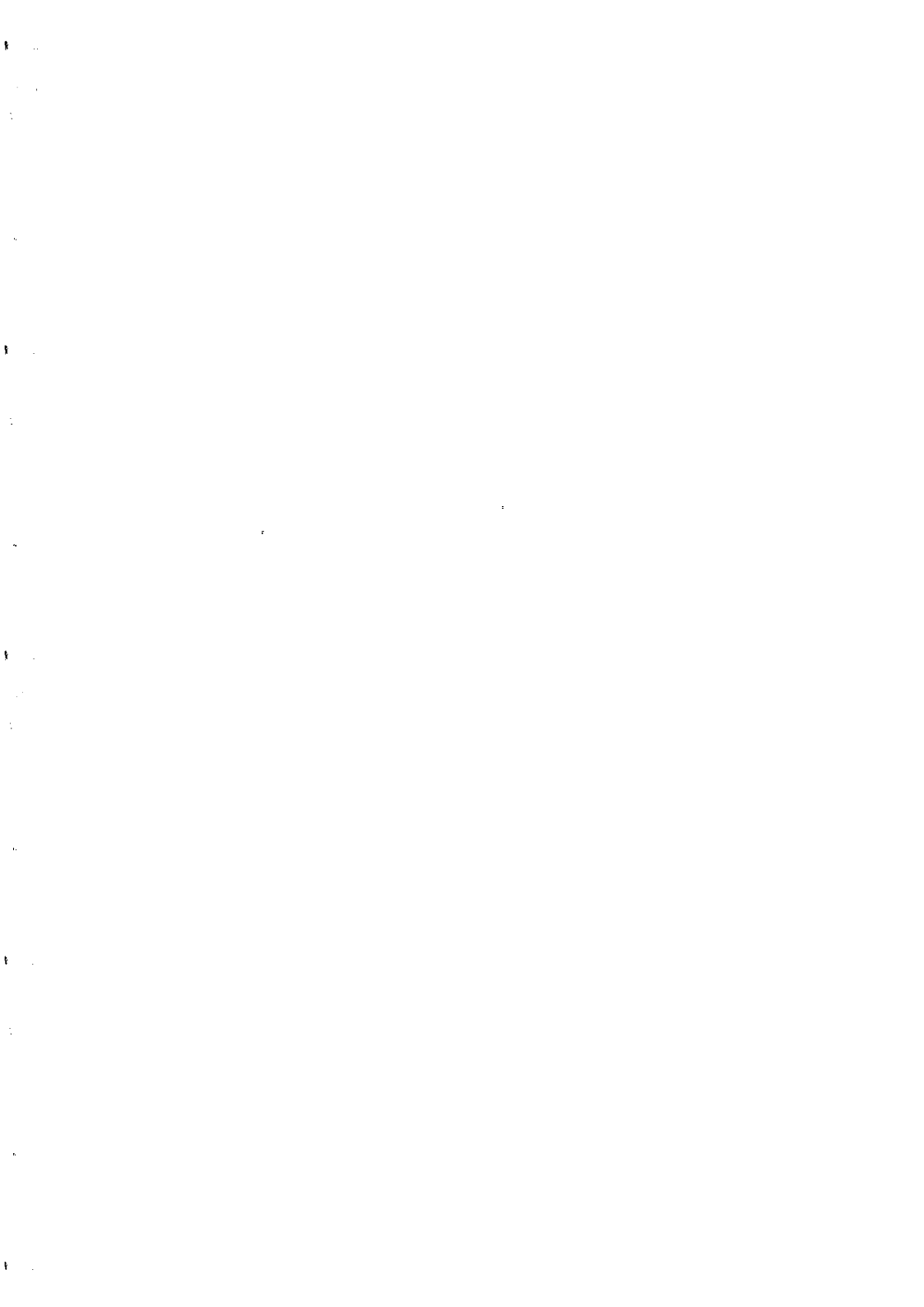
<sup>4</sup>W. J. Elion, J. J. Wachtters, L. L. Sohn, and J. E. Mooij, Phys. Rev. Lett. **71**, 2314 (1993)

<sup>5</sup>L. J. Geerligs, Ph.D. thesis, Delft University of Technology, 1990

<sup>6</sup>L. J. Geerligs, V. F. Anderegg, J. Romijn, and J. E. Mooij, Phys. Rev. Lett. **65**, 377 (1990), P. Joyez, P. Lafarge, A. Filipe, D. Esteve, and M. H. Devoret, Phys. Rev. Lett. **72**, 2458 (1994), T. M. Eiles and J. M. Martinis (to be published)

<sup>7</sup>M. Büttiker, Phys. Rev. B **36**, 3548 (1987)

**QUANTUM INTERFERENCES  
IN SUPERCONDUCTING  
AND NORMAL/SUPERCONDUCTING SYSTEMS**



## MESOSCOPIC PHENOMENA IN SUPERCONDUCTOR/2DEG SYSTEMS

K.-M. H. Lenssen,<sup>1)</sup> P. C. A. Jeekel, C. J. P. M. Harmans, J. E. Mooij  
*Delft University of Technology, Dept. of Applied Physics,*  
*P.O. Box 5046, NL-2600 GA Delft, The Netherlands*

M. R. Leys, J. H. Wolter  
*Eindhoven University of Technology, Dept. of Applied Physics,*  
*P.O. Box 513, NL-5600 MB Eindhoven, The Netherlands*

M. C. Holland  
*University of Glasgow, Dept. of Electronics and Electrical Engineering,*  
*Rankine Building, Glasgow G12 8QQ, United Kingdom*

### 1 Introduction

In the last decades a new branch of solid-state physics arose, studying systems with sizes between microscopic and macroscopic dimensions: mesoscopic physics. This field has yielded many interesting results,<sup>2)</sup> as these proceedings also show. The transport properties of low-dimensional systems are, in fact per definition, strongly determined by the boundaries. Whether we consider a quantum point contact, a quantum wire or a quantum dot, always the confinement is essential. Therefore it is obvious that new effects will be encountered, if some of the boundaries can be formed by superconductors. Due to Andreev reflection<sup>3)</sup> the scattering of electrons at the boundaries will change dramatically.

The aim of our research is to study the interplay of Andreev reflection and the mesoscopic effects which are known to occur in semiconductor nanostructures. We want to use semiconductors, so that the normal N region can be patterned by means of gate structures, and since we want to study phase-coherent effects in particular, we need a semiconductor with a high electron mobility. That is why the use of a two-dimensional electron gas (2DEG) is preferred.

In the past several superconductor/2DEG systems have already been studied: a Si MOS-FET,<sup>4),5)</sup> a native inversion layer on *p*-type InAs,<sup>6)</sup> an accumulation layer in Al<sub>0.5</sub>Ga<sub>0.5</sub>As/GaAs,<sup>7)</sup> an InAs-AlSb quantum well<sup>8)</sup> and GaAs/Al<sub>0.33</sub>Ga<sub>0.67</sub>As heterostructures.<sup>9),10)</sup> Each of these material systems has its own advantages and disadvantages. While it is relatively easy to make contact between InAs and a superconductor because of the absence of a Schottky barrier,

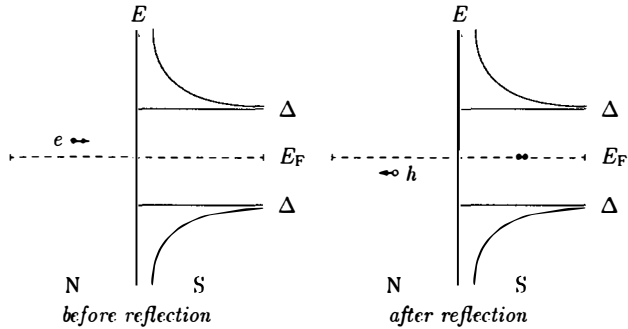


Figure 1: *Schematic view of an Andreev reflection process*

it is certainly not trivial to make good gate structures on this material. In Si MOSFET's supercurrents have indeed been observed and could be modulated by a gate; however, the phase coherence length is so small, that the distance between the superconducting contacts is not enough to place split gate patterns.

We have chosen to use GaAs/Al<sub>0.33</sub>Ga<sub>0.67</sub>As heterostructures, because of its high mobility ( $\mu \sim 10^2$  m<sup>2</sup>/Vs) and its excellent gating properties. The large elastic mean free path ( $l_e \sim 10^{-2}$  mm) gives the possibility to enter the ballistic transport regime, while the distance between the superconducting contacts can be large enough for gate structures like a quantum point contact or a quantum dot. One of the effects which are theoretically predicted to occur in such systems, is the quantization of the critical supercurrent.<sup>11, 12)</sup> However, until now supercurrents in a ballistic superconductor/2DEG/superconductor structure that can be controlled by a gate have not yet been realized. On the other hand, new effects have been observed due to phase-coherent Andreev reflection in mesoscopic systems. This will be the subject of the following, by discussing our experiments on GaAs/AlGaAs heterostructures (section 4). Before that we will shortly describe the most important theoretical concepts (section 2) and the fabrication process of our samples (section 3).

## 2 Theoretical concepts

If an electron from a normal material with an excitation energy  $E$  below the superconducting gap  $\Delta$  reaches the interface with a superconductor (S), it can't enter the superconductor because there are no states available (see figure 1). Andreev<sup>3)</sup> found out that the electron can be reflected as a hole, while a Cooper pair goes on in the S region. While in normal reflection the angle of incidence equals the reflection angle, in an Andreev reflection the hole traces back the path of the incoming electron (the time-reversed path).<sup>13)</sup> It is evident that this retroreflection feature has a large influence on quantum interference. The second important feature of Andreev reflection is the already mentioned particle conjugation. As can be seen in figure 1 we end up with a Cooper pair (charge  $2e$ ) in the superconductor, while we started with an electron ( $e$ ) in the N region. This means that Andreev reflection effectively doubles the current; experimentally this

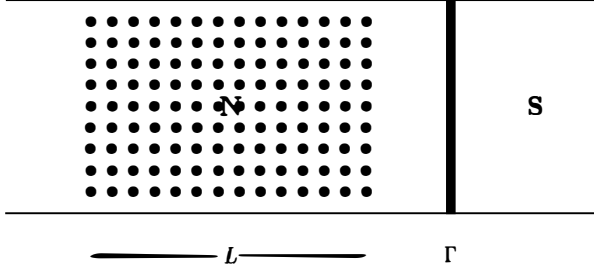


Figure 2: Schematic overview of an NS interface with disordered N region

will be observed as an increase of the conductance.

However, if the NS interface is not ideal, the probability for Andreev reflection will dramatically decrease in the case of a small barrier. Since Andreev reflection is a two-particle process in contrast to normal electron tunneling, the conductance then will decrease at the transition from an NN interface to an NS interface.

So on beforehand we cannot say whether the conductance of the interface will go up or down at the superconducting transition. The net effect depends strongly on the transmission coefficient of the interface.<sup>14)</sup>

For the study of mesoscopic effects it is useful to express the conductance of the NS interface  $G_{NS}$  in terms of the eigenvalues  $T_n$  of the (normal-state) transmission matrix product  $tt^\dagger$ , like Landauer<sup>15)</sup> did for the normal state:

$$G_{NN} = \frac{2e^2}{h} \sum_{n=1}^N T_n. \quad (1)$$

Beenakker<sup>16)</sup> recently found a generalization of this formula for the NS interface ( $B = 0$  T):

$$G_{NS} = \frac{4e^2}{h} \sum_{n=1}^N \frac{T_n^2}{(2 - T_n)^2}. \quad (2)$$

If this expression is applied to a ballistic quantum point contact (that means either  $T_n = 0$  or  $T_n = 1$ ) near an NS interface, it is clear that the conductance will be quantized in units of  $4e^2/h$  instead of the normal value of  $2e^2/h$ .

Now we consider a more specific case, namely an NS interface with a disordered N region. Here “disordered” means that the elastic mean free path  $l_e$  is much smaller than the length  $L$  of the N region. The transmission of an eventual barrier at the NS interface is called  $\Gamma$ . This system has recently theoretically been described by Marmorkos *et al.*<sup>17)</sup> and is schematically shown in figure 2. Classically (i. e. matching currents instead of amplitudes) the resistance in respectively the superconducting and normal state is given by:

$$R_{NS}^{\text{class}} = \frac{h}{2e^2N} (T_d^{-1} + 2(1 - \Gamma)\Gamma^{-2}) \quad (3)$$

and

$$R_N^{\text{class}} = \frac{h}{2e^2N} (T_d^{-1} + (1 - \Gamma)\Gamma^{-1}) \quad (4)$$

with  $T_d$  the transmission of the disordered region. Looking at these formulas we can distinguish two limits:

- high barrier ( $\Gamma \ll 1$ ):  $R_{\text{NS}}^{\text{class}} \gg R_{\text{N}}^{\text{class}}$ , because the contribution of the barrier is  $\propto \Gamma^{-2}$  instead of  $\propto \Gamma^{-1}$
- without barrier ( $\Gamma = 1$ ):  $R_{\text{NS}}^{\text{class}} = R_{\text{N}}^{\text{class}}$ .

However for both limits deviations occur, when quantum interference is taken into account:<sup>(16)–(18)</sup>

- high barrier ( $l_e/L \ll \Gamma \ll 1$ ):  $R_{\text{NS}} \approx R_{\text{N}}^{\text{class}} \ll R_{\text{NS}}^{\text{class}}$ . This is called reflectionless tunneling, because it is as if the Andreev-reflected hole is not reflected by the barrier. Experimentally this will result in a conductance peak
- without barrier ( $\Gamma = 1$ ):  $R_{\text{NS}} > R_{\text{NS}}^{\text{class}}$  due to an enhancement of weak localization: it is as if Andreev reflection effectively doubles the length of the disordered region, which will show up in measurements as an conductance dip.

Experimental observations of three signatures of (phase-coherent) Andreev reflection will be discussed in this paper: conductance quantization in enhanced units, enhancement of weak-localization effects and reflectionless tunneling.

### 3 Sample fabrication

For most samples a “conventional” GaAs/AlGaAs heterostructure has been used. This material is grown by Molecular Beam Epitaxy and consists of a GaAs substrate with a 4  $\mu\text{m}$  undoped GaAs layer, a 40 nm undoped  $\text{Al}_{0.33}\text{Ga}_{0.67}\text{As}$  spacer, a 38 nm  $n$ -doped  $\text{Al}_{0.33}\text{Ga}_{0.67}\text{As}$  layer and a 17 nm undoped GaAs caplayer. The electron mobility is  $\mu \approx 110 \text{ m}^2/\text{Vs}$  and the electron density is  $n_e \approx 2.4 \times 10^{15} \text{ m}^{-2}$  (at  $T \approx 5 \text{ K}$ ).

The major problem is the coupling between a superconductor and the buried 2DEG. We have developed a diffusion process for making highly transmissive superconducting Sn/Ti-contacts, which have shown clear evidence of Andreev reflection.<sup>(9),(19)</sup> Using this process we have made a sample with a layout as shown in figure 3 on this heterostructure. The centre of the sample consists of two 10  $\mu\text{m}$  wide superconducting contacts at a mutual distance of 800 nm. Each of these contacts is attached to two large bond pads for the connection to the outside world. Split gates forming a quantum point contact (width  $\approx 150 \text{ nm}$ , length  $\approx 90 \text{ nm}$ ) are positioned between the small contacts. Outside the contacts the gates are widened, so that they can confine the current flow to the region between the small superconducting contacts. The whole sample is surrounded by a wide gate (a moat gate) for device isolation.

The patterning of all three layers (contacts, wide gate and quantum point contact) is done by 100 keV electron beam lithography in a double PMMA resist layer to reduce negative influences of the lithographic proximity effect. The alignment of these three lithography steps is achieved by automatic marker search on especially prepared gold markers (with an inaccuracy below 30 nm). With this process also six thin gates forming a quantum dot have been fabricated between superconducting contacts (distance  $\approx 900 \text{ nm}$ ) on a test wafer, proving the reliability and flexibility of this nanolithography and alignment technique.

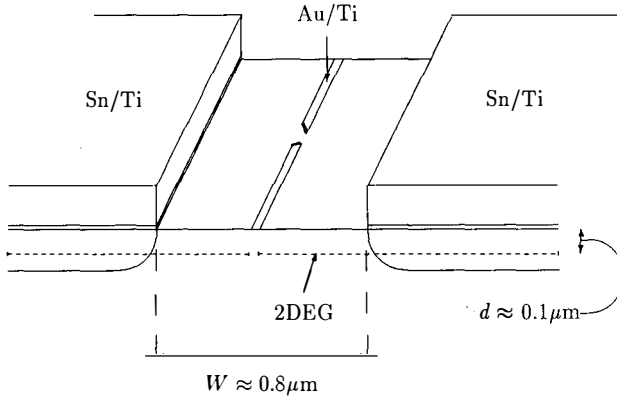


Figure 3: *Side-view of the centre of the sample*

The measurements of reflectionless tunneling have been performed on a different heterostructure with a “shallow” 2DEG. For this material a different layer structure has been grown on a GaAs substrate: respectively, a  $0.5 \mu\text{m}$  undoped GaAs layer, a 10 nm undoped AlAs layer, a  $\delta$ -doped 0.56 nm GaAs layer sandwiched between two 1.13 nm  $\text{Al}_{0.33}\text{Ga}_{0.67}\text{As}$  layers, again a 10 nm undoped AlAs layer and a 5.4 nm undoped GaAs caplayer. In this way the 2DEG (with  $\mu \approx 60 \text{ m}^2/\text{Vs}$  and  $n_e \approx 3.6 \times 10^{15} \text{ m}^{-2}$ ) is situated only  $\approx 28 \text{ nm}$  below the surface. On this material  $200 \mu\text{m} \times 200 \mu\text{m}$  superconducting contacts are placed on a  $200 \mu\text{m}$  wide etched mesa at several mutual distances (a so-called TLM structure).

The resistance measurements on the samples were performed in a dilution refrigerator, employing a current-biased ac lock-in technique as well as dc methods.

## 4 Results of the measurements

### 4.1 Conductance quantization in enhanced units

In figure 4 the conductance of the sample with the quantum point contact is presented as a function of the gate voltage  $V_g$  ( $T = 10 \text{ mK}$ ). It can be clearly seen that at zero magnetic field the conductance is quantized in units larger than  $2e^2/h$ . We think this can only be due to Andreev reflection. In this respect it is important to note that these are the original measurement data, i. e. without a correction for a series resistance.

The fact that the steps are practically equidistant for  $B = 0 \text{ T}$  means that there is no significant series resistance. The figure also shows that the effect is suppressed by small magnetic fields; even the remanent field of the superconducting magnet is enough to destroy the enhancement.

By means of formula (2) we can make an estimation for an effective, averaged transmission probability  $T$  (assuming mode independence). From the fact that the observed quantization unit is  $\approx 2.2e^2/h$  instead of the ideal value  $4e^2/h$ , we find  $T \approx 0.85$ . To check this we can do an

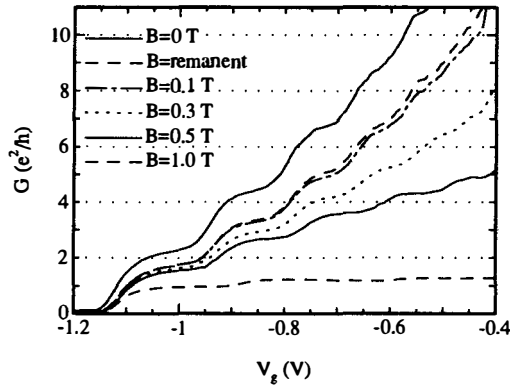


Figure 4: The differential conductance as a function of the voltage on the quantum point contact gates

analogous estimation in the normal state using formula (1), which indeed yields the same value. This suggests that the transmission of an eventual barrier at the NS interface  $\Gamma$  is larger than 0.85. Following the theory<sup>17)</sup> this is in the regime where enhanced weak-localization effects can be expected. Indeed this has been observed as will be discussed in the next section.

#### 4.2 Enhanced weak-localization effects

At zero gate voltage the conductance shows a sharp minimum at zero bias, which is rapidly suppressed by a magnetic field (figure 5) and increased temperature (figure 6). We think this

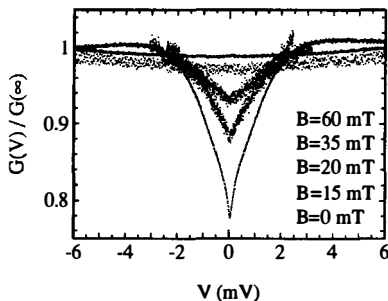


Figure 5: The normalized differential conductance as a function of the bias voltage for several magnetic fields ( $T = 10$  mK)

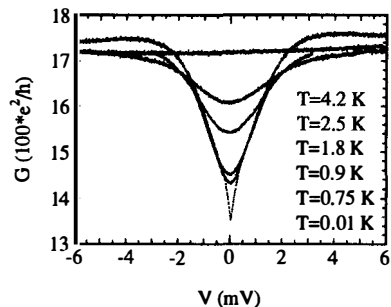


Figure 6: The differential conductance as a function of the bias voltage at several temperatures ( $B = 0$  mT)

minimum consists of two superimposed phenomena: a broad minimum due to the opening of the superconducting gap at a non-ideal NS interface<sup>14)</sup> and a sharp dip caused by enhanced weak localization.<sup>16)</sup> This hypothesis is confirmed by measurements on a sample in which the

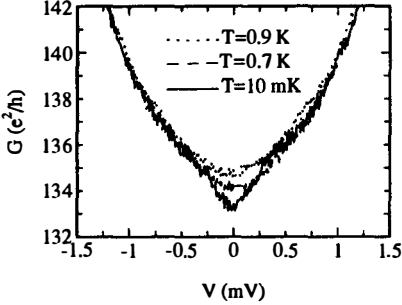


Figure 7: The differential conductance at  $V_g = -400$  mV as a function of the bias voltage at several temperatures ( $B = 0$  mT)

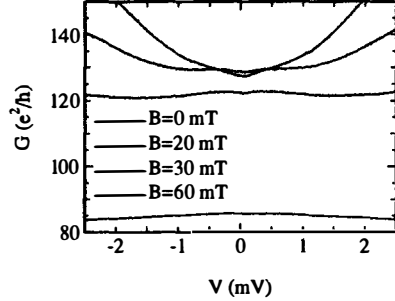


Figure 8: The differential conductance at  $V_g = -400$  mV as a function of the bias voltage for several magnetic fields ( $T = 10$  mK)

major part of the thin gate between the superconducting contacts doesn't function, but in which the current flow still can be confined by means of the wider gates at the sides of the contacts (figures 7 and 8). Figure 7 clearly shows that at temperatures below 0.9 K a small dip arises superimposed on the broad minimum. This dip also vanishes in a small magnetic field (figure 8) which is in agreement with the fact that weak localization is suppressed when time-reversal symmetry is broken. The depth of the dip is also in good agreement with theory which predicts a magnitude in the order of  $e^2/h$ .<sup>20)</sup> The disorder which causes the weak localization is probably introduced near the contacts by the diffusion process.

Also in the original sample (figures 5 and 6) the sharp dip is suppressed at  $B \approx 35$  mT and  $T \approx 0.75$  K. It is difficult to predict the voltage at which the enhanced weak localization is suppressed, since the Fermi velocity and the elastic mean free path of the disordered region are not known. However, the threshold voltage and the threshold temperature should be related by  $eV_{th} \approx 4k_B T_{th}$ . The observed values are in good agreement with this prediction ( $V_{th} \approx 0.25$  mV).

The enhanced weak localization can however also be suppressed by a large negative voltage on the nearby gates. At  $V_g = -890$  mV not a conductance minimum but a maximum is found around zero bias and also the sign of the temperature dependence is opposite.<sup>21),22)</sup> We think the suppression is caused by the formation of a potential barrier in the quantum point contact; this lowers the transmission of the sample, which is then not in the regime of enhanced weak localization anymore. Anyway, it proves that phase coherence is preserved into the 2DEG.

From the theoretical expression for the threshold magnetic field<sup>17)</sup>  $B_{th} = h/(el_\varphi^2)$  we find an estimation for the phase coherence length  $l_\varphi$  of the order of  $0.4 \mu\text{m}$ . This is in agreement with the observed gate influence.

### 4.3 Reflectionless tunneling

Reflectionless tunneling was the first signature of phase-coherent Andreev reflection that was experimentally observed. It was measured for the first time in a Nb/InGaAs junction by Kastalsky *et al.*<sup>23)</sup> Later it has been observed in other material systems.<sup>5),8),22),24)</sup> Van Wees<sup>25)</sup>

was the first to realize that the measured conductance peak could be explained by phase-coherent Andreev reflection; this concept was elaborated by others.<sup>16),17)</sup>

We have observed reflectionless tunneling most clearly in samples on the shallow 2DEG. The data are shown in the figures 9 and 10. Below the critical temperature of tin ( $T_c = 3.7$  K

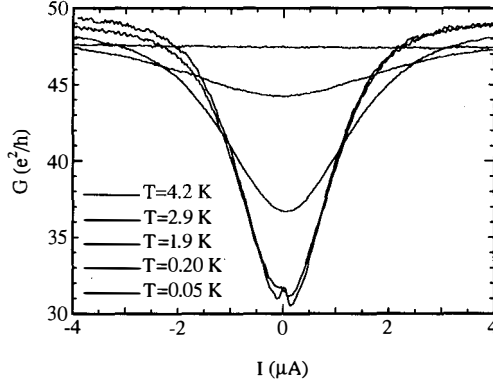


Figure 9: *The differential conductance as a function of the bias current at several temperatures*

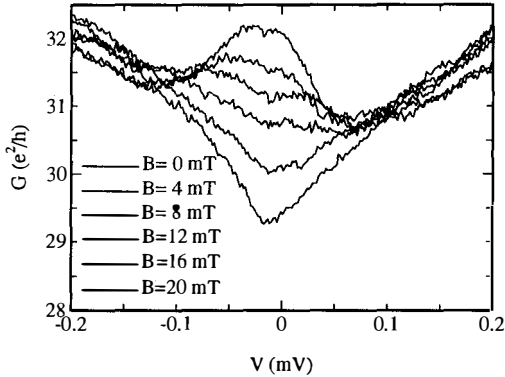


Figure 10: *The differential conductance as a function of the bias voltage for several magnetic fields*

for bulk) a broad conductance minimum arises because of “classical” Andreev reflection at an NS interface with a non-unity transmission.<sup>14)</sup> At very low temperatures ( $T < 0.3$  K), however, a small conductance peak appears, due to phase-coherent Andreev reflection (figure 9). This temperature is in correspondence with the voltage at which the peak vanishes. The peak is also suppressed by a small magnetic field of  $B \approx 20$  mT (figure 10). This suggests that  $l_\varphi \approx 0.45$   $\mu\text{m}$ , which means that phase coherence is preserved into the 2DEG.

The fact that we observe reflectionless tunneling in this shallow 2DEG means that the NS

interface is less transmissive as in the conventional 2DEG. This is in agreement with the higher contact resistances we find on this material, probably due to the different layer structure.

## 5 Conclusions

We have reported the experimental observation of three signatures of phase-coherent Andreev reflection in superconductor/2DEG systems. The conductance of a quantum point contact near a superconductor is quantized in units larger than  $2e^2/h$ . At zero gate voltage an enhancement of weak localization by Andreev reflection has been observed for the first time. In a different heterostructure reflectionless tunneling has been measured for the first time in GaAs/AlGaAs.

The fact that in these effects phase coherence is preserved into the 2DEG shows that GaAs/AlGaAs heterostructures are very promising for the study of the interplay between Andreev reflection and mesoscopics.

## Acknowledgment

We are grateful to C. W. J. Beenakker for valuable discussions, to L. A. Westerling for help with the experiments and analysis of the data, and to the Delft Institute of Micro-Electronics and Submicron technology (DIMES) for the use of their facilities. This research was financially supported by the Dutch Foundation for Fundamental Research on Matter (Stichting FOM).

## References

- [1] Present address: Philips Research Laboratories, Post box WA-14, Prof. Holstlaan 4, NL-5656 AA Eindhoven, The Netherlands
- [2] See, for example, C. W. J. Beenakker and H. van Houten, *Solid State Physics* **44**, 1 (1991) and references therein
- [3] A. F. Andreev, *Zh. Eksp. Teor. Fiz.* **46**, 1823 (1964) [*Sov. Phys. JETP* **19**, 1228 (1964)]; A. F. Andreev, *Zh. Eksp. Teor. Fiz.* **49**, 655 (1965) [*Sov. Phys. JETP* **22**, 455 (1965)]
- [4] T. Nishino, M. Miyake, Y. Harada, and U. Kawabe, *IEEE Electron Device Lett.* **6**, 297 (1985); T. Nishino, M. Hatano, H. Hasegawa, F. Murai, T. Kure, A. Hiraiwa, K. Yagi, and U. Kawabe, *IEEE Electron Device Lett.* **10**, 61 (1989)
- [5] S. J. M. Bakker, E. van der Drift, T. M. Klapwijk, H. M. Jaeger, and S. Radelaar, *Phys. Rev. B* (to be published)
- [6] H. Takayanagi and T. Kawakami, *Phys. Rev. Lett.* **54**, 2449 (1985)
- [7] Z. Ivanov, T. Claeson, and T. Andersson, *Japanese J. Appl. Phys.* **26-3**, 617 (1987)
- [8] C. Nguyen, H. Kroemer, and E. L. Hu, *Phys. Rev. Lett.* **69**, 2847 (1992)
- [9] K.-M. H. Lenssen, M. Matters, C. J. P. M. Harmans, J. E. Mooij, M. R. Leys, W. van der Vleuten, and J. H. Wolter, *IEEE Trans. Appl. Superconductivity* **3**, 1961 (1993)

- [10] J. R. Gao, J. P. Heida, B. J. van Wees, T. M. Klapwijk, G. Borghs, and C. T. Foxon, *Surf. Sci.* (in press)
- [11] C. W. J. Beenakker and H. van Houten, *Phys. Rev. Lett.* **66**, 3056 (1991)
- [12] A. Furusaki, H. Takayanagi, and M. Tsukada, *Phys. Rev. Lett.* **67**, 132 (1991)
- [13] Fundamentally this is only exactly true if the electron energy (and thus the energy of the hole) equals the Fermi energy  $E_F$ ; otherwise small deviations will occur.
- [14] G. E. Blonder, M. Tinkham, and T. M. Klapwijk, *Phys. Rev. B* **25**, 4515 (1982)
- [15] R. Landauer, *IBM J. Res. Dev.* **1**, 223 (1957); R. Landauer, *IBM Res. Dev.* **32**, 306 (1988)
- [16] C. W. J. Beenakker, *Phys. Rev. B* **46**, 12841 (1992)
- [17] I. K. Marmoros, C. W. J. Beenakker, and R. A. Jalabert, *Phys. Rev. B* **48**, 2811 (1993)
- [18] See also C. W. J. Beenakker, elsewhere in these proceedings.
- [19] K.-M. H. Lenssen, M. Matters, C. J. P. M. Harmans, J. E. Mooij, M. R. Leys, W. van der Vleuten, and J. H. Wolter, *Appl. Phys. Lett.* **63**, 2079 (1993)
- [20] In the rough measurement data at  $V_g = 0$  mV the depth of the sharp dip seems to be larger than  $e^2/h$  (figure 6); this probably due to the many parallel pathes between the superconducting contacts that the current can follow.
- [21] K.-M. H. Lenssen, L. A. Westerling, C. J. P. M. Harmans, J. E. Mooij, M. R. Leys, W. van der Vleuten, and J. H. Wolter, *Surf. Sci.* (in press)
- [22] K.-M. H. Lenssen, L. A. Westerling, P. C. A. Jeekel, C. J. P. M. Harmans, J. E. Mooij, M. R. Leys, W. van der Vleuten, J. H. Wolter, and S. P. Beaumont, *Physica B* **194-196**, 2413 (1994)
- [23] A. Kastalsky, A. W. Kleinsasser, L. H. Greene, R. Bhat, F. P. Milliken, and J. P. Harbison, *Phys. Rev. Lett.* **67**, 3026 (1991)
- [24] P. H. C. Magnée, N. van der Post, B. J. van Wees, and T. M. Klapwijk, *Physica B* **194-196**, 1031 (1994)
- [25] B. J. van Wees, P. de Vries, P. Magnée, and T. M. Klapwijk, *Phys. Rev. Lett.* **69**, 510 (1992)

## DIFFERENTIAL RESISTANCE CHARACTERISTICS OF SUPERCONDUCTOR - SEMICONDUCTOR HETEROSTRUCTURES

A.M. Marsh, D.A. Williams\*, B.W. Alphenaar\* and H. Ahmed

Microelectronics Research Centre, University of Cambridge, Cavendish Laboratory,  
Madingley Road, Cambridge CB3 0HE, UK

\*Hitachi Cambridge Laboratory, Cavendish Laboratory,  
Madingley Road, Cambridge CB3 0HE, UK

The transport properties of two dimensional electron gases with superconducting contacts are analysed. A dip in the differential resistance around zero bias is observed, and attributed to Andreev reflection at the interfaces, and higher bias structure is attributed to quasiparticle recombination in the superconducting contacts. The apparent temperature independence of the width of the dip is shown to be due to a balance between the thermal distributions of carriers in the normal and superconducting regions.

### Introduction

At the junction between a normal material (N) and a superconductor (S) at biases less than the superconductor gap energy, there are no states for single electron transport into the superconductor, and so charge transfer can only take place by two electrons, equally spaced in energy around the pair energy, pairing and entering the superconductor. This can be viewed as an incident electron at the Fermi level retroreflecting (Andreev<sup>1</sup> reflecting) as a conduction band hole. Andreev reflection usually results in a dip in the differential resistance around zero bias (see Fig.1), due to the extra hole current. The so-called zero bias anomaly has been observed in a remarkably wide variety of junctions that range<sup>15)</sup> from niobium-silver<sup>2)</sup> through tin-GaAs<sup>3)</sup> to an interface between superconducting and metallic phases of a polymer<sup>4)</sup>. Although the probability of Andreev reflection has been predicted as vanishingly small in junctions with a finite tunnel barrier, van Wees<sup>5)</sup> has shown how the probability can be increased by quantum interference if there is disorder in the normal region. Beenakker<sup>6)</sup> and Marmorkos et al.<sup>7)</sup> extended this for a general

interface disorder potential. It has been predicted that the central dip should end at a bias of  $\Delta/e$  at a single interface, when the Fermi level in the normal region reaches the quasiparticle energy in the superconductor. However, experimentally the width of the central dip has often been found to be a few times greater than this, and explanations of this have generally been device-specific<sup>2,4</sup>).

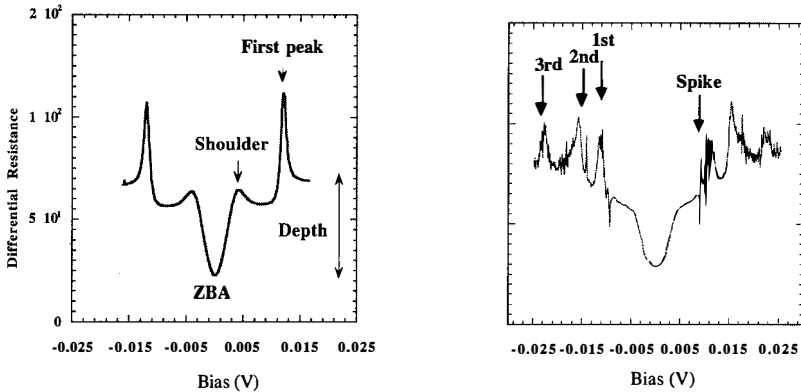


Figure 1:  $dV/dI$  curves for an S-N-S device at 1.6K (l) and 4.2K(r)

We have made differential resistance measurements of S-N-S and S-N devices, and observe a resistance dip around zero bias with a higher bias peak. In addition we observe structure in the differential resistance at higher bias that only occurs in a narrow temperature range. The shoulder of the central dip occurs at a bias of  $4\Delta/e$  in the S-N-S junction and approximately  $2\Delta/e$  in the S-N junction. The width of the central dip is found to be almost independent of temperature below  $T_C$ , rather than following the temperature dependence of the superconductor gap, as predicted<sup>8</sup>). The apparent temperature independence of the shoulder position is due to a balance between the gap reduction with increasing temperature, and thermal broadening in the normal material. The higher bias structure appears to be due to quasiparticle recombination.

## Experiments

A standard modulation-doped AlGaAs/GaAs heterojunction was used with superconducting contacts,  $3\mu\text{m}$  apart, diffused to make a connection between the surface and the two-dimensional electron gas (2DEG), 80nm below. These contacts were formed by evaporating a Sn-Cr-Au multilayer film which was sintered using

rapid electron beam annealing. The contacts have a critical temperature of 7.2K, much higher than that of bulk Sn (3.7K), which is probably due to an alloy in the contact composed of Sn, Al, Ga and As.

The differential junction resistance was measured, and for all devices the normal state resistances ( $R_N$ ) ranged from 40 -100 $\Omega$ . The differential resistance of a junction is shown in Fig.1. The characteristics have three main features: the dip around zero bias, the first peak at higher biases, and further peaks, spikes and noise beyond the first peak. All of these effects disappear above the measured critical temperature of the electrodes at 7.2K.

At 1.6K the central dip has a minimum of approximately  $R_N/3$ , and as temperature increases this minimum gradually increases, then the dip disappears rapidly above 5.0K. The shoulder of the dip becomes less distinct with increasing temperature, becoming a smooth gradient change around 4.2K; at this point the width of the dip has also increased slightly. Above 4.2K the shoulder re-develops and the feature narrows, then rapidly disappears above 5.0K.

The first resistance peak is observed at a higher bias than the shoulder. As temperature increases, the peak shifts consistently inwards, rapidly collapsing above 5.0K. At 1.6K only the first peak is seen, but as temperature increases further structure develops. A second peak starts to appear at 3.5K and is fully developed by 4.2K, at which point a third peak is also seen. No further structure other than the return to the normal state resistance develops beyond the third peak at any temperature. Above 4.2K the second peak changes to a sharp spike which reverts to a small peak at higher temperatures. Spikes also develop just before the first peak at a temperature around 4.2K, and appear to shift inwards with increasing temperature in the same manner as the first peak. The second and third peaks are accompanied by an increase in the measured noise.

## Discussion

At zero temperature, quasiparticle injection begins when the bias across a single interface reaches  $\Delta/e$ . This increases the interface resistance, and hence a shoulder should be observed in  $dV/dI$  at  $V=\Delta/e$ . However, the critical temperature of our electrodes is 7.2K, so  $\Delta=1.1meV$  at 0K, and we observe the shoulder at 4.1mV. This can be explained if we consider that what is normally described as a single S-N interface is in fact a N-S-N junction, as another normal contact must be made to the superconductor to make an electrical measurement. The second S-N interface formed by this contact cannot be ignored in determining the width, depth and temperature dependence of the central dip.

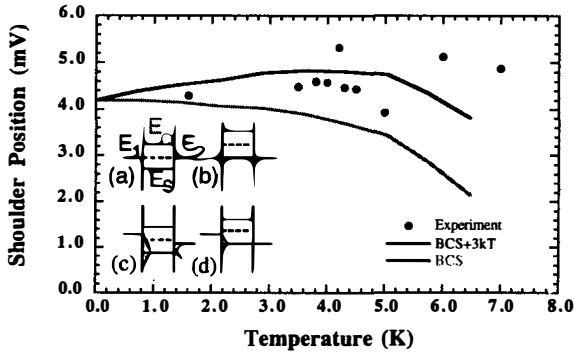


Figure 2: Temperature dependence of the shoulder of the central dip.

The symmetry of the  $dV/dI$  characteristics suggests that the two S-N interfaces are electrically very similar. If both interfaces have a very low Andreev reflection probability then at zero applied bias the equilibrium state would look as inset (a) in Figure 2, but if Andreev reflection is probable, charge will cross the interface and fill the ground state. This will charge the superconductor until the ground state aligns with the Fermi energies in the two leads (inset (b)). When a bias is applied the bands offset as shown in inset (c)-(d). In case (c), no current can flow at zero temperature. Andreev reflection must be possible at both interfaces for excess current to flow in the junction, and in this case (inset (d)), most of the potential drop will be at the upstream interface, as Andreev reflection requires the spatial and temporal overlap of electrons satisfying the energy and wave vector conservation conditions. Pair injection into a continuum of empty states is less restrictive at the downstream interface<sup>9</sup>).

We have also fabricated a single diffused contact overlapped by two Au-Cr bond pads to form an N-S-N device, with no 2DEG normal region. The shoulder occurs at 1.4mV, which falls within the limit predicted by our model (2.2mV). This also agrees well with other observations<sup>2-4,10,11</sup>).

The depth of the anomaly is difficult to account for quantitatively from recent theories<sup>5,6,7</sup>), as the disorder potential and barrier at the interface are not known. However, the number of junctions in series between the current probes will also affect the minimum resistance, as each Andreev reflecting junction creates an excess current through the device, and so multiple junctions in series will have lower resistances. The minimum for our N-S-N-S-N junction ( $R_N/3$ ) is approximately half of that for the N-S-N junction ( $2R_N/3$ ).

The temperature dependence of the central dip is expected to follow that of the BCS energy gap. The temperature independence of the central dip that we observe has been observed by others<sup>3,4,11</sup>), but has not been explained. Finite temperature broadens the Fermi distribution in the normal region, so that instead of an abrupt change in  $dV/dI$  when the Fermi level reaches the quasiparticle energy, there will be a smooth transition. The differential resistance will start to increase at a lower bias and stop at a higher bias than it would if there were no broadening. The shoulder at finite temperature represents the upper end of this change in  $dV/dI$ , and so will move to higher bias with increasing temperature. However, the gap decreases with increasing temperature, and so the two effects compete<sup>16</sup>). An estimate of the change in shoulder position can be obtained by adding a term linear in temperature to the BCS dependence of the energy gap. Figure.2 shows this dependence plotted with the experimental shoulder positions. It can be seen that thermal broadening widens the shoulder slightly and reduces the temperature dependence of the width, until very close to  $T_C$ , which approximately matches the experimental results.

The other generally observed feature in the differential resistance is the first peak outside the shoulder. This has been commonly attributed to a collapse back to the normal state resistance, but an excess current exists after the first peak, and the transition to the normal state happens at a much higher bias. It is likely that the peak results from quasiparticle recombination in the superconducting electrodes.

When the applied bias at the injecting contact is greater than  $\Delta/e$ , hot quasiparticles are injected into the superconductor. These can pair and relax to the ground state by emitting a phonon, or a quasiparticle can recombine to the ground state by pairing with an electron of equal energy below the ground state, in a zero-phonon transition which is essentially internal Andreev reflection. A coherent electron-phonon process leads to a jump in the I-V curve<sup>19</sup>), giving a  $dV/dI$  spike similar to that we observe; the peak appears to be a broadening of this effect by temperature or disorder.

Multiple peaks similar to those we see have been reported<sup>3</sup>) for a SnPd-AlGaAs/GaAs device at the lowest-temperature measurement (1.2K), and were attributed to the collapse of supercurrent paths in the contacts. We observe similar peaks in a similar material structure, but the additional peaks only appear within a small temperature band. The spikes could result from a coherent electron-phonon process as described above, which is strongly dependent on the cooling properties of the environment of the superconductor, and these broaden into the extra peaks.

The increased noise at higher biases is, we believe, due to the generation of local phase slip centres<sup>20</sup>), making small regions of the tin remaining above the alloy resistive, which causes local heating, leading to random changes in the device resistance.

## Conclusions

We have shown that the width of the zero bias anomaly observed in superconductor - normal junctions can be explained by considering the changeover from Andreev reflection to quasiparticle injection at all the junctions present in series independent of material or geometry. The thermal distribution in the normal material slightly widens the central dip and alters the temperature dependence. Quasiparticle recombination in the superconductor determines the structure in the differential resistance at higher applied biases.

The authors would like to acknowledge many useful discussions with Dr Mathias Wagner of the Hitachi Cambridge Laboratory, members of the collaboration between the Microelectronics Research Centre and the Hitachi Cambridge Laboratory, and Dr Trevor Thornton of Imperial College, London University.

## References

1. A.F. Andreev, *Zh. Eksp. Teor. Fiz.* **46** 1823 (1964) *Sov. Phys. JETP* **19** 1228 (1964).
2. P. Xiong, G. Xiao, and R.B. Laibowitz, *Phys. Rev. Lett.* **71** 1907 (1993).
3. J.R. Gao, J.P. Heida, B.J. van Wees, T.M. Klapwijk, G. Borghs, C.T. Foxon, *10th Int. Conf. Electronic Properties of Two-Dimensional Systems*, Rhode Island, U.S.A., (1993).
4. M. Weger, A. Nowack, D. Schweitzer, J. Kubler, J.M. Van Bentum, and C.S. Sommers, in *Organic Superconductivity*, edited by V. Z. Kresin and W. A. Little (Plenum Press, New York, 1990), p. 211-220.
5. B.J. van Wees, P. de Vries, P. Magnée, and T.M. Klapwijk, *Phys. Rev. Lett.* **69** 510 (1992).
6. C.W.J. Beenakker, *Phys. Rev. B* **46** 12841 (1992).
7. I.K. Marmorkos, C.W.J. Beenakker, and R.A. Jalabert, *Phys.Rev..B* **48** 2811 (1993).
8. G.E. Blonder, M. Tinkham, and T.M. Klapwijk, *Phys. Rev. B* **25** 4515 (1982).
9. F.W.J. Hekking and Yu. V. Nazarov, *Phys.Rev.Lett.* **71** 1625 (1993).
10. T. Nishino, M. Hatano, H. Hasegawa, T. Kure, and F. Murai, *Phys.Rev.B* **41** 7274 (1990).
11. C. Nguyen, H. Kroemer, and E.L. Hu, *Phys.Rev.Lett.* **69** 2847 (1992).
12. A.W. Kleinsasser, T.N. Jackson, D.McInturff, F. Rammo, G.D. Pettit, and J.M. Woodall *Appl. Phys. Lett.* **57** 1811 (1990).
13. K.M. Lenssen, M. Matters, C.J.P.M. Harmans, J.E. Mooij, M.R. Leys, W. van der Vleuten, and J.H. Wolter, *Appl. Phys. Lett.* **63** 2079 (1993).
14. A. Kastalsky, A.W. Kleinsasser, L.H. Greene, R. Bhat, F.P. Milliken, and J.P. Harbison, *Phys. Rev. Lett.* **67** 3026 (1991).
15. Also in BiSCO - metal. T. Ekino and J. Akimitsu in *Selected topics in Superconductivity*, edited by L.C. Gupta and M.S. Multani (World Scientific, Singapore, 1992), pp. 477-525.
16. When the ground state energy in the superconductor is within the thermal broadening of the Fermi energy in the normal material an Andreev reflecting electron can be below the pair energy, and the hole above, creating a non-equilibrium carrier distribution in the normal material<sup>17</sup>. This is related to the effects observed in<sup>18</sup>.
17. A.B. Pippard, in *Nonequilibrium Superconductivity, Phonons, and Kapitza Boundaries*, edited by K. E. Gray (Plenum Press, New York, 1981), pp. 341-352.
18. M.G. Blamiré, E.C.G. Kirk, J.E. Evetts and T.M. Klapwijk, *Phys. Rev. Lett.* **66** 220 (1991)
19. V.M. Galitskii, V.F. Elesin, and Y.U. Kopaez, in *Nonequilibrium Superconductivity*, edited by D.N. Langenberg and A.I. Larkin (North-Holland, Amsterdam, 1986), pp. 377-451.
20. W.J. Skocpol, M.R. Beasley, and M. Tinkham, *Journal of Low Temp. Phys.* **16** 145 (1974).

## INTERFERENCE OF PAIRS OF ELECTRONS TUNNELING INTO A SUPERCONDUCTOR

H. Pothier, S. Guéron, D. Esteve, and M.H. Devoret  
*Service de Physique de l'Etat Condensé, CEA-Saclay  
F-91191 Gif-sur-Yvette Cedex, France*

Interest in the transfer process of electron pairs at the interface between normal and superconducting electrodes, first described by Andreev in 1964<sup>1)</sup>, was recently revived by experiments on semiconductor-superconductor contacts<sup>2,3)</sup>. The electrical conductance of such contacts was found to be strongly enhanced at zero voltage, a result which the well accepted ballistic electron model<sup>4)</sup> failed to predict. Recently, Xiong et al.<sup>5)</sup> have shown that the conductance of normal metal-superconductor (NS) contacts depends on the shape of the normal electrode. Furthermore, in experiments on charging effects in superconducting nanostructures, the conductance of NS junctions was found to be much larger than expected from the ballistic model<sup>6,7)</sup>. That multiple attempts for tunneling of electron pairs could enhance the conductance of NS junctions, unlike the case of NN junctions, was pointed out by van Wees *et al.*<sup>8)</sup> and subsequently analysed by several other authors<sup>9,10,11,12)</sup>. In the semiclassical description of an NN junction, even if an electron collides  $n$  times with the barrier, it contributes to the conductance exactly like  $n$  electrons each colliding with the barrier just once. The reason is that the dephasing of the electron wavefunction is random between collisions with the barrier. This is no longer the case in NS junctions in the presence of time reversal symmetry. Consider two electronic wavefunctions on the normal metal side. The phase of the pair tunnel amplitude at each point is the algebraic sum of the phases of the two wavefunctions and of the superconducting order parameter. If the wavefunctions are nearly time-reversed, as depicted in Fig. 1, and if the order parameter of the superconductor is uniform, the total phase is constant along the barrier, and the amplitudes at different points interfere constructively. The total pair tunnel amplitude is thus multiplied by the number of points at which the trajectory hits the barrier. This simple semiclassical model describes how multiple attempts of tunneling of electron pairs near the tunnel barrier enhance the conductance.

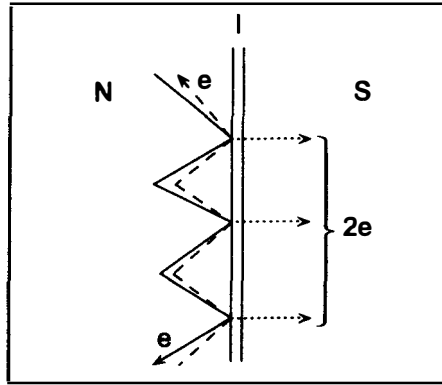


Figure 1: Semiclassical representation of the mechanism responsible for the enhancement of the Andreev current. Two diffusing electrons in the normal electrode, with nearly time-reversed wavefunctions, tunnel through the barrier at different points with the same phase. If the order parameter of the superconductor is uniform, the tunnel amplitudes at these different points contribute constructively to the total current.

Hekking and Nazarov proposed recently<sup>11)</sup> different layouts in which this effect could manifest itself. In particular, they considered the case of two NS junctions in parallel in which the interference between the pair tunnel amplitudes at the two junctions is controlled by the difference between the superconducting phases at the two junctions.

We report here measurements of the Andreev current in such an "NS-QUID" (Normal metal-Superconductor QUantum Interference Device) whose layout is shown in Fig. 2. In NS-QUIDs, the difference between the superconducting phases at the two junctions is monitored by the flux  $\Phi$  threading the loop. The normal electrode near the junctions is long and narrow in order to increase the number of tunnel attempts of electron pairs. Our sample was fabricated using electron beam lithography and shadow-mask evaporation<sup>13)</sup>. The superconducting and normal electrodes consist of a 20 nm thick aluminum film and a 30 nm thick copper film, respectively. The sample was cooled down in a dilution refrigerator. We deduced the normal state conductance  $G_T = 641 \mu\text{S}$  from the large scale normal state current-voltage ( $I$ - $V$ ) characteristic (dashed line in the top-left inset of Fig. 3), measured by applying a field of 0.1 T perpendicular to the films.

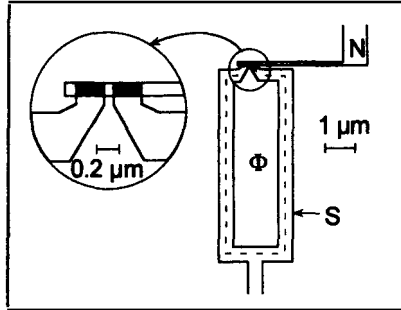


Figure 2: NS-QUID layout: a normal metal wire overlaps an oxidized superconducting fork electrode. The effective area of the loop (enclosed by the dashed line) is  $13 \mu\text{m}^2$ . The superconducting bottom electrode (aluminum) and the normal top electrode (copper) were 20 and 30 nm thick, respectively. Regions where the normal electrode overlaps the superconducting electrode are in dark.

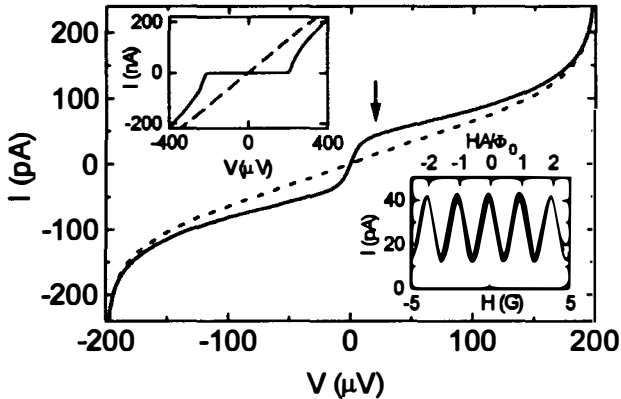


Figure 3: Extremal subgap I-V characteristics measured at  $T=27$  mK. The solid and the dotted lines correspond to maxima ( $\Phi = k\Phi_0$ ) and minima ( $\Phi = (k+1/2)\Phi_0$ ) of the modulation of the current as a function of the magnetic field  $H$  shown in the bottom-right inset, respectively. The arrow indicates the bias voltage at which the modulation pattern was measured (circles: data; solid line: sine function fit). The top-left inset represents the large scale characteristics of the NS-QUID at  $H=0$  (solid line) and  $H=0.1$  T (dashed line).

At zero field, the current decreases considerably below the superconducting gap voltage (solid line in the same inset). As the temperature is decreased below 300 mK, the residual sub-gap current becomes strongly field modulated, as shown in the bottom right inset of Fig. 3 for  $V=20 \mu\text{V}$  and  $T=27$  mK. The magnetic

field dependence of the current follows a sine function (solid line), as predicted in Ref. 11. Assuming a  $\Phi_0 (= h/2e)$ -periodicity for the modulation as a function of the flux  $\Phi$  threading the loop, we deduce an effective field capturing area  $A$  of the loop which agrees within 20% with the area defined in Fig. 2. Note that the positions of the maxima do not exactly correspond with integer multiples of flux  $\Phi_0$ , an offset which we attribute to the residual field in the cryostat. We show in the main plot of Fig. 3 the two extremal  $I$ - $V$  characteristics (solid and dashed lines). The maximal ( $\Phi = k\Phi_0$ ) and minimal ( $\Phi = (k + 1/2)\Phi_0$ ) conductances at  $V=0$  are  $G_{\max} = 4.6 \mu\text{S}$  and  $G_{\min} = 0.66 \mu\text{S}$ , which are much larger than the ballistic upper bound estimate  $G_{\text{bal}} = (\hbar/4e^2)G_T^2/N_{\text{eff}} \approx 25 \text{ nS}$ , where  $N_{\text{eff}} = S/4\pi\lambda^2$  is the effective number of channels calculated with the upper bound estimate  $\lambda = 0.2 \text{ nm}$  for the barrier wavelength cut-off<sup>12</sup>).

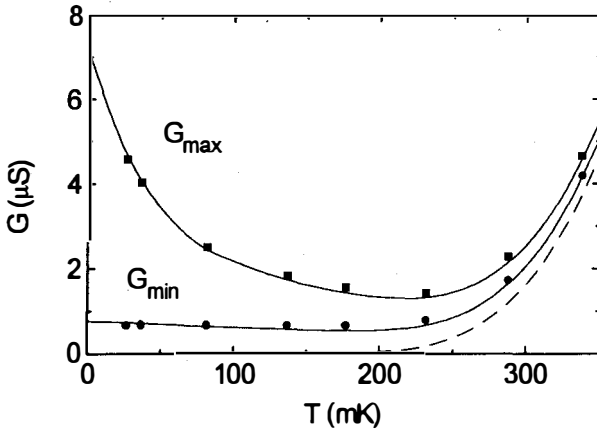


Figure 4: Comparison between the measured (symbols) and predicted (solid lines) temperature dependences of the maximal and minimal conductances  $G_{\max}$  and  $G_{\min}$ . Predicted curves are calculated along the lines of Ref. 12 with a diffusion constant  $D = 59 \text{ cm}^2 \text{ s}^{-1}$  and with a phase-breaking time  $\tau_\phi = 120 \text{ ps}$ . We have used  $n(E_F) = 1.5 \times 10^{47} \text{ J}^{-1} \text{ m}^{-3}$  for the density of states of copper. The dashed line shows the quasiparticle conductance contribution  $G_{\text{qp}}$  to  $G$ .

Figure 4 shows the variations of  $G_{\max}$  and  $G_{\min}$  as a function of the temperature  $T$ , from 27 to 350 mK. In Ref. 12, Hekking and Nazarov establish the link between the current and the return probability of an electron at the barrier. We have made the hypothesis of a diffusive motion of electrons in the normal electrode and have deduced from their formula  $G_{\max}$  and  $G_{\min}$  after solving the diffusion

problem for our particular device layout. The fit parameters are *i*) the diffusion constant  $D = 60 \pm 5 \text{ cm}^2 \text{ s}^{-1}$  and *ii*) the phase-breaking time  $\tau_\phi = 120 \pm 10 \text{ ps}$ , which are compatible with previous measurements<sup>14)</sup>. However, we had to scale the calculated conductances up by a factor 4.7, which is not understood at present. The expected extra contribution to the current arising from phase-coherent diffusion of quasiparticles in the superconducting electrode<sup>12)</sup> is too small to resolve the discrepancy, and should not affect the modulated part of the conductance. Allowing for this adjustment, we find a good agreement between experiment and theory at temperatures between 27 mK and 180 mK. Above 200 mK, the contribution  $G_{\text{qp}}$  of thermally activated quasiparticle tunneling to the conductance is no longer negligible, and we have added it to the Andreev conductance using<sup>15)</sup>

$$G_{\text{qp}} = G_{\text{T}} \sqrt{\frac{2\pi\Delta}{k_{\text{B}}T}} \exp\left(-\frac{\Delta}{k_{\text{B}}T}\right)$$

with  $\Delta = 205 \text{ } \mu\text{eV}$  for the energy gap of our aluminium film. With this added contribution, shown as a dashed line in Fig. 4, the agreement with experimental data is then excellent in the whole temperature range.

#### ACKNOWLEDGEMENTS

We have benefited from many discussions with F. Hekking and Yu. Nazarov. We are grateful to T. M. Klapwijk for useful comments on our results.

#### REFERENCES

- 1) A. F. Andreev, Zh. Eksp. Teor. Fiz. **46**, 1823 (1964) [Sov. Phys. JETP **19**, 1228 (1964)].
- 2) A. Kastalsky, L.H. Greene, J. B. Barner, and R. Bhat, Phys. Rev. Lett. **64**, 958 (1990); A.W. Kleinsasser, T. N. Jackson, D. McInturff, F. Rammo, G.D. Petit, and J.M. Woodall, Appl. Phys. Lett. **57**, 1811 (1990); A. Kastalsky, A.W. Kleinsasser, L.H. Greene, R. Bhat, F. P. Milliken, and J. P. Harbison, Phys. Rev. Lett. **67**, 3026 (1991).
- 3) C. Nguyen, H. Kroemer, and E. L. Hu, Phys. Rev. Lett. **69**, 2847 (1992).
- 4) G. E. Blonder, M. Tinkham, and T. M. Klapwijk, Phys. Rev. **B 25**, 4515 (1982).
- 5) P. Xiong, G. Xiao and R.B. Laibowitz, Phys. Rev. Lett. **71**, 1907 (1993).
- 6) T. M. Eiles, J. M. Martinis, M. H. Devoret, Physica **B 189**, 210 (1993).
- 7) J. M. Hergenrother, M. T. Tuominen, and M. Tinkham, Phys. Rev. Lett. **72**, 1742 (1994).

- 8) B. J. van Wees, P. de Vries, P. Magnée, and T. M. Klapwijk, *Phys. Rev. Lett.* **69**, 510 (1992).
- 9) A. F. Volkov, A. V. Zaitsev, and T. M. Klapwijk, *Physica C* **210**, 21 (1993).
- 10) C. W. J. Beenakker, *Phys. Rev. B* **46**, 12841 (1992).
- 11) F. W. Hekking and Yu. Nazarov, *Phys. Rev. Lett.* **71**, 1625 (1993).
- 12) F. W. Hekking and Yu. Nazarov, *Phys. Rev. B* **49**, 6847 (1994).
- 13) G. J. Dolan and J. H. Dunsmuir, *Physica B* **152**, 7 (1988).
- 14) B. Pannetier, J. Chaussy, and R. Rammal, *Physica Scripta* **T13**, 245 (1986).
- 15) L. Solymar, *Superconductive Tunnelling and Applications* (Chapman and Hall, London, 1972), Chap. 4.

## ELECTRON TRANSPORT IN A SUBMICRON METALLIC WIRE PERIODICALLY IN CONTACT WITH SUPERCONDUCTING ISLANDS

Hervé Courtois, Philippe Gandit and Bernard Pannetier  
C.R.T.B.T., C.N.R.S., 25 Av. des Martyrs, BP 166, 38042 Grenoble, France.  
Laboratoire Associé à l'Université Joseph Fourier, Grenoble.

In this paper, we report electron transport measurements in a long submicron metallic wire periodically in contact with ultrasmall superconducting islands. Evaporation in the same U.H.V. vacuum cycle of Cu and Al with two-axes shadow evaporation technique enables us to obtain high quality interfaces. The separation between Al lines has been varied between 0.4 and 2.5  $\mu\text{m}$  whereas the normal coherence length  $L_T$  is 0.2  $\mu\text{m}$  at 1 K. The existence of a resistance increase below  $T_c$  is discarded. At low temperature, phase coherence extends over the whole system and zero-resistance state is observed. Current-Voltage characteristics show critical currents up to 1  $\mu\text{A}$  at 40 mK and resistance steps, reminiscent of phase-slip centers. Magnetoresistance measurements in 2D arrays of parallel Cu wires coupled by transverse Al lines exhibit fluxoid quantization and interference effects.

There is now a number of puzzling theoretical predictions<sup>1)</sup> and experimental results on Normal-Superconducting systems<sup>2),3)</sup>. In a recent experiment, Petrashov et al<sup>2)</sup> showed an increase of the resistance of a mesoscopic normal wire when a small piece of superconductor in contact with the normal metal goes in the superconducting state, even if the measurement current does not flow under the piece of superconductor. We present here results on a similar system with a larger length and at lower temperature.

If a superconductor is put in clean contact (no oxide barrier) with a normal metal, the proximity effect between the two metals depresses the pair potential in the superconductor while superconductivity appears in the normal metal<sup>4)</sup>. Evaporated metallic layers are usually in the dirty limit, where the mean free path

is of the order of the thickness of the layer and much lower than the coherence lengths of the system. In the normal metal, the characteristic length over which Cooper pairs diffuse is the normal coherence length:

$$L_T = \sqrt{\frac{\hbar D}{2\pi k_B T}} \quad (\text{dirty limit}) \quad (1)$$

In our typical layers, the mean free path in the copper is 30 nm and the normal coherence length is 0.2  $\mu\text{m}$  at 1 K. This scale is now easily attainable with modern lithography techniques. We designed a new type of mesoscopic system made of a single normal metallic wire periodically in contact with superconducting material. The total length  $L$  of our system is 92  $\mu\text{m}$  or 79  $\mu\text{m}$ . The distance between Al strips  $d$  has been varied between 0.4 and 2.5  $\mu\text{m}$ , whereas the width  $w$  of the wires is about 0.2  $\mu\text{m}$ . Figure 1 shows a draw of a part of one sample.

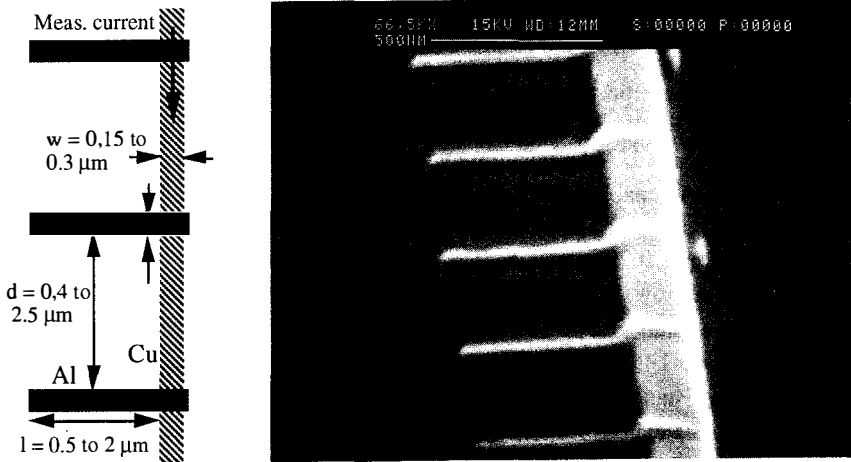


Figure 1: Scheme of our samples and SEM oblique view of a typical sample.

We used e-beam lithography on a bilayer of resist (PMMA/MAA and PMMA) in order to obtain a PMMA mask suspended about 0.5  $\mu\text{m}$  over the silicon substrate<sup>5)</sup>. Angle evaporations with two axes of rotation enable us to choose which metal we evaporate on the substrate for a given direction of a line. The e-beam evaporation were performed in a UHV system with a pressure lower than  $3 \cdot 10^{-8}$  mbar during all the process which lasts about 20 mn. This technique allows us to obtain a high-quality interface between Al and Cu. In order to test the quality of the metal layers and of the interface, we performed Ratio of Residual Resistivity (RRR) tests on extended layers of Cu, Al and a Al-Cu bilayer. The RRR of the layer of Cu and Al were respectively of 3 and 3.4, whereas the bilayer has a RRR of 2.7. The

RRR for the bilayer remains quite good and indicates that the Cu has not been alloyed with deposited Al.

We performed high sensitivity transport measurement on more than 10 samples down to 20 mK in a dilution refrigerator. Lithographed rf filters with a reliable efficiency of more than -60 dB at 300 MHz were integrated in the sample holder<sup>6</sup>). The samples were shielded from earth magnetic field by  $\mu$ -metal shields.

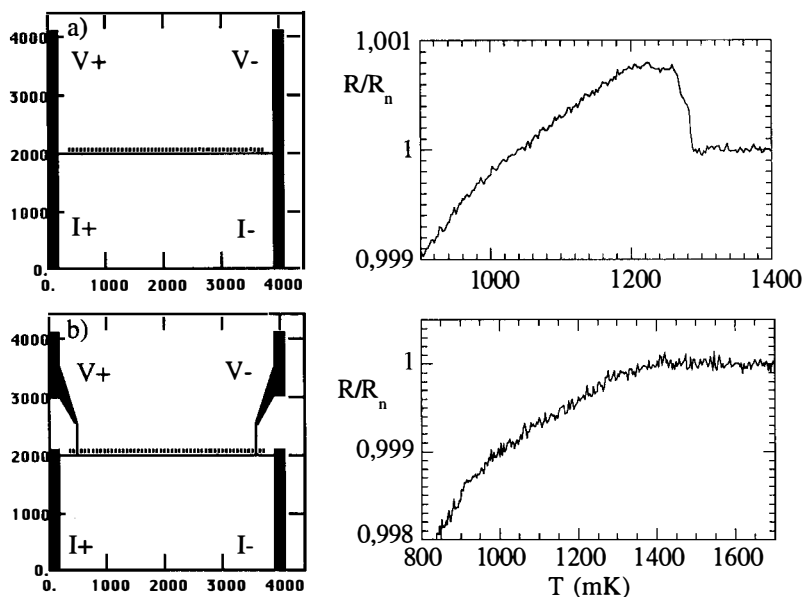


Figure 2: Two kinds of four probes geometry (size of the window  $100 \times 100 \mu\text{m}^2$ ) and the respective  $dV/dI$  behavior near  $T_C(\text{Al})$  with 300Hz measurement frequency.

We first consider the behavior of the measured resistance near the superconducting transition of Al. Due to the fabrication technique, the current and voltage contacts are made of a bilayer of Cu and Al. We found that the design of the contacts was very important to make an accurate measurement of the resistance of our hybrid samples. Figure 2 sketches two different four terminals contact designs and the measured  $dV/dI$  beside. In the H-type geometry (Fig. 2a) we observe an increase of resistance which is related to the superconducting transition of the contacts, which occurs near the  $T_C$  of Al. When the wide line constituting the contacts goes from the superconducting to the normal state, the deformation of the isopotential lines gives a false measure of the resistance above  $T_C$ <sup>7</sup>). In Figure 2a, the relative percentage of the effect is about 0.1 % which is close to the geometrical aspect ratio of contact  $w/L$  (0.2%). No such jump is observed in true four terminals

design (Fig. 2b). One must point out that our samples are much longer than all the characteristic coherence lengths and that mesoscopic fluctuations will be averaged out. The quality of the interface has also some importance if one wants to compare different results.

As temperature is lowered, a zero-resistance state is obtained. Dynamic resistance versus current measurements show a sharp critical current (see fig. 3). We also notice remarkable structures which are not periodic in current or in voltage. If one plots resistance versus the label of the peak, one obtains a straight line (see inset), showing that every peak in dynamic resistance corresponds to the transition to the normal state of an equal length of Cu wire. This behavior is reminiscent of phase-slip centers in conventional superconducting wires. Hence the characteristic length of this normal region where single electrons and Cooper pairs are not in equilibrium is here  $6 \mu\text{m}$ , much larger than the coherence length in Cu but of the order of the phase breaking length  $L_\phi$  in Cu<sup>8</sup>).

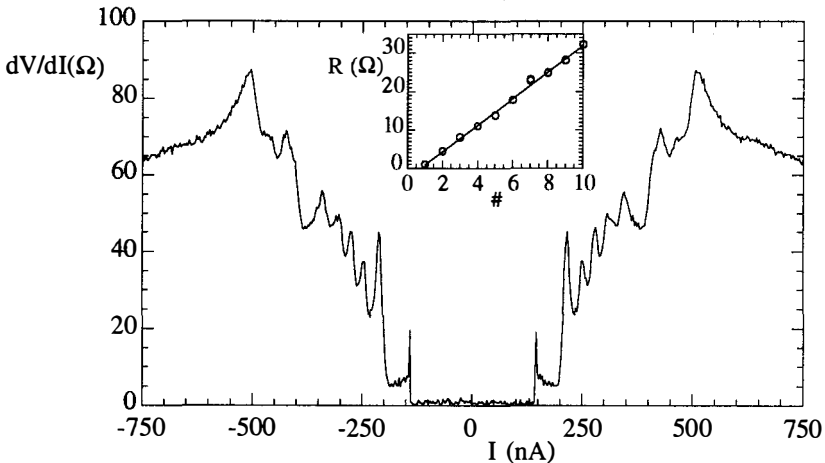


Figure 3: Sample #9,  $d=0.4 \mu\text{m}$ ,  $T=30 \text{ mK}$ . Dynamic resistance versus current. Inset: Value of the resistance at which the peak label # occurs.

We performed a systematic study of the critical current as a function of the temperature for various distances  $d$  between Al strips. Figure 4 shows the critical current of two samples of  $d = 0.4$  and  $1.6 \mu\text{m}$ . At temperature higher than  $600 \text{ mK}$  the critical current of the sample  $d = 0.4 \mu\text{m}$  is smeared out by thermal fluctuations. The measured critical current can be viewed as the critical current of a S-N-S junction between two neighbouring Al islands. In order to evaluate this quantity, one has to know the order parameter in the Cu in contact with Al. We can consider our system locally as a bilayer of Al with a thickness equal to the length of the strip (usually  $1.6 \mu\text{m}$ ) and Cu with a thickness equal to  $d$ . We can then calculate

the critical temperature of our system by the De Gennes-Werthamer<sup>4)</sup> model which is valid in the dirty limit and for thicknesses larger than the coherence lengths:

$$T_{CNS} = T_{CS} \left[ 1 - \frac{\pi^2}{2} \frac{\xi_{GL}^2}{(e_s + L_T)^2} \right] \quad (2)$$

where  $T_{CNS}$  and  $T_{CS}$  are respectively the transition temperature of Al and of the bilayer. Here  $T_{CS} = 1.4$  K and  $T_{CNS} = 1.35$  K. The superconductivity in Al is only slightly affected by the Cu.

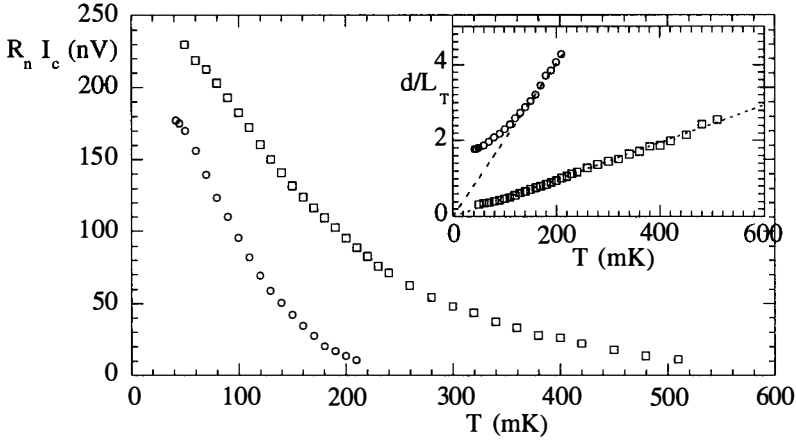


Figure 4:  $R_n I_c(T)$  with a resistance threshold of 3 Ohms and for two different samples; Squares: #10,  $d = 0.4 \mu\text{m}$ . Circles: #11,  $d = 1.6 \mu\text{m}$ . Inset:  $d/L_T$  versus  $T$ .

We can then use the critical current expression of a S-N-S junction<sup>9)</sup>:

$$R_n I_C \propto \left\{ 1 - \frac{T}{T_{CNS}} \right\}^2 e^{-d/L_T} \quad (3)$$

to derive the temperature behavior of  $L_T$  from the experimental data, see the inset of figure 4. One can easily see that  $L_T$  does not follow the expected dirty limit law  $1/\sqrt{T}$  but rather a  $1/T$  law, as would be expected in the clean limit:

$$L_T = \frac{h v_f}{2 \pi k_B T} = \frac{1,6 \mu\text{m}}{T(K)} \quad (\text{clean limit}) \quad (4)$$

This anomalous behavior has already been noticed in other types of proximity systems<sup>10)</sup>. We obtain from our data from sample #10  $L_T = 0.1 \mu\text{m}$  at 1 K. The discrepancy between these two values can be explained by the presence of some diffusion barrier at the interface. Further experiments on other proximity couples are under progress in order to confirm this result.

Finally, we present magnetoresistance measurement on a two-dimensionnal array of parallel Cu wires coupled by transverse Al lines (Fig. 5). The figure is

periodic with a period corresponding to a flux  $\phi$  in one cell equal to a quantum of flux  $\phi_0$ . The rapid oscillations inside one period correspond to quantum interference between the 18 parallel supercurrents which are dephased by a quantity  $f = \phi/\phi_0$ . The result is the well-known Fraunhofer pattern of diffraction that can be observed in large S-I-S junctions with in-plane magnetic field:

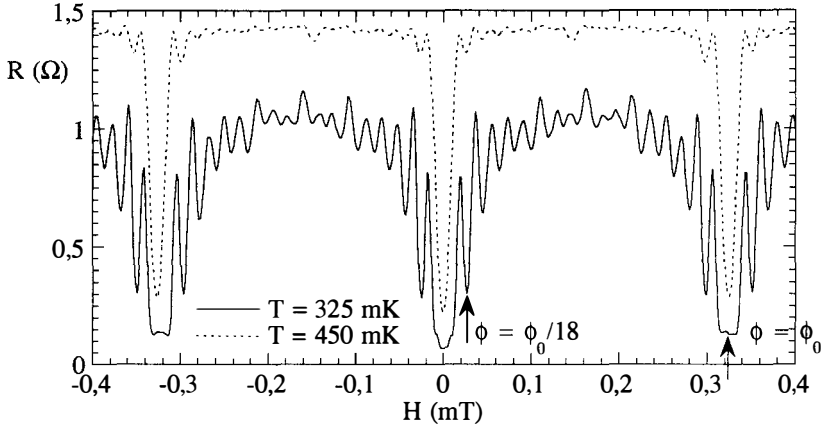


Fig. 5: Sample #5:  $d=2.5 \mu\text{m}$ . Magnetoresistance of a 2D array of Cu and Al wires.

$$I_c = I_{c0} \sum_{i=1}^n \sin(2\pi i f) = I_{c0} \frac{\sin(2\pi n f)}{\sin(2\pi f)} \quad n=18 \quad (5)$$

We can then deduce the  $R(H)$  characteristic from the RSJ (Resistively-Shunted Junction) model.

In summary, we have discussed some transport properties of a new mesoscopic proximity system. In contrast to other experiments made on shorter samples, no resistance increase below  $T_c$  is reliably observed. A  $1/T$  law for  $L_T$  has been found, in contradiction with classical models. It will be interesting to study the effects of Coulomb blockade<sup>11)</sup> or quantum interference on this lateral proximity system. We would like to thank Louis Dumoulin for fruitful discussions.

- 1) B. Spivak and D. E. Kmel'nitskii, JETP Lett **35**-8, 412 (1982).
- 2) V. T. Petrashov, V. N. Antonov, S. Maksimov and R. Shaikhaidarov, JETP Lett. **58**-1 (1993).
- 3) Y. K. Kwong, K. Lin, P.J. Hakonen, M. Isaacson and J. Parpia, Phys. Rev. B **44**, 462 (1991).
- 4) G. Deutscher and P.-G. de Gennes, in "Superconductivity", Parks (1968)
- 5) G. J. Dolan and J. H. Dunsmuir, Physica B **152**, 7 (1988).
- 6) H. Courtois, O. Buisson, J. Chaussy and B. Pannetier, to be published.
- 7) R. Vaglio, C. Attanasio, L. Maritato and A. Ruosi, Phys. Rev. B **47**, 15302 (1993).
- 8) B. Douçot and R. Rammal, Phys. Rev. Lett. **55**, 1148 (1985).
- 9) P.-G. de Gennes, Rev. Mod. Phys. **36**, 225 (1964).
- 10) A. C. Mota, D. Marek and J. C. Weber Helvetica Phys. Acta, **55**, 647 (1982).
- 11) C. Bruder, Rosario Fazio and Gerd Schön, preprint.

MESOSCOPIC EFFECTS IN PROXIMITY INDUCED SUPERCONDUCTING  
CYLINDERS OF COPPER AND SILVER

P. Visani, A. C. Mota, K. Aupke, A. Amann, and B. Lundqvist  
*Laboratorium für Festkörperphysik, ETH- Hönggerberg  
CH-8093 Zürich, Switzerland*

Due to the proximity effect, the properties of a system consisting of a superconducting metal in good electrical contact with another superconductor or a normal metal, are changed within some characteristic distances from the interface of both metals. For the case where the mean free path  $\ell$  in the normal metal is large compared to the induced coherence length (clean limit), Deutscher and de Gennes<sup>1)</sup> have calculated the induced pair amplitude  $F_N(\mathbf{r})$  for the case  $V_N = 0$ . For this case the pair potential  $\Delta(\mathbf{r})$  vanishes in N, but  $F_N(\mathbf{r}) = \Delta(\mathbf{r}) / V(\mathbf{r})$  has a finite "tail" in the N region. For the one dimensional case and for values of  $x$  large compared to the coherence length,  $F_N$  has the asymptotic form:

$$F_N(x) = \phi(x) \exp(-K_N |x|) \quad (1)$$

where  $\phi(x)$  is a slowly varying function of  $x$  and the induced coherence length  $K_N^{-1}$  is given by:

$$K_N^{-1} = \frac{\hbar v_F}{2\pi k_B T} = \begin{cases} \frac{1.7 \mu\text{m} \cdot \text{K}}{T(\text{K})} & \text{for silver} \\ \frac{1.9 \mu\text{m} \cdot \text{K}}{T(\text{K})} & \text{for copper} \end{cases} \quad (2)$$

The importance of the understanding of this limit is readily realized if we consider that at millikelvin temperatures samples in the "clean" limit could have induced coherence lengths of the order of hundreds of microns. Cooper pairs that in the "dirty" limit are described in the phenomenological theories to propagate diffusively into the normal metal, should show in the "clean" limit long range coherent effects.

Recently we have reported<sup>2)3)</sup> the discovery of a novel quantum coherence

effect in cylinders of a normal metal in proximity with a superconductor. In the temperature regime where the induced coherence length  $K_N^{-1}$  becomes greater than the perimeter  $L$  of the cylinders, we have observed that the full diamagnetic screening induced in the normal metal by the proximity effect is reduced below a well defined temperature  $T_{\min}$  following a law of the type  $\Delta\chi = A \exp(-T/T^*)$ . The characteristic temperature  $T^*$  of the new effect is strongly size dependent and given by  $T^* = p (\hbar v_F / 2\pi k_B L)$ , where  $p$  is a measured constant of order one.

Specimens consisting of wires with a superconducting core (Nb or Ta) embedded in a normal metal matrix (Cu or Ag) were prepared similarly to the commercial wires in superconducting magnet technology. With this technique we could achieve excellent transmission coefficients at the N-S surface and long mean free paths of the order of several microns in the normal metal. AC susceptibility, DC isothermal magnetization and Meissner expulsion were measured using SQUID detection in the temperature range  $5\text{mK} < T < 9\text{K}$ .

In Fig. 1 we summarize the result of three different experiments done on a Ag-Nb sample with an external perimeter  $L = 72\mu\text{m}$ . The in-phase component of the AC susceptibility has been measured with a frequency  $f = 80\text{ Hz}$  and an excitation field of  $33\text{ mOe}$ . The DC susceptibility has been obtained from the initial slope of magnetization curves taken at constant temperature. For the Meissner experiment, a

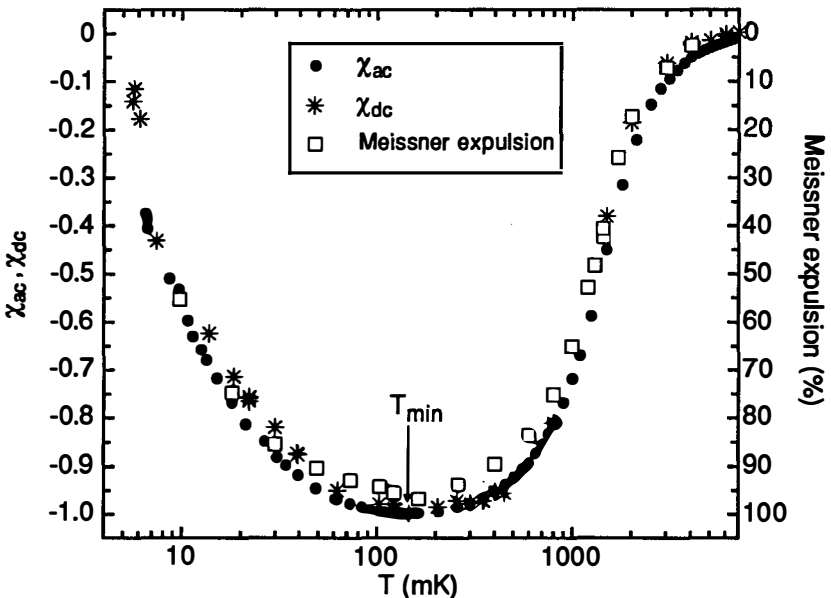


Fig. 1:  $\chi_{ac}$ (●),  $\chi_{dc}$ (\*) and Meissner expulsion(□) as a function of temperature for a Ag-Nb sample with  $L=72\mu\text{m}$ .

magnetic field  $H = 1.7$  Oe was applied at  $T = 6$  K and then the flux change recorded while reducing the temperature. Within the experimental uncertainties, the three experiments are in excellent agreement and show a general behaviour which is common to all the specimens we have investigated. In Fig. 1 the constant value of the diamagnetic contribution due to the superconducting core of Nb has been subtracted from the data so that a value of the susceptibility corresponding in the graph to  $\chi' = 0$  corresponds to full diamagnetism in the superconducting core and no induced superconductivity in the normal metal. A value of the susceptibility corresponding to  $\chi' = -1$  means complete screening or for the Meissner effect experiment 100% flux expulsion in the normal metal. In the temperature interval  $T_{\min} < T < T_c$  all the samples screen the applied magnetic field and the effect is complete at  $T = T_{\min}$ .

Below  $T_{\min}$ , a well defined temperature which is strongly size dependent, we observed a reentrance of the induced diamagnetic screening in the normal metal. The novel behaviour of the susceptibility for  $T < T_{\min}$  is given in Fig. 2 for different samples. Here the quantity  $\Delta\chi' = \chi'(T) - \chi'(T_{\min})$ , corresponding to the deviation of the susceptibility from complete Meissner screening, is plotted as a function of temperature in a semilogarithmic graph. The fitted lines correspond to:

$$\Delta\chi' = A \exp(-T/T^*) \quad (3)$$

Values of  $T^*$  obtained from the slopes of the lines in Fig. 2 are given in Fig. 3. as a function of the quantity  $p(\hbar v_F / 2\pi k_B L)$ . We also give in this graph the

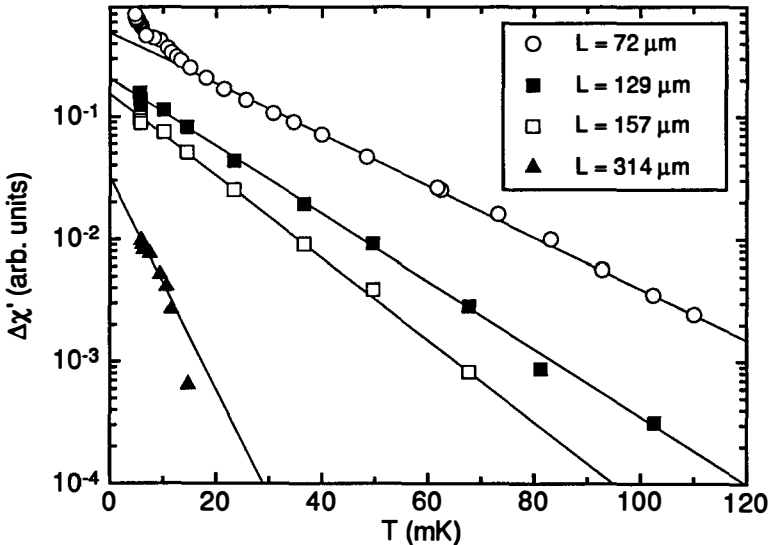


Fig. 2:  $\Delta\chi'(T) = \chi'(T) - \chi'(T_{\min})$  as a function of temperature for four Ag-Nb specimens with different perimeter  $L$ .

temperature  $T_{\min}$  for all the specimens investigated. The numerical constant  $p = (K_N^{-1})_{\text{meas}} / (K_N^{-1})_{\text{theo}}$  is obtained from an independent measurement of breakdown fields  $H_b$  in the temperature range  $T > T_{\min}$  as explained in ref. 2) and 3). From Fig. 3 we can write:

$$T^* = p \frac{\hbar v_F}{2\pi k_B L} = \frac{(K_N^{-1})_{\text{meas}}}{L} T \quad (4)$$

$$\Delta\chi' = A \exp[-L / (K_N^{-1})_{\text{meas}}] \quad (5)$$

Clearly the ratio between the measured induced coherence length  $K_N^{-1}$  and the sample circumference  $L$  characterizes this new form of quantum coherence.

At this moment we do not have an explanation for the origin of the effect observed below  $T_{\min}$ . One scenario for this novel effect could be that for  $T < T_{\min}$ , the induced superconductivity is destroyed in the normal metal on further cooling. On the other hand, for  $T < T_{\min}$ , the condition  $K_N^{-1} > L$  is fulfilled and novel quantum effects on the scale of the perimeter  $L$  can be expected. We have proposed to call this regime, where the induced coherence length  $K_N^{-1}$  is larger than the perimeter  $L$ , mesoscopic<sup>3)</sup>. A second scenario then for the appearance of the reentrance of the

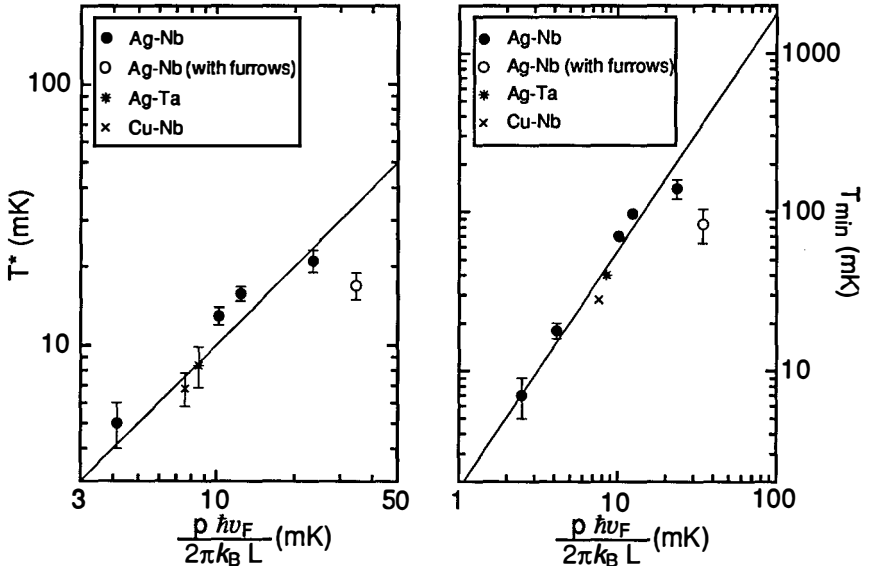


Fig. 3: Characteristic temperature  $T^*$  and reentrance temperature  $T_{\min}$  as a function of  $p(\hbar v_F / 2\pi k_B L)$ . The lines through the points have slopes of 1 and 1.5, respectively. Open symbols correspond to the Ag-Nb sample with furrows.

susceptibility below  $T_{\min}$  could be the building of a paramagnetic persistent current which runs on the external surface of the cylinders and opposes the diamagnetic Meissner current. To test the scenario of a paramagnetic current running on the surface, we have prepared a sample with a different surface respect to the previous ones. A qualitative comparison of the surface structures can be obtained from Fig. 4 where SEM pictures of both types of samples are given. Sample B clearly presents a continuous series of furrows running along the axis of the sample, approximately  $0.5 \mu\text{m}$  apart. An immediate consequence of this corrugated surface is an increase of the effective external perimeter  $L_{\text{eff}}$ . From several SEM pictures we have been able to estimate that the increase in  $L_{\text{eff}}$  respect to the perimeter  $L = 2\pi r$ , assuming a circular section for the cylinder, is roughly of the order of  $\pi/2$ . It is not surprising then to see in Fig. 3 that the points corresponding to the sample with corrugated surface lie to right of the lines that fit very well all the other samples.

It is tempting to compare the results presented here for the proximity induced

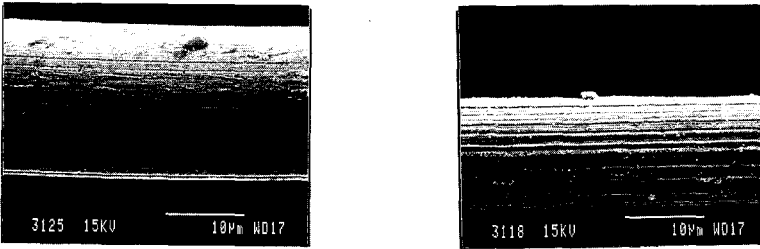


Fig. 4: Lateral surface of two Ag-Nb samples recorded with a scanning electron microscope. Sample A: smooth surface. Sample B: surface with furrows.

superconductors with the predicted behaviour of persistent currents in mesoscopic *normal* metal cylinders. Recently, Cheung, Gefen and Riedel<sup>4)</sup> have analyzed one-channel as well as multichannel systems. For impurity-free multichannel rings they find that the sensitivity of the current to temperature is governed by a characteristic temperature  $T^*$  such that for  $T > T^*$ , the current amplitude is:

$$I \propto I_0 \frac{M}{\sqrt{L/\lambda_F}} \exp\left(-\frac{T}{T^*}\right) \quad (6)$$

with  $I_0 = ev_F/L$  and  $T^*$  proportional to the level spacing of a one-channel ring of the same circumference, rather than the much smaller level spacing of the  $M$ -channel system  $\Delta_M \propto \Delta_1 / M$ . The level spacing for the one-channel system is:

$$\Delta_1 = \frac{2\pi\hbar v_F}{L} \quad (7)$$

and

$$T^* = \frac{\Delta_1}{2\pi^2 k_B} = \frac{\hbar v_F}{\pi k_B L} \quad (8)$$

The number of channels  $M$  is defined as the largest integer  $\leq 2h / \lambda_F$  where  $h$  is the height of the cylinder and  $\lambda_F$  is the Fermi wavelength. Persistent currents in multichannel normal metal systems have not been observed experimentally up to now. The striking similarities of expressions (3) and (4) with expressions (6) and (8) suggest the possibility that, in analogy with persistent currents on mesoscopic normal metal rings, a persistent paramagnetic current is also established in this proximity system, which opposes the Meissner persistent current induced in copper and silver by the proximity effect. In fact, the experimentally determined characteristic temperature  $T^*$ , which gives the energy scale that is relevant in these new phenomena, not only has the same type of size dependence predicted for a persistent current in multichannel normal metal rings, but also agrees quantitatively with the predicted value.

In conclusion, we have found an unexpected manifestation of mesoscopic effects in cylinders of copper or silver in proximity with niobium or tantalum. At a temperature  $T_{\min}$  at which superconductivity has been induced in all the normal metal cylinders by the proximity effect, the diamagnetic response starts decreasing on further cooling. An analysis of the data shows that for all the different specimens, the only parameter characterizing this novel effect is the temperature  $T^*$  which depends solely on the ratio  $K_N^{-1} / L$  between the measured decay length of the induced order parameter in the normal metal and the perimeter of the sample. Undoubtedly we are observing a novel type of quantum coherence which is not present in intrinsic superconductors where the coherence length remains almost constant for  $T \ll T_c$ . Indeed, the fact that the induced coherence length in the normal metal is inversely proportional to the temperature allows the study of quantum coherence at millikelvin temperatures in samples with sizes that are not mesoscopic in the usual sense.

This work was partially supported by the Schweizerischer Nationalfonds zur Förderung der wissenschaftlichen Forschung.

- 
- 1) G. Deutscher and P. G. de Gennes, in *Superconductivity*, R. D. Parks ed., Marcel Dekker, New York (1969), Vol. 2, p. 1005.
  - 2) P. Visani, A. C. Mota, and A. Pollini Phys. Rev. Lett. **65**, 1514-1516 (1990)
  - 3) A. C. Mota, P. Visani, A. Pollini, and K. Aupke, Physica B **197**, 95 (1994)
  - 4) H. F. Cheung, Y. Gefen and E. K. Riedel, IBM J. Res. Develop. **32**, 359 (1988)

## SUPERCONDUCTING PHASE BOUNDARY $T_c(H)$ OF MESOSCOPIC OPEN AND FILLED SQUARES

L. Gielen, V. V. Moshchalkov, C. Strunk, V. Bruyndoncx, R. Jonckheere\*, X. Qiu, C. Van Haesendonck and Y. Bruynseraede. *Laboratorium voor Vaste-Stoffysika en Magnetisme, K. U. Leuven, Celestijnenlaan 200 D, B-3001 Leuven, Belgium.*

\* *Interuniversity Microelectronics Center, Kapeldreef 75, B-3001 Leuven, Belgium.*

### Abstract

The superconducting phase boundary in the presence of a magnetic field,  $T_c(H)$ , has been measured for mesoscopic Al open and filled squares. The critical temperature  $T_c$  of an open square with a circumference comparable to the superconducting coherence length  $\xi(T)$  shows pronounced Little-Parks oscillations as a function of an applied field  $H$ . For a filled square the oscillations are less pronounced and are related to the transitions between superconducting states with different angular momenta. The observed superconducting phase boundary  $T_c(H)$  of the filled square is in good agreement with the theoretical predictions.

### Introduction

The Ginzburg-Landau (GL) theory allows to calculate the spatial variations of the complex superconducting order parameter  $\psi$  in the presence of a magnetic field  $H$ . For cylinders and loops with a circumference comparable to the GL coherence length  $\xi(T)$  and the cross-section area  $S$ , the GL approach predicts that the superconducting transition temperature  $T_c$  oscillates as a function of the applied field  $H$  with the period  $\Delta H = \phi_0/S$  with  $\phi_0$  the superconducting flux quantum. These Little-Parks (LP) oscillations are observed for superconducting cylinders<sup>1,2</sup>, loops<sup>3</sup> and disks<sup>4</sup>). In the case of a filled square, we find that the oscillations of the critical temperature  $T_c$  are related to the transitions between superconducting states with different angular

momenta, analyzed by Saint-James<sup>5</sup>). By comparing the phase boundary  $T_c(H)$  for an open and an filled square made from the same Al film, we show that  $T_c(H)$  is not only material dependent, but also very strongly influenced by the sample topology.

### **Influence of the sample geometry on the phase boundary**

For our study of the phase boundary  $T_c(H)$  of systems with a different topology, we prepared open squares with a side of  $1 \mu\text{m}$  and a linewidth  $w \cong 0.15 \mu\text{m}$  and filled squares with the same side of  $1 \mu\text{m}$ . These Al structures, with thickness  $t \cong 25 \text{ nm}$ , were obtained by thermal evaporation of high purity Al (99,9995 %). The evaporation is performed in a reduced helium atmosphere ( $p \cong 10^{-3} \text{ Torr}$ ) to produce smooth and continuous metallic films.

The normal to superconducting phase boundaries for the open and filled squares, shown in Fig. 1, are obtained by carefully measuring the resistive  $R(T)$  transition in different magnetic fields. It is clear that for the open square  $T_c(H)$  reveals classical Little-Parks oscillations, which are caused by the fluxoid quantization. If the applied flux  $\phi$  is equal to a multiple of the flux quantum  $\phi_0$ , i.e., the flux is quantized in units of  $\phi_0$ , the critical temperature reaches a local maximum. Our experimental data for this geometry, are in good agreement with the theoretical calculations based on the Tinkham model<sup>6</sup>). Furthermore, the phase boundary of the open  $1 \times 1 \mu\text{m}^2$  square shows a quadratic background as function of the applied field  $H$  which is due to the finite width of the structure.

The investigation of the phase boundary for the filled Al square width side  $1 \mu\text{m}$  reveals that the shape of the  $T_c(H)$  phase boundary is very different from the  $T_c(H)$  boundary of the open Al square, as illustrated in Fig. 1. For the filled Al square, the oscillating behavior is still present, but the amplitude is strongly suppressed. Close to the critical temperature, the  $T_c(H)$  phase boundary is a linear function of the applied field. Looking more into detail, the periodicity of the oscillations is no longer equal to a multiple value of  $\phi_0$  and the first period is much larger than the next periods. This behavior can be understood within the framework of the linearized GL theory and will be explained below.

The dashed line in Fig. 1 shows the theoretical phase boundary for bulk Al with  $H_c(T \rightarrow 0) = 100 \text{ G}$ . It is clear that the sample topology defines the structure of the phase boundary for the systems which are all made of the same material under identical conditions.

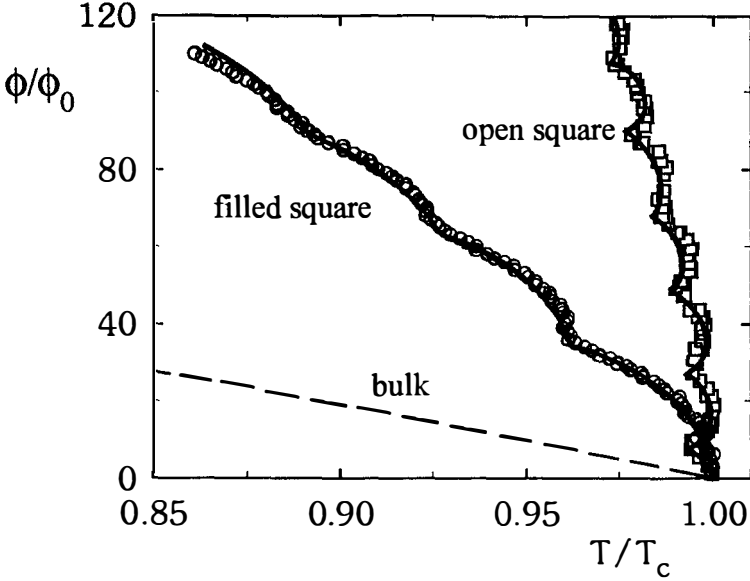


Fig. 1: The measured superconducting phase boundary,  $T_c(H)$ , for the  $1 \times 1 \mu\text{m}^2$  open Al square ( $\square$ ) and for the  $1 \times 1 \mu\text{m}^2$  filled Al square ( $\circ$ ). The dashed line shows the theoretical calculated phase boundary for bulk Al ( $H_C(T \rightarrow 0) = 100$  G). The solid lines correspond to calculations based on Tinkham formula for an open square and a disk<sup>6</sup>).

In order to obtain the phase boundary for a filled square, it is necessary to solve the linearized GL equation:

$$\frac{\hbar^2}{2m} \left( -i\vec{\nabla} - \frac{2\pi\vec{A}}{\phi_0} \right) \psi = -\alpha\psi, \quad (1)$$

with  $\vec{A}$  the vector potential,  $-\alpha = \frac{\hbar^2}{2m\xi^2(0)} \frac{T_c - T}{T_c}$  and taking into account the

boundary condition at the superconducting-insulator interface:

$$\left( -\vec{\nabla} + \frac{2\pi\vec{A}}{\phi_0} \right) \Big|_n \psi = 0. \quad (2)$$

This problem can be considered as the problem of a particle in a box with charge  $2e$  in the presence of a magnetic field. We assume here that the solutions of this problem for a filled square is similar to that for a disk<sup>6</sup>). Given the radial symmetry of the structure, the order parameter  $\psi$  can be written as  $\psi(r, \varphi) = f(r) \cdot \exp(-iL\varphi)$ , where  $L$  is the orbital quantum number. The possible solutions for the eigenvalue  $E \propto -\alpha$ , which correspond to the allowed energy levels for the enclosed electron pairs, are shown in Fig. 2. The envelope of these energy levels will correspond to the experimental phase boundary. For small values of  $\phi/\phi_0$ , the energy of the electron pairs is determined by the state with  $L=0$ . This state corresponds with the first period of the  $T_c(H)$  phase boundary. For higher values of  $\phi/\phi_0$ , the lowest possible energy for the electron pairs is defined by increasing values of the orbital quantum number  $L$ . The phase boundary, which is obtained for the filled Al square (see Fig. 1) is clearly in agreement with the theoretical result shown in Fig. 2, including the difference in periodicity of  $T_c$  as a function of the reduced flux  $\phi/\phi_0$  as well as the suppression of the amplitude.

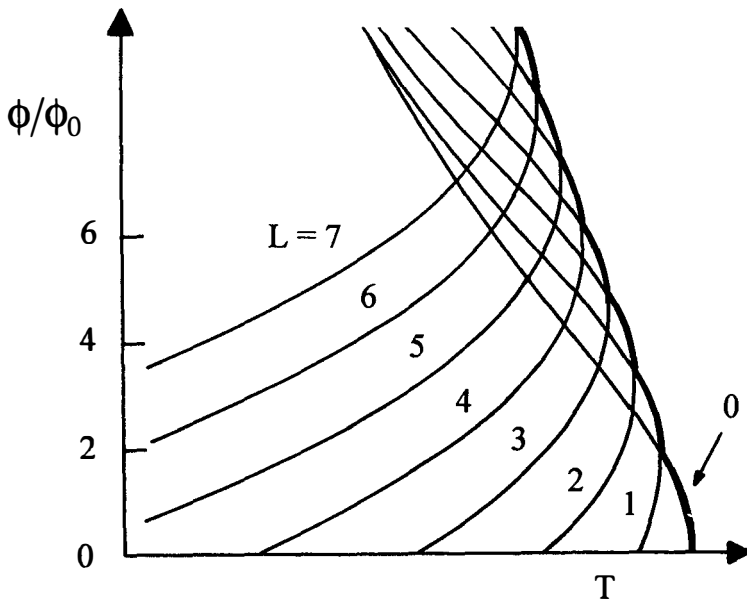


Fig. 2: Solutions of the GL equation (1) with the boundary condition (2) for the angular momenta  $L$  as function of the reduced applied magnetic flux  $\phi_0$ . The tick line gives the oscillating  $T_c(H)$  phase boundary for the filled square (see solid line in Fig. 1).

The macroscopic wave functions  $\Psi_L(r, \varphi)$  for the different orbital quantum numbers  $L$ , are related to the possible energy states, with energy  $E$ . These wavefunctions can be used to find the local density of the electron pairs in the superconducting system. Therefore, we have calculated the dependence for the amplitude of the order parameter  $|\psi|$  for a disk. Fig. 3 shows three-dimensional figures of the amplitude  $|\psi|$  as function of  $|r|$  with  $r$  the radius of the disk. For  $L=0$ , the amplitude reaches a maximum at  $r=0$ , which means that the Cooper pair density is localized around the center of the disk at small fields. By increasing the value  $L$  from 1 to 3, the amplitude  $|\psi|$  is decreasing at  $r=0$  and the maximum is now found at a circle, which moves towards the edge of the disk. Increasing the field results in a growing number of the flux quanta  $L$  and on the average the electron pairs are pushed towards the border of the disk.

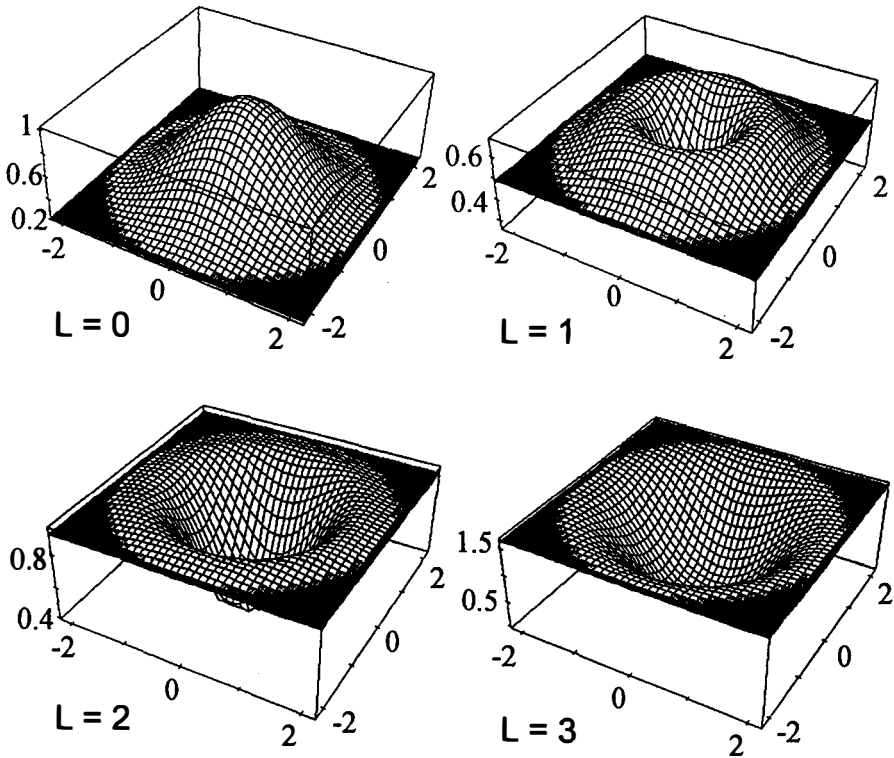


Fig. 3: Three-dimensional representation of the amplitude of the order parameter  $|\psi|$  for different values of the orbital quantum number  $L$ .

In summary, the study of the phase boundary of structures with different topology reveals that it is not only the material which defines the nature of the critical parameters of a mesoscopic superconductor, but the sample geometry must also be taken into account. Experimentally, we find that superconductivity still exists at the boundary of mesoscopic superconducting systems when the applied field is relatively large.

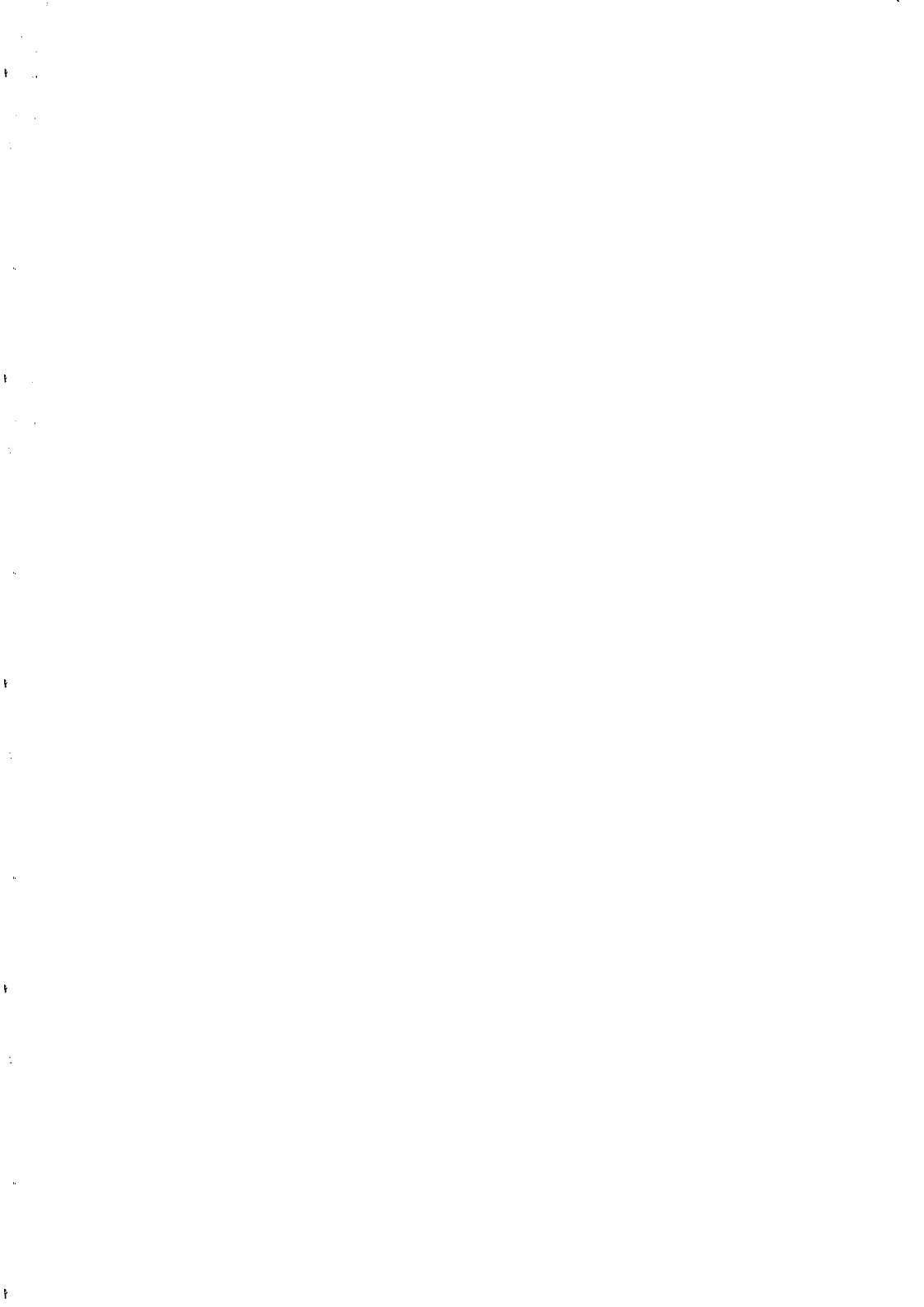
### Acknowledgements

The research was supported by the Belgian Inter-University Attraction Poles (I.U.A.P.) and Concerted Action (G.O.A.) programs. L.G. is a Research Assistant of the Belgian Institute for the Encouragement in Industry and Agriculture (I.W.O.N.L.), C.V.H. is a Senior Research Associate of the Belgian National Fund for Scientific Research (N.F.W.O.).

### References

- 1) W. A. Little and R. D. Parks, Phys. Rev. Lett. **9**, 9 (1962)
- 2) R. P. Groff and R.D. Parks, Phys. Rev. **176**, 567 (1968)
- 3) H. Vloeberghs, V. V. Moshchalkov, M. Dhallé, G. Neuttiens, C. Van Haesendonck, and Y. Bruynseraede, Phys. Rev. Lett. **69**, 1268 (1992)
- 4) B. Pannetier, in "Quantum Coherence in Mesoscopic Systems", 457, Ed. by B. Kramer (Plenum Press, New York, 1991)
- 5) D. Saint-James, Phys. Lett. **15**, 13 (1965)
- 6) M. Tinkham, Phys. Rev. **129**, 2413 (1963)

## ENERGY LEVEL STATISTICS



## QUANTUM CHAOS: ENERGY LEVELS AS FERMIONS

B D Simons, P A Lee and B L Altshuler

Department of Physics, Massachusetts Institute of Technology, 77 Massachusetts Avenue,  
Cambridge, MA 02139

### I. INTRODUCTION

In contrast to classical chaos, it seems impossible to offer a simple yet general definition of quantum chaos. One definition would prescribe systems whose classical dynamics are chaotic. However, a classical description is very often unavailable and attention has focused on finding apparently unique characterizations based on a common behavior of statistical properties.<sup>1,2)</sup> Remarkably, the union of chaos and quantum mechanics leads to an astonishing degree of universality. Our goal will be to extend the existing description to include new characterizations. In doing so we will show some surprising connections to the quantum properties of an *integrable* Hamiltonian.

Universal properties of quantum chaotic systems are characterized by only two time scales. The longest is the Heisenberg time,  $t_H \equiv \hbar/\Delta$  equal to the inverse mean spacing between levels  $\Delta$ . The second,  $t_c \equiv \hbar/E_c$  is less precisely defined and reflects the typical time for all regions of phase space to become connected. In disordered metals it is equal simply to the typical time for an electron to diffuse across the sample, the inverse Thouless energy  $t_c = L^2/D$ , while in ballistic systems such as “quantum billiards” phase space is connected only after scattering several times from an irregular boundary  $t_c \sim L/v$ . At time scales shorter than  $t_c$  chaos is not fully developed and the spectrum reflects quasi-regularities of the system. At longer time scales there is a crossover to “zero-dimensional” behavior in which properties are universal.  $t_c$  therefore plays a role in quantum chaos similar to the Lyapunov exponent in classical chaos.

In recent years the technology of “periodic orbit theory” (POT) has been applied very successfully to describe the transition between the quasi-regular short time scale description and the universal properties that appear at longer times.<sup>3)</sup> In this path integral approach there is

an implicit assumption that only (closed periodic) classical trajectories contribute significantly and the effects of quantum tunneling can be neglected. Numerous experiments have provided strong evidence to justify this semi-classical approximation on short time scales.

However, at scales comparable with  $t_H$ , where quantum tunneling becomes increasingly important, POT appears to break down. At the same time, quantum chaotic systems begin to display a remarkable degree of universality. This coincidence is not accidental but closely related to the effective zero-dimensionality of the system at long times. The description of universality calls for a different approach which treats the quantum mechanics in a rigorous manner. We will show how such a theory reveals a new type of universality which offers fresh insight into quantum chaos.

To introduce our main findings we begin by considering the dispersion of the energy levels of a non-integrable Hamiltonian,  $H(U)$  which depends on an adjustable parameter,  $U$ . One example would be the spectrum of hydrogen in a strong magnetic field.<sup>5)</sup> Beginning with the work of Pechukas<sup>6)</sup> and Yukawa<sup>7)</sup> problems of this kind have attracted great interest<sup>1)</sup> most recently in the study of the level curvature distribution.<sup>8-13)</sup> In Ref. 8 this distribution was argued to become universal after a rescaling of the curvature by the variance of the level gradients. We will argue that on energy scales smaller than  $E_c$  the rescaling of the energy levels and perturbation,<sup>4)</sup>

$$\epsilon_i = E_i/\Delta, \quad \Delta = \langle E_{i+1} - E_i \rangle, \quad (1a)$$

$$u = U\sqrt{C(0)}, \quad C(0) = \langle (\partial E_i/\partial U)^2 \rangle/\Delta^2, \quad (1b)$$

make *all* of the statistical properties of  $\epsilon_i(u)$  universal, dependent only on the symmetry of  $H$ .<sup>14)</sup> The statistical average  $\langle \dots \rangle$  can be performed over a range of energy levels or  $U$ .

A physical interpretation for  $C(0)$  can be found through a universal formula for the rate of energy dissipation in the presence of a time-dependent perturbation,<sup>15,4)</sup>

$$\frac{\partial W}{\partial t} = \frac{\pi\beta\hbar}{2} C(0) \left( \frac{\partial U}{\partial t} \right)^2, \quad (2)$$

where  $\beta$  is defined according to whether  $H$  conserves ( $\beta = 1$ ), or breaks  $T$ -invariance ( $\beta = 2$ ). Systems which conserve  $T$ -invariance but display strong spin-orbit scattering belong to a third ensemble ( $\beta = 4$ ). Following from matrix ensembles, the different symmetry classes are frequently afforded the classification orthogonal, unitary, or symplectic for  $\beta = 1, 2, \text{ or } 4$  respectively. Eq. (3) represents a type of "mesoscopic" fluctuation-dissipation theorem and gives to  $C(0)$  the meaning of a "generalized conductance". Typically  $C(0) \propto t_H/t_c$  which, as we will demonstrate for disordered metals, is analogous to the Thouless formula<sup>16)</sup> with the r.h.s. equal to the dimensionless conductance,  $g$ .<sup>4,17)</sup>

Although it would be desirable to develop these ideas from a microscopic study of quantum Hamiltonians, theoretical progress does not seem possible for studying even average properties on time scales shorter than  $t_H$  where universality is most robust. However, averaging over a

class of different systems which belong to the same statistical ensemble does enable certain properties to be studied analytically. If we accept the “ergodic hypothesis” that ensemble and spectral averaging are equivalent<sup>18)</sup> we can use “disordered” systems to investigate the universality proposed above. In surrendering the generality of POT we will be able to confirm Eq. (1) and derive *exact* results for certain universal correlators.

The effective zero-dimensionality at long time scales suggests a random matrix description in which all states are coupled by some element drawn from a random distribution.<sup>19)</sup> Random matrix theory (RMT) therefore represents a natural starting point for the study of statistical correlations. Indeed since  $t_c \sim N$  where  $N$  denotes the number of eigenvalues, RMT can be regarded as a “fixed point” for universality in quantum chaos.<sup>20)</sup> Since its introduction as a model of complex nuclei more than forty years ago<sup>21)</sup> the Wigner-Dyson statistics of RMT have found considerable success in describing level correlations<sup>2,22)</sup> of a wide variety of non-integrable systems and the universality implied by Eq. (1a) has been firmly established. To interpolate between universal and quasi-regular behavior it is instructive to examine the physical example of disordered metals. In our discussion we will encounter two crucial assumptions related to the time scales  $t_H$  and  $t_c$  which define the regime in which behavior is universal.

In the next section we will develop an approach for studying statistical correlations based on a field theoretic technique in which average properties are expressed in the form of a non-linear  $\sigma$ -model. We will show how zero-dimensionality and universality is manifest and indicate why a random matrix interpretation of spectral correlations is natural.

Remarkably the spectral correlations described in section II coincide with the dynamical properties of an *integrable* one-dimensional many-particle quantum Hamiltonian when the eigenvalues are associated with the coordinates of hard-core particles (fermions) and the perturbation with the Euclidean time.<sup>23)</sup> This striking correspondence can be revealed by a different kind of matrix model. In section III we will discuss this correspondence and its relation to the Brownian motion model of “level dynamics” introduced by Dyson<sup>19)</sup> more than thirty years ago. Finally in section IV we will conclude with a brief discussion of the results presented here and mention some future directions.

## II. SUPERSYMMETRY APPROACH

The goal of this section is to motivate and to some extent justify the ideas discussed in the introduction by examining certain examples of non-integrable or quantum chaotic systems. We begin by examining the behavior of a single electron confined to a weakly disordered metallic ring of size  $L^d$  threaded by an Aharonov-Bohm flux,  $\phi$  (measured in units of the flux quantum,  $hc/e$ ). The corresponding Hamiltonian is given by,

$$H(\phi) = \frac{\hbar^2}{2m} \left( -i\nabla + \frac{2\pi}{L} \phi \mathbf{e}_\phi \right)^2 + V(\mathbf{r}), \quad (3)$$

where  $\mathbf{e}_\phi$  is the unit vector along the azimuthal direction,  $V(\mathbf{r})$  is a Gaussian distributed white-noise impurity potential,  $\langle V(\mathbf{r}) \rangle = 0$ ,  $\langle V(\mathbf{r})V(\mathbf{r}') \rangle = \delta(\mathbf{r} - \mathbf{r}') \hbar/2\pi\nu\tau$ ,  $\nu$  is the average density of states at energy  $E$ , and  $\tau$  is the elastic scattering time. The definition of  $\langle \dots \rangle$  is extended to include the ensemble average. The dimensions of the grain are assumed to be much larger than the elastic mean free path  $l \equiv \nu\tau \ll L$  so that the motion of the electron is diffusive.

Spectral properties of the system can be characterized by density of states (DOS) correlators. We will examine the first non-trivial correlator describing the dimensionless two-point function,

$$k(\Omega, \phi) = \Delta^2 \langle \nu(E + \Omega/2, \bar{\phi} + \phi/2) \nu(E - \Omega/2, \bar{\phi} - \phi/2) \rangle - 1, \quad (4)$$

where  $\nu(E, \phi) = \text{Tr} \delta(E - H(\phi))$ , and  $\Delta = (L^d \nu)^{-1}$  denotes the mean-level spacing. Eq. (4) can be expressed by the product of retarded and advanced Green functions,  $G^{R,A}(E, \phi) = [E - H(\phi) \pm i0]^{-1}$

$$k(\Omega, \phi) = \frac{\Delta^2}{2\pi^2} \Re \langle f(\Omega, \phi) \rangle - \frac{1}{2}, \quad (5a)$$

$$f(\Omega, \phi) = \text{Tr} G^R(E - \Omega/2, \bar{\phi} - \phi/2) \text{Tr} G^A(E + \Omega/2, \bar{\phi} + \phi/2). \quad (5b)$$

To determine an analytical expression for  $k(\Omega, \phi)$  we adopt the supersymmetry approach developed by Efetov to study weakly disordered metals.<sup>24)</sup> Since our aim is not to supplement the many reviews on this method but rather to emphasize certain aspects in the context of quantum chaos we will keep discussion brief and refer to Refs. 24, 25 for a more lengthy pedagogical description. We also draw attention to a recent paper by Altland *et al.*<sup>26)</sup> in which much of the formalism presented here is discussed in detail and whose notation we will adopt.

The starting point is the representation of Green functions as Gaussian integrals over a  $2 \times 2 \times 2$ -component supervector  $\Psi_{\mu d}^T(\mathbf{r}) = (S_{\mu d}(\mathbf{r}), \chi_{\mu d}(\mathbf{r}))$ , where  $S$  and  $\chi$  denote commuting and anticommuting fields respectively,  $\mu$  labels the retarded and advanced components, and  $d$  labels conjugate elements. (The use of supervectors obviates the need for explicit normalizations thereby circumventing possible difficulties associated with the replica approach.<sup>27)</sup>) Following the notation of Ref. 26

$$f(\Omega, \phi) = \int \mathcal{D}\Psi(\mathbf{r}) e^{-L[\Psi]} \left[ \int d\mathbf{r} \Psi^\dagger(\mathbf{r}) P(a, B) \Psi(\mathbf{r}) \int d\mathbf{r}' \Psi^\dagger(\mathbf{r}') P(r, B) \Psi(\mathbf{r}') \right], \quad (6a)$$

$$L[\Psi] = \frac{i}{2} \int d\mathbf{r} \Psi^\dagger(\mathbf{r}) \Lambda^{1/2} \left[ E - \frac{\Omega + i0}{2} \Lambda - \frac{\hbar^2}{2m} (i\nabla + \frac{2\pi}{L} (\bar{\phi} + \frac{\phi}{2}) \Lambda) \mathbf{e}_\phi \tau_3 \right]^2 - V(\mathbf{r}) \right] \Lambda^{1/2} \Psi(\mathbf{r}), \quad (6b)$$

where the matrices  $\tau_3 = (-)^{\delta_{dd'}}$  and  $\Lambda = (-)^{\mu} \delta_{\mu\mu'}$  break time-reversal and the advanced/retarded symmetry respectively. The matrices  $P(a, B)$  and  $P(r, B)$  project onto the advanced and retarded bosonic blocks of  $\Psi$ . We remark that this approach is not restricted to correlators of DOS and can be easily generalized to include properties such as the density response function.<sup>24,28)</sup>

The ensemble average over the disorder potential generates a quartic interaction in the fields  $\Psi(\mathbf{r})$ . To proceed it is crucial to assume that the disorder is weak so that the fields vary

only slowly in comparison to the electron wavelength,  $\lambda = h/mv$ . Within this approximation the interaction can be decoupled by means of a Hubbard-Stratonovitch transformation with the introduction of  $8 \times 8$  supermatrix fields  $Q(\mathbf{r})$  with the symmetry of the dyadic product  $\Lambda^{1/2}\Psi \otimes \Psi^\dagger\Lambda^{1/2}$ . As a result the  $\Psi$  integration becomes Gaussian and can be performed.

Further progress is possible within a saddle-point approximation in which  $Q(\mathbf{r})$  acts as a mean-field self-energy satisfying the equation  $Q(\mathbf{r})^2 = 1$ . The solution is defined by the manifold  $Q = T^{-1}\Lambda T$  where  $T$  denotes unitary matrices which satisfy the symmetry requirements. Allowing for small spatial fluctuations about the saddle-point, and expanding to leading order in  $l/L$  and  $\Omega\tau$ , we obtain the result,

$$\langle f(\Omega, \phi) \rangle = (\pi\nu)^2 \left\{ 1 - \frac{1}{4} \int \mathcal{D}Q(\mathbf{r}) e^{-F[Q]} \times \int d\mathbf{r} \text{STr} [P(a, B)(Q(\mathbf{r}) - \Lambda)] \int d\mathbf{r}' \text{STr} [P(\tau, B)(Q(\mathbf{r}') - \Lambda)] \right\}, \quad (7a)$$

$$F[Q] = \frac{\pi\nu}{2} \int d\mathbf{r} \text{STr} \left[ \hbar D (\nabla Q - i \frac{2\pi}{L} \mathbf{e}_\phi [\tau_3 (\bar{\phi} + \phi\Lambda/2), Q])^2 + 2i (\Omega + i0)\Lambda Q(\mathbf{r}) \right], \quad (7b)$$

where  $D = v^2\tau/d$  is the diffusion constant, the supertrace  $\text{STr}$  is defined in Ref. 24, and the functional integral is constrained to the saddle-point manifold. The expression takes the form of a functional non-linear  $\sigma$ -model, with Goldstone modes related to the breaking of supersymmetry, from which the well known effects of weak localization can be derived. For large values of flux  $\bar{\phi}$  the (Cooperonic) degrees of freedom of  $Q$  which do not commute with  $\tau_3$  acquire a mass and become frozen out. To focus on a fixed (unitary) symmetry class in which  $T$ -reversal symmetry is fully broken we will impose the additional constraint that  $[\tau_3, Q(\mathbf{r})] = 0$ .

To proceed without resort to perturbation theory we restrict attention to  $\Omega \ll \hbar D/L^2 = E_c$ , and  $\phi \ll 1$  when the contribution from the higher spatial modes becomes exponentially small in comparison to the "zero-mode". Up to a trivial gauge transformation,<sup>4,26)</sup> this is given by  $Q$  independent of position. Thus, on time scales  $\hbar/\Omega \gg t_c = \hbar/E_c$  the system behaves as though it were *zero-dimensional*. In this limit we obtain the definite integral expression,

$$\langle f(\Omega, \phi) \rangle = \left( \frac{\pi}{\Delta} \right)^2 \left[ 1 - \frac{1}{4} \int d[Q] e^{-F[Q]} \text{STr} [P(a, B)(Q - \Lambda)] \text{STr} [P(\tau, B)(Q - \Lambda)] \right], \quad (8a)$$

$$F[Q] = i \frac{\pi(\Omega + i0)}{4\Delta} \text{STr} (\Lambda Q) - \frac{\pi^3}{8} g \phi^2 \text{STr} [\Lambda, Q]^2, \quad (8b)$$

where  $g = E_c/\Delta$  denotes the dimensionless conductance. Although the integral can be performed the parametrization of the coset space requires some technology which it would be inappropriate to describe here. Instead we refer to Refs. 24, 26 for a detailed discussion.

A knowledge of  $k(\Omega, \phi)$  allows the distribution of level gradients to be determined from the formula<sup>29)</sup>  $\langle \delta(c - \partial E_i/\partial \phi) \rangle = \lim_{\phi \rightarrow 0} \phi k(c, \phi)$  from which we find the distribution of  $c$  to be Gaussian with a variance  $C(0) = 4\pi g$ . Applying the rescaling of Eq. (1) we obtain the dimensionless integral expression,

$$k(\omega, u) = \Re \frac{1}{2} \int_{-1}^{\infty} d\lambda_1 \int_{-1}^1 d\lambda \exp \left[ -\frac{\pi^2 u^2}{2} (\lambda_1^2 - \lambda^2) + i\pi(\omega + i0)(\lambda_1 - \lambda) \right]. \quad (9)$$

With this derivation we have invoked only the semi-classical assumption that  $\lambda \ll l$ . We remark that, in contrast, diagrammatic perturbation theory is an expansion in the parameter  $\alpha_d \equiv (1/g)^{d/2}(1/\omega)^{1-d/2}$ . In the zero-dimensional case this leads to as unphysical infrared divergences for  $\hbar/\Omega > t_H$  at all orders in perturbation theory.<sup>30,31)</sup>

It is possible to verify that different perturbations with the same symmetry, such as magnetic field, generate the same  $\sigma$ -model but with different prefactors in the free energy.<sup>4)</sup> The effect is merely to change the value of  $C(0)$  and leave the rescaled expression for  $k(\omega, u)$  unaffected and therefore *universal*. Corresponding correlation functions can be determined for orthogonal and symplectic symmetry by examining perturbations which conserve  $T$ -invariance and introducing spin-orbit scattering. Instead of reviewing those results which can be found in Refs. 4 and 23 we turn to a different class of non-integrable Hamiltonians — random matrix ensembles.

An analogous approach can be used to derive the density correlator  $k(\Omega, U)$  for,

$$H = \Phi + U\Phi_c, \quad (10)$$

where  $\Phi$  is a random hermitian matrix drawn from some (say Gaussian) ensemble, and  $\Phi_c$  is some fixed (traceless) matrix chosen from the same ensemble. With zero-dimensional super-vectors, we are lead to the saddle-point constraint  $Q^2 = 1$  ( $[\tau_3, Q] = 0$  for  $\Phi$  unitary,  $[\vec{e}_i, Q] = 0$  for  $\Phi$  symplectic) from which we arrive at the  $\sigma$ -model of Eq. (8) with,<sup>32)</sup>

$$F[Q] = i \frac{\pi(\Omega + i0)}{4\Delta} \text{STr}(\Lambda Q) - \frac{\pi^2 U^2}{8\Delta^2 N^2} \text{Tr}[\Phi_c^2] \text{STr}[\Lambda, Q]^2. \quad (11)$$

Here we have assumed that  $\Omega/\Delta$  and  $U(\text{Tr}[\Phi_c^2])^{1/2}/N\Delta \sim O(N^0)$ . It is straightforward to show that for all three Dyson ensembles the distribution of level gradients is Gaussian with  $C(0) = 2 \text{Tr}[\Phi_c^2]/\beta\Delta^2 N^2$ . Definite integration over the saddle-point manifold yields,

$$k(\omega, u) = \Re \int_{-1}^{\infty} d\lambda_1 \int_{-1}^{\infty} d\lambda_2 \int_{-1}^1 d\lambda \frac{(1-\lambda^2)(\lambda - \lambda_1 \lambda_2)^2}{(2\lambda\lambda_1\lambda_2 - \lambda_1^2 - \lambda_2^2 - \lambda^2 + 1)^2} \times \exp\left[-\frac{\pi^2 u^2}{4}(2\lambda_1^2\lambda_2^2 - \lambda_1^2 - \lambda_2^2 - \lambda^2 + 1) + i\pi(\omega + i0)(\lambda_1\lambda_2 - \lambda)\right], \quad (12)$$

for orthogonal ( $\beta = 1$ ) symmetry, Eq. (9) for unitary ( $\beta = 2$ ) symmetry, and

$$k(\omega, u) = \Re \int_{-1}^1 d\lambda_1 \int_0^1 d\lambda_2 \int_{-1}^{\infty} d\lambda \frac{(\lambda^2 - 1)(\lambda - \lambda_1 \lambda_2)^2}{(2\lambda\lambda_1\lambda_2 - \lambda_1^2 - \lambda_2^2 - \lambda^2 + 1)^2} \times \exp\left[2\pi^2 u^2(2\lambda_1^2\lambda_2^2 - \lambda_1^2 - \lambda_2^2 - \lambda^2 + 1) - i2\pi(\omega + i0)(\lambda_1\lambda_2 - \lambda)\right], \quad (13)$$

for symplectic ( $\beta = 4$ ) symmetry. Setting  $u = 0$  we obtain the results previously obtained for random matrix ensembles<sup>22)</sup> and verified by Efetov<sup>24)</sup> for disordered metallic grains.

Although it is possible to generalize the supersymmetry approach to find an expression for arbitrary moments of density through a generating function expressed in terms of the non-linear  $\sigma$ -model, it does not seem possible to find a general parametrization of the saddle-point manifold. However, the rescaling of Eq. (1) can be applied directly to the generating function

showing *all* higher-point functions to be universal. This suggests that parametric correlations functions provide a new characterization of quantum chaos applying with the same generality as Wigner-Dyson correlations of RMT.

To conclude this section we will apply these results to the spectra of a strongly interacting system of spinless fermions moving on a one-dimensional  $N$ -site ring,

$$H = - \sum_{\mathbf{n}} \left[ e^{i2\pi\phi} c_{\mathbf{n}}^{\dagger} c_{\mathbf{n}+1} + \text{h.c.} \right] + \sum_{\mathbf{n}, \mathbf{m}} V_{\mathbf{m}} n_{\mathbf{n}} n_{\mathbf{n}+\mathbf{m}}. \quad (14)$$

Aharonov-Bohm flux changes the phase of the wavefunction by  $N\phi$  as particles circulate around the ring. Even without disorder, by accounting for certain discrete symmetries (see Ref. 33), a potential  $V_{\mathbf{m}}$  which extends over more than one lattice site makes  $H$  non-integrable. Invariance under  $T$ -reversal and inversion implies “anti-unitary” symmetry<sup>34</sup>) and level correlations are characteristic of the orthogonal ensemble.

With  $\phi$  acting as the adjustable parameter, Fig. 1 shows measurements of the correlator

$$\begin{aligned} \bar{c}(\omega, u) &\equiv \frac{\sum_{ij} \langle \dot{\epsilon}_i(\bar{u} + u) \dot{\epsilon}_j(\bar{u}) \delta(\epsilon_i(\bar{u} + u) - \epsilon_j(\bar{u}) - \omega) \rangle}{\sum_{ij} \langle \delta(\epsilon_i(\bar{u} + u) - \epsilon_j(\bar{u}) - \omega) \rangle}, \\ &= - \frac{1}{1 + k(\omega, u)} \lim_{s \rightarrow \infty} \int_{\epsilon - \omega}^{\epsilon - \omega + s} d\epsilon_1 \int_{\epsilon}^{\epsilon + s} d\epsilon_2 \frac{1}{2} \frac{\partial^2}{\partial u^2} k(\epsilon_1 - \epsilon_2, u). \end{aligned} \quad (15)$$

which demonstrate a close agreement with theory over a wide range of  $u$ . This, as well as results from simulations of Anderson models, quantum billiards,<sup>4)</sup> and hydrogen in a magnetic field,<sup>12,35)</sup> provide compelling evidence for this new type of universality.

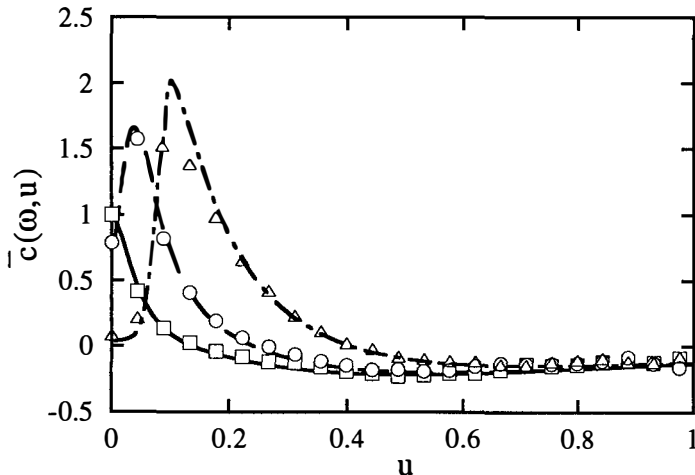


Fig. 1 Measurements of  $\bar{c}(\omega, u)$  together with theory (curves) for  $\omega = 0$  ( $\square$ /continuous),  $\omega = 0.1$  ( $\circ$ /dashed), and  $\omega = 0.25$  ( $\Delta$ /dash-dotted) for flux. A small regularization is included to control the numerics.

### III. CONTINUOUS MATRIX MODEL AND INTERACTING FERMIONS

The manifold of energy levels into which spectra separate have a form reminiscent of particle world lines with the eigenvalues playing the role of coordinates and the perturbation parameter acting as "time". Remarkably an interpretation of this kind is found to be exact. In this section we will demonstrate that correlation functions derived in section II apply equally to the many-particle Hamiltonian introduced by Sutherland,<sup>36)</sup>

$$H_S = - \sum_i \frac{\partial^2}{\partial \lambda_i^2} + \beta \left( \frac{\beta}{2} - 1 \right) \sum_{i < j} \frac{(\pi/N)^2}{\sin^2((\lambda_i - \lambda_j)\pi/N)}. \quad (16)$$

To establish this connection we begin with a matrix model more commonly associated with string theory.<sup>37)</sup> The partition function  $\mathcal{Z} = \int \mathcal{D}\Phi(\tau) \exp\{-S[\Phi(\tau)]\}$  with the action

$$S[\Phi(\tau)] = \int_{-\infty}^{\infty} d\tau \operatorname{Tr} \left[ \frac{1}{4} \left( \frac{\partial \Phi(\tau)}{\partial \tau} \right)^2 + V(\Phi) \right], \quad (17)$$

describes the time evolution of  $N \times N$  matrices in a potential  $V(\Phi)$ . The symmetry of  $\Phi$  is denoted by the Dyson index  $\beta$ , and the potential is for the present left unspecified. Interpreting the matrix model as a path integral it describes the quantum mechanics of the Hamiltonian  $H = -\operatorname{Tr} (\partial/\partial\Phi)^2 + \operatorname{Tr} V(\Phi)$ . As  $N \rightarrow \infty$  the "angular" degrees of freedom of the matrices which diagonalize  $\Phi$  give an exponentially small contribution leaving only the "singlet" component of the Laplace operator.<sup>38)</sup> The resulting Schrödinger equation for the wavefunction,  $P(\{\lambda_j\}, \tau)$  describes a one-dimensional system of interacting eigenvalues or "particles",

$$\frac{\partial}{\partial \tau} P(\{\lambda_j\}, \tau) = \sum_i^N \left[ \frac{1}{J} \frac{\partial}{\partial \lambda_i} J \frac{\partial}{\partial \lambda_i} - V(\lambda_i) \right] P(\{\lambda_j\}, \tau), \quad (18)$$

where  $J = \prod_{i < j} |\lambda_i - \lambda_j|^\beta$  denotes the metric of the group transformation for Dyson ensembles. After a similarity transformation,  $\psi(\{\lambda_j\}, \tau) = J^{1/2} P(\{\lambda_j\}, \tau)$  we obtain  $\partial\psi(\{\lambda_j\}, \tau)/\partial\tau = -H_C \psi(\{\lambda_j\}, \tau)$ , where

$$H_C = - \sum_i \frac{\partial^2}{\partial \lambda_i^2} + \beta \left( \frac{\beta}{2} - 1 \right) \sum_{i < j} \frac{1}{(\lambda_i - \lambda_j)^2} + \sum_i V(\lambda_i). \quad (19)$$

$H_C$  describes the motion of particles with an inverse square pairwise interaction in the presence of a background potential  $V(\lambda_i)$ . Although the *hard-core* nature of the particles suggest fermions, a Jordan-Wigner transformation can be used to assign arbitrary statistics.

For a Gaussian potential,  $V(\lambda_i) = \omega_0^2 \lambda_i^2$  Calogero has shown that the model is separable, and the spectrum integrable.<sup>39)</sup> The ground state wavefunction of  $H_C$ ,

$$|0\rangle \propto \prod_{i < j} |\lambda_i - \lambda_j|^{\beta/2} \exp \left[ - \frac{\omega_0}{2} \sum_i \lambda_i^2 \right], \quad (20)$$

generates a probability distribution which coincides with that of Gaussian random matrix ensembles. The mean particle density corresponds to Wigner's semi-circular density of states distribution,<sup>22)</sup> and the mean interparticle spacing at the origin,  $\Delta = (\pi/2)\sqrt{\beta/N\omega_0}$ .

Although the Hamiltonian depends explicitly on the form of  $V(\lambda_i)$ , as  $N \rightarrow \infty$  correlation functions become universal on a scale comparable to  $\Delta$ . Equivalently, to order  $1/N$ , removing the confining potential and constraining the particles to move on a ring leaves the correlation functions unchanged. The resulting distribution corresponds to Dyson's circular ensemble.<sup>19)</sup> More generally the potential smoothly regulates the average density with particles filling the potential energy surface up to some Fermi energy. To order  $1/N$  the local value of  $\Delta$  is fixed and correlation functions again coincide with those of the circular ensemble.

As  $N \rightarrow \infty$  we thus expect the correlation functions of  $H_C$  to coincide with  $H_S$  when  $\omega_0$  is chosen to set  $\Delta = 1$ . This establishes a precise connection between the continuous matrix model and  $H_S$ . Time-dependent correlation functions of the Sutherland Hamiltonian can therefore be represented by the path integral,

$$\langle 0 | \cdots | 0 \rangle \equiv \mathcal{Z}^{-1} \int \mathcal{D}\Phi(\tau) \cdots e^{-S[\Phi(\tau)]}. \quad (21)$$

The correspondence of ground state correlations of  $H_S$  with level statistics of Dyson ensembles is immediately apparent from the structure of the wavefunction alone. The equivalence of dynamical correlations which depend on the excited states of  $H_S$  is not yet assured. To establish this connection we again make use of the supersymmetry approach of section II to determine the two-point particle density correlator,

$$k(\lambda, \tau) = \sum_{ij} \langle 0 | \delta(\bar{\lambda} + \lambda/2 - \lambda_i(\bar{\tau} + \tau/2)) \delta(\bar{\lambda} - \lambda/2 - \lambda_j(\bar{\tau} - \tau/2)) | 0 \rangle - 1. \quad (22)$$

If we assume that  $\lambda_\alpha$  and  $|\tau_\alpha - \tau_\beta| \sim \mathcal{O}(N^0)$ , we can obtain an expression for  $k(\lambda, \tau)$  which is exact to leading order in  $1/N$  (see Ref. 32 for a detailed discussion). The result is expressed in the form of the zero-dimensional  $\sigma$ -model of Eq. (8) with

$$F[Q] = i \frac{\pi(\lambda + i0)}{4} \text{STr}(\Lambda Q) + \frac{\pi^2 \beta}{8} |\tau| \text{STr}[\Lambda, Q]^2. \quad (23)$$

As  $N \rightarrow \infty$ , when the quantum Hamiltonian converges to  $H_S$ , Eq. (23) generates the *exact* time-dependent correlator of the Sutherland model if we assign

$$\omega = \lambda, \quad u^2 = 2|\tau|. \quad (24)$$

Although not immediately clear from the non-linear relationship of  $u$  and  $\tau$ , we remark that a correspondence can be found for higher-point functions and we refer to Ref. 32 for a discussion.

For unitary ensembles the coupling constant vanishes and  $H_S$  describes non-interacting fermions. The density correlator is determined by a single particle-hole excitation and it is simple to derive Eq. (9) directly.<sup>23)</sup> Orthogonal and symplectic ensembles generate strongly attractive and repulsive interacting models respectively, and the  $\sigma$ -model approach seems to be the only way of determining  $k(\lambda, \tau)$ . However, despite the apparent complexity of Eqs. (12,13) the results indicate a remarkably simple structure which can be interpreted as the separation of a particle (or hole) into a quasi-particle pair.<sup>40,41)</sup>

Thus we have shown that the problem of level statistics in quantum chaotic systems and the ground state properties of  $H_S$  are related through the  $\sigma$ -model. We remark that the Schrödinger equation obtained in Eq. (18) is also interpreted as a Fokker-Planck equation. Indeed, as first recognized by Sutherland<sup>36)</sup> it is in fact equivalent to Dyson's Brownian motion model<sup>19)</sup> of level correlations in random matrix ensembles. The results above give physical meaning to the "fictitious" dynamics of the particles showing the friction coefficient to be related directly to the generalized conductance  $C(0)$ .

#### IV. DISCUSSION

We have focused on the universal properties of quantum chaotic systems. For time scales longer than  $t_c$  spectral correlations of disordered metals and random matrix ensembles were shown to depend on only two parameters,  $\Delta$  and  $C(0)$ . The theory central to our discussion has involved a zero-dimensional non-linear  $\sigma$ -model which we believe applies to chaotic systems with the same generality as Wigner-Dyson statistics.

We have discussed a surprising connection of spectral correlations of chaotic systems and the dynamical properties of an integrable one-dimensional Hamiltonian. This correspondence, which was resolved by a matrix field theory, has provided new results for the physics of strongly interacting systems and has had important ramifications in the properties of quantum spin chains.<sup>41)</sup> Moreover, it has provided a natural interpretation of the fictitious particle dynamics proposed by Dyson,<sup>19)</sup> and suggested a new way of studying spectral correlations, which has already found application (see for example Refs. 42, 43). A summary of different connections made by the  $\sigma$ -model is shown in Fig. 2.

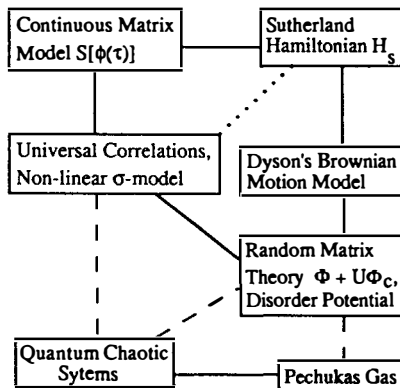


Fig. 2 A schematic diagram showing how the  $\sigma$ -model draws together different branches of physics. The dotted line is established only in limiting cases, and the dashed lines require a statistical hypothesis which has been checked numerically.

To complete our discussion we mention briefly an alternative approach to level dynamics. Pechukas has expressed<sup>6)</sup> the dispersion of the energy levels of a Hamiltonian in response to an external perturbation as a set of first order differential equations, later shown to be integrable.<sup>44)</sup> To make the equilibrium statistical mechanics of the “Pechukas gas” equivalent to RMT, Yukawa<sup>7)</sup> proposed a certain statistical hypothesis (a comprehensive review can be found in Ref. 1, see also Ref. 45 for a recent discussion). In particular a similar approach allowed Gaspard et al.<sup>8)</sup> to obtain the large value tail of the level curvature distribution,  $P(k)$ . Their findings suggested universality of  $P(k)$  after a certain rescaling of the curvature. We remark that this rescaling can be viewed as one application of Eq. (1).

It is instructive to reinterpret the connections in Fig. 2. terms of the appropriate perturbation theory at large  $(\omega, u) \leftrightarrow (\lambda, \tau)$ . For RMT and weakly disordered metals the Cooperon and diffusion modes of diagrammatic perturbation theory generate the leading order contributions. The behavior in this regime is reproduced by the hydrodynamic limit of the Brownian motion model,<sup>46)</sup> and the Sutherland (or Luttinger Liquid) Hamiltonian.<sup>23)</sup> We remark that perturbation theory applies only for time scales shorter than  $t_H$ . More seriously, for symplectic ensembles, the leading contributions derive from a *non-perturbative*  $2k_f$  charge density wave which gives rise to long-range oscillatory correlations. Qualitatively, the leading order of perturbation theory can be viewed as the inclusion of all periodic trajectories in phase space, but with the exclusion of tunneling between trajectories. This same semi-classical interpretation we believe provides the basis of POT and the Gutzwiller trace formula.<sup>3)</sup>

Although we have focused on spectral correlations, universality has been shown to encompass properties of wavefunctions. Complimentary calculations have provided characterizations based on local density and conductance distributions,<sup>47)</sup> time-dependent correlations (“echo”) in spreading wavefunctions,<sup>48)</sup> and the statistics of response functions and oscillator strengths.<sup>28)</sup> (Curiously, the response function can be interpreted as the conductivity of the Sutherland model.) These investigations emphasize the generality of the rescaling of Eq. (1) and the power of the supersymmetry approach.

To conclude we will focus on some new directions which have yet to be fully explored. In section II, we assumed that the average flux,  $\bar{\phi}$  was sufficiently strong that the Cooperonic modes were frozen out. Very often the contribution from these modes can not be completely neglected.<sup>49)</sup> It is therefore natural to ask whether rescaling can be defined for the “crossover” regime. Universal results which involve a third parameter,  $\bar{u}$  and interpolate between unitary — orthogonal, and unitary — symplectic ensembles have been derived.<sup>50,26,51)</sup> For the one-dimensional model these findings can be interpreted as the dynamics of free ( $\beta = 2$ ) particles which satisfy the initial boundary condition  $\psi(\bar{\tau} = 0) \equiv |0\rangle_{\beta=1}$  or  $|0\rangle_{\beta=4}$  respectively.<sup>52)</sup>

The continuous matrix model proposed in section III provides a powerful tool for studying symmetries beyond the usual Dyson ensembles. In particular it is possible to extend consideration to ten symmetric spaces.<sup>53)</sup> Each class is characterized by a different one-dimensional

Hamiltonian. Once again it is possible to derive a  $\sigma$ -model and demonstrate the correspondence of RMT and the generalization of the Sutherland Hamiltonian. However, parametrization of the  $Q$  matrix for the wider symmetry class requires the development of new technology which remains the subject of continuing investigation.

Other than the usual Dyson ensembles, transmission matrices have received most attention because of their connection to the conductance properties of long quasi one-dimensional metallic wires. The Laplace operator of the group of transmission matrices<sup>54)</sup> generates the Dorokhov-Mello-Pereyra-Kumar equation,<sup>55)</sup>

$$\frac{\partial}{\partial \tau} P(\{\lambda_j\}, \tau) = \sum_i^N \frac{\partial}{\partial \lambda_i} \lambda_i (1 + \lambda_i)^J \frac{\partial}{\partial \lambda_i} \frac{1}{J} P(\{\lambda_j\}, \tau), \quad (25)$$

describing the statistics of transmission eigenvalues where  $\tau$  denotes the reduced length of the wire. Recently Beenakker and Rejzai have made considerable progress by obtaining the complete analytical solution of Eq. (25) in the unitary (non-interacting) case.<sup>42)</sup>

To conclude we have shown that a matrix field theory provides a precise correspondence between the universal non-linear  $\sigma$ -model description of spectral correlations in non-integrable systems and an integrable one-dimensional quantum Hamiltonian. These results establish a precise connection between interacting quantum systems, matrix models and quantum chaos.

We are grateful to E. Akkermans, A. Andreev, M. V. Berry, J. T. Chalker, M. Courtney, K. B. Efetov, M. Faas, A. Hashimoto, D. Kleppner, I. V. Lerner, L. Levitov, A. Macêdo, E. R. Mucciolo, A. M. Polyakov, V. N. Prigodin, B. S. Shastry, B. Sutherland, A. Szafer, and N. Taniguchi for valuable discussions. The work was supported through NSF Grant Nos. DMR 92-16007 and DMR 92-04480.

## REFERENCES

- <sup>1</sup> F. Haake, *Quantum Signatures of Chaos*, Springer, Berlin, 1991.
- <sup>2</sup> M. V. Berry, Proc. R. Soc. Lond. A **413**, 183 (1987); O. Bohigas, in *Chaos and Quantum Physics* ed. by M.-J. Giannoni, A. Voros, and Z. Zinn-Justin (North-Holland, 1991).
- <sup>3</sup> For a review see M. C. Gutzwiller, *Chaos in Classical and Quantum Mechanics* (Springer, New York, 1990)
- <sup>4</sup> B. D. Simons, A. Szafer, and B. L. Altshuler, JETP Lett. **57**, 276 (1993); B. D. Simons and B. L. Altshuler, Phys. Rev. Lett. **70**, 4063 (1993); Phys. Rev. B **48**, 5422 (1993).
- <sup>5</sup> J. Goldberg, U. Smilansky, M. V. Berry, W. Schweizer, G. Wunner, and G. Zeller, Nonlinearity **4**, 1 (1991).
- <sup>6</sup> P. Pechukas, Phys. Rev. Lett. **51**, 943 (1983)
- <sup>7</sup> T. Yukawa, Phys. Rev. Lett. **54**, 1883 (1985); Phys. Lett. **116A**, 227 (1986).
- <sup>8</sup> P. Gaspard, S. A. Rice, and K. Nakamura, Phys. Rev. Lett. **63**, 930 (1989); P. Gaspard, S. A. Rice, H. J. Mikeska, and K. Nakamura, Phys. Rev. A **42**, 4015 (1990).
- <sup>9</sup> T. Takami and H. Hasegawa, Phys. Rev. Lett. **68**, 419 (1992).
- <sup>10</sup> D. Saher, F. Haake, and P. Gaspard, Phys. Rev. A **44**, 7841 (1991).
- <sup>11</sup> E. Austin and M. Wilkinson, Nonlinearity **5**, 1137 (1992)
- <sup>12</sup> J. Zakrzewski and D. Delande, Phys. Rev. E **47**, 1650 (1993).
- <sup>13</sup> F. Von Oppen, unpublished
- <sup>14</sup> Strictly the average slope of the levels,  $(\partial E_i(U)/\partial U) = 0$  is required to vanish but this does not have to be crucial.
- <sup>15</sup> M. Wilkinson, J. Phys. A **21**, 4021 (1988); Phys. Rev. A **41**, 4645 (1990); M. Wilkinson and E. J. Austin, Phys. Rev. A **46**, 64 (1992).
- <sup>16</sup> J. T. Edwards and D. J. Thouless, J. Phys. C **5**, 807 (1972); D. J. Thouless, Phys. Rep. **13**, 93 (1974).
- <sup>17</sup> E. Akkermans and G. Montambaux, Phys. Rev. Lett. **68**, 642 (1992).
- <sup>18</sup> A. Pandey, Ann. Phys. **119**, 170 (1979).
- <sup>19</sup> F. J. Dyson, J. Math. Phys. **3**, 140, 157, 166, 1191 (1962)
- <sup>20</sup> E. Brezin and A. Zee, Nucl. Phys. **B402** [FS], 613 (1993).
- <sup>21</sup> E. P. Wigner, Ann. Math. **53**, 36 (1953); C. E. Porter, *Statistical Theory of Spectra: Fluctuations*, (Academic Press, NY) 1965
- <sup>22</sup> For a review see M. L. Mehta, *Random Matrices* (Academic Press, New York, 1991).
- <sup>23</sup> B. D. Simons, P. A. Lee, and B. L. Altshuler, Phys. Rev. Lett. **70**, 4122 (1993); Phys. Rev. B **48**, 11450 (1993).
- <sup>24</sup> K. B. Efetov, Adv. in Phys. **32**, 53 (1983).
- <sup>25</sup> J. J. M. Verbaarschot, H. A. Weidenmüller, and M. R. Zirnbauer, Phys. Rep. **129**, 367 (1985).
- <sup>26</sup> A. Altland, S. Iida and K. B. Efetov, J. Phys. A **26**, 3545 (1993).
- <sup>27</sup> J. J. M. Verbaarschot and M. R. Zirnbauer, J. Phys. A **17**, 1093 (1985).
- <sup>28</sup> N. Taniguchi and B. L. Altshuler, Phys. Rev. Lett. **71**, 4031 (1993); "Statistics of Oscillator Strengths in Chaotic Systems", Preprint.
- <sup>29</sup> V. E. Kravtsov and M. R. Zirnbauer, Phys. Rev. B **46**, 4332 (1992).
- <sup>30</sup> B. L. Altshuler, and B. I. Shklovskii, Zh. Eksp. Teor. Fiz. **91**, 220 (1986) [Sov. Phys. JETP **64**, 127 (1986)].
- <sup>31</sup> A. Szafer, and B. L. Altshuler, Phys. Rev. Lett. **70**, 587 (1993).

- <sup>32</sup> B. D. Simons, P. A. Lee and B. L. Altshuler, Nucl. Phys. **B409**, 487 (1993); Phys. Rev. Lett. **72**, 64 (1994).
- <sup>33</sup> M. Faas, B. D. Simons, X. Zotos, and B. L. Altshuler, Phys. Rev. B **48**, 5439 (1993).
- <sup>34</sup> M. Robnik and M. V. Berry, J. Phys. A **19**, 669 (1986).
- <sup>35</sup> B. D. Simons, A. Hashimoto, M. Courtney, D. Kleppner, and B. L. Altshuler, Phys. Rev. Lett. **71**, 2899 (1993).
- <sup>36</sup> B. Sutherland, J. Math. Phys. **12**, 246 (1971); **12**, 251 (1971); Phys. Rev. A **4**, 2019 (1971); **5**, 1372 (1972).
- <sup>37</sup> For a review see P. Ginsparg and G. Moore, "Lectures on 2D Gravity and 2D String Theory", Lectures given at TASI summer school, Boulder, Colorado (1992).
- <sup>38</sup> E. Brezin, C. Itzykson, G. Parisi, and J. Zuber, Comm. Math. Phys. **59**, 35 (1978).
- <sup>39</sup> F. Calogero, J. Math. Phys. **10** 2191, 2197 (1969).
- <sup>40</sup> E. R. Mucciolo, B. S. Shastry, B. D. Simons, and B. L. Altshuler, "Exact Dynamical Correlations of the  $1/r^2$  Model", to appear in Phys. Rev. B
- <sup>41</sup> F. D. M. Haldane and M. R. Zirnbauer, Phys. Rev. Lett. **71**, 4055 (1993)
- <sup>42</sup> C. W. J. Beenakker and B. Rejaei, Phys. Rev. Lett. **71**, 3689 (1993)
- <sup>43</sup> A. M. S. Macêdo, "Universal Parametric Correlations in the Transmission Eigenvalue Spectra of Disordered Conductors", Preprint; "Universal Parametric Correlations at the Soft Edge of the Spectrum of Random Matrix Ensembles", Preprint
- <sup>44</sup> K. Nakamura and M. Lakshamanan, Phys. Rev. Lett. **57**, 1661 (1986).
- <sup>45</sup> H. Hasegawa and M. Robnik, Europhys. Lett. **23**, 171 (1993)
- <sup>46</sup> C. W. J. Beenakker, Phys. Rev. Lett. **70**, 4126 (1993).
- <sup>47</sup> K. B. Efetov and V. N. Prigodin, Phys. Rev. Lett., **70**, 1315 (1993); V. N. Prigodin, K. B. Efetov and S. Iida, Phys. Rev. Lett. **71**, 1230 (1993).
- <sup>48</sup> V. N. Prigodin, K. B. Efetov, B. L. Altshuler, and S. Iida, Phys. Rev. Lett. **72**, 546 (1994).
- <sup>49</sup> U. Sivan *et al.*, "Spectroscopy, Electron-Electron Interaction and Level Statistics in Disordered Quantum Dots", to appear in Europhys. Lett.
- <sup>50</sup> A. Pandey and M. L. Mehta, Comm. Math. Phys. **87**, 449 (1983); M. L. Mehta and A. Pandey, J. Phys. A **16**, 2655 (1983).
- <sup>51</sup> N. Taniguchi, A. Hashimoto, B. D. Simons, and B. L. Altshuler, unpublished
- <sup>52</sup> J. B. French, V. K. B. Kota, A. Pandey, and S. Tomsovic, Ann. Phys. **181**, 198 (1988).
- <sup>53</sup> M. A. Olshanetsky, Int. J. Mod. Phys. A. **7**, 4259 (1992).
- <sup>54</sup> A. Huffmann, J. Phys. A **23**, 5733 (1990).
- <sup>55</sup> O. N. Dorokhov, Pis'ma Zh. Eksp. Teor. Fiz. **36**, 259 (1982) [JETP Lett. **36**, 318 (1982)]; P. A. Mello, P. Pereyra and N. Kumar, Ann. Phys. **181**, 290 (1988).

## SPECTRAL PROPERTIES OF DISORDERED QUANTUM DOTS

*U. Sivan*

*Physics Department and Solid State Institute, Technion - Israel Institute of Technology, Haifa 32000, Israel.*

- \* *The experiment reported in section II was carried out in collaboration with F. P. Milliken, K. Milkove, S. Rishton, Y. Lee, J. M. Hong, V. Boegli, D. Kern, and M. deFranza. It appeared in Europhys. Lett. 25, 605 (1994).*
- \*\* *The experiment reported in section III was carried out in collaboration with Y. Aloni and M. Tischler, unpublished (1993).*
- \*\*\**The calculations of the dephasing rate presented in the appendix were done in collaboration with Y. Imry and A. G. Aronov, unpublished (1994).*

## Abstract

We report on two experiments that probe the quasi particle level spectrum and the ground state level statistics of disordered quantum dots. The quasi particle spectrum is found to be discrete only in close vicinity to the Fermi level. Levels farther than  $O(10)$  levels away are broadened, probably by electron - electron interaction, beyond the average level spacing and merge to form a continuous spectrum. For the discrete part of the spectrum we study level statistics as a function of magnetic field and find it to agree remarkably well with recent predictions of the random matrix theory. The ground state energy is measured as a function of dot population. Its fluctuations are considerably larger than those predicted by the constant interaction model. The fluctuations are probably due to mesoscopic fluctuations ... the many body interaction.

## I. Introduction.

In the study of spectral properties of disordered quantum dots one may carry out two generically different spectroscopic experiments. In one of them, the spectrum is studied at a constant number of particles while in the other, the energy needed to add

one electron at a time is measured (so called addition spectrum). The information contained in each experiment is different. In the first case, under most circumstances, the quasi particle excitation spectrum is measured while the second experiment probes the many body ground state energy. This difference is overlooked in many studies where Coulomb blockade data are analyzed in terms of a constant charging energy plus a quasi particle level spacing.

In the present paper we report on both types of experiments. In section II we present an experiment that measures the quasi particle excitation spectrum at a constant number of electrons. To that end we have developed a new spectrometer which is insensitive to charging effects. We find discrete spectrum only in close vicinity to the Fermi energy,  $E_F$ , in the dot. Levels which are farther than roughly  $7\Delta$  ( $\Delta$  is the average level spacing) from  $E_F$  are broadened beyond  $\Delta$  and merge to form quasi continuous spectrum. The breakdown of a simple single particle picture is attributed to electron-electron interaction<sup>1)</sup>. Calculations of the electronic dephasing time in the dot that support that interpretation are presented in the appendix and show that the life time of levels farther than a fraction of the Thouless energy,  $E_C = 4\pi^2 D/L^2$ , from  $E_F$  is shorter than  $\Delta^{-1}$  ( $\hbar = 1$  in our notation). Here  $D$  is the diffusion coefficient and  $L$  is dot dimension.

In the energy range where single particle picture is valid we study the correlation between two spectra taken at different magnetic fields. The measured correlation function agrees well with recent calculations for disordered dots<sup>2)</sup> and in particular, the flux range over which levels are correlated is found to be  $\Phi_0 \sqrt{\Delta/E_C}$  ( $\Phi_0 = h/e$  is the quantum flux unit) times a geometrical factor.

In section III we present a Coulomb blockade type of experiment from which the fluctuations in the ground state energy vs. number of electrons can be deduced. We find these fluctuations to be a factor of five larger than those given by the constant interaction model and hence conclude that they probably originate from mesoscopic fluctuations in the many body interaction rather than fluctuations in the quasi particle level spacing.

## II. Quasi Particle Spectrum.<sup>3)</sup>

The structure used in the experiment is schematically shown in Fig. 1a. It comprises of a quantum dot and spectrometer separated by a tunnel barrier. The layers as grown (bottom to top) include an  $n^+$  GaAs substrate, a thick  $2 \times 10^{18} \text{cm}^{-3}$   $n^+$  GaAs buffer layer, a  $5\text{nm}$  intrinsic GaAs spacer, a  $10\text{nm}$  intrinsic GaAs well cladded between two  $6\text{nm}$   $\text{Al}_{0.35}\text{Ga}_{0.65}\text{As}$  barriers, a  $10\text{nm}$  intrinsic GaAs spacer, and

an 85 or 45nm (two different growths)  $n^{++}$  top GaAs layer. The latter layer is doped to  $2 \times 10^{18} \text{cm}^{-3}$  next to the spacer and up to  $5 \times 10^{18} \text{cm}^{-3}$  near the surface.

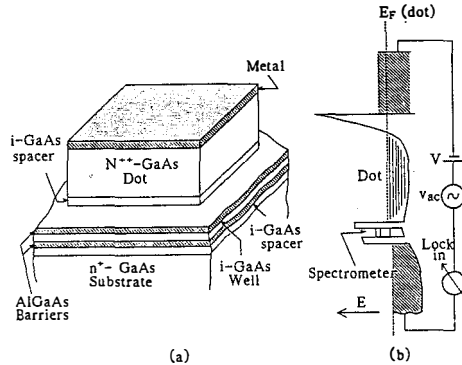


Fig. 1 - (a) The structure (b) Band diagram.

The fabrication process is detailed in ref. 3. A schematic cross section of the potential along the structure is depicted in Fig. 1b. The quantum dot is vertically confined between the Schottky barrier and the top AlGaAs barrier. The Schottky barrier width at the Fermi level is approximately 15nm, implying electrical dot thicknesses of  $W = 80$  and 40nm for the two growths. The Fermi energies in the dot and in the well are 90meV and a few meV, respectively. The elastic mean free path in the dot,  $\ell \approx 50$  nm, deduced from the doping level, is considerably shorter than  $L$ . For  $W = 80$  nm the average level spacing in the dot is approximately 10 times smaller than the level spacing in the well,  $\delta$ . For a  $200 \times 200 \text{nm}^2$  square dot, for instance,  $\delta \approx 175 \mu\text{eV}$  and  $\Delta \approx 18 \mu\text{eV}$ . The calculated charging energy for adding or removing one electron from the well is  $\approx 0.7\delta$ . The conductance scales well with dot area over almost six orders of magnitude (insert to Fig. 4) except for the smallest dot ( $L = 140$  nm) which is partially depleted by the surface potential.

The differential conductance,  $g$ , vs. dc bias,  $V_{dc}$ , is depicted in Fig. 2 for a  $200 \times 200 \text{nm}^2$  square dot. The trace is reproducible in a given cool down and changes when the sample is thermally cycled. However, the average peak spacing is not affected by thermal cycling. At small voltages ( $|V_{dc}| \leq 0.1 \text{mV}$  in Fig. 2) there is no spectrometer state available for tunneling and the current vanishes. Upon increasing the bias, one spectrometer state starts conducting and the current peaks whenever that state resonates with a dot level. At even higher bias, more spectrometer states become available for transport and a complicated trace resulting from incommensurate, overlapping spectra is expected. Experimentally, however, we find no change in

periodicity over a range of a few  $mV$ . We return to that point shortly. Finally, for  $|V_{dc}| \geq 4.5mV$ , the structure associated with dot levels is hardly observable. Measurements of different dots indicate that the peak spacing is independent of dot shape, but inversely proportional to dot area and thickness. The average level spacing agrees with the calculated one, assuming that 30% of the external voltage drops between the dot and the well. All data reported here were taken at temperatures below  $70mK$ , where results are independent of temperature, and with an ac excitation voltage,  $v_{ac} \leq 2\mu V$ .

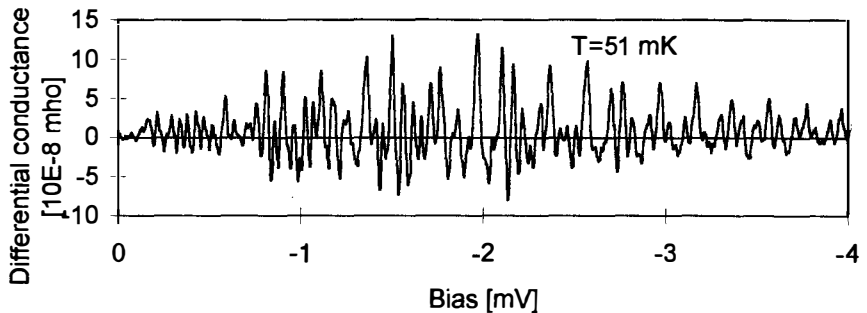


Fig. 2 - Differential conductance vs. dc bias across the device.

The lack of complex structure expected for tunneling via several spectrometer states is also evident from the total current vs. bias curve (thick line in Fig. 3) obtained by integrating Fig. 2. Current increases in steps of nearly equal height, each corresponding to an opening of additional conducting spectrometer state. The fine structure superimposed on a step is due to that level scanning dot states. A closer look reveals two types of steps, a shorter (e.g., between  $-1.1$  and  $-1.3mV$ ) and a longer (e.g.,  $-1.3$  to  $-1.7mV$ ) one, corresponding, we believe, to the two possible charge states of a system composed of two quantum dots. A crucial clue to the interpretation of the tunneling data is provided by the autocorrelation function,  $\int dV g(V)g(V + \Delta V)$ , depicted in Fig. 3 by thin line. A pronounced correlation with a periodicity of  $0.6mV$  and a weaker one, shifted by  $0.2mV$ , are evident and correspond to the step spacings discussed above. The correlation stems from the fact that the fine structure superimposed on equivalent plateaus is due to the **same dot levels** scanned by consecutive spectrometer states. The number of electrons in the dot and spectrometer is fixed along a given plateau and the fine structure is measured at a fixed number of electrons. It is therefore free of obscuring charging effects.

Puzzled by the lack of fine structure due to tunneling via spectrometer states other than the top one, Sivan *et al.*<sup>1)</sup> have calculated the level width,  $\Gamma$ , due to electron-

electron interaction in the dot (see appendix). It turns out that for energies  $\varepsilon \geq 0.1E_C$  the level width becomes larger than the level spacing. We therefore believe that the lack of complex structure is due to the fact that all dot states resonating with spectrometer levels other than the top one are already broadened by e-e interaction beyond  $\Delta$ . Stairs, on the other hand, being a result of spectrometer level discreteness, are hardly affected by this broadening.

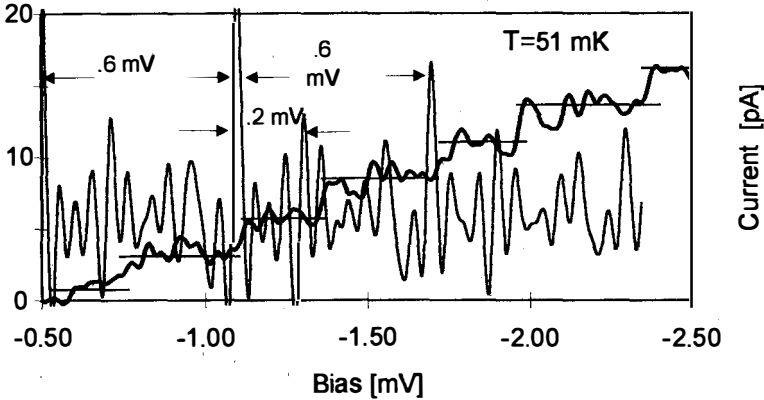


Fig. 3 - Thick line-current vs. bias. Thin line-conductance correlation vs. bias separation (arbitrary units).

We turn now to discuss correlation between discrete levels. Calculations<sup>2)</sup> as well as numerical simulations show that for non-interacting electrons, level statistics follows random matrix theory.<sup>4)</sup> The major characteristics of that level statistics are remarkable spectral rigidity and universality that depend solely on the global symmetries of the system. Such level statistics has been known to apply to large nuclei;<sup>4)</sup> and non-interacting particles in chaotic cavities.<sup>5)</sup> Recently, some features of that level statistics were observed in electrons scattering off a ballistic, chaotic cavity.<sup>6)</sup>

The spectrum is very sensitive to magnetic field<sup>3)</sup> and application of less than one flux quantum shifts levels by roughly one level spacing. To quantify the correlation between two spectra taken at different magnetic fields we have carefully mapped the conductance as a function of both dc bias and magnetic field in the range  $-2\text{mV} \leq V_{\text{dc}} \leq -1\text{mV}$  and  $0 \leq B \leq 70\text{G}$ . At higher fields, Zeeman effect is dominant and we therefore confine ourselves here to weak fields. The resulting level correlation function

$$K(\Phi, \Delta\Phi) = \int dV [g(V, \Phi) - \bar{g}(\Phi)][g(V, \Phi + \Delta\Phi) - \bar{g}(\Phi + \Delta\Phi)], \quad (1)$$

normalized to its value at  $\Delta\Phi = 0$  is depicted in Fig. 4 for several values of  $B = \Phi/L^2$ . Here,  $\bar{g}$  is the average differential conductance. In our geometry electrons pass two dots and hence,  $g(V, \Phi) \propto \partial_V \int dV' \nu(V - V', \Phi) f(V')$ , where  $\nu(V, \Phi)$  is the dot's density of states and  $f(V)$  is the line shape of a spectrometer level. The partial derivative with respect to  $V$  results from the fact that we measure the differential conductance rather than the conductance itself. Since energy is proportional to the bias one obtains with the aid of Eq. 1

$$\begin{aligned}
 K(\Phi, \Delta\Phi) &\propto \int d\varepsilon' d\varepsilon'' f(\varepsilon) f(\varepsilon'') S(\varepsilon' - \varepsilon'', \Phi, \Delta\Phi), \\
 S(\varepsilon' - \varepsilon'', \Phi, \Delta\Phi) &= \int d\varepsilon \partial_\varepsilon \nu(\varepsilon - \varepsilon', \Phi) \partial_\varepsilon \nu(\varepsilon - \varepsilon'', \Phi + \Delta\Phi) \\
 &\quad - \int d\varepsilon \partial_\varepsilon \nu(\varepsilon, \Phi) \int d\varepsilon \partial_\varepsilon \nu(\varepsilon, \Phi + \Delta\Phi)
 \end{aligned}
 \tag{2}$$

The physics is contained in  $S(\varepsilon' - \varepsilon'', \Phi, \Delta\Phi)$  which measures the correlation between the derivative of the density of states with respect to energy at two different energies and fluxes. It also depends, in accordance with the random matrix theory,<sup>4)</sup> on the total flux,  $\Phi$ , which determines time reversal symmetry and hence the statistics.

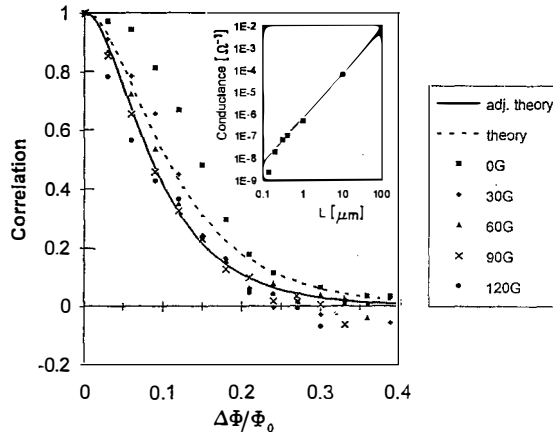


Fig. 4 -Correlation function vs. flux. Insert -conductance of square dots vs. dot length.

To compare our results with theory we note<sup>2)</sup> that  $S$  is a universal function of energy and flux separation, provided they are measured in units of  $\Delta$  and  $\Phi_0 \sqrt{r \Delta / E_C}$ , respectively. The factor  $r$  depends solely on the geometry and, for a cubic dot, equals  $\pi^3/3$ . Assuming  $f(E/\Delta) = \eta / ((E/\Delta)^2 + \eta^2) \pi$ , with  $\eta = 1/4$  estimated from the experiment, Eq. 2 yields the dashed line in Fig. 4. Since

$E_C/\Delta \approx 400$  is estimated from the doping level and lithography, there are no adjustable parameters in the theory. The agreement between theory and experiment is hence remarkable. Alternatively, one can treat  $\sqrt{E_C/\Delta r}$  as a single fitting parameter and adjust it to yield best fit to the experiment. The results of such a procedure are displayed by the thick line in Fig. 4 and give  $\sqrt{E_C/\Delta r} = 7.8$  compared with the 6.4 value estimated from doping level and lithography. This discrepancy can easily result from deviations in geometry and/or doping level. In fact, the agreement is good enough to suggest a new method for measuring conductance of a microscopic object which can't be otherwise measured.

Note that the  $B = 0$  and, to some extent, the  $B = 30G$ , curves in Fig. 4 are different from higher field ones. We attribute this deviation to these cases being members of a different universality class,<sup>4)</sup> namely, the orthogonal rather than the unitary one. Similar behavior is observed in numerical simulations.<sup>2)</sup>

### III. Ground State Level Statistics<sup>7)</sup>

We turn now to discuss measurements of the ground state energy as a function of number of electrons residing in the dot. The dot is schematically depicted in the left part of fig. 5. It is fabricated using a standard modulation doped two dimensional electron gas formed in the interface between GaAs and AlGaAs layers. Confinement is provided by biased Schottky gates (dark areas in the figure) deposited on top of the structure. A low frequency ac voltage is applied between electrodes 8 and 16 and the resulting current is measured as a function of the dc bias applied to gate 3.

Due to the small capacitance, at temperatures below  $\approx 0.5K$ , the charging energy needed in order to drive current through the dot is usually larger than the temperature. The quantum dot is hence insulating except for special values of dot potential for which the ground state energy with  $N$  electrons is degenerate with that of  $N + 1$  electrons. Since the dot potential depends on gate voltages, the conductance oscillates, for instance, as a function of the voltage applied to gate 3 (fig. 5). Each peak corresponds to an addition of one electron to the dot. Such oscillations are known as Coulomb blockade oscillations and have been observed in recent years by many groups (e.g. refs. 8,9).

To extract information from the peak position we note that the total energy of a dot with  $N$  electrons is given by

$$E_N = \varepsilon_N - eN\Phi ; \Phi = \Phi_0 + \alpha V_{G3} , \quad (3)$$

where  $\varepsilon_N$  is the many body ground state energy of the dot with  $N$  electrons,  $\Phi$  is the total electrostatic potential,  $\Phi_0$  is the electrostatic potential induced by donors etc.

and by all gates except gate 3.  $\alpha V_{G3}$  is the potential induced by gate 3 with  $V_{G3}$  being the bias applied to the gate and  $\alpha$  a proportionality factor to be determined from the experiment. At the peak conductance,  $E_N = E_{N+1}$ , thus  $\varepsilon_{N+1} - \varepsilon_N = e\Phi_0 + e\alpha V_{G3}^N$  where  $V_{G3}^N$  is the bias satisfying the above degeneracy condition. Subtracting two expressions for consecutive electron number we find an expression for the pair energy in terms of peak spacing

$$\varepsilon_{N+1} - 2\varepsilon_N + \varepsilon_{N-1} = e\alpha(V_{G3}^N - V_{G3}^{N-1}). \quad (4)$$

Since  $\alpha$  is measured very accurately either by fitting the peak shape to a derivative of the Fermi function<sup>8)</sup> or by measurements in the quantum Hall effect regime, eq. 4 provides an accurate method for measuring the ground state energy as a function of  $N$ .

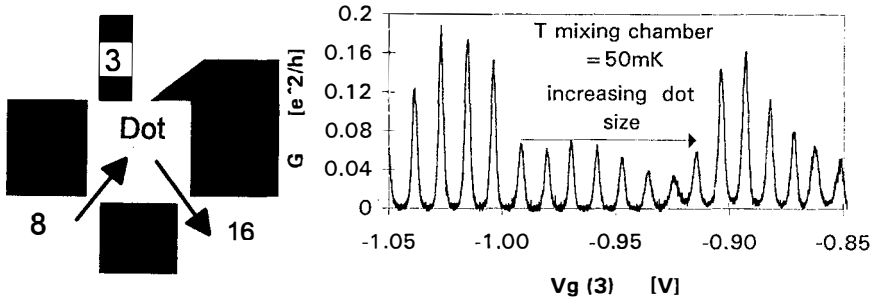


Fig. 5 -left-Dot schematics. right-conductance vs. bias applied to gate 3

For non interacting fermions with spin  $1/2$  the pair energy is the level spacing for even  $N$  and zero for odd  $N$ . Adding a constant Coulomb interaction adds a constant,  $e^2/C$ , to each term ( $C$  is the capacitance). Based on the results of section II, which strongly suggest a random matrix theory statistics, we thus expect in the constant interaction model a constant pair energy for odd  $N$  and Wigner surmise<sup>4)</sup> statistics for even  $N$ . The experimental results, however, are very different. The measured pair energy calculated from curves like fig. 5 is presented in fig. 6 after subtraction of the average spacing. For comparison with the constant interaction model one bare level spacing is marked on the graph. This is a generous upper bound on the fluctuations predicted by this model. It is clearly seen that the actual fluctuations are considerably larger. Moreover, we have not observed any significant difference between the fluctuations at even and odd  $N$ . It is therefore concluded that the constant interaction model fails to describe the ground state level statistics. The observed fluctuations are probably due to mesoscopic fluctuations in the many body energy rather than quasi

particle level fluctuations. In retrospect, this result is rather expected. The Coulomb interaction in these objects is roughly an order of magnitude larger than the average quasi particle level spacing. Mesoscopic fluctuations in the interaction can therefore easily exceed the bare level spacing. It is interesting to note that upon application of a strong magnetic field, the fluctuations are greatly reduced and replaced by oscillations which reflect the Landau level structure. The constant interaction model works much better in this case as already noticed by several authors (e.g. McEuen et al.<sup>9</sup>). We feel that full theoretical and experimental understanding of these fluctuations sets a challenge for practitioners in the field.

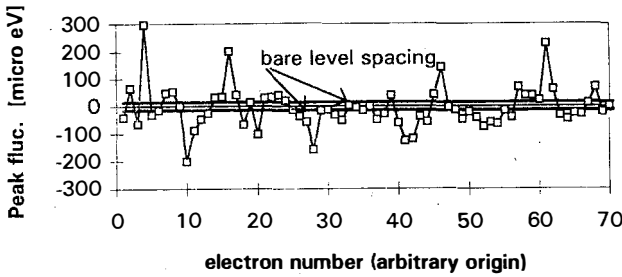


Fig. 6 - Fluctuations in peak spacing. Note magnitude compared with a level spacing (two horizontal lines).

#### Appendix - Dephasing Time Due to Electron Electron Interaction in the Dot.<sup>1)</sup>

In second order perturbation theory the probability that the environment changes its initial state due interaction with a test electron is given by<sup>10,11)</sup>

$$P(\tau_0) = \sum_{|n\rangle \neq |0\rangle} \int_0^{\tau_0} \int_0^{\tau_0} dt' \langle 0 | \Psi_I(x_1(t), t) - V_I(x_2(t), t) | n \rangle \langle n | V_I(x_1(t'), t') - V_I(x_2(t'), t') | 0 \rangle, \quad (5)$$

where  $V_I(x, t) = \int \frac{\hat{\rho}_I(r', t)}{|x - r'|} d^3 r'$  is the Coulomb interaction between the probe electron and the rest of the electrons in the dot,  $\hat{\rho}_I(r', t)$  is the density operator,  $|0\rangle$  and  $|n\rangle$  are the ground state and the  $n$ -th excited state of the Fermi sea, respectively, and  $x_1, x_2$  stand for two different real space paths available for the electron. In the infinite case, eq. 5 reproduces previous bulk results.<sup>12)</sup> Similarly to ref. 12 we consider pairs of paths of equal length only. The dephasing time,  $\tau_\Phi$ , is the value of  $\tau_0$  for which  $P$  is on the order of unity. We arbitrarily choose  $P = 0.5$ . Following the steps leading from Eq. (8) to (12) in ref. 10, one obtains for a rectangular box of a side  $L$  and quasi particle energy  $\epsilon$

$$P = \frac{1}{L^3} \int_0^{\tau_0} dt \int_0^{\tau_0} dt' \int_0^{\epsilon} d\omega \sum_{q_j \neq 0} \frac{4e^2}{q_j^2} \text{Im} \left( \frac{1}{\epsilon(q_j, \omega)} \right) (S_1 + S_2 - S_3 - S_4) e^{i\omega(t-t')}, \quad (6)$$

with  $S_1 = e^{iq_j \cdot (x_1(t) - x_1(t'))}$ ,  $S_2 = e^{iq_j \cdot (x_2(t) - x_2(t'))}$ ,  $S_3 = e^{iq_j \cdot (x_1(t) - x_2(t'))}$ ,

$S_4 = e^{iq_j \cdot (x_2(t) - x_1(t'))}$ , and  $q_j = \frac{\pi}{L} j\hat{x} + \frac{\pi}{L} l\hat{y} + \frac{\pi}{L} m\hat{z}$ ;  $j, l, m = 0, 1, 2, \dots$ ;  $j + l + m > 0$ .

The  $q = 0$  mode is excluded due to charge neutrality.

For  $q_j \ell \gg 1$ , the proper dielectric function is the ballistic one and typical exchanged momentum is on the order of the Thomas Fermi screening wave vector,  $q_{TF} = \sqrt{\frac{4k_F}{\pi a_B}} \gg \ell^{-1}$  ( $a_B$  is the effective Bohr radius and  $k_F$  is the Fermi wave vector). Since  $q_{TF} L \gg 1$ , the finite dot dimensions play no role and the resulting dephasing rate for a 3D dot is identical to the one characteristic to an infinite system,  $\tau_{\Phi}^{-1} \approx \frac{\pi^2}{16} \frac{\epsilon^2}{E_F} \frac{q_{TF}}{k_F}$ . This result is four times larger than the electron-electron rate calculated by Quinn and Ferrell.<sup>13</sup>) To calculate the small exchanged momenta contribution we define new variables,  $t^{\pm} = t \pm t'$ , and substitute  $\omega/4\pi\sigma$  ( $\sigma$  being the conductivity) for  $\text{Im}(1/\epsilon(q, \omega))$ , For diffusive dots,  $L \gg \ell$ , eq. (6) then takes the form

$$P_i = \frac{e^2}{2\pi L^3 \sigma} \left\{ \int_0^{\tau_0} dt^+ \int_{-t^+}^{t^+} dt^- + \int_0^{2\tau_0} dt^+ \int_{-2\tau_0+t^+}^{2\tau_0-t^+} dt^- \right\} \int_0^{\epsilon} d\omega \sum_{q_j \neq 0}^{|q_j| \leq 2\pi/\ell} \frac{S_i}{q_j^2} e^{i\omega t^-}; \quad i=1..4. \quad (7)$$

Obviously,  $P_1 = P_2$  and  $P_3 = P_4^*$ . We start by calculating  $P_1$ . The integrand in this case is independent of  $t^+$  and the temporal integrations can be combined to yield

$$P_1 = \frac{\Delta}{\pi D} \int_0^{\tau_0} dt^+ \int_{-t^+}^{t^+} dt^- \int_0^{\epsilon} d\omega \sum_{q_j \neq 0}^{|q_j| \leq 2\pi/\ell} q_j^{-2} e^{iq_j \cdot x(t^-)} e^{i\omega t^-}. \quad (8)$$

Here,  $\nu_3$  is the 3D density of states.

The coordinate  $x(t^-)$  executes a random walk with a probability distribution  $\Pi(x, t^-)$  satisfying the diffusion equation with the boundary condition  $\nabla_{\perp} \Pi|_{\text{surface}} = 0$ .

The solution is

$$\Pi(x, t) = \sum_{jlm} \Pi_{jlm} \cos\left[j \frac{\pi}{2} \left(\frac{2x-L}{L}\right)\right] \cos\left[l \frac{\pi}{2} \left(\frac{2y-L}{L}\right)\right] \cos\left[m \frac{\pi}{2} \left(\frac{2z-L}{L}\right)\right] e^{-\left(\frac{\pi}{L}\right)^2 (j^2 + l^2 + m^2) D|t|}, \quad (9)$$

where  $\Pi_0$  and  $\Pi_{jlm}$  are determined by  $\Pi(x, t = 0)$ . The Fourier transformed Coulomb interaction can now be averaged using Eq. (9) to yield

$$\left\langle \sum_{q_j \neq 0} \frac{e^{iq_j \cdot x(t)}}{q_j^2} \right\rangle = \frac{\sum_{j+l+m > 0}^{\sqrt{j^2 + l^2 + m^2} \leq L/\ell} L^3 (-1)^{j+l+m} \Pi_{2j, 2l, 2m} e^{-\left(\frac{2\pi}{L}\right)^2 (j^2 + l^2 + m^2) D|t|}}{\left(\frac{2\pi}{L}\right)^2 (j^2 + l^2 + m^2)}, \quad (10)$$

In particular, for  $\Pi(x, t = 0) = \delta(x)$ ,  $\Pi_{2j, 2l, 2m} = 8L^{-3} (-1)^{j+l+m}$ . Substituting  $\Pi_{2j, 2l, 2m}$  into Eq. (10) and then Eq. (10) into Eq. (8) one obtains

$$P_1 = \frac{16\Delta}{\pi E_C} \tau_0 \int_0^{t^+} dt^+ \int_0^{t^+} dt^- \int_0^\varepsilon d\omega \omega \sum_{j+l+m > 0}^{\sqrt{j^2 + l^2 + m^2} \leq L/\ell} \frac{e^{-\left(\frac{2\pi}{L}\right)^2 (j^2 + l^2 + m^2) D|t^-|}}{j^2 + l^2 + m^2} \cos(\omega t^-), \quad (11)$$

The integrals in Eq. (11) can all be calculated analytically and for  $E_C \tau_0 \gg 1$  we find

$$P_1 = \frac{8}{\pi} \Delta \tau_0 \sum_{j+l+m > 0}^{\sqrt{j^2 + l^2 + m^2} \leq L/\ell} \ln\left\{1 + \left[\frac{\varepsilon}{E_C (j^2 + l^2 + m^2)}\right]^2\right\}. \quad (12)$$

To calculate  $P_3$  we note that  $\langle S_3 \rangle$  is a function of  $t^+$  only. A straightforward calculation then gives

$$P_3 = \frac{4\Delta}{\pi E_C} \sum_{j+l+m > 0}^{\sqrt{j^2 + l^2 + m^2} \leq L/\ell} \frac{\ln\left\{1 + \left[\frac{\varepsilon}{E_C (j^2 + l^2 + m^2)}\right]^2\right\}}{j^2 + l^2 + m^2}. \quad (13)$$

In all cases,  $P_3 \ll P_1$ ; for  $\varepsilon \ll E_C$  by a factor of  $\tau_0 E_C \gg 1$  and for  $\varepsilon \gg E_C$  by a factor of  $\tau_0 \varepsilon \gg 1$ . Hence,  $P_3$  can be neglected.

The dephasing time is the value of  $\tau_0$  for which  $P \approx 2P_1 = 1/2$ , thus

$$\tau_\Phi^{-1} = \frac{32}{\pi} \Delta \sum_{j+l+m > 0}^{\sqrt{j^2 + l^2 + m^2} \leq L/\ell} \ln\left\{1 + \left[\frac{\varepsilon}{E_C (j^2 + l^2 + m^2)}\right]^2\right\}. \quad (14)$$

For  $\varepsilon \gg E_C$  the sum can be replaced by an integral to reproduce a rate similar to the 3D bulk one<sup>12)</sup>

$$\tau_{\Phi}^{-1} = \frac{16\sqrt{2}\pi}{3} \Delta \left(\frac{\varepsilon}{E_C}\right)^{3/2}. \quad (15)$$

For  $\varepsilon \ll E_C$  we obtain a new, 0D result

$$\tau_{\Phi}^{-1} \equiv \frac{32\Delta}{\pi} \Xi \left(\frac{\varepsilon}{E_C}\right)^2; \quad \Xi = \frac{\sqrt{j^2 + l^2 + m^2} \leq L/\ell}{\sum_{j+l+m>0} (j^2 + l^2 + m^2)^{-2}} \approx 5. \quad (16)$$

The total dephasing rate is given by the sum of Eq. (14) and the large momenta

contribution,  $\tau_{\Phi}^{-1} \approx \frac{\pi^2 \varepsilon^2 q_{TF}}{16 E_F k_F} = \frac{2\pi^4}{9} \Delta \left(\frac{\varepsilon}{E_C}\right)^2 \frac{q_{TF} \ell^2}{L}$ .

#### References

- 1U. Sivan, Y. Imry, and A. G. Aronov, unpublished (1994).
- 2B. D. Simons, and B. L. Altshuler, Phys. Rev. **B48**, 5422 (1993) and private communication.
- 3U. Sivan, F. P. Milliken, K. Milkove, S. Rishton, Y. Lee, J. M. Hong, V. Boegli, D. Kern, and M. deFranza, Europhys. Lett. **25**, 605 (1994).
- 4M. L Mehta, *Random Matrices* (Academic, NY, 1967).
- 5M. V. Berry, Proc. R. Soc. London, Ser. A **400**, 229 (1985).
- 6C. M. Marcus, A. J. Rimberg, R. M. Westervelt, P. F. Hopkins, and A. C. Gossard, Phys. Rev. Lett. **69**, 506 (1992).
- 7Y. Aloni, U. Sivan, and M. Tischler, unpublished (1993).
- 8U. Meirav, M. A. Kastner, S. J. Wind, Phys. Rev. Lett. **65**, 771 (1990).
- 9P. L. McEuen, E. B. Foxman, U. Meirav, M. A. Kastner, Y. Meir, N. Wingreen, and S. J. Wind, Phys. Rev. Lett. **66**, 1926 (1991).
- 10A. Stern, Y. Aharonov, and Y. Imry in *Quantum Coherence in Mesoscopic Systems*, pp. 99-104, edited by B. Kramer, Plenum Press, NY (1991).
- 11Eq. 5 is a straight forward generalization of Eq. 8 in ref. 10 which includes interaction in either path available for the electron.
- 12B. Altshuler, A. G. Aronov, and D. E. Khmel'niskii, Solid State Commun. **39**, 619 (1981); J. Phys. **C15**, 7367 (1982).
- 13D. Pines and P. Nozie' res "The Theory of Quantum Liquids" Vol. 1, Addison-Wesley Publishing Company, Inc., p.309 (1989).

## MOTION OF ENERGY LEVELS IN DIFFUSIVE ELECTRONIC SYSTEMS

Daniel Braun<sup>1</sup>, Gilles Montambaux<sup>1</sup> and Alex Kamenev<sup>2</sup><sup>1</sup> Laboratoire de Physique des Solides, Associé au CNRS, Université Paris–Sud, 91405 Orsay, France<sup>2</sup> Department of Condensed Matter Physics, The Weizmann Institute of Science, Rehovot 76100, Israel**Abstract**

We examine numerically and by means of random matrix theory (RMT) the statistical properties of the spectra of mesoscopic systems in the diffusive regime pierced by an Aharonov–Bohm flux  $\varphi$ . The quantities considered are the statistics of single level curvatures  $c_n(\varphi)$  at zero and finite flux, the square of the typical single level current  $\langle i_n^2(\varphi) \rangle$ , and single level current correlation functions. The curvature distribution function decays as  $c_n^{-3}$  for large curvatures, such that its second moment, which is commonly regarded as a measure of the Thouless energy  $E_c$ , *diverges*. The square of the typical single level current shows a logarithmic low–flux behavior, and a corresponding behavior is observed for the single level current autocorrelation function. We discuss the consequences of these results for the universal conductance ratio proposed in Ref. 1.

**Introduction**

Let us consider a parameter dependent Hamiltonian  $H(\lambda)$  of the form  $H(\lambda) = H_1 + \lambda H_2$  where  $H_1$  and  $H_2$  are two independent random Hermitian matrices. The parametric motion of energy levels  $e_n(\lambda)$  of such a Hamiltonian has recently been investigated by numerous authors<sup>2,3,4,5,6</sup> and various statistical properties of the spectra have been calculated, like distributions of the first and second derivatives of  $e_n(\lambda)$ , or correlation functions of these quantities. It has been shown<sup>2)</sup> that the motion of the energy levels corresponds to the classical motion of interacting particles, when  $\lambda$  is regarded as a fictitious time, and classical Hamiltonians which govern this dynamics have been derived. Most of the cited work dealt

with what we will call “pure symmetry cases”, i.e. cases in which  $H_1$  and  $H_2$  belong both to the same universality class of random matrices, i.e. for example both to GOE or both to GUE (Gaussian orthogonal and Gaussian unitary ensembles, respectively).

In this article we investigate the situation, where  $H_1$  and  $H_2$  belong to *different* symmetry classes (we will call this case the “transition case”), in particular a Hamiltonian of the form

$$H(\alpha) = H_1(S) + i\alpha H_2(A), \quad (1)$$

where  $H_1(S)$  is a random symmetric matrix and  $H_2(A)$  a random antisymmetric matrix. The parameter  $\alpha$  thus allows for a continuous transition between GOE ( $\alpha = 0$ ) and GUE ( $\alpha = 1$ )<sup>7,8</sup>. Such a form of the Hamiltonian is physically particularly interesting, since it corresponds to a situation, where the time reversal symmetry of the system is gradually broken. A physical realization of such a situation is a mesoscopic ring in the diffusive regime, i.e. a ring with a circumference  $L$  much larger than the elastic mean free path  $l_e = v_F \tau_e$  but smaller than the dephasing length  $L_\varphi$ . It is well known that the low energy ( $E \leq \hbar/\tau_e$ ) spectral correlations are well described by Random Matrix Theory (RMT)<sup>9,10</sup>. Dupuis and Montambaux showed that the unique parameter which drives the transition from GOE to GUE and which is proportional to  $\alpha$  is given by  $\varphi/\varphi_c$  with  $\varphi_c = \frac{1}{\sqrt{E_c/\Delta}}$ , where  $E_c = \frac{\hbar D}{L^2}$  is the so called Thouless energy,  $D$  the diffusion constant and  $\Delta$  the mean level spacing. With this mapping they demonstrated that the fluctuation of the number of levels in a given energy range  $E$ ,  $\Sigma^2(E, \varphi)$ , is a universal function of  $\varphi/\varphi_c$ <sup>11</sup>.

One of the interests in mesoscopic rings pierced by an AB flux comes from an argument by Thouless<sup>12</sup>. The AB flux may be thought of as introducing generalized boundary conditions along the circumference of the ring:  $\psi(x + L, y, z) = e^{i2\pi\varphi}\psi(x, y, z)$ . Thouless showed that the average conductance  $G$  of the system can be related to the sensitivity of the spectrum of the system’s Hamiltonian to a change of the boundary conditions. More precisely, defining the “level curvature”  $c_n(\varphi) = \frac{\partial^2 \epsilon_n(\varphi)}{\partial \varphi^2}$ , he showed that the width of the distribution  $P_\varphi(c_n(\varphi)/\Delta)$  at  $\varphi = 0$  is proportional to the dimensionless conductance  $g_c = \frac{G}{e^2/\hbar}$ . This “Thouless relation” has henceforth often be quoted in the form  $g_c = \frac{1}{\Delta} \langle c_n^2(0) \rangle^{\frac{1}{2}}$ <sup>1,13,14</sup>. We show here that this choice of the typical curvature to describe the conductance is not correct, since the curvature distribution  $P_0(c_n(0))$  decays too slowly, so that its second moment does not exist.

Another measure of the sensitivity of the spectrum to a change of the boundary conditions has been introduced by Akkermans and Montambaux <sup>1)</sup>. They showed that the dissipative conductance  $g_d$  of the system (equivalent to the one obtained from the Kubo formula) is given by  $g_d = \frac{1}{\Delta^2} \langle \overline{i_n^2(\varphi)} \rangle$ , where  $i_n(\varphi) = -\frac{\partial e_n(\varphi)}{\partial \varphi}$  is a single level current and the overline denotes an average over one flux period. Making certain assumptions about the current correlation function  $C(\varphi, \varphi') = \frac{1}{\Delta^2} \langle i_n(\varphi) i_n(\varphi') \rangle$ , they also showed that  $g_d$  is proportional to the typical curvature of the levels and thus to  $g_c$ . Since the typical curvature actually diverges, this argument, based on a perturbative hypothesis, should be rephrased and the typical curvature replaced by the width of the curvature distribution, as originally proposed by Thouless. It is therefore worthwhile to reconsider the assumptions made about  $C(\varphi, \varphi')$ . Similar correlation functions have been considered before, e.g. by Szafer and Altshuler <sup>15)</sup> and Simons and Altshuler <sup>13)</sup>, who considered the auto correlation function  $C(\varphi_-) = \int_0^1 C(\varphi, \varphi + \varphi_-) d\varphi$ . They predicted a universal behavior of  $C(\varphi_-)$  in the parameter region  $\varphi_c \ll \varphi \ll \frac{1}{2}$  <sup>15)</sup> and a universal behavior for all fluxes after appropriate rescaling <sup>13)</sup>. Using the method of supersymmetry, Simons and Altshuler found the low-flux behavior of  $C(\varphi_-)$  in the pure GUE case (with an additional transversal flux applied). In the case of a GOE-GUE crossover a RMT model predicts a logarithmic low flux behavior of  $C(\varphi, \varphi')$  <sup>16)</sup>.

In this paper we study the distribution of curvatures for zero and finite flux,  $P_\varphi(c_n(\varphi))$ . We show numerically that  $C(\varphi, \varphi')$  has a logarithmic behavior at low flux, and confirm numerically a linear relation between  $\langle |c_n(0)| \rangle$  and  $\frac{1}{\Delta^2} \langle \overline{i_n^2(\varphi)} \rangle$  <sup>4)</sup>. A more detailed version of this work, also comprising numerical results for the distributions of  $i_n(\varphi)$  and  $\overline{i_n^2(\varphi)}$ , will be published in Ref. 17.

### Curvature distributions

The large curvature behavior of  $P_\varphi(c_n(\varphi))$  ( $0 \leq \varphi < \varphi_c$ ) is easily obtained from solving a  $2 \times 2$  RMT model <sup>16)</sup>. The results of such a simple model are expected to become exact for  $\frac{1}{\Delta} c_n(\varphi) \rightarrow \infty$ , since large curvatures arise from avoided crossings with very small level spacings, such that the interaction with next levels can be neglected <sup>3,5,16)</sup>. The result for  $\varphi = 0$  is given by <sup>16)</sup>

$$P_0(c_n(0)) = \frac{3}{8v} \sqrt{\frac{2v}{c_n(0)}} e^{\frac{1}{4} \left( \frac{c_n(0)}{2v} \right)^2} D_{-\frac{5}{2}} \left( \frac{c_n(0)}{2v} \right), \quad (2)$$

where  $v = \frac{\Delta}{\sqrt{2\pi}}$  is the variance of the randomly chosen matrix elements, and  $D_\alpha(x)$  a

Whittaker parabolic cylinder function. The same result has been obtained for the pure GOE case in Ref. 3. The asymptotic behavior of eqn. (2) — and only its asymptotic behavior should be taken seriously — reads  $P_0(c_n(0)) \simeq \left(\frac{v}{c_n(0)}\right)^3$  for  $c_n(0) \gg v$ . Concerning the scale  $v$  of this algebraic decay, note that in a  $2 \times 2$  RMT model the Thouless-energy is comparable to the mean level spacing ( $\frac{E_c}{\Delta} \sim N$ , where  $N$  is the size of the matrix). We therefore cannot determine from this model the scaling of  $P_0(c_n(0))$  for large matrices, but we will see below that the relevant scale is  $E_c$ , not  $\Delta$ .

A  $c_n^{-3}(0)$  decay was also obtained for the tail of the curvature distribution function in the pure GOE case<sup>2,3,5</sup>). In fact, one can show that the complete distribution function  $P_0(c_n(0))$  is identically the same as in the pure GOE case for all curvatures<sup>17</sup>). This is a priori not obvious, since the curvatures calculated at  $\varphi = 0$  probe infinitesimally small fluxes to both sides of  $\varphi = 0$ , where the level statistics is changed already. Up to our knowledge, no analytical formulas have been derived for the whole distribution function in the pure symmetry cases<sup>21</sup>), only the limiting behavior for large curvatures is well established. However, in Ref. 3 a distribution function was guessed which fits the numerical data remarkably well. It has the form of a generalized Lorentzian,

$$P_\beta(c_n) = N_\beta \frac{1}{\left(1 + \left(\frac{c_n}{\gamma_\beta}\right)^2\right)^{(\beta+2)/2}}, \quad (3)$$

with  $\gamma_\beta = \beta\pi\frac{v}{\Delta}$  and  $\beta = 1, 2, 4$  for GOE, GUE, GSE, respectively<sup>21</sup>).  $N_\beta$  is a normalization factor. Thus we expect to find for the GOE-GUE transition case the same distribution as above with  $\beta = 1$ .

$$P_0(c_n(0)) = \frac{1}{\gamma} \frac{1}{\left(1 + \left(\frac{c_n(0)}{\gamma}\right)^2\right)^{3/2}}, \quad (4)$$

in agreement with the predicted  $1/c_n^3(0)$  tail.

In order to verify these predictions numerically, we have calculated the curvatures of the energy levels of many tight binding Anderson Hamiltonians with diagonal disorder distributed in a box like distribution from  $-\frac{w}{2}$  to  $\frac{w}{2}$ . In Fig. 1 we show the result for  $P_0(c_n(0))$  together with the generalized Lorentzian eqn. (4) for a 3D sample<sup>18</sup>). The width  $\gamma$  was used as a fitting parameter. We will show below that it is related to  $\frac{1}{\Delta} \langle \overline{i_n^2(\varphi)} \rangle$ . Corresponding results were found for all samples examined, independent of their geometry and their disorder, as long as we stayed in the diffusive regime.

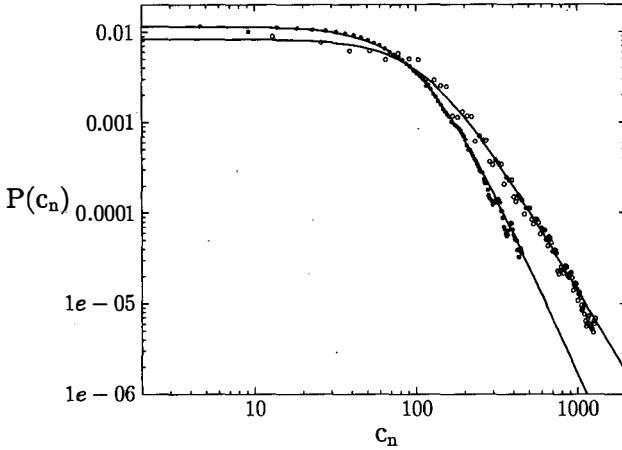


Figure 1: The numerically calculated curvature distributions at  $\varphi = 0$  (empty circles) and  $\varphi = 0.24$  (full circles) for  $100\ 8^*8^*8$  samples with  $w = 5$ . The full lines are fits to the generalized Lorentzians known from the pure GOE and GUE case with the widths as fitting parameters.

As a consequence of eqn. (4), the second moment of  $P_0(c_n(0))$  diverges logarithmically with an upper cut-off  $c_{max}$ .

In the transition regime,  $0 < \varphi \ll \varphi_c$ , the curvature distribution is completely different from the one in either the pure GOE and the pure GUE cases <sup>16)</sup>. It has a Gaussian tail, such that  $\langle c_n^2(\varphi) \rangle$  is finite for every finite  $\varphi$ :  $P_\varphi(c_n(\varphi)) \propto \frac{c_n(\varphi)}{v} e^{-g(\varphi) \frac{c_n^2(\varphi)}{v^2}} \frac{c_n^2(\varphi)}{v^2}$  for  $c_n(\varphi) \gg \frac{v}{\sqrt{2\varphi/\varphi_c}}$ .  $g(\varphi)$  is a fourth order polynomial slowly varying in the flux range  $0 < \varphi < \varphi_c/\sqrt{2}$  <sup>19)</sup>. For curvatures between  $v$  and  $\frac{v}{\sqrt{2\varphi/\varphi_c}}$  the  $c_n^{-3}(\varphi)$  decay found for  $\varphi = 0$  prevails. Such Gaussian tails have been found numerically <sup>17)</sup>.

For  $\varphi > \varphi_c$  but close to  $\varphi_c$ , a transition back to an algebraic decay of  $P_\varphi(c_n(\varphi))$  must take place, which we haven't studied yet. However, for  $\varphi \gg \varphi_c$  the transition to GUE is completed and the formulas for the pure GUE case should apply. Thus we expect a  $c_n^{-4}$  decay of  $P_\varphi(c_n(\varphi))$  for  $\varphi \simeq \frac{1}{4}$ . This is indeed what is found numerically, as shown in Fig. 1 for  $\varphi = 0.241$ . The numerical data are well fitted by the generalized Lorentzian guessed for the pure GUE regime, Eq. (3) with  $\beta = 2$  <sup>3)</sup>.

### Current Correlation Functions

We now consider the single level current correlation function  $C(\varphi, \varphi') = \frac{1}{\Delta^2} \langle i_n(\varphi) i_n(\varphi') \rangle$ . If the broadening of the levels or  $E_c \varphi_{\pm}^2$  with  $\varphi_{\pm} = \varphi \pm \varphi'$  are much larger than  $\Delta$ , it may be related to spectral density correlations by  $C(\varphi, \varphi') = \frac{\delta^2}{\partial \varphi \partial \varphi'} \int_0^{E_f} d\epsilon \int_0^{E_f} d\epsilon' K(\epsilon, \varphi; \epsilon', \varphi')$ , where  $K(\epsilon, \varphi; \epsilon', \varphi') = \langle \rho(\epsilon, \varphi) \rho(\epsilon', \varphi') \rangle - \langle \rho(\epsilon, \varphi) \rangle \langle \rho(\epsilon', \varphi') \rangle$ , and  $\rho(\epsilon, \varphi)$  is the energy and flux dependent density of states <sup>15</sup>. Under the above conditions  $K(\epsilon, \varphi; \epsilon', \varphi')$  was expressed diagrammatically by Al'tshuler and Shklovskii <sup>10</sup> in terms of Cooperon and Diffuson contributions as  $K(\epsilon, \varphi; \epsilon', \varphi') = \tilde{K}(\epsilon, \epsilon'; \varphi_+) + \tilde{K}(\epsilon, \epsilon'; \varphi_-)$ , such that  $C(\varphi, \varphi')$  can be written as  $C(\varphi, \varphi') = f(\varphi_+) - f(\varphi_-)$ , where  $f(\varphi + 1) = f(\varphi) = f(-\varphi)$ .

Here we are interested in the low-flux behavior  $0 \leq \varphi, \varphi' < \varphi_c$ . At zero temperature, RMT results show that the effective low energy cut-off is of the order of  $\Delta$  <sup>11</sup>, so that the perturbation theory breaks down <sup>10</sup>. The following low-flux behavior can be obtained from RMT <sup>16</sup>:

$$C(\varphi, \varphi') \propto -\frac{E_c^2}{\Delta^2} \varphi \varphi' \ln\left(\frac{\varphi + \varphi'}{\varphi_c}\right) \text{ for } 0 \leq \varphi, \varphi' \ll \varphi_c. \quad (5)$$

Note that this expression leads to  $\langle c_n^2(\varphi) \rangle \propto -E_c^2 \ln \frac{2\varphi}{\varphi_c}$  for  $\varphi \ll \varphi_c$  and thus back to a divergence of  $\langle c_n^2(0) \rangle$ , but to a finite value for all finite fluxes.

For  $\varphi = \varphi'$  we get the square of the typical single level current:

$$\frac{1}{\Delta^2} \langle i_n^2(\varphi) \rangle = -N \frac{\varphi^2}{\varphi_c^4} \ln\left(\frac{2\varphi}{\varphi_c}\right), \quad (6)$$

with a constant prefactor  $N$ . We compared this expression to numerical data by using  $N$  and  $\varphi_c$  as fitting parameters and found excellent agreement. The agreement is much better than with a simple power expansion in  $\varphi^2$  containing also two free parameters and fitted in the same parameter range. This latter form would be obtained by an extension of the perturbational results to  $\varphi < \varphi_c$  as well as by a low-flux expansion of a formula recently suggested by Delande et al. for the pure GOE case <sup>6</sup>. Also, the dependence of  $N$  and  $\varphi_c$  on the disorder parameter  $w$  is as expected: Since  $\varphi_c = \frac{1}{\sqrt{E_c/\Delta}}$ ,  $E_c = \frac{\hbar v_f l_e}{dL^2}$  ( $d$  is the dimensionality of the sample) and  $l_e \propto \frac{1}{w^2}$  <sup>20</sup>, we have  $\varphi_c \propto w$ .  $N$  is independent of disorder. Both relations are well observed numerically ( $N \simeq 17.78 \pm 2.40$ ). The error margin is a simple standard deviation calculated from seven macroscopically different samples with 25 to 100 disorder realizations each.

Eqn. (6) implies the following rescaling:

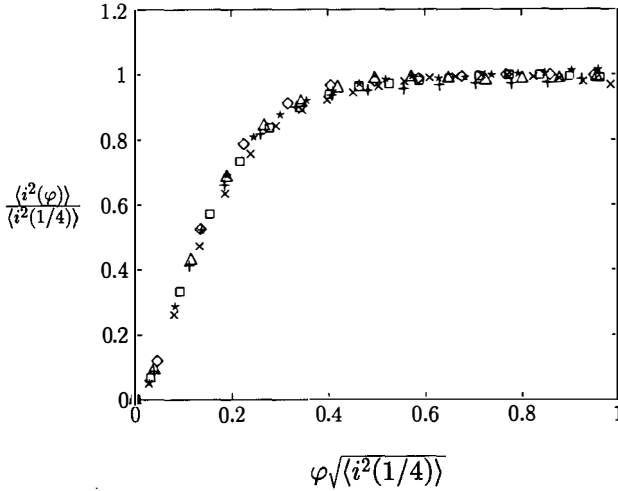


Figure 2: The rescaled function  $\langle i_n^2(\varphi) \rangle / \langle i_n^2(1/4) \rangle$  as a function of  $\varphi \sqrt{\langle i_n^2(1/4) \rangle}$  for several two and three dimensional samples.

$$\frac{1}{\Delta^2} \langle i_n^2(\varphi) \rangle \varphi_c^2 = -N x^2 \ln 2x, \quad (7)$$

with  $x = \frac{\varphi}{\varphi_c}$ . Thus,  $\frac{1}{\Delta^2} \langle i_n^2(\varphi) \rangle \varphi_c^2$  is a universal function of  $\varphi / \varphi_c$ , independent of any system specifications like geometry or disorder, as long as we stay in the diffusive regime. Due to the RMT origin of eqn. (7), we conjecture its validity more generally for any chaotic system. Furthermore, since it is found numerically that  $\langle i_n^2(\varphi) \rangle$  is basically constant for  $\varphi \geq \varphi_c$ , the universality holds for a much larger flux range and is in fact only restricted by the periodicity of  $\langle i_n^2(\varphi) \rangle$  (see Fig. (2), where we made use of the fact that  $\varphi_c \propto 1 / \sqrt{\langle i_n^2(1/4) \rangle}$ , see Ref. 17). Note that  $\langle i_n^2(\varphi) \rangle$  is non-perturbative for all fluxes ( $\varphi_- = 0$ ).

From  $C(\varphi, \varphi')$  the auto correlation function  $C(\varphi_-) = \frac{1}{\Delta^2} \int_0^1 \langle i_n(\varphi) i_n(\varphi + \varphi_-) \rangle d\varphi = \int_0^1 C(\varphi, \varphi + \varphi_-) d\varphi$  proposed by Szafer and Altshuler<sup>15)</sup> can be derived. They found the universal behavior  $C(\varphi_-) = -\frac{1}{\pi^2 \varphi_-^2}$  for  $\varphi_c \ll \varphi \ll 1/2$ . Later it was shown<sup>13)</sup> that  $c(X) = \frac{C(\varphi)}{C(0)}$  is a universal function of  $X = \varphi \sqrt{C(0)}$  for all fluxes. However, so far no analytical formulas could be

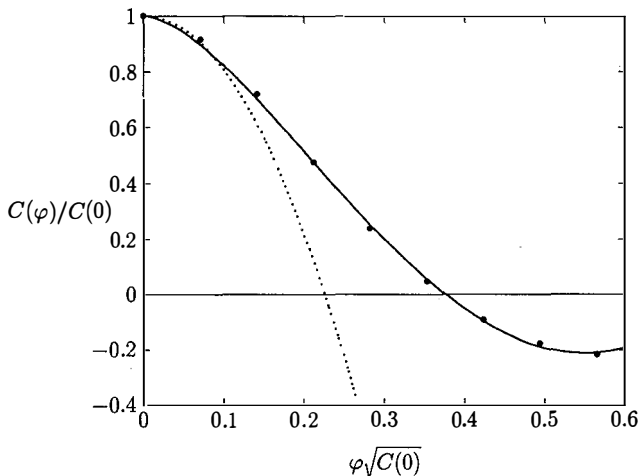


Figure 3: The low flux behavior of  $C(\varphi)/C(0)$  (full circles) is well described by  $1 + N'\varphi^2 \ln(\varphi/\varphi'_c)$  (full line). The dotted line represents the pure GUE behavior:  $C(\varphi)/C(0) = 1 - 2\pi^2 C(0)\varphi^2$ .

derived for  $C(\varphi_-)$  which are valid for all fluxes. In Ref. 6 a formula was proposed without derivation which amounts to a quadratic low flux behavior. A corresponding behavior was obtained in Ref. 13 for the pure GUE case (a transversal flux was applied in order to enforce unitary symmetry even for  $\varphi = 0$ ):  $c(X) = 1 - 2\pi^2 X^2 + \bullet(X^4)$ , whereas more general formulas were obtained by the method of supersymmetry for a different correlation function, measuring the correlations of single level currents within a fixed slice of energy.

The success of eqn. (6) in describing  $\langle i_n^2(\varphi) \rangle$  suggests to try a corresponding behavior for  $C(\varphi)$ , with parameters  $N'$  and  $\varphi'_c$  possibly different from  $N$  and  $\varphi_c$ :  $C(\varphi) = C(0) + N' \frac{\varphi^2}{\varphi_c^2} \ln\left(\frac{\varphi}{\varphi_c}\right)$ . A fit to this function works indeed extremely well (see Fig. 3), and, like for  $\langle i_n^2(\varphi) \rangle$ , much better than a power expansion to the fourth order in  $\varphi$ .

Due to the universality of  $C(\varphi)/C(0)$  as a function of  $\varphi\sqrt{C(0)}$ , the coefficients  $\varphi'_c$  and  $N'$  depend in the same way as  $\varphi_c$  and  $N$  on the disorder ( $\varphi'_c \propto w$ ,  $N'$  independent of  $w$ ), and we may identify  $\varphi'_c \propto \frac{1}{\sqrt{C(0)}}$ , thus  $E_c \propto \frac{1}{\Delta} \langle i_n^2(\varphi) \rangle$  (up to numerical coefficients). We therefore propose the universal low flux behavior  $C(\varphi)/C(0) \simeq 1 + N'x'^2 \ln x'$  with  $x' = \frac{\varphi}{\varphi'_c}$  and  $N' \simeq 6.67 \pm 0.14$ . The error margin is the simple standard deviation calculated from four

macroscopically different samples with up to 100 disorder realizations each.

**The universal conductance ratio**  $a = g_c/g_d$

In Ref. 1 it was shown that  $a = \frac{g_c}{g_d} = \frac{\langle c_n^2(0) \rangle \Delta}{\langle i_n^2(\varphi) \rangle}$  should be a universal ratio, independent of any system specifications (in the diffusive regime), if  $C(\varphi, \varphi')$  can be written in the form  $C(\varphi, \varphi') = f(\varphi + \varphi') - f(\varphi - \varphi')$  for all  $\varphi, \varphi'$ . According to RMT, its value is given by  $\pi\sqrt{12}$ . Having shown that  $\langle c_n^2(0) \rangle$  diverges, whereas  $\frac{1}{\Delta^2} \langle i_n^2(\varphi) \rangle$  is the average dissipative conductance of the system, it is clear that this relation cannot hold. Therefore the assumption made for its derivation must be wrong, and eqn. (5) shows indeed that  $C(\varphi, \varphi')$  can *not* be written in the form  $f(\varphi + \varphi') - f(\varphi - \varphi')$  for  $0 < \varphi, \varphi' < \varphi_c$ . An even more direct way of showing this is the following: Let us *assume* that  $C(\varphi, \varphi') = f(\varphi + \varphi') - f(\varphi - \varphi')$  for all  $\varphi, \varphi'$ . Then one immediately finds  $\frac{1}{\Delta^2} \langle i_n^2(\varphi) \rangle = f(2\varphi)$  and  $C(\varphi_-) = -f(\varphi_-)$ . Thus,  $\frac{1}{\Delta^2} \langle i_n^2(\varphi) \rangle = C(0) - C(2\varphi)$  for all  $\varphi$ . However, it is easily seen numerically that this relation does not hold: Whereas  $\frac{1}{\Delta^2} \langle i_n^2(\varphi) \rangle$  is basically constant for  $\varphi > \varphi_c$ ,  $C(0) - C(2\varphi)$  reaches a maximum and then decays again, corresponding to the universal  $-\frac{1}{\pi^2\varphi^2}$  behavior of  $C(\varphi)$  <sup>15</sup>. Therefore,  $C(\varphi, \varphi')$  cannot be written in the form  $f(\varphi + \varphi') - f(\varphi - \varphi')$  for all  $\varphi, \varphi'$ , which is equivalent to the statement that the harmonics of  $i_n(\varphi)$  are correlated.

The idea of the universal ratio  $g_c/g_d$  was that the GOE  $\rightarrow$  GUE transition is driven by the unique parameter  $\varphi/\varphi_c$ , such that different measures of the sensitivity of the spectrum to a change of the boundary condition should be equivalent. If we measure this sensitivity by means of curvatures at  $\varphi = 0$ , an appropriate quantity is  $\gamma_1 = \langle |c_n| \rangle$  <sup>4</sup>). Indeed, we found numerically a linear relationship between  $\frac{1}{\Delta} \langle |c_n| \rangle$  and  $\frac{1}{\Delta^2} \langle i_n^2(\varphi) \rangle$ :  $\frac{1}{\Delta} \langle |c_n| \rangle \simeq 13.4 + 6.7 \frac{1}{\Delta^2} \langle i_n^2(\varphi) \rangle$ . The error margin of the coefficients is estimated to be of the order of 10%. The ratio of the two conductances is thus universal in the diffusive regime where the offset can be neglected. As a consequence, the width of the curvature distribution is related to  $g_d$  and the rescaled distribution  $g_d P(\frac{c_n}{\Delta})$  should be a universal function of  $\frac{c_n}{\Delta g_d}$ . Similar relations have been reported earlier, like in Ref. 4, where a linear relation between  $\frac{1}{\Delta} \langle |c_n| \rangle$  and  $\frac{1}{\Delta^2} \langle i_n^2(\frac{1}{4}) \rangle$  was found.

## Conclusions

We examined various measures of the flux sensitivity of spectra of diffusive mesoscopic systems using numerical simulations and RMT description. We found that  $P_0(c_n(0))$  decays as  $1/c_n^3(0)$  for large curvatures, leading to a diverging second moment.  $P_0(c_n(0))$  is identical to the curvature distribution in the pure GOE case.  $P_\varphi(c_n(\varphi))$  with  $\varphi_c \ll \varphi \ll \frac{1}{2}$  is identical

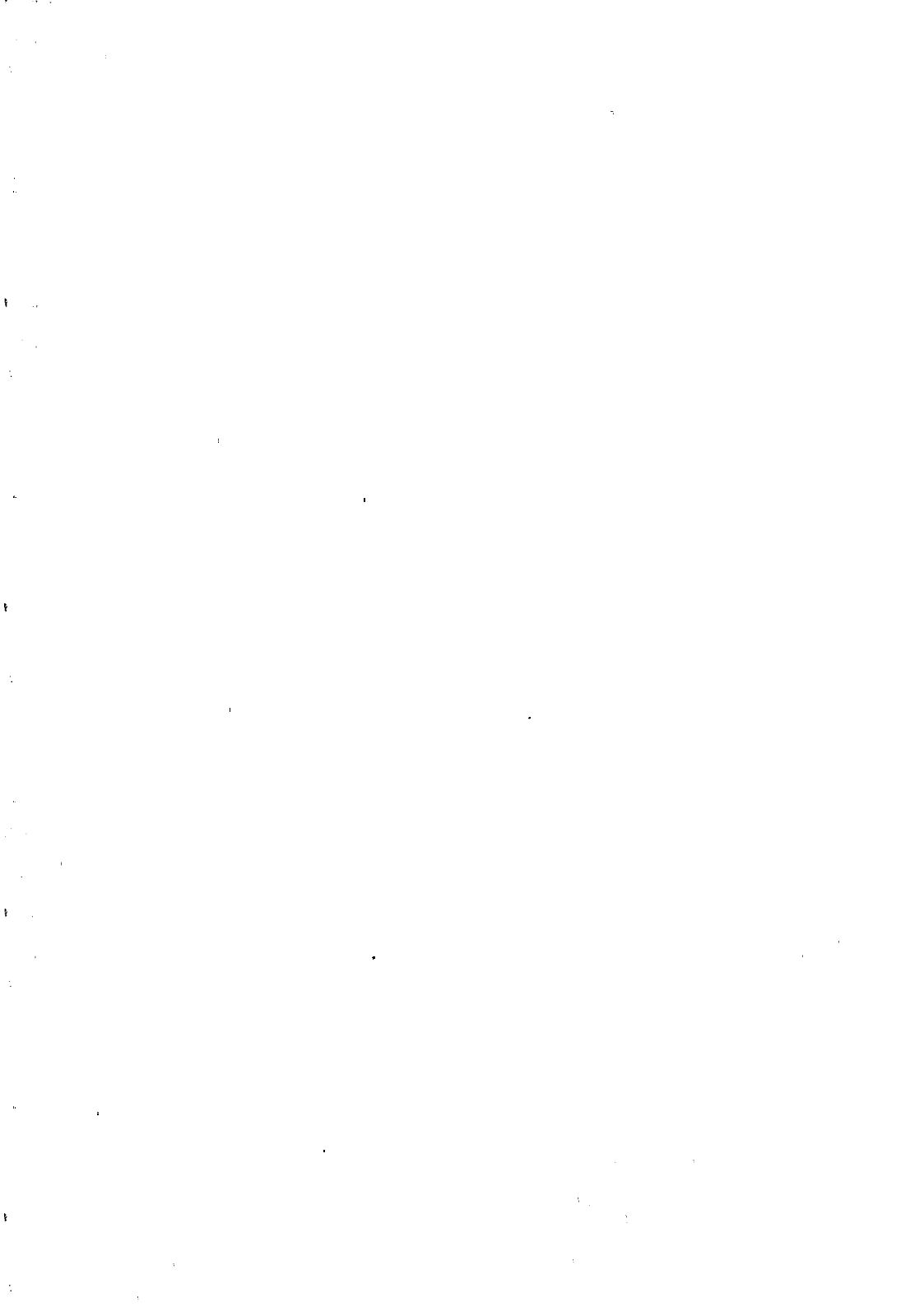
to the one of the pure GUE case. For  $0 < \varphi \ll \varphi_c$ ,  $P_\varphi(c_n(\varphi))$  has Gaussian tails, leading to a finite second moment of the curvature distribution. We also showed that the current correlation function  $C(\varphi, \varphi')$  has a logarithmic low-flux behavior. This function becomes universal after appropriate rescaling. A logarithmic low-flux behavior was also found for the single level current auto correlation function  $C(\varphi)$  introduced in Ref. 15. Finally, a universal linear relationship between  $\frac{1}{\Delta} \langle |c_n(0)| \rangle$  and  $\frac{1}{\Delta^2} \langle \overline{i_n^2(\varphi)} \rangle$  was found.

*Acknowledgments:* We have benefitted from many helpful discussions with E. Akkermans, H. Bouchiat, Y. Gefen and B. Shklovskiĭ. Numerical calculations were performed on the CRAY computer of the Centre de Calcul Vectoriel pour la Recherche at Palaiseau. This work was supported in part by the EC Science program under grant number SSC\_CT90\_0020. A.K. was partly supported by German-Israel Foundation (GIF) and U.S.-Israel Binational Science Foundation (BSF).

## References

- 1 E. Akkermans, and G. Montambaux, *Phys. Rev. Lett.* **68**, 642 (1992).
- 2 P. Gaspard, S.A. Rice, and K. Nakamura, *Phys. Rev. Lett.* **63**, 930, (1989); P. Gaspard, S.A. Rice, H.J. Mikeska, and K. Nakamura, *Phys. Rev. A* **42**, 4015, (1990).
- 3 J. Zakrzewski, and D. Delande, *Phys. Rev. E* **47**, 1650, (1993).
- 4 K. Życzkowski, L. Molinari, F.M. Izrailev: preprint; G. Casati, I. Guarneri, F. M. Izrailev, L. Molinari, K. Życzkowski: preprint
- 5 D. Saher, F. Haake, *Phys. Rev. A* **44** 7841 (1991)
- 6 D. Delande, J. Zakrzewski: preprint
- 7 M. L. Mehta, "Random Matrices", second edition, *Academic Press, New York*, 1991.
- 8 A. Pandey and M. L. Mehta, *Commun. Math. Phys.* **87**, 449 (1983); J. B. French, V. K. Kota, A. Pandey, S. Tomsovic, *Ann. Phys.* **181**, 198, (1988).
- 9 K. B. Efetov, *Adv. Phys.* **32**, 53 (1983).
- 10 B. L. Al'tshuler, B. I. Shklovskiĭ, *Sov. Phys. JETP* **64**, 127 (1986).

- 11 N. Dupuis, and G. Montambaux, Phys. Rev. B **43**, 14390 (1991).
- 12 J.T. Edwards, D.J. Thouless, J. Phys. C **5**, 807 (1972); D.J. Thouless, Phys. Rep. **13 C**, 95 (1974); D.J. Thouless, Phys. Rev. Lett. **39**, 1167 (1977).
- 13 B. D. Simons, B. L. Al'tshuler, Phys. Rev. B **48**, 5422 (1993).
- 14 Y. Hatsugai, and P. A. Lee, Phys. Rev. B **48** 4204 (1993); Y. Imry in *Quantum Coherence in Mesoscopic Systems*, ed. B. Kramer, NATO ASI Series, Plenum Press (1991)
- 15 A. Szafer, and B. Altshuler, Phys. Rev. Lett **70**, 587 (1993).
- 16 A. Kamenev, D. Braun, to be published in Journal de Physique (Paris)
- 17 D. Braun and G. Montambaux, to be published
- 18 In principle, an AB flux is only equivalent to the simple form  $\psi(x+L, y, z) = e^{i2\pi\varphi}\psi(x, y, z)$  of the change of boundary conditions for quasi-1D samples. In higher dimensions the phase-shift induced by an AB flux depends not only on  $\varphi$  but also on the radial coordinate. In our simulations we did not include this radial dependence of the phase shift for 2D or 3D samples, which amounts to neglecting the curvature of the samples.
- 19 Note that our definition of  $\varphi_c$  differs by a factor  $1/\sqrt{2}$  from the one given in Ref. 16.
- 20 H. Bouchiat, G. Montambaux, D. Sigeti, Phys. Rev. B **44**, 1682 (1991)
- 21 Note added: When preparing the manuscript we received a preprint of F. von Oppen, who calculates the whole distribution function for the pure GUE case, confirming the conjecture by Delande et al. (Ref. 3).



# Spectral Correlations in Diffusive and Ballistic Systems

Alexander Altland, Institut für theoretische Physik,  
Zülpicher Straße 77, D-50937 Köln, Germany

## Abstract

Spectral correlations exhibited by disordered but non-interacting systems are analyzed in terms of the two level correlation function ( $Y_2$ ) and the fluctuation of the number of levels contained in energy intervals of given width  $E$  ( $\Sigma_2$ ). The analysis extends to non-diffusive regimes, including  $E$  larger than the inverse elastic scattering time  $\hbar/\tau$  and ballistic (but not perfectly clean) systems. It is shown that ballistic systems show a variety of inequivalent spectral correlations which necessitate the definition of different correlation functions. The relevance of this observation for the calculation of physical observables is discussed.

## 1 Introduction

The quantum mechanical spectra of *diffusive* metallic systems exhibit strong correlations which are responsible for a large variety of mesoscopic fluctuation phenomena. Among these are persistent currents [1], universal conductance fluctuations [2] or anomalously large diamagnetic susceptibilities [3, 4] just to mention a few of the most prominent examples. Recently it has been shown [5] that the correlation functions characterizing the statistical properties of these systems contain even information about the time evolution of individual charge carriers, thus providing an efficient tool to interpret seemingly complex mesoscopic effects in terms of elementary physical concepts. In consideration of these facts, it is natural to ask, whether spectral correlations are of relevance for the physics of *ballistic* mesoscopic systems too, but most surprisingly this question has not been adressed so far.

A reason for this ignorance may be that the elastic mean free path  $l$  characterizing the disorder strength in a given mesoscopic system is often interpreted in a too naive sense, i.e. as the “typical spacing between neighboring scatterers”. This identification implies that disorder is inessential or may at least be treated perturbatively once the system size  $L$  is smaller than  $l$ . In order to refute this assumption one may compare the clean system’s level spacing  $\Delta$  with the size of a typical disorder matrix element  $M := \langle k|V|k' \rangle$  taken between electronic states  $|k\rangle, |k'\rangle$  at the Fermi energy. Modeling the disorder by short range scatterers, one easily obtains

$$\frac{|M|^2}{\Delta^2} \sim \frac{L}{l} (p_F L)^{d-1}, \quad (1)$$

i.e. even if  $L \simeq l$ , the disorder matrix element exceeds the level spacing by a large factor  $(p_F L)^{d-1}$ . From this observation, one may conclude that (i) disorder in ballistic systems must generally not be treated perturbatively, whence it can be expected that (ii) it is capable of inducing strong spectral correlations in these systems, too. (iii) It makes sense to define a class

of "perturbative" systems by the condition  $L < l_p := p_F^{-1}(lp_F)^{1/d} \ll l$  [6]. Systems of this size are nearly clean in the sense that disorder may indeed be regarded as a small perturbation.

Before turning to the concrete analysis of spectral correlations in the ballistic case, it is worthwhile to classify all regimes with expectedly different spectral properties. For the sake of completeness, I will include the diffusive regime in this discussion as well. As long as no magnetic fields are taken into account, the various regimes may be classified with respect to two parameters, length and energy. Considering a completely idealized mesoscopic system at zero temperature and with no dephasing, the following length and energy scales are of relevance ( $\hbar = 1$ ):

*Length scales:*

$L$ : The size of the system.

$\xi$ : The localization length (localization always occurs in systems of dimensionality  $d \leq 2$  or, otherwise, for sufficiently strong disorder).

$l$ : The elastic mean free path. For "soft" scattering potentials one has to distinguish between the mean free path between subsequent scattering events, and the (longer) scale characterizing the randomization of the particle's original momentum, the latter is of relevance for transport coefficients.

$\lambda_F$ : The Fermi wave length (the inverse Fermi momentum,  $\lambda_F \equiv 2\pi p_F^{-1}$ ). Unless we are in the strong disorder limit the inequality  $p_F l \gg 1$  holds.

*Energy scales:*

$E_F$ : The Fermi energy

$\tau^{-1}$ : The inverse elastic mean free time. Similarly to our preceding remarks one may distinguish between the elastic scattering time and the transport mean free time  $\tau_t$ .

$t_F^{-1}$ : The inverse time of flight of electrons at the Fermi energy through a ballistic system,  $t_F^{-1} \equiv v_F L^{-1}$ . Here  $v_F$  is the Fermi velocity.

$E_c$ : The Thouless (or correlation) energy,  $E_c = DL^{-2}$ , equal to the inverse diffusion time through a diffusive system.

$\Delta$ : The mean level spacing at the Fermi energy.

Combining length and energy to a two-dimensional parameter space, one obtains sort of a phase diagram which is displayed in fig.1. In the diffusive ( $l < L < \xi$ ) and ballistic ( $l_p < L < l$ ) case one obtains respectively three regimes, denoted by  $Di$  and  $Bi$ ,  $i = 1, 2, 3$ , resp., with different spectral behaviour. To understand the physical meaning of these regimes, it is essential to know the connection between spectral statistics and the *dynamics* of electrons [5]: In a sense to be precised a few paragraphs further down, spectral correlations over a given energy range  $\omega$  contain information about the probability that an electron released somewhere in the system returns to its initial phase space coordinates after times  $1/\omega$ . In consideration of this fact, the different regimes may be interpreted as follows:

*Diffusive systems:*

$D1$ :  $\omega < E_c$ . Time scales larger than the inverse diffusion time  $E_c^{-1}$  are probed. As a consequence, the system behaves fully ergodic and can be described in terms of random matrix theory.

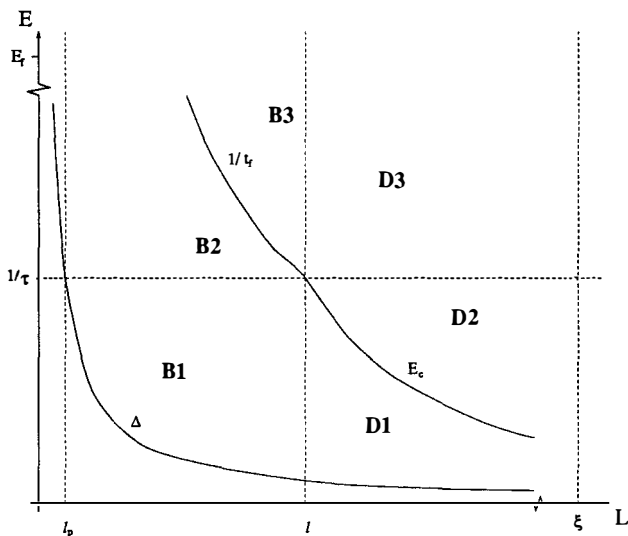


Figure 1: On the definition of regimes with different spectral statistics. Explanation, see text.

**D2**:  $E_c < \omega < 1/\tau$ . Corresponds to time scales larger than the scattering time, but smaller than the inverse diffusion time; electrons move diffusively but do not yet feel the presence of the system's boundaries.

**D3**:  $\omega > 1/\tau$ . The electron motion is no longer diffusive but governed by only a few impurity scattering events.

*Ballistic systems:*

**B1**:  $\omega < 1/\tau$ . The same what was said under **D1** applies.

**B2**:  $1/\tau < \omega < 1/t_f$ . Corresponds to times larger than the time of flight through the system but smaller than the scattering time, i.e. electrons bounce multiply off the boundaries but not significantly off impurities. The system geometry is of relevance in this regime.

**B3**:  $\omega > 1/t_f$ . The motion is fully ballistic.

## 2 Quantitative Analysis

In most cases the probability distribution of the energy eigenvalues is unknown and one has to characterize the spectrum in terms of correlation functions. Here I will restrict myself to the discussion of the two functions

$$\begin{aligned}
 Y_2(\omega) &= \frac{1}{\nu^2} \langle \nu(E_0 + \omega) \nu(E_0) \rangle - 1, \\
 \Sigma_2(E) &= \Delta^{-2} \int_{E_0 - E/2}^{E_0 + E/2} d\epsilon_1 d\epsilon_2 Y_2(\epsilon_1 - \epsilon_2), \quad E_0 = \mathcal{O}(E_f),
 \end{aligned} \tag{2}$$

where the angular brackets denote a configurational averaging over the disorder and  $\nu := \langle \nu(E_0 + \omega) \rangle \simeq \langle \nu(E_0) \rangle$ . The reason for this choice is that (i) these functions play the by far most important role for practical calculations in the field of mesoscopic physics (cf. Refs. [1, 2, 3] and references cited therein) and (ii) the Fourier transform of  $Y_2$ ,  $Y_2(t)$  establishes the above mentioned correspondence to the return probability via the equation [5]

$$Y_2(t) \propto tP(t). \tag{3}$$

Precisely speaking,  $P(t)$  is the probability for a classical particle released at time  $t = 0$  somewhere in the system to return to its initial *phase space* coordinates after time  $t$ , averaged over all initial coordinates. As is obvious from their definition, the functions  $Y_2$  and  $\Sigma_2$  measure correlations in the density of states at different energies and the fluctuation in the number of energy levels contained in an interval of width  $E$ , resp.

In a seminal paper [2], Altshuler and Shklovskii have analyzed these two correlation functions for regimes *D1* and *D2* by means of diagrammatic perturbation theory. In the following I will sketch a generalization of the approach taken in ref. [2] which yields  $Y_2$  and  $\Sigma_2$  for *all* above mentioned regimes simultaneously. Details of the derivation can be found in ref. [7] and readers who are not interested in technicalities are invited to turn directly to the final result Eqs.(9) and (10).

To begin with the density of states is represented in a somewhat unusual fashion as

$$\nu(\epsilon) = -\frac{1}{\pi} \partial_\epsilon \Im \text{tr} \ln \mathcal{G}^+(\epsilon), \tag{4}$$

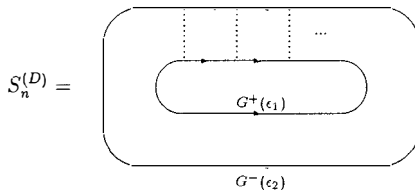
where  $\mathcal{G}^+(\epsilon) = (\epsilon^+ - H)^{-1}$  is the single electron Green function,  $H = H_0 + V$  the system's Hamiltonian,  $H_0 = p^2/(2m)$ ,  $V$  the disorder potential and  $\epsilon^\pm = \epsilon \pm i\gamma$ ,  $\gamma = \mathcal{O}(\Delta)$ . The width  $\gamma$  has to be introduced in order to cut off unphysical divergences appearing in diagrammatic analyses for small values  $\omega < \Delta$ . To study correlations on these scales one has to resort to non-perturbative techniques, e.g. supersymmetry[8]. As long as  $\omega > \Delta$ , the smearing  $\gamma$  is inessential (see below). Most regimes are universal in the sense that results do not depend on microscopic details of the disorder. To be specific, one may model it by a white noise potential

$$\begin{aligned} \langle V(x) \rangle &= 0, \\ \langle V(x)V(y) \rangle &= \frac{1}{2\pi\nu\tau} \delta(x - y). \end{aligned} \tag{5}$$

The effect of different types of disorder will be discussed below. Expanding Eq. (4) in powers of  $V$  and taking only diagrams with avoided crossings of impurity lines, i.e. diagrams of leading order in  $pFl$  into account, we are led to the result

$$Y_2(\omega) = -\frac{\Delta^2}{\pi^2} \partial_\omega^2 \Re \sum_{n=2}^{\infty} \frac{1}{n} S_n^{(D)}(\omega). \tag{6}$$

The quantities  $S_n^{(D)}$  can be represented diagrammatically as



where the inner and the outer ring are mutually connected by  $n$  impurity lines. The solid arrows represent impurity averaged Green functions:

$$\underline{\overset{x}{\leftarrow} \langle \mathcal{G}^\pm \rangle \overset{x'}{\rightarrow}} = \langle \mathcal{G}^\pm(\epsilon; r, r') \rangle =: G^\pm(\epsilon; r, r') = \left\langle r \left| \left( \epsilon \pm \frac{i}{2\tau} - H_0 \right)^{-1} \right| r' \right\rangle. \quad (8)$$

Depending on the regime under consideration the evaluation of the diagrams  $S_n^{(D)}$  may or may not depend on the system's geometry. Specializing the analysis to the relatively simple case of a *two-dimensional square geometry* one obtains [7]:

$$\begin{aligned} Y_2(\omega) &= \frac{\Delta^2}{\pi^2} \partial_\omega^2 \Re \sum_q \hat{\ln}(1 - \lambda(q, \omega)), \\ \Sigma_2(E) &= \frac{1}{\pi^2} \Re \sum_q 2 \left( \hat{\ln}(1 - \lambda(q, E)) - \hat{\ln}(1 - \lambda(q, 0)) \right), \end{aligned} \quad (9)$$

where  $\sum_q$  is an abbreviation for the summation over all values of the two-dimensional vector  $\vec{q}^T = \pi L^{-1}(n_1, n_2)$ ,  $n_i = 0, 1, \dots$ ,  $q = |\vec{q}|$ ,  $\hat{\ln}(1+x) = \ln(1+x) - x$  and

$$\lambda(q, \omega) = \left( (1 - \gamma\tau + i\omega\tau)^2 + (ql)^2 \right)^{-\frac{1}{2}}. \quad (10)$$

In the following, I will briefly discuss the results obtained by evaluating Eqs. (9) approximately in the various regimes.

*Diffusive systems:*

D1: Retaining only the most important  $q = 0$  contribution to the sums appearing in Eqs. (9) one gets

$$\begin{aligned} Y_2(\omega) &= \frac{\Delta^2}{\pi^2} \frac{\gamma^2 - \omega^2}{(\gamma^2 + \omega^2)^2} \\ \Sigma_2(E) &= \frac{1}{\pi^2} \ln \left( \frac{E^2 + \gamma^2}{\gamma^2} \right) \end{aligned} \quad (11)$$

in agreement with results obtained for the Gaussian Orthogonal Ensemble of random matrix theory[2].

D2: Order of  $(L/l)^2 \gg 1$  modes contribute. An approximation of the sum over  $\vec{q}$  by an integral, leads to [2]

$$\begin{aligned} Y_2(\omega) &\simeq \frac{2(\Delta\tau)^2}{\pi} \left( \frac{L}{2\pi l} \right)^2 \ln(\omega\tau) \\ \Sigma_2(E) &\simeq \left( \frac{L}{2\pi l} \right)^2 E\tau. \end{aligned} \quad (12)$$

D3: Here the diagram  $S_2^{(D)}$  involving only two impurity scattering events gives the most important contribution. This reflects the fact that we are probing trajectories shorter than the elastic mean free path. The result obtained for  $S_2^{(D)}$  depends crucially on the microscopic features of the disorder potential  $V$ . A calculation based on a white noise potential, results in

$$\begin{aligned} Y_2(\omega) &= -\frac{1}{2\pi} \left( \frac{L}{2\pi l} \right)^2 \frac{\Delta^2}{\omega^2} \\ \Sigma_2(E) &= \frac{1}{2\pi} \left( \frac{L}{2\pi l} \right)^2 \left( \ln(E\tau) + \frac{3}{2} \right), \end{aligned} \quad (13)$$

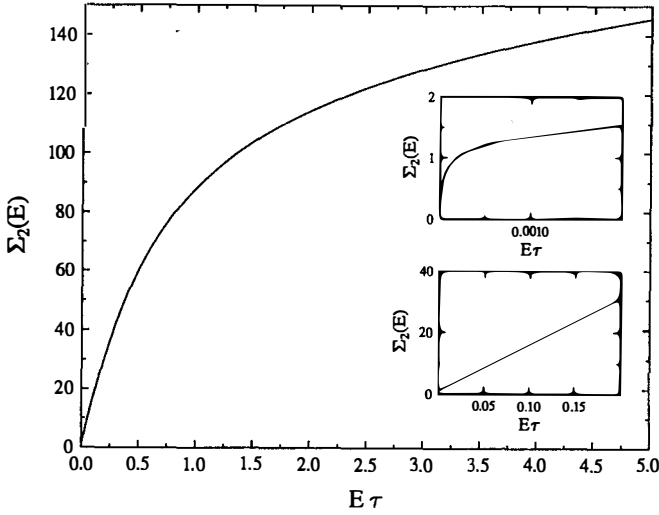


Figure 2:  $\Sigma_2(E)$  in the diffusive case ( $p_F l = 100$ ,  $L/l = 100$ ,  $d = 2$ )

i.e. a logarithmically increasing result for  $\Sigma_2$ . In the case of a potential with finite correlation length  $a > p_F^{-1}$ , however,  $\Sigma_2$  saturates at a constant which is parametrically of the order of  $\Sigma_{2, \text{whitenoise}}(1/\tau_{\text{tr}})$ . Thus, one may conclude that the large energy behaviour of the correlation functions depends non-universally on microscopic details. Note, however, the existence of a general sum rule [9] which enforces that  $\Sigma_2(E)/E \xrightarrow{E \rightarrow \infty} 0$ .

A plot of  $\Sigma_2$  for a square of size  $L = 100l$  is shown in fig.2.

*Ballistic Systems:*

B1: Again, the zero mode  $q = 0$  dominates whence we obtain the same result as in D1: *On time scales longer than  $1/\tau$ , the presence of disorder leads to complete ergodicity, even though the system is ballistic.*

B2: In this regime the motion is indeed ballistic. Still the  $q = 0$  mode dominates and we obtain

$$Y_2(\omega) = \frac{3\Delta^2}{2\pi^2\tau^2} \frac{1}{\omega^4},$$

$$\Sigma_2(E) = -\frac{2}{\pi^2} \ln(\gamma\tau) - \frac{1}{2\pi^2} \frac{(E\tau)^2}{1 + (E\tau)^2}. \quad (14)$$

B3: As soon as  $\omega$  becomes comparable with  $1/t_f$ ,  $q \neq 0$  modes contribute to the sum in Eq. (9). Replacing the summation by an integral we obtain the same asymptotic behaviour as in D3 (and the same what was said there concerning non-universality applies). A close look at Eqs. (9), however, reveals that an approximation of  $\Sigma_q$  by an integral is a poor approximation. Fortunately the sum converges rapidly and can easily be computed

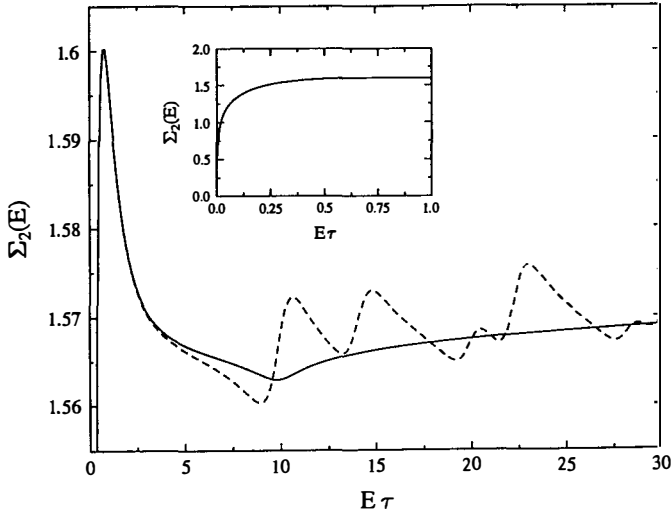


Figure 3:  $\Sigma_2(E)$  in the ballistic case ( $pFl = 10^4$ ,  $L/l = 0.1$ ,  $d = 2$ ).

numerically. As a result one obtains fluctuations with typical period  $1/t_f$  around the integral approximation (cf. fig.3). These fluctuations can be interpreted semiclassically [10] as due to periodic orbits bouncing off the system boundaries. Needless to say that they depend non-universally on the geometry.

The different types of spectral correlations discussed above (regimes  $D1, \dots, B3$ ) have recently been observed numerically by direct diagonalization of the Hamiltonian representing a  $64 \times 64$  disordered tight binding lattice [11]. Having obtained these results, one might be tempted to proceed and apply them directly to the calculation of physical observables. As will be explained in the following section, however, this may lead to incomplete or even wrong results if the systems under consideration are ballistic.

### 3 Novel Types of Spectral Correlations in Ballistic Systems

In order to understand the statement made in the last paragraph of the preceding section, one has to step back and review the whole concept of spectral correlations in mesoscopic physics. The point is that there is a lot of *freedom in the averaging procedure* necessary to characterize correlations between levels. As is indicated in fig.4, one may e.g. take two energy levels at fixed positions  $E$  and  $E + \omega$ , resp., and average over all microscopic disorder configurations; this procedure leads to the correlation function  $Y_2 \equiv Y_2^d$  which has been discussed so far. Alternatively one may average over  $E$  but keep the disorder configuration fixed, thereby arriving at another correlation function  $Y_2^E$ . A third possibility is to generate a function  $Y_2^H$  by averaging over an external magnetic field for fixed  $E$  and disorder. In fact, the situation is even more difficult, as all sorts of combined averaging procedures can be applied. As long as one is concerned with diffusive systems these ambiguities in the averaging procedures do not cause

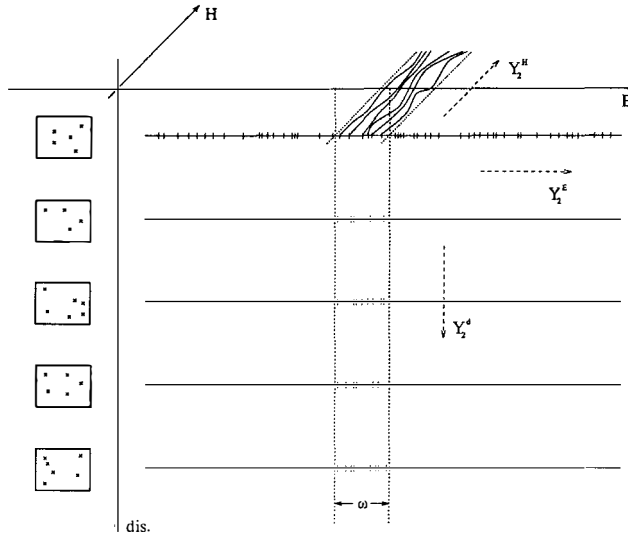


Figure 4: On the existence of different spectral correlation functions in mesoscopic physics. Explanation, see text.

problems since there is a well established ergodicity hypothesis (cf.e.g.Ref. [12]) stating that  $Y_2^d = Y_2^E = Y_2^H$ , at least in regimes  $D1$  and  $D2$ . In the ballistic regime, however, the situation is much more complex: Even in the field free case,  $H = 0$ , there exist qualitatively different types of spectral correlations. This phenomenon is due to *fluctuations in the disorder averaged density of states*: Consider the general expression for the disorder averaged density of states of a two-dimensional square

$$\langle \nu(E_F) \rangle = \frac{1}{\pi L^2} \Im \langle \text{tr} (G^-(E_F)) \rangle \simeq \frac{m}{\pi L^2 p_F l} \sum_p \frac{1}{(p - p_F)^2 + (2l)^{-2}}, \quad (15)$$

where the last equation is valid up to corrections in  $1/(E_F \tau) \ll 1$ . Eq. (15) means that the density of states is given by the number of discrete  $p$ -modes contained in a ring of width  $\sim l^{-1}$  and radius  $p_F$ . In the diffusive regime, the ring's width exceeds the inter-mode spacing  $\sim L^{-1}$ , whence the sum can be approximated by an integral resulting in a constant density of states  $\langle \nu(E_F) \rangle \equiv \bar{\nu} = m/(2\pi)$ . In the ballistic case, however, the number of captured modes and thereby the density of states fluctuate as functions of  $p_F$  or equivalently as functions of  $E_F$ . These fluctuations can be described quantitatively in terms of the function

$$Y_2'(\omega) \equiv \frac{1}{\bar{\nu}^2} \langle \langle \nu(E + \omega) \rangle \langle \nu(E) \rangle \rangle - 1, \quad (16)$$

where  $\langle \nu(E) \rangle$  is given by Eq. (15) and  $\langle \dots \rangle_{E_0}$  denotes averaging over a sufficiently large ( $\gg t_f^{-1}$ ) energy interval. Note that this object is an example of a correlation function employing composite averaging procedures. The calculation of  $Y_2'$  is detailed in ref. [7] and results in

$$Y_2'(\omega) = \frac{1}{\pi} \sum_{k \neq 0} \frac{1}{p_F L_k} e^{-L_k/l} \cos \left( \frac{L_k}{v_f} \omega \right), \quad (17)$$

where  $L_k = 2L\sqrt{k_1^2 + k_2^2}$ ,  $k_i = 0, \pm 1, \dots$  and  $\sum_k$  is an abbreviation for the summation over all tuples  $(k_1, k_2) \neq (0, 0)$ . For small energies  $\omega t_f^{-1}$ , the sum may be approximated by an integral leading to

$$Y_2'(\omega) \stackrel{\omega \ll t_f^{-1}}{\simeq} \frac{2}{\rho F l} e^{-\frac{L}{l}} \frac{1}{\left(\frac{L}{l}\right)^2 + (\omega t_f)^2}. \quad (18)$$

Note the presence of the damping term  $\exp(-L/l)$  expressing the irrelevance of  $Y_2'$  in the diffusive regime.

Besides  $Y_2$  and  $Y_2'$  various other correlation functions characterizing different types of fluctuations may be defined [7]. One thus encounters a relatively complex scenario of various inequivalent types of correlations, and may ask how to apply the concept of spectral statistics to the calculation of physical observables in the ballistic regime. This question will be adressed in the final section.

## 4 Applications and Conclusive Remarks

How does one use the theory presented in the preceding sections in physical applications? In many cases one is concerned with expressions of the type

$$\int_0^{E_F} d\epsilon d\epsilon' \langle \nu(\epsilon, \dots) \nu(\epsilon', \dots) \rangle, \quad (19)$$

where the dots indicate a possible dependence of  $\nu$  on other parameters, most typically external magnetic fields. The correlator Eq. (19) appears e.g. in the calculation of averaged and typical persistent currents [1], orbital susceptibilities [3, 4] or conductance fluctuations [2]. At least, it may serve as fairly general example for the present discussion. At first sight, it may seem that the formalism discussed above, being restricted to correlations on energy scales  $\ll E_F$ , is inapplicable to the analysis of Eq. (19) since both energy arguments  $\epsilon_i$  are integrated independently over the whole range  $0, \dots, E_F$ . This, however, is not the case. In all cases of interest, it turns out that only the region  $\epsilon_i \simeq E_F$  contributes significantly to the integral in Eq. (19) (which is a consequence of a sum-rule mentioned in the discussion of regime *D3*).

The answer to the question raised in the final section of the preceding section may now be formulated as follows: The type of correlation functions entering the calculation of expressions like Eq. (19),  $Y_2^d, Y_2^E, Y_2^H$  or functions involving multiple averages like  $Y_2'$ , is uniquely prescribed by the modelling of the averaging procedure  $\langle \dots \rangle$ . Even if no averages over external parameters like magnetic fields are involved,  $\langle \dots \rangle$  need not at all correspond to a simple average over a random potential. Individual samples belonging to an array of mesoscopic systems, for instance, do not only differ in the distribution of microscopic scatters but also in their size. Thus, even if the samples appear to be macroscopically identical, one has to perform a simultaneous average  $\langle \dots \rangle_{\text{dis., sampl. siz.}}$  over the disorder configuration and the system size. In reality, the sample size fluctuations may be of the order of a few percent but for the present discussion it suffices to allow for fluctuations on atomic scales. The important point is that sample size fluctuations bring other correlation functions besides  $Y_2^d$  into play. To see this, one has to know two properties of the combined average: (i) Sample size and disorder average can be regarded as approximately statistically independent [7], i.e.  $\langle \dots \rangle_{\text{dis., sampl. siz.}} \simeq \langle \langle \dots \rangle_{\text{dis.}} \rangle_{\text{sampl. siz.}}$ . (ii) The sample size average is equivalent to an average over the Fermi energy [7]. Qualitatively, the last point is evident from the remarks made in connection with Eq. (15): Instead of changing the radius of the Fermi sphere (energy-averaging) one may quench or stretch the lattice of discrete  $p$ -modes (sample

size averaging); both procedures lead to the same fluctuations in the disorder averaged density of states. Knowing these two properties, it is easy to see that

$$Y_2^{\text{ens}} = Y_2^d + Y_2' \quad (20)$$

where  $Y_2^{\text{ens}}$  denotes the density of states correlation function calculated with respect to the realistic ensemble average  $\langle \dots \rangle_{\text{dis.,sampl.size}}$ ,  $Y_2^d$  is the disorder correlation function which has been discussed in the first sections (an has been simply denoted by  $Y_2$  there) and  $Y_2'$  has been defined in the previous section. The appearance of the correlation function  $Y_2'$  upon sample size averaging has been recently been observed numerically by analyzing the spectra of tight binding lattices of slightly different size [11].

In the general case with account for magnetic fields, it may happen that more complex combinations of correlation functions appear. At this point it may be appropriate to mention that magnetic fields applied to ballistic systems are notoriously difficult to handle within the Green function approach taken here. Even in simple cases like homogeneous fields applied to a square geometry one has to resort to semiclassical techniques [13]. Thus, very little can be said about the field dependence of spectral correlations exhibited by ballistic systems in general. The important exception are Aharonov-Bohm (AB) geometries: It turns out that the present formalism, with account for magnetic fields, can straightforwardly be extended to the description of AB-cylinders. A detailed analysis will be published elsewhere [14]. In fact, it turns out that some long standing puzzles related to canonical persistent currents [1] in ballistic geometries are solved once correlation functions like  $Y_2'$  are taken into account.

In conclusion, it has been shown that disorder in ballistic systems induces strong spectral correlations and may thus play an important role in the analysis of various physical observables. On energy scales  $< 1/\tau$ , the spectrum is *fully chaotic* and can be described in terms of random matrix theory. This imposes constraints on the feasibility of quantum-chaos experiments intending to probe trajectories which exist the idealized, clean system's geometry: time scales larger than  $\tau$  cannot be probed due to the inevitable randomization of trajectories due to disorder scattering. The description of spectral correlations in ballistic systems turns out to be more complex than in the diffusive case since there exists a variety of inequivalent *types* of fluctuations. As for practical applications, however, the situation is not too confusing since the physically prescribed averaging procedure determines the proper choice of correlation functions uniquely.

## References

- [1] A.Schmid, Phys.Rev.Lett. **66**, 80 (1991); B.L. Altshuler, Y. Gefen and Y. Imry, Phys. Rev. Lett. **66**, 88 (1991); F.von Oppen, E.K.Riedel, Phys.Rev.Lett. **66**, 84 (1991).
- [2] B.L. Altshuler and B.I. Shklovskii, Sov. Phys. JETP **64**, 127 (1986).
- [3] B.L. Altshuler, Y. Gefen and Y. Imry and G.Montambaux, preprint; Y.Gefen, B.Reulet and H.Bouchiat, Phys.Rev.B **46**, 15922 (1992).
- [4] S. Oh, A. Yu. Zyuzin and R.A. Serota, Phys. Rev. B **44**, 8858 (1991); R.A.Serota and A.Y.Zyuzin, preprint.
- [5] N.Argaman, Y.Imry, U.Smilansky, Phys.Rev.B **47**, 4440 (1993).
- [6] U.Sivan and Y.Imry, Phys.Rev.B **35**, 6074 (1987).

- [7] A.Altland and Y.Gefen, Phys. Rev. Lett. **71**, 3339 (1993); to be published.
- [8] K.B.Efetov, Adv.Phys. **32**, 53 (1983).
- [9] B.L.Altshuler, A.Aronov, V.Kravtsov, I.V.Lerner. Phys.Rev.Lett. **72**, 888 (1994).
- [10] M.V.Berry Proc.Roy.Soc. London A 400 (1985).
- [11] A.Altland, R.Loosen, to be published.
- [12] P.A.Lee, D.Stone, H.Fukuyama, Phys.Rev.B **35**, 1039 (1987)
- [13] Y.Gefen, preprint; R.Jalabert, preprint; F.von Oppen, preprint.
- [14] A.Altland, Y.Gefen, G.Montambaux, in preparation.



**THERMODYNAMICS OF MESOSCOPIC SYSTEMS  
AND PERSISTENT CURRENTS**



## EXPERIMENTAL OBSERVATION OF PERSISTENT CURRENTS

C. Chapelier<sup>(1)</sup>, A. Benoit<sup>(2)</sup>, D. Mailly<sup>(3)</sup>.

*1-Servive de Physique Statistique, Magnétisme et Supraconductivité  
Centre d'Etudes Nucléaires de Grenoble-France*

*2-Centre de Recherche sur les Très Basses Températures  
Centre National de la Recherche Scientifique-Grenoble-France*

*3-Laboratoire de Microstructures et de Microélectronique  
Centre National de la Recherche Scientifique-Bagneux-France*

**Abstract**

We have detected the presence of persistent currents of about 4 nA in a mesoscopic single loop etched in a GaAs-GaAlAs heterojunction. For this purpose a dedicated device with an integrated DC-SQUID has been developed.

**1 INTRODUCTION**

The ground state energy of a mesoscopic normal-metal ring has been predicted in 1983 by Büttiker, Imry and Landauer <sup>1)</sup> to be a periodic function of the magnetic flux  $\Phi$  enclosed by the loop with a period  $\Phi_0 = h/e$ , the flux quantum. Following Byers and Yang <sup>2)</sup>, they showed that, due to the periodic boundary conditions imposed by the doubly connected geometry, the electron wavefunctions  $\Psi_n$ , the energy levels  $E_n$  and then any thermodynamical quantities such as the equilibrium magnetization, exhibit the same periodic dependance with  $\Phi$ . This can be seen as the consequence of persistent currents  $I_n = -\partial E_n / \partial \Phi$  carried by each electrons in the loop.

For a perfect one dimensional ring with a circumference  $L$  smaller than the phase coherence length  $L_\Phi$ , each successive energy level gives a contribution of opposite sign and the currents carried by every electrons almost cancel each other. The net current depends on the total number of electrons, but an order of magnitude of the amplitude is given by

$$I_0 = e v_F / L \quad (1)$$

where  $v_F$  is the Fermi velocity <sup>3</sup>).

Considerable theoretical work has since been devoted to a more realistic system, namely a disordered 3D ring <sup>4-6</sup>).

In the ballistic case, the effect of the finite transverse dimension  $L_y$  of the ring can be accounted for with a correcting factor  $\sqrt{M}$ , where  $M \propto k_F L_y$  is the number of independent channels and  $k_F$  is the Fermi wavevector. In the diffusive regime, the disorder introduces correlations between the energy levels and mixes the different channels. According to these early theoretical models, after averaging over all the microscopic configurations, the typical current in this regime is given by

$$I_{typ} = I_0 (l_e/L) = e/\tau_D \quad (2)$$

where  $l_e$  is the electronic mean free path and

$$\tau_D = L^2 / v_F l_e = L^2 / D \quad (3)$$

is the diffusive time along the ring perimeter.  $D$  is the one dimensional diffusion constant. Numerical simulations have also addressed the impurity scattering issue and showed that the typical current does not depend any longer on the number of channels <sup>7</sup>).

The first effect of a non zero temperature is to mix the contribution of different energy levels within an interval  $k_B T$  and to decrease exponentially the persistent current. Due to energy correlations, the scale of this decay is given by the Thouless energy  $E_C$ . The second influence of the temperature is to reduce the phase coherence length  $L_\Phi$  via phonon scattering. Here also, the current vanishes exponentially with  $L/L_\Phi$ .

## 2 PREVIOUS EXPERIMENTS

In 1990, L. Levy et al. <sup>8)</sup> reported the first experimental evidence of persistent currents in an ensemble of  $10^7$  Cu rings. Since these currents are sample specific the ensemble-averaging is not a trivial issue and it can be shown that the amplitude of the mean current is dominated by the even harmonics which give an always positive contribution <sup>9-11)</sup>. Actually, the persistent current period was found to be half a flux quantum and the mean current per ring measured was found to be  $3 \cdot 10^{-3} I_0$ .

More recently, the magnetization response of one single gold loop has been measured by Chandrasekhar et al. and the authors found a persistent current of about  $0.3$  to  $2 I_0$  <sup>12)</sup>. Both of these two results are more than an order of magnitude larger than the theoretical calculations in the diffusive regime. In order to understand these two experimental results and to solve the discrepancies with the theoretical models, a lot of work has been published to give a better description of the role of the disorder and to take into account the Coulomb interaction between electrons as well <sup>13-19)</sup>.

We report here magnetization measurements of a single loop fabricated from the two dimensional electron gas (2 DEG) of a high mobility GaAs-GaAlAs heterojunction. Contrary to the two preceding experiments, this is a very clean system near the ballistic regime, i.e.  $L \approx L\Phi$ .

## 3 EXPERIMENTAL SET-UP

Our device is fabricated by etching a GaAs-Ga<sub>0.7</sub>Al<sub>0.3</sub>As heterojunction grown by molecular beam epitaxy. The geometry is the following : 720 nm GaAs buffer layer, 24 nm undoped GaAlAs spacer layer, 48 nm Si doped GaAlAs and 10 nm undoped GaAs cap layer. When cooled down at liquid Helium temperature in the dark, the 2 DEG has an electron concentration  $n = 3.6 \cdot 10^{11} \text{ cm}^{-2}$  and a mobility  $\mu = 1.14 \cdot 10^6 \text{ cm}^2 / \text{V.s}$  which give a Fermi velocity  $v_F = 2.6 \cdot 10^5 \text{ m.s}^{-1}$ , a Fermi wavelength  $\lambda_F = 42 \text{ nm}$  and an elastic mean free path  $l_e = 11 \mu\text{m}$ . Weak localization experiments performed with 80  $\mu\text{m}$  long wires of different widths patterned in this 2DEG yield at T=0K a coherence length  $L\Phi = 25 \mu\text{m}$  and no observable spin-orbit scattering.

The mean free path and the electronic density evaluated by conductance measurements and Shubnikov-de-Haas oscillations are not significantly modified compared with the original 2 DEG and give a depletion length of the order of  $0.27 \mu\text{m}$ . These wires as well as the mesoscopic loop are fabricated in the following manner.

Electron beam lithography performed with a JEOL 5 DII on PMMA and a conventional liftoff technique are used to draw a Titanium mask before a 10 nm deep Argon ionic etching. The mask is then chemically removed. The mean diameter of the ring is  $2.7 \mu\text{m}$  (I.D.  $2 \mu\text{m}$ , O.D.  $3.4 \mu\text{m}$ ) and its arm width  $0.7 \mu\text{m}$  (see fig.1a). Because of the depletion this gives a real width of  $0.16 \mu\text{m}$ . Its electrical resistivity can be measured by a usual four-probe technique with the help of four leads also patterned in the 2DEG and ended with AuGeNi ohmic contacts.

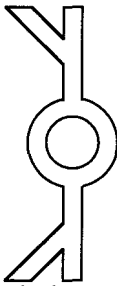


Fig.1a : etched mesoscopic loop.

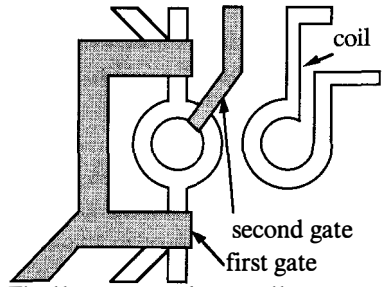


Fig.1b : gates and test coil.

A first Schottky gate in Gold is vapor-deposited on these wires. This allows to locally deplete the 2DEG by applying a negative electrostatic voltage and isolate a fixed number of electrons in the ring. A second gate is simultaneously deposited on one arm of the ring in order to open it and to destroy any quantum interference effect in the loop, such as the Aharonov-Bohm effect or the persistent currents. A test coil in Gold with the same geometry than the ring is also deposited nearby it (see fig.1b). The device is then covered with a 150 nm thick resist layer (AZ 1350) which plays the role of an electrical insulator.

On the top, an Aluminium DC-SQUID is patterned. This SQUID is composed of two counter-wound loops. The inner and outer diameters of each loop are  $2.3 \mu\text{m}$  and  $3.1 \mu\text{m}$ . One of them is superposed with the ring while the other one with two microbridge Josephson junctions is just above the test coil. Therefore it works like a magnetic gradiometer which in principle is insensitive to an uniform magnetic field.

Actually the lack of compensation is of a few percents. The previous attempts of measurements with a single loop SQUID and lithographed field coils have all been limited by current-induced field penetration in the superconductive films. It's the reason why we have built magnetic gradiometers and used an external coil to produce an uniform magnetic field. In order to connect the two loops without shortcutting them at the center of the device, the first lithographic level is made of two half loops (see fig.1c). An insulating layer is then spun (100 nm of AZ 1350) and the circuit is closed with the two opposite half loops (see fig.1d). The contact between the two aluminium layers is ensured by covering them with aluminium pads deposited after an Argon ionic etching has been performed in the same vacuum in order to remove the aluminium oxyde (see fig.1e). Each layer of this SQUID is made of 50 nm thick aluminium.

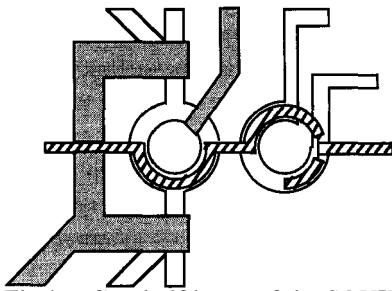


Fig.1c : first half loops of the SQUID.

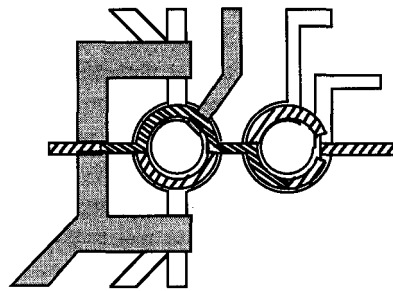


Fig.1d : second half loops.

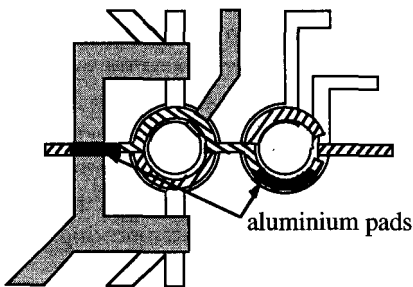


Fig.1e : electrical contacts between the two aluminium layers.

A detailed description of our SQUID and of our measurement method has already been given in Ref. 20. In summary, the two Dayem microbridges have a typical width of 30 to 50 nm, a thickness of 50 nm and a length of 200 nm. The critical currents  $I_C$  range from  $I_C = 10 \mu\text{A}$  to  $300 \mu\text{A}$  and the inductance  $L_S$  of the SQUID is typically a few pH. These values yield a  $\beta$  parameter close to one.

$$\beta = 2\pi L_S I_C / \Phi'_0 \quad (4)$$

where  $\Phi'_0 = h/2e$  is the superconductive quantum flux, and an optimum modulation of the critical current with the magnetic flux.

The sensitivity which is achieved is about  $S = 8 \cdot 10^{-6} \Phi'_0 / \sqrt{\text{Hz}}$ .

#### 4 MEASUREMENT METHOD

The key point of the method consists in measuring simultaneously the resistance and the susceptibility of the mesoscopic loop versus an external magnetic field while changing the voltage applied to the gate evaporated on the top of one of its arm. When this voltage is slightly positive (+40 mV), the ring is closed and exhibits quantum coherence effects such as Aharonov-Bohm oscillations, related to its doubly connected geometry. On the contrary, when the gate voltage is negative (-330 mV), the electron gas is depleted under it and this rotational symmetry is broken.

The device is cooled in a dilution fridge around 15 mK. The actual sensitivity of the SQUID is measured by sending a known current through the calibration coil. This allows to directly convert its critical current in terms of current in the ring. Then, an external magnetic field of +/- 2.1 mT corresponding to  $4 \Phi_0$  in the ring is swept. The modulation is triangular at a frequency of 0.1 Hz to avoid heating by eddy currents. The response of the SQUID is measured synchronously (see fig.2). The main part of the signal is due to the lack of compensation of the gradiometer, but doesn't depend on the voltage of the gate. Therefore it can be easily removed by subtracting a measurement when the ring is closed to another one with the ring open. Then it remains only the magnetization signal of the mesoscopic ring (see fig.3).

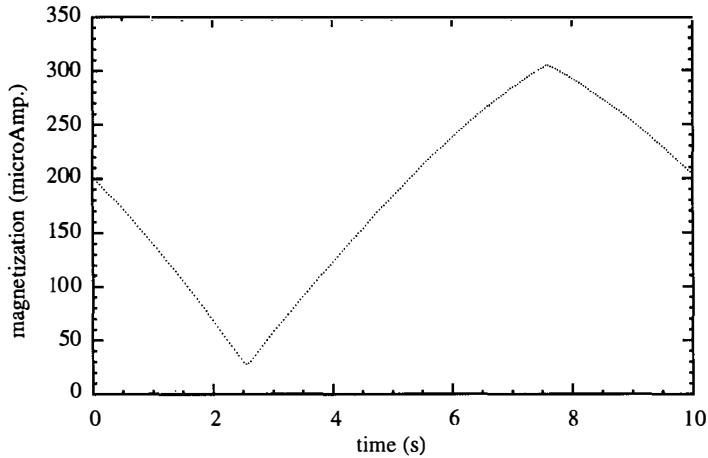


Fig. 2 : Response of the gradiometer to a uniform time dependent magnetic field. The modulation is triangular between  $\pm 2$  mT at 0.1 Hz. The magnetization is converted in equivalent current in the mesoscopic loop after calibration with the test coil.

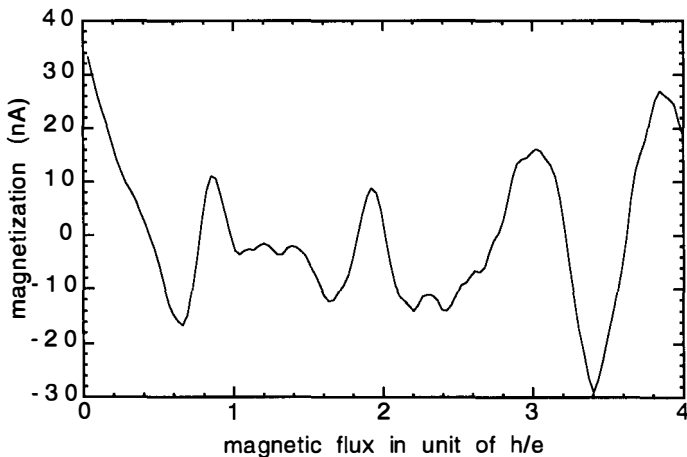


Fig. 3 : Magnetization of the mesometer of the loop given in equivalent persistent current after subtraction of the non compensated signal of the gradiometer. The field is calibrated in quantum flux with an arbitrary origin.

It should be emphasized that the signal displayed in figure 3 is one of the strongest ever measured. Usually the component of the magnetization at the frequency  $h/e$  is only visible after averaging several Fourier transformed signals.

A dc current of 1.5 nA is supplied to the ring and the voltage is recorded in order to measure its magneto-resistance whose mean value is around  $1 \text{ k}\Omega$ . When the ring is closed, the observation of the Aharonov-Bohm oscillations allows us to check the electronic temperature and the coherence of the mesoscopic loop (see fig.4). Although our SQUID is directly coupled without any pick-up coil, it seems that neither the current injected in it nor the Josephson oscillations affect the ring since no related modifications of the Aharonov-Bohm oscillations have been observed.

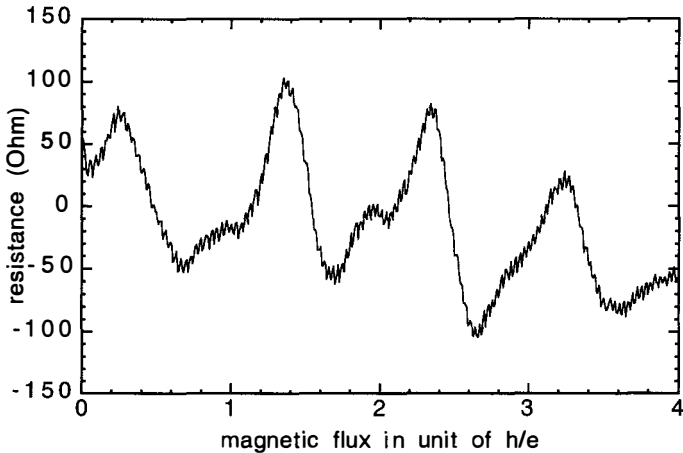


Fig. 4 : Aharonov-Bohm signal. The variation of the resistance is given in Ohm after subtraction of an offset.

The magnetization and the resistance signals are both extracted by Fourier transform of the difference between measurements with the ring open or closed, while the noise is evaluated from differences between measurements with the ring always open.

## 5 EXPERIMENTAL RESULTS

Typical results are presented in figure 5 for the magneto-resistance of the ring and in figure 6 for its susceptibility. In both cases, the vertical scale is the squareroot of the spectrum power, expressed respectively in the equivalent resistance fluctuations in Ohm and in equivalent persistent currents in nA. Our modulation of  $4 \Phi_0$  gives a pitch of  $1/4 \Phi_0$  for the horizontal scale. When the ring is closed, clear Aharonov-Bohm oscillations with a period  $h/e$  and their first harmonic ( $h/2e$ ) allow us to calibrate the magnetic flux in it. The width of the peak is due to the aspect ratio of the mesoscopic loop <sup>21</sup>). The low frequency signal of the spectrum is the signature of aperiodic fluctuations due to quantum interferences within the same branch. Therefore, contrary to the Aharonov-Bohm peaks, they do not disappear when the ring is open.

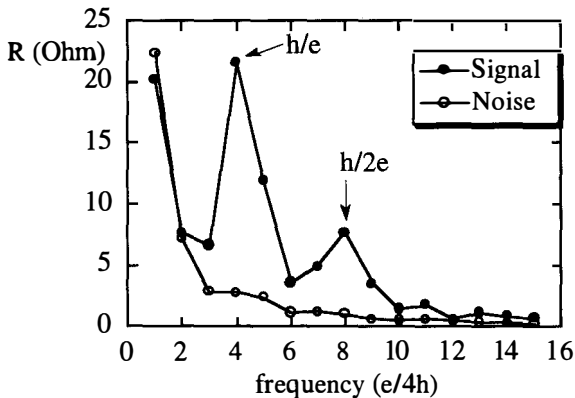


Fig.5 : Fourier transform of the Aharonov-Bohm signal

Similarly, the  $h/e$  peak in the Fourier spectrum of the susceptibility is a signature of persistent currents. Their amplitude which is sample specific is sometimes not detectable but averaging different measurements and subtracting the noise give a typical amplitude of  $4 \pm 2$  nA comparable to the theoretical value  $I_0 = e v_F / L = 5$  nA, computed using our experimental parameters. Moreover, this peak is never present when the ring is open. This is a clear indication of its mesoscopic origin.

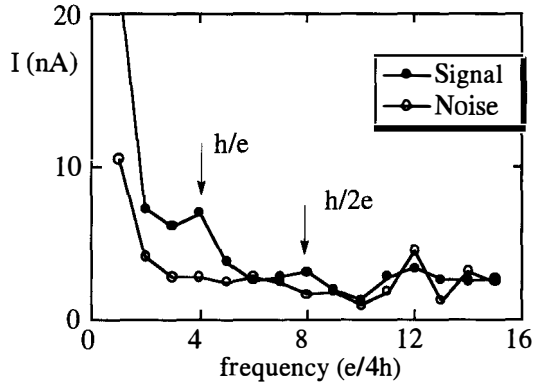


Fig.6 : Fourier transform of the magnetization

The main experimental difficulties with this kind of mesoscopic ring come from the microscopic instabilities of the semi-conductor. We have observed random modifications of the Aharonov-Bohm oscillations on a time scale of 10 to 40 hours. These conductance fluctuations can be attributed to some slow relaxation process of impurities inducing changes in the electrostatic scattering potential configuration or in the Fermi level <sup>22</sup>). Since the amplitude and even the sign of the persistent currents are very sensitive to this configuration it becomes impossible to integrate the signal on a too long period otherwise it averages to zero. The data were therefore accumulated only during the period of time when the Aharonov-Bohm signal was stable enough. This problem causes the main limitation of our signal to noise ratio.

Although we were able to check the randomness of the amplitude and of the sign of the persistent currents, the first harmonic signal at  $h/2e$  was too weak to determine whether it vanishes or not after averaging on different disorder configurations.

Some measurements were made with the ring isolated from the leads, with the help of the first gate. Although the experiment became very difficult without the possibility of controlling the Aharonov-Bohm signal, the preliminary results do not seem to show a significant difference between the canonical ensemble (number of electron fixed, ring isolated) and the grand canonical ensemble (Fermi level fixed, ring connected to the contacts).

## 6 DISCUSSION AND CONCLUSION

We have observed persistent currents in a mesoscopic loop in the quasi-ballistic regime. Because of the very weak disorder,  $l_e/L \approx 1.3$  we find a typical amplitude close to  $I_0 = e v_F / L = 5$  nA, in good agreement with the theory. Since the number of channels in our ring is very low:  $M \approx 4$ , the expected correction is  $\sqrt{M}=2$  which is not significant since we are dealing with typical values.

The electron-electron interactions are known to be important in our samples because of the low electronic density. Although these interactions have been proposed<sup>3-19)</sup> to explain the large values of the persistent currents measured previously in metallic samples, it is now clear that they do not play a major role in the ballistic regime.

Other experiments to investigate the temperature dependence, the effect of disorder and of the geometrical dimensions are currently under way. For this purpose, improvement of our SQUID performance should be obtained with the help of shunting resistors.

We are indebted to B. Etienne and V. Thierry-Mieg for the supply of very good quality heterojunctions. We wish to acknowledge R. Webb, H. Launois, H. Bouchiat, G. Montambaux, L. Levy, and B. Shapiro for helpful discussions and F.R. Ladan and C. Mayeux for technical assistance.

This work has been partly supported by grants from DRET n°56466 and from European ESPRIT Latmic 3043.

## References

- [1] M. Büttiker, Y. Imry, and R. Landauer, Phys. Lett. **96A**, 365 (1983); R. Landauer and M. Büttiker, Phys. Rev. Lett. **54**, 2049 (1985).
- [2] N. Byers and C.N. Yang, Phys. Rev. Lett. **7**, 46 (1961).
- [3] H.F. Cheung, Y. Gefen, E.K. Riedel, and W.H. Shih, Phys. Rev. **B 37**, 6050 (1988); Cheung and E.K. Riedel, Phys. Rev. **B 40**, 9498 (1989).
- [4] N Trivedi and D.A. Browne, Phys. Rev. **B 38**, 9581 (1988).
- [5] Y Imry, in Directions in Condensed Matter Physics, edited by G. Grinstein and G. Mazenkov, World Scientific, Singapore (1986), p101.
- [6] H.F. Cheung and E.K. Riedel, Phys. Rev. Lett. **62**, 587 (1989); H. F.

- [7] G. Montambaux, H. Bouchiat, D. Sigeti and R. Friesner, *Phys. Rev. B* **42**, 7647 (1990).
- [8] L.P. Levy, G. Dolan, J. Dunsmuir, and H. Bouchiat, *Phys. Rev. Lett.* **64**, 2074 (1990).
- [9] H. Bouchiat and G. Montambaux, *J. Phys. (Paris)* **50**, 2695 (1989)
- [10] B.L. Altschuler, Y. Gefen, and Y. Imry, *Phys. Rev. Lett.* **66**, 88 (1991).
- [11] E Akkermans, *Europhys. Lett.* **15**, 709 (1991).
- [12] V. Chandrasekhar, R.A. Webb, M. J. Brady, M.B. Ketchen, W. J. Gallagher, and A. Kleinsasser, *Phys. Rev. Lett* **67**, 3578 (1991).
- [13] F. von Oppen and E.K. Riedel, *Phys. Rev. Lett.* **66**, 84 (1991).
- [14] V. Ambegaokar and U. Eckern, *Phys. Rev. Lett.* **65**, 381 (1990).
- [15] A. Schmidt, *Phys. Rev. Lett.* **66**, 80 (1991).
- [16] U. Eckern and A. Schmid, *Europhys. Lett.* **18**, 457 (1992).
- [17] P. Kopietz, *Phys. Rev. B* **46**, 2280 (1992).
- [18] D. Loss, *Phys. Rev.Lett.* **69**, 343 (1993).
- [19] A. Müller-Groeling, H.A. Weidenmüller and C.H. Lewenkopf, *Europhys. Lett.* **22**, 193 (1992); A. Müller-Groeling, H.A. Weidenmüller and C.H. Lewenkopf, *Phys. Rev. B* **49**, 4752 (1994).
- [20] C. Chapelier, M. El Khatib, P. Perrier, A. Benoit, and D. Mailly, in *SQUID 91, Superconducting Devices and Their Applications*, edited by H. Koch and H. Lübbig (Springer-Verlag, Berlin, 1991) pp 286-291.
- [21] S.A. Washburn and R.A. Webb, *Advance Physics* **35**, 375 (1986).
- [22] D. Mailly and M. Sanquer, *J Phys. France* **2**, 357 (1992).

# SEMICLASSICAL APPROACH TO THE THERMODYNAMICS OF MESOSCOPIC SYSTEMS

*Felix von Oppen*

*Max-Planck-Institut für Kernphysik, 69117 Heidelberg, Germany*

Semiclassical theory provides a useful and physically intuitive framework to understand the thermodynamic properties of mesoscopic systems. This is illustrated by results for persistent currents and the magnetic susceptibility of ballistic microstructures.

## 1 Introduction

Two recent experiments focused attention on the thermodynamics of mesoscopic systems in the ballistic regime, where the elastic mean free path exceeds the sample size. Mailly et al. [1] observed persistent currents [2, 3] in a single GaAs/AlGaAs ring. Lévy et al. [4] measured the magnetic susceptibility of an array of isolated GaAs squares and found a paramagnetic susceptibility far exceeding Landau diamagnetism [5]. When considering these systems within the independent-electron model, semiclassics is a natural approximation because the Fermi wavelength is much smaller than the system size. While the theory for the persistent-current experiment [6] had been developed without explicit reference to the semiclassical approximation, semiclassics proved to be very valuable in understanding the susceptibility experiment [7, 8, 9].

In the following, I outline the general semiclassical approach to the thermodynamics of mesoscopic systems, first employed by Argaman et al. [10] in the context of diffusive systems. The method is then applied to persistent currents in the ballistic regime [11] where it is shown that the current is much larger in integrable billiard geometries than in (completely) chaotic ones, and to the susceptibility of ballistic microstructures in order to understand the experiment by Lévy et al. [4].

## 2 General formulation

Within the independent-electron approximation, the (grand) thermodynamic potential  $\Omega$  can be written in terms of the spectral density  $\rho(E) = \sum_n \delta(E - E_n)$  (the  $E_n$  denote the single-particle energy levels),

$$\Omega = -\frac{1}{\beta} \int_0^\infty dE \rho(E) \ln \{1 + \exp[-\beta(E - \mu)]\}. \quad (1)$$

Here  $\beta = 1/k_B T$  denotes the inverse temperature. The leading contribution to  $\Omega$  comes from the energy-averaged spectral density  $\langle \rho(E) \rangle$ . In mesoscopic systems the discrete nature of the spectrum leads to quantum-coherence corrections  $\delta\Omega$  to the bulk potential. Semiclassically, the discreteness of the spectrum is reflected in the oscillatory periodic-orbit contributions to the density of states, first calculated by Gutzwiller [12],

$$\delta\rho(E) = \frac{1}{\hbar^\nu} \sum_\gamma A_\gamma \exp\left\{\frac{i}{\hbar} S_\gamma(E)\right\}. \quad (2)$$

Here the sum is over all periodic orbits  $\gamma$  of the system and  $S_\gamma(E)$  denotes the classical action of the periodic orbit. For billiards it is given in terms of the length  $L_\gamma$  of the orbit,  $S_\gamma = \hbar k L_\gamma$ . The exponent  $\nu$  and the amplitude  $A_\gamma$  depend on the type of periodic orbit. While  $\nu = (d+1)/2$  for the non-isolated periodic orbits of integrable systems ( $d$  denotes the dimensionality of the system), one has  $\nu = 1$  for the unstable and isolated periodic orbits of chaotic systems. Useful expressions for the amplitude  $A_\gamma$  were derived by Gutzwiller [12] for chaotic and by Berry and Tabor [13] for integrable systems. Inserting the Gutzwiller formula into Eq. (1), linearizing the action around the chemical potential  $\mu$ , and performing the energy integration using contour integration one has

$$\delta\Omega = \frac{1}{\hbar^{\nu-2}} \sum_\gamma \frac{A_\gamma}{T_\gamma^2} \exp\{ik_F L_\gamma\} \left(\frac{\pi T_\gamma}{\hbar\beta}\right) \sinh^{-1}\left(\frac{\pi T_\gamma}{\hbar\beta}\right), \quad (3)$$

where

$$T_\gamma = \frac{dS_\gamma}{dE} \quad (4)$$

denotes the orbit traversal time. The contribution of each periodic orbit oscillates with chemical potential with a period equal to the orbit correlation energy  $\hbar/T_\gamma = \hbar v_F/L_\gamma$ . In general, infinitely many classical periodic orbits contribute to Eq. (3). Its usefulness derives from the fact that finite temperature and inelastic scattering rapidly restrict the number of orbits that must be considered. A periodic orbit contributes significantly only if the orbit length  $L_\gamma$  is of the order of or shorter than both the thermal length  $L_T = \hbar v_F/k_B T$  and the phase-coherence length  $L_\Phi$ .

Our terminology “orbit correlation energy” for  $\hbar/T_\gamma$  stresses the analogy with the Thouless correlation energy  $\hbar/\tau_D$  of diffusive systems ( $\tau_D$  is the diffusion time through the system). The semiclassical approximation is so successful for mesoscopic systems because it directly involves these mesoscopic correlation energies. By contrast, these relevant energy scales are masked in expressions involving sums over exact eigenenergies.

### 3 Persistent Currents

Ballistic microstructures allow for the experimental investigation of billiard systems of different geometries. In particular, it is an interesting question whether there are differences between integrable and chaotic billiards. Semi-classics can be used to demonstrate that mesoscopic persistent currents are a sensitive probe of quantum chaos: their amplitude has different universal dependences on the Fermi energy for integrable and for completely chaotic billiards [11]. For our purposes the main difference between integrable and completely chaotic billiards lies in the nature of the periodic orbits. In integrable systems, they form continuous families. Each member of the family contributes with the same phase and hence their contribution is enhanced due to constructive interference. This constructive interference is absent in completely chaotic systems where *all* periodic orbits are isolated and unstable. Hence, the persistent current is larger in integrable than in completely chaotic billiards.

Using a simple scaling relation for the density of states and sum rules for the amplitudes  $A_\gamma$  in the Gutzwiller formula (2), this physical argument can be made more precise [11]. One finds that the typical persistent-current amplitude is characterized by different dependences on the Fermi wave vector  $k_F$ ,

$$\langle I^2 \rangle^{1/2} \sim I_0 (k_F L)^\nu, \quad (5)$$

where  $I_0 = ev_F/L$  denotes a natural current scale,  $L$  a typical length of the system. The exponent  $\nu$  reflects the nature of the classical dynamics. One has  $\nu = (d + 1)/2$  for integrable and  $\nu = 1$  for completely chaotic systems ( $d$  is the dimensionality). It follows by dimensional analysis that Eq. (5) fixes the persistent-current amplitude up to functions of ratios of geometric length scales.

It should be apparent that the arguments in this section are not specific to mesoscopic persistent currents. Similar results can be obtained for the magnetic susceptibility [7, 8].

### 4 Magnetic susceptibility

Lévy et al. [4] recently measured the magnetic susceptibility of an array of  $10^5$  isolated GaAs/AlGaAs squares, and observed a striking zero-field peak of the susceptibility. The peak amplitude was about two orders of magnitude larger than Landau diamagnetism, and decreased with temperature on the scale of 0.5K. The width of the peak corresponded to magnetic fields such

that roughly one flux quantum is threading each square.

These experimental results can be (partially) understood in terms of the semiclassical approach outlined above. Details of the calculation will be published elsewhere [7, 8]. The strategy of the calculation follows from the following observations:

- Semiclassics should be an excellent approximation because the Fermi wavelength  $\lambda_F \simeq 50\text{nm}$  is much smaller than the system size  $L = 4.5\mu\text{m}$ .
- For the magnetic fields of the experiment, the classical cyclotron radius is roughly 50 times larger than the system size. Hence, to a very good approximation, the periodic orbits can be taken as those for zero field.
- The magnetic field enters only via Aharonov-Bohm phases due to the flux enclosed by the periodic orbits.
- The experiment measures the ensemble-averaged susceptibility which is vanishingly small for fixed chemical potential, but finite for fixed number of electrons per square [14, 15, 16].
- Only the shortest nontrivial (rectangular) orbit needs to be considered due to finite temperature and inelastic scattering. (However, it is not difficult to go beyond this approximation.)

In terms of the Landau susceptibility  $\chi_{\text{Landau}}$  the average mesoscopic susceptibility of an array of square billiards becomes

$$\langle \delta\chi \rangle \simeq \frac{4\sqrt{2}}{5\pi} (k_F L) |\chi_{\text{Landau}}| \frac{(T/T^*)^2}{\sinh^2(T/T^*)} g(BL^2/\phi_0) \quad (6)$$

with characteristic temperature

$$k_B T^* = \frac{\hbar v_F}{4\sqrt{2}\pi^2 L}. \quad (7)$$

The damped oscillations as function of the magnetic field are described by the function

$$g(\varphi) = 30 \left\{ \int_0^1 dx \cos[4\pi\varphi x(1-x)] \int_0^1 dx x^2(1-x)^2 \cos[4\pi\varphi x(1-x)] - \left( \int_0^1 dx x(1-x) \sin[4\pi\varphi x(1-x)] \right)^2 \right\}. \quad (8)$$

One feature of this result is particularly noteworthy. One observes that for  $T = 0$  the finite-size corrections (6) to the susceptibility increase faster with the system size than the bulk (Landau) contribution. This result which may

seem counterintuitive at first can be understood as a consequence of phase coherence. Since the magnetic field enters the mesoscopic corrections to the thermodynamic potential  $\delta\Omega$  only via the Aharonov-Bohm phases, one notes that

$$\delta\chi \sim \frac{\hbar^2}{\partial B^2} \cos(2\pi B A_\gamma / \phi_0) \sim \left( \frac{2\pi A_\gamma}{\phi_0} \right)^2 \cos(2\pi B A_\gamma / \phi_0). \quad (9)$$

For billiards the enclosed areas  $A_\gamma$  scale with the system size. Hence, even though one calculates corrections to the thermodynamic limit for the thermodynamic potential, these finite-size corrections can dominate the susceptibility because of the additional area factors due to the derivatives with respect to the magnetic field. We conclude that the order of the limits  $T \rightarrow 0$  and  $V \rightarrow \infty$  (thermodynamic limit) is important.

For a detailed comparison with experiment the reader is referred to Ref. [7]. Here we only mention that the results for the amplitude and the magnetic-field dependence are consistent with the experimental results of Lévy et al. [4]. By contrast, the theoretical temperature scale appears to be too small by about an order of magnitude compared to experiment.

Clearly, the approach is not restricted to square billiards. In fact, it is interesting to note that already in 1952 Dingle [17] found related results for the susceptibility of a cylinder subject to an axial magnetic field without using the semiclassical approximation explicitly. One can also consider the finite-size corrections to the magnetic susceptibility of completely chaotic systems [7, 8, 18]. A special case of completely chaotic systems are diffusive samples whose susceptibility had been discussed extensively by diagrammatic techniques [19].

## 5 Summary

The semiclassical approach to the thermodynamics of mesoscopic systems has been outlined and applied to persistent currents and the magnetic susceptibility. It was shown that persistent currents are much larger in integrable than in completely chaotic billiard geometries and universal dependences on the Fermi energy were derived. Mesoscopic corrections to the susceptibility were found to be much larger than the bulk Landau susceptibility. While this explains the amplitude of the susceptibility in a recent experiment by Lévy et al. on an array of GaAs squares, the theory predicts a faster decrease with temperature than observed experimentally.

## References

- [1] D. Mailly, C. Chapelier, and A. Benoit, Phys. Rev. Lett. **70**, 2020 (1993).
- [2] F. Hund, Ann. Phys. (Leipzig) **32**, 102 (1938).
- [3] M. Büttiker, Y. Imry, and R. Landauer, Phys. Lett. **96A**, 365 (1983).
- [4] L.P. Lévy, D.H. Reich, L. Pfeiffer, and K. West, Physica B **189**, 204 (1993).
- [5] L.D. Landau, Z. Phys. **64**, 629 (1930).
- [6] H.F. Cheung, Y. Gefen, and E.K. Riedel, IBM J. Res. Dev. **32**, 359 (1988).
- [7] F. von Oppen, PhD thesis, University of Washington (1993); and preprint.
- [8] D. Ullmo, K. Richter, and R. Jalabert, preprint.
- [9] Y. Gefen, D. Braun, and G. Montambaux, preprint.
- [10] N. Argaman, Y. Imry, and U. Smilansky, Phys. Rev. B **47**, 4440 (1993).
- [11] F. von Oppen and E.K. Riedel, Phys. Rev. B **48**, 9170 (1993).
- [12] M. Gutzwiller, in “*Chaos and Quantum Physics*”, ed. by M.-J. Giannoni, A. Voros, and J. Zinn-Justin, (Elsevier, Amsterdam 1991), p. 201.
- [13] M.V. Berry and M. Tabor, J. Phys. A **10**, 371 (1977).
- [14] B.L. Altshuler, Y. Gefen, and Y. Imry, Phys. Rev. Lett. **66**, 88 (1991).
- [15] A. Schmid, Phys. Rev. Lett. **66**, 80 (1991).
- [16] F. von Oppen and E.K. Riedel, Phys. Rev. Lett. **66**, 84 (1991).
- [17] R.B. Dingle, Proc. Roy. Soc. Lond. A **212**, 47 (1952).
- [18] O. Agam, preprint.
- [19] B.L. Altshuler, Y. Gefen, Y. Imry, and G. Montambaux, Phys. Rev. B **47**, 10335 (1993).

## ORBITAL MAGNETISM IN QUANTUM DOTS: A SEMICLASSICAL APPROACH

Rodolfo A. Jalabert, Klaus Richter, and Denis Ullmo; Division de Physique Théorique<sup>†</sup>  
 Institut de Physique Nucléaire, 91406 Orsay Cedex, France.

In this communication we review our recent work<sup>1),2)</sup> on the magnetic response of ballistic microstructures. The study of orbital magnetism in an electron gas has a long history, and was initiated by Landau<sup>3)</sup> only four years after the discovery of the Schrödinger equation. For a free electron gas the low-field susceptibility is diamagnetic. In three and two dimensions it attains, respectively, the values  $\chi_L^{3D} = -(1/12\pi^2)e^2k_F/mc^2$  and  $\chi_L^{2D} = -(1/12\pi)e^2/mc^2$ , where  $k_F$  is the Fermi wavevector. The modifications of these results arising from constraining the electron gas in a finite volume have been the object of several studies<sup>4)</sup>. On the other hand, in the last few years the field known as Quantum Chaos has been dealing with questions regarding the differences at the quantum level between systems whose underlying classical mechanics is chaotic and those where it is regular. Nakamura and Thomas<sup>5)</sup> were the first to address the problem of orbital magnetism from a Quantum Chaos point of view by numerically studying the differences in the magnetic response of circular and elliptic billiards.

The interest on the orbital magnetism of confined systems, and its connection with Quantum Chaos has recently been renewed with the experimental realization of ballistic quantum dots lithographically defined on high mobility semiconductor heterojunctions. Experiments by Lévy *et al*<sup>6)</sup> yielded, for an ensemble of  $10^5$  microscopic ballistic squares<sup>7)</sup>, a paramagnetic low-field susceptibility being more than an order of magnitude larger than  $|\chi_L^{2D}|$ . Combining a thermodynamic formalism that closely follows that developed in the context of persistent currents with a semiclassical approach, we are able to show that *the enhancement of the low-field susceptibility with respect to the Landau value is due to large modulations in the density of states caused by families of periodic orbits* present in integrable systems.

<sup>†</sup>Unité de recherche des Universités de Paris XI et Paris VI associée au CNRS

The magnetic susceptibility of a two-dimensional system of  $N$  electrons occupying an area  $A$  is given by the change of the free energy  $F$  under the effect of a magnetic field,

$$\chi = -\frac{1}{A} \left( \frac{\partial^2 F}{\partial H^2} \right)_{N,T}. \quad (1)$$

In the macroscopic limit of very large  $N$  and  $A$  the choice of the ensemble is a matter of convenience, we can equally well work in the grand canonical ensemble (GCE) at fixed chemical potential and obtain the susceptibility as a derivative of the thermodynamical potential  $\Omega$ ,

$$\Omega(T, \mu, H) = F(T, N, H) - \mu N = -\frac{1}{\beta} \int dE \rho(E, H) \ln(1 + \exp[\beta(\mu - E)]). \quad (2)$$

$\rho(E, H)$  is the density of states and  $\beta = 1/k_B T$ . The above mentioned equivalence between the ensembles breaks down in the mesoscopic regime of small structures<sup>8)</sup>, and therefore it is important to work with the canonical expression (1). Separating  $\rho$  into a mean part  $\rho^0$  (that scales as the area of the system) and an oscillatory component  $\rho^{\text{osc}}$  (that in a semiclassical approach is given by the sum over periodic trajectories), we define a mean chemical potential  $\mu^0$  from  $N = \int dE \rho(E) f(E - \mu) = \int dE \rho^0(E) f(E - \mu^0)$ . ( $f$  is the Fermi-Dirac distribution function.) Since  $\rho^0$  and  $\rho^{\text{osc}}$  have different order in the semiclassical parameter  $\hbar$ , we can expand the terms in Eq. (2) up to second order in  $\rho^{\text{osc}}/\rho^0$  obtaining<sup>9)</sup>

$$F(N) \simeq F^0 + \Delta F^{(1)} + \Delta F^{(2)}, \quad F^0 = \mu^0 N + \Omega^0(\mu^0), \quad (3)$$

$$\Delta F^{(1)} = \Omega^{\text{osc}}(\mu^0), \quad \Delta F^{(2)} = \frac{1}{2\rho^0(\mu^0)} \left[ \int dE \rho^{\text{osc}}(E) f(E - \mu^0) \right]^2. \quad (4)$$

$\Omega^0$  and  $\Omega^{\text{osc}}$  are defined by using respectively  $\rho^0$  and  $\rho^{\text{osc}}$  instead of  $\rho$  in Eq. (2).  $F^0$  is field independent to leading order in a semiclassical expansion. Higher order terms in  $\hbar$  give rise to the standard two-dimensional diamagnetic Landau susceptibility  $\chi_L^{2D}$  regardless of the confining potential<sup>2)</sup>. The decomposition (3)-(4) has the advantage of that the corrections  $\Delta F^{(1)}$  and  $\Delta F^{(2)}$  are expressed as simple functions of the oscillatory part of the density of states which can be evaluated semiclassically.

In order to calculate the oscillating part of the density of states we use a semiclassical approach starting from the expression of  $\rho^{\text{osc}}$  in terms of the trace of the semiclassical Green function<sup>10)</sup>,

$$G_E^{\text{sc}}(\mathbf{r}', \mathbf{r}) = \sum_t D_t \exp \left[ i \left( \frac{S_t}{\hbar} - \left( \eta_t - \frac{1}{2} \right) \frac{\pi}{2} \right) \right]. \quad (5)$$

The sum runs over all classical trajectories  $t$  joining  $\mathbf{r}$  to  $\mathbf{r}'$  at energy  $E$ .  $S_t$  is the action integral along the trajectory. For billiards without magnetic field we simply have  $S_t/\hbar = kL_t$  where  $k = \sqrt{2mE}/\hbar$  and  $L_t$  is the length of the trajectory. The amplitude  $D_t$  takes care of the classical probability conservation and  $\eta_t$  is the Maslov index.

The free energy corrections  $\Delta F^{(1)}$  and  $\Delta F^{(2)}$  are therefore given as sums over classical trajectories, each term being the convolution in energy of the semiclassical contribution (oscillating as  $kL_t$ ) with the Fermi factor (smooth on the scale of  $\beta^{-1}$ ). This implies that the contribution of a given trajectory to  $\Delta F^{(1)}$  at finite temperature is reduced with respect to its  $T=0$  counterpart by a multiplicative factor  $R(T) = (L_t/L_c) \sinh^{-1}(L_t/L_c)$ , with  $L_c = \hbar^2 k_F \beta / (\pi m)$ . A factor  $R^2(T)$  is needed for  $\Delta F^{(2)}$ . At high temperatures  $R(T)$  yields an exponential suppression of long trajectories. Therefore the fluctuating part of the free energy, and  $\chi$ , are dominated by trajectories with  $L_t \leq L_c$ , which are the only ones considered in our analysis.

The square constitutes the generic case of a regular system: it is integrable at zero magnetic field, but a perturbing field breaks the integrability. This implies that in calculating the susceptibility we cannot use neither the standard Berry-Tabor trace formula<sup>11)</sup> (valid for integrable systems) nor the Gutzwiller trace formula<sup>10)</sup> (applicable when the periodic orbits are well separated). On the other hand, we can directly use Eq. (5) since the simplicity of the geometry allows the enumeration of all closed trajectories and the evaluation of the field dependence of their contribution to  $\rho^{\text{osc}}$ . Given the exponential suppression of long trajectories, the finite-temperature susceptibility will be dominated by the contribution to  $\rho^{\text{osc}}$  of the family of closed trajectories which, for  $H \rightarrow 0$ , tends to the family of shortest periodic orbits with non-zero enclosed area. We note this family as (1,1) since the trajectories bounce once on each side of the square (upper inset, Fig. 1). Their length is  $L_{11} = 2\sqrt{2}a$ , which is of the order of the cut off length  $L_c \approx 2a$  at the temperature of the experiment of Ref. 6.<sup>12)</sup>

Applying classical perturbation theory for the change in the action  $S_t$  of trajectories (1,1) under the effect of a small magnetic field (such that the cyclotron radius  $r_c$  verifies  $r_c \gg a$ ), and performing the energy integrations of Eqs. (4) we obtain for the contributions to the susceptibility coming from  $\Delta F^{(1)}$  and  $\Delta F^{(2)}$  respectively

$$\frac{\chi^{(1)}}{|\chi_L^{2D}|} = \frac{3}{(\sqrt{2}\pi)^{5/2}} (k_F a)^{3/2} \sin\left(k_F L_{11} + \frac{\pi}{4}\right) \frac{d^2 \mathcal{C}}{d\varphi^2} R(T), \quad (6)$$

$$\frac{\chi^{(2)}}{|\chi_L^{2D}|} = -\frac{3}{\sqrt{2}\pi^3} k_F a \sin^2\left(k_F L_{11} + \frac{\pi}{4}\right) \frac{d^2 \mathcal{C}^2}{d\varphi^2} R^2(T). \quad (7)$$

The field dependence enters through the function

$$\mathcal{C}(\varphi) = \frac{1}{\sqrt{2}\varphi} [\cos(\pi\varphi) C(\sqrt{\pi\varphi}) + \sin(\pi\varphi) S(\sqrt{\pi\varphi})] . \quad (8)$$

$C$  and  $S$  are respectively the cosine and sine Fresnel integrals, and  $\varphi = \Phi/\Phi_0$  is the total flux  $\Phi = Ha^2$  inside the square measured in units of  $\Phi_0 = hc/e$  (the fundamental flux).  $\chi^{(1)}$  is the leading contribution to the susceptibility of a given square since its typical magnitude is much larger than  $|\chi_L^{2D}|$  and that of  $\chi^{(2)}$ . On the other hand,  $\chi^{(1)}$  can be paramagnetic or diamagnetic (Fig. 1) and it will vanish by averaging over an ensemble of squares where the dispersion of  $k_F L_{11}$  is of the order of  $2\pi$ . Since  $\sin^2(k_F L_{11} + \pi/4)$  averages to  $1/2$ , the average susceptibility is given by  $\chi^{(2)}$  (solid line, Fig. 2). In particular, the zero-field susceptibility of the ensemble is paramagnetic and has a value  $4\sqrt{2}/(5\pi)k_F a R^2(T)^{13}$ . For ensembles with a wide distribution of lengths (in the experiment of Ref. 6 the dispersion in size across the array is estimated between 10 and 30%) the dependence of  $\mathcal{C}$  on  $a$  (through  $\varphi$ ) has to be considered. Since the scale of variation of  $\mathcal{C}$  with  $a$  is much slower than that of  $\sin^2(k_F L_{11} + \pi/4)$  we can effectively separate the two averages and obtain the total mean by averaging the local mean. The low-field oscillations of  $\langle\chi\rangle$  with respect to  $\varphi$  are suppressed under the second average (performed for a gaussian distribution with a 30% dispersion, dashed line in Fig. 2), while the zero-field behavior remains unchanged.

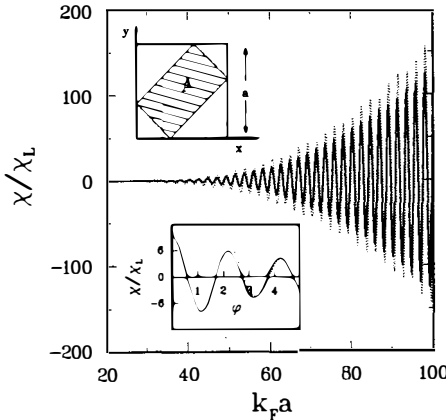


**Fig.1:** Magnetic susceptibility of a square as a function of  $k_F a$  at zero field and a temperature equal to 10 level-spacings from numerical calculations (dotted), and from semiclassical calculations (solid). The period  $\pi/\sqrt{2}$  indicates the dominance of the shortest periodic orbits enclosing non-zero area with length  $L_{11} = 2\sqrt{2}a$  (upper inset). Lower inset: amplitude of the oscillations (in  $k_F L_{11}$ ) of  $\chi$  as a function of the flux through the sample from Eq. (6) (solid) and numerics (dashed).

We have checked the above semiclassical results by calculating the partition function  $Z = \exp(-\beta F)$  after direct diagonalization of the hamiltonian. As shown in Figs. 1 and 2, the agreement between semiclassical theory and exact quantum mechanical calculations is excellent, demonstrating that the concept of classical trajectories is essential for the physical understanding of the phenomenon and showing the importance of the family (1,1) in the finite-temperature,

low-field regime of interest.

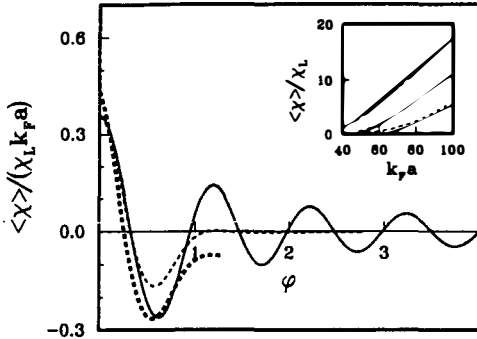


**Fig.2:** Average magnetic susceptibility for an ensemble of squares with a small dispersion of sizes (solid) and with a large dispersion (dashed) from semiclassical calculations. Thick dashed: average from numerics. The shift of the numerical with respect to the semiclassical results reflects the Landau susceptibility (due to  $F^0$ ). Inset: average susceptibility as a function of  $k_F a$  for various temperatures (4,6 and 10 level spacings) and a flux  $\varphi = 0.15$ , from semiclassics (solid) and numerics (dashed).

The generic case of an integrable system perturbed by a weak magnetic field can be treated more generally within a semiclassical approach<sup>2)</sup>, and one obtains the same qualitative behaviour as for the square geometry (Eqs. (6)-(7)). That is, a  $(k_F a)^{3/2}$  dependence for the typical value of  $\chi^{(1)}$  (which can be diamagnetic or paramagnetic) and  $k_F a$  dependence for  $\chi^{(2)}$  which gives the average susceptibility of an ensemble. The numerical prefactors obviously depend on the particular geometry in consideration. Circles and rings, for instance, which have the same parametric dependence constitute a particularly simple case since the rotational symmetry avoids that a perturbing magnetic field breaks integrability, and we can calculate the magnetization by a direct application of the Berry-Tabor trace formula. In ring geometries it is customary to measure the magnetic response in terms of the persistent currents, and our semiclassical calculations are in reasonable agreement with the existing experiments in the ballistic regime<sup>14)</sup>.

For chaotic systems (of typical length  $a$ ) the Gutzwiller Trace Formula provides the appropriate path to calculate  $\rho^{\text{osc}}(E, H)$ . For temperatures at which only a few short periodic orbits are important,  $\chi^{(1)}$  can be paramagnetic or diamagnetic and its typical value is of the order of  $k_F a \chi_L^{2D}$ <sup>15)</sup>. Extending this analysis to the case of an ensemble of chaotic systems we obtain  $\langle \chi \rangle \propto |\chi_L^{2D}|$ . The individual  $\chi$  are larger, by a factor  $(k_F a)^{1/2}$  in regular geometries than in chaotic systems. For  $\langle \chi \rangle$  the difference is of the order of  $k_F a$ . These differences are due to the large oscillations of  $\rho$  in regular systems induced by families of periodic trajectories. Therefore, the different magnetic response according to the geometry does not arise as a long-time

property (linear vs. exponential trajectory divergences) but as a short-time property (family of trajectories vs. isolated trajectories).

It is important to notice that the semiclassical concepts that we have outlined can be extended outside the weak-field regime. For the case of the square<sup>2)</sup> the essential physical behavior can be understood from only one kind of trajectories in each field regime: the family (1,1) for weak fields  $r_c \gg a$ , the bouncing trajectories of electrons that are reflected between opposite sides of the square for  $r_c \approx a$ , and the cyclotron orbits that give the standard de Haas - van Alphen oscillations when  $r_c < a/2$ .

We have so far ignored the possibility of impurity scattering. Our model of a clean system is quite appropriate from a Quantum Chaos point of view and also constitutes a good first order approximation to the physics of quantum dots. In order to get a more realistic description of the actual microstructures we consider the corrections to the above picture due to the presence of weak disorder scattering. Including the effect of the disorder in our semiclassical framework we obtain<sup>2)</sup> the rather natural result that the two contributions to the susceptibility coming from the (1,1) family are reduced with respect to their clean counterparts as  $\chi^{(1)} = \chi_{cl}^{(1)} e^{-L_{11}/2l}$  and  $\chi^{(2)} = \chi_{cl}^{(2)} e^{-L_{11}/l}$ , where  $l$  is the elastic mean free path. We have checked these relationships numerically and in Fig. 3 we present the results of the typical susceptibility for  $\delta$ -function impurities and various  $l$ 's. We have an excellent agreement with the semiclassical prediction for very weak disorder, while for  $l \approx a$  the semiclassical approximation tends to overestimate the reduction. It is important to notice that the long trajectories, very sensitive to the presence of disorder, are completely irrelevant at finite temperatures.

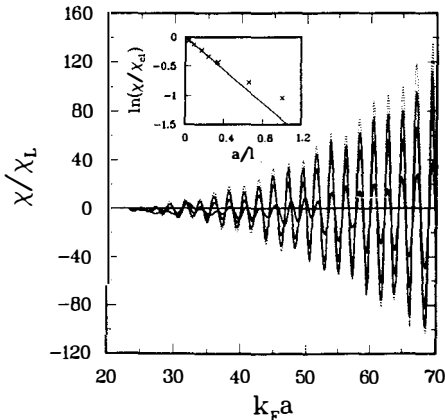


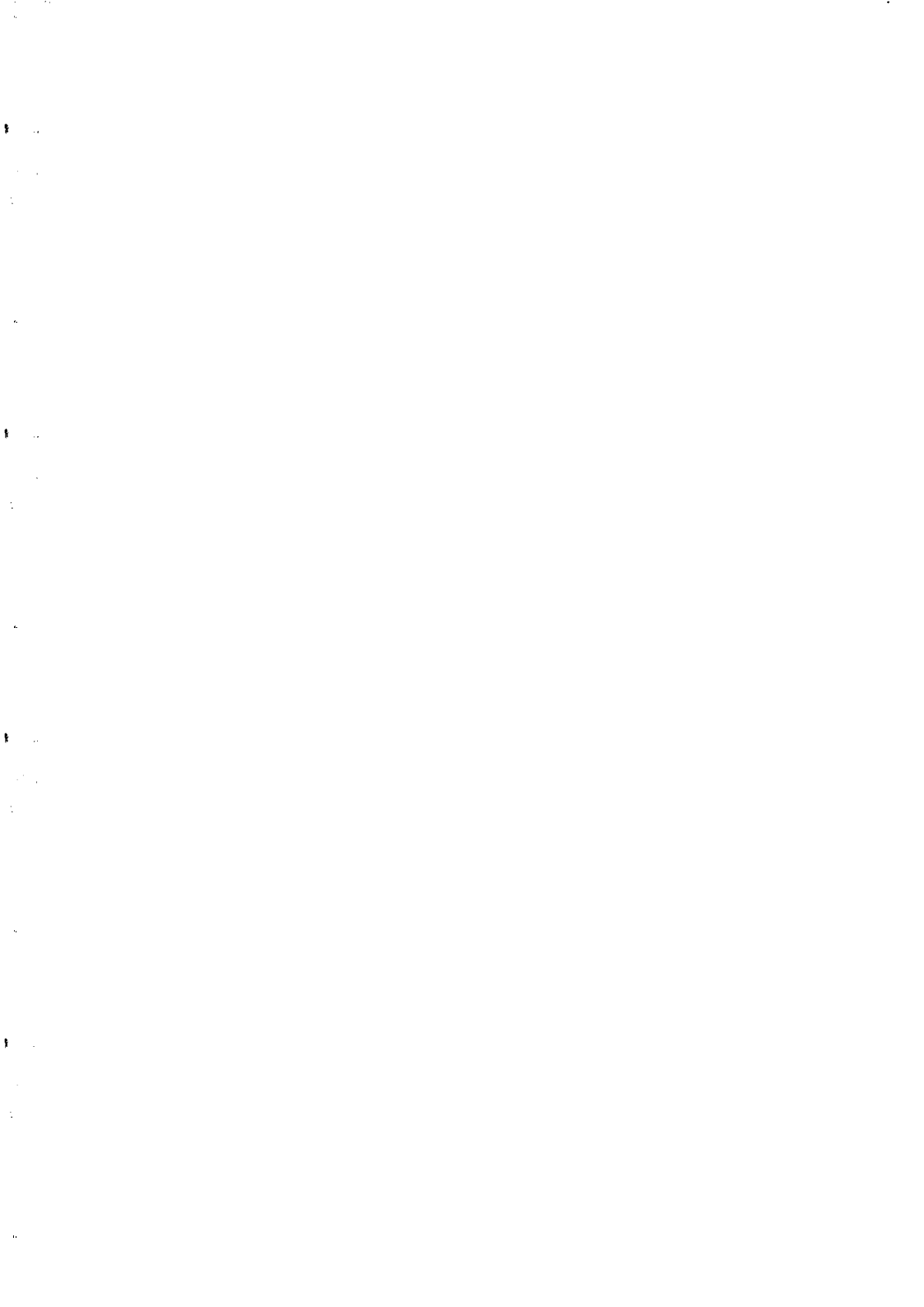
**Fig.3:** Zero-field susceptibility of a disordered square as a function of  $k_F a$  from numerical calculations with  $l/a = 12, 3$  and  $1$  (solid). The temperature is equal to 6 level spacings, the potential scattering is  $\delta$ -like, and in each case an average over five impurity configurations has been performed. The clean case ( $l = \infty$ ) is shown for comparison (dotted). Inset: logarithm of the reduction factor as a function of the inverse mean free path from numerical calculations (crosses). The straight line is the semiclassical prediction.

Ref. 6 yielded a paramagnetic susceptibility at  $H = 0$  with a value of approximately 100 (with an uncertainty of a factor of 4) in units of  $\chi_L$ . The two electron densities considered in the experiment are  $10^{11}$  and  $3 \times 10^{11} \text{cm}^{-2}$  corresponding to approximately  $10^4$  occupied levels per square. For a temperature of  $40 \text{mK}$  Eq. (7) gives, respectively, for the zero-field susceptibility values of 60 and 170. A further reduction arises from the effect of disorder and we are then within the order of magnitude of the experiment (given the experimental uncertainties in the magnitude of the susceptibility and in the determination of the elastic mean free path). The field scale for the decrease of  $\langle \chi(\varphi) \rangle$  is of the order of one flux quantum through each square, in reasonable agreement with our theoretical findings. A better knowledge of the actual impurity potential and the inclusion of interaction effects are desirable in order to attempt a more precise comparison with experiment. These more refined theories should necessarily incorporate the simple physics that we have discussed: the enhancement of the weak field susceptibility due to families of short periodic orbits.

KR acknowledges financial support by the A. von Humboldt foundation.

#### References:

- 1) D. Ullmo, K. Richter, and R.A. Jalabert, submitted to Physical Review Letters.
- 2) K. Richter, D. Ullmo, and R.A. Jalabert, to be submitted to Physical Review B.
- 3) L.D. Landau, Z. Phys. **64**, 629 (1930).
- 4) For a very complete account of the history of orbital magnetism see A.D. van Leeuwen, Thesis, University of Leiden (1993).
- 5) K. Nakamura and H. Thomas, Phys. Rev. Lett. **61**, 247 (1988).
- 6) L.P. Lévy, D.H. Reich, L. Pfeiffer, and K. West, Physica B **189**, 204 (1993).
- 7) The size of the squares is  $a = 4.5 \mu\text{m}$ , the phase-coherence length is estimated between 15 and  $40 \mu\text{m}$  and the elastic mean free path between 5 and  $10 \mu\text{m}$ . Therefore, the experiments are in the phase-coherent, ballistic regime.
- 8) H. Bouchiat and G. Montambaux, J. Phys. (Paris) **50**, 2695 (1989).
- 9) Y. Imry, in *Coherence Effects in Condensed Matter Systems*, edited by B. Kramer (Plenum, 1991); A. Schmid, Phys. Rev. Lett. **66**, 80 (1991); F. von Oppen and E.K. Riedel, *ibid* **84**; B.L. Altshuler, Y. Gefen, and Y. Imry, *ibid* **88**.
- 10) M.C. Gutzwiller, *Chaos in Classical and Quantum Mechanics*, (Springer-Verlag, Berlin, 1990).
- 11) M.V. Berry and M. Tabor, J. Phys. A **10**, 371 (1977).
- 12) For lower temperatures we will have a larger  $L_e$ , however, the strong flux cancellation of long trajectories in a square geometry makes that the family (1,1) will give the main contribution to the susceptibility at any nonzero temperature.
- 13) This result has been independently proposed in Ref. 1 and by F. von Oppen [unpublished].
- 14) D. Mailly, C. Chapelier, and A. Benoit; Phys. Rev. Lett. **70**, 2021 (1993).
- 15) B. Shapiro, Physica A, **200**, 498 (1993); O. Agam, preprint 1993.



## Macroscopic Tunneling of a Pinned Wigner Crystal-Ring: Anomalous Temperature Behaviour

I.V.Krive,<sup>(1)\*</sup> R. I. Shekhter,<sup>(1)</sup> S. M. Girvin,<sup>(2)</sup> and M. Jonson<sup>(1)</sup>

<sup>(1)</sup>*Department of Applied Physics, Chalmers University of Technology  
and Göteborg University, S-412 96 Göteborg, Sweden*

<sup>(2)</sup>*Department of Physics, Indiana University, Bloomington, Indiana 47405, USA*

In recent experiments<sup>1,2</sup> persistent currents have been observed in the ballistic transport regime of mesoscopic rings formed in the laterally confined two-dimensional electron gas of certain AlGaAs heterostructures. The current  $I$  and the associated magnetic moment were found to oscillate as a function of magnetic flux with period  $\Phi_0 = hc/e$  — the quantum unit of flux — and amplitude  $I_0 \sim ev_F/L$  ( $e$  is the electronic charge,  $v_F$  the Fermi velocity, and  $L$  the length of the circumference of the ring). These results are in excellent agreement with a theory of such Aharonov-Bohm (AB) oscillations based on a free electron model of the ballistic electrons<sup>3,4</sup>. Since electron-electron interactions in the semiconductor ring are not weak, and since electron correlations must play an important role when the density of conducting electrons is low, this agreement is quite surprising. In diffusive metal rings, for example, where the electronic mean free path is short ( $\ell \ll L$ ), it has been suggested that electron correlations significantly enhance the amplitude of the AB oscillations<sup>5</sup>. Thus the question of how Coulomb correlations in a system of ballistic electrons affect the magnitude of the persistent current is of significant interest.

In this paper we study persistent currents and AB oscillations in systems of spinless interacting electrons confined to a one-dimensional ring; the electrons are assumed to be so strongly correlated that they form a Wigner crystal. In an ideal ring the mechanism of the persistent current is a dissipationless sliding of the crystal as a whole. We demonstrate that the resulting current oscillates as a function of magnetic flux with period  $\Phi_0$ . Its amplitude at zero temperature is exactly the same as for the noninteracting electrons of the same density in accordance with general theorem<sup>6</sup>. If the temperature is raised, the amplitude of the oscillations is exponentially suppressed:  $I(T) \sim I_0 \exp(-\pi T/2T_0)$ , where  $I_0 \equiv ev_F/L$ ,  $T_0 \equiv \hbar v_F/L$  is the characteristic crossover temperature and  $v_F \equiv \pi \hbar/ma$  ( $a$  is the period of the Wigner crystal,  $m$  is the electron mass).

The situation changes drastically if a potential barrier, somewhere along the ring, impedes the motion of the electrons. Charge transport in this case requires that electrons tunnel through the barrier — the process which in the limit of strong repulsion can be viewed as a macroscopic tunneling of a Wigner crystal-ring. It is convenient to think of the motion of the crystal as a two-step process, where first a single electron tunnels through the barrier producing a deformation of a finite portion of the Wigner crystal, which then is relaxed<sup>7,8</sup>. This process necessarily depends on the elastic properties of the crystal, and as a result the magnitude of

the persistent current will depend on the sound velocity,  $s$ , in the Wigner lattice. As our analysis below will show, the temperature dependence of the amplitude of the AB oscillations is also affected in a qualitative way. The presence of the tunnel barrier, which pins the Wigner crystal and makes charge transfer possible only by macroscopic tunneling, strongly decreases the zero temperature value of the persistent current since for a repulsive interaction quantum fluctuations in a strongly correlated electron system renormalize the barrier upward. The finite ring circumference cuts off the divergent renormalization of the barrier height which occurs in the thermodynamic limit of a Luttinger liquid<sup>9</sup> or Wigner crystal<sup>7,8</sup>. Thus the persistent current of a pinned Wigner crystal at zero temperature is greatly reduced but is still finite. At finite temperatures the effective barrier for tunneling is diminished which enhances the tunneling probability. The competition between two effects of an increased temperature — a reduced renormalized barrier height for tunneling and a loss of phase coherence due to the destructive interference — leads to a sharp maximum in the temperature dependence of the persistent current. For a rigid crystal this maximum occurs at  $T \sim 0.5 T_s$ , where  $T_s \equiv \hbar s/L \gg T_0$ . This effect makes it possible to measure the Wigner crystal sound velocity in a ring with an ‘adjustable barrier’ (height controlled by a gate voltage).

The starting point of our analysis is a model system, where the Wigner crystal is regarded as an elastic chain of spinless electrons forming a ring. In the presence of a potential barrier, smooth on the scale of  $a$  but well localized on the scale of  $L$ , and the AB interaction the Lagrangian of such a system in the long wavelength approximation is

$$L = \frac{ma^2}{8\pi^2} \left\{ \dot{\varphi}^2 - s^2(\varphi')^2 \right\} - V_0 \delta(x) \cos(\varphi) + \frac{\hbar}{L} \frac{\Phi}{\Phi_0} \dot{\varphi}. \quad (1)$$

Here  $\varphi = 2\pi u(x)/a$  is the dynamical displacement field of the crystal,  $V_0$  is the magnitude of the pinning potential (without loss of generality placed at the point  $x = 0$ ) and  $\Phi$  is the magnetic flux through the ring.

We emphasize that (1) is an effective Lagrangian that describes the long wavelength aspects of the quantum dynamics of the Wigner crystal. The short wavelength fluctuations do not affect the global dynamics of the system, and only result in a renormalization of the magnitude,  $V_0$ , of the potential, (already included in (1) but negligible for a stiff Wigner crystal<sup>8</sup>). We assume that the ring circumference is large enough to justify dropping terms from (1) which are irrelevant in an infinite system.

The flux-induced persistent current  $I(\Phi) = -c\partial F/\partial\Phi$ , is defined in terms of the sensitivity of the free energy of the ring to a magnetic flux. For the following analysis, it is convenient to express the free energy  $F$  as a functional integral over quantum- and thermal fluctuations of the displacement field,

$$F = -k_B T \ln \left\{ \sum_{n=-\infty}^{\infty} (-1)^{n(N-1)} \int D\varphi_n e^{-S_E[\varphi_n]/\hbar} \right\}, \quad (2)$$

where the action  $S_E$  derives from the Lagrangian (1) in the imaginary time representation. ‘Twisted’ boundary conditions in imaginary time are imposed on the field  $\varphi$  (see, e.g.<sup>10</sup>):  $\varphi_n(\tau + \beta, x) = \varphi_n(\tau, x) + 2\pi n$ . Here  $n = 0, \pm 1, \pm 2 \dots$  is the topological (winding) number, classifying homotopically inequivalent trajectories. The physical meaning of this boundary condition follows from the definition of the field  $\varphi = 2\pi u(x)/a$ ; a uniform shift of the crystal by a distance equal to an integer times the lattice constant  $a$  leads, in the ring geometry, to a state identical to the initial state after certain permutations of electrons. For the minimum shift by  $1 \times a$  ( $\Delta\varphi = 2\pi$ ), the initial state is recovered after  $(N - 1)$  successive permutations of pairs of electrons. The corresponding extra phase  $\pi(N - 1)$ , that appears in the many-particle

wavefunction because the electrons obey Fermi statistics, generates the factor  $(-1)^{n(N-1)}$  in (2). As we will see below, this factor properly accounts for the parity effects in the response of one-dimensional interacting electrons to a magnetic field<sup>11-13</sup>. We note in passing that the analogous twisted boundary conditions appear when the Luttinger model is applied to a ring geometry<sup>12</sup>. The appearance of the homotopic index  $n$  in the boundary condition suggests that the functional integral should first be calculated for trajectories belonging to a definite homotopic class, and then the homotopically non-equivalent classes of trajectories should be summed over.

In every homotopic class we will calculate the functional integral using the saddle point approximation, assuming the saddle point action to be large,  $S_n \gg \hbar$ , on the extremal trajectory given by the solution of the classical equations of motion in imaginary time. Below we will show that this assumption is justified for a stiff Wigner crystal.

First we calculate the persistent current in the ideal, unpinned crystal ( $V_0 = 0$ ). In a perfect ( or weakly pinned ) Wigner crystal, long-wave quantum fluctuations are cut off at the wavelength of the order of inverse crystal size  $L$ . It is physically evident that we can imagine ordered crystal structures until the mean square fluctuations of the dimensionless field  $\varphi$ ,

$$\langle \varphi^2 \rangle \sim \alpha \int_{\pi/L}^{\pi/a} \frac{dk}{k} \coth \left( \frac{s\hbar}{2k_B T} k \right), \quad (3)$$

are small  $\langle \varphi^2 \rangle \ll 1$  ( $T$  is the temperature,  $\alpha = \pi\hbar/msa$  denotes the dimensionless parameter that determines the intensity of quantum fluctuations in the Wigner crystal). For  $T \rightarrow 0$  this inequality imposes an upper bound to the chain length  $L \ll ae^{1/\alpha}$ . One can easily check that for such samples the thermal fluctuations are suppressed up to the temperature  $T \lesssim T_s/\alpha$  ( $T_s \equiv \hbar s/L$ ). The situation is changed drastically for a strongly pinned Wigner crystal where an "intermediate" cut off scale appears<sup>8</sup>.

One can readily calculate the persistent current of an ideal ring as the problem in the long wavelength limit is described by a quadratic Lagrangian. The extremal trajectory corresponding to the twisted boundary condition is linear in imaginary time and independent of the  $x$ -coordinate,

$$\varphi_n(\tau) = 2\pi n (\tau/\hbar\beta). \quad (4)$$

By substituting (4) into (1) and (2), it is easy to find an exact solution for the free energy in terms of the Jacobi function  $\vartheta_3$  (see e.g.<sup>14</sup>). The asymptotic expressions for the persistent current at high- and low temperatures are

$$\frac{I_{WC}}{I_0} \simeq \begin{cases} 2\frac{T}{T_0} e^{-\frac{\pi}{2}\frac{T}{T_0}} (-1)^N \sin \left( 2\pi \frac{\Phi}{\Phi_0} \right), & T \gtrsim T_0 \\ 1 - 2\{ \frac{\Phi}{\Phi_0} + \delta_N \}, & T \ll T_0 \end{cases} \quad (5)$$

Here  $\{ \{x\} \}$  denotes the fractional part of  $x$ , and the parity dependent term  $\delta_N$  is 1/2 (0) for  $N$  odd (even). Thus the persistent current carried by an ideal Wigner crystal is a periodic function of flux with period  $\Phi_0 = hc/e$  and amplitude  $I_0 = ev_F/L$  at low temperatures. The oscillations are exponentially damped at  $T \gtrsim T_0 = \hbar v_F/L$ . The current has a paramagnetic character when there is an even number of electrons in the ring (i.e. the induced magnetic moment is parallel to the external magnetic field) and diamagnetic for an odd number of electrons. All these properties of the persistent current exactly coincide with those calculated using the model of an ideal Fermi gas. For  $T = 0$ , this was first shown in Ref.<sup>6</sup> for a general case of arbitrary Coulomb-like interaction. At finite temperatures there are in general contributions due to crystal deformations produced by thermally excited phonons. It is possible to show<sup>15</sup>

that, even in a perfect Wigner crystal ring, the contribution of phonon fluctuations to the action results in a correction to the persistent current which is small if the temperature is less than  $mv_F s/2$ .

Now let us consider the persistent current in a Wigner crystal in the presence of a potential barrier. A uniform sliding motion of the crystal is impossible in this case, and the persistent current is inevitably accompanied by a local deformation in a small region adjacent to the barrier. The mechanism for charge transport around the ring includes electron tunneling through the barrier, as well as elastic relaxation of the associated deformed state of the crystal. The relevance of such a partition of the macroscopic tunneling of the system into two processes becomes especially clear in the case of strong pinning,  $\alpha V_0 \gg T_s$ . The above mechanism for macroscopic tunneling was first considered in connection with the tunneling of commensurate charge density waves<sup>7</sup> and has also been used to describe the tunneling conductivity of a Wigner crystal<sup>8</sup>. In these contexts it was shown<sup>7,8</sup> that in the case of strong pinning the dominating tunneling process is the elastic relaxation of the deformed state arising in the near-barrier region.

Thus to evaluate the persistent current of a strongly pinned Wigner crystal at  $T \neq 0$  we need to find the instanton solution of the free equation of motion ( $V_0 = 0$ ) satisfying twisted boundary conditions imposed at the finite interval of imaginary time  $[0, \beta]$ . It is easy to verify that the desired exact solution is given by

$$\varphi_\sigma^{(s)}(\tau) = 2\sigma \arctan \left[ \coth \left( \frac{\pi|x|}{\hbar s \beta} \right) \tan \left( \pi \left( \frac{\tau}{\hbar \beta} - \frac{1}{2} \right) \right) \right], \quad \sigma = \pm 1. \quad (6)$$

Equation(6) transforms into the Larkin-Lee instanton<sup>7</sup> at low temperatures and describes a uniform sliding of the Wigner crystal-ring, Eq.(4), in the high-temperature region. A description of the dominating relaxation process in terms of this 'periodic instanton'-solution is valid in the region outside the interval  $[-\ell_0, \ell_0]$  containing the part of the crystal deformed by the initial tunneling process. The length  $\ell_0$ , which is inversely proportional to the potential  $V_0$ , appears only as a limit of the integration over coordinate  $x$ ; we assume that  $\ell_0 \ll L/2$ , a criterion which one can show to be equivalent to a restriction on temperature,  $T \ll \alpha V_0$ .

At  $T \rightarrow 0$  the one-instanton action for the solution, Eq.(6), reduces to the expression derived in<sup>7</sup>.

$$S_i \simeq \frac{\hbar}{\alpha} \ln \left( \frac{\alpha V_0}{T_s} \right) \quad (7)$$

This action is large,  $S_i/\hbar \gg 1$ , in the strong pinning case and we can use the well-known dilute instanton gas approximation (see e.g.<sup>16</sup>) when evaluating the flux-dependent part of the ground state energy. In this manner we get the zero temperature value of the persistent current as

$$I_{WC}(T=0) \sim (-1)^N \frac{e s}{L} \left( \frac{T_s}{\alpha V_0} \right)^{1/\alpha} \sin(2\pi \Phi / \Phi_0). \quad (8)$$

This result for the persistent current of a Wigner crystal in the presence of a pinning potential barrier, clearly shows that the effect of the barrier is simply to suppress and smoothen the zero temperature current. The suppression of the current reflects the fact that due to the barrier, charge transport in the ring is not caused by a sliding rotation of the Wigner crystal as a whole. Rather, it is due to macroscopic quantum tunneling of the system through a deformed state of the crystal. Notice that the size dependence of the oscillation amplitude  $\propto (1/L)^{1+1/\alpha}$  is intermediate ( $\alpha \ll 1$ ) between the regimes of Aharonov-Bohm oscillations in metals<sup>3,4</sup> ( $I \propto 1/L$ ) and in dielectrics<sup>17,14</sup> ( $I \propto \exp(-L/l_g)$ ,  $L \gg l_g$ ,  $l_g \equiv \hbar s / \Delta_g$ ,  $\Delta_g$  being the gap in the energy spectrum on the Fermi level).

Except at very low temperatures,  $T \ll T_s$ , the main contribution to the oscillating part of the free energy of a stiff Wigner crystal provided by trajectories with minimal winding number ( $n = \pm 1$ ). By using the periodic instanton solution, Eq.(6), one gets for the normalized temperature-dependent current in the strong pinning case

$$\frac{I_{WC}(T)}{I_{WC}(0)} = \frac{T}{T_s} \exp\left(\frac{1}{\alpha} f(T/T_s)\right), \quad f(x) = \frac{\pi}{2}x - \ln\left(\frac{\sinh(\pi x)}{\pi x}\right). \quad (9)$$

This result implies a non-monotonic temperature dependence of the persistent current; for a stiff crystal (small  $\alpha$ ) the current has an exponentially sharp maximum at  $T \sim 0.5T_s$ , with a width of the order of  $\sqrt{T_0 T_s}$ . The physical reason for this non-trivial temperature dependence — shown in Fig. 1 for different values of  $\alpha$  — can be explained as follows: It is easy to see from (6) that as the temperature is increased the picture of the elastic deformation propagating as a ‘sharp’ instanton changes (at  $T \sim T_s$ ) into a picture of a homogeneous sliding of the crystal as a whole.

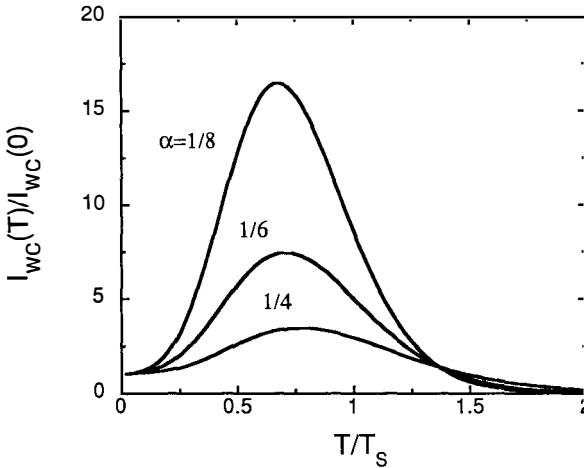


FIG. 1 Temperature dependence of the normalized persistent current in a strongly pinned Wigner crystal of different stiffness (measured by  $\alpha^{-1} = 2msa/h$ ;  $T_s = \hbar s/k_B L$ , see text). The sharp peak for stiff crystals is a result of a competition between two effects of temperature: a reduced renormalized tunneling barrier and enhancement of destructive interference.

This temperature-induced ‘softening’ of the instanton reduces the contribution to the action from the elastic deformation of the crystal. Hence, the persistent current should increase with temperature. On the other hand this effect competes with a thermal smearing of the phase coherence which — as we showed for the unpinned crystal — tends to reduce the current. The sharp peak in the temperature dependence of the persistent current carried by the pinned Wigner crystal, is a result of this very competition.

Formula (9) is valid in the strong pinning limit, when temperature is much smaller than  $\alpha V_0$ . At high temperatures,  $T \gtrsim \alpha V_0$ , the pinning potential can be treated as a perturbation when

calculating the depinning of the Wigner crystal. In this case we find unimportant corrections to the persistent current in an ideal Wigner crystal. Note, however, that the perturbation theory calculations have revealed that the result for the low temperature limit of a persistent current in a perfect stiff Wigner crystal-ring is unstable if an arbitrary small pinning potential ( $V_0 > T$ ;  $T \rightarrow 0$ ) is accounted for (the details of this calculation will be published elsewhere<sup>15</sup>).

By measuring the dependence of the persistent current on the barrier height at zero temperature (8) and its temperature dependence (9), one has an opportunity to determine independently the stiffness parameter,  $\alpha = h/2msa$ , and the sound velocity,  $s$ , in this system of strongly correlated electrons. This gives us strong reasons to propose an experiment using a gate-controlled barrier in a mesoscopic semiconductor ring in order to study Wigner crystallization and to measure the parameters of the crystal.

In conclusion we have shown that in an ideal ring with no impurity scattering, the persistent current carried by interacting electrons — so strongly correlated that they form a Wigner crystal — is indistinguishable from the current carried by a non-interacting Fermi gas. By incorporating a potential barrier in the ring structure, a qualitative change of the magnitude and temperature dependence of the persistent current appears. With an adjustable barrier, these differences can be used for detecting and investigating the properties of the Wigner crystal.

We gratefully acknowledge discussions with L. Glazman, A. Nersisyan, A. Sjölander, and A. Zagoskin. This work was supported by the Swedish Royal Academy of Sciences, the Swedish Natural Science Research Council, the Swedish National Board for Industrial and Technical Development, and by the NSF through grant DMR-9113911. One of us (I.K.) acknowledges the hospitality of the Department of Applied Physics, CTH/GU.

\* Permanent address: B. Verkin Institute for Low Temperature Physics and Engineering, Academy of Sciences of Ukraine, 310164 Kharkov, Ukraine

<sup>1</sup> D. Mailly, C. Chapelier, and A. Benoit, Phys. Rev. Lett. **70**, 2020 (1993).

<sup>2</sup> J. Liu, W. X. Gao, K. Ismail, K. Y. Lee, J. M. Hong, and S. Washburn, Phys. Rev. B (unpublished).

<sup>3</sup> L. Günter and Y. Imry, Solid State Commun. **7**, 1391 (1969).

<sup>4</sup> I. O. Kulik, JETP Lett., **11**, 275 (1970).

<sup>5</sup> V. Ambegaokar and U. Eckern, Phys. Rev. Lett. **65**, 381 (1990).

<sup>6</sup> A. Müller-Groeling, H. A. Weidenmüller, and C. H. Lewenkopf, Europhys. Lett. **22**, 193 (1993).

<sup>7</sup> A. I. Larkin and P. A. Lee, Phys. Rev. **B17**, 1596 (1978).

<sup>8</sup> L. I. Glazman, I. M. Ruzin, and B. I. Shklovskii, Phys. Rev. **B45**, 8454 (1992).

<sup>9</sup> C. L. Kane and M. P. A. Fisher Phys. Rev. **B46**, 15233 (1992).

<sup>10</sup> I. V. Krive and A. S. Rozhavsky, Int. J. Mod. Phys. **B6**, 1255 (1992).

<sup>11</sup> N. Byers and C. N. Yang, Phys. Rev. Lett. **7**, 46 (1961).

<sup>12</sup> D. Loss, Phys. Rev. Lett. **69**, 343 (1992).

<sup>13</sup> A. J. Leggett, in *Granular Electronics*, Eds. D. K. Ferry, J. R. Barker, and C. Jacoboni, NATO ASI Ser. B vol. 251 (Plenum, New York, 1991), p. 297.

<sup>14</sup> E. N. Bogachek, I. V. Krive, I. O. Kulik, and A. S. Rozhavsky, Phys. Rev. **B42**, 7614 (1990); Sov. Phys. JETP, **70**, 336 (1990).

<sup>15</sup> I. V. Krive, R. I. Shekhter, S. M. Girvin, and M. Jonson, (unpublished).

<sup>16</sup> R. Rajaraman, *Solitons and Instantons. An Introduction to Solitons and Instantons in Quantum Field Theory* (North Holland, Amsterdam, 1982).

<sup>17</sup> I. O. Kulik, A. S. Rozhavsky, and E. N. Bogachek, JETP Lett., **47**, 303 (1988).

## TUNNELING AND THE BAND STRUCTURE OF CHAOTIC SYSTEMS

P. Leboeuf and A. Mouchet, Division de Physique Théorique<sup>†</sup>  
Institut de Physique Nucléaire, 91406 Orsay Cedex, France.

As is well known, the quantum motion of electrons in periodic potentials gives rise to energy bands. A precise determination of the density of states is necessary in order to obtain an appropriate description of the elementary physical properties, like the transport and magnetic properties. However, a direct calculation of the dispersion laws is in general difficult, like for example in the case of a chaotic underlying dynamics.

Our purpose here is to consider the band structure of classically chaotic periodic systems from the point of view of periodic orbit theory. In this approach, the trace of the evolution operator – which can be related to the density of states – is expressed, in the semiclassical limit, as a sum over classical periodic paths <sup>1),2)</sup>. As shown below, the dependence of the dispersion laws on the quasimomenta (or Bloch angles) is related to the winding numbers of the periodic orbits (p.o.'s) around the elementary cell. Trajectories with winding numbers different from zero are associated to open diffusive processes through the periodic lattice. However, in some cases these processes are classically forbidden, or not well described by the real p.o.'s. The relevant features of the band structure can however be recovered going one step beyond this approximation by including some tunneling effects in the semiclassical trace formula. This is done by taking into account the complex p.o.'s (by complex or ghost p.o.'s we mean the periodic solutions of Hamilton's equations having at least one complex phase-space coordinate). Moreover, the inclusion of ghost orbits extends the range of validity of the semiclassical approximation. As an illustration we present an example in which, in spite of being far from a classical behaviour, including the complex p.o.'s we obtain very good results for the dependence of the (quasi-)energies on the Bloch-numbers, while only taking into account the real p.o.'s gives a very crude approximation to the true solution.

---

<sup>†</sup>Unité de recherche des Universités de Paris XI et Paris VI associée au CNRS

In the standard WKB theory – valid for integrable systems – complex classical paths have been used in the past in different contexts, as in the study of the band structure of one-dimensional periodic potentials. To our knowledge, the existence and relevance of ghost orbits in the semiclassical trace formula was pointed out for the first time in <sup>3),2)</sup>. More recently, these orbits were studied in more detail in Refs. <sup>4),5)</sup> in connection to the trace of the evolution operator of the kicked top and the standard map, respectively. Here, we also consider a dynamics described by a discrete (chaotic) map, inspired by the study of the motion of an electron in a two-dimensional periodic potential in the presence of a uniform and constant magnetic field perpendicular to the crystal plane. For a strong magnetic field, the lowest Landau level approximation leads to the motion of a 1D-particle whose phase space is a 2D-torus  $\mathcal{T}$ . If Planck's constant is rational,  $\hbar = M/N$ , then the corresponding evolution operator  $U$  is doubly periodic and its spectrum is made of  $N$  bands  $\epsilon_\alpha(\vec{\theta})$  given by  $U|\psi_\alpha(\vec{\theta})\rangle = \exp(i\epsilon_\alpha(\vec{\theta}))|\psi_\alpha(\vec{\theta})\rangle$ ,  $\alpha = 1, \dots, N$ . For simplicity, in the following we take  $M = 1$  and  $\mathcal{T}$  will be of unit length in both directions. The Bloch parameters  $\vec{\theta} = (\theta_1, \theta_2)$  are associated to generalized periodic boundary conditions  $\psi(q+1) = \exp(i\theta_1)\psi(q)$ ,  $\psi(p-1) = \exp(i\theta_2)\psi(p)$ . The classical limit is obtained when  $N \rightarrow \infty$ .

In order to mimic the motion of the electron as the magnetic field is lowered, we consider the kicked Hamiltonian  $H = f(p) + g(q) \sum_{n=-\infty}^{\infty} \delta(t - n\tau)$ , which leads to a discrete map on the torus

$$q_{i+1} = q_i + \tau f'(p_{i+1}) \pmod{1}; \quad p_{i+1} = p_i - \tau g'(q_i) \pmod{1}, \quad (1)$$

where  $(q_j, p_j) \in [0, 1]^2$  are the phase-space coordinates of the particle at time  $t = j\tau$  while  $f$  and  $g$  are two smooth functions of period one. One can interpret the two integers  $w_q^{(i+1)} = [q_i + \tau f'(p_{i+1})]$ ,  $w_p^{(i)} = -[p_i - \tau g'(q_i)]$  (square brackets denote integer part) as the winding numbers of the orbit around the torus for the iteration  $(q_i, p_i) \rightarrow (q_{i+1}, p_{i+1})$  in the  $q$  and  $p$  directions, respectively. As we shall see in the following these two integers – which arise from the toroidal topology of phase space by the identification of points differing by an integral number of phase-space cells – play a crucial role in the semiclassical interpretation of the bands (see also Ref. <sup>6)</sup>).

Quantum mechanically the map is implemented by the one-step evolution operator  $U = e^{-i\tau f(\hat{p})/\hbar} e^{-i\tau g(\hat{q})/\hbar}$ . In order to make explicit the dependence on the parameters  $\vec{\theta}$ , instead of  $U$  we consider the operator  $\tilde{U}(\vec{\theta})$  which is obtained from the expression of  $U$  by making the substitutions  $\hat{q} \rightarrow \hat{q} + \hbar\theta_2, \hat{p} \rightarrow \hat{p} + \hbar\theta_1$  <sup>7)</sup>. Then the dispersion laws  $\epsilon_\alpha(\vec{\theta})$  are given by the roots  $z_\alpha(\vec{\theta}) = \exp(i\epsilon_\alpha(\vec{\theta}))$ ,  $\alpha = 1, \dots, N$  of the spectral determinant

$\det(z - \tilde{U}(\vec{\theta})) = \sum_{k=0}^N a_k(\vec{\theta})z^k$ , where  $a_N(\vec{\theta}) = 1$  by construction. The coefficients of this characteristic polynomial can be obtained from the trace of the first  $N$  powers of  $\tilde{U}$  through the formula  $a_{N-k} = -\frac{1}{k} \sum_{n=1}^k a_{N-k+n} \text{tr}(\tilde{U}^n)$ , ( $k = 1, \dots, N$ ) whose interest comes from the fact that in the semiclassical limit  $N \rightarrow \infty$  the trace of the powers of  $\tilde{U}$  can be computed in terms of a finite number of classical p.o.'s (which are assumed to be isolated)<sup>1),8)</sup>. In our case, by considering the special topology of phase space, we get

$$\text{tr}(\tilde{U}^n) = i^n \sum_{\text{p.o.}} \frac{T}{\sqrt{|\det(M-1)|}} \exp\left(\frac{i}{\hbar} S + i w_p \theta_2 + i w_q \theta_1 - i \frac{\pi}{2} \nu\right). \quad (2)$$

In this formula the sum extends over all the real p.o.'s of the map (1) whose period  $T$  is an integer fraction of  $n$ ,  $w_p$  and  $w_q$  are the total winding numbers of the p.o.,  $w_p = \sum_{j=0}^{n-1} w_p^{(j)}$ ,  $w_q = \sum_{j=0}^{n-1} w_q^{(j)}$ ,  $S = \sum_{j=0}^{n-1} \{-\tau(g(q_j) + f(p_j)) + p_{j+1}(q_{j+1} - q_j) - w_p^{(j)} q_j - w_q^{(j)} p_j\}$  is the classical action of the p.o.,  $M$  is the monodromy matrix (related to its stability) and  $\nu$  is the number of negative eigenvalues of the Hessian of  $S$  (a  $2n \times 2n$  matrix assumed to be non singular). The information concerning the band structure (i.e., the dependence on  $\vec{\theta}$  of the dispersion laws) is thus recovered, semiclassically, through the factor  $\exp(i(w_q \theta_1 + w_p \theta_2))$ . This factor, which is different from zero for open diffusive p.o.'s, can be interpreted for each  $\vec{\theta}$  as a unitary representation of the homotopy group of  $\mathcal{T}$ . The fact that the representation of that group appears in  $\text{tr}(\tilde{U}^n)$  when one deals with path integrals (or their discrete equivalent) in multiply-connected spaces is well known<sup>9)</sup>. Eq.(2) was obtained from the exact expression of  $\text{tr}(\tilde{U}^n)$  replacing the sums by integrals using the Poisson summation formula and then computing the integrals by the stationary phase approximation. One step further is to deform the contour of integration of the path integral in order to reach the stationary orbits lying in the complex plane. The outcome of this procedure is to include in the summation (2) complex p.o.'s, whose contribution is exponentially small. However, as we shall now see, they cannot be neglected if  $\hbar$  is not too small or if we are close to a (first order) bifurcation of a p.o. .

For the sake of definiteness, we consider the kicked-Harper model where we have  $g(x) = f(x) = -\gamma \cos(2\pi x)/(2\pi\tau)$ . Phase-space plots of the classical trajectories of the kicked-Harper map for different values of  $\gamma > 0$  can be found in<sup>7)</sup>: for  $\gamma \rightarrow 0^+$  the dynamics is integrable (it tends to the Harper Hamiltonian); for  $\gamma \simeq 0.4$  it is a mixture of regular and chaotic orbits, while for  $\gamma \geq 0.6$  unstable chaotic trajectories dominate. At the quantum level, some spectral and transport properties of the model were studied in<sup>7),10)</sup>.

We now compute the trace of  $\tilde{U}$  for this model. The exact result is

$$\text{tr } \tilde{U} = N \left\{ J_0(\gamma N) + 2 \sum_{w=1}^{\infty} e^{-iwN\pi/2} \cos(w\theta_1) J_{wN}(\gamma N) \right\} \times \{\theta_1 \Rightarrow \theta_2\}, \quad (3)$$

where the second curly brackets in the r.h.s. is identical to the first one except for the fact that  $\theta_1$  is replaced by  $\theta_2$ . In order to compute (3) semiclassically, we need to find all the p.o.'s of period one of the map. Their location  $(q, p) \in [0, 1]^2$  is given by the solutions of the set of equations  $\sin(2\pi q) = w_p/\gamma$ ;  $\sin(2\pi p) = w_q/\gamma$ , where  $(w_q, w_p) \in \mathbb{Z}^2$ . For a fixed  $\gamma > 0$ , there is an infinite number of complex p.o.'s (all integers  $(w_q, w_p)$  whose modulus is larger than  $\gamma$ ). Since the imaginary part of the coordinate is proportional to  $\text{Arch}|w_i/\gamma|$ , the complex p.o.'s with large winding number  $|w_i| \gg \gamma$  are deeply located in the complex plane. As  $\gamma$  increases (starting from  $1/2$ , for example), a complex orbit becomes real if  $\gamma$  becomes larger than the modulus of both winding numbers. This will happen at each integer value of  $\gamma$  through a first-order bifurcation (fold catastrophe), where several orbits coalesce in at least one phase-space coordinate. The total number of real p.o.'s increases with  $\gamma$  as  $(4[\gamma] + 2)^2$ .

Concerning the stability of those orbits, generically  $\text{tr } M = 2$  at  $\gamma_n = n \in \mathbb{N}^*$  for all the real p.o.'s emerging at that value of  $\gamma$ . When  $\gamma$  is increased, half of them are initially stable, the other half unstable; but very rapidly they become all unstable<sup>11)</sup>.

Using the information described above we have computed semi-classically the trace of  $\tilde{U}$  (for fixed  $\gamma$  and arbitrary  $N$ ) including all the real as well as complex p.o.'s. The result is

$$\text{tr } \tilde{U} = \frac{2}{\pi\gamma} F(\theta_1)F(\theta_2) + \mathcal{O}(1/N) \quad (4)$$

where

$$\begin{aligned} F(\theta) &= 2 \sum_{w=0}^{[\gamma]} e^{-iwN\pi/2} \frac{\cos(w\theta)}{\sqrt{\cos(x_w)}} \cos \{ N(\gamma \cos(x_w) - w(x_w - \pi/2)) - \pi/4 \} \\ &+ \sum_{w=[\gamma]+1}^{\infty} e^{iwN\pi/2} \frac{\cos(w\theta)}{\sqrt{\sinh(y_w)}} e^{-N(wy_w - \gamma \sinh(y_w))} \end{aligned} \quad (5)$$

and  $x_w = \arcsin(w/\gamma)$ ;  $y_w = \text{Arch}(w/\gamma)$ . In Eq.(4),  $F(\theta_2)$  is related to the  $q$ -coordinate of the orbit, while  $F(\theta_1)$  contains the information about its momentum. The first sum in Eq.(5) ( $w \leq [\gamma]$ ) comes from p.o.'s having a real coordinate (which reproduces the oscillating part of Bessel functions occurring in Eq.(3)), while the second sum ( $w > [\gamma]$ ) comes from those having a complex coordinate (reproducing the exponentially decreasing part of the Bessel functions). The symbol  $\sum'$  indicates that the term  $w = 0$  must be multiplied by a factor  $1/2$ . The product of both functions in Eq.(4) gives rise to four different sums, one related to real p.o.'s, the other three to complex ones. The dependence on  $\vec{\theta}$  in Eq.(4) is the same for both kinds of orbits,

but the complex orbits are exponentially damped by a factor (or a product of factors) of the form  $\exp(-NS_I)$ , where  $S_I = wy_w - \gamma \sinh(y_w) > 0$ . Because of that, complex p.o.'s with large winding number can in general be neglected. On the other hand, as  $\gamma$  approaches some integer value  $n$  from below, the contribution of the complex p.o.'s becoming real at  $\gamma_n = n > 0$  is particularly important, since the imaginary part of their action tends to zero. In fact, they remain important for parameter values relatively far from  $\gamma_n$ , since  $S_I \simeq \sqrt{2/n}(\gamma_n - \gamma)^{3/2}/3\pi$  as  $\gamma \rightarrow \gamma_n$  from below (the exponent  $3/2$  was also found for the kicked top and the standard map <sup>4),5)</sup>). Moreover, because of the  $1/\sqrt{n}$  dependence, the parameter interval in which complex orbits are important increases with  $\gamma$  (at a fix  $N$ ). Exactly at  $\gamma = \gamma_n$  Eq.(5) is not defined since the denominator in both sums vanishes due to the coalescence of several orbits. In order to avoid divergences we must improve the approximation, and include third order terms in the computation of the integrals for  $\gamma \simeq \gamma_n$  using Airy functions <sup>12),3)</sup>. Including these corrections, we find that Eq.(4) reproduces extremely well the exact  $\text{tr } \tilde{U}$ , even for small values of  $N$ .

In order to illustrate this, let us consider the extreme quantum limit  $N = 2$ . For the kicked-Harper map, it can be shown that for  $N = 2$  all the information concerning the spectrum of  $\tilde{U}$  is contained in  $\text{tr } \tilde{U}$ , since the characteristic polynomial is of second degree with coefficients  $a_2 = 1, a_1 = -\text{tr } \tilde{U}, a_0 = 1$ . The two dispersion relations obtained from that equation are  $\epsilon_{\pm}(\vec{\theta}) = \pm \arccos(\text{tr } \tilde{U}(\vec{\theta})/2)$ . Although our results are valid for arbitrary  $\gamma > 0$ , the role of the complex p.o.'s is particularly stressed in  $0 < \gamma < 1$ . In that parameter interval there exist only four real p.o.'s of period one, located at  $(0,0), (0,1/2), (1/2,0), (1/2,1/2)$ . But these orbits do not introduce any  $\vec{\theta}$  dependence in  $\text{tr } \tilde{U}$  (and therefore in  $\epsilon_{\pm}(\vec{\theta})$ ) since for all of them  $w_q = w_p = 0$ , leading to flat bands. In fact, the exact dispersion laws for  $N = 2$  have a strong and non-trivial  $\vec{\theta}$ -dependence; in particular, for an arbitrary  $\gamma$  there is at least one linear contact (diabolical point) between the two bands. In order to introduce semiclassically a  $\vec{\theta}$  dependence in the dispersion laws one must include complex p.o.'s. Fig.1(a) plots the exact result and the semiclassical dispersion laws computed from Eq.(4) with and without complex orbits for  $\gamma = 0.86$  and  $\theta_2/2\pi = 0.5$  as a function of  $\theta_1/2\pi$  (only complex p.o.'s up to winding number two were included). The result obtained with complex p.o.'s is extremely good even near the diabolical point, which is the worst situation for semiclassical analysis. Part (b) of that Figure shows the case  $\gamma = 4.86$ . It is also possible to compute, using only the  $\text{tr } \tilde{U}$ , the dispersion laws for  $N = 3$  since the coefficients of the characteristic polynomial are now given by  $a_3 = 1, a_2 = -\text{tr } \tilde{U}, a_1 = \overline{\text{tr } \tilde{U}}, a_0 = 1$ . Fig.1(c)-(f) illustrate the results obtained in this case for the dispersion laws and the trace of  $\tilde{U}$ .

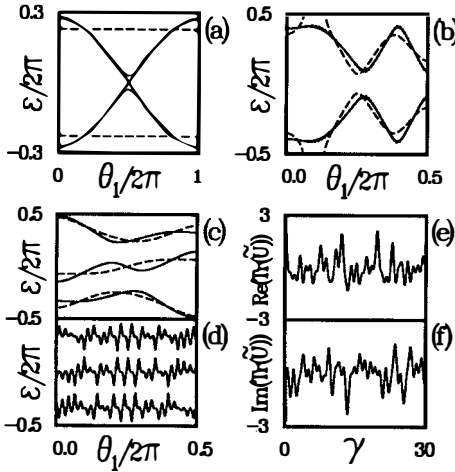


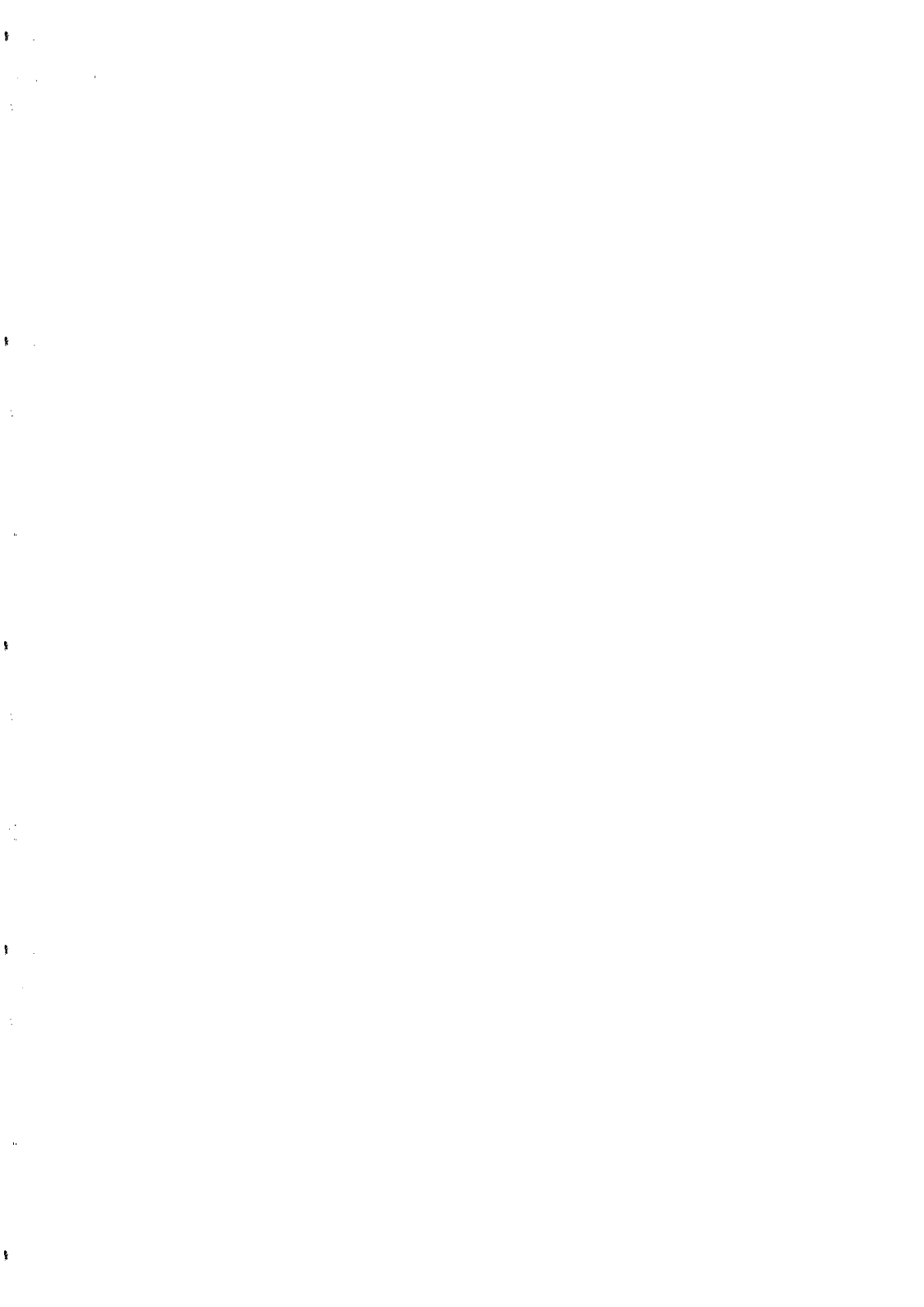
**Fig.1:** Band structure and trace of the evolution operator for the kicked-Harper model. (a) dispersion laws  $\epsilon(\theta)$  as a function of  $\theta_1/2\pi$  for  $\theta_2/2\pi = 0.5$ ,  $N = 2$  and  $\gamma = 0.86$ . Full line: exact; dotted line: semiclassical theory including the real and complex p.o.'s; dashed line: semiclassical theory including only the real p.o.'s. (b) same as in part (a) but for  $\gamma = 4.86$  and  $\theta_2/2\pi = 0.25$ . (c)-(d) same as in part (a) but for  $N = 3$ ,  $\theta_2/2\pi = 0.25$ ,  $\gamma = 2.86$  and  $\gamma = 52.1$ , respectively. (e)-(f) real and imaginary part of  $\text{tr}(\tilde{U})$  as a function of  $\gamma$  for  $\theta_1/2\pi = 0.55$ ,  $\theta_2/2\pi = 0.32$  and  $N = 3$ . The semiclassical result using only the real p.o.'s is not shown in (e)-(f). Except near the diabolical point in part (a), in all the other plots the dotted line cannot in general be distinguished from the full line.

As a final remark, let us point out that the approach presented in this Letter is also relevant in systems where the topology producing the band structure is not toroidal, but for example cylindrical. This occurs in particular in the context of persistent currents, where the Aharonov-Bohm flux threading the ring plays the role of the Bloch-parameter and the winding number of the p.o.'s is precisely the winding number around that flux (see Ref. <sup>13</sup>) for a more detailed discussion).

#### References:

- 1) M. C. Gutzwiller, *J. Math. Phys.* **12**, 343 (1971).
- 2) R. Balian and C. Bloch, *Ann. Phys. (NY)* **85**, 514 (1974).
- 3) R. Balian and C. Bloch, *Ann. Phys. (NY)* **69**, 76 (1972).
- 4) M. Kuś, F. Haake and D. Delande, *Phys. Rev. Lett.* **71**, 2167 (1993).
- 5) R. Scharf and B. Sundaram, preprint.
- 6) J. M. Robbins, *Phys. Rev. A* **40**, 2128 (1989).
- 7) P. Lebœuf, J. Kurchan, M. Feingold and D.P. Arovav, *Phys. Rev. Lett.* **65**, 3076 (1990); *CHAOS* **2**, 125 (1992).
- 8) M. Tabor *Physica* **6D**, 195 (1983); G. Junker and H. Leschke *Physica D* **56**, 135 (1992).
- 9) L. S. Schulman *Techniques and Applications of Path Integration* (Wiley, New York, 1981), chap. 23.
- 10) R. Lima and D.L. Shepelyansky, *Phys. Rev. Lett.* **67**, 1377 (1991); T. Geisel et al, *Phys. Rev. Lett.* **67**, 3635 (1991); R. Artuso, G. Casati and D. Shepelyansky, *Phys. Rev. Lett.* **68**, 3826 (1992); R. Artuso et al, *Phys. Rev. Lett.* **69**, 3302 (1992).
- 11) However, the existence of a small parameter range (whose size decreases with  $\gamma$ ) above each integer value of  $\gamma$  around which some of the period-one p.o.'s are stable demonstrates that the kicked-Harper map, even for large values of  $\gamma$ , is never completely hyperbolic.
- 12) M. V. Berry and K. E. Mount *Rep. Prog. Phys.* **35** 315 (1972); A. Ozorio de Almeida and J. Hannay, *J. Phys. A* **20**, 5873 (1987).
- 13) P. Lebœuf and A. Mouchet, in preparation.

**LOCALIZED REGIME  
AND METAL-INSULATOR TRANSITION**



## QUANTUM COHERENT EFFECTS IN FERMI-GLASSES

A. Frydman and Z. Ovadyahu, The Racah Institute of Physics,  
The Hebrew University, Jerusalem 91904, Israel.

### *1. Introduction.*

The low-temperature transport properties of electronic systems may be appreciably modified by quantum-coherent effects. This issue has been intensively investigated for the last 15 years and is, by now, fairly well understood. In particular, quite well established theories exist for the weak scattering regime due to the applicability of a perturbation treatment. Quantum mechanical corrections to the Boltzmann theory in this regime arise from interference phenomena that are usually referred to as "Weak-Localization" (WL) effects. These are believed to be a precursor to the disorder-driven, "true" Localization in which spatial disorder causes the electronic wave-functions to be confined to a particular site with envelopes that decay exponentially away from it. The spatial decay length,  $\xi$ , called the localization length, is a function of disorder and diverges at the transition.

When  $\xi$  becomes the smallest length in the problem, the system is "strongly-localized" (SL) and electronic transport is only possible by some sort of hopping. This regime is much less understood than the diffusive one despite substantial theoretical and experimental efforts over several decades. Nevertheless, in many uniformly disordered electronic systems, it is established that transport is governed by Variable Range Hopping (VRH) as originally described by Mott.<sup>1)</sup> The problem is a complicated one even under ideal conditions (gaussian disorder) and may be further complicated by electron-electron interactions that are likely to be important in insulating media. These issue will not be considered here. We shall also omit from discussion granular systems and semi-continuous films where the transport mechanism is not of the "simple" VRH kind.

Evidence for quantum interference effects in the transport properties of several VRH systems has been published by a number of researchers. Almost every phenomenon that is known to exist in WL system has been established in the SL regime as well. The most widely studied effect is the magnetoresistance (MR) which involves macroscopic samples. Some of the main features of the MR are summarized in the next section.

Observation of Conductance Fluctuations and  $h/e$  oscillations, on the other hand, require mesoscopic structures and in section 3 we bring a brief account of the experimental attempts to observe these phenomena and discuss the inherent difficulties that may be encountered. Finally, in section 4 we elaborate on a more recent manifestation of quantum coherence in the SL regime which involves a mediation of Cooper-pairs between two superconducting banks.

## 2. Magnetoresistance

Most of the evidence for quantum interference in the hopping regime is based on MR measurements. This issue has been described elsewhere quite extensively<sup>2-5)</sup> so we restrict the discussion here to what we regard as the main features. A MR in the insulating regime may originate from "de-localization" (i.e., an increase of  $\xi$  due to the field, in close analogy with WL). This is apparently the dominant mechanism near the metal-insulator transition where  $\xi$  is large. Indeed, once  $L_H=(ch/eH)^{1/2}$  is smaller than  $\xi$ , the MR should be qualitatively similar to that of WL.<sup>2)</sup> Accordingly, one expects the

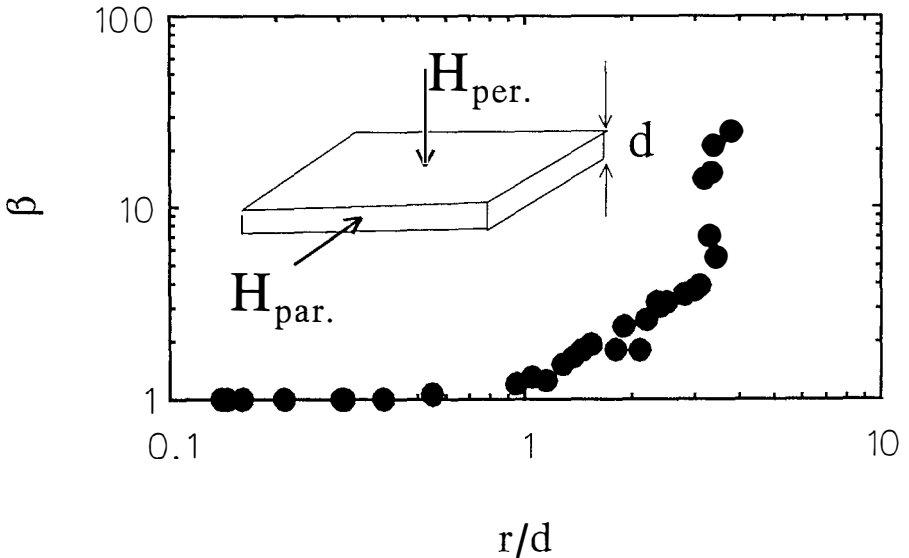


Figure 1: The MR anisotropy parameter,  $\beta$  (the ratio between the MR in perpendicular field,  $H_{per}$  and a parallel one,  $H_{par}$ ) for a thin film of thickness  $d$ . Data are for crystalline  $In_2O_{3-x}$  with  $d$ 's of 100, 200, 300, 500 and 1200 Å measured at the liquid helium temperature range. The range of  $r$ 's for these samples is 150-400 Å.

MR to be negative or positive dependent on the strength of spin-orbit scattering as indeed observed.<sup>8)</sup> In the limit of strong disorder, however, compelling arguments suggest that another MR mechanism, proposed by Nguyen et al<sup>4)</sup>, should take over and only negative MR is observed (neglecting wave-function shrinkage). This regime has been studied only in few cases<sup>9)</sup> due to the difficulties in measuring highly disordered VRH systems at low temperatures. For either mechanism, the most convincing case for the MR being due to an orbital effect, comes from the anisotropy of the phenomenon when the system is 2D (or 1D). Figure 1 depicts the dependence of the MR anisotropy on the hopping length,  $r$ , in units of the sample thickness,  $d$ .

Such experiments are very useful in empirically estimating the phase-coherent length,  $L_\phi$ , in a VRH system. In WL,  $L_\phi$  is essentially the inelastic diffusion length,  $L_{in}$  and the well established theories for this regime enable a fairly convincing determination of this length from a fit to MR data. In VRH, this length turns out to be just  $r$  as illustrated in the above figure and established in many different experiments.<sup>2)</sup> The hopping length,  $r$ , may be controlled by either the temperature or be the electric field used in the measurement.<sup>2,10)</sup> At liquid helium temperatures and small fields,  $r$  is typically 100-300Å. It is noteworthy that this  $L_\phi$  is only 20-60 times smaller than  $L_{in}$  of "good" metals while the resistivity of a VRH medium under such conditions can be 10 (or more) orders of magnitude bigger.

### 3. Conductance fluctuations and $h/e$ oscillations

The phenomenon of Conductance Fluctuation (CF) is well known in WL where universal features<sup>11)</sup> are predicted and observed as characteristic modulations of the sample conductance. CF are also observed in the VRH regime and, in fact, are much more prominent. The prominence of CF in this regime has been anticipated by Imry<sup>13)</sup> and was experimentally established by demonstrating the existence of measurable CF in macroscopic samples,<sup>14)</sup> with spatial extent much bigger than  $L_\phi$ . The orbital (Aharonov-Bohm) nature of the CF can be appreciated from their dependence on the field orientation as shown in figure 2.

The main goal of these experiments was to detect  $h/e$  (or  $h/2e$ ) oscillations in multiply-connected objects. Using crystalline  $In_2O_{3-x}$  samples enabled a control of the amount of disorder of a given sample by employing UV and heat-treatments.<sup>12)</sup> In particular, a given array could be made WL or SL reversibly so the evolution of the various quantum interference effects could be studied systematically. The following facts were found:

1. Both  $h/e$  and CF are observed in the WL regime and their relative magnitude, i.e.,  $\Delta G/G$ , actually increases with disorder up to, and including, the crossover to SL.
2. For SL samples, the rms.  $\Delta G/G$  of the CF is of order unity and remains so up to the highest disorder. At the same time, the  $h/e$  modulation behaves differently. For just-

insulating arrays, the rms.  $\Delta G/G$  is large and can be seen at the entire range of the magnetic field used (0 to 14T). But, with further increase of disorder, it seems to disappear from the  $G(H)$  traces, or, to be observable only at rare regions of  $H$ .

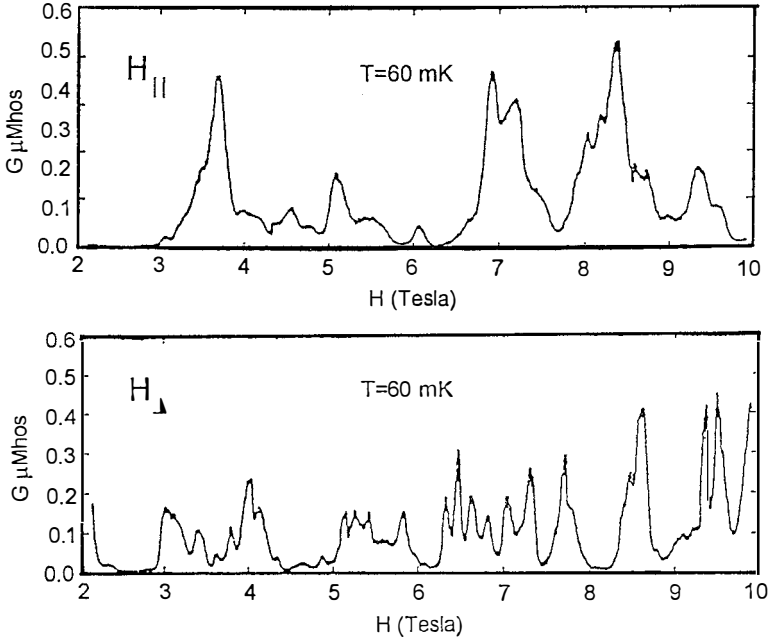


Figure 2: Conductance,  $G$ , versus field traces for a crystalline  $\text{In}_2\text{O}_{3-x}$  film with thickness  $170\text{\AA}$  that was patterned as an array composed of  $25 \times 28$  square "rings". The mesh periodicity is  $3000\text{\AA}$  and the line width is  $500\text{\AA}$ . The difference in characteristic field of the CF between the two different field orientation is about 3 which is quite close to the ratio between the line width and the film thickness as might be expected from an orbital, Aharonov-Bohm effect. (Ovadyahu, Milliken and Webb, unpublished).

It should be noted that the  $h/e$  oscillation is, topologically, exactly the same quantum interference mechanism as the CF. Thus, it is puzzling that one persists as disorder increases while the other seems to have vanished at moderate values of it. We believe that the absence of  $h/e$  modulation in the strong disorder regime is inherent to VRH transport. Basically, the  $h/e$  oscillation in a ring results from interference between the two probability-amplitudes of the quasi-particle (one for each arm) to cross from "side to side". The modulus of each such amplitude is proportional to the conductivity of the respective "arm". In the VRH regime, the local conductivities are spread over an enormous (exponentially wide) range. As a result, the probability that one will

encounter a situation where both arms have comparable conductivities is exponentially small. Clearly, the most likely situation is that the two amplitudes in question will be vastly different and the result of interfering them will give a negligible small modulation. This is just like a two-slit experiment with grossly different light intensity emanating from each slit. The problem in the  $h/e$  case is further complicated due to the modulation of the amplitudes themselves by the applied field: Let us assume that by some chance the ring in question is "balanced" such that the conditions for  $h/e$  oscillations are favorable. To observe this modulation, the field must be swept. But then, the ever-present CF (from the singly-connected parts of the ring), come into their own, and since they are uncorrelated between the two arms, will quickly take the arms away from being balanced. The  $h/e$  oscillation can then be observable only under these rare occasions where the field is such that the arms are accidentally balanced.

#### *4. Superconducting contacts and Andreev reflections*

The various manifestations of quantum interference discussed above have the Aharonov-Bohm effect as an essential ingredient. In this section we describe a different approach to the problem of quantum coherence in the hopping regime. This is based on some properties of SIS devices where S is a superconducting electrode and I is a VRH system. In particular, we demonstrate the existence of a regime where a superconducting current flows through the device that cannot be accounted for by the usual Josephson effect. The results are interpreted as evidence for an indirect Josephson coupling involving a quantum-coherent diffusion through the VRH system.

Our experimental observations were made on structures fabricated as follows. A  $\approx 1000\text{\AA}$  strip of Ag-doped Pb film was thermally evaporated onto room temperature glass-slide, previously cleaned and  $O_2$ -ion-bombarded, in the vacuum chamber, prior to the actual deposition. Then, a thin film of either a-Ge or amorphous indium oxide was e-gun evaporated on the middle section of the Pb film. Finally, another cross-strip of Pb was evaporated to complete a 4-probe tunneling junction through the amorphous Ge or indium-oxide layer. The latter is the oxygen-rich, non-superconducting phase of indium-oxide. Silver doping of the Pb films was used to improve the uniformity and mechanical stability and did not appreciably change the superconducting properties of the lead films. Junction area was typically  $100 \times 100 \mu\text{m}$ . The samples were mounted in an immersion  $He^4$  cryostat and measured by a 4-probe lock-in techniques employing ac modulation of  $\approx 10 \mu\text{V}$ .

I-V curve and  $dV/dI$  versus voltage,  $V$ , typical of our samples, are depicted in figure 3. One notes that up to some critical current,  $I_c$ , no voltage appears across the sample. Above  $I_c$ , the dynamic resistance increases with  $V$  and reveals a superimposed structure that can be classified as follows:

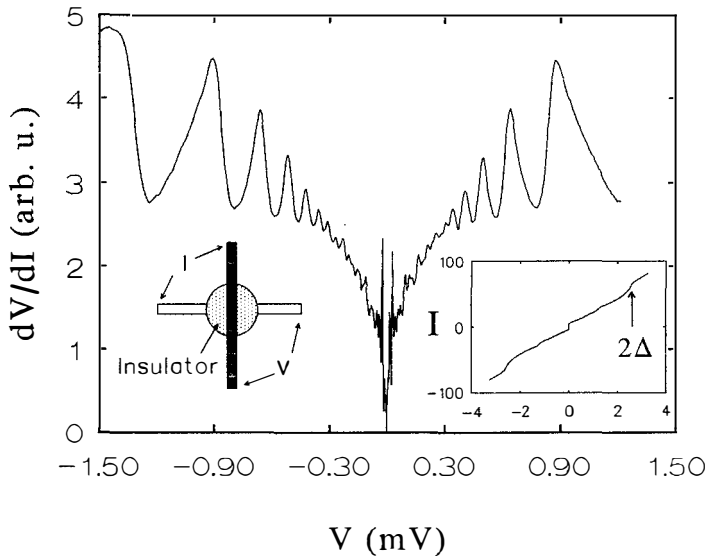


Figure 3: Dynamic resistance versus voltage for a typical Pb/InO<sub>x</sub>/Pb junction measured at T=4.11K. The inserts depict the sample geometry and the I-V curve (current in mA). The barrier thickness in this case is 150Å.

1. For thin barriers (70-250Å for InO<sub>x</sub> and 50-150Å for Ge), a clear dip at  $2\Delta$  is observed. This feature is common in S-S junctions and presumably reflects the existence of a single-particle tunneling-current, and, by inference, the lack of significant superconducting "shorts" in our devices.
2. A series of peaks in  $dV/dI$  are observed at the superconducting gap sub-harmonics, i.e., at  $V_p=2\Delta/n$  with  $n$  between 2 and up to 8.
3. Another modulation, fairly periodic-with- $V$ , is observed at relatively small voltages. This feature is common in Josephson junctions and is believed to result from self generating Shapiro steps.<sup>15)</sup>

Lowering the temperature below 4K increased the amplitude of the periodic modulations but otherwise has only a small effect (mainly through  $\Delta(T)$ ) on the above features. Applying a magnetic field affected the observed structure appreciably. In particular, a field perpendicular to the plane of the Pb strips caused a monotonous reduction in the  $2\Delta/n$  peaks amplitude at fields that are much smaller than  $H_{c2}$  of the electrode (the latter is typically 3kOe).

Not surprisingly, a sensitive parameter in these experiments is the barrier spatial extent,  $L$ . The evolution of the I-V characteristics as a function of  $L$  is described in figure 4 and some relevant junction parameters are summarized in figure 5.

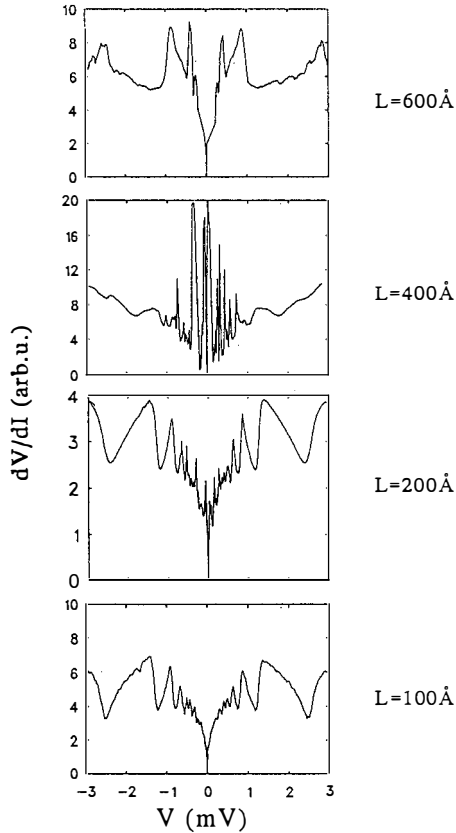


Figure 4: Characteristics of Pb/InO<sub>x</sub>/Pb junctions (at  $T=4.11\text{K}$ ) for samples with different barrier length,  $L$ . Note the strong quasi-periodic modulation at small voltages ( $|V| \leq 0.5\text{mV}$ ) that becomes very prominent for  $L=400\text{Å}$ .

The key observation here is the following.  $I_c$  is still finite for  $L$  as large as  $600\text{Å}$  while the feature at  $2\Delta$  is already washed out for  $L \geq 300\text{Å}$ . In other words, the "direct" single-particle tunneling is rapidly vanishing with  $L$  which is natural for such a process. But, one then expects that *pair*-tunneling, which is a higher-order process and thus

much less likely, is effectively shut-out even sooner. Therefore, to account for the finite  $I_c$  at large  $L$ 's in these samples, one is compelled to look for a non-direct Josephson coupling. The validity of this conclusion does not depend on the actual  $L$ .

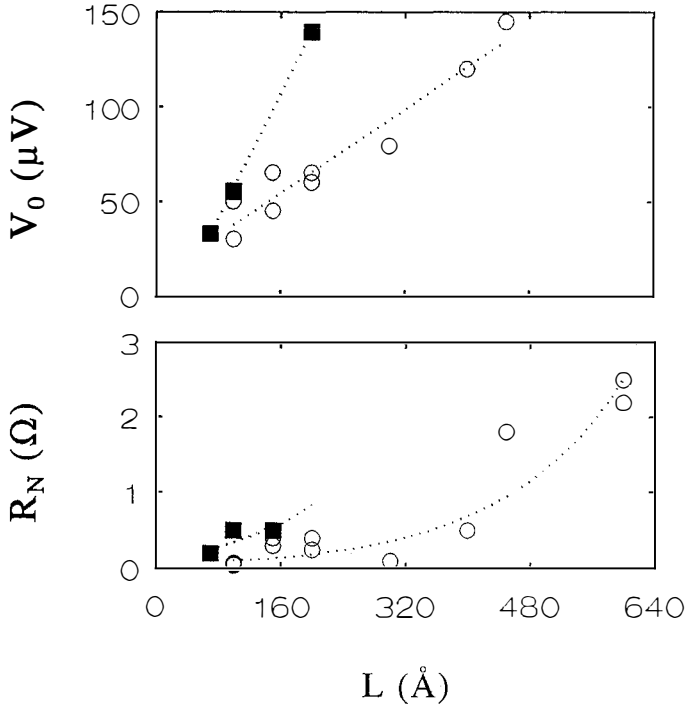


Figure 5: The dependence of the S-I-S, normal-state resistance,  $R$  (measured at  $V=3\text{mV}$  and  $T=4.11\text{K}$ ), and the quasi-period of the low voltage modulation,  $V_0$ , (see text), on the barrier length,  $L$ , for  $\text{InO}_x$  samples (circles) and a-Ge (squares).

A possible solution for this mystery is the Andreev reflection mechanism that has been recently proposed by several authors.<sup>16)</sup> The physical model discussed in these papers is based on a S-N-S structure where N is a normal metal, i.e., a degenerate Fermi system capable of sustaining quasi-particles and quasi-holes. Superconducting coupling between the two S electrodes is mediated by the coherent diffusion of these quasi-particles that are Andreev-reflected at each S-N boundary in turn. Further, the same process may lead to the  $2\Delta/n$  series discussed above: When a finite  $V < \Delta$  is imposed on the junction, a quasi-particle gains an energy of  $eV$  on each S to S trip and so does a quasi-hole. After  $n$  such trips, and provided no inelastic event has occurred,

the diffusive quasi-charge may acquire an energy of  $2\Delta$ , sufficient to escape the N-region and modulate the dynamic resistance at  $V=2\Delta/n$ .

In the systems studied here, however, the region between the two superconductors is a VRH system rather than a "metal". It can be easily shown that the observed  $2\Delta/n$  structure must involve transport via localized states rather than through "metallic-bridges". There are several reasons why such an artifact is a dubious suggestion for our samples. In particular, let us consider the corollary that follows from such an alleged scenario. Assume that a metallic "filament" of length,  $L$ , and made from a metal with resistivity,  $\rho$ , does connect the two superconductors. Let the cross-section of this conducting channel at the N-S interface be  $A$ . In order to observe a structure at a voltage  $V$ , a finite current,  $VA/\rho L$ , must be maintained through this filament. If Andreev reflection is involved, this current must be much smaller than the critical current of the superconductor (or else there would be no  $\Delta$  to affect the process). It is easy to see that the condition  $\rho \gg V/LJ_c$  must be obeyed, where  $J_c$  is the critical current-density of the superconducting electrode. Putting in  $V=10^{-3}$  volt,  $L=100\text{\AA}$ , and the measured,  $J_c=10^5$  A/cm<sup>2</sup>, one obtains  $\rho \gg 10^{-2}$   $\Omega\text{cm}$ . This value is, practically, much too large to be reconciled with "metallic conductivity" of *any* of the substances involved in our structures. It seems, then, that transport through localized states has to be considered which we do next.

A VRH system, just like a metal, has a finite density of states<sup>1)</sup>, DOS, at the Fermi level. "Quasi-particle" and "quasi-hole" are then, fundamentally, still a valid description of an excitation above and below the Fermi energy respectively. The main difference between a metal and a VRH system is the structure of the electronic wave-functions which in the latter case are localized i.e., their envelope decay in space as:  $\exp[-x/\xi]$ . For both, a-Ge and a-InO<sub>x</sub>,  $\xi$  is of the order of few  $\text{\AA}$ , i.e.,  $\xi \ll L$ . This has a number of consequences relevant for charge transport in the medium. The most obvious one is that the conductivity on scales larger than  $\xi$  is exponentially small. But since  $L$  is finite, quasi-electrons and quasi-holes can still diffuse from side to side just like in a dirty metal. A more subtle requirement is the issue of quantum-phase coherence that *must* exist over distances comparable with  $L$  (and thus *much larger* than  $\xi$ ) for the model to explain both, the Josephson coupling and the  $2\Delta/n$  series. As explained above, quantum coherence in VRH systems persists on scales as large as  $r$ . This length is, typically, 100-300 $\text{\AA}$  at 4K which is comparable with  $L$  in our devices. Energy exchange with the environment occur on the scale of  $r$ . One therefore expects that if quasi-particles have to traverse  $n$ -times a length of  $L$  in such medium, only a fraction of the order of  $\exp[-nL/r]$  will do so without loss of energy. This, in turn, should reflect on the magnitude of the structure of the  $2\Delta/n$  series which is amenable to an immediate critical test. Figure 6 depicts the experimental dependence of the  $2\Delta/n$  peaks magnitude on  $n$  for three typical samples which reproduce the expected

functional dependence and, with values for  $r$  that agree quantitatively with the other measurements mentioned in previous sections.

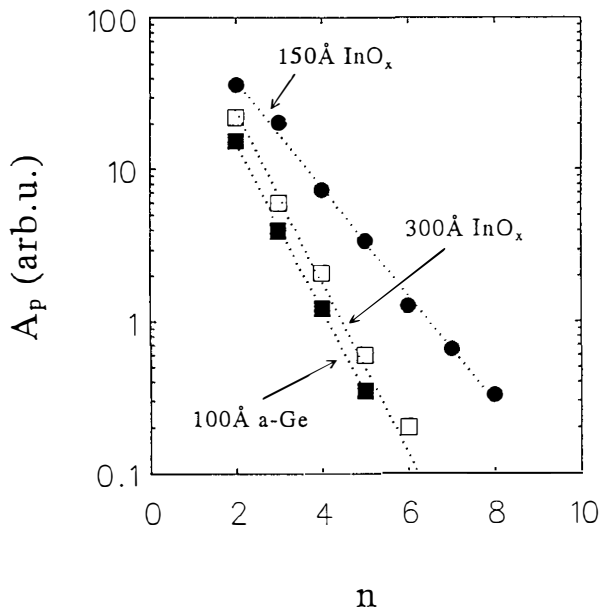


Figure 6: The dependence of the amplitude,  $A_p$ , of the resistance peaks in the  $2\Delta/n$  series of several structures with different barrier length, on the order of the Andreev reflection,  $n$ . The logarithmic slopes yield  $r \approx 200 \text{ \AA}$  for the  $\text{InO}_x$  samples and  $r \approx 90 \text{ \AA}$  for the a-Ge sample which are very reasonable values at  $T=4\text{K}$ . We note that these estimates neglect the possibility that the Andreev-reflection coefficient is smaller than 1 which is most likely to be the case, especially for a-Ge where the DOS is smaller.

Further in support of this physical picture, we cite the lack of a significant temperature dependence (below 4K) on the  $2\Delta/n$  structure which would be natural for a Hopping medium: Note that this structure appears at  $V$ 's of the order of  $10^{-3}$  volt thus imposing electric fields that are typically  $10^3$  volt/cm across the insulating layer. Such fields are sufficient to make the hopping length *field* rather than *temperature* dependent.<sup>10)</sup> Thus, both the junction resistance and the  $2\Delta/n$  structure should be essentially *temperature independent* as observed. On the strength of all these points, we conclude that the "multiple Andreev reflection" model, augmented by ideas pertinent to hopping conductivity may be a plausible explanation for the  $2\Delta/n$  structure and the "long-scale" Josephson effect observed in our experiments.

An intriguing question arises from the above picture that concerns the microscopic mechanism of the Andreev reflection in such cases. The localized nature of the electronic states and the concomitant weakening of screening in the medium render pairing in it energetically unfavorable. In the first place this eliminates the need to consider modifications due to "proximity-effects" in the bulk of the barrier region. However, some sort of pairing near the S-N interface seems to be needed for the Andreev reflection itself. Whether this becomes possible due to the screening by the superconducting electrode or another scenario is involved is not known at present.

In summary, we have detailed several types of experiments that demonstrate the role played by quantum coherence in VRH systems. These include Aharonov-Bohm interference phenomena as well as a quantum-diffusion mediated superconductivity. The latter may prove to be a powerful new technique to study quantum coherence in the insulating regime as well as other fundamental issues such as electron-electron interactions and screening.

We gratefully acknowledge illuminating discussions with Y. Imry, A. Aronov, B. Laikhtman and M. Raikh. This research has been supported by a grant administered by the Israeli Academy for Sciences and Humanities.

### *References*

- 1 N. F. Mott, *J. Non-Crys. Solids*, **1**, 1 (1968).
- 2 Z. Ovadyahu and Y. Imry, *J. Phys. C: Solid State Phys.*, **16**, L471 (1983); Z. Ovadyahu, *Phys. Rev. B* **33**, 6552 (1986); O. Faran and Z. Ovadyahu, *Phys. Rev. B* **38**, 5457 (1988)
- 3 E. I. Laiko, A.O. Orlov, A.K. Savchenko, E.A. Il'ichev and E.A. Poltoratskii, *Sov. Phys. JETP*, **66**, 1258 (1987).
- 4 V. I. Nguyen, B.Z. Spivak and B.I. Shklovskii, *JETP Lett.*, **41** 42 (1985) and *Sov. Phys. JETP*, **62** 1021 (1985).
- 5 U. Sivan, O. Entin-Wohlman and Y. Imry, *Phys. Rev. Lett.*, **60**, 1566 (1988).
- 6 B. Shapiro, *Phil. Mag.* **B50**, 241 (1984).
- 7 J. L. Pichard, M. Sanquer, K Slevin and P. Debray, *Phys. Rev. Lett.*, **65**, 1812 (1990).
- 8 Y. Shapir and Z. Ovadyahu, *Phys. Rev. B* **40**, 12441 (1989), F. Trambly, M. Pepper, R. Newbury, D.A. Ritchie, D.C. Peacock, J.E.F. Frost and G.A.C. Jones, in *"Hopping and Related Phenomena"* Hellmut Fritzsche and Michael Pollak eds., World Scientific Publishing Company (1990).
- 9 Z. Ovadyahu, in *"Localisation 1990"* K.A. Benedict and J.T. Chalker eds, Institute of Physics conference series number 108.

- 10 D. Shahar and Z. Ovadyahu, Phys. Rev. Lett., 64, 293 (1990).
- 11 C. Umbach, S. Washburn, R.B. Laibowitz and R.A. Webb, Phys. Rev B30, 4048 (1984).
- 12 V. Chandrasekhar, Z. Ovadyahu and R.A. Webb, Phys. Rev. Lett, 67, 2862 (1991).
- 13 Y. Imry, Europhys. Lett, 1,249 (1986).
- 14 F. P. Milliken and Z. Ovadyahu, Phys. Rev. Lett, 65, 911 (1990).
- 15 M. D. Fiske, Rev. Mod. Phys., 36, 221 (1964).
- 16 T. M. Klapwijk, G.E. Blonder, M. Tinkham, Physica 109 & 110B, 1657 (1982).

## SPECTRAL CORRELATIONS IN THE VICINITY OF THE ANDERSON TRANSITION

Igor V. Lerner

*School of Physics, University of Birmingham, Birmingham B15 2TT, UK*

We demonstrate the level statistics in the vicinity of the Anderson transition in  $d > 2$  dimensions to be universal and drastically different from both Wigner–Dyson in the metallic regime and Poisson in the insulator regime. The two-level correlation function is shown to have the asymptotic behavior  $R(\omega) \sim (\Delta/\omega)^{2-\gamma}$ , and hence the levels number variance  $\Sigma_2(E) \sim \langle N \rangle^\gamma$  in an energy interval of the width  $E$ , containing in average a large number of the levels  $\langle N \rangle \equiv E/\Delta \gg 1$ , where  $\Delta$  is the mean levels spacing, and  $\gamma = 1 - (\nu d)^{-1}$  with  $\nu$  being the correlation length exponent.

### 1 Introduction

One of the most surprising facts about the Wigner–Dyson (WD) statistics<sup>1</sup> is their applicability to a wide variety of supposedly different situations<sup>2</sup>). These statistics describe, *e.g.*, the distributions of prime numbers and of zeros of the Riemann  $\zeta$  function, and the spectra of compound nuclei, of quantum billiards and of electrons in small metallic particles. In all these cases, the distributions of appropriate eigenvalues (energy levels) are too complicated to be known exactly. The only common feature for all these cases is the presence of some general symmetries which impose certain correlations between the levels. The knowledge of these symmetries turns out to be sufficient for a full statistical description of the spectral properties. Three symmetry classes introduced by Dyson<sup>1</sup>) correspond to the general unitary ensemble (GUE), the general orthogonal ensemble (GOE), and the general symplectic ensemble (GSE) of random matrices.

The main characteristics of the WD statistics are levels rigidity and levels repulsion. The rigidity is reflected by the long-range character of the two-level correlation function. In the simplest GUE case this function is given by

$$Y_2(s) = \sin^2(\pi s)/(\pi s)^2, \quad s \equiv \omega/\Delta, \quad (1)$$

where  $\omega$  is a level separation and  $\Delta$  is the mean level spacing. The level rigidity suppresses the level number fluctuations  $\Sigma_2 \equiv \langle (\delta N)^2 \rangle$  (here  $\delta N \equiv N - \bar{N}$ , and  $N = E/\Delta$  is the number, and  $\bar{N} = \langle N \rangle$  is the average number of energy levels in a given energy interval of the width  $E$ ):

$$\Sigma_2(E) = \frac{2}{\beta\pi^2} \ln \langle N(E) \rangle + C \quad (2)$$

where  $\beta = 1, 2, \text{ or } 4$  for the GOE, GUE, or GSE, respectively, and  $C$  is a certain constant<sup>2)</sup> that is irrelevant for what follows.

The levels repulsion reveals itself in a probability  $P(s)$  to find the nearest-neighbor level at the distance  $s$  from a given one. The famous Wigner surmise for this probability,

$$P(s) = Bs^\beta \exp(-As^2), \quad (3)$$

is very accurate for all  $s$ , although not exact<sup>2)</sup> (the coefficients  $B$  and  $A$  in Eq. (3) are defined by normalizing this distribution and noting that the first moment, *i.e.* the average distance between levels,  $s = \omega/\Delta = 1$ ).

The universal Poisson statistics describe spectral properties of systems with uncorrelated random eigenvalues. In this case,  $R(s) = 0$ ,  $\Sigma_2 = \overline{N}$ , and  $P(s) = e^{-s}$ . In general, the WD statistics are applicable to the quantum chaotic systems, while the Poisson statistics are applicable to the quantum integrable systems. A lot of efforts has been put to describing a crossover between the two universal statistics with changing some of parameters governing a quantum system. Naturally, statistics in the crossover regime are not universal.

In this presentation we will discuss the spectral properties of a quantum particle in a random potential. For this problem the WD statistics are known to be applicable in the metallic region<sup>3,4,5)</sup>. With increasing the random potential, the system undergoes the Anderson transition into the insulator phase<sup>6)</sup>, where all states are localized. In this region, the statistics of energy levels are expected to be Poisson. In the thermodynamic limit  $L \rightarrow \infty$  ( $L$  is the sample size) both statistics are exact. No smooth crossover between them is possible, as in this limit the disordered system is either an ideal metal for  $g > g_c$ , or an ideal insulator for  $g < g_c$  where  $g$  is a dimensionless conductance of the system, and  $g_c$  is its critical value. Obviously, at the mobility edge, where  $g = g_c$ , the statistics could be neither Wigner–Dyson nor Poisson. On the other hand, it is naturally to expect this statistics to be universal since the disordered systems at the mobility edge depend on no parameters at all.

The existence of the universal statistics at the mobility edge has been first conjectured in Ref. 7 where the number variance  $\Sigma_2$  has been considered. The dimensional scaling estimation made in Ref. 7 has resulted in  $\Sigma_2 = a\overline{N}$ , which differs from the Poisson statistics only by a certain number  $a < 1$ . Later<sup>8)</sup>, it has been surmised on the basis of numerical simulations that the nearest-level-spacing distribution  $P(s)$  is a certain universal ‘hybrid’ of the Poisson distribution for large  $s$  and the Wigner surmise for small  $s$ .

We will show here basing on the *analytical* results of Refs. 9, 10 that, indeed, there exist universal statistics, exactly applicable near the Anderson transition point (the mobility edge). However, in contrast to the conjectures of Refs. 7, 8, they are entirely new and drastically different from both the Wigner–Dyson and the Poisson limit. Before going to this, we will recall how to describe the statistical properties of electrons in disordered metals using the perturbative approach<sup>5)</sup>, and show how to obtain within this limit the number variance (2) for a closed disordered system.

## 2 Spectral statistics in the metallic regime

A finite disordered sample is characterized by a set of relevant energy scales that obey in the metallic limit the following inequalities:

$$\Delta \ll E_c \ll \hbar/\tau \ll \varepsilon_p \quad (4)$$

where  $E_c = \hbar/v$  is the Thouless energy,  $\tau_D = L^2/D$  is the time of diffusion through the sample,  $D$  is the electronic diffusion coefficient in the classical limit,  $D = v_p^2\tau/d$ , and  $\tau$  is the elastic scattering rate.

The spectral properties in the metallic regime could be very different depending on what interval is considered on the energy scale or, via the Fourier transform, on the time scale<sup>11)</sup>. The energy region

$\omega > \hbar/\tau$  (or, equivalently,  $s > \hbar/\tau\Delta$ ) corresponds to the ballistic behavior, as the appropriate time is shorter than the mean time of the elastic scattering  $\tau$ . The region  $E_c < \omega < \hbar/\tau$  (equivalently,  $g < s < \hbar/\tau\Delta$ , where the average dimensionless conductance  $g = E_c/\Delta$  equals the average number of levels in the energy window of the width  $E_c$ ) corresponds to the diffusive behavior. The region  $\omega < E_c$  (or  $s < g$ ) is ergodic where the appropriate time is much longer than the average time of diffusion through the sample  $\tau_D$ . Part of this region,  $\omega < \Delta$  ( $s < 1$ ), corresponds to the quantum regime where neither perturbative<sup>5)</sup>, nor quasiclassical<sup>11)</sup> technique is applicable.

Altshuler and Shklovskii have shown<sup>5)</sup> that in the whole region  $\Delta \ll \omega \ll \hbar/\tau$  the main

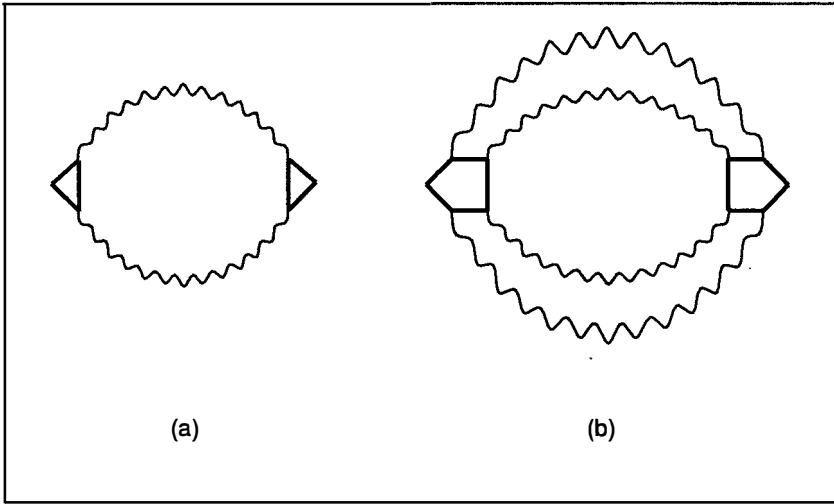


Fig. 1. Diagrams for  $R(s)$ .

contribution to the spectral correlation function  $R_E(\omega)$  is made by the “two-diffuson” diagram (and an equivalent “two-cooperon” one, if allowed by symmetry) shown in Fig. 1a. The wavy line corresponds to the standard diffusion (or cooperon) propagator, while the triangles are made of the one-particle Green’s functions. Here the spectral density correlation function is defined as

$$R_E(\omega) \equiv \frac{1}{\nu_0^2} \langle \nu(\varepsilon)\nu(\varepsilon + \omega) \rangle - 1, \quad (5)$$

where  $\nu(\varepsilon)$  is the exact density of states at the energy  $\varepsilon$ , and  $\langle \dots \rangle$  denotes the ensemble average over the realizations of the random potential. In the whole region  $\omega < \hbar/\tau$ , the average density of states  $\nu_0$  is a constant (which the mean level spacing  $\Delta$  is related to as  $\Delta = (\nu_0 L^d)^{-1}$ ), and  $R_E(\omega) \equiv R(\omega)$  depends only on the distance  $\omega$  between the two levels. Note that this function contains the  $\delta(\omega)$  term resulting from the self-correlation of energy levels. This term is relevant for the integral properties of  $R(s)$ . In general,  $R(\omega)$  is related to the function  $Y_2$ , which is given for the GUE case by Eq. (1), as

$$R(\omega) = -Y_2(\omega) + \Delta \cdot \delta(\omega) \quad (6)$$

On calculating the constants represented by the triangles, one reproduces the result of Ref. 5:

$$R(\omega) = \frac{\Delta^2}{\beta\pi^2} \text{Re} \sum_{\mathbf{q}} (Dq^2 - i\omega)^{-2}. \quad (7)$$

Each vector component of the momentum  $\mathbf{q}$  takes the values  $q_\alpha = (2\pi/L)n_\alpha$  where  $n_\alpha$  is an integer. For a closed system (*i.e.* a finite disordered sample without leads to the reservoir)  $n_\alpha$  takes all integer values. In the ergodic region  $\omega \ll E_c$ , the summation in Eq. (7) reduces to the  $q = 0$  term only which results in

$$R(\omega) = -\frac{\Delta^2}{\beta\pi^2\omega^2} \equiv -\frac{1}{\beta\pi^2s^2} \quad (8)$$

Corrections from the  $2n$ -diffusons diagrams like that in Fig. 1b (for  $n = 2$ ) are proportional to  $s^{-2n}$  which reveals the failure of the perturbative approach in the quantum regime. Even in the ergodic region,  $1 < s < g$ , this approach gives only the envelope of the exact correlation function (1). For the electrons in the ergodic region, this function has been calculated by Efetov<sup>4</sup>) within a non-perturbative technique of the "zero-dimensional" nonlinear  $\sigma$  model. Such a technique, however, could not be extended even to the diffusive region  $\omega \gg E_c$ , not speaking about the region of the Anderson transition.

Although the oscillating factor in Eq. (1) is obviously non-perturbative as the diagrammatic expansion is going on in inverse powers of  $s$ , the levels number variance  $\Sigma_2$  may be found perturbatively. It is given in terms of  $R(\omega)$  as

$$\Sigma_2(E) = \frac{2}{\Delta^2} \int_0^E (E - |\omega|) R(\omega) d\omega. \quad (9)$$

A naive lower-limit cutoff  $\omega \sim \Delta$  in this integral would be disastrous having led to an (absent)  $\bar{N}$ -proportional contribution to the variance. In Ref. 5 the lower cutoff has been provided by changing  $\omega$  to  $\omega + i\Gamma$  in the diffuson pole, that gives  $\Sigma_2$  for  $\Gamma \gg \Delta$  (*e.g.*, for an open sample). In this way one would not be able to compare this directly to the WD result for the levels number variance  $\Sigma_2$  at  $\Gamma = 0$ , Eq. (2).

Nevertheless, one can restore the expression (2), using the perturbative result (8) and the following sum rule

$$\int_{-\infty}^{\infty} R_{\text{ex}}(s) ds = 0, \quad s \equiv \omega/\Delta, \quad (10)$$

which results from the conservation of the total number of energy levels for any non-singular random potential,  $\int_{-\infty}^{\infty} [\nu(\varepsilon + \omega) - \nu_0] d\omega = 0$ , and holds for the exact correlation function  $R_{\text{ex}}(s)$ .

Now suppose that we know  $R_{\text{ex}}(s)$ . Then using the sum rule for the first term in Eq. (9) and splitting the second one into the sum of the two terms, one has:

$$\Sigma_2(\bar{N}) = -2 \left\{ \frac{1}{\bar{N}} \int_{-\infty}^{\infty} R_{\text{ex}}(s) ds + \left( \int_0^a s R_{\text{ex}}(s) ds + \int_a^{\bar{N}} s R_{\text{ex}}(s) ds \right) \right\}, \quad (11)$$

where  $\bar{N} = E/\Delta$  is the average number of the levels in a wide enough energy window with  $\Delta \ll E < E_c$  (*i.e.*  $1 \ll \bar{N} < g$ ), and a constant  $a$  is chosen so that  $1 \ll a \ll \bar{N}$ . Now one may substitute the asymptotic expression (8) for  $R_{\text{ex}}(s)$  into both the first and the third integrals. The second integral, where such a substitution is impossible, is reduced to some  $\bar{N}$ -independent constant. The first integral also gives a constant (neglecting small corrections coming out of the integration of the ballistic tail of  $R$  in the region  $s > 1/\Delta\tau$ ), while the third one reproduces with the accuracy up to a constant the WD result (2):

$$\Sigma_2(E) = \frac{2}{\beta\pi^2} \ln \bar{N} + \text{const}, \quad 1 \ll \bar{N} \lesssim g. \quad (12)$$

In the diffusive region, the perturbative approach is naturally applicable. In this case, the summation in Eq. (7) may be replaced by the integration:  $\sum_{\mathbf{q}} \rightarrow L^d \int d^d q (2\pi)^{-d}$ . Introducing the dimensionless variable of integration  $k = qL\omega$ , with the diffusive length given by

$$L_\omega \equiv \sqrt{D/\omega}, \quad (13)$$

one obtains the following estimation for  $R(\omega)$ :

$$R(\omega) = -\frac{\Delta^2}{\beta\pi^2\omega^2} \left(\frac{L}{L_\omega}\right)^d \operatorname{Re} \int \frac{d^d k}{(2\pi)^d} (1 + ik^2)^{-2} \sim \frac{1}{g^{d/2}} \left(\frac{1}{s}\right)^{2-d/2}, \quad s \gg g. \quad (14)$$

Naturally, it is easy to calculate the dimensionless integral here in order to obtain an exact coefficient of proportionality but for a moment we prefer to leave Eq. (14) as a dimensional estimation. Then  $\Sigma_2$  in the diffusive region is obtained straightforwardly with the help of Eq. (9) to reproduce the result of Ref. 5:

$$\Sigma_2(E) \sim \frac{1}{g^{d/2}} \overline{N}^{d/2}, \quad g \ll \overline{N} \lesssim \frac{1}{\Delta\tau}. \quad (15)$$

In contrast to the variance in the ergodic region (12), the last one is not universal, as it depends on the conductance  $g$ .

The universal WD statistics become exactly applicable to *the entire metallic regime* in the thermodynamic limit

$$L \rightarrow \infty, \quad \overline{N} \equiv E/\Delta = \text{const} \gg 1, \quad (16)$$

when the mean level spacing  $\Delta = (\nu_0 L^d)^{-1}$  tends to zero but the number of levels in the energy window of the width  $E$  is kept finite, although very large. Indeed, as  $g = E_c/\Delta \sim \nu D L^{d-2} \rightarrow \infty$  for  $d > 2$ , the region of validity of the nonuniversal statistics (15) in the diffusive region vanishes.

### 3 Universal spectral statistics in the critical regime

Let us recall what is the scaling description of the Anderson transition<sup>6</sup>). The standard Gell-Mann – Low equation near the transition has the form

$$\frac{dg}{d \ln \lambda^{-1}} = \beta(g) = \frac{1}{\nu}(g - g_c), \quad (17)$$

where  $g_c$ , the critical value of  $g$ , is of order 1 for  $d = 3$ ,  $\lambda$  is the scaling parameter,  $0 < \lambda < 1$ , and  $1/\nu \equiv \beta'(g_c)$ . The solution to this equation may be written down at the metallic side of the transition ( $g > g_c \equiv g_0(\varepsilon_c)$ ) as

$$g = g_c \left[ 1 + \left(\frac{\mathcal{L}}{\xi}\right)^{1/\nu} \right], \quad \xi \equiv l \left(\frac{g_c}{g_0 - g_c}\right)^\nu = \bar{l} \left(\frac{\varepsilon_c}{\varepsilon - \varepsilon_c}\right)^\nu. \quad (18)$$

Here  $\xi$  is the correlation length (with  $l$  being the elastic mean free path, and  $\bar{l}$  being a certain length of order  $l$ ), and  $\mathcal{L}$  is the coherence length (the shortest of  $L$ ,  $L_\omega$ , the phase-breaking length  $L_\phi$ , etc). For a given  $L$ , the correlation length diverges only when the energy  $\varepsilon$  is exactly at the mobility edge  $\varepsilon_c$ . However, the critical region includes all energies obeying  $\xi(\varepsilon) > L$ . For the energy window of any fixed width  $E$  centered at the mobility edge,  $\xi \geq \xi(E/2) \sim \bar{l}(\varepsilon_c/E)^\nu$ . Then the ratio

$$\xi(E)/L = \text{const} \overline{N}^{-\nu} (L/l)^{d\nu-1} \quad (19)$$

diverges in the limit (16) due to the Harris criterion<sup>12)</sup>  $\nu > 2/d$ . This ensures that an infinitesimal energy window centered at the mobility edge may contain an arbitrary large number of the levels.

We have shown that in the limit (16) statistics of the levels in the infinitesimal energy window centered at the energy  $\varepsilon$  such that  $g(\varepsilon) > g_c$  were exactly Wigner-Dyson (the disordered system is an ideal metal with  $g \rightarrow \infty$ ). Similarly, statistics in the energy window with  $g(\varepsilon) < g_c$  are exactly Poisson (the system is an ideal insulator with  $g \rightarrow 0$ ). Now we see that in the very same limit there is a possibility for the existence of new, critical statistics for the energy window centered at the mobility edge  $\varepsilon_c$ .

Let us return to the energy scale picture, Eq. (4). When the disorder increases so that the bare value of the dimensionless conductance decreases down to  $g_c \sim 1$  in the vicinity of the Anderson transition, the whole ergodic region shrinks to  $s \lesssim 1$ , while the ballistic region is shifted to  $s \gtrsim \varepsilon_p / \Delta$ . So the whole region of interest,  $\Delta \lesssim \omega \lesssim \varepsilon_p$  is arising from the nonuniversal diffusive region in the metallic regime. Statistics in this parameter-free region may be analyzed within the standard scaling approach.

The first attempt of this sort has been made in Ref. 7. It follows from Eq. (18) and the Einstein relation  $g = \nu_0 D L^{d-2}$  that at the mobility edge

$$L_\omega = (g_c / \nu_0 \omega)^{1/d} \sim (\nu_0 \omega)^{-1/d}. \quad (20)$$

Comparing this with Eq. (13), one restores the well-known<sup>13)</sup> result at the mobility edge:

$$D(\omega) \propto L_\omega^{2-d} \propto \omega^{1-2/d}. \quad (21)$$

This result has been converted in Ref. 7 to the statement that one can substitute  $g = \nu_0 D L^{d-2} \propto E^{1-2/d}$  into Eq. (12) obtained in the metallic regime. Had such a scaling been correct, it would lead to a sub-Poisson behavior  $\Sigma_2 = \alpha \bar{N}$  at the mobility edge. (A coefficient  $\alpha$  has been claimed equal 0.25 in Ref. 7).

However, the diffusion coefficient depends on the distance  $\omega$  between the two levels rather than on the width of the energy window. Moreover, it should also depend on the momentum  $q$  so that the diffusion propagator that enters Eq. (7) for the two-diffusion diagram may be expressed as

$$P(\omega, \mathbf{q}) = [D(\omega, \mathbf{q}) q^2 - i\omega]^{-1}. \quad (22)$$

which is the most general expression compatible with the particle conservation law. Now, even without knowing this propagator exactly, we can estimate the two-diffusion contribution (7) at the mobility edge. It is actually similar to the estimation (14) made for the diffusion region in the metallic regime. Although the integral could be totally different, dimensional analysis gives the same expression in terms of  $D$  and  $L_\omega$

$$R_2(\omega) \sim \frac{\Delta^2}{\beta D^2(\omega)} \frac{L_\omega^d}{L_\omega^{d-4}} \sim \frac{\Delta}{\omega} \equiv \frac{1}{s}, \quad s \gg 1, \quad (23)$$

where the final estimation is quite different, though, due to the  $\omega$ -dependence of  $D$ , Eq. (21). On substituting this into Eqs. (9), (11), one obtains a very unpleasant result:  $\Sigma_2 \sim \bar{N} \ln \bar{N}$  at the mobility edge.

The subscript 2 in Eq. (23) is to stress that it describes the contribution of the two-diffuson and two-cooperon diagrams only. Naturally, one expects many-diffuson diagrams to be also important at the mobility edge. A similar dimensional estimation for the contribution of the  $2n$ -diffuson diagram in Fig. 2a yields

$$R_{2n}(\omega) \sim \frac{\Delta^{2n}}{D^{2n}(\omega)} \frac{L_\omega^{(2n-1)d}}{L_\omega^{d(2n-1)-4n}} = \left(\frac{\Delta}{\omega}\right)^{2n} \left(\frac{L}{L_\omega}\right)^{d(2n-1)} \sim \frac{\Delta}{\omega}, \quad (24)$$

as at the mobility edge  $(L/L_\omega)^d \sim \omega/\Delta$ , Eq. (20). Note that the same diagrams lead to the inapplicability of the perturbative approach in the quantum region in metals,  $\omega < \Delta$ . At the mobility edge, the contribution (24) of each diagram is of the same order,  $\propto 1/s$ , as that of the two-diffusion diagram (23). One can check that there are no diagrams that could give a bigger contribution to  $R(s)$ . Then, on the face of it, the “unpleasant estimation”  $\Sigma_2 = A_\Sigma \bar{N} \ln \bar{N}$  persists at the mobility edge, with  $A_\Sigma$  being a dimensionless coefficient given by the sum of all diagrams.

Let us argue now that this result is no more unpleasant than that of the Ref. 7,  $\Sigma_2 = \alpha \bar{N}$ , described above. Both of them are forbidden *at the mobility edge* by the sum rule (10). Indeed, one obtains from Eqs. (9) and (10) that

$$\frac{d\Sigma_2(\bar{N})}{d\langle N \rangle} = 2 \int_0^{\bar{N}} R(s) ds = -2 \int_{\bar{N}}^{\infty} R(s) ds. \quad (25)$$

The function  $R(s)$  must be universal at the mobility edge (in a sense that it does not depend on any other parameter but  $s$ ). For such a function the sum rule (10) is fulfilled only if the integral in the r.h.s. of Eq. (25) tends to 0 with increasing  $N$ . Therefore, in this case  $\Sigma_2(\bar{N})/\langle N \rangle \sim o(\bar{N})$  for  $\bar{N} \gg 1$ .

Note that were  $R(s)$  to contain a long flat tail (proportional to some small parameter), the sum rule could impose no limitation on the value of the integral in the r.h.s. of Eq. (25). Indeed, it is just the case for the insulator regime where this small parameter is  $\Delta/\Delta_\xi$ , with  $\Delta_\xi$  being the mean level spacing within a localization volume  $\xi^d$ , and just the existence of the tail ensures, as we have shown,<sup>9)</sup> the Poisson behavior of  $\Sigma_2$ . However, the only small parameter at the mobility edge is  $\tau\Delta \sim \Delta/\varepsilon_p$ . Within the standard one-parameter scaling<sup>6)</sup> such a dependence is forbidden as all microscopic parameters are absorbed by the dimensionless conductance  $g$  that is of order 1 near the mobility edge. Moreover, were any contribution proportional to this parameter to exist, it would be almost the same in the metallic regime, as it could only be originated from the ballistic region  $\omega > \hbar/\tau$  which is hardly sensitive to the transition, thus leading to the sub-Poisson behavior of  $\Sigma_2$  in this regime as well. Therefore, it is hardly possible to believe in the existence of such a tail that could justify the sub-Poisson behavior at the mobility edge.

The dimensionless estimation above has given  $\Sigma_2 = A_\Sigma \bar{N} \ln \bar{N}$  which is absolutely unacceptable. A proverbial “poor man hope” would be that contributions of different diagrams cancel each other so that  $A_\Sigma = 0$ . Again, it is hard to believe in such a miracle: the cancellation, if any, should happen for all the three ensembles,  $\beta = 1, 2, 4$ .

The *real result* is that the  $1/s$ -proportional contribution of each diagram to  $R(s)$  does not exist. Dimensionless estimations are usually quite reliable, until an appropriate coefficient appears to be equal to 0. It is just the case for the problem under consideration. The key is the analytical properties of the diffusion propagator (22) *resulting from the causality*. The analyticity and certain scaling relations at the mobility edge similar to that in Eq. (20) ensure vanishing these  $1/s$ -proportional contributions. The same considerations will allow to find what is left after the cancellation of the  $1/s$  terms.

The causality means that the propagator  $\tilde{P}(t, \mathbf{r} - \mathbf{r}')$ , that is the space-time Fourier-transform of  $P(\omega, \mathbf{q})$ , Eq. (22), is zero for  $t < 0$ . Then  $P(\omega, \mathbf{q})$  is analytical in the upper half-plane of the complex variable  $\omega$ . It satisfies also the relation  $P^*(\omega, \mathbf{q}) = P(-\omega, -\mathbf{q})$ , as  $\text{Im } \tilde{P}(t, \mathbf{r} - \mathbf{r}') = 0$ . Using also the spatial isotropy, one has  $P^*(\omega, q) = P(-\omega, q)$ . Then the conventional scaling arguments allow to express  $P(\omega, q)$  at the mobility edge ( $\xi \rightarrow \infty$ ) in the limit  $L \rightarrow \infty$  in terms of the dimensionless scaling function  $F$  depending on  $qL_\omega$ , the ratio of the only two lengths characterizing the system<sup>14)</sup>:

$$P(\omega, q) = \frac{1}{(-i\omega)} \tilde{F}(qL_\omega) \equiv \frac{1}{(-i\omega)} F(\zeta), \quad \zeta \equiv \frac{q^d}{-i\omega\nu_0}, \quad (26)$$

where due to the above analyticity requirements,  $\omega$  contains an infinitesimal imaginary part, and the function  $F(\zeta)$  is analytical for  $\text{Re } \zeta > 0$  and satisfies the condition

$$F^*(\zeta) = F(\zeta^*). \quad (27)$$

In the static limit  $P(\omega \rightarrow 0, q) \propto q^{-d}$  at the critical point<sup>15</sup>). In the opposite limit,  $L_\omega q \ll 1$ , the diffusion propagator has the form (22) with the diffusion coefficient (21) depending only on  $\omega$ . That results in the asymptotics

$$F(\zeta) = \begin{cases} \alpha_1 \zeta^{-1}, & |\zeta| \gg 1 \\ [1 + \alpha_2 \zeta^{2/d}]^{-1} \approx 1 - \alpha_2 \zeta^{2/d}, & |\zeta| \ll 1 \end{cases} \quad (28)$$

where  $\alpha_{1,2}$  are real coefficients of order 1.

Now we can show the  $1/s$ -proportional contributions to vanish. Before coming to this, let us return to the dimensional estimation in the diffusive regime, Eq. (14). Calculating the integral in that equation exactly, one finds that it is pure imaginary at  $d = 2$ . Therefore, correlations between two levels are absent at  $d = 2$  to the first order in  $1/g$ .<sup>5</sup>) We can show this in a different way. Namely, we change the variable of integration in Eq. (14) to  $\zeta$ , Eq. (26), using that  $\zeta = iq^2 L_\omega^2/g \equiv ik^2/g$  for  $d = 2$ :

$$\text{Re} \int \frac{d^2 k}{(2\pi)^d} (1 + ik^2)^{-2} \sim \int_0^\infty \frac{dk^2}{(2\pi)^d} \text{Re} (1 + ik^2)^{-2} \sim \int_0^\infty \frac{d\zeta}{(2\pi)^d} \text{Re} (1 + \zeta/g)^{-2} \quad (29)$$

As the real part of the integrand is an even function of  $\zeta$ , one extends the integration to the entire axis. Then, closing the contour of integration in the right half-plane of  $\zeta$ , one shows the original integral to be equal to 0. A crucial point for this proof is that in the diffusive regime the integration at  $d = 2$  is reduced to that over  $d\zeta$ , with no additional dependence on  $\zeta$ .

From this viewpoint, the integration in the two-diffuson diagram at the mobility edge is similar to that at  $d = 2$  in the diffusive regime. Indeed, using Eq. (26) one obtains:

$$R_2(s) = \frac{\Delta^2}{2\pi^2 \beta} L^d \text{Re} \int \frac{d^d q}{(2\pi)^d} [P(\omega, q)]^2 \sim -\frac{i}{s} \int_0^\infty \frac{d\zeta}{(2\pi)^d} \text{Re} F^2(\zeta). \quad (30)$$

Eq. (27) ensures that the real part of the integrand is even, so that again the integration may be extended to the entire axis. Since the integrand is analytical for  $\text{Re} \zeta > 0$  and decreases fast enough at  $z \rightarrow \infty$ , Eq. (28), the original integral equals 0. A straightforward extension of these arguments allows to prove that the  $2n$ -diffuson contributions vanish in the same approximation<sup>9</sup>).

So, what is left after the main contributions having been cancelled? It transpires that one should calculate the same diagrams, Fig. 1, with the higher accuracy. Indeed, we have considered the limit (16) in calculating the integral in Eq. (30). However, in this limit  $\Delta \rightarrow 0$ , and thus  $1/s \rightarrow 0$ . To keep corrections in powers of  $1/s$ , one should keep  $L$  finite, although large. We can consider the crossover regime where both the correlation length  $\xi$  and the system size  $L$  are much larger than  $L_\omega$ . In practice, it is more convenient to begin with the limit  $L \gg \xi \gg L_\omega$ . In this case any scaling function depends on the appropriate lengths measured in  $\xi$ . In particular, the diffusion propagator becomes a function of  $q\xi$  and  $L_\omega\xi$ . As  $L_\omega\xi$  is a small parameter, it is convenient to rearrange it as a function of  $\zeta \sim i(qL_\omega)^d$  and  $L_\omega\xi$ , and expand in  $L_\omega\xi$  (such an expansion being not necessarily analytic):

$$P(\omega, q) = (-i\omega)^{-1} \left[ F(\zeta) + (\Delta_\xi / -i\omega)^{1-\gamma} \Phi(\zeta) \right], \quad (31)$$

where  $\Delta_\xi \equiv (1/\nu_0 \xi^d)$  is the mean spacing withing the correlation volume  $\xi^d$ . Here  $\Delta_\xi / -i\omega = i(L_\omega\xi)^d$  is chosen to be the parameter of the expansion to ensure that the scaling function  $\Phi(\zeta)$  has the same analytical properties as  $F(\zeta)$ .

To define the exponent  $\gamma$  in Eq. (31), one finds the diffusion propagator (22) in the limit  $L_\omega q \ll 1$ . For  $\xi = \infty$ , an asymptotic behavior at small  $\zeta$  has been given by Eq. (28). For finite  $\xi$ , one uses

$D(\omega) = (g/\nu_0 L_\omega)^{d-2}$ , and substitutes  $g$  from Eq. (18) with  $\mathcal{L} = L_\omega$ . (The analyticity requirements mean, as above, that one always substitutes  $(i/\omega\nu_0)^{1/d}$  for  $L_\omega$ ). It results for finite  $\xi$  in

$$P(\omega, q) = \frac{1}{-i\omega} \left[ 1 - \alpha_2 \zeta^{2/d} - \alpha_2 \zeta^{2/d} \left( \frac{\Delta_\xi}{-i\omega} \right)^{1/\nu d} \right], \quad |\zeta| \ll 1. \quad (32)$$

Comparing Eqs. (32) and (31), we have:

$$\gamma = 1 - (\nu d)^{-1}. \quad (33)$$

Note that  $1/2 < \gamma < 1$  due to the Harris criterion<sup>12</sup>).

Now, Eq. (31) can be used for estimating the first integral in (30). As the real part of the integrand is no more an even function of  $\zeta$ , the integral does not vanish. The main non-vanishing contribution is obviously proportional to  $(\Delta_\xi^{1-\gamma} \Delta / \omega^{2-\gamma})$ . A coefficient of proportionality could not be found as one does not know an explicit expression for the diffusion propagator near the mobility edge. Anyway, this coefficient is irrelevant by itself since all  $2n$ -diffuson diagrams give the same-order contributions to  $R(s)$ , see Ref. 9. Finally, the standard crossover reasoning allows to substitute  $\Delta$  for  $\Delta_\xi$  in the universality limit (16) when  $\xi \gg L$ , Eq. (19), which leads to

$$R(s) = -c_{d\beta} s^{-2+\gamma}, \quad s \gg 1, \quad (34)$$

where  $c_{d\beta}$  is some numerical factor which depends on the universality class ( $\beta$ ) and dimensionality.

Now we can use Eq. (11), based on the sum rule (10), for calculating  $\Sigma_2$ . Again, for both the first and the third integrals we can use the asymptotic expression (34). Thus, neglecting an irrelevant constant that depends on the arbitrary cutoff  $a$  in Eq. (11), we arrive at

$$\langle (\delta N)^2 \rangle = a_{d\beta} \bar{N}^\gamma, \quad (35)$$

that holds exactly at the mobility edge. Here  $a_{d\beta} = 2c_{d\beta}/\gamma(1-\gamma)$ , and  $\gamma$ , Eq. (33), depends only on the dimensionality and the correlation length exponent  $\nu$ . Since the coefficient  $a_{d\beta}$  must be positive,  $c_{d\beta} > 0$ , and the correlator  $R(\omega)$  is negative for  $\omega \gg \Delta$ . For small  $\omega \ll \Delta$  one can use the same zero-mode approximation<sup>4</sup>) as in the metal region for  $\omega \ll 1/\tau_D$ , so that the correlation function  $R(s)$  should have the Wigner-Dyson form. We can conclude, therefore, that the energy levels are repelling at all energy scales.

## 4 Conclusion

We have obtained that the statistics at the mobility edge are intermediate between the Wigner-Dyson and Poisson cases. It seems to be in line with our general understanding of behavior of the wave function at the transition. Indeed, in the absence of the level correlations in the insulator phase, where wave functions corresponding to different localized states have no overlapping in the limit (19), the variance  $\Sigma_2 = \bar{N}$ . A strong overlapping of the wave functions in the metallic phase leads to the logarithmic suppression of the level number fluctuations, Eq. (12). At the mobility edge the states are not localized but appear to be very patchy so that the overlapping is in general smaller, that leads to the level number fluctuations (35) that much larger than in the metallic phase but much smaller than in the insulator one.

Note in conclusion that, having known the asymptotic behavior of the correlation function (34), we could use a Dyson-like plasma model to restore the asymptotic behavior of the nearest-level-spacing distribution  $P(s)$ .<sup>10</sup>) Since for  $s \ll 1$  the distribution should have the same behaviour  $P(s) \sim s^\beta$  at

the mobility edge as in the metallic phase<sup>8)</sup> which follows from the general symmetry theorem proved by Dyson<sup>1)</sup>, the entire distribution could be described by the following surmise:

$$P(s) = Bs^\beta \exp(-A_{d\beta}s^{2-\gamma}). \quad (36)$$

The coefficients  $B$  and  $A_{d\beta}$  in Eq. (3) are defined by the normalization and the first moment, similar to that for the Wigner surmise (3). On the other hand,  $A_{d\beta}$  is directly related<sup>10)</sup> to the coefficient  $c_{d\beta}$  in the correlation function (34). So, provided that the surmise (36) is valid, we would be able to gain quite a thorough knowledge of the new universal statistics at the mobility edge.

The author acknowledges travelling support under the EEC grant No. SSC-CT90-0020.

## References

- 1) E. P. Wigner, Proc. Cambridge Philos. Soc. **47** (1951) 790; F. J. Dyson, J. Math. Phys. **3** (1962) 140.
- 2) M. L. Mehta, *Random matrices*, Academic Press, Boston (1991).
- 3) L. P. Gor'kov and G. M. Eliashberg, Zh. Eksp. Teor. Fiz. **48** (1965) 1407 [Sov. Phys. JETP **21** (1965) 940].
- 4) K. B. Efetov, Adv.Phys. **32** (1983) 53.
- 5) B. L. Altshuler and B. I. Shklovskii, Zh. Eksp. Teor. Fiz. **91** (1986) 220 [Sov. Phys. JETP **64** (1986) 127].
- 6) P. A. Lee and T. V. Ramakrishnan, Rev. Mod. Phys. **57** (1985) 287.
- 7) B. L. Altshuler, I. K. Zharekeshev, S. A. Kotochigova, and B. I. Shklovskii, Zh. Eksp. Teor. Fiz. **94** (1988) 343 [Sov. Phys. JETP **67** (1988) 625].
- 8) B. I. Shklovskii, B. Shapiro, B. R. Sears, P. Lambrianides, and H. B. Shore, Phys. Rev. B **47** (1993) 11487.
- 9) V. E. Kravtsov, I. V. Lerner, B. L. Altshuler, and A. G. Aronov, Phys. Rev. Lett. **72** (1994) 888.
- 10) A. G. Aronov, V. E. Kravtsov, and I. V. Lerner, Pis'ma v ZhETF **59** (1994) 39 [JETP Letters **59** (1994) 40].
- 11) N. Argaman, Y. Imry, and U. Smilansky, Phys. Rev. B **47** (1993) 4440.
- 12) A. B. Harris, J. Phys. C **7**, (1974) 1671; J. T. Chayes, L. Chayes, D. S. Fisher, and T. Spencer, Phys. Rev. Lett. **57**, (1986) 299; B. Kramer, Phys. Rev. B **47**, (1993) 9888.
- 13) F. Wegner, Z. Phys. B **25** (1976) 327; B. Shapiro and E. Abrahams, Phys. Rev. B **24** (1981) 4889; Y. Imry, Y. Gefen, and D. J. Bergman, Phys. Rev. B **26** (1982) 3436.
- 14) J. T. Chalker and C. J. Daniell, Phys. Rev. Lett. **61** (1988) 593.
- 15) F. Wegner, Phys. Repts. **67** (1980) 15.

# CORRELATION EFFECT ON HOPPING CONDUCTION WITH SPIN-ORBIT INTERACTION

Mikio Eto

*Department of Physics, Faculty of Science and Technology, Keio University,  
3-14-1 Hiyoshi, Kohoku-ku, Yokohama 223, Japan*

## Abstract

Correlation effect is investigated theoretically in the strongly Anderson-localized regime in the presence of spin-orbit (SO) interaction. Based on numerical studies on the Hubbard model with disordered on-site energies, we suggest the magnetic-field-dependence of hopping conduction. In the absence of SO interaction the magnetoconductance (MC) is positive through the Zeeman effect. In its presence the MC can be negative in low magnetic fields while it becomes positive in high magnetic fields. This result is in good agreement with a recent experimental result of nearest neighbor hopping conduction in a Cu-particle film.

## 1 Introduction

In the strongly Anderson-localized regime both the interference and the correlation effects play important roles. As for the interference effect, the positive magnetoconductance (MC) of the hopping conduction has been suggested.<sup>1,2,3)</sup> While the electron-electron interaction affects the localized electronic states in various ways: (i) The long range Coulomb interaction makes a gap of the density of states at the Fermi level, Coulomb gap, which changes the  $T$  dependence of the variable range hopping conduction.<sup>4)</sup> (ii) The short range correlation has been studied to explain the  $T$  dependence of the spin susceptibility and specific heat.<sup>5,6,7)</sup>

In this paper we investigate the correlation effect of short range on the hopping conduction based on numerical studies on the Hubbard model having disordered on-site energies. We have shown that the correlation effect makes the positive MC through the Zeeman effect in the absence of spin-orbit (SO) interaction.<sup>8)</sup> The proposed MC is independent of the direction of the magnetic field. Here we extend the calculation to SO-interacting systems. The spin flip processes are taken as random variables.<sup>9,3)</sup> We indicate that the MC can be negative in low magnetic fields while it becomes positive in high fields. Then we explain an experimental result of the nearest neighbor hopping conduction in a Cu-particle film<sup>10)</sup> for the first time.

## 2 Model and Calculation Method

To treat the many-body effect of short range in a quantum mechanical way, we adopt the Hubbard model with disordered on-site energies in two-dimensional square lattice. The Hamiltonian is,

$$H = \sum_{i,\sigma} \varepsilon_i a_{i,\sigma}^\dagger a_{i,\sigma} + \sum_{\langle i,j \rangle, \sigma, \sigma'} (T_{ij})_{\sigma, \sigma'} a_{i,\sigma}^\dagger a_{j, \sigma'} + U \sum_i n_{i,\uparrow} n_{i,\downarrow}, \quad (1)$$

$$-W/2 < \varepsilon_i < W/2, \quad (2)$$

where  $\langle i, j \rangle$  denotes the nearest neighbor sites  $i$  and  $j$ . Hopping terms are assumed to be constant without SO interaction,  $(T_{ij})_{\sigma, \sigma'} = t \delta_{\sigma, \sigma'}$ , while they can be written as below with SO interaction;

$$T_{ij} = \begin{pmatrix} \alpha_{ij} & \beta_{ij} \\ -\beta_{ij}^* & \alpha_{ij}^* \end{pmatrix}, \quad (3)$$

where  $\alpha_{ij}$  and  $\beta_{ij}$  are taken as random variables. We only consider the Zeeman effect when a magnetic field is applied.

Electronic states are calculated by the unrestricted Hartree-Fock method in non-SO-interacting case. By the method not only mean field but also part of the correlation effect can be taken into account because the orbitals for up-spin electrons can be different from those for down-spin electrons.<sup>8)</sup> We determine the one-electron orbitals in a self-consistent way for all the total spin ( $S_z$ ) states independently.

In SO-interacting case we adopt the following approximation;

$$U n_{i,\uparrow} n_{i,\downarrow} \longrightarrow U \langle n_{i,\uparrow} \rangle n_{i,\downarrow} + U n_{i,\uparrow} \langle n_{i,\downarrow} \rangle - U \langle n_{i,\uparrow} \rangle \langle n_{i,\downarrow} \rangle \\ - U \langle a_{i,\uparrow}^\dagger a_{i,\downarrow} \rangle a_{i,\downarrow}^\dagger a_{i,\uparrow} - U \langle a_{i,\downarrow}^\dagger a_{i,\uparrow} \rangle a_{i,\uparrow}^\dagger a_{i,\downarrow} + U \langle a_{i,\uparrow}^\dagger a_{i,\downarrow} \rangle \langle a_{i,\downarrow}^\dagger a_{i,\uparrow} \rangle.$$

This is a natural expansion of the unrestricted HF method. Although  $S_z$  is no longer a good quantum number, its average is determined automatically by the self-consistent calculation.

To estimate the degree of localization in the real space we calculate the participation ratio. It is defined as

$$\langle \psi^4 \rangle = \int |\psi(\mathbf{r})|^4 d\mathbf{r} = \sum_i^{\text{all-site}} |\psi(i)|^4, \quad (4)$$

$$\sum_i^{\text{all-site}} [|\psi_\uparrow(i)|^2 + |\psi_\downarrow(i)|^2]^2, \quad (5)$$

in the absence and presence of SO interaction, respectively. Here the lattice constant is unity. The larger the value is, more localized is the orbital.

### 3 Calculated Results

#### 3.1 Absence of SO interaction

First we present the calculated results for two electrons in an  $8 \times 8$  square lattice ( $W = 10$ ,  $U = 20$ ,  $t = -1$ ). The boundary condition is free. The calculation is done for  $S_z = 0$  and  $S_z = 1$  states independently. In Fig.1 we show the wavefunctions in both states. The orbitals in the low spin state are more localized than those in the high spin state. The reason is as follows: the electrons with antiparallel spins are interacting with each other through the  $U$  term in the Hamiltonian (1) while the electrons having parallel spins do not interact, that is, the correlation effect is stronger for the former. Thus spin-antiparallel electrons tend to be apart from each other, as a result, to be localized.

Next we perform the calculation for eight electrons in  $4 \times 4$  sites to investigate the magnetic field ( $H$ ) dependence of the localization length. We calculate the total energy including the Zeeman term,  $2\mu_B H S_z$ , for states of  $S_z = 0, 1, 2, 3, 4$  and determine the ground state as a function of  $H$ . The values of  $W$ ,  $U$  and  $t$  are the same as before and the boundary condition is free. Taking ensemble average over 200 samples, we get the magnetization ( $\langle S_z \rangle$ ) and the participation ratio of the electrons at the Fermi level ( $E_F$ ), the highest occupied orbitals.

The result is indicated by solid lines in Fig.2 as a function of the magnetic field. As the magnetic field increases, the magnetization increases due to the Zeeman effect (Fig.2 (a)). With the field, the averaged participation ratio is reduced and hence the orbitals are more extended, reflecting the increased number of the high spin states (in Fig.2 (b) the ratio becomes smaller in the

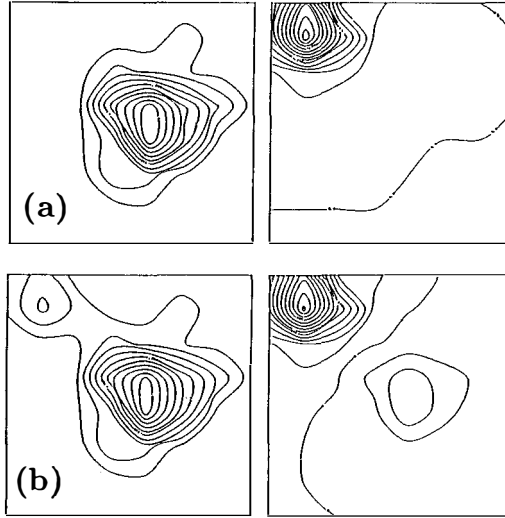


Figure 1: The one-electron orbitals for a two-electron system of  $8 \times 8$  sites; (a) (upper two figures) the spin-antiparallel state ( $S_z = 0$ ) and (b) (lower two figures) the spin-parallel state ( $S_z = 1$ ). The contour lines are drawn every 0.05.

vertical direction). The  $H$  dependence of the localization length seems to be almost linear.

The extension of the orbitals with the magnetic field causes the positive MC of the hopping conduction. It is estimated to be a few % in the nearest neighbor hopping conduction.<sup>8)</sup> The proposed MC is independent of the direction of the magnetic field in contrast to the interference mechanism in which only the component of  $H$  perpendicular to the orbitals is effective.<sup>1,2,3)</sup>

### 3.2 Presence of SO interaction

For spin flip processes, we take a model of Ref. 3:  $\alpha_{ij}$  and  $\beta_{ij}$  in eq.(3) are randomly distributed under the condition

$$\det(T_{ij}) = |\alpha_{ij}|^2 + |\beta_{ij}|^2 = |t|^2. \quad (6)$$

The SO disorder is independent of the site disorder. This model corresponds to a large SO interaction case. We consider eight electrons in a  $4 \times 4$  square lattice with  $W = 10$ ,  $U = 20$ ,  $|t| = 1$  and free boundary condition. The ensemble average is taken over 200 samples.

The calculated results are indicated by broken lines in Fig.2. Although the  $H$  dependence of the magnetization is almost the same as in non-SO-interacting case (Fig.2 (a)), that of the averaged participation ratio at  $E_F$  is

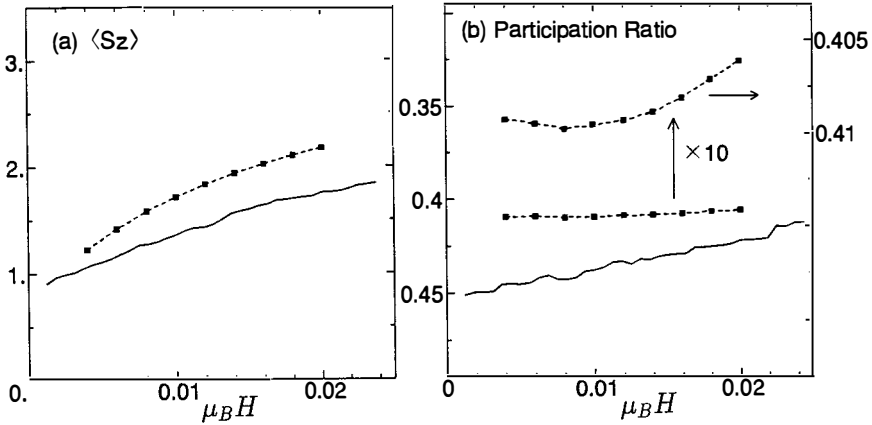


Figure 2: The magnetic field ( $H$ ) dependence of the averaged  $S_z$  (magnetization) per a system (a) and of the participation ratio (b) for systems of eight electrons in  $4 \times 4$  sites. The ensemble average is taken over 200 samples. Solid and dotted lines indicate the cases in the absence and presence of SO interaction, respectively. The unit of  $\mu_B H$  is  $|t|$ . In (b) the value becomes smaller in the vertical direction.

much changed by the SO interaction, as seen in Fig.2 (b): (i) its  $H$  dependence becomes much weaker, and (ii) it increases first and then it decreases with the magnetic field.

This is due to the interplay between the SO interaction and the correlation effect. It is well known that the SO interaction weakens the localization of electrons in the weak localization regime. The tendency seems to be the same in the strong localization regime. (It should be noted that the absolute value of the participation ratio is smaller with SO interaction than without SO interaction in Fig.2 (b).) In low magnetic fields the spin flip processes are suppressed because the ratio of one-component of the electron spin is reduced and, as a result, the orbitals are localized. In high magnetic fields the correlation effect becomes dominant, which extends the orbitals with increasing the magnetic field, as mentioned before.

It indicates that the MC is negative in low fields while it becomes positive in high fields. This result is in good agreement with the recent experimental result of nearest neighbor hopping conduction in a Cu-particle film.<sup>10)</sup>

The model we have adopted represents a large SO interaction. We are now examining another model for spin-flip processes<sup>9)</sup> to study a case of small SO interaction.

## 4 Conclusions

We have investigated the correlation effect on the strongly-localized orbitals with and without SO interaction based on numerical studies on the Hubbard model. Taking account of the Zeeman effect, we have suggested a new mechanism of the positive MC of the hopping conduction in the absence of the SO interaction: the Zeeman effect increases the number of the high spin states in which the orbitals at  $E_F$  are more extended owing to the weaker correlation effect of short range, than in the low spin states. The proposed MC is independent of the direction of the magnetic field and thus it can be distinguished from the orbital MC in experiments.

In the presence of the SO interaction the MC through the Zeeman effect has more interesting features; it is negative in low fields and positive in high fields at least in strongly SO-interacting case. The  $H$  dependence of the MC has been observed in the nearest neighbor hopping conduction in a Cu-particle film.<sup>10)</sup> The proposed MC of the hopping conduction will be also observable in other systems, *e.g.* doped semiconductors, an array of artificial quantum dots, if some condition is satisfied.<sup>8)</sup>

## References

- 1) V. L. Nguyen, B. Z. Spivak and B. I. Shklovskii, JETP Lett. **41**, 42 (1985); U. Sivan, O. Entin-Wohlman and Y. Imry, Phys. Rev. Lett. **60**, 1566 (1988).
- 2) J.-L. Pichard, M. Sanquer, K. Slevin and P. Debray, Phys. Rev. Lett. **65**, 1812 (1990).
- 3) Y. Meir, N. S. Wingreen, O. Entin-Wohlman and B. L. Altshuler, Phys. Rev. Lett. **66**, 1517 (1991).
- 4) A. L. Efros and B. I. Shklovskii, in *Electron-electron interactions in disordered systems*, eds. A. L. Efros and M. Pollak (North-Holland, Amsterdam, 1985) p.409; M. Pollak and M. Ortuno, *ibid.* p.287.
- 5) H. Kamimura, in Ref. 4, p.555.
- 6) K. Andres, *et al.*, Phys. Rev. **B24**, 244 (1981); R. N. Bhatt and P. A. Lee, Phys. Rev. Lett. **48**, 344 (1982).
- 7) M. Eto and H. Kamimura, Phys. Rev. Lett. **61**, 2790 (1988); J. Phys. Soc. Jpn. **58**, 2826 (1989); in *Hopping and Related Phenomena*, eds. H. Fritzsche and M. Pollak (World Scientific, 1990) p.111.
- 8) M. Eto, Phys. Rev. **B48** (Rapid Comm.) 4933 (1993); Physica B, to appear.
- 9) N. Zanon and J.-L. Pichard, J. Phys. France **49**, 907 (1988).
- 10) R. Yamada, Ph.D. thesis (Univ. of Tokyo, 1993).

**Persistent photoconductivity in the Coulomb glass”.**

**E.L.Altshuler**

***Department of Nuclear Physics. The Weizmann Institute of Science,  
Rehovot, 76100, Israel***

The subject of the Coulomb gap and its experimental manifestations were extensively investigated for the last two decades [4, 5, 6, 7]. Though many works were devoted to the form of the gap and the influence of multiparticle transitions for the samples of various dimensionality [8, 9, 10, 11, 12, 13], the dynamics of the correlation processes leading to the Coulomb gap were not studied in such detail. The relaxation process for a system of interacting localized electrons was discussed in [14].

These dynamics could be responsible for the persistent photoconductivity observed in recent experiments [1, 2]. In these experiments, relaxation of the photoconductivity of Anderson insulators was studied. The sample, a 2-d indium oxide film, was excited by light [2] or by an external electric field [1] and the slow relaxation of the induced conductivity ( $\delta\sigma$ ) was observed ( $\delta\sigma/\sigma \sim 10^{-2}$  at the time scale  $\sim 10^3$  sec after the excitation;  $\sigma$  is the conductivity of the material) (Fig. 1).

We will consider the following model for electron states in the insulator. The states (sites) of characteristic size  $a$  are randomly distributed in space and energy in the absence of interaction. An interaction between electrons is purely Coulombic:  $u_{ij} = e^2/r_{ij}$ , where  $e$  is the effective electron charge and  $r_{ij}$  is the distance between the sites. The characteristic distance between sites  $r$  is supposed to be greater than the localization length  $a$ .

The ground state for such a system is, by definition, the state where any electron transition from one site to another corresponds to a non-negative change of the energy of the system.

This condition provides the following inequality for a transition from site  $j$  to  $i$  [18]:

$$\epsilon_i - \epsilon_j - e^2/r_{ij} \geq 0 \quad (1)$$

where  $e^2/r_{ij}$  is the energy of Coulomb interaction between the two sites and  $\epsilon_i$  is the single particle energy of the site  $i$ , i.e. the energy necessary to deliver one electron to site  $i$  from infinity while all the others are frozen.

To find the density of states which satisfies the restriction (1) the selfconsistent equation was proposed [8, 9]:

$$g(\epsilon) = g_0 \exp\left(-e^{2d}(\nu_d/2) \int_0^\infty g(\epsilon') \frac{e^2}{(\epsilon + \epsilon')^d} d\epsilon'\right), \quad (2)$$

here  $g(\epsilon)$  is the single particle density of states as a function of energy measured from the Fermi level (hereafter all the energies will be measured from the Fermi level),  $g_0$  is the density of states far from the Fermi level,  $d$  is the dimensionality of the sample,  $\nu_d$  is the volume of unit  $d$ -dimensional sphere .

The solution for this equation for  $\epsilon \ll W$ , where  $W \sim (g_0/e^2)^{1/(d-1)}$  is the width of the Coulomb gap, has the form

$$g(\epsilon) = (d/\pi)\epsilon^{d-1}/e^{2d} \quad (3)$$

Such a behavior of the density of states is referred to as a Coulomb gap and is supposed to be responsible for the  $\exp-(T_1/T)^{1/2}$  temperature behavior of the conductivity [18]. Now we discuss the time dependent density of states  $g(\epsilon, t)$  for a system of interacting electrons which was excited at time  $t = 0$  to such a degree that the Coulomb gap has completely disappeared.

To estimate the relaxation time to such a correlated state from an initial homogeneous energy distribution we recall that the jump time between sites  $i$  and  $j$  is:

$$t_{ij} = \tau_0 \exp(r_{ij}/a). \quad (4)$$

where  $\tau_0 \sim 10^{-12}$ sec is the characteristic time for electron site-to-site jumps. Here we neglect the energy term in the exponent since in the following we will only be concerned with long relaxation times. Eq.(4) introduces characteristic distance, and energy for the problem:

$$r(t) = a \ln \frac{t}{\tau_0}, \quad \epsilon(t) = \frac{e^2}{a \ln \frac{t}{\tau_0}}. \quad (5)$$

In the following we present two approaches for calculating the time dependent density of states. Both of them imply that for large time scale  $g(\epsilon, t) = g(-\epsilon, t)$ .

Relaxation of the density of states was considered previously in [14]. It was assumed that in a time interval  $(t, t + \delta t)$  only electron jumps of the range  $(r(t), r(t) + \delta r)$  take place. The balance equation was written and solved in [14] for the  $g(\epsilon, t)$  using this assumption. The form of the nonequilibrium density of states obtained in [14] is presented in Fig.2. Below, calculating conductivity, we will use the following interesting feature of  $g(\epsilon, t)$  obtained in [14]. In the derivation of  $g(\epsilon, t)$  only jumps of distance  $r(t)$  were taken into account. During these jumps the changes of the energy for the abandoned and occupied sites are less than  $e^2/r(t)$ . Thus all the jumps between sites will take place within an energy strip  $|\epsilon_{i,j}| < e^2/r(t)$ . This leads to the conservation of the number of states within this strip.

Another approximation for calculating non-equilibrium density of states could be the following. Suppose that in a time  $t$  after excitation all the correlations at distances shorter than  $a \ln(t/\tau_0)$  are established. The problem becomes similar to the problem of the Coulomb gap for a cut off Coulomb potential  $U$ :

$$U = \begin{cases} e^2/r & \text{for } r < r(t); \\ 0 & \text{for } r > r(t) \end{cases}$$

The problem can be solved with a help of Efros selfconsistent equation analogous to (2) by methods developed in [17] for the case of screened Coulomb potential, and the result is somewhat different from the one of [14] (see Fig.2). Note that the density of states calculated with this method demonstrates unrealistic behavior. Namely, there exists a domain of energies  $E$  for which  $\int_{-E}^E (g(\epsilon, t) - g(\epsilon, \infty)) d\epsilon < 0$ . One can see that if the jump from site  $j$  to site  $i$  is possible when  $\epsilon_i - \epsilon_j - e^2/r_{ij} \leq 0$ , then the energy of the abandoned state  $\epsilon_j + e^2/r$  becomes higher than the energy of the occupied one before the jump  $\epsilon_i$ . This means that in single particle jumps approximation each jump causes the states to move away from the Fermi level, thus implying non-negative value for the integral. However, the negative values of the integral are small (in a sense that will be clarified later), and we will be able to neglect it.

We now calculate the conductivity relaxation according to the derivation of the variable range hopping conductivity presented in [19]. The whole sample can be considered as a set of random resistors connecting sites. Two sites  $i$  and  $j$  are connected with the resistor  $R_{ij}$ :

$$R_{ij} = R_0 \exp(r/a + \epsilon_{ij}/kT) \quad (6)$$

here  $\epsilon_{ij} = 1/2(|\epsilon_i| + |\epsilon_j| + |\epsilon_j - \epsilon_i|)$ ;  $\epsilon_{i,j}$  are the energies of the sites,  $T$  is the temperature and  $k$  is the Boltzmann constant. The conductivity of the sample  $\sigma$  has the form:

$$\sigma = \sigma_0 e^{-\xi}, \quad (7)$$

here  $\xi$  is the critical value for which pairs of sites obeying the bonding criterion

$$r_{ij}/a + \epsilon_{ij}/kT < \xi$$

form an infinite cluster. We find  $\xi(t) = \xi_0 + \xi_1(t)$  substituting the time dependent DOS in the derivation [19]:

$$\xi_1(t) = \alpha \left( \frac{T_1}{T} \right)^{1+d/2} \frac{1}{\ln^{d+1}(t/\tau_0)}. \quad (8)$$

Here

$$T_1 = \frac{\epsilon^2}{a}$$

is the characteristic energy for the problem,  $\alpha \sim 10^{-2}$  is the numerical constant. Time dependent conductivity is :

$$\sigma(t) = \sigma_0 e^{-\xi_0 - \xi_1} \quad (9)$$

The system achieves equilibrium when the characteristic width of the energy band where the relaxation takes place  $\epsilon \sim e^2/r(t)$  turns out to be of the order of the temperature. The corresponding time

$$t_{eq} = \tau_0 e^{T_1/T}.$$

We expect, for the systems discussed in [1, 2, 16], localization lengths to be several  $\text{\AA}$ , and hence  $T_1 \sim 1000K$  ( dielectric constant for the sample is of order 10). This leads to the relaxation time that somewhat exceeds the age of the Universe (actually measured relaxation times are determined by the accuracy of measurements).

This means that even before the illumination the system was not in an equilibrium state and its conductivity should be described by equations Eq.(9) and Eq.(8), where instead of  $t$  one should substitute the time of preparation of the sample  $t_{prep}$  which in actual experiments was  $\sim 10^4 \div 10^5$ sec. Thus to understand the experimental results we will choose certain reference time  $t_0$  and study the relative variation of conductivity. This gives the following result for the excess conductivity due to the perturbation of the sample :

$$\frac{\sigma(t) - \sigma(t_0)}{\sigma(t_0)} = \alpha \left( \frac{T_1}{T} \right)^{d/2+1} \left( \left( \ln \frac{t_0}{\tau_0} \right)^{-d-1} - \left( \ln \frac{t}{\tau_0} \right)^{-d-1} \right) \quad (10)$$

where  $\sigma$  is the conductivity of the material after the preparation.

Fitting the experimental data with expression (10) ( see Fig.1 ), one gets for  $T_1$  the value  $\sim 1000K$ . The corresponding localization length  $a$  is  $\sim 10\text{\AA}$ .

I would like to thank Prof. Zvi Ovadyahu for the numerous helpful discussions and acquainting me with the unpublished experimental data. I am very grateful to Prof. M.E. Raikh for

valuable comments and discussions on this work. I am very grateful to Profs. B.D. Laichtman, A.G. Aronov, Y. Imry, M. Pollak and B.I. Shklovskii for the interesting and helpful discussions. This work was supported by the German-Israeli foundation for Research (GIF), Jerusalem, Israel.

## References

- [1] M. Ben-Chorin and Z. Ovadyahu Phys. Rev. B **44** 3420, (1992)
- [2] M. Ben-Chorin Z. Ovadyahu and M.Pollak, to be published in Phys.Rev.B, November (1993).
- [3] C.J. Adkins in *Hopping and Related Phenomena* edited by H. Fritzsche and M. Pollak, World Scientific, pp.93 (Singapur–New Jersey–London–Hong Kong), (1990).
- [4] M. Pollak, *Discuss.Faraday Soc.*, **50**, 11 (1970).
- [5] G. Srinivasan Phys. Rev. B **4**, 2581, (1971).
- [6] A. L. Efros and B. I. Shklovskii in *Electron-electron Interactions in Disordered Systems*, edited by A.L Efros and M. Pollak ( Amsterdam: North Holland), chap 5; (1987)
- [7] M. Pollak Phyl. Mag. B **65**, 657, (1992).
- [8] A.L. Efros J. Phys. C **9**, 2021, (1976)
- [9] S.D. Baranovskii, B.I. Shklovskii and A.L. Efros, Sov.Phys.–JETP **51**, 199, (1980) [Zh.Eksp.Teor. Fiz. **78**, 395,(1980) ].
- [10] P. Gosar, Physica A **120**, 339, (1983)
- [11] J.H. Davies Phyl. Mag. B **52**, 511, (1985)
- [12] R. Chicon, M. Ortuño and M. Pollak Phys. Rev. B **37**, 10520, (1988).
- [13] M.E. Raikh and A.L. Efros Sov.Phys.–JETP Lett. **45**, 280, (1987) [Pis'ma Zh.Eksp.Teor. Fiz. **45**, 225,(1987) ].
- [14] A.A. Mogilyanskii and M.E. Raikh Sov.Phys.–JETP **68**, 1081, (1989) [Zh.Eksp.Teor. Fiz. **95**, 1870,(1989) ].
- [15] Z. Ovadyahu J. Phys. C **19**, 5187 (1986).
- [16] Ju-Jin Kim and Hu Jong Lee, Phys. Rev. Lett., **70** 2798, (1993)
- [17] V.L Nguen, M.E. Raikh and A.L. Efros Sov. Phys.–Solid State **28**, 1129, (1986) [Fiz. Tverd. Tela **28**, 2019,(1986) ].
- [18] A.L. Efros and B.I. Shklovskii, J. Phys. C **8**, L49, (1975).
- [19] B.I. Shklovskii and A.L. Efros *Electronic Properties of Doped Semiconductors* ( Nauka, Moskva), (1979) [Engl. transl.: Heidelberg, (1984) ].

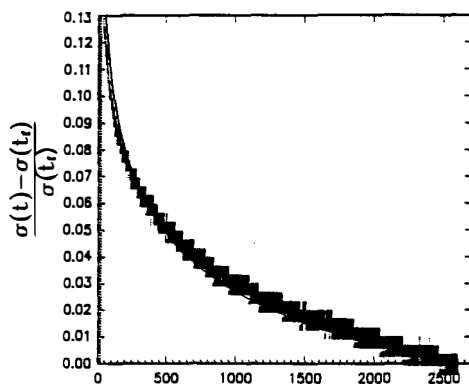


Fig.1 The plot represents the time dependence of the excited conductivity. The Y-axis is the relative difference between the conductivity at a given time  $\sigma(t)$  and the conductivity at time  $t_f = 2685$  sec. The X-axis is the time after the excitation. The gray area shows the experimental data from [2]. The solid line corresponds to a fit of Eq.(18), with parameters  $\tau_0 = 10^{-12}$ sec and  $\alpha^{1/2}T_1 = 1608K$ .

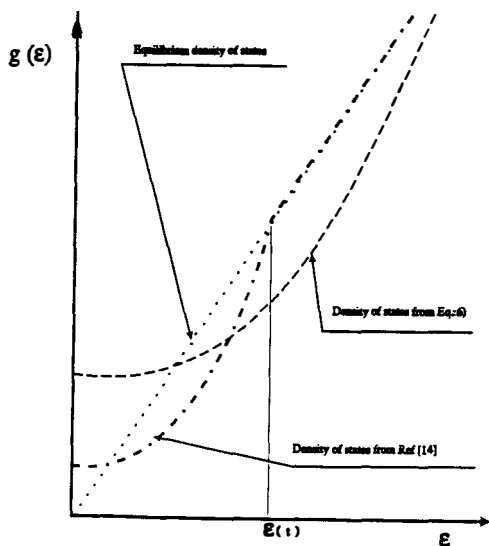


Fig.2 The time dependent density of states from [14] and calculated from equation (6).  $\epsilon_0(t) = e^2/\tau(t)$ .

FROM CHAOTIC SCATTERING TO LOCALIZATION:  
A BRIEF REVIEW OF RANDOM MATRIX APPROACHES.

Jean-Louis Pichard

Service de Physique de l'État Condensé, C.E.A. Saclay, 91191, Gif sur Yvette cedex, France.

**Abstract**

The statistics of the transmission eigenvalues of a complex many-channel scatterer are reviewed, assuming different random matrix ensembles for its scattering matrix  $S$  or transfer matrix  $M$ . We derive the distributions corresponding to the Dyson circular ensembles for  $S$ , which we compare to those given by the global maximum entropy approach for  $M$  and to those yielded by the multiplication of isotropically distributed transfer matrices. Following the considered ensemble, one gets the conductance distribution for ballistic dots with chaotic dynamics and for quasi-1d disordered conductors and insulators. We show in conclusion how some level repulsion persists in the transmission spectra of 3d Anderson insulators and how localization appears in the two level form factor of the scattering phase shifts.

We consider a complex scatterer which is connected to two electron reservoirs by two identical leads where electron fluxes have a quantized transverse momentum. This quantization defines  $N$  channels by which the carriers can be injected through each lead. The sample between the two leads is represented by a  $2N \times 2N$  scattering matrix  $S$  (giving the outgoing fluxes in terms of the incoming ones) or by a  $2N \times 2N$  transfer matrix  $M$  (giving the fluxes in one of the lead in terms of the flux in the opposite lead). Introducing a certain polar parametrization of  $M$  and  $S$ , one can define  $N$  real positive parameters  $\lambda_a$ , hereafter mentioned as the radial parameters, which are particularly convenient<sup>1,2)</sup> since:

(i). They give the transmission eigenvalues  $T_a = (1 + \lambda_a)^{-1}$  of  $t.t^\dagger$ , where  $t$  is a submatrix of  $S$  describing how the flux amplitudes are transmitted from one reservoir to the other. Using

a two-probe Landauer formula, the sample conductance  $g$  (in units of  $2e^2/h$ ) reduces in this parametrization to a linear statistics of the radial parameters:

$$g = \sum_{a=1}^N \frac{1}{1 + \lambda_a}. \quad (1)$$

as other physical quantities of interest (shot-noise power, conductance when one of the reservoir becomes superconducting, Josephson effect between two superconducting reservoirs).

(ii). Their joint probability distribution  $P(\{\lambda_a\})$  is given, assuming for  $M$  a statistical ensemble of maximum information entropy with a given average density  $\rho(\lambda)$ , hereafter mentioned as the global approach, by:

$$P(\{\lambda_a\}) = Z^{-1} \exp[-\beta \mathcal{H}(\{\lambda_a\})], \quad (2)$$

$$\mathcal{H}(\{\lambda_a\}) = - \sum_{a < b} \ln |\lambda_a - \lambda_b| + \sum_a V(\lambda_a), \quad (3)$$

where  $Z$  is a normalization constant. One can view this distribution as the Gibbs factor of a fictitious Coulomb gas. The parameter  $\beta$ , which plays the role of an inverse temperature, can take three possible values depending on the system symmetries:  $\beta = 1$  when the system is invariant under time reversal symmetry and spin rotation symmetry (orthogonal case),  $\beta = 4$  when a strong spin-orbit scattering removes spin rotation symmetry (symplectic case) and  $\beta = 2$  if a magnetic field breaks time reversal symmetry (unitary case). The one-body potential  $V(\lambda)$  can be related, in the large  $N$ -limit, to the constraint  $\rho(\lambda)$  of this maximum entropy ensemble by:

$$V(\lambda) = \int_0^\infty \rho(\lambda') \ln |\lambda - \lambda'| d\lambda' + O(N^0). \quad (4)$$

In this description, the radial parameters  $\{\lambda_a\}$  are distributed like the energy levels of a complex system with Wigner-Dyson statistics<sup>3</sup>. This allows us to use the powerful methods first developed for the energy levels statistics of complex nuclei, with two major differences: the  $\lambda_a$  are confined to the positive part of the real axis and their density  $\rho(\lambda)$  contains a more direct information about transport than the Hamiltonian spectra. The average conductance  $\langle g \rangle = \int_0^\infty \rho(\lambda)(1 + \lambda)^{-1} d\lambda$  indicates indeed whether the system is metallic or insulating. When  $V(\lambda)$  strongly confines the radial parameters to small values, one can for instance describe a chaotic ballistic quantum dot or one can give a somewhat simplified picture of a diffusive quasi-1d conductor with elastic mean free path  $l$  and size  $L$  (global approach). When  $V(\lambda)$  weakly confines the  $\lambda_a$  to exponentially large value  $\exp(2L/\xi_a)$ , one simply gets the statistics of an insulator with a localization length defined by the largest of the characteristic decay length  $\xi_a$ . For weakly disordered wires, we discussed in section 4 the merits and the weaknesses of this simplified description.

(iii) The radial parameters are related to the logarithms  $\nu_a = 2L/\xi_a$  of the eigenvalues of  $M^\dagger M$  through the relation

$$\lambda_a = \frac{\cosh \nu_a - 1}{2}. \quad (5)$$

The  $\nu_a$  obey a law of large numbers if one has a multiplicative combination law for  $M$  (Oseledec's theorem) and are normally distributed in the localized regime.

The purpose of this contribution is to shortly review recent advances in the understanding of the validity and of the limit of Wigner-Dyson statistics for these radial parameters, concerning chaotic ballistic dots<sup>4</sup>, quasi-1d disordered conductors and insulators<sup>1,2</sup>, and disordered systems in higher dimensions (e.g. 3d insulators<sup>5</sup>).

## 1 Polar decomposition of $S$ and $M$ .

Using system symmetries (current conservation, time reversal symmetry, spin rotation symmetry) one can show<sup>6,7</sup> that both  $S$  and  $M$  can be expressed in terms of the  $N$  radial parameters  $\{\lambda_a\}$  of  $M$  and 4 (2 in the presence of time reversal symmetry) auxiliary unitary matrices. Writing  $S$  as usual in terms of the 4  $N \times N$  reflection (transmission) matrices  $r, r'$  ( $t, t'$ ) and similarly the  $2N \times 2N$  transfer matrix in terms of 4  $N \times N$  blocks, the polar decomposition of  $S$  and  $M$  is defined by:

$$S = \begin{pmatrix} r & t' \\ t & r' \end{pmatrix} = \begin{pmatrix} u^{(3)} & 0 \\ 0 & u^{(4)} \end{pmatrix} \begin{pmatrix} -\sqrt{\mathcal{R}} & \sqrt{\mathcal{T}} \\ \sqrt{\mathcal{T}} & \sqrt{\mathcal{R}} \end{pmatrix} \begin{pmatrix} u^{(1)} & 0 \\ 0 & u^{(2)} \end{pmatrix} \quad (6)$$

$$M = \begin{pmatrix} u^{(4)} & 0 \\ 0 & u^{(2)\dagger} \end{pmatrix} \begin{pmatrix} (I + \lambda)^{1/2} & \lambda^{1/2} \\ \lambda^{1/2} & (I + \lambda)^{1/2} \end{pmatrix} \begin{pmatrix} u^{(1)} & 0 \\ 0 & u^{(3)\dagger} \end{pmatrix}. \quad (7)$$

The  $u^{(l)}$  ( $l = 1, \dots, 4$ ) are arbitrary  $N \times N$  unitary matrices.  $\lambda$ ,  $\mathcal{R}$  and  $\mathcal{T}$  are real diagonal  $N \times N$  matrices with non-zero elements being respectively the radial parameters  $\lambda_a$ , the reflection eigenvalues  $R_a = \lambda_a(1 + \lambda_a)^{-1}$  and transmission eigenvalues  $T_a = (1 + \lambda_a)^{-1}$ .

This decomposition applies to the unitary case. In the orthogonal case,  $S$  is symmetric and the polar decomposition requires only two independent unitary matrices:

$$u^{(3)} = u^{(1)\text{T}}, \quad (8)$$

$$u^{(4)} = u^{(2)\text{T}}. \quad (9)$$

In the symplectic case, the spin degeneracy is removed and each matrix element becomes a  $2 \times 2$  quaternion matrix, which doubles the size of  $M$  and  $S$ , but  $u^{(3)}$  and  $u^{(4)}$  are also given<sup>6</sup> in terms of  $u^{(1)}$  and  $u^{(2)}$  and the  $\lambda$  have a twofold degeneracy (Kramers degeneracy).

## 2 Invariant measure of $S$ in the polar parametrization.

In the original work of Dyson<sup>8)</sup>, the measures  $\mu_\beta(dS)$  of an infinitesimal volume element of the matrix-space where  $S$  is defined, given the system symmetries, are expressed as a function of the  $2N$  eigenvalues  $\{\exp i\theta_a\}$  and of the eigenvector coordinates. This is suitable to obtain the distribution of the scattering phase shifts  $\{\theta_a\}$ , but not to study a transport property  $A$  which can be expressed as a linear statistic  $A = \sum_{a=1}^N f(\lambda_a)$  of the radial parameters. For having the measure  $\mu_\beta(dS)$  in terms of the  $\{\lambda_a\}$  and of the  $u^{(l)}$ , we have adapted<sup>7)</sup> the original method of Dyson, as sketched here only for the orthogonal ensemble ( $\beta = 1$ ), where  $S$  is unitary symmetric and can be represented in the form  $S = YY^T$ , where  $Y$  is unitary. Note that this decomposition is not unique. An infinitesimal neighborhood  $dS$  of  $S$  is given by  $dS = iY dQ Y^T$ , with  $dQ$  a real symmetric matrix. It has been shown by Dyson<sup>7)</sup> that if the matrix elements  $dQ_{ij}$  vary through some small intervals of lengths  $d\mu_{ij}$ , the measure  $\mu_1$  equals  $\mu_1(dS) = \prod_{i \leq j} d\mu_{ij}$ , independent of  $Y$ . We use this freedom to choose  $Y$  in a form convenient for the polar parametrization

$$Y = \mathcal{U}\mathcal{O}\mathcal{I} = \begin{pmatrix} u & 0 \\ 0 & u' \end{pmatrix} \begin{pmatrix} (\frac{1-\sqrt{\kappa}}{2})^{1/2} & -(\frac{1+\sqrt{\kappa}}{2})^{1/2} \\ (\frac{1+\sqrt{\kappa}}{2})^{1/2} & (\frac{1-\sqrt{\kappa}}{2})^{1/2} \end{pmatrix} \begin{pmatrix} \mathbf{1} & 0 \\ 0 & i\mathbf{1} \end{pmatrix}. \quad (10)$$

Since  $idQ = dY^T Y^* + Y^\dagger dY$ , and since  $Y$  and  $dY$  can be expressed in terms of the matrices  $\mathcal{U}$ ,  $\mathcal{O}$ ,  $\mathcal{I}$  and their neighborhoods  $d\mathcal{U}$  and  $d\mathcal{O}$ , one can easily get  $dQ$  in this parametrization. The result is an expression for  $\mu_1(dS)$  in terms of the measures  $\mu(d\mathcal{U})$  and  $\mu(d\lambda)$  associated with the matrices  $\mathcal{U}$  and  $\lambda$ , times a Jacobian  $P(\{\lambda_a\})$ :

$$\mu_1(dS) = P(\{\lambda_a\})\mu(d\lambda)\mu(d\mathcal{U}). \quad (11)$$

The calculations in the unitary<sup>3)</sup> and symplectic<sup>9)</sup> ensembles proceed similarly and give for the Jacobian  $P(\{\lambda_a\})$  an expression valid for the three ensembles which we write under the form of a Gibbs distribution,

$$P(\{\lambda_a\}) = Z^{-1} \exp[-\beta\mathcal{H}(\{\lambda_a\})], \quad (12)$$

$$\mathcal{H}(\{\lambda_a\}) = -\sum_{i < j} \ln |\lambda_i - \lambda_j| + \sum_i V_\beta(\lambda_i), \quad (13)$$

$$V_\beta(\lambda) = \left( N + \frac{2-\beta}{2\beta} \right) \ln(1 + \lambda). \quad (14)$$

## 3 Ballistic quantum dots with chaotic dynamics.

A quantum dot is essentially a mesoscopic electron billiard connected by two small holes to two electron reservoirs. In contrast to a disordered wire with bulk scattering and constant section

considered in the next section, there is not a natural multiplicative combination law for the corresponding transfer matrix, in the case of an arbitrary complex shape of the chaotic billiard.

An electron which is injected through one of the holes will either return through the same hole, with probability  $R$ , or be transmitted through the other hole, with probability  $T$ . Classically, if the electron dynamics is chaotic, the uniform (ergodic) exploration of the boundaries yields  $T = R$ , if the two holes are of the same size and sufficiently small that direct transmission (without boundary reflections) can be ignored.

For a *closed* quantum dot (without holes), it is well known that one of the quantum signatures of its classically chaotic character consists in the Wigner-Dyson distribution of the energy levels<sup>10</sup>. The quantum dot with holes is an *open*, rather than a closed system. Just as the Wigner-Dyson distribution describes the Hamiltonian  $H$  of the closed system, Dyson's circular ensemble<sup>8</sup>) provides the statistical properties of the scattering matrix  $S$  of the open system. To have spectral or scattering properties given by Wigner-Dyson distributions can be actually regarded as a precise definition of the somewhat vague concept of "quantum chaos". To what extent a real ballistic cavity is close to this precise universal-limit is the subject of the theory of quantum billiards<sup>11,12</sup>).

Assuming this definition of a quantum chaotic system, the statistics of the radial parameters characterizing the circular ensembles and their implications have been derived in Ref. 4, which we summarize. Dyson's circular ensemble applies to a system where all scattering processes are equally probable (subject to the constraints of current conservation and time-reversal and spin-rotation symmetry). The probability  $P_\beta(dS)$  to find  $S$  in a neighborhood  $dS$  of some given  $S$  is just

$$P_\beta(dS) = \frac{1}{V_\beta} \mu_\beta(dS), \quad (15)$$

where  $V_\beta = \int \mu_\beta(dS)$  is the total volume of the  $S$ -matrix space. Then, the circular ensembles consist in auxiliary matrices  $u^{(l)}$  which are independent from each other (excepted symmetries related to time reversal invariance) and distributed according to the invariant Haar measure on the unitary group. The  $N$  parameters  $\lambda_\alpha$  are statistically independent from the  $u$ -matrices and have a joint probability distribution identical to the Jacobian  $P(\{\lambda_\alpha\}) = Z_\beta^{-1} \exp(-\beta\mathcal{H}(\{\lambda_\alpha\}))$  given by Eq. (12-14). The Hamiltonian of this Gibbs factor has a one-body potential  $V_\beta(\lambda)$  which is symmetry-independent to order  $N$ , while the term of order  $N^0$  depends on  $\beta$ . This distribution is universal; i.e. does not contain any physical parameter, excepted the number  $N$  of channels in the leads.

The expectation value  $\langle A \rangle = \int_0^\infty a(\lambda)\rho(\lambda)d\lambda$  of a linear statistics  $A = \sum_{n=1}^N a(\lambda_n)$  is given

by the density  $\rho(\lambda)$  characterizing the circular ensembles. Decomposing  $\rho = \rho_N + \delta\rho$  into a contribution  $\rho_N$  of order  $N$  (giving the “Boltzmann conductance”) and a symmetry-dependent correction  $\delta\rho$  of order  $N^0$  (responsible for the “weak-localization effect”), one finds:

$$\rho_N(\lambda) = \frac{N}{\pi(1+\lambda)\sqrt{\lambda}}, \quad (16)$$

$$\delta\rho(\lambda) = \frac{\beta-2}{4\beta} \delta_+(\lambda), \quad (17)$$

where the one-sided delta-function satisfies  $\int_0^\infty \delta_+(\lambda) d\lambda = 1$ .

This gives for the expectation value  $\langle g \rangle$  of the conductance:

$$\langle g \rangle = \frac{1}{2}N + \delta g, \quad \delta g = \frac{\beta-2}{4\beta}. \quad (18)$$

For  $\beta = 2$ , one finds  $\langle T \rangle = \frac{1}{2}N = \langle R \rangle$  (where  $\langle R \rangle = N - \langle T \rangle$  is the total reflection probability). This is the quantum analog of what we expect from the “ergodic” exploration of the dot boundaries by the classical trajectories. Quantum interference then breaks the equality  $\langle T \rangle = \langle R \rangle$  by an amount  $\delta T$ , due to weak localization ( $\beta = 1$ ) or anti-localization ( $\beta = 4$ ). In the same way one can compute the average of any other linear statistics<sup>4</sup>.

Fluctuations around the average in this ensemble can be computed using the general formulas of Ref. 13, which hold for any ensemble with a logarithmic interaction (regardless of the form of the one-body potential). The variance in the large- $N$  limit is given by

$$\text{Var } A = -\frac{1}{\beta} \frac{1}{\pi^2} \int_0^\infty d\lambda \int_0^\infty d\lambda' \left( \frac{da(\lambda)}{d\lambda} \right) \left( \frac{da(\lambda')}{d\lambda'} \right) \ln \left| \frac{\sqrt{\lambda} - \sqrt{\lambda'}}{\sqrt{\lambda} + \sqrt{\lambda'}} \right|. \quad (19)$$

One gets the analogue of the “Universal Conductance Fluctuations” (UCF) in a ballistic chaotic cavity, which can be induced by a change of the Fermi energy, of the applied magnetic field, or of the boundary spin-orbit scattering, as well as by a slight deformation of the shape of the dot, with  $\text{Var } g = 1/8\beta$ .

Another remarkable result mentioned in Ref. 4 (see also Ref. 14), which might be experimentally confirmed without difficulty, applies to a semiconductor quantum dot which is coupled to the reservoirs by two quantum point contacts with a quantized conductance of  $2e^2/h$ . For  $N = 1$ , the probability distribution (2) reduces to  $P(\lambda) = \frac{1}{2}\beta(1+\lambda)^{-1-\beta/2}$ , giving for  $g$  the distribution

$$P(g) = \frac{\beta}{2} g^{-1+\beta/2}, \quad 0 \leq g \leq 1. \quad (20)$$

In the presence of magnetic field ( $\beta = 2$ ), any value of the conductance between 0 and  $2e^2/h$  is equally probable. In non-zero field it is more probable to find a small than a large conductance, provided that the boundary scattering preserves spin-rotation symmetry ( $\beta = 1$ ). In the

presence of spin-orbit scattering at the boundary ( $\beta = 4$ ), however, a large conductance is more probable than a small one.

## 4 Quasi-1d wires with weak bulk disorder.

It is remarkable that the pairwise interaction for the radial parameters in the circular ensembles is the same than in the global approach (see Eq. 2), originally introduced for describing bulk diffusion with elastic mean free path  $l$ . However, with bulk disorder, the  $V(\lambda)$  of the circular ensemble, which does not contain  $l$ , is not appropriate: the presence of many impurities in the sample strongly favors the reflection of the carriers back into their reservoir, while very few of them can reach the opposite reservoir and the conductance  $\approx Nl/L$  (metal) or  $\approx \exp(-2L/\xi)$  (insulator). This has to be contrasted with a ballistic cavity where an injected carrier is subjected to many chaotic boundary reflections before finding with almost equal chance one of the two injection leads, when  $N$  is large. The appropriate form for the potential of a disordered wire is given <sup>2)</sup> by:

$$V_d(\lambda) = (Nl/L) \ln^2(\sqrt{\lambda} + \sqrt{1+\lambda}) + \mathcal{O}(N^0). \quad (21)$$

Of little practical importance, but of great theoretical interest, the pairwise interaction  $u(\lambda_a - \lambda_b)$  occurring in a quasi-1d disordered system is not exactly the simple Wigner-Dyson logarithmic interaction assumed by the global approach, but is given <sup>15)</sup> by:

$$u(\lambda_a - \lambda_b) = -\frac{1}{2} \ln |\lambda_a - \lambda_b| - \frac{1}{2} \ln |\operatorname{arcsinh}^2 \sqrt{\lambda_a} - \operatorname{arcsinh}^2 \sqrt{\lambda_b}| \quad (22)$$

at least in the unitary case. One can see that this interaction reduces to the usual logarithmic interaction if  $|\lambda_a - \lambda_b| < 1$ , but is halved if  $|\lambda_a - \lambda_b| > 1$ . It is worth to note that this modified interaction does not introduce a new parameter, in contrast to the one describing in a metallic particle the energy-level interaction which is controlled by the time it takes for an electron to diffuse in the sample<sup>16)</sup>. This discrepancy is responsible for the slightly different U.C.F. values characterizing ballistic quantum dots with chaotic dynamics ( $2/16\beta$ , logarithmic interaction) and quasi-1d disordered conductors ( $2/15\beta$ , local logarithmic interaction only).

Let us mention how to obtain these results for a long disordered wire of constant transverse section in the limit of weak disorder, such that the total  $M$ -matrix can be regarded as the product of the transfer matrices of many slices. This multiplicative combination law for  $M$  is at the basis of many works, either numerical or analytical, as those developed by Dorokhov<sup>17)</sup> from purely microscopic considerations and by Mello et al<sup>3)</sup> from a local maximum entropy assumption. Contrary to their numerical counterparts, the analytical works we refer to assume that the

radial part of  $M$  is statistically decoupled from the  $u$ -matrices, which are supposed to remain distributed with the Haar measure on the unitary group, independently of the sample length. The radial part of  $M$ , characterized by the distribution  $P(\{\lambda_a\})$ , has its length dependence given by a Fokker-Planck equation. <sup>†</sup> This isotropy hypothesis makes sense only for weak disorder and quasi-one dimension (one gets the same UCF and weak-localization corrections than diagrammatic calculations based on quasi-1d microscopic models). Using Sutherland's transformation, Beenakker and Rejzaj<sup>15)</sup> have mapped this diffusion equation onto a Schrodinger equation (with imaginary time) of a quantum set of point like particles free to move on a half line (the positive part of the real axis) within a certain potential. For arbitrary values of  $\beta$ , these particles have a pairwise interaction, attractive for  $\beta = 1$  and repulsive for  $\beta = 4$ , making difficult the solution of the Schrodinger equation. Fortunately, this interaction vanishes for  $\beta = 2$ , and the solution of the diffusion equation is reduced to an exactly solvable quantum  $N$ -body free fermion problem, giving the interaction defined by Eq.(22).

In the localized regime, the global approach (with the potential given by Eq. (21)) and the Fokker-Planck equation give identical symmetry dependence<sup>19)</sup> of the localization lengths, though the (log) conductance fluctuations differs by a factor 2 in the quasi-1d localized limit<sup>1)</sup>. This later point again is consistent with the halving of the pairwise interaction  $u(\lambda_a - \lambda_b)$  when  $|\lambda_a - \lambda_b| \gg 1$ . For metals and insulators far from a quasi-one dimensional shape, a more dramatic shrinkage of the logarithmic repulsion has been observed<sup>20)</sup>. This means that transverse diffusion (or even more transverse localization<sup>5)</sup> yields a more significant reduction of the logarithmic pairwise interaction than the one obtained in quasi one dimension by Rejzaj and Beenakker. We have to deal with a more difficult case where the  $u$ -matrices and the radial parameters are correlated, such that the length dependence of the statistics does not reduce to an "isotropic" Brownian motion in the  $M$ -matrix space.

Using the polar parametrization of  $S$  and  $M$ , we have exactly shown the similarity and the difference between the distributions implied by the Dyson circular ensembles, which are suitable for describing quantum ballistic dots with underlying chaotic classical dynamics, and those describing in the weak scattering limit long quasi-1d disordered conductors and insulators where  $M$  has a multiplicative combination law. In the two cases, the  $u$ -matrices are decoupled from the radial part and are distributed with the Haar measure on the unitary group. The

<sup>†</sup>One can say that the multiplicative combination law of  $M$  induces an isotropic Brownian motion on the Lobachesky plane, as understood<sup>18)</sup> a long time ago in radio-electrical engineering for  $N = 1$  (C.W.J Beenakker, private communication). For arbitrary  $N$ , one has the heat equation on a space of negative curvature, with a diffusion constant related to  $l$  in front of the radial part of the Laplace-Beltrami operator.

statistics of the radial parts differ essentially because of the one-body potential  $V(\lambda)$ , and slightly because of the long range part of the pairwise interaction.

## 5 Disordered insulators in three dimensions.

In the quasi-1d localized regime, when the sample length is larger than the symmetry dependent quasi-1d localization length  $\xi = \beta N l$ , the pairwise interaction, logarithmic with infinite range in the global approach, or locally logarithmic only as implied by matrix multiplication (Eq (22)), remains unchanged for a fixed number  $N$  of channels. The statistics is only governed by the weakening of the confining potential as  $L$  increases, eventually giving exponentially large values for all the  $\lambda_a$ , with exponentially large separations between them. Those very large spacings only prevent to observe the persistence of the pairwise interaction.

It is therefore interesting to consider strongly disordered  $L * L * L$  cubes where the number  $N$  of channels is not kept constant, but scales as  $L^2$ , in order to numerically check the persistence of some repulsion in the presence of localization. In figure 1, one can see the ensemble averaged values of the variables  $\nu_a$  (essentially the  $\log \lambda_a$ , see Eq. (5)) given in Ref. 5 for intermediate and strong disorder. One can see indeed that exponentially large values coexist with small spacings, such that the pairwise repulsion should be felt, and the spacing distribution between nearest neighbours should be close to the Wigner surmises.

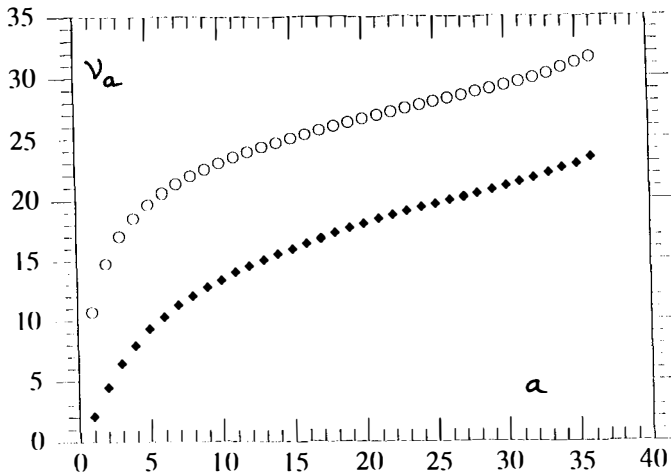


Fig.1: Ensemble averaged  $\nu_a$  for a  $6 \times 6 \times 6$  cube ( $N = 36$ ). Diamonds:  $\xi \approx L = 6$ ; Circles:  $\xi \approx 1 < L$ .

This can be seen in figure 2: the transmission eigenvalues still repel each other when they are exponentially small, but close to each other. This has been obtained from a  $3d$ -network of disordered quantum wires as explained in Ref. 5. Using the usual microscopic Anderson model, one gets similar behaviours. The persistence of a strong repulsion between transmission modes with extremely short characteristic decay lengths is quite noticeable, though weaker than the Wigner–Dyson repulsion. We can note that weak magnetic fields (about one flux quantum through the sample) have no clear effects on the spacing fluctuations. For moderate disorder, we observe a change of the spacing statistics and an increase of the localization length for a cross-over field of the order of a flux quantum per localization domain, considerably larger than the cross-over field characterizing a good conductor (one flux quantum through the whole sample only). A study of the long range rigidity indicates that the random matrix correlations persist only for small  $\lambda$  separations, but disappear on a larger scale, recalling to some extent the situation encountered with energy level statistics (Wigner–Dyson statistics persisting on energy interval smaller than  $g$  times the level spacing<sup>21</sup>). However, this analogy cannot be pushed very far, since we have seen, for the quasi- $1d$  wire, that the range of validity of the Wigner–Dyson statistics for the transmission spectra is independent of any physical parameter (see Eq.(22)), in contrast to the hamiltonian spectra.

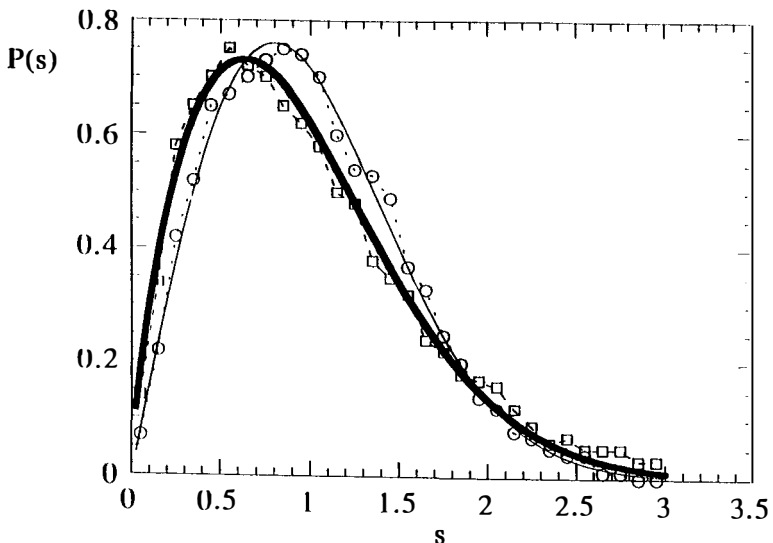


Fig.2: Distribution  $P(S)$  of the spacing  $S = \nu_2 - \nu_1$ , measured in units of its average, for the same cubes than in Fig. 1. When  $\xi \approx L$ , one gets the Wigner surmise (circles). When  $\xi \ll L$  (squares), the fat curve indicates a weakening of the level repulsion.

## 6 Scattering phase shift form factor and localization.

Diagonalizing  $S$ , one gets  $2N$  scattering phase shifts  $\{\theta_a\}$ . Their density  $\rho(\theta)$  and two point correlation function  $R_2(\theta_1, \theta_2)$  have been studied in Ref. 7, for  $2d$  samples with bulk disorder and different aspect ratios  $L/L_t$  ( $L$  and  $L_t$  denoting respectively the longitudinal and transverse lengths). The two level form factor<sup>7)</sup>:

$$b(k) = \int_{-\infty}^{\infty} dr Y_2(\theta) \exp(2\pi i k \theta) \quad (23)$$

is the Fourier transform of the 2 point cluster function  $Y_2(\theta) = 1 - \frac{1}{\Delta^2} R_2(\theta)$ , where  $\theta$  is measured in units of the average spacing  $\Delta$ . Numerically, the form factor  $b(k)$  calculated from a microscopic Anderson model turns out to be well described by the corresponding functions of the circular ensembles, in the quasi-1d metallic limit ( $L_t \ll L \ll \xi$ ). This observation cannot be easily anticipated, since we have seen how quasi-1d disordered ensembles differ from Dyson statistics, if one uses the polar parametrization. This might mean that these differences mostly matter for the eigenvector statistics of  $S$ . Easier to understand, if one assumes isotropy, quasi-1d localization ( $L_t \ll \xi \ll L$ ) breaks  $S$  into two uncorrelated reflection matrices  $r$  and  $r'$ , each one them distributed with a Dyson measure. One has just to look at Eq. (6), setting  $\mathcal{T} \approx 0$  and  $\mathcal{R} \approx 1$ , to see that the distribution of the  $2N$  phase shifts will be broken into the incoherent superposition of two Dyson series of  $N$  phase shifts. Figure. 3 presents this phenomenon for the form factor when  $L \approx \xi$  (cross-over regime between the metal and the insulator). One can see the evolution between the behaviour of two uncoupled circular ensembles (small  $k$ ) to the behaviour of a single circular ensemble (large  $k$ ), showing in the harmonics of  $Y_2(\theta)$  how reflection by opposite edges is statistically decorrelated by longitudinal localization. Outside the weak-disorder quasi-1d limit, we find that the phase shift density is not uniform and that  $S$  remains nonzero after disorder averaging (non isotropy). Another correction to the circular ensemble behaviour of  $b(k)$  can be observed in addition of the crossover phenomenon related to longitudinal localization, more pronounced for sample shape far from the quasi-1d limit, in the low harmonics of  $Y_2(\theta)$ . This deviation to the Dyson behaviour visible in Fig.4 is reminiscent of the non universal regime found by Altshuler and Shklovskii for energy-level separation larger than the Thouless energy  $E_C$  (with  $b(k) \propto k^{1-d/2}$  for small  $k$ ). One can relate<sup>7)</sup> under certain assumptions the energy level form factor to the scattering phase shift form factor. Numerical check of the proposed relation between the dimensionality dependent corrections to the universal random matrix behaviours of the energy levels and of the scattering phase shifts for disordered systems are given in Ref. 7.

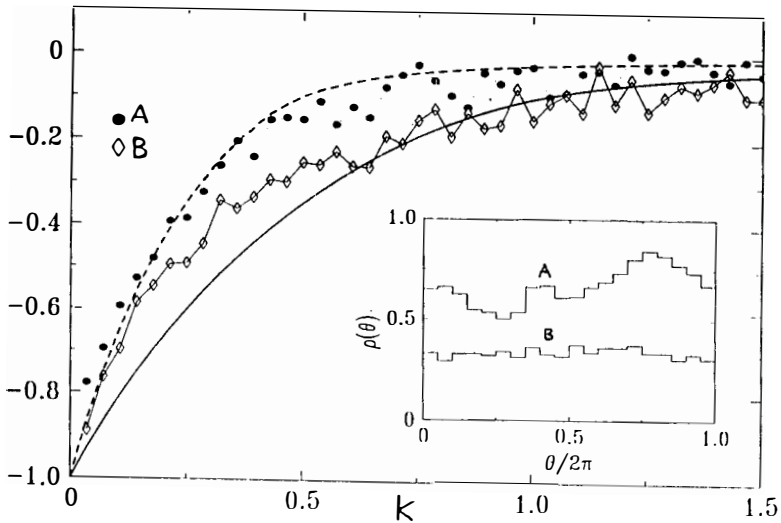
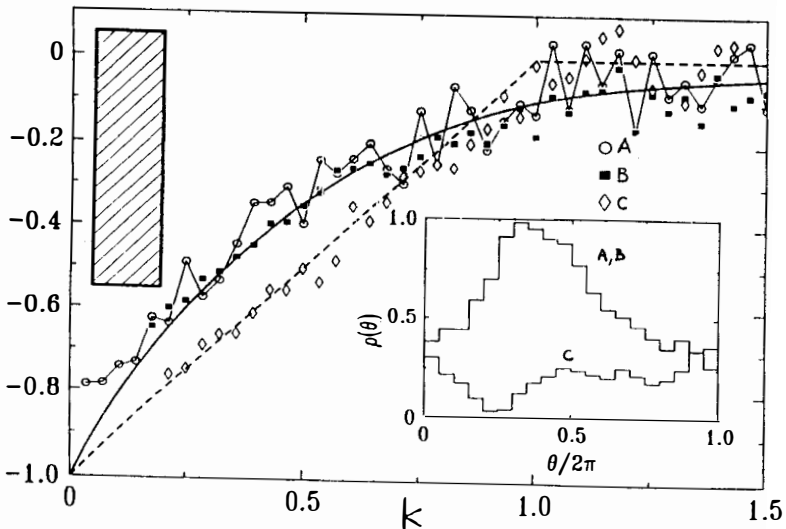


Fig.3: Phase Shift Form Factor  $b(k)$  for quasi-1d systems: (A) full circles:  $L \gg \xi$  and (B) diamonds  $L \approx \xi$ . The solid line corresponds to a single circular orthogonal ensemble (C.O.E.) and the dashed line to the incoherent superposition of two C.O.E. The inset indicates uniform densities  $\rho(\theta)$ .

Fig.4: Phase Shift Form Factor  $b(k)$  for a short sample ( $L_t = 4L$  with magnetic field (diamond) and without (solid square and circle). The dashed and solid curves gives the C.U.E and C.O.E. behaviours. One can notice that  $b(k)$  behaves as  $k^{1-d/2}$  with  $d = 2$  for small  $k$ . The inset indicates highly non uniform  $\rho(\theta)$ .

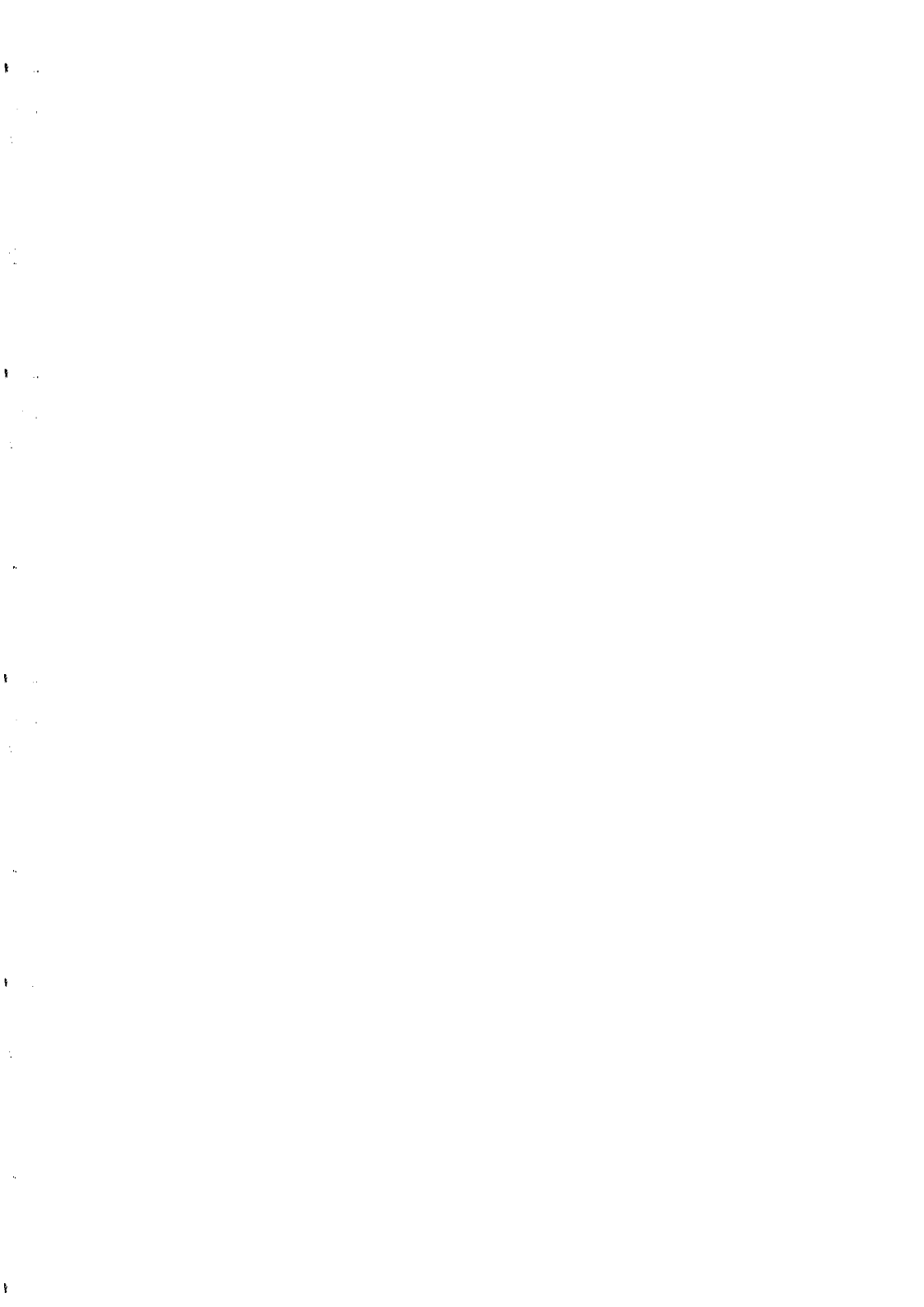


## Acknowledgments

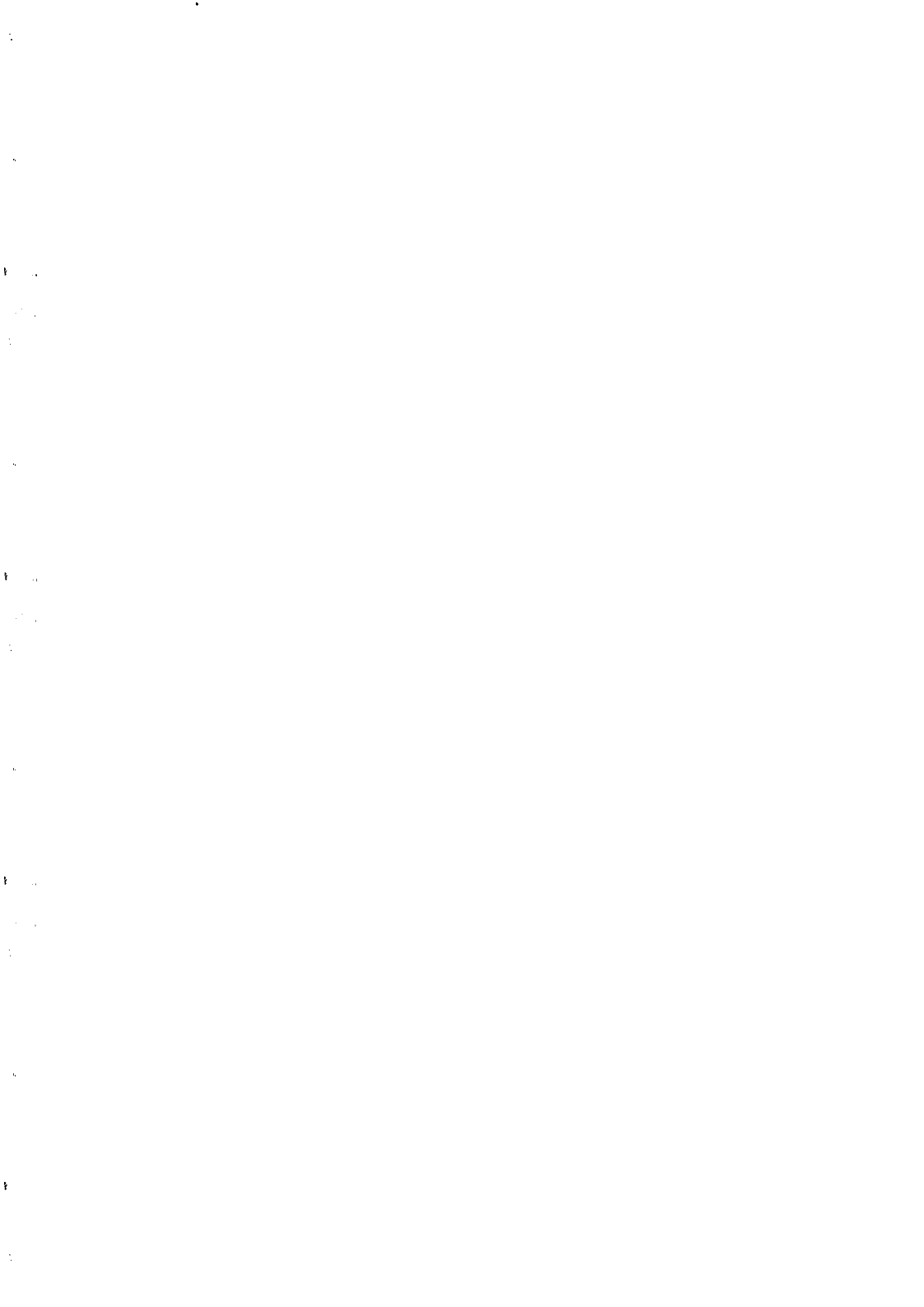
I gratefully acknowledge the collaboration of Y. Avishai, C.W.J. Beenakker, K. Muttalib and more particularly of R. Jalabert, with whom most of the results summarized in this review has been obtained. More details can be found in the references 4,5 and 7.

## References:

- 1) J.-L. Pichard, in *Quantum Coherence in Mesoscopic Systems*, (NATO ASI series, Plenum, New York), ed. by B. Kramer (1991).
- 2) A. D. Stone, P. A. Mello, K. Muttalib and J.-L. Pichard in *Mesoscopic Phenomena in Solids* (North-Holland, Amsterdam), ed. by B. L. Althshuler, P. A. Lee and R. A. Webb (1991).
- 3) M.-L. MEHTA, *Random Matrices* (Academic Press, New York) second edition (1991).
- 4) R. Jalabert, J.-L. Pichard and C.W.J. Beenakker, to appear in *Europhys. Lett.* .
- 5) Y. Avishai, J.-L. Pichard and K. Muttalib, *J. Phys. France*, **3**, 2343 (1993).
- 6) P. A. Mello and J.-L. Pichard, *J. Phys. France*, **bf 1**, 493 (1991).
- 7) R. A. Jalabert and J.-L. Pichard, Saclay preprint.
- 8) F. J. Dyson, *J. Math. Phys.*, **3**, 140 (1962).
- 9) K. Frahm. unpublished.
- 10) O. Bohigas, M.-J. Giannoni and C. Schmit, *Phys. Rev. Lett.*, **52**, 1 (1984).
- 11) M. V. Berry, *Proc. Roy. Soc. Lond. A*, **400**, 229, (1985).
- 12) R. Blumel and U. Smilansky, *Phys. Rev. Lett.*, **64**, 241, (1989).
- 13) C. W. J. Beenakker, *Phys. Rev.*, **bf B 47**, 15763, (1993).
- 14) H. U. Baranger and P. A. Mello, preprint.
- 15) C. W. J. Beenakker and B. Rejaei, *Phys. Rev. Lett.*, **71**, 3689, (1993).
- 16) R. A. Jalabert, J.-L. Pichard and C.W.J. Beenakker, *Europhys. Lett.*, **24**, 1, (1993).
- 17) O. N. Dorokhov, *J. E. T. P. Lett.* **36**, 259, (1982).
- 18) M. E. Gertsenshtein and V. B. Vasil'ev, *Theor. Probab. Appl.*, **4**, 391, (1959).
- 19) J.-L. Pichard, M. Sanquer, K. Slevin and P. Debray, *Phys. Rev. Lett.*, **65**, 1812, (1990).
- 20) K. Slevin, J.-L. Pichard and K. Muttalib, *J. Phys. France*, **3**, 1387, (1993).
- 21) I. V. Lerner, these proceedings.



**CHARGING EFFECTS AND RESONANT  
TUNNELLING IN QUANTUM DOTS  
OR NORMAL METAL ISLANDS**



LOW TEMPERATURE TRANSPORT THROUGH A QUANTUM DOT:  
FROM THE COULOMB BLOCKADE TO THE KONDO EFFECT

Yigal Meir

Department of Physics, University of California at Santa Barbara, CA 93106

Low temperature transport through a quantum dot is investigated theoretically. At relatively high temperatures the conductance exhibits periodic peaks as a function of an external gate voltage, due to Coulomb blockade of tunneling through the dot. It is shown that as the temperature is lowered there is a crossover from multi-level to single-level transport, leading to nonmonotonic temperature dependence and the possibility of experimental spectroscopy of the quantum dot. At even lower temperatures correlation effects such as the Kondo effect are shown to play a significant role in the transport through the dot.

I. INTRODUCTION

Since the first experimental realization of an artificially constructed semiconductor quantum dot, our theoretical understanding of the experiments have progressed significantly [1]. The key ingredient in the experimentally explored regime is the interplay between the Coulomb interactions and the discrete spectrum [2-4]. Taking that into account explains most experimental results.

A simple model which includes these effects is an Anderson-like model

$$\begin{aligned}
 H = & \sum_{n\sigma} \epsilon_{n\sigma} \mathbf{d}_{n\sigma}^\dagger \mathbf{d}_{n\sigma} + \frac{1}{2} \sum_{\substack{n,n' \\ \sigma,\sigma'}} U_{n\sigma,n'\sigma'} n_{n\sigma} n_{n'\sigma'} \\
 & + \sum_{\substack{k \in L,R \\ \sigma}} \epsilon_k \mathbf{c}_{k\sigma}^\dagger \mathbf{c}_{k\sigma} + \sum_{\substack{k \in L,R \\ n\sigma}} (V_{k\sigma} \mathbf{c}_{k\sigma}^\dagger \mathbf{d}_{n\sigma} + h.c.). \quad (1)
 \end{aligned}$$

The first two terms describe the isolated quantum dot. The first term describe the discrete spectrum, with states denoted by the quantum number  $n$  and spin  $\sigma$ , while the second term describes the interactions between electrons occupying these states. The third term describes the free electrons in the two leads, while the fourth term accounts for tunneling in and out of the quantum dot. While the interaction  $U$  may depend on the particular states the electrons occupy, a fact that must be taken into account in order to explain some experimental observations in the quantum Hall regime (see Van der Vaart's contribution in this volume), I am going to assume for simplicity a constant  $U$ . This simplified model does indeed capture much of the physics involved (see Fig. 1).

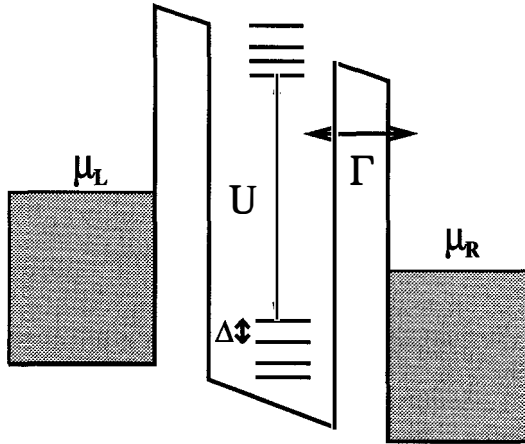


Fig.1: A schematic representation of the energy scales associated with the transport through a quantum dot

For a typical quantum dot [1]  $U \sim 1 - 5K$ , the typical level spacing  $\Delta \sim 0.2 - 0.5K$ , while the coupling to the leads  $\Gamma \equiv 2\pi V^2 \rho$ , where  $\rho$  is the density of states in the leads, can be of the order of  $100mK$ . These energy scales determine the different experimental temperature scales: (1)  $kT > U$ : the system behaves like a metal. (2)  $U > kT > \Delta$ : Coulomb blockade plays a significant role. The conductance through the quantum dot consists of isolated peaks, where each peak corresponds to tunneling via several levels.

(3)  $\Delta > kT > \Gamma$  : each isolated peak corresponds to tunneling through a single level. (4)  $\Gamma > kT$  : correlation effects such as the Kondo effect start to play an important role in the transport. In the following section I will briefly describe the physics underlying the “high-temperature regime”,  $kT > \Gamma$ , where the Coulomb blockade controls the transport. Then I will describe the expected signature of the Kondo effects in the measured current.

## II. THE COULOMB BLOCKADE

The conductance through a quantum dot exhibits spectacularly well separated and periodic peaks as a function of an external gate voltage,  $V_G$ . This effect can be attributed [5] to the Coulomb blockade: in order to add another electron into the quantum dot, one has to supply enough energy to compensate for the repulsion from all the other electrons. In the constant  $U$  model, the ground-state energy of  $N$  electrons on the quantum dot is given by

$$E_g(N) = \frac{N(N-1)}{2}U + \sum_{n\sigma} \epsilon_{n\sigma} - NeV_G, \quad (2)$$

where the sum is over the lowest  $N$  energies. Since transport occurs when the number of electrons can fluctuate between  $N$  and  $N+1$ , then  $V_G$  has to be adjusted so that  $E_g(N) = E_g(N+1)$ , or  $eV_G = NU + \epsilon_{N+1}$ . If  $U \gg \Delta$ , the peaks will look periodic in gate voltage.

One of the big puzzles in the original experiment [6] was the nonmonotonic temperature dependence of the peak amplitudes. This was later explained [3] in terms of a temperature crossover from the the single-level tunneling regime ( $\Delta > kT$ ) to the multilevel tunneling regime ( $kT > \Delta$ ). In the first regime, each conductance peak corresponds to tunneling via a single level — when the chemical potential aligns with one of the energy levels, resonant tunneling takes place and there is a peak in the conductance; once the chemical potential is larger than the energy of that level, this level is filled, and no other level can participate in the transport. As temperature increases all the levels within  $kT$  of the chemical potential start to contribute to the transport because of the width of the Fermi-Dirac distribution. Still, only a single electron can tunnel at a time, so the peak amplitude will depend on a weighted average of the couplings of these levels to the leads. Thus depending whether the levels which start to participate in the transport are more strongly coupled to the leads or more weakly coupled than the single level that contributed in the

low temperature regime, the peak amplitude may increase or decrease. As the temperature increases, more and more levels participate in the transport. As higher gate voltage corresponds to transport via higher-energy states, and levels with energies closer to the top of the barrier will be, on average, more strongly coupled to the leads than in the high-temperature ( $kT \gg \Gamma$ ) regime the peak amplitudes should monotonically increase with gate voltage, as is indeed observed experimentally.

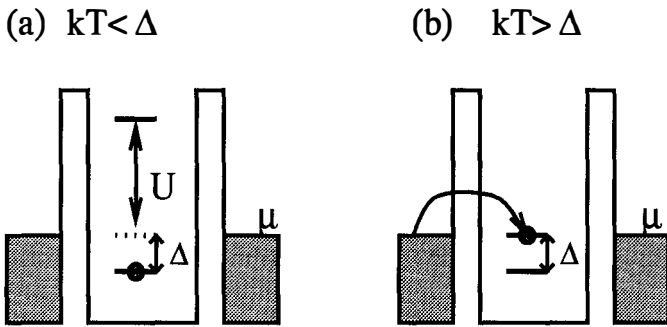


Fig.2: The two temperature regimes discussed in the text. In (a) temperature is smaller than the level spacing, so when the chemical potential aligns with the second level, the first level is full, and the chemical potential has to be increased by another  $U$  to add an electron to the quantum dot. In (b) temperature is larger than the level spacing, so the lower level might not be occupied and an electron can tunnel through the second level. In this regime every peak in the conductance corresponds to tunneling through several levels.

The fact that for  $kT < \Delta$  each peak corresponds to transport through a single level suggests that by studying the characteristics of a single peak, one may obtain information about that specific level. Indeed this idea was implemented by McEuen et al. [7], who have studied the dependence of the peak position and its amplitude on magnetic field. The data shows that in the quantum Hall regime the amplitudes of the peaks depend sensitively on whether the chemical potential aligns with a lower Landau level state or a higher one, or through the lower spin state or the higher one, as expected. Moreover, the peak position also oscillates as a function of magnetic field as one expects from the depopulation of the spin-resolved Landau levels.

This experiment suggests, however, that the amplitude of these oscillations are larger than expected from a constant  $U$  model, and one has to take a more sophisticated account of the interactions [10]. Additional information about the excitation spectrum of the quantum dot can be obtained via nonlinear I-V measurements, as one expects a signature in the current every time the chemical potential crosses one of the quantum dot levels [8,9].

### III. THE KONDO EFFECT

Since the Anderson model seems to describe very well the transport through a quantum dot, it was pointed out [11,12] that the Kondo effect may play a significant role in the low-temperature transport through the dot. For the case of symmetric barriers, the current can be directly related to the local density of states,  $\rho_{loc}(\epsilon)$  [13],

$$J = \frac{e}{\hbar} \sum_{\sigma} \int d\epsilon [f_L(\epsilon) - f_R(\epsilon)] \Gamma(\epsilon) \rho_{loc}(\epsilon), \quad (3)$$

where  $f_L(\epsilon)$  [ $f_R(\epsilon)$ ] is the Fermi distribution in the left (right) lead. Consider a single degenerate level ( $\epsilon_0 \equiv \epsilon_{0\sigma}$ ). Since the Kondo effect leads to an enhanced density of states at the Fermi energy, this will lead to an enhanced conductance for all  $\epsilon_0 \leq \mu \leq \epsilon_0 + U$ . Using the Friedel sum rule, these authors argued that the periodic peak structure will become a set of plateaus at zero temperature (see Fig. 3). At finite temperatures, it was argued, the plateaus will become peaks with asymmetric line shape.

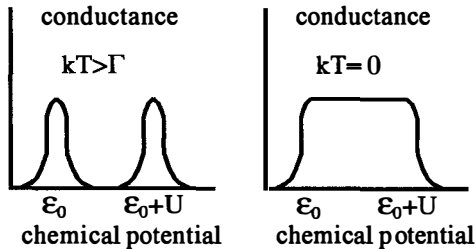


Fig.3: The high-temperature ( $kT > \Gamma$ ) conductance (a) vs. the zero temperature conductance (b). The enhanced density of states at the Fermi energy gives rise to an enhanced conductance at zero temperature for all  $\epsilon_0 < \mu < \epsilon_0 + U$ .

Recently, we [14,15] have carried out a quantitative calculation of the density of state and the current at low temperatures,  $kT < \Gamma$ , using the non-crossing approximation [16] and the equation-of-motion method [17,3]. Fig. 4 displays the conductance through a quantum dot at relatively low temperatures, down to  $kT = \Gamma/200$ . It is quite clear that the peak remains symmetric at these temperature. There is, nevertheless, an enhancement of the peak width and a shift in the peak position at low temperatures (Fig. 5), in contrast to the behavior in the absence of interactions (broken curves). However, in order to definitely resolve that behavior one has to go to temperatures of  $kT \sim \Gamma/40$ , a rather difficult experimental

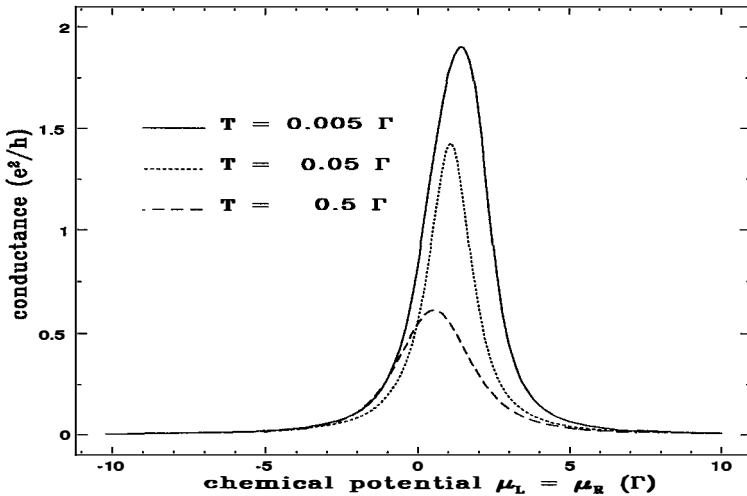


Fig.4: Linear-response conductance through an Anderson impurity for three different temperatures as a function of chemical potential. The impurity has two degenerate spin states at  $\epsilon_0 = 0$ . The conductance peak first narrows then broadens with decreasing temperature.

The quantum dot present a unique opportunity to study the Kondo effect out of equilibrium, as the two leads may be maintained at different chemical potentials. This is a situation which is not readily achieved in the usual systems that exhibit the Kondo effect — magnetic impurities in metals. Thus new theoretical questions arise concerning the nature of the Kondo effect out of equilibrium. In fact the calculation suggests that in nonequilibrium the signature of the Kondo effect in the transport is more easily traceable than

the linear response measurements. The reason is that in linear response one only probes the density of states at the Fermi energy, and as the Kondo peak is always exactly at the Fermi energy, one may obtain information only on the maximal value of the density of states at the peak. On the other hand, by having two different chemical potential, one can probe peak(s) associated with one chemical potential by sweeping the other chemical potential.

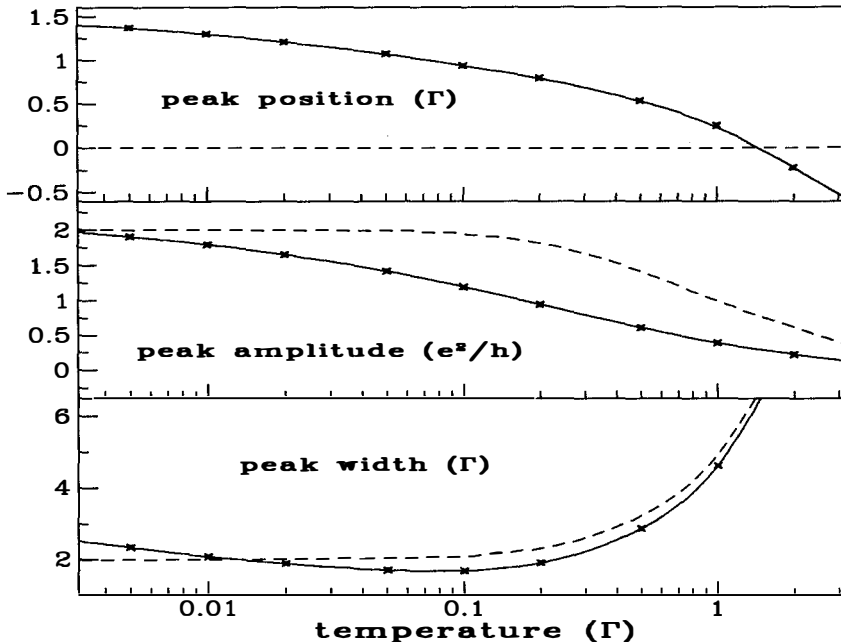


Fig.5: (a) Temperature dependence of linear-response conductance peak position. (b) Temperature dependence of conductance peak amplitude. (c) Temperature dependence of conductance peak full-width at half maximum. In all three panels, the non-crossing approximation results are the data points and the solid curve is a guide to the eye. For comparison, the dashed curves are the exact results for non-interacting levels.

The density of states in equilibrium and in the presence of a finite bias ( $\mu_L \neq \mu_R$ ) and in the presence of a magnetic field ( $\epsilon_{0\uparrow} \neq \epsilon_{0\downarrow}$ ) is depicted in Fig. 6. The sharp peak at the Fermi energy in equilibrium is split upon application of a bias and is suppressed due to dissipative processes where an electron is transferred from the high chemical potential lead to the lower

chemical potential one. A magnetic field shifts the peaks away from the chemical potential by the Zeeman splitting, and suppress them even further.

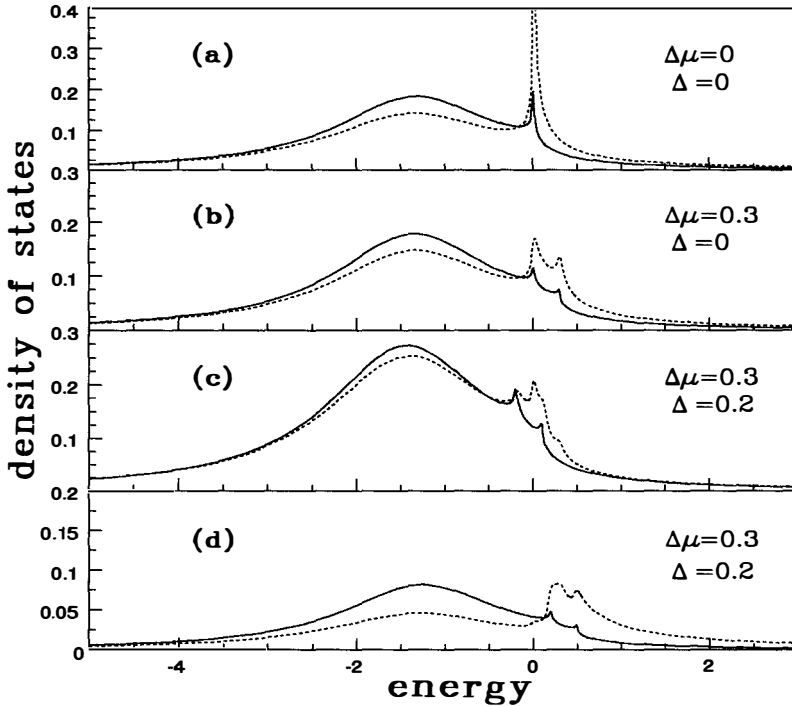


Fig.6: Density of states for an Anderson impurity symmetrically coupled to two leads with chemical potentials  $\mu_L$  and  $\mu_R (= 0)$  and Lorentzian bandwidth  $2W$ , from the equation-of-motion method (continuous line) and the non-crossing approximation (dashed line). The impurity has two spin states with energies  $\epsilon_{0\uparrow}$  and  $\epsilon_{0\downarrow}$  and an on-site interaction  $U \rightarrow \infty$ . All energies are in units of the total coupling to the leads,  $\Gamma$ . The band width is  $W = 100$  and the temperature is  $T = 0.005$ . (a) The equilibrium ( $\mu_L = 0$ ) density of states at zero magnetic field  $\epsilon_{0\uparrow} = \epsilon_{0\downarrow} = -2.0$ , exhibiting a single peak at the Fermi level. (b) The non-equilibrium ( $\mu_L = 0.3$ ) density of states at zero magnetic field  $\epsilon_{0\uparrow} = \epsilon_{0\downarrow} = -2.0$ , with a suppressed Kondo peak at each chemical potential. (c),(d) The non-equilibrium ( $\mu_L = 0.3$ ) density of states for spin up (c) and spin down (d) at finite magnetic field  $\epsilon_{0\uparrow} = -1.9, \epsilon_{0\downarrow} = -2.1$ . The Kondo peaks shift away from the chemical potentials by the Zeeman splitting  $\Delta\epsilon = 0.2$ ; the shift is up in energy for the up spin and down in energy for the down spin.

The implications of these results on the transport are quite striking. In zero magnetic field the differential conductance will exhibit a peak at zero bias – zero-bias anomaly [18] – due to the enhanced density of states at the chemical potential (Fig. 7). At a finite magnetic field, the peaks in the density of states are shifted away from the chemical potentials, so they will only contribute to the current once the bias,  $\Delta\mu$ , is larger than the Zeeman splitting,  $\Delta$  (Fig. 8). Thus we predict that the differential conductance will exhibit two peaks as a function of the bias, for  $\Delta\mu = \pm\Delta$ .

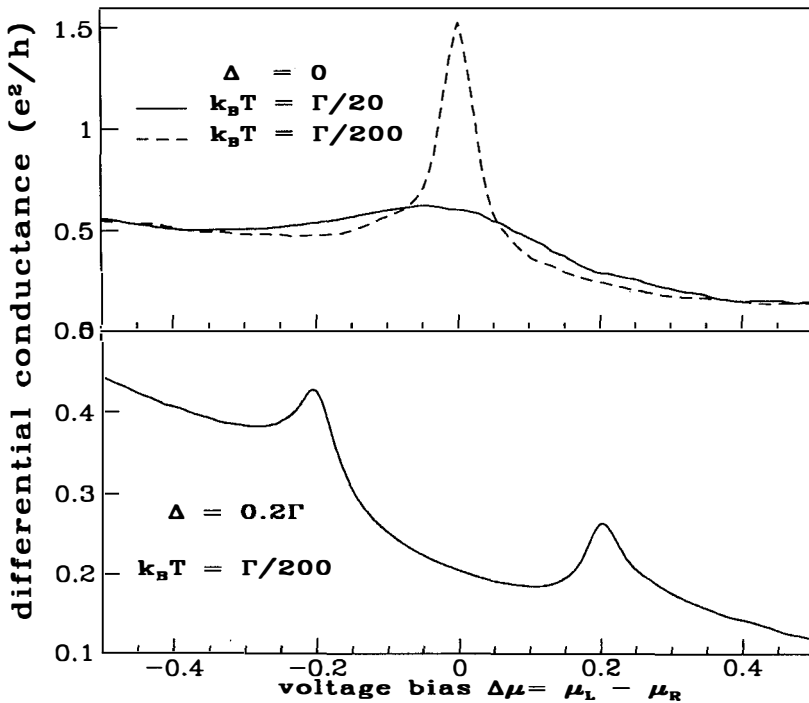


Fig.7: Differential conductance,  $e dJ/d\Delta\mu$ , with  $\mu_R = 0$ , vs. applied bias. (a) Zero magnetic field differential conductance via the non-crossing approximation. (b) Differential conductance at the finite magnetic field,  $\Delta = 0.2$ , used in Figs. 1 (c) and (d), via equations of motion. When the chemical potential difference,  $\Delta\mu$ , reaches the Zeeman splitting,  $\Delta$ , the Kondo peaks in the density of states enter the region between the chemical potentials, giving rise to a peak in the differential conductance.

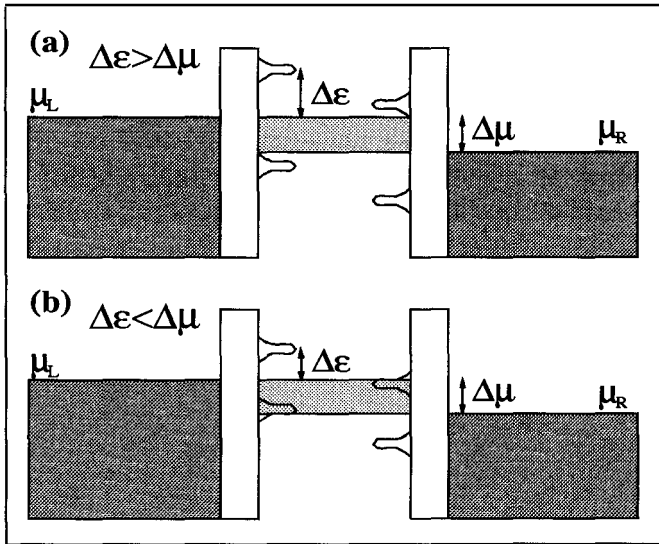


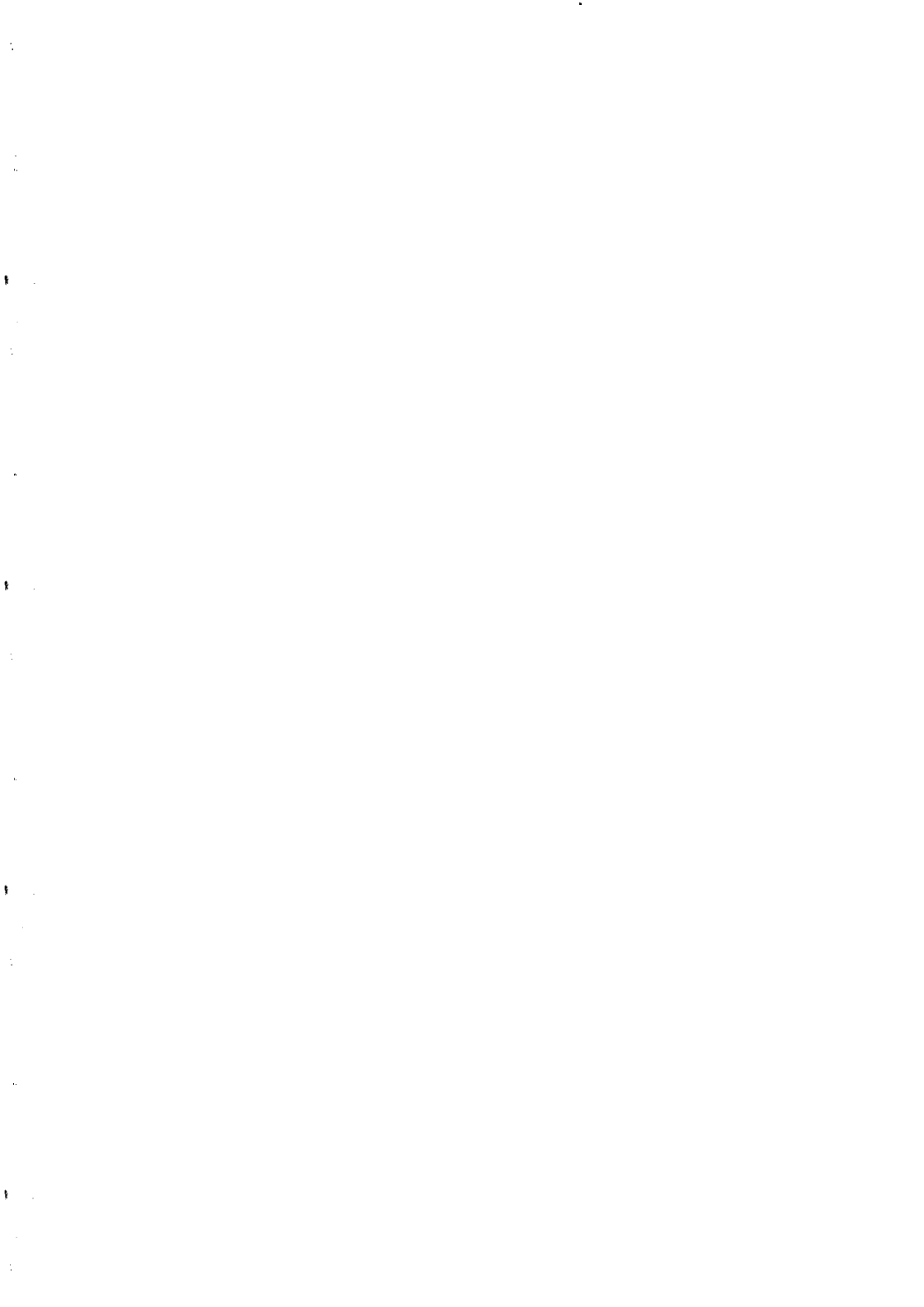
Fig. 8: Schematic picture of the Kondo peaks in the density of states at finite magnetic field. When the chemical potential difference,  $\Delta\mu$ , reaches the Zeeman splitting,  $\Delta$ , the Kondo peaks in the density of states enter the region between the chemical potentials, giving rise to a peak in the differential conductance (see Fig. 7).

To date, no experiment on quantum dots has revealed any signature of the Kondo effect. Interestingly, though, a recent experiment by Ralph and Buhrman [19], where the current through a point contact has shown behavior typical of tunneling through a single magnetic impurity, which might reside in the barrier near the point contact. The results of this experiment, in particular the splitting of the peak in the differential conductance by a magnetic field, are consistent with the calculations presented in this work.

*Acknowledgments:* This work has been carried out in collaboration with Ned S. Wingreen and Patrick A. Lee. Work at U.C.S.B. was supported by NSF Grant No. NSF-DMR-9308011, by the NSF Science and Technology Center for Quantized Electronic Structures, Grant No. DMR 91-20007, and by NSF, ONR, and ARO at the Center for Free Electron Laser Studies.

## REFERENCES

- [1] For a review see M. A. Kastner, *Physics Today*, January 1993, p.24.
- [2] D. V. Averin and A. N. Korotkov, *Zh. Eksp. Teor. Fiz.* **97**, 927 (1990) [*Sov. Phys. JETP* **70**, 937 (1990) ].
- [3] Y. Meir, N. S. Wingreen, and P. A. Lee, *Phys. Rev. Lett.* **66**, 3048 (1991).
- [4] C. W. J. Beenakker, *Phys. Rev. B* **44**, 1646 (1991).
- [5] H. van Houten and C. W. J. Beenakker, *Phys. Rev. Lett.* **63**, 1893 (1989).
- [6] U. Meirav, M. Kastner, and S. J. Wind, *Phys. Rev. Lett.* **65**, 771 (1990).
- [7] P. L. McEuen, E. B. Foxman, U. Meirav, M. A. Kastner, Y. Meir, N. S. Wingreen, and S. J. Wind, *Phys. Rev. Lett.* **66**, 1926 (1991).
- [8] A. T. Johnson, L. P. Kouwenhoven, W. de Jong, N. C. van der Vaart, C. J. P. M. Harmans, and C. T. Foxon, *Phys. Rev. Lett.* **69**, 1592 (1992).
- [9] E. B. Foxman, P. L. McEuen, U. Meirav, N. S. Wingreen, Y. Meir, P. A. Belk, N. R. Belk, M. A. Kastner, and S. J. Wind, *Phys. Rev. B* **47**, 10020 (1993).
- [10] P. L. McEuen, E. B. Foxman, J. Kinaret, U. Meirav, M. A. Kastner, N. S. Wingreen, and S. J. Wind, *Phys. Rev. B* **45**, 11419 (1992).
- [11] L. I. Glazman and M. E. Raikh, *JETP lett.* **47**, 452 (1988).
- [12] T. K. Ng and P. A. Lee, *Phys. Rev. Lett.* **61**, 1768 (1988).
- [13] Y. Meir and N. S. Wingreen, *Phys. Rev. Lett.* **68**, 2512 (1992).
- [14] Y. Meir, N. S. Wingreen, and P. A. Lee, *Phys. Rev. Lett.* **70**, 2601 (1993).
- [15] N. S. Wingreen and Y. Meir, *Phys. Rev. B*, in press.
- [16] N. E. Bickers, *Rev. Mod. Phys.* **59**, 845 (1987).
- [17] C. Lacroix, *J. Phys. F* **11**, 2389 (1981).
- [18] S. Hershfield, J. H. Davies, and J.W. Wilkins, *Phys. Rev. Lett.* **67**, 3720 (1991); *Phys. Rev. B* **46**, 7046 (1992).
- [19] D. C. Ralph and R. A. Buhrman, unpublished.



## A FERMI-EDGE SINGULARITY PROBED BY RESONANT TUNNELLING SPECTROSCOPY

N. La Scala Jr., A. K. Geim, P. C. Main, T. J. Foster, P. H. Beton,  
J. W. Sakai, F. W. Sheard, N. Mori and L. Eaves  
Department of Physics, University of Nottingham, Nottingham NG7 2RD,  
England

A Fermi-edge singularity is observed in the tunnelling current between a two-dimensional electron gas (2DEG) and a zero-dimensional localized state. The effect is observed in a double barrier resonant tunnelling structure in which there is a low but significant density of shallow donor impurities in the quantum well. A sharp peak in the tunnel current is observed when the energy of the localized state matches the Fermi energy of the 2DEG. The peak grows and becomes sharper as the temperature is decreased to 70 mK. We attribute the singularity to the Coulomb interaction between the tunnelling electron on the localized site and the Fermi sea of the 2DEG. The localised state occurs at an energy significantly below that expected for an isolated donor in the quantum well and is attributed to a closely spaced donor pair.

PACS: 73.40.Gk, 71.45.Gm, 71.35.+z, 73.20.Dx.

## 1. Introduction

The Coulomb interaction between conduction electrons leads to various anomalies in the properties of a metal which involve the energy spectrum near the Fermi energy ( $\varepsilon_F$ )<sup>1</sup>). The X-ray spectra of metals shows a Fermi-edge singularity (FES) which has become known as the Mahan exciton or Mahan-Nozières-Dominicis (MND) singularity<sup>2</sup>). In the case of X-ray emission, an electron in the Fermi sea recombines with an inner shell "core" hole. Conservation of momentum is maintained in the recombination process because of the momentum spread of the strongly localised hole. This enables electrons at the Fermi energy (with wavevector  $k_F \sim 10^8 \text{ cm}^{-1}$ ) to recombine.

Recently, there has been much interest in a similar anomaly seen at low temperatures in the optical spectra of doped semiconductor quantum wells, in which one of the carriers (usually a photo-excited hole) is localised by disorder<sup>3</sup>). The tunnel current in such a system may also be influenced by electron-electron interactions and a number of mechanisms have been proposed which could lead to singularities at  $\varepsilon_F$ . In disordered metals electron-electron interactions cause the well-known singularity in the single-particle density of states which has been observed as a zero-bias anomaly in the tunnelling conductance between high-resistivity metals (for refs., see [4]). In the last few years it has been suggested that tunnelling through a quantum dot may emerge as a new tool for studying electron-electron interactions. Fermi-edge singularities have been predicted due to either on-site Coulomb repulsion of electrons with different spins (Kondo resonance)<sup>5,6</sup>) or the interaction between a tunnelling electron and the Fermi sea in the contacts<sup>7</sup>). Although a large number of effects due to single electron transport and Coulomb blockade phenomena have been seen in metallic and semiconducting submicron tunnelling devices<sup>8</sup>), no evidence for a Fermi-edge singularity has been reported to date.

In this paper we report the observation of a Fermi-edge singularity in resonant

tunnelling between a two-dimensional electron gas (2DEG) and a strongly localised zero-dimensional (0D) state. The electron-electron interaction leads to a remarkable enhancement of the tunnel current. To investigate the 0D-2D tunnelling process we have employed our recent observation that the onset of the tunnel current at low bias voltages in mesoscopic and also conventional, macroscopic resonant tunnelling devices (RTD) is determined by tunnelling through random impurity-related states in the quantum well<sup>9</sup>). These states occur at energies well below that of the edge of the continuum of two-dimensional bound states of the quantum well formed by the two tunnel barriers. The 2DEG is created in the negatively biased emitter accumulation layer which forms adjacent to one of the tunnel barriers when the device is biased. The number of impurity channels may be successfully controlled by intentional doping and by careful design of the RTD layers<sup>9,10</sup>). Our technique is an alternative to the nanofabrication of quantum dots<sup>8</sup>) and provides much more strongly confined 0D states.

## 2. Details of the device

The double barrier RTDs were grown by molecular beam epitaxy on  $n^+$ GaAs substrates with substrate temperatures between 480°C and 550°C to inhibit donor segregation from the doped contact regions into the active region of the device<sup>11</sup>). The thickness of both  $(\text{Al}_{0.4}\text{Ga}_{0.6})\text{As}$  barriers is 5.7 nm, the quantum well width is 9 nm and there is a 20 nm undoped spacer layer between each barrier and the doped contact regions. Figure 1 shows a schematic energy band diagram for our devices under bias. Tunnelling occurs from the 2DEG, formed in an accumulation layer near the left-hand emitter-barrier, into the electron states in the well. We also grew samples in which the centre plane of the quantum well was  $\delta$ -doped with Si donors at concentrations between 2 and  $8 \times 10^{13}\text{m}^{-2}$ . At these sheet densities the donors have an average separation of at least 100 nm and most, though not all, are essentially non-interacting. Square mesas of side lengths varying from 6  $\mu\text{m}$  to 100  $\mu\text{m}$  were fabricated using photolithography and dry or wet etching.

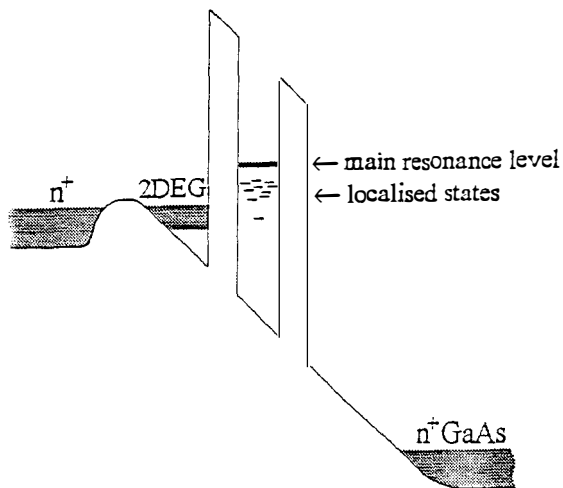


**Figure 1** Schematic diagram of the conduction-band profile of our devices under bias. Tunnelling occurs from a two-dimensional electron gas through the ground state in the quantum well (for the main resonance) or highly localised impurity levels at lower energies.

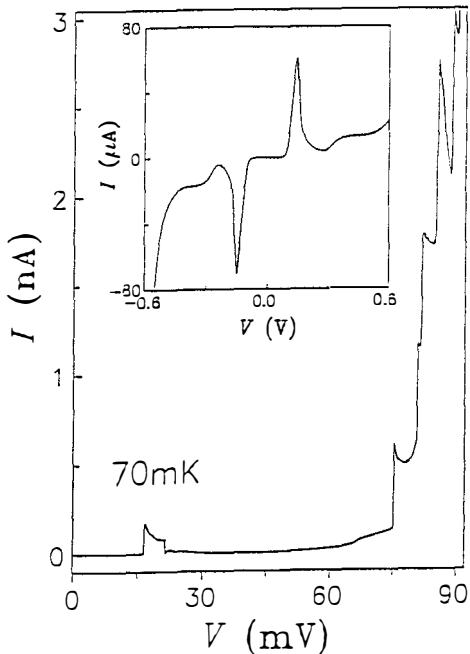


**Figure 2**  $I(V)$  characteristic at 70 mK and at low bias for a device 12  $\mu$ m across. The inset shows the main resonance.

### 3. Experiments and discussion

A current-voltage characteristic  $I(V)$  for a  $12 \mu\text{m}$  square device is shown in Figure 2. This device has no intentional doping in the quantum well. A current flows when the energy of an electron in the emitter 2DEG is resonant with a state in the quantum well<sup>12)</sup>. The inset shows the main resonance due to the lowest 2D subband in the quantum well. This resonance has a large peak-to-valley ratio indicating the high quality of our structures. At biases below the main resonance near the onset of the tunnel current we have found additional steplike structure which is shown also in Figure 2 ( $V > 70\text{mV}$ ) for this undoped sample. Similar structure is seen in all devices, although details are unique to a particular device, characteristic of a mesoscopic system. Similar features occur in both directions of the applied bias but their exact form is different. For the  $\delta$ -doped samples the additional features are more numerous and extend to lower values of applied bias. In many, but not all, of the devices with undoped quantum wells isolated peaks occur such as that shown in Figure 2 for  $V \cong 20\text{mV}$ . We consider the additional features to be due to tunnelling through localised 0D states in the quantum well of the RTD with energies well below the edge of the lowest 2D subband, as shown schematically in Fig. 1<sup>9,10,13)</sup>. The localised state giving rise to structure at  $20 \text{ mV}$  is at an energy well below the expected binding energy of an isolated donor in the quantum well ( $\sim 12 \text{ meV}$  for a donor in the centre of a  $9 \text{ nm}$  quantum well<sup>10,14)</sup>). A more tightly bound localised state of this kind can arise from a closely-spaced donor pair, which is statistically likely in a mesa of this size, due to the presence of the unintentional donor doping background. Naturally, the population of such pairs increases enormously in intentionally  $\delta$ -doped quantum wells. Assuming a background volume doping density in the quantum well of around  $10^{21} \text{ m}^{-3}$ , the sheet density in the well would be  $n = 10^{13} \text{ m}^{-2}$ , corresponding to an average separation of  $0.3 \mu\text{m}$ . At this separation donors can be regarded as isolated. However, a pair with separation  $d \cong 1/\sqrt{n}$  can be expected for a mesa area  $S$ . Hence for a device with  $S = 12 \mu\text{m}$  square, it is statistically probable to find a donor pair with separation around  $100 \text{ \AA}$ .

This is comparable with the donor Bohr radius ( $a_{2D} = 7$  nm for an ideal 2D donor in GaAs) and hence such a pair would have a binding energy larger than that of an isolated donor.

To illustrate this point further, Figure 3 plots the probability of finding a donor pair at separation  $r$  or less for a  $7 \mu\text{m}$  square mesa at different sheet doping densities in the well. Figure 4 plots the results of a variational calculation, based on effective mass theory, of the binding energy of a donor pair (separation  $d$ ) and a triangular arrangement of donors (triangle side =  $d$ ). Note that in both cases, there is a significant increase in binding energy when  $d < 2a_{2D}$ . Thus, the presence of the deep localised states in our structures can be *naturally* explained by the cluster model.

Two examples of the step structure in  $I(V)$  characteristics are plotted in Figure 5 for several temperatures. In Figure 5(a) we show in more detail the isolated peak of Figure 2 and Figure 5(b) is the current onset for a  $\delta$ -doped RTD with  $2 \times 10^{13}\text{m}^{-2}$  Si donors in the quantum well. The unexpected feature in the observed  $I(V)$  dependences is the singular enhancement of tunnelling near the threshold, when the localised state is resonant with the emitter Fermi energy (see Figure 5). Note that every current step in Fig. 2 is accompanied by such an enhancement. The characteristic width of the peaks at threshold biases can be as small as  $0.2\text{mV}$  at the lowest temperature (e.g. see the marked feature in Fig. 5(b)). The low voltage edge of each step is thermally activated down to  $70$  mK indicating that the 2DEG remains in thermal equilibrium with the main heat bath. In general, as in Figure 5(b), there is some additional oscillatory structure within the step at voltages above the threshold voltage  $V_{th}$ . However, in contrast to the singularity this structure does not depend on temperature. The Fermi-edge singularity is seen in *all* devices at temperatures below  $1$  K.

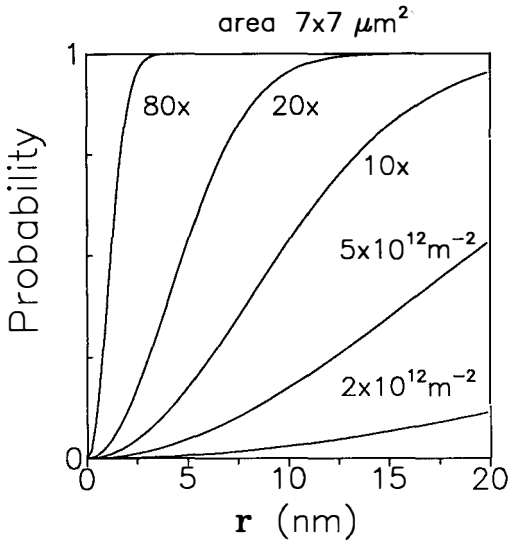


**Figure 3** Probability of finding, for different well sheet densities, a pair of donors with separation of  $r$  or less in a  $7 \mu\text{m}$  square mesa.

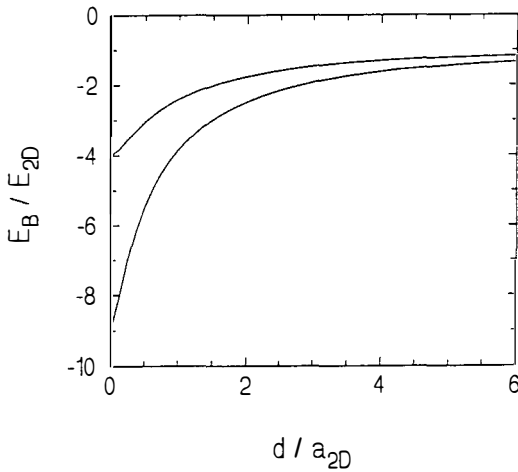


**Figure 4** Upper curve: binding energy as a function of donor separation  $d$ , of an electron on a shallow donor pair. Lower curve: binding energy for three donors arranged as an isosceles triangle of side-length  $d$ .

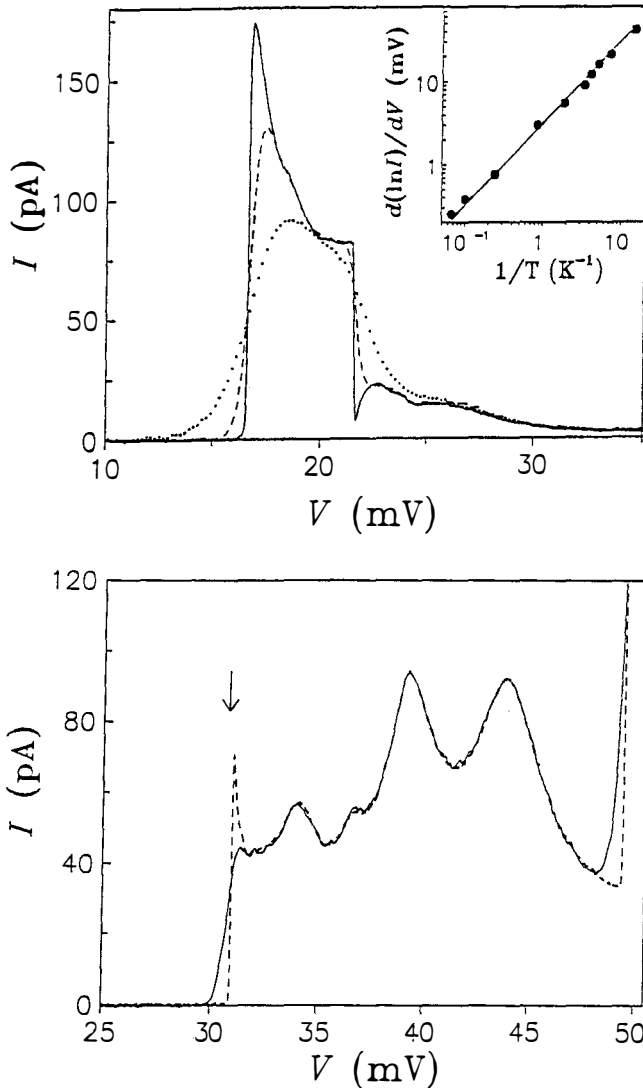


**Figure 5** Detailed  $I(V)$  characteristics at low biases when the first localised level is resonant with the emitter 2DEG. (a) (top) - the same device as in Fig. 2 at three different temperatures of 70 mK (solid line), 1.3 K (dashed line) and 5 K (dots). Inset - temperature dependence of the logarithmic slope of the tunnel current near the threshold voltage. (b) (below) - another device 6  $\mu\text{m}$  across at 70 mK (dashed line) and 1.2 K (solid line).

The general behaviour of the tunnel current, i.e. without the singularity, can be understood as follows. Under a typical applied bias of tens of mV, the collector barrier is lower than the emitter barrier. Also the 3D density of states in the collector available to the electron tunnelling from the localised state is larger than the equivalent density of states in the emitter 2DEG. Consequently, the current is limited by tunnelling through the emitter barrier and the states in the quantum well are empty most of the time. We estimate the escape rate  $\tau_c^{-1}$  from the impurity into the collector contact to be considerably larger than the tunnelling rate  $\tau_e^{-1}$  from the 2DEG into the impurity-related site. The latter rate can be found from a value of the single electron current through an impurity<sup>7-9,13</sup>,  $I \cong 100\text{pA}$ , yielding  $\tau_e = e/I \cong 2\text{ns}$ . This is consistent with the barrier height and thickness. As the bias increases, the impurity level moves downwards relative to the energy of the emitter 2DEG (see Fig. 1) and the tunnel current exhibits a step increase when the localised state coincides with the highest filled state, i.e. the Fermi level of the 2DEG. As the voltage is increased further and the energy of the 0D state becomes lower than the lowest energy state of the emitter, no states are available for resonant tunnelling and the current falls sharply (see Fig. 5(a)). However, this sharp fall-off is not common to all devices. In Figure 5(b) a second impurity channel comes into resonance with the 2DEG (at  $V \cong 50\text{mV}$ ) before the first channel has passed away. The latter behaviour is also seen above 75mV in Fig. 2.

For quantitative analysis, we discuss first the behaviour expected for impurity-assisted tunnelling of non-interacting electrons. The tunnel current is given by<sup>11)</sup>

$$I = \frac{e}{\hbar} \Gamma(\varepsilon_i) \theta(\varepsilon_i) f(\varepsilon_i) \quad (1)$$

where  $f(\varepsilon) = \{1 + \exp[(\varepsilon - \varepsilon_F)/k_B T]\}^{-1}$  is the Fermi-distribution function,  $\theta(\varepsilon)$  is the unit step-function and  $\varepsilon_i$  is the energy of the impurity state measured from the bottom of the 2DEG subband. For the case of tunnelling from a 2DEG, the tunnelling coefficient  $\Gamma$  can be written as<sup>15)</sup>

$$f(\varepsilon_i) = t \exp(-\varepsilon_i / \varepsilon_0) \quad (2)$$

where  $\varepsilon_0$  is the binding energy of the localised state and  $t$  is a coefficient which includes parameters of the localised state and the tunnel barrier but is independent of the kinetic energy  $\varepsilon_i$  of tunnelling electrons within a 2DEG subband. Near the onset of the tunnel current, Eq.(1) varies as the Fermi function which fits very well the observed  $I(V)$  characteristics and their temperature dependence. This allows us to convert the voltage across the device into the energy difference between the impurity state and  $\varepsilon_F$ . We use  $\varepsilon_F - \varepsilon_i = \alpha e(V - V_{th})$  where the constant  $\alpha$  is characteristic of the distribution of electrostatic potential across the device<sup>12)</sup>. Experimental curves yield  $\alpha = 0.25 \pm 0.05$  for all devices. The inset in Figure 5(a) shows an example of temperature dependence of the tunnel current below the threshold at biases when  $I \propto f(\varepsilon_i) \cong \exp[(\varepsilon_F - \varepsilon_i)/k_B T]$  and one can write  $d \ln(I)/dV \cong \alpha/k_B T$ . The linear dependence of the logarithmic slope down to the lowest temperature of 70 mK indicates that the localised state has a very narrow linewidth. This is in agreement with the linewidth  $\Gamma_e = \hbar/\tau_e \cong 4$  mK estimated from the tunnelling time. We note that the sharp fall of the current which is seen at  $V \cong 22$  mV in Fig. 5(a) is not a common feature for the isolated peaks and, usually, the decrease is much smoother.

Equation 2 shows that, for non-interacting electrons, the tunnel current within the step varies on the energy scale of the binding energy  $\varepsilon_0 \geq 13$  meV<sup>10)</sup>. On the other hand, typical values of the Fermi energy in the emitter accumulation layer for the first few steps in the  $I-V$  characteristics are between 1 - 4 meV in our experiment, corresponding to 4 - 20 mV in bias. Therefore, according to Eqs.(1) and (2), variation of the current within the step has to be small. The dashed line in Figure 6 shows the  $I(V)$  characteristic for non-interacting electrons, calculated using Eqs.(1) and (2) for the sample in Fig. 5(a). The binding and Fermi energies were estimated using the value of  $\alpha \cong 0.2$  for this sample, found by fitting the temperature dependence of the current onset. From Fig. 6 we conclude that the observed

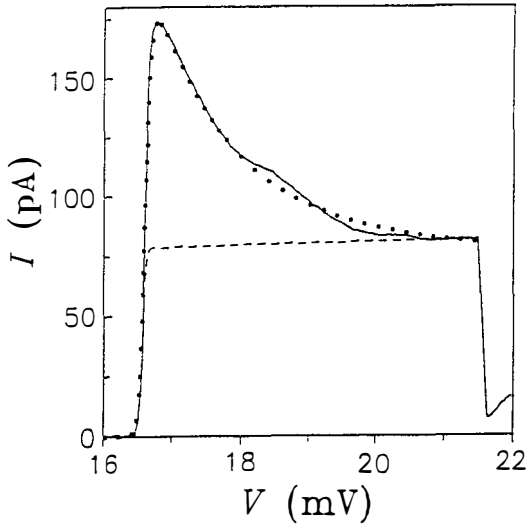


**Figure 6** Comparison of the observed singularity with theory. The solid line is the experimental curve at 70 mK for the same device as in Figures 2 and 5(a). The dotted curve is the behaviour expected from the theory of Matveev and Larkin<sup>7)</sup>. The dashed curve: if the electron-electron interaction is neglected, the tunnel current within the step exhibits only a very small increase with increasing bias.

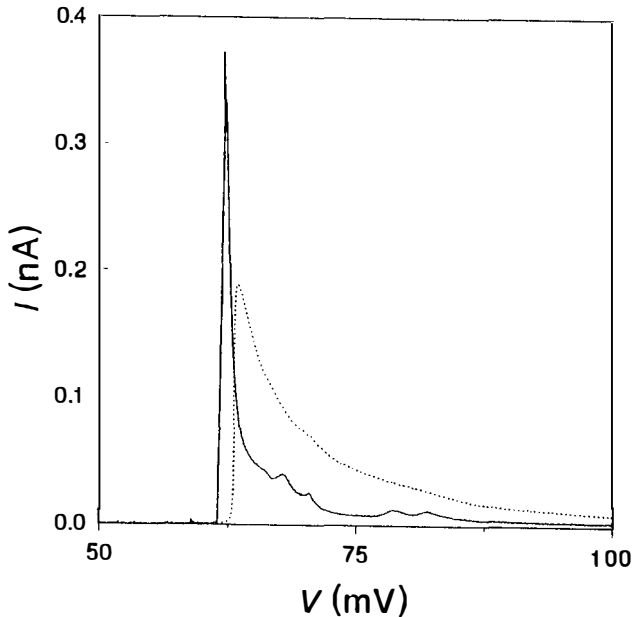


**Figure 7**  $I(V)$  curve at 0.3 K (dotted line is reverse bias) for a  $7 \mu\text{m}$  square diode.

singularity in the tunnel current cannot be explained within a model involving only non-interacting electrons. Therefore, we attribute the FES to the influence of the electron-electron interaction.

Three models leading to a FES for the case of impurity assisted tunnelling have been considered recently. First, the interaction between conduction electrons in the emitter 2DEG yields a logarithmic singularity in the tunnelling density of states<sup>4</sup>). Secondly, repulsion between electrons with the opposite spins on the impurity site may give rise to a Kondo resonance<sup>5,6</sup>). Finally, the interaction between an electron on the impurity site and the Fermi sea in the emitter contact may cause the MND singularity<sup>7</sup>). The first effect is important if the electron mean free path is short,  $l \sim \lambda_F$ , but is expected to be negligibly small for our 2DEG at the emitter interface. In addition, we would expect a negative contribution to the tunnel current near  $\epsilon_F$  rather than the increase which is observed<sup>4</sup>). The Kondo resonance also leads to  $I(V)$  qualitatively different from that observed (see Ref. 6 for the corresponding  $I(V)$  characteristics). The FES in our experiments is very similar to the behaviour predicted by Matveev and Larkin (ML)<sup>7</sup>). The singularity originates from extra tunnelling processes due to the Coulomb interaction between the fluctuating charge on the localised site and the Fermi sea in the contacts. The interaction allows an electron to violate the requirement of energy conservation between its initial and final states in the tunnel process. In addition to the direct tunnelling, the electron can tunnel into the localised site from an initial state which does not participate in tunnelling in a model of non-interacting particles. The difference in the energies is transferred to or from the Fermi sea. A singularity arises at  $\epsilon_F$  because scattering processes with small energy transfer are most effective (Fermi's golden rule) while the Pauli principle allows them only near the Fermi energy. The ML theory is basically analogous to the Mahan problem which considers the interaction between the Fermi sea and a positively charged virtual hole. The calculations take into account all many-body processes such as shake-up of the Fermi sea, excitonic effects,

etc.

The ML theory yields a power-law singularity of the form<sup>7)</sup>

$$I \propto (\varepsilon_F - \varepsilon_i)^{-\beta} \theta(\varepsilon_F - \varepsilon_i) \quad (3)$$

$$\beta \cong 3/4\pi(k_F d)^{-1} \quad (4)$$

where  $k_F = 2\pi/\lambda_F$  is the Fermi wavevector and  $d$  is the distance from the plane of the 2DEG to the localised site. The parameter  $\beta$  is characteristic of the strength of the Coulomb interaction and can be found directly from the experimental data. We estimate  $d \cong 25$  nm assuming the Fang-Howard approximation for the emitter 2DEG and that the localised states are in the middle of the quantum well. For the first few steps which occur at biases  $V$  between 15-90mV, we found  $\beta$  between 0.1 and 0.3.

The interaction lasts a finite time  $\tau_c$ , before an electron escapes from the impurity state into the collector contact, and this leads to smearing of the singularity on the energy scale  $\Gamma_c = \hbar/\tau_c$ . The smearing is described by adding the imaginary part  $i\Gamma_c$  to  $\varepsilon_i$  in Eq.(3), leading to the expression<sup>7)</sup>

$$I \propto \left( \sqrt{(\varepsilon_F - \varepsilon_i)^2 + \Gamma_c^2} \right)^{-\beta} \left[ \frac{\pi}{2} + \arctan \frac{\varepsilon_F - \varepsilon_i}{\Gamma_c} \right] \theta(\varepsilon_F - \varepsilon_i) \quad (5)$$

Referring to the estimates for the ratio between the tunnelling rates  $\tau_e^{-1}$  and  $\tau_c^{-1}$  in our structures, we expect  $\Gamma_c$  to be of the order 0.1meV ( $\tau_c \cong 10$ ps).

To describe the observed form of FES we assume that the net current includes both single-particle and many-body contributions given by Equations 1 and 5, respectively. The absolute value of the many-body current in Eqs. (3-5) is unknown and used as a fitting parameter. Also, we vary  $\Gamma_c$  around 0.1meV to obtain the best agreement with the experimental data. Figure 6 shows the best fit to the low-temperature  $I(V)$  characteristic from Figure 5(a). The coefficient  $\beta$  is  $\cong 0.22$  for this sample and the fit yields  $\Gamma_c \cong 0.2$ meV. For other samples, the singularities are also described by

values of  $\Gamma_c$  within a factor of two close to 0.1meV.

For completeness, to describe the temperature smearing at the onset of tunnelling in Figure 6 we have multiplied Eq.(5) by the Fermi function  $f(\epsilon_i)$ , instead of using the theta-function as in ref. [7]. For higher temperatures, when  $k_B T \cong \Gamma_c$ , the smearing of FES is due to the effect of both temperature and  $\Gamma_c$ . Essentially, the singularity increases in size with decreasing temperature until it is limited by  $\Gamma_c$ . Further reduction in the temperature results in only minor modifications to the peak, although the current onset is still thermally activated. Although Figure 6 shows quantitative agreement between the experiment and ML theory, we note that Eqs.(3-5) are derived for biases close to the threshold. In addition, the numerical coefficient  $3/4\pi$  in Eq.(4) is valid for the case  $k_F d \gg 1$ , while we deal with the situation when the interaction is strong and  $k_F d \cong 1$ <sup>16)</sup>.

We also note that some of our devices show another unusual form of  $I(V)$ , as shown in Figure 7 for both bias directions. This exhibits an extended and smooth fall-off of current beyond the FES with some weak peaks superimposed on it. We postulate that the current at voltages well above the FES may also be related to electron-electron interaction processes, such as a plasmon-emission process in the 2DEG, in which the tunnelling carrier transfers some of its excess energy to a collective excitation of the 2DEG in the emitter accumulation layer. Plasmon-assisted tunnelling has been reported repeatedly in large area resonant tunnelling diodes<sup>17)</sup>.

#### 4. Conclusions

We have found that the electron-electron interaction has a remarkable effect on tunnelling between a degenerate 2DEG and a strongly localised 0D state. We have observed this effect in small area ( $\sim 10 \mu\text{m}$  square) double barrier resonant tunnelling devices. The localised state is most probably associated with a closely spaced pair of shallow donor impurities situated in the quantum well. This provides a distinct

0D tunnelling channel at an energy well below that of both the 2D continuum and of isolated donors. A distinct and strongly temperature-dependent singular feature is observed in the current-voltage characteristics when the Fermi energy matches the energy of the localised state. We attribute this feature to the Coulomb interaction between the fluctuating charge on the impurity site and the 2DEG and describe the results in terms of the Matveev-Larkin theory. The experimental system offers the possibility of investigating details of 0D tunnelling and properties of the 2DEG on the spatial scale of a few nanometres.

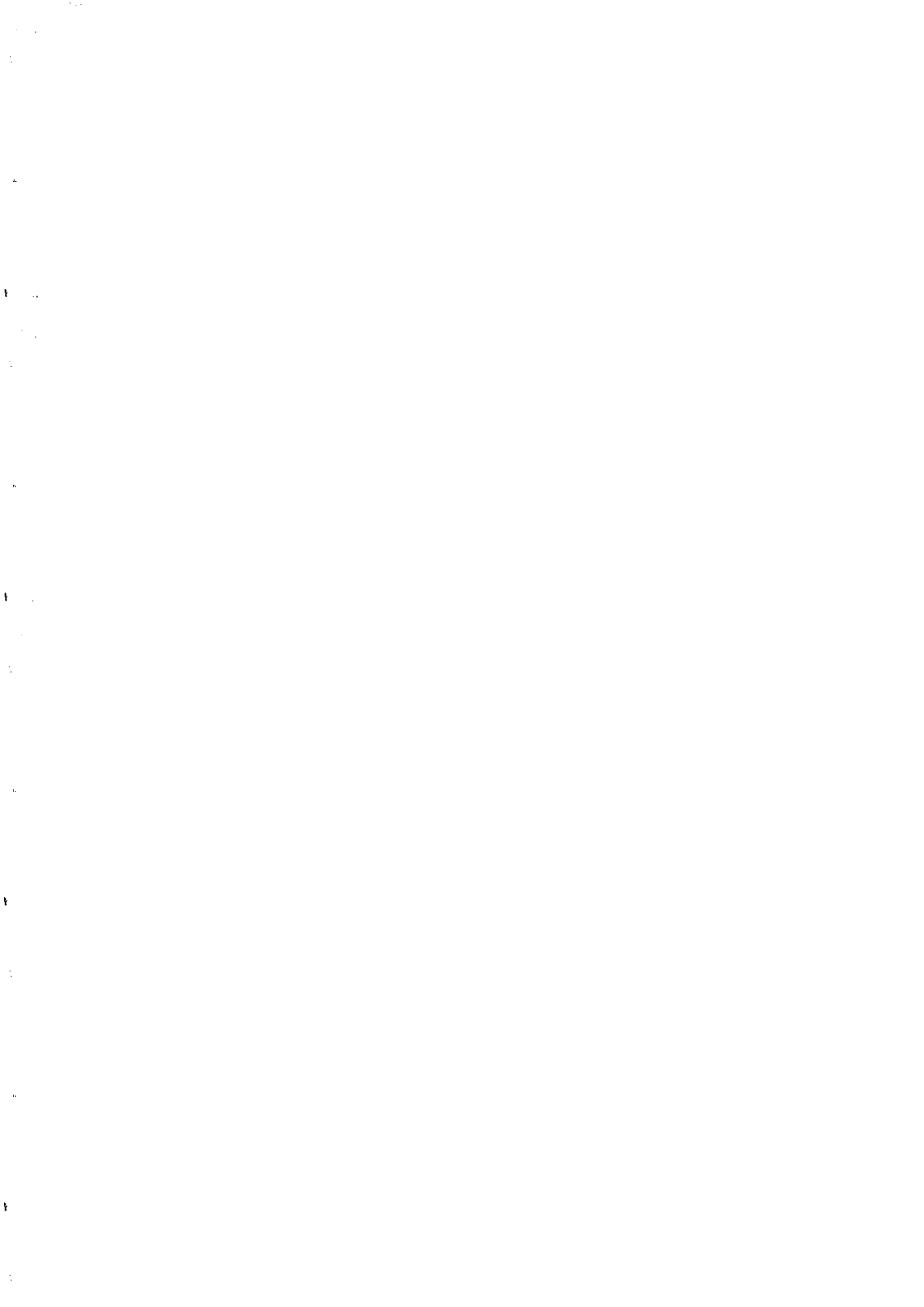
This paper describes the topic covered in the first part of the talk given by L. Eaves at the Recontres de Moriond Condensed Matter Physics Meeting. The second part, concerning tunnelling spectroscopy of chaotic electron states in a quantum well, is described in a paper by T. M. Fromhold, L. Eaves, F. W. Sheard, M. L. Leadbeater, T. J. Foster and P. C. Main, submitted to *Phys. Rev. Letters*.

This work is supported by SERC (UK). Two of us, (LE and PHB) are grateful to the Royal Society for financial support. We are grateful to V. I. Falko and P. Hawrylak for useful discussions. NLSJ and JWS thank CNPq (Brasil) for financial support.

## List of references

1. For an extensive review, see *Electron-electron Interactions in Disordered Systems*, edited by A. L. Efros and M. Pollak (Elsevier Science, Amsterdam, 1985).
2. K. Ohtaka and Y. Tanabe, *Phys. Rev. B* **28**, 6833 (1983). G. D. Mahan, *Many Particle Physics* (Plenum, New York, 1981).
3. There is vast literature on this problem and we refer only to recent papers which would allow one to trace the references. M. S. Skolnick *et al.*, *Phys. Rev. Lett.* **58**, 2130 (1987). J. S. Lee *et al.*, *Semicond. Sci. Technol.* **2**, 675 (1987). G. Livescu *et al.*, *Superlattices and Microstructures* **4**, 359 (1988). W. Chen *et al.*, *ibid.*, 4237 (1992). P. Hawrylak, *Phys. Rev. B* **45**, 8464 (1992). For a recent review see P. Hawrylak, *Optical Phenomena in Semiconductor Structures of Reduced Dimensions*, ed. D. J. Lockwood and A. Pinczuk, NATO ASI Series E **248**, 295 (1993).
4. For a review, see B. L. Altshuler and A. G. Aronov, in Ref. [1].
5. T. K. Ng and P. A. Lee, *Phys. Rev. Lett.* **61**, 1768 (1988). L. I. Glazman and M. E. Raikh, *Pis'ma Zh. Eksp. Teor. Fiz.* **47**, 378 (1988) [*JETP Lett.* **47**, 452 (1988)].
6. L. I. Glazman and K. A. Matveev, *Pis'ma Zh. Eksp. Teor. Fiz.* **48**, 403 (1988) [*JETP Lett.* **48**, 445 (1988)]. S. Hershfield, J. H. Davies, and J. W. Wilkins, *Phys. Rev. Lett.* **67**, 3720 (1991). A. L. Yeyati, A. Martin-Rodero, and F. Flores, *Phys. Rev. Lett.* **71**, 2991 (1993). D. C. Ralph and R. A. Buhrman, *Phys. Rev. Lett.* **69**, 2118 (1992).
7. K. A. Matveev and A. I. Larkin, *Phys. Rev. B* **46**, 15337 (1992).
8. M. A. Reed *et al.*, *Phys. Rev. Lett.* **60**, 535 (1988). U. Meirav *et al.*, *ibid.* **65**, 771 (1990). B. Su, V. J. Goldman *et al.*, *App. Phys. Lett.* **58**, 747, (1991). M. Tewordt *et al.*, *Phys. Rev. B* **45**, 14407 (1992). P. Guéret *et al.*, *Phys. Rev. Lett.* **68**, 1986 (1992). R. C. Ashoori *et al.*, *ibid.*, 3088 (1992).
9. J. W. Sakai *et al.*, in *Workbook of Sixth International Conference on Modulated Semiconductor Structures*, Garmisch-Partenkirchen, Germany, 1993 (to appear in *Solid State Elect.*). P. H. Beton, L. Eaves, and P. C. Main, *Phys. Rev. Lett.* **69**, 2995 (1992).
10. J. W. Sakai *et al.*, *Phys. Rev. B* **48**, 5664 (1993).
11. J. J. Harris *et al.*, *J. Cryst. Growth* **111**, 239 (1991).
12. For a review on resonant tunnelling see *Resonant Tunneling in Semiconductors - Physics and Applications*, ed. L. L. Chang, E. E. Mendez and C. Tejedor, NATO ASI Series B Physics **227** (Plenum, New York, 1991).
13. Impurity-assisted tunnelling has been reported earlier by several groups. S. J. Bending and M. R. Beasley, *Phys. Rev. Lett.* **55**, 324 (1985). A. B. Fowler *et al.*, *ibid.* **57**, 138 (1986). T. E. Kopley, P. L. McEuen, and R. G. Wheeler, *ibid.* **61**, 1654 (1988). M. W. Dellow *et al.*, *ibid.* **68**, 1754 (1992).
14. R. L. Greene and K. K. Bajaj, *Solid State Commun.* **45**, 825 (1983).
15. F. W. Sheard *et al.* (to be published elsewhere).

16. The strong interaction has been considered for the case of the optical FES but there is no corresponding theory for resonant tunnelling. Nevertheless, we note that our results are qualitatively similar to the optical singularities calculated by P. Hawrylak, *Phys. Rev. B* **44**, 3821 (1991).
17. C. Zhang, M. L. F. Lerch, A. D. Martin, P. E. Simmonds and L. Eaves; submitted to *Phys. Rev. Lett.* 1994.



## TWO-CHANNEL RESONANT TUNNELING

M. E. Raikh and T. V. Shahbazyan

*Department of Physics, University of Utah, Salt Lake City, UT 84112*

Resonant tunneling through a single energy level in a barrier has been subject of considerable interest during the last decade.<sup>1-12</sup>) The essential manifestation of the resonant tunneling is that a single impurity, located in the barrier between metallic contacts, may increase the conductance significantly. The experimental observations of the resonant tunneling were reported in Refs. 1-7. The effect is most dramatic when the impurity forms a localized state with energy  $E_0$  close to the Fermi level  $E_F$  in the contacts. Then the conductance is given by a Breit-Wigner type expression<sup>8-12</sup>)

$$G(E_F) = \frac{e^2}{\pi\hbar} \frac{\Gamma^L \Gamma^R}{(E_F - E_0)^2 + \frac{1}{4}(\Gamma^L + \Gamma^R)^2}, \quad (1)$$

where  $\Gamma^L$  and  $\Gamma^R$  are the widths of the impurity level due to the tunneling into the left and right contacts respectively. If the impurity is located in the middle between the contacts, so that  $\Gamma^L = \Gamma^R$ , then at exact resonance,  $E_F = E_0$ , the conductance reaches its maximal value  $G = e^2/\pi\hbar$ . Eq. (1) was derived neglecting the Hubbard interaction of electrons at the impurity and the Coulomb interaction of electrons in the contact and at the impurity. These many-body effects, resulting in the anomalies in the conductance, were studied in Refs. 13-20.

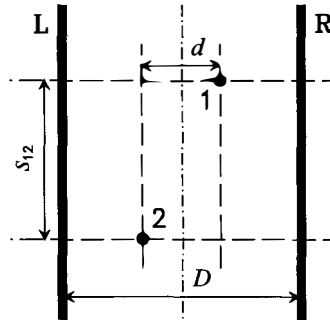


Fig. 1. Schematic representation of the tunneling junction with two resonant impurities (top view). The length of the barrier is  $D$ , and  $d/2$  is the displacement of impurities from the symmetry axis (dash-dotted line).

In the present paper we study two-channel resonant tunneling. The geometry under consideration is schematically shown in Fig. 1. We consider a simplest case, when each channel contains a single resonant level, so that the tunneling from the left to the right metallic contact can occur through either channel 1 or channel 2. The crucial point is that if the de Broglie wavelength of electron in the contacts,  $\lambda_d$ , is of the order of, or much larger than the distance between the two impurities,  $s_{12}$ , then the resonant tunneling involves multiple virtual transitions of electron between the impurity states and the continuum of the states in the contacts. In other words, in the process of tunneling electron visits each impurity many times. Thus, the impurities are coupled to each other not only by the direct overlap of their wave function, but also via the continuum of states in the contacts. The latter coupling, as we will show, results in the dramatic change in the shape of the conductance near the resonance.

We will be working with the following Hamiltonian of the tunneling junction

$$H = \sum_{\nu} E_{\nu}^L C_{L\nu}^{\dagger} C_{L\nu} + \sum_{\nu} E_{\nu}^R C_{R\nu}^{\dagger} C_{R\nu} + \sum_i E_i C_i^{\dagger} C_i + \sum_{\nu,i} (V_{\nu i}^L C_{L\nu}^{\dagger} C_i + V_{i\nu}^L C_i^{\dagger} C_{L\nu}) + \sum_{\nu,i} (V_{\nu i}^R C_{R\nu}^{\dagger} C_i + V_{i\nu}^R C_i^{\dagger} C_{R\nu}) + \sum_{i \neq j} V_{ij} C_i^{\dagger} C_j, \quad (2)$$

where  $E_{\nu}^L$  ( $E_{\nu}^R$ ),  $C_{L\nu}^{\dagger}$  ( $C_{R\nu}^{\dagger}$ ) and  $C_{L\nu}$  ( $C_{R\nu}$ ) are the energy and creation and annihilation operators of the left (right) continuum state  $\nu$ ,  $E_i$ ,  $C_i^{\dagger}$  and  $C_i$  are the energy and creation and annihilation operators of the  $i$ -th impurity state ( $i = 1, 2$ ),  $V_{\nu i}^L$  ( $V_{\nu i}^R$ ) is the matrix element of the impurity potential between left (right) continuum state  $\nu$  and  $i$ -th impurity state, and  $V_{ij}$  is the overlap matrix element between the impurities. One can express the exact time-dependent wave function  $\Psi$  in terms of the wave functions in the contacts,  $\Psi_{\nu}^L$ ,  $\Psi_{\nu}^R$ , and the wave functions of impurities,  $\Psi_i$ , as follows

$$\Psi = \sum_{\nu} A_{\nu}^L(t) \Psi_{\nu}^L + \sum_{\nu} A_{\nu}^R(t) \Psi_{\nu}^R + \sum_i A_i(t) \Psi_i, \quad (3)$$

where the coefficients  $A(t)$  satisfy the following system of equations

$$i\hbar \dot{A}_{\nu}^L = E_{\nu}^L A_{\nu}^L + \sum_i V_{\nu i}^L A_i, \quad (4a)$$

$$i\hbar \dot{A}_{\nu}^R = E_{\nu}^R A_{\nu}^R + \sum_i V_{\nu i}^R A_i, \quad (4b)$$

$$i\hbar \dot{A}_i = E_i A_i + \sum_{\nu} V_{i\nu}^L A_{\nu}^L + \sum_{\nu} V_{i\nu}^R A_{\nu}^R + \sum_{j \neq i} V_{ij} A_j. \quad (4c)$$

The rate of the electron transfer from some state  $\nu_0$  in the left contact to some state  $\mu_0$  in the right contact can be expressed as

$$W(L\nu_0|R\mu_0) = \lim_{t \rightarrow \infty} \left[ \frac{d}{dt} |A_{\mu_0}^R(t)|^2 \right], \quad (5)$$

where  $A_{\mu_0}^R(t)$  is the solution of the system (4) with the initial conditions

$$A_{\nu}^L(0) = \delta_{\nu\nu_0}, \quad A_{\nu}^R(0) = 0, \quad A_i(0) = 0. \quad (6)$$

The expression for the resonant conductance  $G(E_F)$  is obtained by summing Eq. (5) over all the initial and final states at the Fermi level

$$G(E_F) = 2e^2 \sum_{\mu, \nu} W(L\nu|R\mu) \delta(E_F - E_\nu^L). \quad (7)$$

The solution of system (4) can be easily found. Substituting it into Eq. (5) and, then, into Eq. (7), the conductance can be conveniently presented in the following form

$$G(E_F) = \frac{e^2}{\pi \hbar} \text{Tr}(\hat{\Gamma}^L \hat{S} \hat{\Gamma}^R \hat{S}^\dagger), \quad (8)$$

where  $\hat{\Gamma}^L$  and  $\hat{\Gamma}^R$  are  $2 \times 2$  matrices, defined as

$$\Gamma_{ij}^L = \pi \sum_\nu V_{i\nu}^L V_{\nu j}^L \delta(E_F - E_\nu^L), \quad \Gamma_{ij}^R = \pi \sum_\nu V_{i\nu}^R V_{\nu j}^R \delta(E_F - E_\nu^R). \quad (9)$$

The matrix  $\hat{S}$  is expressed through the matrices  $\hat{\Gamma}^L$  and  $\hat{\Gamma}^R$  as

$$\hat{S} = \left[ E_F - \hat{E} - \hat{V} + \frac{i}{2}(\hat{\Gamma}^L + \hat{\Gamma}^R) \right]^{-1}, \quad (10)$$

where we also introduced an energy and overlap matrices  $\hat{E}$  and  $\hat{V}$

$$\hat{E} = \begin{pmatrix} E_1 & 0 \\ 0 & E_2 \end{pmatrix}, \quad \hat{V} = \begin{pmatrix} 0 & V_{12} \\ V_{21} & 0 \end{pmatrix}. \quad (11)$$

The matrix elements  $\Gamma_{ij}$  satisfy a certain relation, which is a consequence of the coupling of the channels through the continuum. To specify this relation, consider the matrix element  $V_{i\nu}^L$ , entering into the definition (9) of  $\Gamma_{ij}^L$

$$V_{i\nu}^L = \int d\mathbf{r} \Psi_i(\mathbf{r}) V(\mathbf{r}) \Psi_\nu^L(\mathbf{r}) \simeq \Psi_\nu^L(x_i, y_i) \int d\mathbf{r} \Psi_i(\mathbf{r}) V(\mathbf{r}), \quad (12)$$

where  $(x_i, y_i)$  are the coordinates of the  $i$ -th impurity. In the  $x$  direction  $\Psi_\nu^L$  decays as  $e^{-\kappa x}$ ,  $\kappa$  being the decay constant, while in the  $y$  direction  $\Psi_\nu^L$  represents a plane wave  $e^{ik_y y}$ ,  $k_y$  being the  $y$ -component of the wave-vector. Thus, we have

$$V_{i\nu}^L = e^{ik_y y_i - \kappa x_i} \Psi_\nu^L(0, 0) \int d\mathbf{r} \Psi_i(\mathbf{r}) V(\mathbf{r}) = e^{ik_y y_i} \beta_i^L. \quad (13)$$

The summation over  $\nu$  in Eq. (9) reduces, in fact, to an averaging over the orientation of the wave vector  $\mathbf{k}$ , since  $|\mathbf{k}| = k_F = 2\pi/\lambda_d$  - the Fermi wave vector. For the diagonal elements,  $\Gamma_{ii}^L$ , the product  $V_{i\nu}^L V_{\nu i}^L$  is independent of the orientation of  $\mathbf{k}$ , so that we have

$$\Gamma_{ii}^L = \pi g(E_F) (\beta_i^L)^2, \quad (14)$$

with  $g(E_F)$  being the density of states at the Fermi level. For  $\Gamma_{12}^L$  the product  $V_{1\nu}^L V_{\nu 2}^L$  contains a factor  $e^{ik_y(y_1 - y_2)}$ , averaging of which results in

$$\Gamma_{12}^L = \pi g(E_F) \beta_1^L \beta_2^L J_0(k_F s_{12}), \quad (15)$$

where  $J_0$  is the Bessel function. A similar formula can also be written for  $\Gamma_{ij}^R$ . Combining Eqs. (14) and (15), we obtain the following relation between diagonal and non-diagonal elements of matrix  $\hat{\Gamma}$

$$\Gamma_{12}^L = \Gamma_{21}^L = \alpha\sqrt{\Gamma_{11}^L\Gamma_{22}^L}, \quad \Gamma_{12}^R = \Gamma_{21}^R = \alpha\sqrt{\Gamma_{11}^R\Gamma_{22}^R}, \quad (16)$$

where we introduced a coupling parameter

$$\alpha = J_0(k_F s_{12}) = J_0(2\pi s_{12}/\lambda_d). \quad (17)$$

We see from Eqs. (16) and (17) that when the two channels are well separated, i.e.,  $s_{12} \gg \lambda_d$ , one can replace the Bessel function by its asymptotics, so that  $\Gamma_{12}$  is small as compared to  $\Gamma_{ii}$  by a factor  $\alpha \sim \sqrt{\lambda_d/s_{12}} \ll 1$ . In this case the coupling of channels through the continuum is weak. Then the conductance (8) represents a sum of two Lorentzians with the widths  $\Gamma_{11}^L + \Gamma_{11}^R$  and  $\Gamma_{22}^L + \Gamma_{22}^R$ .

However, when  $s_{12} \lesssim \lambda_d$ , the parameter  $\alpha$  in Eq. (17) is of the order of unity, and all elements  $\Gamma_{ij}$  are of the same order of magnitude. The latter condition can be satisfied in the resonant tunneling junctions, with the contacts representing heavily doped semiconducting regions. Such type of structures, with  $E_F$  varying by the gate voltage, were studied, e.g., in Refs. 2, 4, and 7. In the case  $s_{12} \sim \lambda_d$ , the two channels should be viewed as a single quantum mechanical system. As a result, the shape of the conductance,  $G(E_F)$ , near the resonance undergoes a drastic transformation, as  $\alpha$  approaches unity. To demonstrate it, let us consider the most symmetrical situation, namely, when the two identical impurities, with no direct overlap ( $V_{12} = V_{21} = 0$ ), are located exactly at the middle of the barrier. Setting  $E_1 = E_2 = E$ ,  $\Gamma_{ii}^L = \Gamma_{ii}^R = \Gamma$ , and  $\Gamma_{12}^L = \Gamma_{12}^R = \alpha\Gamma$  in Eqs. (7) - (11), we obtain

$$G(E_F) = \frac{2e^2}{\pi\hbar} \left\{ \frac{\mathcal{E}^2\Gamma^2(1+\alpha^2) + \Gamma^4(1-\alpha^2)^2}{\mathcal{E}^4 + 2\mathcal{E}^2\Gamma^2(1+\alpha^2) + \Gamma^4(1-\alpha^2)^2} \right\}. \quad (18)$$

where we denoted  $\mathcal{E} = E_F - E$ .

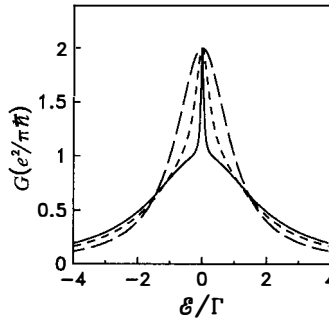


Fig. 2. The conductance, as a function of  $\mathcal{E} = E_F - E$ , is shown for the case of two identical impurities in the middle of the barrier for different values of the coupling strength  $\alpha$ :  $\alpha = 0$  (long-dashed curve),  $\alpha = 0.75$  (dashed curve), and  $\alpha = 0.95$  (solid curve).

The conductance, as a function of  $E_F$ , exhibits a strong dependence on the coupling strength,  $\alpha$ . In the absence of coupling, i.e., at  $\alpha = 0$ , the conductance represents a lorentzian with the width  $\Gamma$  and peak value  $2e^2/\pi\hbar$ , as it should be for two independent channels. However, with an increasing  $\alpha$  the shape of  $G(E_F)$  undergoes a dramatical transformation. The evolution of the conductance peak with increasing  $\alpha$  is shown in Fig. 2.

We see that a drastical narrowing of the resonant peak occurs as  $\alpha$  approaches unity. The conductance curve looks like a narrow peak on top of the wide lorentzian. In the limit  $\alpha = 1$  the upper peak becomes infinitesimally narrow and the conductance represents a simple lorentzian with the height  $e^2/\pi\hbar$  and the width  $2\Gamma$ . Note that the area under the resonant curve is independent of  $\alpha$ .

The narrowing of the resonant peak is the main result of our paper. To clarify the underlying physics, let us consider a related problem, namely, a decay of the localized state 1 into the continuum. We assume that at time  $t = 0$  an electron occupies the state 1, while the state 2 is empty. Then evolution of the population,  $n(t)$ , of the state 1 with time is given by

$$n(t) = |A_1(t)|^2, \quad (19)$$

where  $A_1(t)$  is the solution of system (4) with the initial conditions

$$A_\nu^L(0) = 0, \quad A_\nu^R(0) = 0, \quad A_i(0) \equiv \delta_{i1}. \quad (20)$$

This solution can be expressed through the matrix  $\hat{S}$ , defined by Eq. (10), as follows

$$A_1(t) = \frac{\hbar}{2\pi} \int_{-\infty}^{\infty} d\omega e^{-i\omega t} \left[ \hbar\omega - \hat{E} - \hat{V} + \frac{i}{2}(\hat{\Gamma}^L + \hat{\Gamma}^R) \right]_{11}^{-1}. \quad (21)$$

For the case  $E_1 = E_2 = E$ ,  $\Gamma_{ii}^L = \Gamma_{ii}^R = \Gamma$ , and  $\Gamma_{12}^L = \Gamma_{12}^R = \alpha\Gamma$ , considered above, we obtain

$$A_1(t) = \frac{e^{-iEt/\hbar}}{2i} \left( e^{-t\Gamma_1/\hbar} + e^{-t\Gamma_2/\hbar} \right), \quad (22)$$

with  $\Gamma_1$  and  $\Gamma_2$  defined as

$$\Gamma_1 = (1 + \alpha)\Gamma, \quad \Gamma_2 = (1 - \alpha)\Gamma. \quad (23)$$

We see that the proximity  $\alpha$  to unity causes a slow-decay component of the population  $n(t)$ . This long tail of the population decay manifests itself as a narrow peak in  $G(E_F)$ . Indeed, it can be easily seen that the conductance (18) can be presented as a sum of two lorentzians

$$G(E_F) = \frac{e^2}{\pi\hbar} \left( \frac{\Gamma_1^2}{\mathcal{E}^2 + \Gamma_1^2} + \frac{\Gamma_2^2}{\mathcal{E}^2 + \Gamma_2^2} \right), \quad (24)$$

with the widths  $\Gamma_1$  and  $\Gamma_2$ , given by Eq. (23).

The origin of the slow-decay component can be explained as follows. In the absence of coupling to the continuum, the state of an electron at impurity 1 can be presented as a superposition  $(\Psi^+ + \Psi^-)/\sqrt{2}$  of a symmetric and antisymmetric combinations of  $\Psi_1$  and  $\Psi_2$ . With the coupling taken into account, the amplitude  $A_1$  represents a sum  $A^+ +$

$A^-$  of amplitudes, corresponding to these combinations. Note now that the closer is the parameter  $\alpha$  to unity (i.e., the smaller is the ratio  $s_{12}/\lambda_d$ ), the smaller is the matrix element of coupling of the antisymmetric combination to the continuum. Indeed, for  $s_{12}/\lambda_d \ll 1$  the contributions from  $\Psi_1$  and  $\Psi_2$  to this matrix element almost compensate each other. As a result, the decay time for the amplitude  $A^-$  is much larger than that for  $A^+$ .

The latter argument, in fact, goes back to Dicke.<sup>21)</sup> Forty years ago he considered a spontaneous radiation of an excited atom in the presence of another atom at a distance  $r_{12}$ , much smaller than the radiation wavelength  $\lambda$ . Dicke pointed out that the radiation time increases drastically as  $r_{12}/\lambda \rightarrow 0$ . Namely, the probability that one of the atoms remains in an excited state changes with time according to Eqs. (19) and (22) with  $\Gamma_1 \rightarrow 2\Gamma$  and  $\Gamma_2 \rightarrow 0$ .

We are strongly grateful to V. I. Perel for drawing our attention to the paper by Dicke. The useful discussions P. von Brentano, A. I. Larkin, and D. E. Khmel'nitskii are gratefully acknowledged.

1. S. J. Bending and M. R. Beasley, Phys. Rev. Lett. **55**, 324 (1985).
2. A. B. Fowler, G. L. Timp, J. J. Wainer, and R. A. Webb, Phys. Rev. Lett. **57**, 138 (1986).
3. M. Naito and M. R. Beasley, Phys. Rev. B **35**, 2548 (1987).
4. T. E. Kopley, P. L. McEuen, and R. G. Wheeler, Phys. Rev. Lett. **61**, 1654 (1988).
5. Y. Xu, A. Matsuda, and M. R. Beasley, Phys. Rev. B **42**, 1492 (1990).
6. D. Ephron, Y. Xu, and M. R. Beasley, Phys. Rev. Lett. **69**, 3112 (1992).
7. E. B. Foxman, P. L. McEuen, U. Meirav, N. S. Wingreen, Y. Meir, P. A. Belk, N. R. Belk, and M. A. Kastner, Phys. Rev. B **47**, 10 020 (1993).
8. A. Chaplik and Entin, Zh. Eksp. Teor. Fiz. **67**, 208 (1974) [Sov. Phys. JETP **40**, 106 (1974)].
9. I. M. Lifshitz and V. Ya. Kirpichenkov, Zh. Eksp. Teor. Fiz. **77**, 989 (1979) [Sov. Phys. JETP **50**, 499 (1979)].
10. M. Ya. Azbel, Phys. Rev. **8**, 4106 (1983).
11. A. D. Stone and P. A. Lee, Phys. Rev. Lett. **54**, 1196 (1985).
12. W. Xue and P. A. Lee, Phys. Rev. **38**, 3913 (1988).
13. L. I. Glazman and M. E. Raikh, Pis'ma Zh. Eksp. Teor. Fiz. **47**, 378 (1988) [JETP Lett. **48**, 446 (1988)].
14. T. K. Ng and P. A. Lee, Phys. Rev. Lett. **61**, 1768 (1988).
15. L. I. Glazman and K. A. Matveev, Pis'ma Zh. Eksp. Teor. Fiz. **48**, 403 (1988) [JETP Lett. **48**, 445 (1988)].
16. Y. Meir, N. S. Wingreen, and P. A. Lee, Phys. Rev. Lett. **66**, 3048 (1991).
17. S. Hershfield, J. H. Davies, and J. W. Wilkins Phys. Rev. Lett. **67**, 3720 (1991).
18. K. A. Matveev and A. I. Larkin, Phys. Rev. B **46**, 15 337 (1992).
19. Y. Meir, N. S. Wingreen, and P. A. Lee, Phys. Rev. Lett. **70**, 2601 (1993).
20. T. K. Ng, Phys. Rev. Lett. **70**, 3635 (1993).
21. R. H. Dicke, Phys. Rev. **93**, 99 (1954).

## ANTI-CORRELATED OSCILLATIONS IN A THREE-LEAD QUANTUM DOT

A. Kumar, J. Kinaret,\* C. Eugster, T. Orlando, D. Antoniadis, M. Rooks,† M. Melloch‡

Department of Electrical Engineering and Computer Science  
Massachusetts Institute of Technology  
Cambridge, Massachusetts 02139, U.S.A.

We present results of transport measurements on a quantum dot in which a novel gate geometry allows the dot to be contacted by *three*, rather than two, leads. When the dot charge is well-confined, periodic conductance oscillations due to Coulomb charging are observed in-phase with each other at two of the leads in response to a small excitation voltage at the third. As the tunnel barriers are made softer by changing the gate voltage, a strikingly different phenomenon is observed: conductance peaks at the two output leads evolve from perfect *correlation* to perfect *anti-correlation* with each other. A simple model incorporating polarization states of the dot-lead system is presented as a possible explanation.

Transport measurements have found that the conductance of a quantum dot structure is a periodic function of an external gate voltage.<sup>1)</sup> This striking modulation of the conductance results from the condition that the dot charge is an integer multiple of the electron charge. If the gate voltage is such that the electrochemical potential of the dot lies between the quasi-Fermi levels of the leads, the number of electrons in the dot can fluctuate classically by one and hence the current is at maximum. For all other gate voltages, there is a Coulomb charging energy associated with the tunneling of an additional electron from the input lead, and current flow is suppressed.

The above Single Electron Tunneling (SET) picture of electron transport has been highly successful in explaining the majority of conductance experiments to date<sup>1)</sup> in which a quantum dot is coupled to *two* electron reservoirs. In this paper, we present results of transport

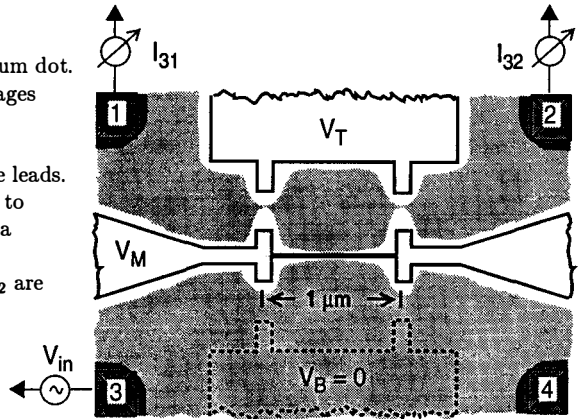
---

\*Nordita, Blegdamsvej 17, DK-2100, Copenhagen Ø, Denmark.

†National Nanofabrication Facility, Knight Laboratory, Cornell University, Ithaca, New York 14853-5403.

‡School of Electrical Engineering, Purdue University, West Lafayette, Indiana 47907.

Figure 1: Schematic of the gate geometry of our three-lead quantum dot. Application of negative gate voltages  $V_T$  and  $V_M$  depletes the 2DEG underneath, leaving behind an electron “island” coupled to three leads. Four ohmic contacts allow access to the 2DEG. In our measurements a voltage  $V_{in}$  is applied at contact 3 and currents  $I_{31}$  and  $I_{32}$  are measured simultaneously.



measurements on a structure in which a novel gate geometry allows us to study a quantum dot coupled via tunnel barriers to *three* leads. A small voltage excitation at one lead results in currents at the other two leads, which can be measured simultaneously. We find that the first several Coulomb blockade oscillations in the two currents line up with each other as the gate voltage is swept, as expected from the simple SET picture. However, the main finding of this work is that, as the gate voltage is increased further, the oscillations undergo a striking transition from being lined up with each other to being perfectly *out-of-phase* with each other.

Figure 1 shows a schematic of our gate geometry, fabricated over a standard GaAs/AlGaAs heterostructure with mobility  $25 \text{ m}^2 \text{ V}^{-1} \text{ s}^{-1}$  and carrier density  $3 \times 10^{15} \text{ m}^{-2}$  at 4.2 K. Application of a negative bias voltage to the top gate,  $V_T$ , and thin ( $\sim 40 \text{ nm}$  linewidth) middle gate,  $V_M$ , depletes the high-mobility 2DEG formed in a GaAs/AlGaAs modulation-doped heterostructure, resulting in an “island” of electrons coupled to narrow channels on the left and right, and to a semi-infinite 2DEG on the bottom. The currents at the output leads (lead 1 and lead 2) are measured in response to a small ac voltage  $V_{in}$  applied at the input lead (lead 3). Two low noise current amplifiers are used to measure simultaneously the currents  $I_{31} = G_{31}V_{in}$  and  $I_{32} = G_{32}V_{in}$  at the output leads. Each current amplifier outputs a voltage which is measured using an ac lock-in technique at frequency 7.7 Hz. Blocking capacitors are used at the inputs of the current amplifiers to shield the device from offset voltages; each output lead is therefore a virtual ground. As a check that the offset voltages are properly compensated, essentially no change is observed in  $I_{31}$  and  $I_{32}$  if the two amplifiers are interchanged. All measurements are carried out at a base cryostat temperature of 300 mK.

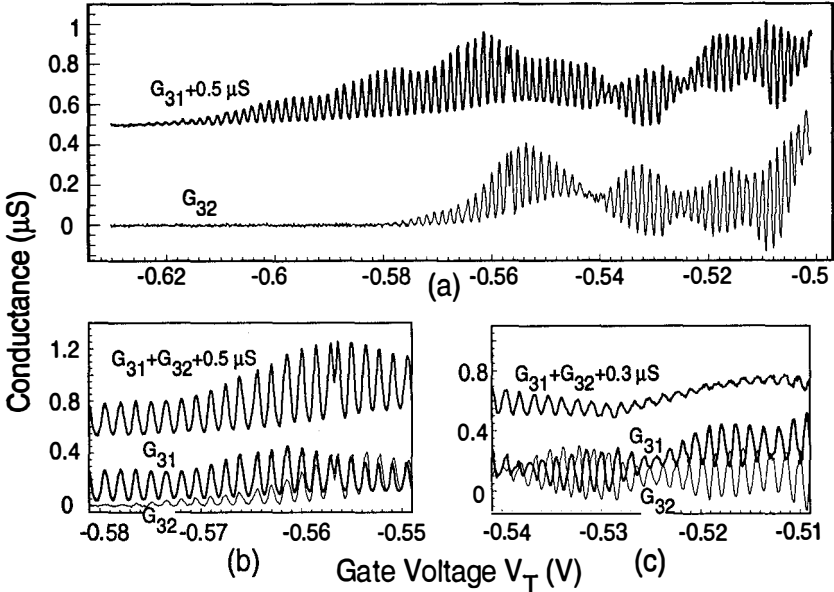


Figure 2: (a) Conductances  $G_{31}$  (offset by  $0.5\mu\text{S}$ ) and  $G_{32}$  as the top gate voltage  $V_T$  is swept. The middle gate voltage  $V_M = -0.7\text{V}$  is fixed in the tunnel regime. (b) Detailed plot of the first several resonances in (a), indicating that they are in-phase with each other. (c) Detailed plot of resonances at higher  $V_T$ , indicating that they have evolved from almost perfect *correlation* to almost perfect *anti-correlation* in gate voltage.

Figure 2(a) shows the conductances  $G_{31}$  and  $G_{32}$ , measured concurrently, as the top gate voltage  $V_T$  is swept. The middle gate voltage  $V_M = -0.7\text{V}$  is kept fixed in the tunnel regime, as determined by an exponential tail in its pinchoff characteristic.<sup>2)</sup> Due to some intrinsic, unintentional asymmetry in our structure, the quantum point contact near lead 2 has a turn-on voltage about 40 mV higher than the one near lead 1.

The first several conductance oscillations in  $G_{31}$  and  $G_{32}$ , along with the total conductance  $G_{31} + G_{32}$  through the dot, are shown in detail in Fig. 2(b). The perfect alignment of the oscillations in  $G_{31}$  and  $G_{32}$  for  $V_T < \sim -0.555\text{V}$  can be understood simply from standard SET theory. At a conductance maximum, an electron which has tunneled into the dot from the input lead has some probability of being transmitted through either one of the two output leads. As the gate voltage is increased in Fig. 2(c), the peak-to-valley ratio in the total dot conductance  $G_{31} + G_{32}$  drops markedly. However, instead of broadening accordingly, resonances in the individual conductances  $G_{31}$  and  $G_{32}$  evolve from being perfectly correlated to being perfectly anti-correlated with each other. Another striking feature of the anti-correlated regime is that

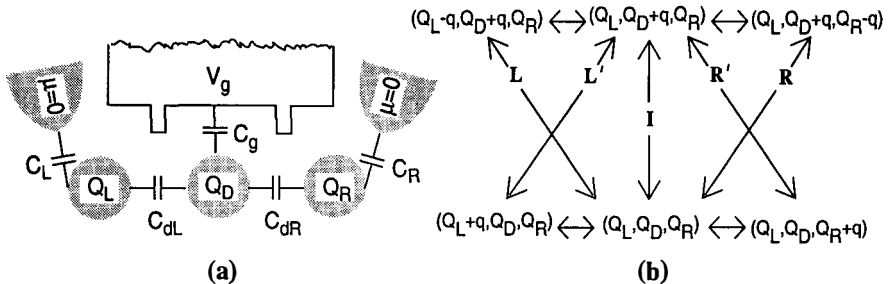


Figure 3: (a) Lumped element circuit containing dot and two quasi-reservoirs to model effect of unequal electrochemical potentials on left and right sides of the dot. (b) Set of states used in calculation and possible transitions between them. The set of states includes the lowest-energy unit polarization fluctuations of the states  $(Q_L, Q_D, Q_R)$  and  $(Q_L, Q_D + q, Q_R)$ . The unlabeled transitions show no resonant structure because of the strong coupling between the quasi-reservoirs and the reservoirs.

$G_{32}$  actually changes sign at some of the deep valleys. The total conductance through the dot  $G_{31} + G_{32}$  is, however, always positive.

We have fitted the lineshapes of  $G_{31} + G_{32}$ . In the correlated regime we find an excellent fit of the lineshapes to the derivative of the Fermi-Dirac function. As the gate voltage is increased so that the oscillations become anti-correlated, we find that the Fermi fit to  $G_{31} + G_{32}$  progressively worsens, predicting valleys much deeper and linewidths much narrower than given by the data. Foxman et al.<sup>3)</sup> have found that such a transition from thermally to intrinsically broadened resonances is accompanied by a rapid increase in the capacitance between the dot and one of the leads.

We now turn to a preliminary model to account for the separation of the peaks in the left and right currents with gate voltage. The crucial ingredient of the model is that there is some intrinsic, unintentional asymmetry between the right and left tunnel barriers which causes the local chemical potentials to be different on the left and the right sides of the dot. We can associate an effective capacitance with each barrier, the value of which depends on the barrier thickness and height. As the barriers are made softer by increasing the top gate voltage  $V_T$ , the barrier capacitances increase, and the relative barrier asymmetry becomes more important. In this regime it is no longer obvious that the transitions necessary to produce current peaks at the left and right leads will resonate at the same gate voltage.

Figure 3(a) depicts a lumped-element circuit used as a first approximation to model the effect of unequal electrochemical potentials. In addition to the dot with quantized charge  $Q_D = -N_{DE}$ , the model contains two quasi-reservoirs which are coupled to the actual reservoirs

by large capacitances  $C_L$  and  $C_R$ . Physically, we expect that a test charge placed in a quasi-reservoir, representing the part of the lead nearest the barrier, will be partially imaged in the dot and partially imaged in the actual reservoir.

The electrostatic energy of the circuit in Fig. 3(a) is

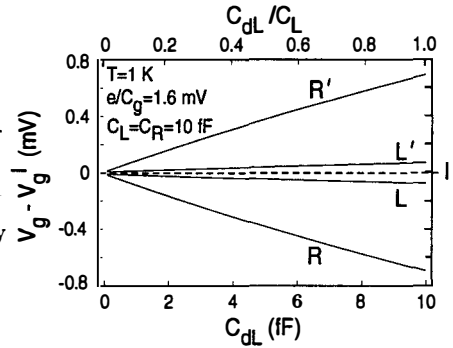
$$W(Q_D, Q_L, Q_R, V_g) = \frac{1}{2\tilde{C}_d}(Q_D + \gamma_L Q_L + \gamma_R Q_R)^2 + \frac{1}{2\tilde{C}_L}Q_L^2 + \frac{1}{2\tilde{C}_R}Q_R^2 + \frac{C_g}{\tilde{C}_d}V_g(Q_D + \gamma_L Q_L + \gamma_R Q_R), \quad (1)$$

where  $\tilde{C}_{L(R)} = C_{L(R)} + C_{dL(dR)}$ ,  $\gamma_{L(R)} = C_{dL(dR)}/\tilde{C}_{L(R)}$ , and  $\tilde{C}_d = C_g + (1 - \gamma_L)C_{dL} + (1 - \gamma_R)C_{dR}$ . Figure 3(b) shows the set of states used in the model and the possible transitions between them. The set of states includes the lowest-energy unit polarization fluctuations of the states  $(Q_L, Q_D, Q_R)$  and  $(Q_L, Q_D + q, Q_R)$ . The procedure for finding the resonant gate voltages for each of the 5 transitions I, L, L', R, R' is as follows. The electrostatic energies of the two states involved in each transition are equated, relating the resonant gate voltage  $V_g$  to the charges  $(Q_L, Q_D, Q_R)$ . To find the charges, it is assumed that the time-average charges  $\bar{Q}_{L(R)} = \sum_i P_i Q_{L(R)}^{(i)}$  are given by the classical electrostatics relations  $\partial W/\partial Q_{L(R)} = 0$ , where the occupancy probability  $P_i$  for state  $i$  is taken in the grand canonical ensemble.

This procedure yields a set of coupled transcendental equations. In the limit  $C_L, C_R \gg C_g, C_{dL}, C_{dR}$ , we recover the conventional SET theory result that all transitions are at resonance at the same gate voltage  $V_g = e(N_D + 1/2)/C_g$ . As the tunnel barriers become softer with increasing gate voltage, the capacitances  $C_{dL}, C_{dR}$  become comparable to  $C_L, C_R$ , in which case the equations must be solved numerically. Figure 4 shows the results of such a calculation, in which the resonant gate voltage positions for the transitions L, L', R, R' are plotted as a function of  $C_{dL}$  for the highly asymmetric case  $C_{dL} = 10C_{dR}$ . With increasing  $C_{dL} = 10C_{dR}$ , the injector transition I is unchanged and the transitions L, L' are shifted only a little. However, the transitions R, R' are strongly shifted; in the limiting case  $C_{dL}/C_L \simeq 1$ , when the left barrier has nearly disappeared, transitions R, R' are at resonance almost midway between successive resonances of the injector transition I.

This polarization model suggests a mechanism by which a phase shift in the resonances can occur. For a peak to occur in the current measured at the right lead, there must be a chain of events involving transition I and either transition R or R', which no longer occur at the same gate voltage. The currents  $I_{31}, I_{32}$  versus gate voltage can be found numerically by replacing the equilibrium probabilities  $P_i$  with a non-equilibrium distribution function determined by a rate equation.<sup>1)</sup> Such a calculation has been carried out<sup>4)</sup> and indeed yields anti-aligned oscillations

Figure 4: Gate voltages at which each of the transitions L,L',R,R' are at resonance (relative to the position of the I resonance) as capacitances  $C_{dL}$  and  $C_{dR}$  are increased, for the highly asymmetric case  $C_{dL} = 10C_{dR}$ . For  $C_{dL} = C_{dR} = 0$ , we recover the standard SET result that all transitions occur at the same gate voltage. As  $C_{dL}/C_L$  approaches 1, so that the left barrier has nearly disappeared, transitions R,R' occur almost midway between neighboring I transitions.



in the limit that  $C_{dL}$  and  $C_{dR}$  are large but asymmetric. However, the currents do not change sign.

In summary, we have fabricated and studied a three-lead quantum dot. When the dot confinement is strong, the two output leads behave as two independent, parallel channels for current flow, resulting in Coulomb blockade oscillations which are aligned with each other in gate voltage. As the leak rates to the output leads increase, peaks in the total incident current broaden accordingly, but peaks in the two output currents evolve from being correlated with each other to being anti-correlated with each other. In this regime the simple single electron tunneling picture is inadequate to explain our results, and we suggested a simple circuit model which reproduces many of the observed features.

The authors wish to thank N.R. Belk, M. Burkhardt, D.J. Carter, M.K. Mondol, R.R. Perilli, and G.E. Rittenhouse for help at various stages of this work. We have also benefited from discussions with P. Debray, E.B. Foxman, D.C. Glatli, and H.I. Smith. This work was sponsored by the U.S. Air Force Office of Scientific Research under agreement F49620-92-J-0064. This work was performed in part at the National Nanofabrication Facility which is supported by the National Science Foundation under Grant ECS-8619049, Cornell University, and industrial affiliates. One of us (A.K.) gratefully acknowledges support from a SRC fellowship.

- 1) For a review, see H. van Houten, C.W.J. Beenakker, and A.A.M. Staring, in *Single Charge Tunneling*, ed. by H. Grabert and M.H. Devoret (Plenum, New York, 1991).
- 2) C.C. Eugster and J.A. del Alamo, *Phys. Rev. Lett.* **67**, 3586 (1991).
- 3) E.B. Foxman, P.L. McEuen, U. Meirav, N.S. Wingreen, Y. Meir, P.A. Belk, N.R. Belk, M.A. Kastner, and S.J. Wind, *Phys. Rev. B* **47**, 10020 (1993).
- 4) J. Kinaret (private communication).

## CONDUCTANCE SPECTROSCOPY OF A QUANTUM DOT IN WEAK MAGNETIC FIELDS

M. Persson<sup>(1)</sup>, B. von Sydow<sup>(2)</sup>, P. E. Lindelof<sup>(3)</sup>, A. Kristensen<sup>(3)</sup> and J. Pettersson<sup>(1)</sup>

<sup>(1)</sup>Department of Physics, <sup>(2)</sup>Department of Applied Physics, Chalmers University of Technology and University of Göteborg, S-41296 Göteborg, Sweden

<sup>(3)</sup>The Niels Bohr Institute, University of Copenhagen, Universitetsparken 5, Dk-2100 Copenhagen Ø, Denmark

Transport spectroscopy is presented for a quantum dot confined by an electrostatic potential in a two-dimensional electron gas. The conductance oscillated quasi-periodically when the magnetic field or the size of the dot were changed. The measured data reflect the density of states at the Fermi energy in the quantum dot. This was observed without interference of charging effects, due to a high conductivity between the dot and the surrounding electron gas. The conductance oscillations agree with a simplified resonant tunneling model, where the energy levels are calculated for an isolated circular disc.

### INTRODUCTION

Many new effects have recently been observed in low-dimensional mesoscopic systems: Quantization of conductance in ballistic point contacts, spatial energy quantization in zero-dimensional quantum dots, electron-electron interactions and single electron charging effects<sup>1)</sup>. Experimental characterizations of energy levels by transport measurement<sup>2)</sup> and capacitance spectroscopy<sup>3)</sup> have been reported. An addition spectra can be deduced from the positions of Coulomb blockade oscillation peaks or capacitive resonances. The distances between peaks give the separations between adjacent levels added to a constant charging energy term. Dots with few electrons where electron interactions can be modeled, have attracted much interest.

Semiclassical theories of the spectra and eigenstates of quantum dots have been developed<sup>4,5)</sup>, in which the electrons move as classical ballistic particles and carry phase information that can be affected by a magnetic vector potential. The geometric form of the confining walls determines the scattering of electrons and strongly affects the energy spectra. Stone and Bruus<sup>5)</sup> have found that minor distortions of the boundary may dramatically change the energy levels of a quantum dot. The statistics of transport properties

have been analyzed experimentally<sup>6)</sup> and theoretically<sup>4, 7)</sup> by means of evaluating power spectra of magnetoconductance. A classically integrable system, for example a circular disc, was found to have higher amplitude of the high-frequency components in the power spectrum than a chaotic irregular structure.

The eigenstates of a circular disc in weak magnetic fields<sup>8)</sup> can be deduced by perturbation theory. This model does not take into account the imperfections or irregularities of the boundary and has been considered as irrelevant for describing the energy levels of quantum dots. We have, however, measured the conductance of a quantum dot as a function of gate voltage and magnetic field and compared it with this simplified model and found qualitative agreement between measured and calculated magnetoconductance. One or more modes were transmitted through the point contact and therefore charging effects were not significant. The levels of the dot may be well-defined even when the total conductance is higher than the conductance quantum, provided there are many levels in the dot that individually have a low transmission probability<sup>9)</sup>. The measured conductance oscillations remain up to a temperature of 2 K. The calculated conductance showed high frequency oscillations at low temperatures that were not clearly observed in the measurement and the oscillations with longer period had a stronger temperature dependence than the measurement. Two energy scales of the oscillations can be identified; one is related to the separation between angular modes and the other to the average separation between discrete states in the dot.

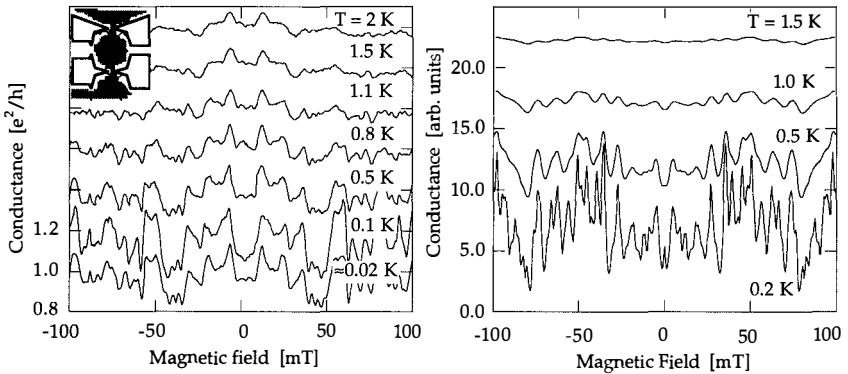


Figure 1. (a) Measured and (b) calculated magnetoconductance at various temperatures. Quasi-periodic oscillations are observed that resemble universal conductance fluctuations, but they have a regular dependence in both magnetic field and size of the dot. The long period oscillations persist up to 2 K. The high frequency fluctuations that appear in the calculated sweeps (b), below  $T=0.2$  K, is not observed in the measurements even at base temperature  $\approx 20$  mK. High frequency oscillations appear in the calculations sweeps below  $T=0.2$  K. The traces are offset for clarity.

## MEASUREMENTS

The experiment was performed on a quantum dot, confined in a two-dimensional electron gas (2DEG) by the electrostatic potential of four Schottky gates (see inset of fig. 1 (a)). The gate geometry had a lithographically defined inner diameter of  $1\ \mu\text{m}$ . The gates formed a quantum dot of circular shape, with a diameter that may be estimated to be  $0.8\ \mu\text{m}$  at pinch off. The 2DEG was formed in a GaAs/Ga<sub>x</sub>Al<sub>1-x</sub>As heterostructure grown by molecular-beam epitaxy and had a mobility of  $63\ \text{m}^2/\text{Vs}$  and an electron density of  $3.7 \cdot 10^{15}\ \text{m}^{-2}$ . The mean free path is estimated to be  $6\ \mu\text{m}$ , which is longer than the perimeter of the dot. The gates (150 Å Ti/ 150 Å Au) were made by electron-beam lithography and lift-off.

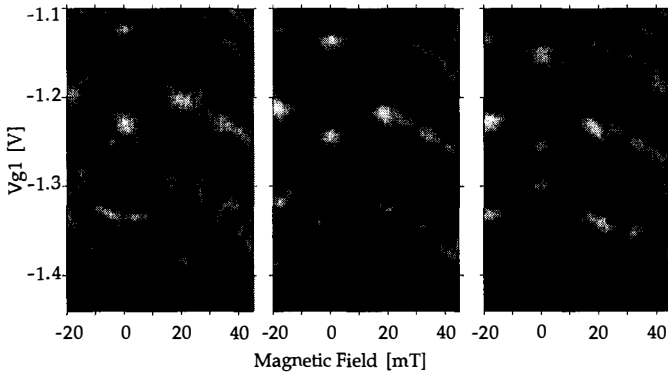


Figure 2. The conductance of the quantum dot as a function of magnetic field and gate voltage  $V_{g1}$ , displayed as a gray-scale image. The bright regions indicate higher conductance. The voltage on the other gate pair is changed: in (a)  $V_{g2} = -1.34\text{V}$ , (b)  $= -1.33\text{V}$ , (c)  $= -1.32\text{V}$ . The dark regions that appear periodically at zero magnetic field are shifted when  $V_{g2}$  is changed. The periodic variation is thus not due to a change of the number modes in the point contact, but to a change of the area of the dot. The variations are clearly periodic in some regions and a zigzag pattern can be seen.

We determined the two-terminal conductance by measuring the current and the voltage over the sample with two lock-in amplifiers, while the magnetic field or the voltages on one gate-pair ( $V_{g1}$ ) were swept. The dot was biased symmetrically by an ac-voltage over two  $100\ \text{k}\Omega$  resistors, connected in series with the sample. The ac-voltage over the sample was of the order of  $10\ \mu\text{V}$ . The measurements presented in figure 2 were done at base the temperature of the dilution refrigerator  $T \approx 20\ \text{mK}$ , but the effective temperature is estimated (based on other experiments) to have been in the range  $100$  to  $300\ \text{mK}$ . The temperature dependence of the magnetoconductance oscillations is shown in figure 1. Note that any major differences between base temperature and  $0.1\ \text{K}$  cannot be observed. The variations have a regular dependence in magnetic field and size. This is seen in figure

2 as quasi-periodic oscillations. High conductance is indicated by bright image. The characteristic pattern shifted and was distorted when  $V_{g2}$  was varied, but it can still be recognized. A third order polynomial is subtracted from the sweeps in the gate voltage direction to remove the influence of an increasing conductance of the point contact and to enhance the oscillatory behaviour.

### CALCULATIONS

The calculation is based on a double-barrier resonant tunneling model. The dot is modeled as a perfectly circular disc with hard walls, where imperfection of the boundary is neglected. The conductance was calculated as a resonant transmission through bound states in the quantum dot, even though the conductance of each point contact was higher than or comparable to the conductance quantum. The temperature used in the calculations was 0.4 K. In the measurements, the swept gate voltage affected the area, the conductance of the point contacts, as well as the electron density in the dot. In the calculations, we vary only the radius.

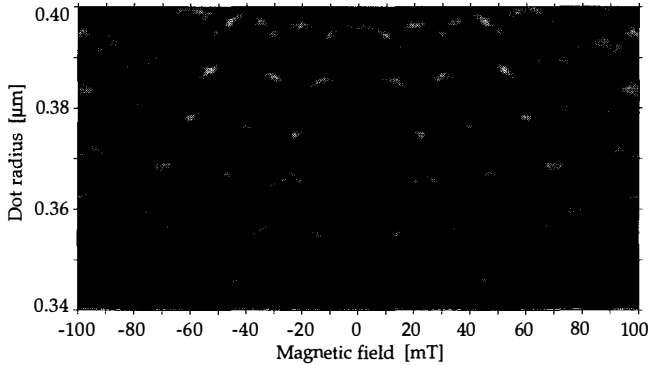


Figure 3. Calculated conductance through resonant states of an isolated circular disc. The variations are very complex, but still quasi-periodic. The characteristic zigzag pattern can be seen in these calculations. Bright regions indicate high conductance. The dot radius can be related approximately linearly to the gate voltage in the measurements. The radial change in figure 2 is estimated to be 0.03  $\mu\text{m}$ .  $T=0.4\text{K}$

The energy levels of the bound states were calculated by solving the Schrödinger equation for a circular geometry in weak magnetic fields. The energy levels of the system can be expressed as <sup>8, 9)</sup>

$$E_{m,n} = E_0 \left[ \gamma_{m,n}^2 + 2m\alpha + \frac{1}{3}\alpha^2 \left( 1 + \frac{2(m^2 - 1)}{\gamma_{m,n}^2} \right) \right]$$

where  $E_0 = \hbar^2 / 2m^* a^2$ , if the applied magnetic field is sufficiently small such that the cyclotron radius is much larger than the dot radius  $r_C \gg a$ . The classical cyclotron radius,

$r_c = \hbar(2\pi m_s)^{1/2} / eB$ , equals the dot radius at a magnetic field  $B=0.25$  T.  $\gamma_{m,n}$  is the  $n$ :th root to the  $m$ :th Bessel function,  $J_m(\gamma_{m,n})=0$ ,  $n=1,2,\dots$ ,  $m=0,\pm 1,\pm 2,\dots$ . For a given magnetic field  $B$ , the flux through the dot is  $\Phi = \pi a^2 B$ , which can be normalized by the magnetic flux quantum  $\Phi_0 = h/e$ , giving the dimensionless parameter  $\alpha = \Phi/\Phi_0$ .

To find the conductance of the double barrier structure we use an expression for the current [10]

$$J = 2 \frac{e}{2\pi} \int dk v(k) T_{12}(k) [n_F(E(k) - \mu_1) - n_F(E(k) - \mu_2)]$$

where  $\mu_i = E_F \pm eV/2$  are the chemical potentials of the reservoirs and  $n_F$  is the Fermi-Dirac distribution.  $v(k)$  is the group velocity of the incident electron to the double barrier structure. The Lorentian shaped energy dependence of the discrete tunneling probability ( $T_{12}$ ) is approximated by a delta function. The tunneling probability at resonance  $T_{res}$  is assumed to be a constant. After evaluating the integral and summing the contributions from all resonance energies  $E_{m,n}$ , the final expression for the current density is

$$J = \frac{e}{2\hbar} \Gamma T_{res} \sum_{m,n} [n_F(E_{m,n} - \mu_1) - n_F(E_{m,n} - \mu_2)]$$

where  $\Gamma$  is the full width at half maximum of the resonant levels. This gives the conductance at zero bias voltage,

$$G = \left. \frac{\partial J}{\partial V} \right|_{V=0} = \frac{e^2 \beta}{2\hbar} \Gamma T_{res} \sum_{m,n} \frac{\eta_{m,n}}{(1 + \eta_{m,n})^2}, \text{ where } \eta_{m,n} = \exp[\beta(E_{m,n} - E_F)] \text{ and } \beta = 1/k_B T.$$

This expression was used to calculate the conductance as a function of both radius of the dot and magnetic field (figure 3).

## DISCUSSION

The conductance through a resonant tunneling structure is proportional to the density of states at the Fermi energy. In figure 3 it can be seen that it has a complex dependence of magnetic field and size, but clearly has regular features. The conductance is strongly affected even by small changes of the radius or the magnetic field. Two magnetic field sweeps may seem uncorrelated after a gate voltage change of only a few tenths of mV. From the gray-scale images we see that the measured conductance has the same complex dependence as the calculated data. It is periodic at zero magnetic field, with a period corresponding to a change of the number of angular modes in the dot. The quantity  $k_F a$  gives approximately the number of angular modes in the circular dot, where  $k_F = (2\pi m_s)^{1/2}$  is the Fermi wavevector and  $a$  is the dot radius. For this dot  $k_F a = 60$  ( $a = 0.4 \mu\text{m}$ ). Two different energy scales can be distinguished: the average separation between discrete energy levels and the separation between angular modes ( $E_F/(k_F a)$ ). They will give different temperature and flux dependence of the conductance. The second will give a contribution that is quasi-periodic in  $\Phi_0$ , whereas the first will lead to oscillations or spikes with higher

frequencies. The corresponding temperature scales were about 0.08 K and 2.6 K respectively in our experiment. The effective temperature of the sample, however, was  $\approx$  0.2 K and therefore the high frequency oscillation was consequently not observed.

The bound states of the dot are well defined if the transmission probability for each state is small,  $|t|^2 \ll 1$ . This can be satisfied for a system with a large number of particles even when the total conductance  $G \approx (2e^2/h)(|t|^2 N) > 2e^2/h$  <sup>9)</sup> We therefore find it reasonable to use the simplified model of a double-barrier resonant tunneling structure and compare it with the transport properties of the quantum dot.

## CONCLUSION

We have observed conductance oscillations that are due to variations of the density of states close to the Fermi energy. The oscillations were seen even though the conductance of one point contact was higher than the conductance quantum. That means that spectroscopy of bound states in a quantum dot can be done without the interference of charging effects. The measurements agree qualitatively with a simple resonant tunneling model where the energy spectrum is calculated for an isolated circular disc. We find that the spectra of perfectly shaped integrable geometries can be relevant for real systems that have roughness of the confining walls and contacts to the dot.

## ACKNOWLEDGMENTS

We thank K.-F. Berggren, P. Delsing and M. Jonson for useful discussions and C. B. Sørensen and M. Bøgelund for technical assistance. We utilized the Swedish Nanometer Laboratory for electron beam lithography. The work is supported by the Swedish and Danish Natural Science Research Councils and the Swedish National Board for Technical and Industrial Development.

## REFERENCES

- 1) C. W. Beenakker and H. van Houten, in *Solid State Physics*, ed. H. Ehrenreich and D. Turnbull. Vol 44. (Academic Press, San Diego, 1991).
- 2) U. Meirav, M. A. Kastner and S. J. Wind, *Phys. Rev. Lett.*, **65**, 771, (1990).
- 3) R. C. Ashoori, H. L. Stormer, J. S. Weiner, L. N. Pfeiffer, K. W. Baldwin and K. W. West, *Phys. Rev. Lett.*, **71**, 613, (1993).
- 4) R. A. Jalabert, H. U. Baranger and D. Stone, *Phys. Rev. Lett.*, **65**, 2442, (1990).
- 5) A. D. Stone and H. Bruus, *Physica B*, **189**, 43, (1993).
- 6) C. M. Marcus, A. J. Rimberg, R. M. Westervelt, P. F. Hopkins and A. C. Gossard, *Phys. Rev. Lett.*, **69**, 506, (1992).
- 7) H. A. Baranger, R. A. Jalabert and A. D. Stone, *Chaos* **3**, 665 (1993).
- 8) R. B. Dingle, *Proc. Roy. Soc. A*, **212**, 47, (1952).
- 9) T. Swahn, Chalmers Univ. of Tech. and Univ. of Göteborg, Ph.D. Thesis, 1993.
- 10) M. Jonson and A. Grincwajg, *Appl. Phys. Lett.*, **51**, 1729, (1987).

**SHELL STRUCTURE IN GaAs/AlGaAs QUANTUM DOTS**

P.E. Lindelof, A. Kristensen and C.J. Kennedy  
The Niels Bohr Institute, University of Copenhagen  
Universitetsparken 5, DK-2100 Copenhagen Ø  
and

M. Persson  
Department of Physics, Chalmers University of Technology  
S-41296 Göteborg, Sweden

**ABSTRACT**

The conductance through a quantum dot made in a 2-dimensional electron gas of a GaAs HEMT structure exhibit a quasiperiodic variation as a function of the gatevoltage, reflecting the level density as a function of the number of electrons in the dot. This has been seen in rather open dots, where Coulomb blockade does not play an important role. We and others observe it in the amplitude modulation of the Coulomb blockade oscillations for quantum dots. These results are suggested to be the result of shell effects in samples with a shape, which comes close to a circle. The results are consistent with a confinement potential, which is parabolic for small quantum dots and with hard walls for larger quantum dots.

**INTRODUCTION**

Lately there has been considerable interest in the electronic spectrum of semiconductor quantum dots with a countable number of electrons<sup>1)</sup>. The interest has in particular been focused on the finestructure within the energy range set by one Coulomb blockade period. The methods are in these cases based on a variable bias across the quantum dot<sup>2,3)</sup> or by capacitive charging<sup>4)</sup>. Both methods investigate the spectrum inside one Coulomb blockade energy period,  $e^2/C$ . Recently it has turned out possible to watch the spectral density over a much larger energy range. The overall spectrum density may be studied in a quantum dot, which has a high conductance (in terms of  $e^2/h$ )

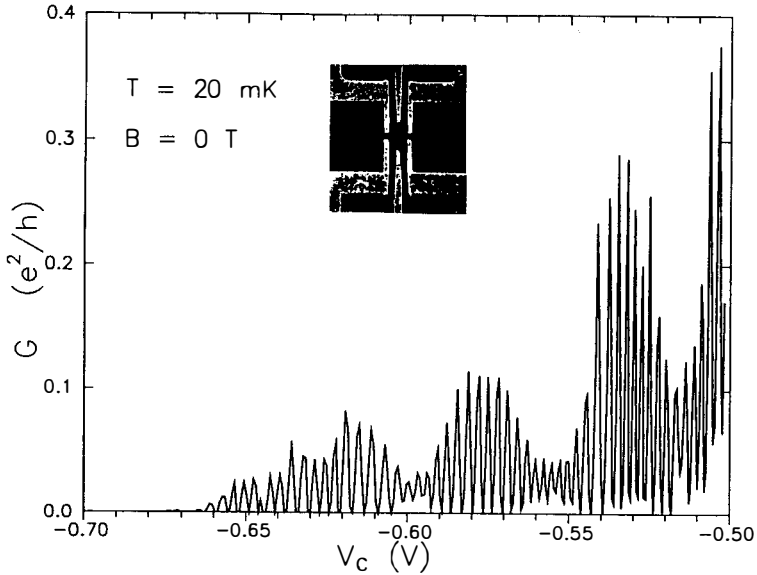


Fig. 1. Conductance,  $G$ , through a 3-splitgate quantum dot plotted as a function of the center splitgate voltage,  $V_C$ . The 2-dimensional electron gas is formed in a GaAs/AlGaAs heterostructure with a mobility,  $\mu=1 \cdot 10^6 \text{ cm}^2/\text{Vs}$ , and a carrier density,  $n_2=1.4 \cdot 10^{11} \text{ cm}^{-2}$ . The split gate configuration is shown on the inserted SEM micrograph. The splitgates to the left and right defines two quantum point contacts; the distance (center to center) between these quantum point contacts is  $1.2 \mu\text{m}$ . The conductances of these split gates were individually adjusted to values below  $e^2/h$ , corresponding to the two split gate voltages  $-0.23\text{V}$  and  $-0.18\text{V}$ . The size of the quantum dot is adjusted with the middle split gate voltage,  $V_C$ , along the abscissa. The amplitudes of the Coulomb blockade oscillations have a characteristic periodically varying envelope, which is ascribed to a penduling semiclassical orbit (see text).

to the external 2-dimensional electron gas<sup>5,6)</sup> or via the envelope of the peaks of the Coulomb blockade oscillations<sup>2,7,8)</sup>. In the last mentioned case one has to be cautious due to the irregular properties of the quantum point contacts<sup>2)</sup>. We have experimentally studied the amplitude in Coulomb blockade oscillations, and we generally find a complicated envelope. In one particular sample we have, however, observed the regular

behaviour displayed in fig. 1, which cannot be ascribed to the quantum point contacts. It turns out that other examples exist in the literature of such quasiperiodic behaviour<sup>6,7,8</sup>). In the following we describe our experiment and put our results and the available data from the literature in the perspective of a spectral density of a circular quantum dot with a billiard or parabolic type confinement.

#### EXPERIMENTAL DETAILS

The quantum dot is formed in a low carrier density ( $n_{2D}=1.4 \cdot 10^{11}$   $\text{cm}^{-2}$ ) 2-dimensional electron gas with high mobility ( $\mu=1 \cdot 10^6$   $\text{cm}^2/\text{Vs}$ ). 3 split gates form the quantum dot into a roughly circular shape with a diameter of 0.6  $\mu\text{m}$  and holding 350 (or less) electrons for the bias conditions of fig. 1 and 2. A SEM micrograph of the split gate configuration is seen as an insert to fig. 1. The two quantum point contacts act as source and drain for the quantum dot. The quantum point contact split gate voltages were adjusted to obtain significantly different conductances, when  $V_c < -0.5\text{V}$ . The center split gate voltage was adjusted to obtain a suitable quantum dot. The depletion voltage of the gates were  $-0.17\text{V}$ , and the quantum point contacts pinched off at split gate voltages  $-0.23\text{V}$  and  $-0.29\text{V}$ , when biased separately, whereas the center splitgate had a pinch off voltage of  $-1.65\text{V}$ , with zero bias on the two outer split gates. The self-capacitance of the quantum dot is  $C_0 \approx \pi \epsilon_r \epsilon_0 2R \approx 6 \cdot 10^{-16}\text{F}$  corresponding to a Coulomb energy of  $e^2/C_0 \approx 0.3\text{meV}$ . The experiment was carried out at very low temperatures,  $T \approx 20\text{mK}$ . The sample was well shielded from higher temperatures by filters in the leads, and we estimated the noise

temperature of the sample to be below 40mK from watching the temperature dependence of the fractional quantum Hall effect in another experiment. The conductance was measured by an a.c. lock-in technique with an excitation current of 1 nA and a lock-in frequency of 33 Hz.

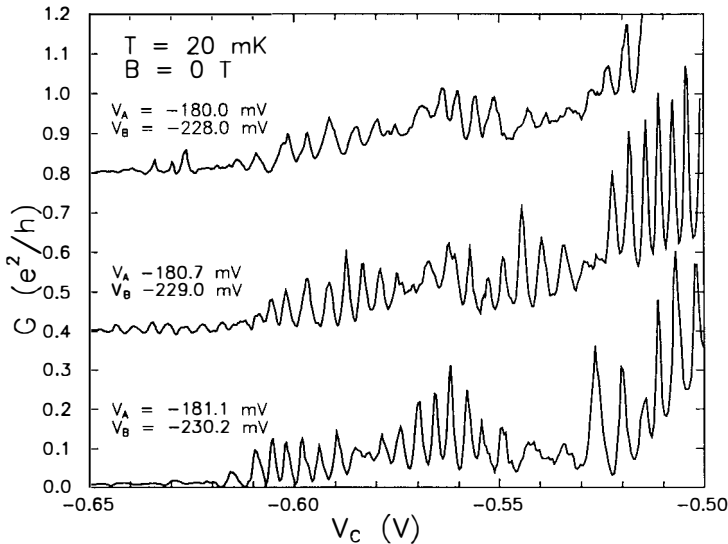


Fig.2. 3 conductance versus center gate voltage curves with different settings of the quantum point contact split gates. The sample is the same as used for fig. 1.  $B=0T$ ,  $T=20mK$ . The periodic envelope of the Coulomb blockade oscillations is very sensitive to the status of the quantum point contacts.

In fig.2 we show another set of data on the same sample as used for fig.1. The conductance through the quantum dot is measured as a function of the center split gate voltage for three split gate voltage settings for the two quantum point contacts. It turns out that the envelope of the Coulomb blockade oscillations shown in fig.1 is a very sensitive function of the split gate settings of the two quantum point contacts. Changes of

only 1mV on the values -230mV and -180mV made considerable change and almost washed out the periodic envelope.

#### SEMICLASSICAL TRAJECTORIES IN A CIRCULAR QUANTUM DOT

A classical billiard with a long mean free path and perfect specularity at the confinement has been predicted to have non-periodic (chaotic) orbits except for particularly symmetric confinements such as a circle<sup>9)</sup>. GaAs quantum dots have been considered a possible testground for such calculations and their quantum mechanical analogues<sup>5,6)</sup>. We attempt to interpret our experimental results fig.1 and fig.2 in terms of a circular confinement. It is wellknown that the eigen-energy spectrum can be represented by Bohr-Sommerfeld quantization on classical periodic trajectories as indicated in the insert to fig.3. This has been particularly developed for nuclei<sup>10)</sup> and 3-dimensional clusters<sup>11)</sup>, where it turns out that triangular and quadratic orbits dominates the spectrum leading to shell and supershell effects.

Solving the Schrödinger equation for the circular confinement with hard walls is straightforward. The large dominance of one or a few types of orbits makes it however possible in a simple way to extract the main features of the density of states for the quantum dot. This approach is used to calculate the periodicity of the level density with the number of electrons in the dot. As the simplest approach we only consider the dominant penduling orbit (see insert to fig. 3). For a circular quantum billiard penduling orbits (see insert to fig.3) can be shown to have a 3 times larger Fourier amplitude than the triangular

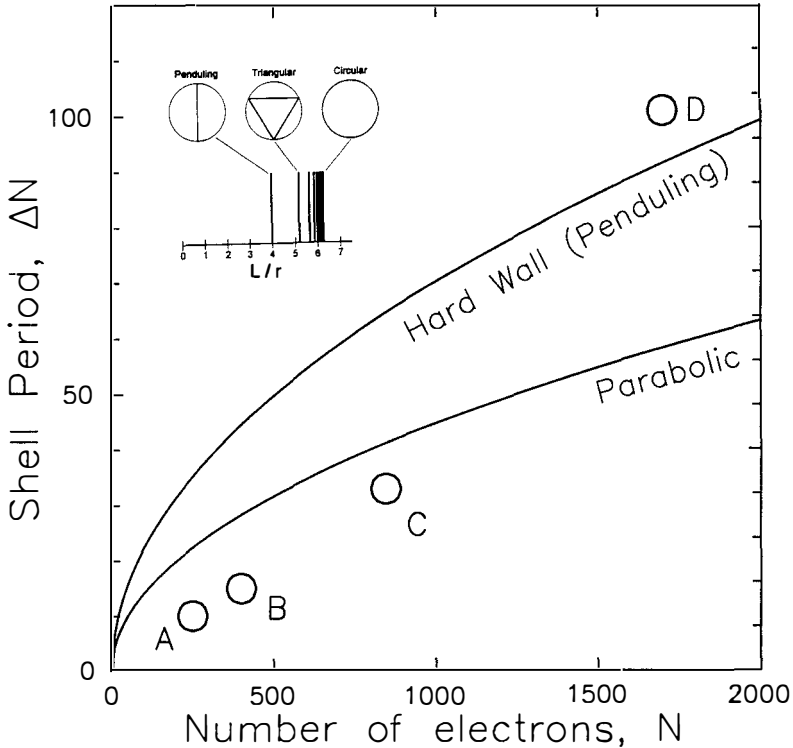


Fig.3. Shell period ( $\Delta N$ , in number of electrons) as a function of the number of electrons in a quantum dot,  $N$ . The two curves are for a quantum dot with a circular shape. The upper curve is for a hard wall flat bottom confinement potential, where the pendling semiclassical orbit dominates in the Bohr-Sommerfeld quantization condition ( $\Delta N = \pi(N/2)^{1/2}$ ). The lower curve corresponds to a parabolic confinement potential ( $\Delta N = (2N)^{1/2}$ ). The 4 circles are experimental points. A is from ref.7, B is from this work (fig. 1 and 2), C is from ref.8 and D is taken from ref.6. Note that it is expected that quantum dot confinement potentials are parabolic for small dots and hard walled for large dots. The insert shows three circular hardwalled quantum dots with a pendling orbit, a triangular orbit and a circular orbit. The circular orbit may be considered the limit of a periodic orbit with infinitely many scatterings at the hard-walled potential. For a sphere the triangular and quadratic orbit has the largest (by a factor of 10) Fourier amplitudes<sup>10</sup>. For a circular disk the pendling orbit has a 3 times larger Fourier component than the triangular orbit, which in turn is much larger than any of the subsequent orbits<sup>12</sup>.  $L/r$  is the length of the orbits measured in units of the radius.

orbit, which again has a much larger Fourier amplitude than orbits with 4 or more boundary touches<sup>12)</sup>. Applying the Bohr-Sommerfeld quantization rule  $\oint (2mE_f)^{1/2} dr = nh$ , where the integral is taken over twice the diameter, we find shells corresponding to integer  $n$  as deltafunctions in the density of states at Fermienergies  $E_f = (hn/a)^2/32m$ , where  $a$  is the radius of the dot. The total number of electrons becomes  $N = (\pi n)^2/8$  leading to a periodicity in the density of states,  $\Delta N = \pi(N/2)^{1/2}$ , as a function of total number,  $N$ , of electrons. In fig.3 we have plotted this shell period for a circular billiard as a function of  $N$ . The billiard model is only expected to be valid for large quantum dots. For smaller quantum dots a parabolic confinement potential is more appropriate. For a parabolic confinement,  $\frac{1}{2}m\omega^2 r^2$ , all the different classical orbits gives a series of shells with the energies  $\hbar\omega(n+\frac{1}{2})$ . The total number of electrons is  $N = \frac{1}{2}n^2$  and the number of electrons in each shell is  $\Delta N = (2N)^{1/2}$ . This shell period is also plotted in fig.3 as a function of  $N$ . The shell period of the sample, fig.1 and fig.2, is shown in fig.3 as the point marked B. We have also plotted the shell period extracted from conductivity of a quantum dot without Coulomb blockade from ref.6 as point D. In the literature on Coulomb blockade of quantum dots periodic variation of the envelope has been reported several times. Pronounced are the results of ref.7 and 8, from which we have extracted the points A and C.

#### CONCLUSION

We have experimentally investigated a quantum dot, which has a particularly pronounced periodic variation of the Coulomb

blockade conductance peaks. The peaks are interpreted as reflecting a maximum in the electronic level density. We therefore believe to have found a shell structure for particular electron numbers in a quantum dot. In a separate article, we have also extracted a shell period from conductivity oscillations without Coulomb blockade interference<sup>6</sup>. We have extracted 2 datapoints from articles in the literature on quantum dots, which also reports a periodic variation of the coulomb blockade envelope. The 4 point fall on a curve, which for low numbers of electrons in the dots (A, B, and C) are close to the expected shell period of a quantum dot with a parabolic confinement potential and at high electronic number (D) is close to the shell period expected for a circular billiard.

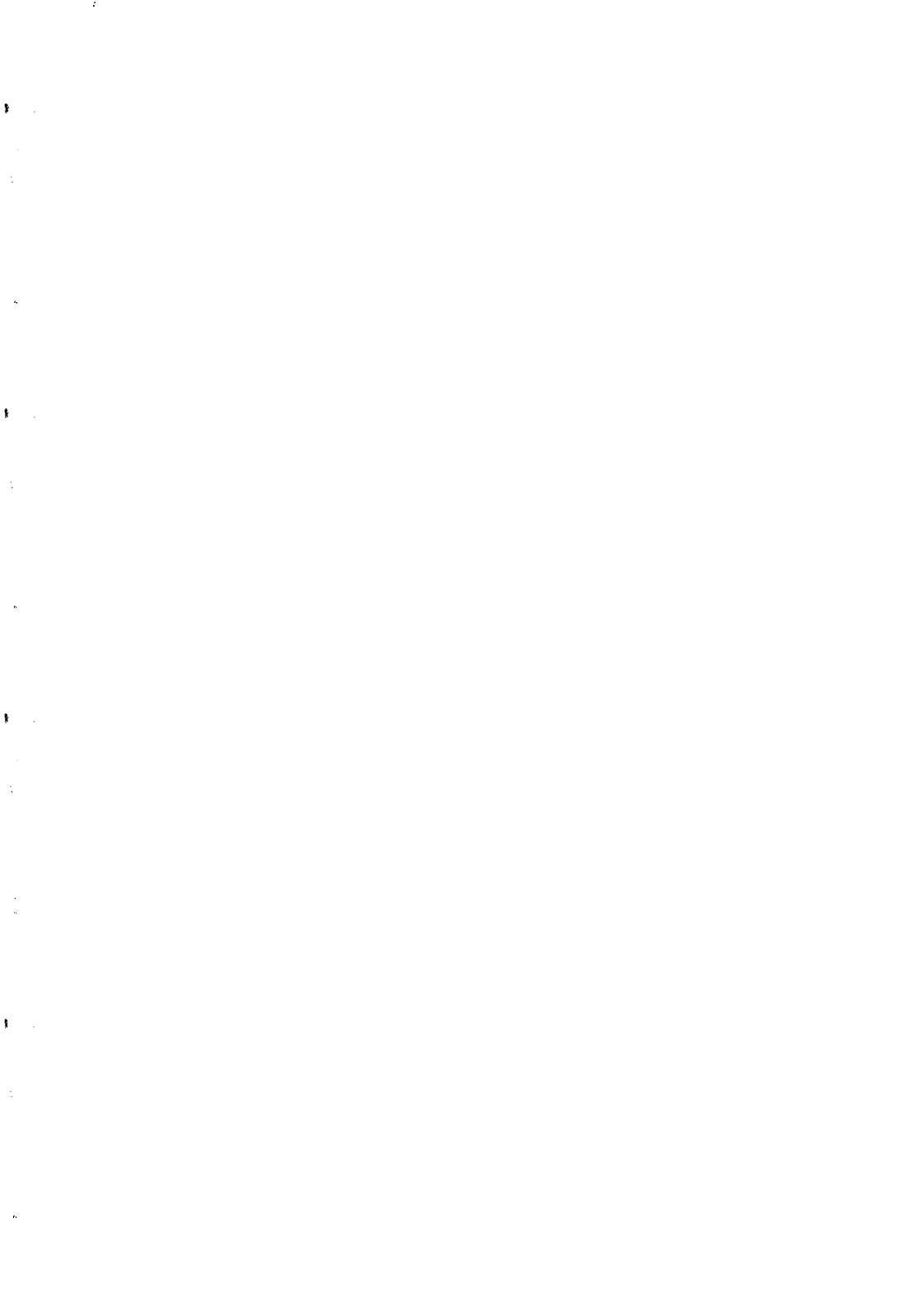
#### ACKNOWLEDGEMENT

Our research was supported by the joint III-V Nanolab of the Danish Microelectronic Centre and the Niels Bohr Institute. C.B. Sørensen has furnished us with MBE samples and M. Bøgelund Jensen has been technical assistant on the project. Discussions with Mathias Brack (Regensburg) on shell effects in 2 dimensions and with R. Taboryski about III-V mesoscopics has been valuable.

#### REFERENCES

1. M.A. Kastner, *Physics Today*, Vol.46(1), pp.24-31 (1993).
2. A.T. Johnson, L.P. Kouwenhoven, W. de Jong, N.C. van der Vaart, and C.J.P. Harmans, *Phys.Rev.Lett.* 69, 1592 (1992).
3. E.B. Foxman, P.L. McEuen, U. Meirav, N.S. Wingreen, Y. Meir, P.A. Belk, N.R. Belk, M.A. Kastner, and S.J. Wind, *Phys.Rev. B* 47, 10020 (1993).

4. R.C. Ashoori, H.L. Stormer, J.S. Weiner, L.N. Pfeiffer, W. Baldwin, and K. West, *Phys.Rev.Lett.* 71, 613 (1993).
5. C.M. Marcus, A.J. Rimberg, R.M. Westervelt, P.F. Hopkins, A.C. Gossard, *Phys.Rev.Lett.* 69, 506 (1992).
6. M. Persson, P.E. Lindelof, B. von Sydow, J. Pettersson, T. Claeson, and A. Kristensen: "Conductance oscillations of a circular quantum dot as a function of size and weak magnetic fields", preprint; M. Persson, B. von Sydow, P.E. Lindelof, J. Pettersson, A. Kristensen, and T. Claeson, *Recontres de Moriond*, this volume.
7. L.P. Kouwenhoven, A.T. Johnson, N.C. van der Vaart, C.J.P. Harmans, and C.T. Foxon, *Phys.Rev.Lett.* 67, 1626 (1991).
8. A.A.M. Staring, B.W. Alphenaar, H. van Houten, L.W. Molenkamp, O.J.A. Buyk, M.A.A. Mabe-soone, and C.T. Foxon, *Phys.Rev.(RC) B* 46, 12869 (1992).
9. A.D. Stone, and H. Bruus, *Physica B* 189, 43 (1993).
10. R. Balian and C. Bloch, *Annals of Physics* 69, 76 (1972).
11. H. Nishioka, K. Hansen, and B.R. Mottelson, *Phys.Rev. B* 42, 9377 (1990).
12. S.M. Reimann, M. Brack, A.G. Magner, and M.V.N. Murthy: "Limitation of periodic orbit theory in quantum billiards with small scattering centers", preprint.



# TUNNELING SPECTROSCOPY ON THE LIGAND STABILIZED METAL CLUSTER $\text{Pt}_{309}\text{Phen}_{36}^*\text{O}_{30}$

J.G.A. Dubois<sup>1</sup>, J.W. Gerritsen<sup>1</sup>, E.J.G. Boon<sup>1</sup>, G. Schmid<sup>2</sup>, and H. van Kempen<sup>1</sup>

<sup>1</sup> *Research Institute for Materials, University of Nijmegen, Toernooiveld, 6525 ED Nijmegen, The Netherlands*

<sup>2</sup> *Institut für Anorganische Chemie, Universität Essen, Universitätstrasse 5-7, 4300 Essen 1, Germany*

## Abstract

We performed low temperature (4.2 K) scanning tunneling microscopy and spectroscopy on  $\text{Pt}_{309}\text{Phen}_{36}^*\text{O}_{30}$  clusters, that were deposited on a bare Au[111] surface. Spectroscopic curves above the clusters showed clear charging effects, indicating that the cluster core is metallic and the ligand shell surrounding the cluster is insulating.

## 1 Introduction

The invention of scanning tunneling microscopy (STM) by Binnig and Rohrer (for a review on scanning tunneling microscopy and spectroscopy see e.g. [1]) has opened the possibility of very local tunneling spectroscopy, even down to an atomic scale. Furthermore STM allows to combine this spectroscopic capability with topographic information: high resolution topographic images (0.1 Å) can be obtained and spectroscopy can be performed on specific sites of the sample. In this contribution we describe STM results, performed at 4.2 Kelvin, on ligand stabilized metallic particles that are deposited on a Au[111] surface.

Many STM experiments have been reported on small isolated metallic particles [2, 3, 4, 5, 6, 7]. In this type of experiments we obtain a situation with two tunnel junctions in series: one between the tip and the cluster and one between the cluster and the substrate (fig. 1). The main feature that is observed in this situation is a stepwise increase of the tunnel current as a function of bias voltage. This effect is called the Coulomb

staircase (CSC). The origin of this CSC are the small capacitances between tip and cluster and between cluster and substrate. Since these capacitances are very small (order  $10^{-18}$  F), the energy for charging such a small capacitance with one single electron ( $e^2/2C$ ) may be large compared to the thermal energy ( $k_B T$ ). Especially at liquid helium temperatures this charging effect may dominate the tunnel characteristics. As a result the tunnel current will show the above mentioned stepwise increase. For a recent review on this subject we refer to ref. [8].

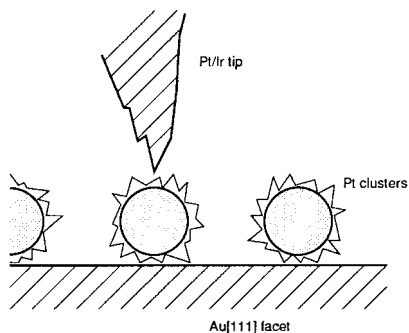


Fig. 1. Experimental situation in a tunnel experiment through an isolated metallic particle. There are two tunnel barriers in this situation: one between the tip and the cluster and one between the cluster and the substrate. Both tunnel junction have a very small capacitance.

The experiments on small isolated metallic particles are usually performed on a sample consisting of *substrate-thin oxide-evaporated islands*. Here we report results on a different type of sample consisting of a *bare Au[111] surface with ligand stabilized clusters on top*. An advantage of these samples is that we do not need an insulating oxide.

## 2 Experimental

The STM used in this study is a home-built stainless steel design, that routinely operates at 1.3 and 4.2 Kelvin. The STM is in the center of a 9.5 Tesla superconducting magnet. Rough approach is achieved with a differential screw.

The clusters that we used are full shell ligand stabilized  $\text{Pt}_{309}\text{Phen}^*_36\text{O}_{30}$  clusters (named  $\text{Pt}_{309}$  hereafter). These clusters consist of a core of 309 Pt atoms (ordered in a fcc lattice), that is surrounded by a ligand shell of phenanthroline and  $\text{O}_2$  molecules. There are some advantages of this type of clusters above the normally used evaporated islands on an insulating oxide. First of all the size and geometry of the clusters is very well known and the same for all clusters. Secondly the ligands that stabilize the cluster can be used as a tunnel barrier, instead of the normally used oxides. These oxides have impurity levels, that may get charged and discharged, thus giving rise to time dependent effects (see e.g. [4]). Because of these two advantages the experimental situation in our experiment might be less complicated. However, the unknown nature of the ligand shell may complicate the situation. For a review on the physical aspects of ligand stabilized clusters we refer to [9].

The substrate on which the clusters are deposited is a Au[111] surface. This surface is produced by melting gold and cooling it down fast. In this way facets of about  $0.5 \times 0.5 \text{ nm}^2$  form. On these facets we deposited a droplet of the solution with the clusters in water. This droplet was blown off after a few seconds with nitrogen gas and some clusters remain on the surface. STM images of samples that were produced in this way mostly showed either densely packed clusters or an uncovered Au[111] surface, but sometimes single clusters were observed. Due to the interaction between the STM tip and the clusters, topographic images were only reproducible at high tunnel resistance (typically 1 GOhm) [10, 11].

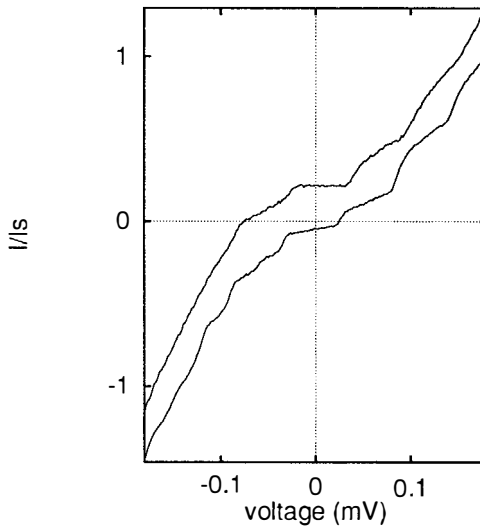


Fig. 2. Spectroscopic curves above a  $\text{Pt}_{309}$  cluster at 4.2 K. The two different curves are taken at different distance between tip and cluster. For both curves the set point for the voltage is 0.18 Volt and for the current: 20 pA for the upper curve and 30 pA for the lower curve. The current indicated in the picture is normalized to this set point value  $I_*$ . The curves are offset for clarity. At small distances between tip and cluster a sharpening of the features occurs and additional steps in the current are resolved (these additional steps are best resolved at negative bias).

### 3 Results

Figure 2 shows spectroscopic results obtained above a single cluster at 4.2 Kelvin. The different curves are taken at different tip-cluster distance. At large tip-cluster distance (high resistance between tip and cluster) we observe a regular CSC (see figure 2, upper curve). However, when the distance between tip and cluster is decreased we observe a sharpening of the features and irregular steps occur. Both effects are not predicted by the orthodox theory (see for example [8]). First of all the theory predicts a flattening of steps if the tip-cluster resistance is decreased, since then the two different resistances of the two tunnel junctions are closer to each other (in regular STM operation the resistance between tip and cluster is much larger than the resistance

between cluster and substrate, since otherwise the feedback system will not work). The irregularity of the steps is also not predicted in the theory for particles that have a constant density of states. However, when the clusters are small enough to cause level splitting of the electron states inside the cluster, irregular steps associated with the discrete levels inside the cluster may occur [12, 13, 14]. Quantum size effects may indeed become important in cluster of the size we studied. A rough estimate of the splitting due to this effect gives  $4E_F/3N \approx 3$  meV (where  $E_F$  is the Fermi energy of bulk platinum and  $N$  is the number of electrons inside the cluster (3090 in our case)).

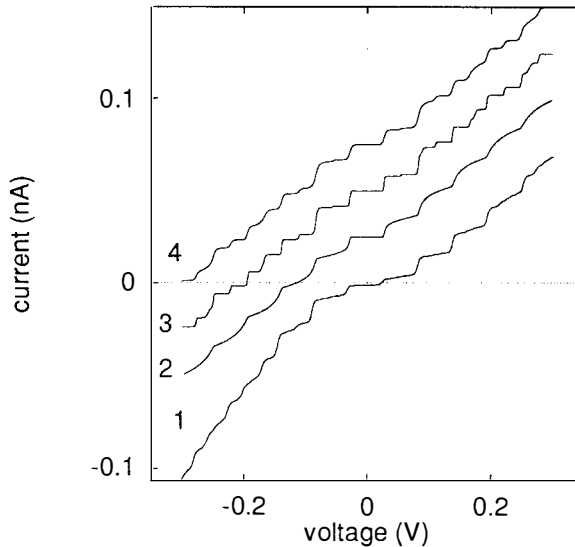


Fig. 3. Tunnel characteristic obtained above a single  $P_{309}$  cluster at 4.2 K (curve 1) and three theoretical fits. Curve 2 is calculated using the orthodox theory without taking into account discrete energy levels of the cluster. The fit parameters for this curve are:  $R_1 = 200$  MOhm,  $R_2 = 3300$  MOhm,  $C_1 = 1$  aF,  $C_2 = 2.9$  aF and  $Q_0 = -0.01$ . Curve 3 takes into account a level splitting of 21 meV and the other parameters are the same as for curve 2. Curve 4 has the same parameters as curve 3, but takes into account heating effects due to the high current density (the effective temperature for this fit is  $T^* = 15$  K). All curves are offset for clarity and have zero current at zero bias.

Figure 3 shows a measurement and calculations. The curve that does not take any discrete levels of the cluster into account (curve 2) is not very close to the measurement. Especially the additional steps at negative bias side are not present in this calculation. However, both curves that take discrete levels into account (3 and 4) show these additional steps. The difference between these two last curves is that curve 4 is calculated at a higher effective temperature  $T^*$  (15 Kelvin in instead of the bath temperature of 4.2 Kelvin) and thus takes heating effects into account that may be caused by the high current densities through the cluster. At negative bias side this curve is very close to the measured data. From this fit we see that the level splitting that we extract from the data (21 meV) is considerably larger than the estimated value. There are several effects that may cause this discrepancy. First of all it is not likely that the outer platinum shell is contributing to the conduction electrons

due to the bonding of the ligands [15]. This would reduce the number of electrons to 1470 and hence double the estimated splitting. A second effect that may play a role is that the clusters are highly symmetric which causes degeneracies and therefore increases the level splitting. The last effect that may be important is that it is expected that the level splitting around the Fermi level (which is the energy range that we are looking at in our experiment) is larger than the average level splitting [16].

However, for some clusters we observe CSC's that indicate an even larger splitting of about 50 meV (figure 4). Although the irregular steps are in good agreement with the theory if we take discrete energy levels into account, the differences between the estimated and measured values of this energy splitting is very large. Therefore we don't want to exclude other effects that possibly might cause irregular steps. Especially the ligand shell might cause additional effects. There might for example be localized electron states in this ligand shell which cause additional structure. It is also possible that, although the ligands are good insulators, there are more spots on the cluster where tunneling to the substrate occurs. If this is the case we obtain a situation of a few double tunnel junctions in series which also may complicate the interpretation of the data.

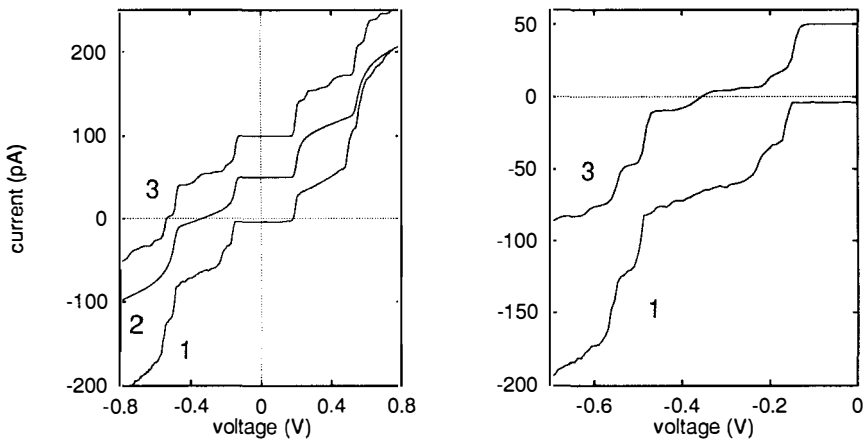


Fig. 4. A measured spectroscopic curve that shows a very large splitting of the steps (curve 1). Also indicated are two calculated curves: one without level splitting of the cluster (2) and one with level splitting (3). The fit parameters are:  $C_1=0.47$  aF,  $C_2=0.16$  aF,  $R_1=3.6$  MOhm,  $R_2=0.18$  MOhm,  $Q_0=-0.08$ ,  $T^*=40$  K and the level splitting (only used in the upper curve) 50 meV. The figure on the right shows the negative bias part of the measurement and the curve calculated with level splitting

## 4 Conclusions

Tunneling spectroscopy on  $\text{Pt}_{309}\text{Phen}_{36}\text{O}_{30}$  clusters showed clear charging effects. From this observation we can conclude that the core of these clusters is metallic. Furthermore it shows that the ligands that stabilize these clusters are good insulators. However, in addition to the charging effect we observed structure on a smaller energy scale. Although this structure is consistent with discrete energy levels of the clusters, also other effects

may cause the observed structure.

This work is supported by the Dutch Foundation for Fundamental Research of Matter FOM, which in turn is financially supported by the Dutch Organization for Scientific Research NWO. This research is also part of an EC Science Project SCI-CT92-0788. We would like to thank J.G.H. Hermesen for technical support.

## References

- [1] L.E.C. van de Leemput and H. van Kempen, *Rep. Progr. Phys.* **55**, 1165 (1992).
- [2] P.J.M. van Bentum, R.T.M. Smokers and H. van Kempen, *Phys. Rev. Lett.* **60**, 2543 (1988).
- [3] R. Wilkins, E. Ben-Jacob and R.C. Jaklevic, *Phys. Rev. Lett.* **63**, 801 (1989).
- [4] J.G.A. Dubois, E.N.G. Verheijen, J.W. Gerritsen, and H. van Kempen, *Phys. Rev.* **B48**, 11260 (1993).
- [5] K.A. McGreer, J.-C. Wan, N. Anand, and A.M. Goldman, *Phys. Rev.* **B39**, 12260 (1989).
- [6] A.E. Hanna and M. Tinkham, *Phys. Rev.* **B44**, 5919 (1991).
- [7] C. Schönenberger, H. van Houten and H.C. Donkersloot, *Europhys. Lett* **20**, 249 (1992).
- [8] D.V. Averin and K.K. Likharev, in *Mesoscopic Phenomena in Solids*, edited by B.L. Altshuler, P.A. Lee and R.A. Webb (Elsevier Science Publisher, 1991), p.173.
- [9] L.J. de Jongh, H.B. Brom, J.M. van Ruitenbeek, R.C. Thiel, G. Schmid, G. Longoni, A. Ceriotti, R.E. Benfield, and R. Zanon, in *Cluster Models for Surface and Bulk Phenomena*, edited by G. Pacchioni, P.S. Bagus and F. Parmigiani (Plenum Press, New York, 1992), p. 151.
- [10] H.A. Wierenga, L. Soethout, J.W. Gerritsen, L.E.C. van de Leemput, H. van Kempen, and G. Schmid, *Adv. Mater.* **2**, 482 (1990).
- [11] L.E.C. van de Leemput, J.W. Gerritsen, P.H.H. Rongen, R.T.M. Smokers, H.A. Wierenga, G. Schmid, and H. van Kempen, *J. Vac. Sci. Technol.* **B9**, 814 (1991).
- [12] D.V. Averin and A.N. Korotkov, *J. Low Temp. Phys.* **80**, 173 (1990).
- [13] D.V. Averin, A.N. Korotkov and K.K. Likharev, *Phys. Rev.* **B44**, 6199 (1991).
- [14] M. Amman, R. Wilkins, E. Ben-Jacob, P.D. Maker, and R.C. Jaklevic, *Phys. Rev.* **B43**, 1146 (1991)
- [15] F.A. Mulder, T.A. Stegink, R.C. Thiel, L.J. de Jongh, and G. Schmid, *Nature in press*.
- [16] O.B. Christensen, K.W. Jacobsen, J.K. Nørskov, and M. Manninen, *Phys. Rev. Lett.* **66**, 2219 (1991).

## CRYOGENIC PRECISION CAPACITANCE BRIDGE USING A SINGLE ELECTRON TUNNELING ELECTROMETER

R.N. Ghosh,\* A.F. Clark, B.A. Sanborn, and E.R. Williams  
*National Institute of Standards and Technology  
Gaithersburg, Maryland 20899, USA*

The value of the electronic charge can be determined by placing a known number of electrons on a calibrated capacitor and measuring the resulting voltage, which can lead to a measure of the fine structure constant,  $\alpha$ . Single electron tunneling (SET) electrometers with sufficient sensitivity for this application have been fabricated. We report on the design and preliminary results of a capacitance bridge experiment using an SET electrometer as a detector to measure two capacitors in a dilution refrigerator. AC measurements of the capacitance ratio have a precision of one part in  $10^4$  and DC measurements provide information on the leakage rate of the standard capacitors.

### I. INTRODUCTION

The single-electron-tunneling (SET) transistor can be used as a highly sensitive electrometer,<sup>1)</sup> and noise figures of  $10^{-4}e/\sqrt{\text{Hz}}$  at 10 Hz have been reported.<sup>2)</sup> We have proposed an experiment<sup>3)</sup> to measure the fine structure constant  $\alpha$  by counting electrons on a standard capacitor. This experiment<sup>3)</sup> uses the sensitivity of the SET electrometer to small changes in charge on a coupling capacitor in order to monitor the voltage on an isolated island while electrons are being pumped onto the island. For the technique to be successful, the amount of charge pumped onto the island must be a well-defined quantity throughout the measurement time. Therefore, the leakage rate of charge from the island must be small in order to achieve metrological accuracy. In this paper, we report on a cryogenic capacitance bridge balance experiment which is a prerequisite to a precision measurement of  $\alpha$ . We determined the AC and DC capacitance ratio of two standard capacitors in a dilution refrigerator, as well as the leakage rate of the capacitors.

## II. THE SET ELECTROMETER

The SET electrometer, shown schematically in the left portion of Fig. 1a, consists of two nanoscale normal metal/insulator/metal tunnel junctions in series, represented by the double-box symbols. If the junctions are designed so that their tunneling resistances are large compared to the resistance quantum  $h/e^2$ , and if the capacitance  $C_\Sigma$  seen by the island between the junctions is small compared to  $e^2/2k_B T$ , the tunneling probability is greatly reduced for  $|V_E| < e/2C_\Sigma$ , the Coulomb blockade region. Under these conditions, the tunneling current  $I$  through the junctions can be sensitively controlled by varying the gate voltage  $U$  across the capacitor  $C_0$ . At constant bias  $V_E$ , the SET current undergoes oscillations as  $U$  is varied, with period  $\Delta U = e/C_0$ . To use the transistor as an electrometer, the voltages  $V_E$  and  $U$  are fixed at levels chosen to maximize sensitivity of the device, so that  $I$  is linearly proportional to small changes in charge induced on the interjunction region. The electrometer is then highly sensitive to charge induced on the coupling capacitor  $C_c$ , and it provides a high impedance technique to measure the potential controlling the charge on  $C_c$ .

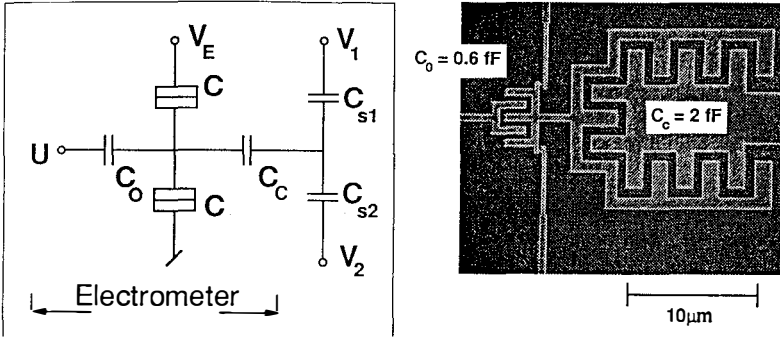


FIG. 1. a) Schematic of capacitance bridge circuit for determining the ratio of the standard capacitors  $C_{s1}$  and  $C_{s2}$ . b) Scanning electron micrograph of the SET electrometer.

The electrometer can be used as a null voltage detector in order to balance the two arms of a bridge circuit. The proposed experiment<sup>3)</sup> to determine  $\alpha$  uses an SET pump to place  $n$  electrons on a standard capacitor  $C_s$  and then measures the resulting voltage  $V_s$ . In terms of this voltage and capacitance,  $e$  is determined from the relationship  $ne = C_s V_s$ . If  $V_s$  is related to the Josephson voltage standard, then  $\alpha$  can be determined by comparing  $C_s$  to the calculable capacitor. The circuit in reference 3 is a variant of a bridge balance with the SET pump on one arm and the standard capacitor on the other arm. An SET electrometer is used to maintain a constant potential at the isolated island while electrons are pumped onto the island.

### III. AC CRYOGENIC CAPACITANCE BRIDGE

In order to explore issues relevant to the experiment to measure  $\alpha$ , we have experimented on a cryogenic capacitance bridge using an SET electrometer to determine the capacitance ratio of two fused silica capacitors at 10 mK. The electrometer in the left portion of Fig. 1a, including the coupling capacitor  $C_c$ , was fabricated on a single chip. Electron beam lithography and a shadow evaporation technique<sup>4)</sup> were used to fabricate Al/AIO/Al tunnel junctions on an oxidized Si substrate. We can make  $(30 \text{ nm})^2$  junctions which are reproducible across several  $1 \text{ cm}^2$  dies. The electrometer chip has four electrodes, two for voltage leads and one each for the gate capacitor  $C_0$ , and the coupling capacitor  $C_c$ . The chip was placed inside one chamber of a three chamber copper box with each standard capacitor in a separate chamber. The standard capacitors are metallized fused silica disks with a grounded guard ring and have a nominal capacitance of 1 pF. By separating the two standard capacitors from one another and the electrometer chip, we insured that  $C_{s1}$  and  $C_{s2}$  each have a well defined capacitance. Coaxial leads were used for the two voltage leads  $V_1$  and  $V_2$ . The assembled copper box was then thermally anchored to the platform of the dilution refrigerator.

In order to make precision measurements, a ground shield must be provided to prevent the potentials  $V_1$  and  $V_2$  from affecting the electrometer except through their respective capacitances. Stray capacitance to ground will degrade the electrometer sensitivity, and therefore it must be kept small. The sensitivity of the electrometer to the bridge balance point is proportional to  $C_c/(C_{s1} + C_{s2} + C_g)$ , where  $C_g$  represents all stray capacitance to ground. We have measured  $C_g$  to be 5 pF, which is reasonably close to our target of a few pF. Choosing  $C_s = C_{s1} + C_{s2}$  to be small both increases  $V_s$  and maximizes the electrometer sensitivity. A practical choice for  $C_s$  is 1 pF, because it is of similar magnitude to  $C_g$  as well as a convenient value to compare with existing capacitance standards. Our tunnel junction capacitances are typically a few tenths of a femtofarad. A large value for  $C_c$  would increase the electrometer sensitivity, however  $C_c$  also contributes directly to the electrometer island capacitance, thus reducing the Coulomb charging energy. We measured  $C_c$  to be 2 fF in our experiment.

For the AC bridge balance experiment, an inductive divider together with a 1:1 doubly-shielded transformer and an AC signal generator ( $V_{cap}$ ) was used to supply the potentials  $V_1$  and  $V_2$ .<sup>5)</sup> At balance,  $C_{s2}/C_{s1} = V_1/V_2 = Z_1/Z_2$  where  $Z_1$  is the setting of the inductive divider and  $Z_2 = 1 - Z_1$ . In order to improve our signal to noise ratio, a lock-in amplifier was used to detect the AC electrometer current that was in phase with  $V_{cap}$ . We also slowly ramped the gate voltage  $U$  to ensure that the electrometer was functioning properly. Fig. 2 shows the capacitance bridge data at 10 Hz and a platform temperature of 10 mK. We deduce from these data that the ratio

of the two capacitors is  $C_{s2}/C_{s1} = 1.0377 \pm 0.0001$  (one  $\sigma$ ), where the precision of our measurements is one part in  $10^4$ . Bridge balance measurements were also made at 270 Hz. Our precision was limited by the magnitude of the out-of-phase or quadrature signal. We therefore performed a double bridge experiment to determine both the in-phase and quadrature signals by introducing an orthogonal component to  $V_{cap}$  to cancel the quadrature signal. The large dissipation in the standard capacitors affected the SET oscillations and prevented an increase in the sensitivity of the bridge.

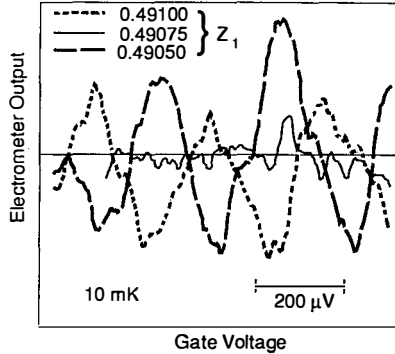


FIG. 2. AC bridge balance data. The solid line is the electrometer output at balance,  $Z_1 = 0.49075$ . The dashed and dotted lines are the off-balance traces which show SET oscillations due to charge accumulation on the island between the two standard capacitors.

#### IV. DISSIPATION

One of the advantages of our cryogenic capacitance bridge is the ability to make both AC and DC measurements. The DC capacitance ratio of the standard capacitors was measured using a resistive divider together with a battery ( $V_{cap}$ ).<sup>5</sup> With the platform temperature at 10 mK, we found  $C_{s2}/C_{s1} = 1.036 \pm 0.25\%$ . Our precision was limited by a slow decay of the applied bias  $V_{cap}$  at balance. A second DC experiment was performed to measure the leakage rate of the standard capacitors at cryogenic temperatures. The two voltage leads  $V_1$  and  $V_2$  shown in Fig. 1a were connected together and a step voltage  $V_{step}$  was applied to the standard capacitors in parallel. In this configuration, the electrometer is sensitive to the charge induced on  $C_c$  by the potential  $V_c = V_{step}[1 + C_g/(C_{s1} + C_{s2})]^{-1}$ . If there were no leakage current at all, the electrometer output as a function of time would show rapid initial SET oscillations in response to the polarization charge induced by the step, but would detect no subsequent charge motion. In fact, after the initial response, we observed continued SET oscillations with increasing period as time progressed. This indicates

that the electrometer was responding to charge on  $C_c$  controlled by a potential that was decaying with time.

The inset to Fig. 3 shows the SET oscillations against time observed after a 1.35 V step voltage was applied to the standard capacitors in parallel ( $C_{s1} + C_{s2} = C_s$ ). Since each oscillation corresponds to one electron charge induced on the coupling capacitor  $C_c$ , the trace represents a voltage decay across  $C_s$ . Plotted in Fig. 3 is  $N(t)$ , the number of zero crossings as a function of time between  $t$  and  $T$ , where  $T$  is the final observation time. The times  $t$  were chosen so that  $t \geq t_o$ , where  $t_o$  is a time after the initial polarization response.  $N(t)$  equals twice the number of charges induced at times between  $t$  and  $T$ . If charge leaked from  $C_s$  and induced charge on  $C_c$  at random times in the interval  $(t_o, T)$ , then the curve would correspond to a simple exponential form with a single leakage rate. Fig. 3 shows that the data do not fit this form. However,  $N(t)$  fits remarkably well to a sum of two exponentials, which indicates that the rates of two mutually dependent processes are governing the SET current. One model that is consistent with the two-exponential form is a two-level system subject to a decay process. Random telegraph switching between two charge states is frequently observed in SET devices<sup>2)</sup> and the rate for this process could be folded into the measured leakage rate.

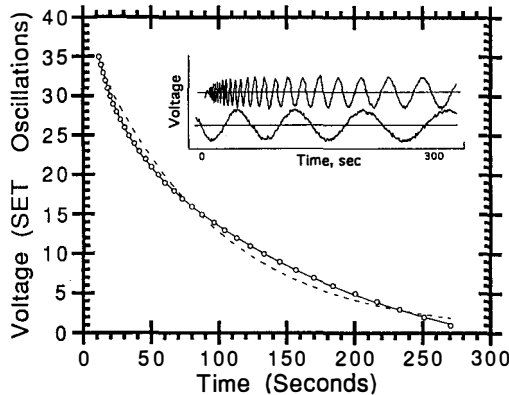


FIG. 3. SET oscillations vs time after application of 1.35V step voltage. The open circles are the experimental data points. The fit to a single exponential is shown by the dashed curve and the sum of two exponentials is shown by the solid curve.

From the data in Fig. 3, the apparent leakage rate measured by the SET electrometer is on the order of one charge per second, which is equivalent to a leakage resistance of  $10^{12}\Omega$  for the parallel combination of  $C_{s1}$  and  $C_{s2}$ . Using a standard laboratory electrometer and a 45 V battery outside the cryostat, we obtain a lower

bound of  $10^{14} \Omega$  for the leakage resistance across  $C_{a1}$  and  $C_{a2}$  in series at cryogenic temperature. Environmental noise caused by excessive dissipation could influence the SET electrometer signal and may be the reason we were limited in our ability to increase the voltage ( $V_{cap}$ ) applied to the bridge. We are currently investigating the mechanisms responsible for the measured DC leakage and AC quadrature signal. If the dissipative signal is due to the leakage across the standard capacitors, alternative fabrication techniques, such as an air capacitor, can greatly improve the situation. To obtain a precision measurement of  $\alpha$  as described in reference 3, we will need many orders of magnitude improvement on our standard capacitors.

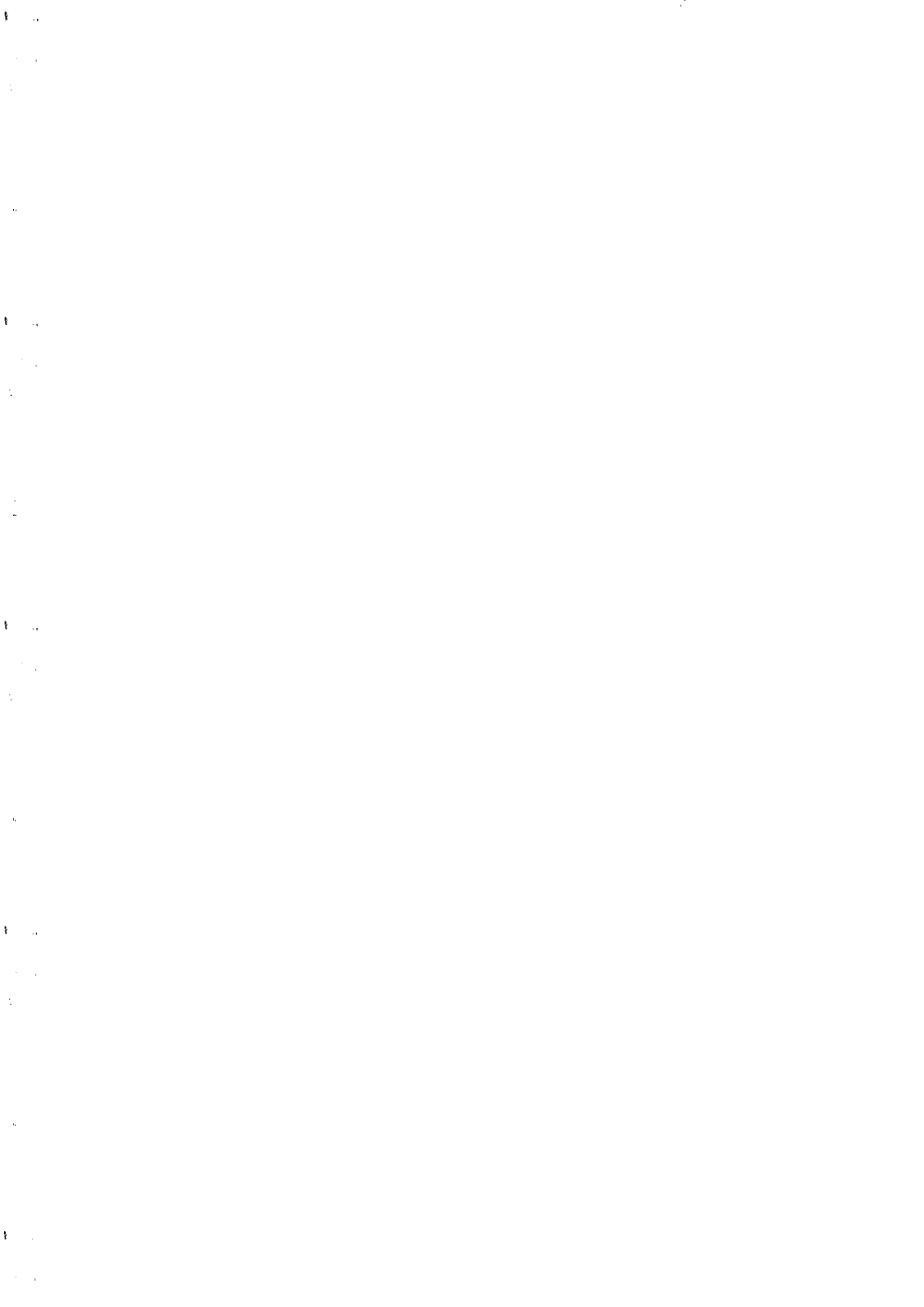
In conclusion, we have used an SET electrometer in a capacitance bridge experiment to measure the AC ratio of two standard capacitors to one part in  $10^4$  in a dilution refrigerator. The stray capacitance to ground which limits the sensitivity of the electrometer was found to be 5 pF in our first design. DC capacitance and leakage rate measurements demonstrate that the SET electrometer is a very sensitive detector of any time-varying potentials that induce changes in the charge state of the bridge balance point. This experiment is a first step towards a precision measurement of  $\alpha$ , but it is clear that greatly improved capacitors will be required for success in this experiment.

Acknowledgements: We thank Richard Tiberio of the National Nanofabrication Facility at Cornell University for help with the tunnel junction fabrication. We also thank William Fogel, Robert Soulen, Jr., and John Martinis for their advice and assistance with this work.

\* Present Address: AT&T Bell Laboratories, 600 Mountain Ave., Murray Hill 07974, USA.

- 1) P. Lafarge, H. Pothier, E.R. Williams, D. Esteve, C. Urbina, and M.H. Devoret, *Z. Phys. B* **85**, 327 (1991); T.A. Fulton, P.L. Gammel, and L.N. Dunkelberger, *Phys. Rev. Lett.* **67**, 3148 (1991).
- 2) G. Zimmerli, T.M. Eiles, R.L. Kautz, and J.M. Martinis, *Appl. Phys. Lett.* **61**, 237 (1992).
- 3) E.R. Williams, R.N. Ghosh, and J.M. Martinis, *J. Res. Nat. Inst. Stand. Technol.* **97**, 299 (1992).
- 4) T.A. Fulton and G.J. Dolan, *Phys. Rev. Lett.* **59**, 109 (1987).
- 5) B.P. Kibbel and G.H. Rayner, *Coaxial AC Bridges* (Adam Hilger, Bristol, 1984).

**COULOMB INTERACTIONS  
AND QUANTUM HALL EFFECT**



## Atomic Spectroscopy of a Single Quantum Dot

R.C. Ashoori

*Dept. of Physics, M.I.T.*

H.L. Stormer, J.S. Weiner, L.N. Pfeiffer, K.W. Baldwin, and K.W. West

*AT&T Bell Laboratories, Murray Hill, NJ 07974*

### Abstract

We have recently developed a spectroscopic technique which allows direct measurement of quantum energy levels. The method is based on observation of the capacitance signal resulting from single electrons tunneling into discrete quantum levels. The electrons tunnel between a metallic layer and confined states of a microscopic capacitor fabricated in GaAs. Charge transfer occurs only for bias voltages at which a quantum level resonates with the Fermi energy of the metallic layer. This creates a sequence of distinct capacitance peaks whose bias positions directly reflect the electronic spectrum of the confined structure. Using this “single-electron capacitance spectroscopy”, we map the magnetic field dependence of the ground state energies of a single quantum dot containing from 0 to 50 electrons. Along with a spectroscopic measurement of the dot’s ground states, we probe tunneling rates of electrons to individual quantum states. The experimental spectra reproduce many features of a noninteracting electron model with an added fixed charging energy. However, in detailed observations deviations are apparent: exchange induces a two-electron singlet-triplet transition, self-consistency of the confinement potential causes the dot to assume a quasi two-dimensional character. Finally, broad features seen as the magnetic field strength is varied suggest changes in the shape and size of the dot induced by the magnetic field.

Several years ago, it became evident that semiconductor technology had, at least in one sense, began to touch the ultimate limits of miniturization. Several experiments, such as the resonant tunneling system of Reed et al.,[1] made it clear that it might be feasible to produce a “quantum dot or artificial atom” containing as few as one electron. Over the last few years, many other methods have been developed to study these systems. Among these are gated resonant tunneling devices [2], far infrared spectroscopy [3, 4], conventional capacitance studies of arrays [5, 6], and photoluminescence spectroscopies [7]. Recently, two techniques have been developed which allow spectroscopic study of the ground state (GS) energies in *individual* quantum dots with a resolution limited only by the temperature of the electronic system.[8, 9]

A key question to be answered by spectroscopic studies on quantum dots is the role of the electron-electron interaction in modifying the dot’s electronic level structure. Bryant[10] has addressed this question for quantum dots containing just two electrons. He finds a continuous evolution of the level structure, from single-particle like states in the limit of a very small dot, to a level structure dominated by the electron-electron interaction in larger dots. Since the confinement potential in semiconductor quantum dots can be controlled at will, a large range of this continuum which is not accessible in atomic physics can be examined.

In the presence of magnetic field (B), the electron-electron interaction is expected to affect the electronic level structure of a quantum dot in interesting ways. For instance, Maksym and Chakraborty[11] find in their calculations that electrons in their GS in a quantum dot undergo discrete increases of angular momentum of several  $\hbar$  as B is increased, reminiscent of transitions between different fractional quantum Hall states. In order to investigate experimentally such novel phenomena, we have undertaken a high resolution study of the GS energy levels and tunneling rate spectra of a single quantum dot in magnetic field.

In a previous paper,[8] we have introduced single-electron capacitance spectroscopy (SECS). The method allows the direct measurement of the energies of quantum levels of an individual small structure (dot) as a function of magnetic field (B). When the Fermi energy

of an electrode becomes resonant with a quantum level of a nearby dot, single electrons can tunnel back and forth between the electrode and the dot through a tunnel barrier (see Fig. 1a). The resulting charge induced by this motion on the opposite electrode of a “tunnel capacitor” is detected by an on-chip, highly sensitive transistor. Using this technique we were able to detect spatially distinct localized states in a small tunnel capacitor. We now use SECS to measure the GS energies of a single quantum dot containing  $N$  electrons in which charge nucleates in only one central location.

To measure the capacitance signal from single electrons moving back and forth across the tunnel barrier, we have incorporated our device into a “bridge on a chip”, with a standard capacitor and detector located very close to the tunnel capacitor. As a detector, we use a cryogenic high electron mobility transistor (HEMT) with input shunt capacitance of  $\approx 0.3$  pF. It is positioned within 2 mm of the bridge. We mount the HEMT with its two-dimensional electron gas parallel to the magnetic field, and we find its characteristics practically unaffected by an applied field in this geometry.

The basic configuration of our GaAs samples has been described previously,[8] although the semiconductor structure has been slightly modified for the present experiments. A schematic of the sample is shown in Fig. 1a. The layer sequence is as follows: 3000 Å  $n^+$ -doped ( $4 \times 10^{17} \text{cm}^{-3}$ ) GaAs bottom electrode; 600 Å undoped GaAs spacer layer; 125 Å undoped  $\text{Al}_{0.3}\text{Ga}_{0.7}\text{As}$ /GaAs superlattice tunnel barrier; 175 Å quantum well (vertically confines the quantum dot); 500 Å  $\text{Al}_{0.3}\text{Ga}_{0.7}\text{As}$  blocking barrier; and a 300 Å GaAs cap layer. The blocking barrier contains a Si delta doped layer 200 Å from the well edge. The wide 600 Å spacer layer and the superlattice tunnel barrier[12] were implemented to prevent Si atoms from migrating into the well.[8] Lateral confinement is provided by first patterning a 3500 Å diam. circular metallic disk on top of the sample surface and using this as an etch mask to etch down to the AlGaAs blocking barrier surface. The 3500 Å diam. top electrode is contacted for measurement by overlaying it with a 1.5  $\mu\text{m}$  diam. metal disk. All measurements are taken at 0.35 K.

Figure 1b displays capacitance vs. gate bias data for the quantum dot sample. The top trace is the signal observed in-phase with the excitation voltage. A first peak appears at -373 mV and arises as the lowest electronic state of the dot becomes resonant with the Fermi energy of the  $n^+$  electrode. With increasing positive gate bias subsequent electrons tunnel onto the quantum dot. Unlike our previous results in a larger dot, the peaks are spaced rather uniformly, with their separation decreasing slightly with increasing electron number. The constancy of the peak heights attests to the quantization of charge that is being moved onto the dot.

Beyond the 25<sup>th</sup> peak, the peak heights in the top trace of Fig. 1b drop due to a decrease in the tunneling rate. This interpretation is confirmed by measuring the signal at the dot in 90° lagging phase, shown in the bottom trace of Fig. 1b, where peaks occur only for  $N \geq 25$ . This behavior is unambiguous evidence that the tunneling rate of electrons is becoming smaller than the 210 kHz excitation frequency. A slow tunneling rate causes an electron to “wait” a length of time before it tunnels in response to the excitation voltage, and its motion thus lags the excitation. The present experiment thus allows both a tunneling rate spectroscopy based on the height and phase of capacitance peaks as well as an energy level spectroscopy based on the positions of the peaks.

We have developed an understanding of why the tunneling rates decrease in these samples with increasing electron number based upon studies of different wafers with different undoped spacer layers just below the tunnel barrier. Briefly, the geometry of our samples suggests that the tunneling problem can be separated into transverse (in the plane of the quantum well) and longitudinal (in the direction of tunneling) parts.[13] The large 600 Å spacer layer acts as a long and low (<20 meV high) tunnel barrier. As the dot fills up with electrons, their bound state energy in the quantum well is lowered with respect to this barrier, reducing the tunneling rate.

The regime of a few electrons in a dot has been probed by relatively few experiments.[14] We now use SECS in B-field to study this domain with unprecedented resolution. Figure 2

is a grey scale image of the dot capacitance as a function of gate bias and B-field applied perpendicular to the plane of the dot. The white and black regions correspond to the highest and lowest capacitance respectively. The gate bias scale is converted to an energy scale[8] by division by a lever-arm of  $2.0 \pm 0.1$  for this structure. This lever-arm was determined from capacitance measurements on large area mesas made on the same wafer.

Fig. 2 represents the B-field evolution of the first 35 N-electron GS energies of the quantum dot. The field dependence of the lowest energy state in Fig. 2a is smooth and is well described by the first electron in a cylindrically symmetric parabolic potential[15]  $\frac{1}{2}m^*\omega_0^2r^2$  with  $\hbar\omega_0 = 5.4$  meV. The high field asymptote of this curve follows the dashed line in Fig. 2a with slope  $\hbar\omega_c/2$ . From the classical turning points of the lowest bound state we deduce a dot diameter of  $408 \text{ \AA}$ .

In contrast to the first electron, the evolution of the ground state energy of two electrons shows a pronounced “bump” and a change of slope at about 1.5 T (see dot on 2nd electron). We interpret this feature as a singlet-triplet crossing. Considering noninteracting states, the first two electrons in the dot fall into a two-fold (spin) degenerate ground state for  $B=0$ . At higher field, the energy difference between the ground orbital state and the first excited state shrinks, and the Zeeman effect causes a level crossing at 25 Tesla for  $\hbar\omega_0 = 5.4$  meV.

Electron-electron interactions significantly reduce the B-field for this singlet-triplet crossing. Wagner, Merkt, and Chaplik[16] have calculated its position for parabolic quantum dots. For  $\hbar\omega_0 = 5.4$  meV, the crossing is expected at 3.6 T, about a factor of 2 higher than seen in Fig. 2a. The discrepancy may arise from the assumption of a strictly parabolic potential in the calculation. Such a singlet-triplet crossing has not been observed in atomic physics experiments due to the exceedingly high B-field required ( $4 \times 10^5$ T for He). The weak binding of electrons in our quantum dot along with the small electronic mass shifts it to attainable fields.

The singlet-triplet crossing should exist *even in the absence* of a Zeeman splitting, arising solely from the electron-electron interaction.[16] The angular momentum quantum number

$m$  of the two electrons in the ground state increases with  $B$ , being equal to zero only at low field.[11, 16] The energy difference between single-particle states of progressively larger angular momenta decreases with increasing  $B$ ; in higher fields, it becomes advantageous for the system to place electrons in states of successively higher angular momenta (larger orbit radii) in order to decrease the Coulomb repulsion between electrons. To maintain exchange antisymmetry of the two-electron wavefunction, the system undergoes singlet-triplet (triplet-singlet) crossings as  $m$  switches from even (odd) to odd (even) numbers.

The Zeeman energy moves the first singlet-triplet crossing to yet lower fields. Moreover, at higher fields the Zeeman effect may force for the system to remain in a spin triplet, allowing only transitions between odd  $m$  states. For our GaAs dot, the nature of transitions beyond the initial singlet-triplet crossing depends sensitively on the value of  $\hbar\omega_0$  for the dot as well as on the precise shape of the bare confining potential. These transitions cause smaller changes of slope in the two-electron GS energy, and we do not attempt to label them here.

The data of Fig. 2a, display several unexpected features. The bump seen in the GS energy of the two-electron system seems to progress through the few-electron system (white dots). Its position shifts monotonically to higher fields with increasing  $N$ , producing a clear “ripple” through the data set. It seems likely that these features are also spin related. Finally, selected traces of Fig. 2a show a distinct intensity loss with increasing  $B$  resulting from an unexplained decreased tunneling rate. At a lower excitation frequency (65 kHz rather than 210 kHz), all capacitance peaks continue smoothly to our maximum field of 10.8 T, except at  $N=2$ , for which the tunneling rate drops precipitously at 8 T.

Figure 2b shows the ground state energies of the dot for  $N=6-35$  on an expanded field scale. In order to interpret the general features of this data set, we turn first to Fig. 3. This graph reproduces the highly intertwined single-particle states of a cylindrically symmetric parabolic potential with  $\hbar\omega_0 = 1.12 \text{ meV}$  in a  $B$ -field.  $N$  electrons in this system fill the  $N$

lowest energy states. The GS energy of the  $N^{\text{th}}$  electron should thus oscillate as levels cross as indicated in bold for the 35<sup>th</sup> electron GS. The oscillations cease at about 2 T.

In magnetic field, Landau level structure develops in the dot. Because the density is higher near the dot center than at the edges, and in magnetic field, levels of larger Landau index  $\nu$  may be filled there than at the dot edge. As the field is increased, the degeneracy of the lower  $\nu$  levels increases, and electrons move from the higher  $\nu$  states at the dot center to the lower  $\nu$  states which become available at the dot edge. Taking the Landau level index  $\nu$  for the dot to be given by the Landau level occupancy at the dot center, the position of the last crossing in Fig. 3 can thus be identified with  $\nu = 2$ . At this field, all electrons have moved into the lowest Landau level, and at the dot center, there are two electrons (one spin up and one spin down) per flux-quantum passing through the dot.

In order to incorporate the electron-electron interaction to lowest order into this picture, we follow the constant interaction (CI) model.[9, 17, 18] It consists of single-particle states each separated by a magnetic field independent charging energy. In Fig. 2b, the development of the  $\nu = 2$  positions are clearly visible (white triangles). Beyond  $N=10$ , the  $\nu = 2$  positions for each successive electron agree well with the CI model using a constant  $\hbar\omega_0 = 1.12$  meV. Curiously, the tunneling rates are attenuated around  $\nu = 2$  at large  $N$ . At  $\nu = 2$ , the electrons in the dot center are in a quantum Hall state, and we speculate that tunneling suppression arises from the incompressibility of this state.

Figure 4 zooms in on the  $\nu = 2$  region for  $N=21-33$ . These data are taken at 125 kHz to achieve well developed capacitance peaks. The oscillations expected from the CI model are clearly visible. Although the qualitative agreement between experiment and the simple model of Fig. 3 is satisfying, there exist some remarkable differences: oscillations in the GS energy appear only very close to  $\nu = 2$ , and GS energies drop abruptly as the field is increased beyond  $\nu = 2$ . While we presently have no explanation for the existence of oscillations only close to the  $\nu = 2$  region and their relative phases, we believe that the energy drop beyond  $\nu = 2$  is related to the nonparabolicity of the self-consistent potential.

Hartree calculations[19] show that the bottom of the dot's confinement potential is "flattened" considerably by the presence of electrons, and in the interior can be considered as a small two-dimensional (2D) system. In a 2D system there exist well known sudden drops in the chemical potential as Landau levels depopulate in B-field. As  $N$  is increased, the dot approaches a 2D system, giving rise to the enhanced chemical potential drop at  $\nu = 2$  seen in our data.

The identification of the  $\nu = 2$  position allows us to determine the size of the dot, calculate its charging energy and compare it with the observed gate bias spacing between successive electrons.[17] Since for large  $N$  the potential around the dot center is approximately constant, we can define a capacitance of the dot to external electrodes. With capacitances  $C_{top}$  and  $C_{bott}$  of the dot to the top and bottom plates respectively, the electrostatic lever-arm is  $(C_{bott} + C_{top})/C_{bott}$ . Ignoring the comparably small quantum level spacings, successive electron additions occur when the electrostatic potential in the dot changes by an amount,  $e/(C_{top} + C_{bott})$ . Accounting for the lever-arm, electron additions are spaced by  $e/C_{top}$  in gate bias.

In a dot with a flat-bottom potential, the area of the dot  $A$  is related to the Landau level filling fraction  $\nu$  by  $A = N(h/eB\nu)$ . For the 30<sup>th</sup> electron,  $\nu = 2$  occurs at about 2.2 T, which translates into a dot diameter of 1900 Å. Assuming parabolic confinement with  $\hbar\omega_0 = 1.1$  meV rather than flat-bottom confinement decreases the dot area by only 2%. A simple parallel plate capacitor model neglecting fringing fields yields  $e/C_{top} = 4.2$  mV, only ~25% larger than the measured gate bias spacing of 3.3 mV between capacitance peaks. The dot sizes determined this way compare very well with sizes calculated using our own classical relaxation method[20] computer simulations. An alternate way of determining the dot size is by looking at Fig. 4 and noting that each oscillation seen here corresponds to adding an additional flux quantum to the dot.[21] The size of the dot determined from the oscillation period is, to within experimental error, the same as that determined above.

As we move to yet higher  $N$ , approaching the 2D limit, additional features become apparent in our spectra. Figure 5, taken at 125 kHz, displays the chemical potentials of the dot containing 33-50 electrons. Similar to Fig. 4, we observe the steep drop in chemical potential at B-fields just beyond  $\nu = 2$  (at about 2.3 T for  $N=33$ ). The same behavior is now apparent at  $\nu = 4$  (at about 1.2 T for  $N=33$ ). We attribute the accentuation of these features to the increasingly 2D character of the system at high filling. A more precise understanding of the chemical potential steps will require a self-consistent calculation of the dot's edges.[22]

Pursuing further the transition between a quantum dot and a finite-sized 2D electron system, we now examine the region  $\nu < 2$  at B above 4 T. We observe a sequence of "bumps" shifting only slightly to higher B with higher  $N$ . These features are inexplicable in terms of any CI model which all predict that successive traces oscillate  $180^\circ$  out of phase.[9, 18] We note also, that unlike the predictions of a single particle model which predicts features with a periodicity of one flux quantum through the dot, the bumps seen in the  $\nu < 2$  regime have a periodicity of about three flux quanta. The origin of these bumps is at present unclear. They may result from the transfer of electrons between the spin states of the lowest Landau level such as has been observed previously by McEuen et al.[18] Alternatively, these features may be of many-particle origin reminiscent of the fractional quantum Hall effect (FQHE). In the FQHE the chemical potential of the system undergoes maxima between FQHE steps and minima at the steps.[23] The features seen in Fig. 5 are 0.2-0.5 meV in height, not unlike the characteristic energy range of the FQHE at such B-fields. Moreover, the decrease in tunneling rates (intensity) between the bumps, may reflect the energy gaps in the FQHE. These features grow monotonically in prominence as more electrons are added to the dot, suggesting a two-dimensional origin. The size and distribution of the electron density within the dot vary with B-field, and it is thus difficult to assign a precise value of  $\nu$  at dot center for fields beyond  $\nu = 2$ . Finally, given the nonuniformity of the electron density, we expect the electron gas to form incompressible and compressible regions, with the FQHE chemical

potential minima occurring with the central portion of the dot is at a  $\nu$  value appropriate for the FQHE.[24]

Between 5.0 T and 5.6 T for the lowest trace of Fig. 5 (33rd electron trace) displays a broad dip, and the tunneling rate is also attenuated. Because the dip commences at 5.0 T, which is precisely twice the field for  $\nu = 2$ , the start of the dip can be identified as the onset of the  $\nu = 1$  regime. It is interesting that  $\nu = 1$  forms such a broad minimum. As the magnetic field is increased in the  $\nu = 1$  regime, the increased degeneracy of the lowest Landau level allows the dot to shrink in size. The electrons in the dot remain at a fixed filling fraction of  $\nu = 1$  as the electronic density in the dot increases with field. At around 5.6 T the electronic density cannot increase any further; the dot is held at a fixed size by the repulsion of electrons within the dot. The electron density in the dot may approach that of a "maximum density droplet".[25]

Beyond the  $\nu = 1$  region, other features appear. For the lowest trace of Fig. 5, a "glitch" appears at 6.5 T. This feature clearly persists at higher electron numbers, and it occurs at fixed Landau level filling fraction. Recently, Klein et al.[26] have observed similar behavior in laterally confined quantum dots probed by transport. They attribute such glitches to a sudden reformation of the edges of the quantum dot predicted by Hartree-Fock calculations.

In summary, SECS has permitted a detailed survey of the N-electron ground states of a quantum dot in magnetic field. There are several salient features of the data set. We observe the singlet-triplet transition in the two electron dot. An unusual "ripple" is seen to run through the data for fewer than 10 electrons in the dot, and it appears that the ripple is caused by correlations between spin-flips in the dot containing different numbers of electrons. Anomalous behavior is seen in both the ground state energies and the tunneling rates to the dot around integer Landau level filling fractions. Finally, features appear at high magnetic field and large electron number which are suggestive of the development of the FQHE.

We thank S.J. Pearton for help preparing the quantum dots and L.I. Glazman, P. Hawrylak, P.A. Lee, A.H. MacDonald, B.I. Shklovskii, and N. Wingreen for helpful discussions.

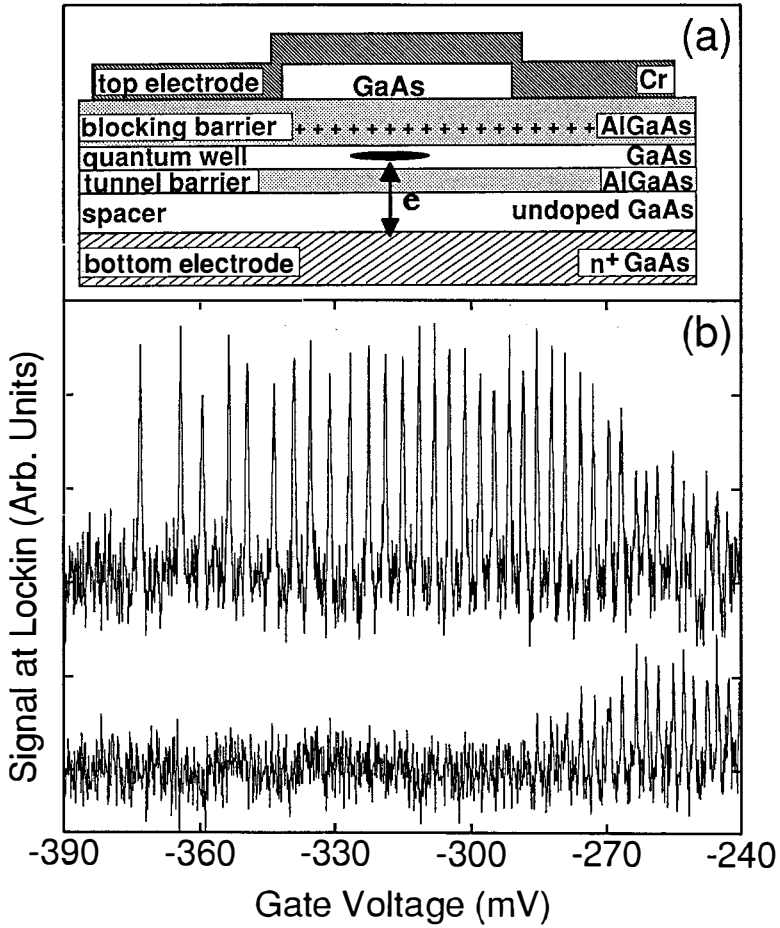
## References

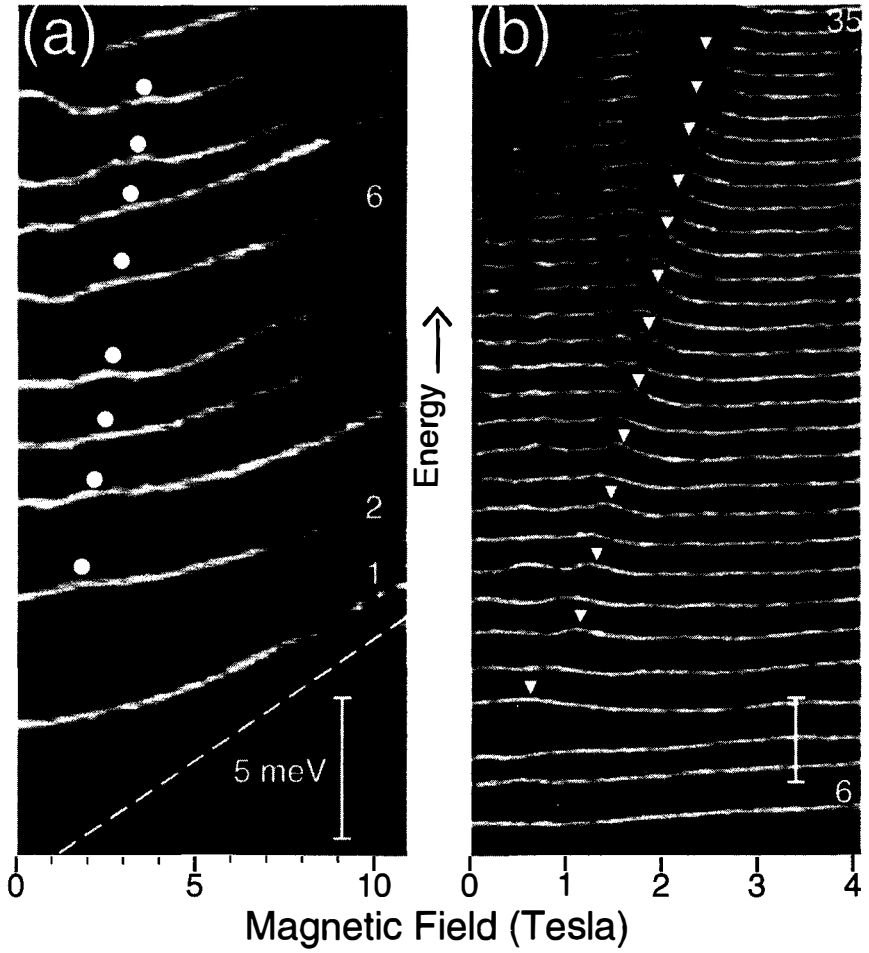
1. M.A. Reed, J.N. Randall, R.J. Aggarwal, R.J. Matyi, T.M. Moore, and A.E. Wetsel, *Phys. Rev. Lett.* **60**, 535 (1988)
2. M.W. Dellow et al. *Phys. Rev. Lett.* **68**, 1754 (1992)
3. Ch. Sikorski and U. Merkt, *Phys. Rev. Lett.* **62**, 2164 (1989)
4. B. Meurer, D. Heitmann, and K. Ploog, *Phys. Rev. Lett.* **68**, 1371 (1992)
5. W. Hansen, T.P. Smith, III, K.Y. Lee, J.A. Brum, C.M. Knoedler, J.M. Hong, and D.P. Kern, *Phys. Rev. Lett.* **62**, 2168 (1989); see comment by R.H. Silsbee and R.C. Ashoori, *Phys. Rev. Lett.* **64**, 1991 (1990)
6. R.C. Ashoori, R.H. Silsbee, L.N. Pfeiffer, and K.W. West in *"Nanostructures and Mesoscopic Systems"* pp. 323-334, edited by M. Reed and W. Kirk (Academic Press, 1992)
7. K. Brunner, U. Bockelmann, G. Abstreiter, M. Walther, G. Böhm, G. Tränkle, and G. Weimann, *Phys. Rev. Lett.* **69**, 3216 (1992)
8. R.C. Ashoori, H.L. Stormer, J.S. Weiner, L.N. Pfeiffer, K.W. Baldwin, and K.W. West, *Phys. Rev. Lett.* **68**, 3088 (1992)
9. P.L. McEuen, E.B. Foxman, U. Meirav, M.A. Kastner, Yigal Meir, Ned S. Wingreen, and S.J. Wind *Phys. Rev. Lett.* **66**, 1926 (1991)
10. Garnett W. Bryant, *Phys. Rev. Lett.* **59**, 1140 (1987)
11. P.A. Maksym and Tapash Chakraborty, *Phys. Rev. Lett.* **65**, 108 (1990)
12. U. Meirav, M. Heiblum, and Frank Stern, *Appl. Phys. Lett.* **52**, 1268 (1988)
13. J.A. Lebens, R.H. Silsbee, and S.L. Wright, *Appl. Phys. Lett.* **51**, 840 (1987)
14. B. Meurer, D. Heitmann, and K. Ploog, *Phys. Rev. Lett.* **68**, 1371 (1992); Bo Su, V.J. Goldman, and J.E. Cunningham, *Science* **255**, 313 (1992)
15. C.G. Darwin, *Proc. Cambridge Philos. Soc.* **27**, 86, (1930)
16. M. Wagner, U. Merkt, and A.V. Chaplik, *Phys. Rev. B* **45**, 1951 (1992)
17. R.H. Silsbee and R.C. Ashoori, *Phys. Rev. Lett.* **64**, 1991 (1990)
18. P.L. McEuen, E.B. Foxman, Jari Kinaret, U. Meirav, M.A. Kastner, Ned S. Wingreen, and S.J. Wind, *Phys. Rev. B* **45**, 11419 (1992)
19. Arvind Kumar, Steven E. Laux, and Frank Stern, *Phys. Rev. B* **42**, 5166 (1990)
20. K.J. Binns and P.J. Lawrenson, *Analysis and Computation of Electric and Magnetic Field Problems* (Pergamon Press, 1973)
21. U. Sivan and Y. Imry, *Phys. Rev. Lett.* **61**, 1001 (1988)

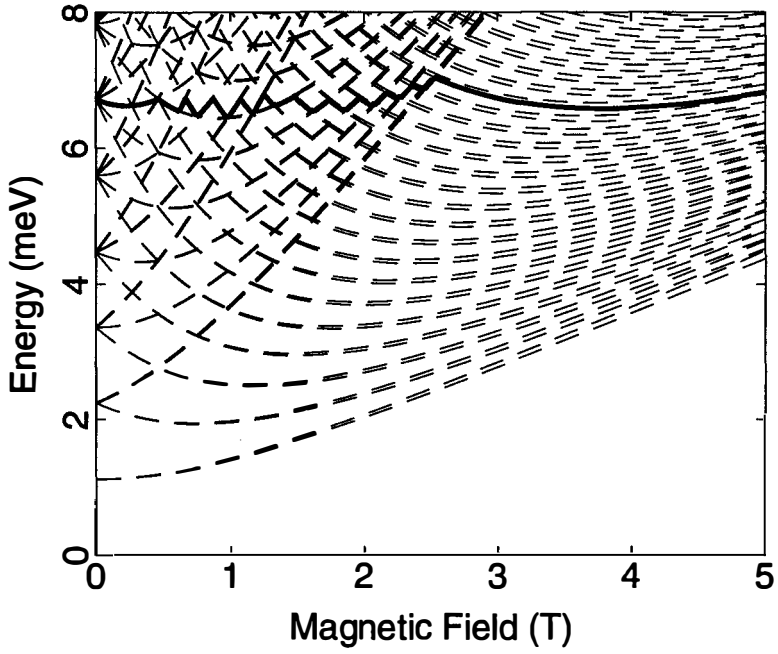
22. D.B. Chklovskii, B.I. Shklovskii, and L.I. Glazman, *Phys. Rev. B* **46**, 4026 (1992)
23. T. Chakraborty and P. Pietiläinen, "The Fractional Quantum Hall Effect," (Springer Verlag, 1988)
24. Jari M. Kinaret, Yigal Meir, Ned S. Wingreen, Patrick A. Lee, and Xiao-Gang Wen, *Phys. Rev. B* **45**, 9489 (1992); A.H. MacDonald and M.D. Johnson, *Phys. Rev. Lett.* **70**, 3107 (1993)
25. A.H. MacDonald, S.-R. Eric Yang, and M.D. Johnson, *Aust. J. Phys.* **46**, 345 (1993).
26. O. Klein, C. de C. Chamon, D. Tang, D.M. Abusch, X.-G. Wen, and M.A. Kastner, to be published

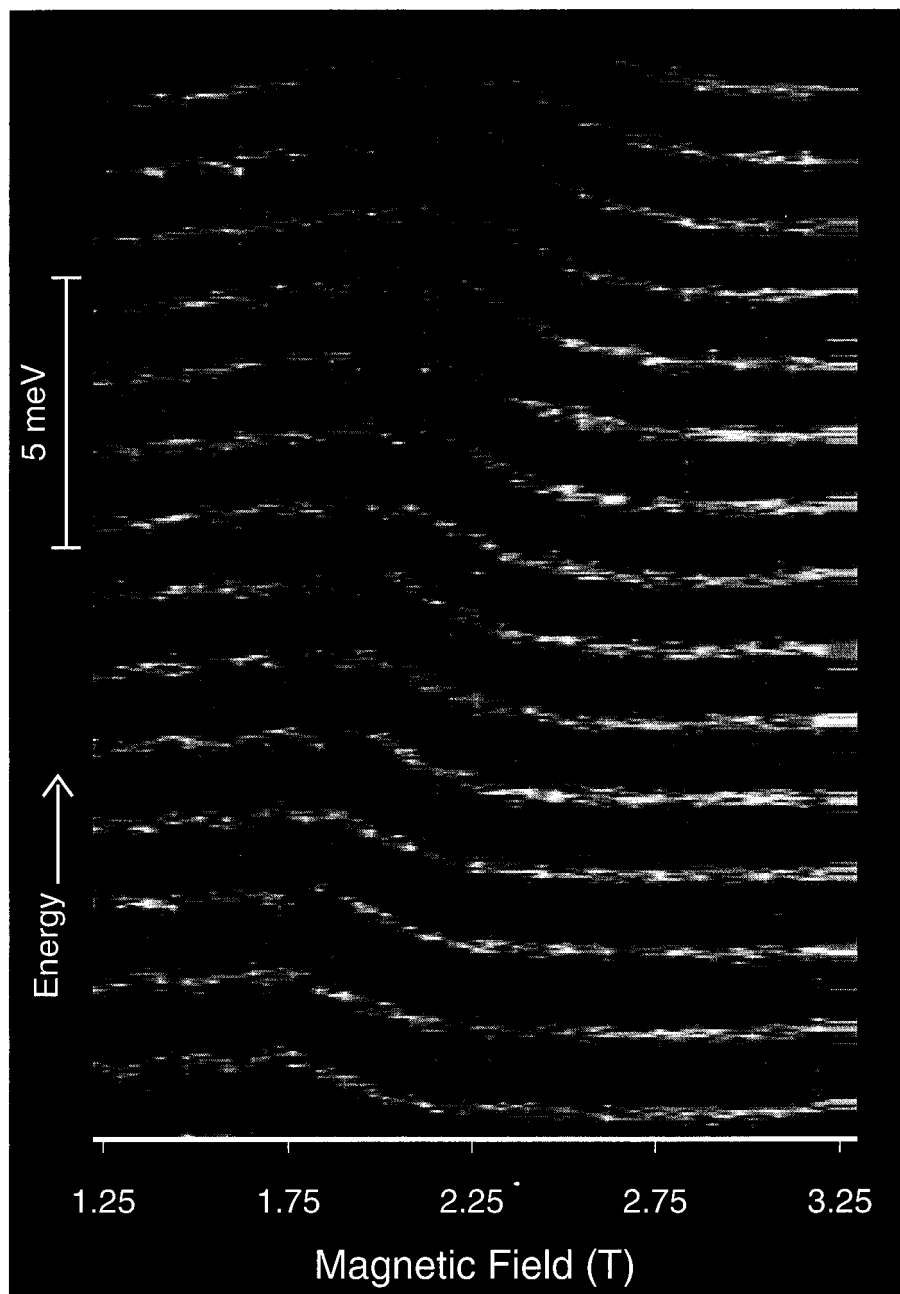
### Figure Captions

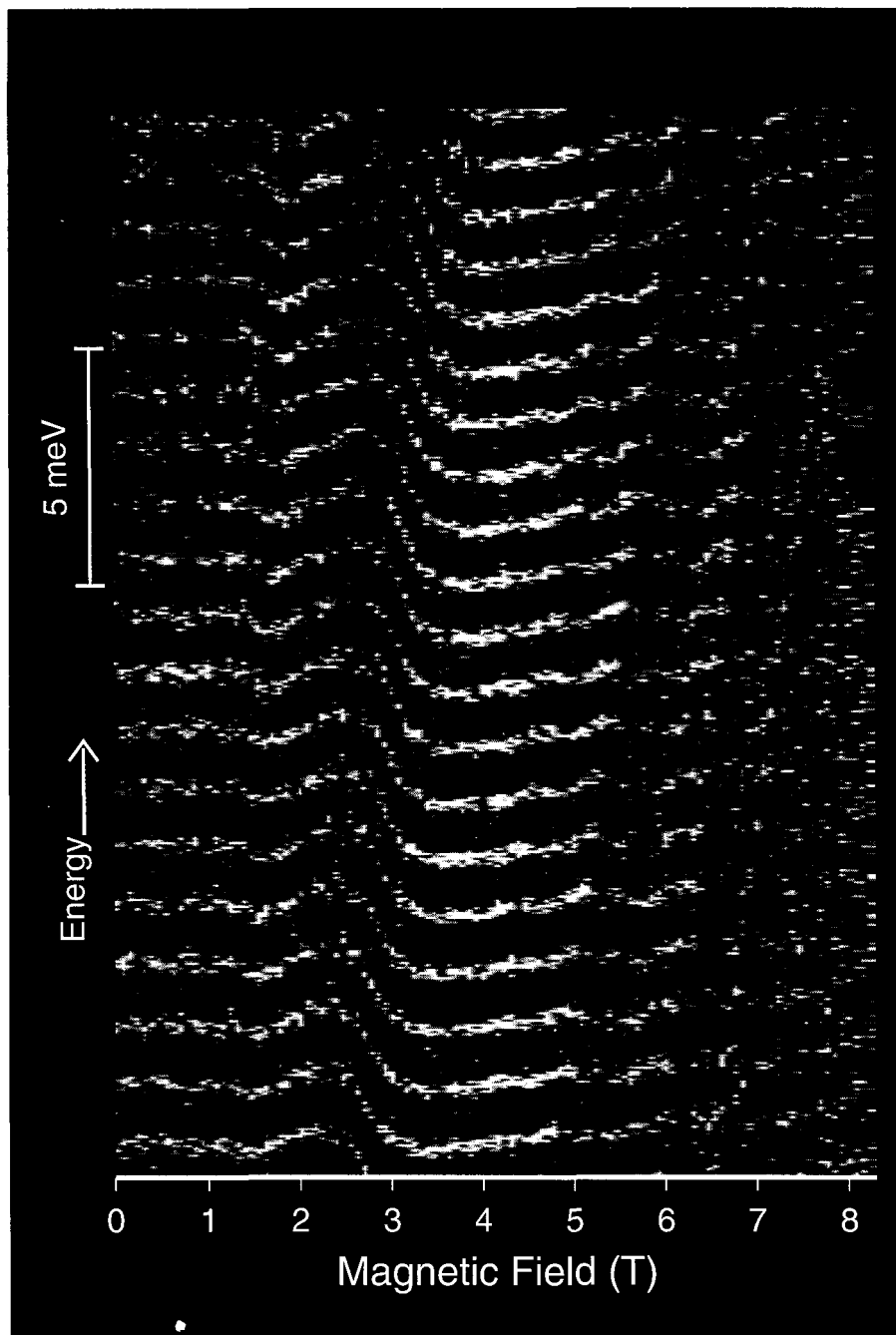
- Fig. 1** (a) Schematic of sample. (b) Capacitance data vs. gate bias for the quantum dot sample in zero magnetic field. The top and bottom traces show the signal resulting from electron tunneling in-phase and electron tunneling in  $90^\circ$  lagging phase with the 210 kHz excitation voltage respectively.
- Fig. 2** Grey scale plots of the sample capacitance as a function of both magnetic field and gate bias. The vertical bars in both (a) and (b) represent an energy of 5 meV. The dashed line follows the zero point energy in magnetic field for a free electron,  $\hbar\omega_c/2$ .
- Fig. 3** (a) Theoretical Darwin-Fock states for a parabolic quantum dot with  $\hbar\omega_0 = 1.12$  meV (dotted curves). The bold solid curve displays the magnetic field evolution of the  $35^{\text{th}}$  electron.
- Fig. 4** Grey-scale capacitance data for  $N=21-33$ . The data set zooms in on the  $\nu = 2$  region.
- Fig. 5** Sample capacitance as a function of gate bias and magnetic field for  $N=33$  (lowest full trace) up to 50. The vertical bar represents an energy of 5 meV.

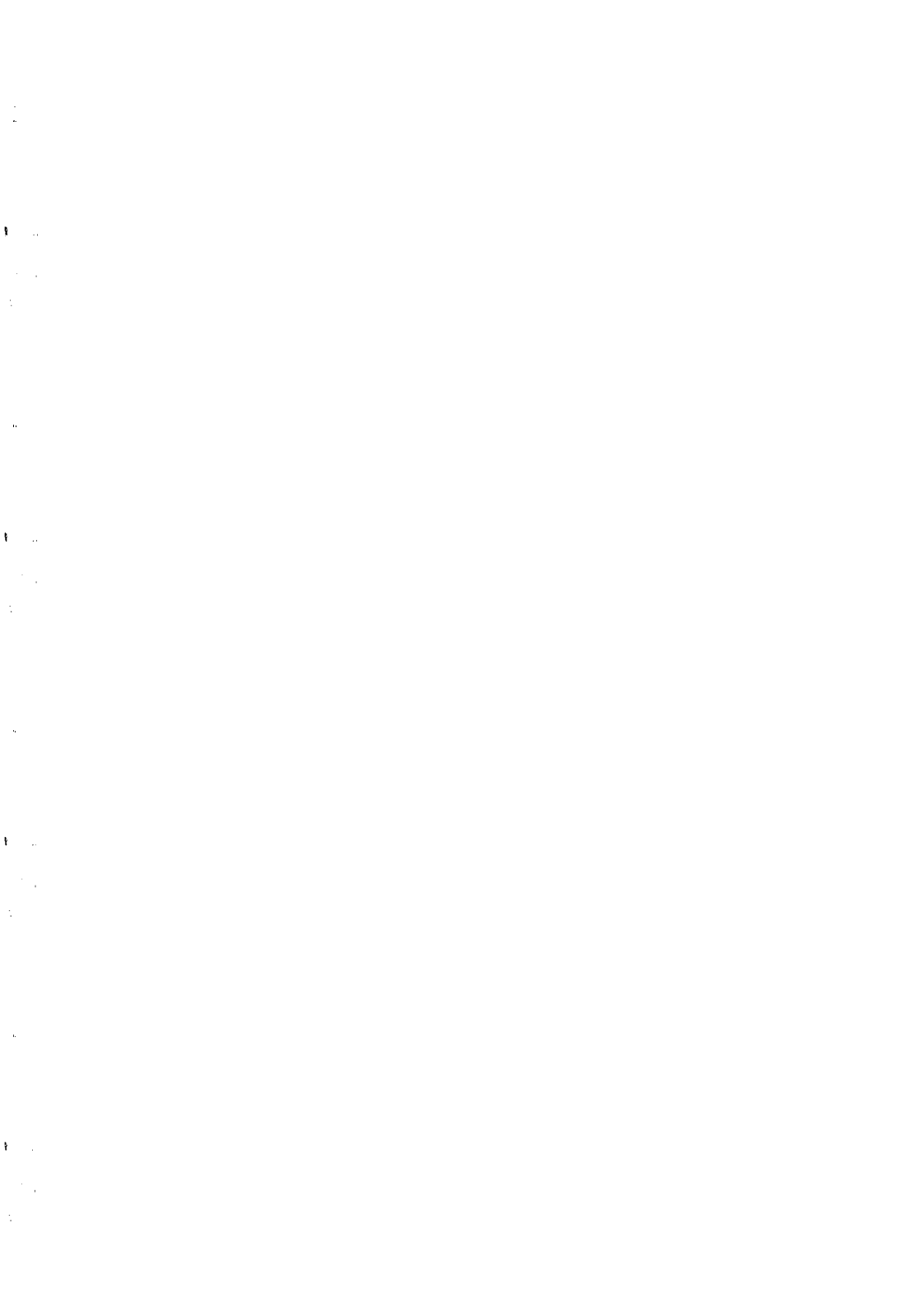












PERIODIC MODULATION OF COULOMB BLOCKADE OSCILLATIONS  
IN A QUANTUM DOT AT HIGH MAGNETIC FIELDS

T. Heinzel, D.A. Wharam, S. Manus, and J.P. Kotthaus, (Sektion Physik der LMU, 80539 München, Germany), G. Böhm, W. Klein, G. Tränkle, and G. Weimann, (Walter Schottky Institut, Technische Universität München, 85748 Garching, Germany)

Transport measurements of laterally defined semiconductor quantum dots are currently the subject of considerable interest and show several striking effects<sup>1</sup>. Conductance oscillations as a function of the Fermi energy inside the dot have their origin in the discreteness of the charge transport through the dot and in the Coulomb interaction between the electrons. These oscillations are usually called Coulomb blockade oscillations (CBO), each peak corresponding to a change in the occupation number of the dot by one electron. The peak conductance is determined by the coupling of the the current-carrying state in the dot to the external leads. The peak separation is a measure of the energy required to add an additional electron to the dot. This energy is determined by the sum of two components: the electrostatic energy necessary to add an additional electron to the dot, usually expressed as  $e^2/C_t$  ( $C_t$  is the total capacitance of the dot), and a discrete energy  $\delta E_i$ , depending upon the state  $i$  the electron occupies in the dot<sup>2,3</sup>. At zero magnetic field the discrete energy contribution is usually of the order of 10% of the charging energy and gives rise to a statistical variation in the peak separation.

In this paper we report on Coulomb blockade oscillations in the presence of a high perpendicular magnetic field. At low fields and high filling factors the amplitude of the CBOs shows a significant modulation, whose period is inversely proportional to the applied magnetic field. Staring et al.<sup>4</sup> have previously reported such a periodic modulation of the peak conductance at high filling factors, and were able to explain this modulation by the different coupling of the (spin degenerate) Darwin-Fock states to the leads as a function of the associated Landau level. At filling factors  $\nu \leq 4$  we observe not only a periodic modulation of the CBOs that can no longer be explained within a single particle picture, but in addition a dramatic periodic modulation of the peak separations

which can become as large as 25%. To interpret our data we apply a recently developed charge-density model<sup>5-7</sup> which has been shown to be in good agreement with previously reported experimental results<sup>8</sup>.

The lithographically defined dot geometry (illustrated in Figure 1) is defined by metallic gates on the surface of a GaAs/AlGaAs heterostructure. Nominally the dot structure is a square of length 500 nm however we expect that, at definition, the actual size of the dot structure taking account for lateral depletion effects will be approximately 300 nm square. The dot is coupled to the reservoirs via two weakly conducting tunneling barriers which can be independently tuned using the finger gates. The central dot is controlled via the centre gate which simultaneously sweeps both the Fermi energy as well as the dot geometry itself.

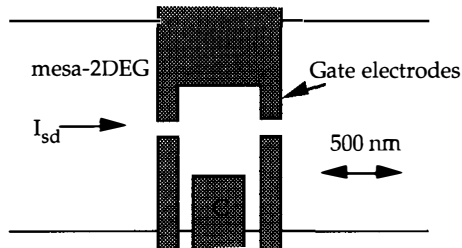


Figure 1. A schematic illustration of the gate electrode structure used to define the quantum dot structure investigated.

The completed structure was inserted directly into the mixing chamber of a top-loading dilution refrigerator with a base temperature of approximately 25 mK. Conductance measurements were then performed using a low-frequency Lock-In technique ( $f \sim 31$  Hz) and low excitation voltages ( $V_{sd} \leq 4 \mu\text{V}$ ). The current resolution thus obtained was of the order of 200 fA and limited by the noise properties of the operational amplifier used as a current-voltage pre-amp.

The finger gates were adjusted such that the conductance of each point contact was less than  $e^2/h$  and the conductance of the dot itself then measured as a function of the voltage applied to each of the gate electrodes. Coulomb blockade oscillations were observed in all measured conductances; the period of the observed oscillations was then used to determine the partial capacitances of the gates to the dot and the resulting total capacitance, neglecting the influence of the two two-dimensional reservoirs, was determined to be  $\sim 144$  aF. This value of capacitance compares favourably with the self-capacitance of a two-dimensional dot of radius 150 nm which we calculate to be 140 aF. Assuming the geometry of our dot structure to lie somewhere between a square and a

circle and using the two-dimensional electron density ( $3.5 \cdot 10^{15} \text{ m}^{-2}$ ) we estimate the number of electrons in our dot at definition to be about 250 ( $\pm 10$ ). In Figure 2 the measured dot conductance is plotted as a function of the centre gate voltage for typical Coulomb-blockade conditions. Of particular interest here is the number of oscillations observed between definition of the dot structure and "pinch-off", where the oscillations finally disappear. At a gate voltage of approximately -200 mV the dot becomes defined as can be seen by a significant change in the periodicity of the observed conductance oscillations (not visible under the resolution provided in Figure 2). The number of subsequent conductance oscillations observed before "pinch-off" is 240 suggesting that we have realised a dot structure where it is possible to study the charging effects of a dot with only a few electrons in the dot using transport experiments.

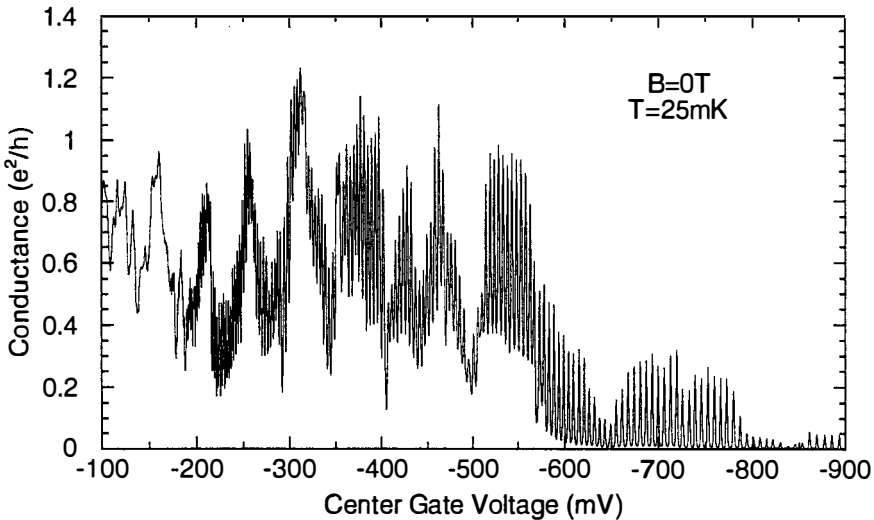


Figure 2. Typical conductance oscillations are plotted as a function of the applied centre gate voltage at zero magnetic field

Under the influence of a perpendicular magnetic field the observed conductance oscillations show an extremely rich and complex behaviour. In weak magnetic fields (i.e. for high filling factors) the conductance oscillations show an additional sinusoidal modulation where the number of coulomb peaks per period scales with the reciprocal of the magnetic field (see e.g. the conductance trace for  $B = 2 \text{ T}$  in Figure 3). This structure has been previously observed<sup>4</sup> and can be readily understood as the sequential filling of the Landau levels within the dot. Within the context of this model the amplitude of the

conductance oscillations reflects the coupling of the dots within the states to the external leads.

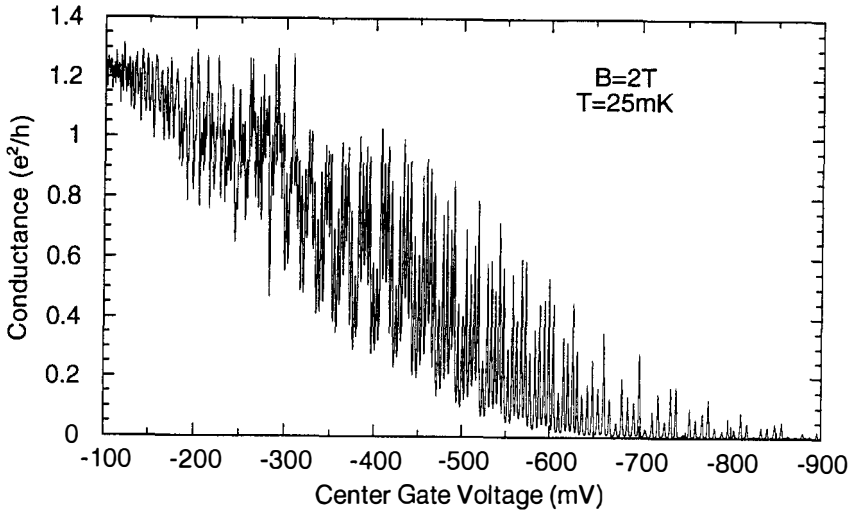


Figure 3. The low-field conductance oscillations are shown as a function of the voltage applied to the centre gate. The sinusoidal modulation of the peak structure is clearly illustrated.

For higher magnetic fields the modulation is no longer sinusoidal and, in addition, the peaks positions are also significantly modulated. This behaviour is clearly illustrated in the traces of Figure 4 where the conductance of the dot is plotted as a function of the applied centre gate voltage for a number of magnetic fields. In order to understand this behaviour in detail it is necessary to consider the self-consistent electronic distribution of the electrons within the dot<sup>5</sup>.

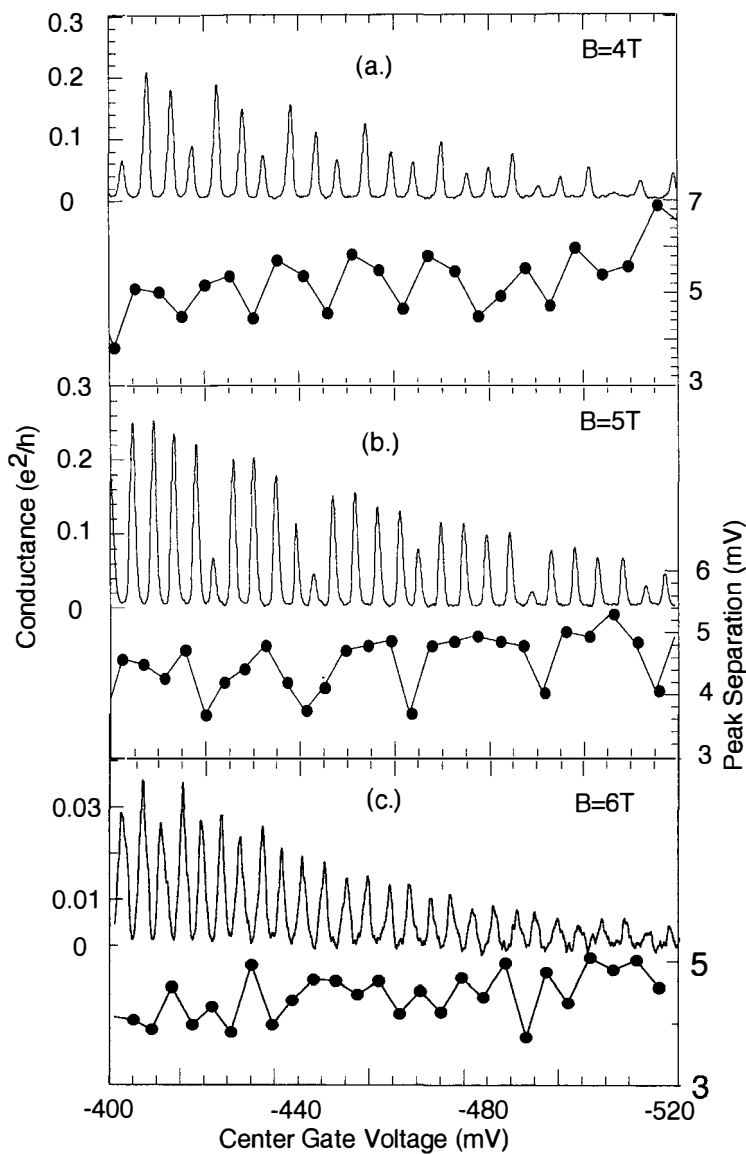


Figure 4. High-field conductance oscillations are plotted as a function of the centre gate voltage. The periodic modulation of both the Coulomb peak amplitudes as well as the peak separation is clearly observed.

At  $B = 0$  the self-consistent solution of the Poisson equation for a system consisting of a single gate and a conducting two-dimensional electron gas (2DEG) gives rise to a charge density distribution of the form<sup>5</sup>

$$(1) \quad n(r) = n_0 \sqrt{\frac{r_0 - r}{r_0 + 2l - r}} \quad \forall r \leq r_0$$

where  $r_0$  is the lithographically defined dot radius (for the structure discussed here  $r_0 = 240$  nm),  $2l$  is the depletion length between gate and 2DEG, and  $n_0$  the 2D electron density. The estimation of the dot size from the self-capacitance leads to  $l = 45$  nm at definition, in agreement both with the depletion lengths observed for the two single quantum point contacts as well as with electrostatic considerations<sup>5</sup>, which give  $l = \epsilon\epsilon_0 V_g / \pi n_0 e$ . In this analysis we make the approximation that the local density is determined by the closest gate. This is justified since  $l$  is small compared with the electrostatic dot diameter. In the presence of a magnetic field the screening properties of the 2DEG are significantly modulated. The electron gas divides into compressible rings separated by incompressible rings with integer filling factor. The filling factor decreases from its maximum value at  $r = 0$  to zero at the edge of the dot, thus traversing incompressible regions which act as insulators. As a consequence the confined electrons form intra-dot capacitances,  $C_{ij}$ , where  $i$  and  $j$  denote the compressible zones. Each zone  $i$  has a partial capacitance with respect to the surrounding metallic gates,  $C_{ig}$ , as illustrated in Figure 5. The width,  $w_k$ , of the insulating rings can be estimated to be<sup>5</sup>

$$(2) \quad w_k = 4 \sqrt{\frac{2\epsilon\epsilon_0 \hbar}{\pi e^3}} \sqrt{1 \frac{\Delta E}{B} \frac{v_0 \sqrt{k}}{v_0^2 - k^2}}$$

located at

$$(3) \quad r_k = r_0 - l \left( \frac{v_0^2 + k^2}{v_0^2 - k^2} + 1 \right)$$

where  $\Delta E$  is either the Zeeman energy if  $k$  is odd, or the cyclotron energy for even  $k$ .

Within the context of this model the peak separation modulation observed in the experiments reflects the energetic stability of particular electronic configurations within the dot determined by the interplay of the  $C_{ij}$  and  $C_{ig}$ . For the case of  $\nu \leq 2$  the problem is analytic and the separation modulation becomes most pronounced when  $C_{1g} = C_{2g}$ . We can thus estimate

$$(4) \quad (\alpha \delta V_g)_{\max} \leq \frac{e}{4C_{12}}$$

provided that an incompressible ring exists between the two Landau levels. This means that the width of the incompressible ring must be comparable to the magnetic length,  $l_B$ . Here  $\delta V_g$  is the amplitude of the CBO peak separation and  $\alpha$  the conversion factor as determined from the ratio between the total capacitance and the partial capacitance of the centre gate. From our measurements we find  $\delta V_{g,\max} = 0.6$  mV at  $V_g = -480$  mV leading to  $C_{12} \leq 290$  aF. This value may be compared directly with the intra-dot capacitance derived from purely electrostatic considerations

$$(5) \quad C_{12} = 4\epsilon\epsilon_0 r_1 \ln\left(\frac{4d}{w_1}\right).$$

From (3) the position of the insulating ring can be calculated,  $r_1 = 130$  nm. The width of the ring we set equal to the magnetic length (10.5 nm at  $B = 6$  T) corresponding to an effective  $g$ -factor of 3, and the characteristic distance between dot and gates we estimate to  $200 \text{ nm} \leq d \leq 400 \text{ nm}$ . For the range of  $d$  assumed we calculate  $260 \text{ aF} \leq C_{12} \leq 300 \text{ aF}$  in good agreement with the intra-dot capacitance as obtained from the measurement. However the information obtained about the width within this model is limited, not only due to the logarithmic dependence of  $C_{12}$  on  $w_1$  but also due to the uncertainty of the screening length  $d$ . Hence, our main conclusion is that the modulation of the CBO peak separation observed at 6 T can be well explained if we assume a spatial separation of the spin-split Landau levels of the order of the magnetic length. This corresponds to an enhanced  $g$ -factor of reasonable magnitude.

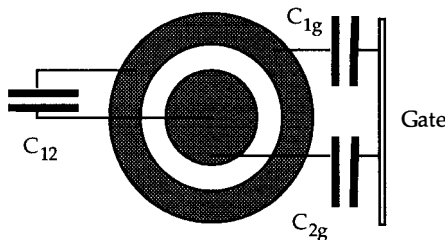


Figure 5. A schematic illustration of the compressible regions within the dot arising from the self-consistent charge distribution.

While the above model is reasonable for the estimation of the characteristic lengths of the dot, a more physical picture is given by the recently developed phase diagram<sup>7</sup> in

the  $B$ - $V_g$  plane. In this diagram each phase is characterised by the number of electrons in each compressible region. In a gate voltage sweep, a transition between phases always corresponds to a change in the total number of electrons,  $N$ , inside the dot. The boundaries between phases with the same value of  $N$  are parallel to  $V_g$  (see Figure 6). As the gate voltage is reduced the two compressible regions are cyclically depopulated and the peak separation is modulated as observed.

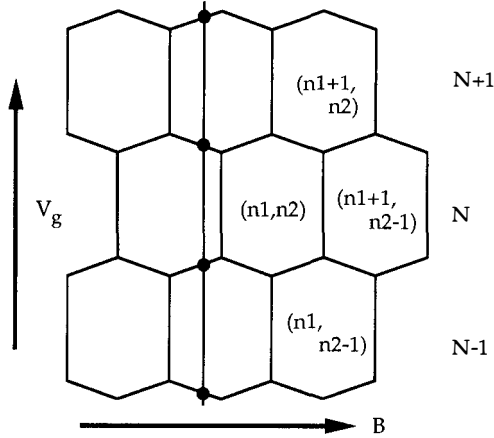


Figure 6. A schematic illustration of the phase diagram derived using the capacitance model of Ref. 7. The vertical line represents a typical gate voltage sweep showing the expected peak separation modulation as discussed in the text.

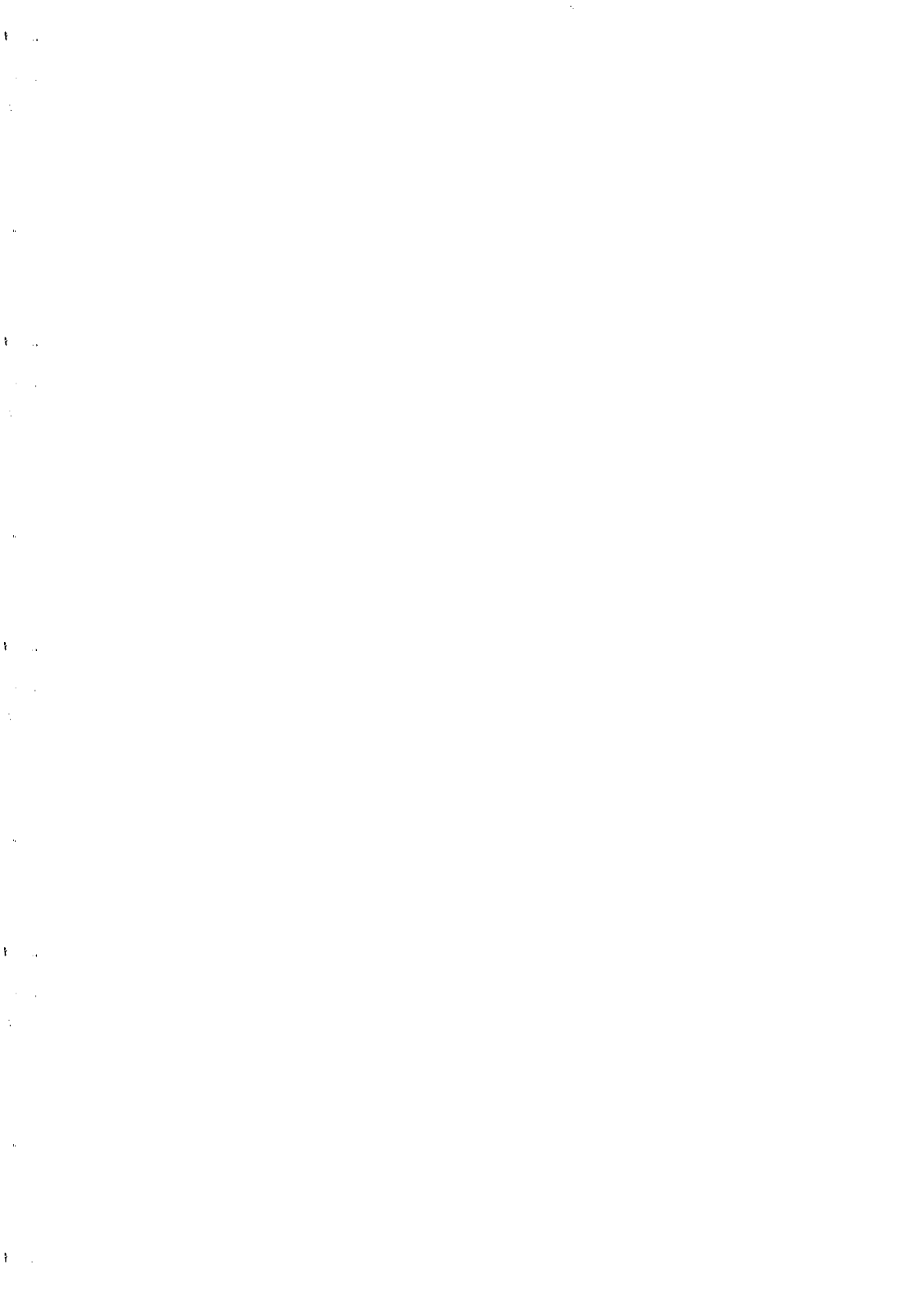
A cyclic depopulation is also observed over a wide range of gate voltages at higher filling factors ( $2 \leq \nu \leq 4$ ). In this regime we clearly observe the spin-splitting of the Landau levels and observe a striking modulation of both the CBO peak amplitude and peak separation. Here however the intra-dot capacitances cannot be connected to the measured modulation of the peak separation in a simple way. To obtain a more quantitative understanding the electrostatic energy of such a system should be minimised by varying the charge in each compressible region, taking into account that charge transfer between regions can only occur in integer multiples of the elementary charge. Such a calculation is beyond the scope of this paper, however many of the qualitative features of the results can be explained within the framework of the phase diagram. Of particular interest is the observation that at filling factors  $\sim 3$  ( $B = 4$  T) the number of peaks per period clearly suggests that we are able to resolve the spin-splitting of the Landau levels within the dot. This observation is in clear disagreement with the single particle picture developed using the Darwin-Fock states and shows the necessity to consider the electrostatic interaction between electrons. This observation is further substantiated by

the clear switch in filling sequence observed at  $-470$  mV. Another interesting feature which can be derived from an extended phase diagram is illustrated in the data at  $B = 5$  T. It has been suggested<sup>7</sup> that the boundaries between phases with constant  $N$  are only parallel to  $V_g$  as long as additional capacitances to the reservoirs can be safely ignored. Preliminary calculations which take such additional capacitances into account have shown that the situation can arise where it is energetically more favourable to successively remove electrons from the same compressible region. Such a tilted phase diagram is clearly able to explain the modulation of the peak amplitudes observed at  $B = 5$  T where we suggest that for each electron removed from the inner region four electrons are removed from the outermost compressible region.

In conclusion, we have investigated the Coulomb blockade oscillations in a semiconductor quantum dot structure at high magnetic fields and have found strong modulations both in the amplitude as well as in the separation of the conductance peaks. A self-consistent charge density model is shown to be an appropriate description of the system. Within this model the modification of the screening properties of the 2DEG by the magnetic field leads to the formation of intra-dot capacitances. The electrostatic energy necessary for the rearrangement of charge inside the dot is shown to be the reason for the modulation of the conductance peak separations. To explain our data we must assume that the separation between spin-split Landau levels is of the order of the magnetic length. This requirement leads to an estimate of an enhanced  $g$ -factor within the dot.

#### References:

1. Special Issue on Single Charge Tunneling, *Z. Phys.* **B 85**, 3 (1991).
2. C.W.J. Beenakker, *Phys. Rev.* **B 44**, 1646 (1991).
3. A.T. Johnson, L.P. Kouwenhoven, W. de Jong, N.C. van der Vaart, C.J.P.M. Harmans, and C.T. Foxon, *Phys. Rev. Lett.* **69**, 1592 (1992).
4. A.A.M. Staring, B.W. Alphenaar, H. van Houten, L.W. Molenkamp, O.J.A. Buyk, M.A.A. Mabeoone, and C.T. Foxon, *Phys. Rev.* **B 46**, 12869 (1992).
5. D.B. Chklovskii, B.I. Shklovskii, and L.I. Glazman, *Phys. Rev.* **B 46**, 4026 (1992).
6. D.B. Chklovskii, K.A. Mateev, and B.I. Shklovskii, *Phys. Rev.* **B 47**, 12605 (1993).
7. A.K. Evans, L.I. Glazman, and B.I. Shklovskii, *Phys. Rev.* **B 48**, 11120 (1993). J.M. Kinaret and N.S. Windgreen, *Phys. Rev.* **B 48**, 11113 (1993).
8. P.L. McEuen, E.B. Foxman, U. Meirav, M.A. Kastner, N.S. Windgreen, and S.J. Wind, *Phys. Rev. Lett.* **66**, 1926 (1991).  
P.L. McEuen, E.B. Foxman, J.M. Kinaret, U. Meirav, M.A. Kastner, N.S. Windgreen, and S.J. Wind, *Phys. Rev.* **B 45**, 11419 (1992).



# Suppression of Josephson Effect and Little-Parks Experiments in the Fractional Hall Liquid

Shechao Feng, Alex Levine, Lan Yin, and Shou-Cheng Zhang

*Department of Physics, University of California, Los Angeles, California 90024-1547, USA*

## Abstract

We use the Chern-Simons gauge theory for the fractional quantum Hall effect (FQHE) to calculate the Josephson current for two weakly coupled subsystems separated by a thin tunnel barrier where each subsystem is in a primary quantum Hall state  $\nu = \frac{1}{(2k+1)}$  ( $k = 0, 1, 2, \dots$ ), at zero temperature. We find that the Josephson current is strongly suppressed by the long-range quantum fluctuations of the Chern-Simons gauge field. We also show that this theory leads to the prediction that an applied gate voltage coupled to an isolated region in a two-dimensional electron gas can induce Little-Parks oscillations of the longitudinal conductance in the quantum Hall devices at odd denominator filling fractions.

## I. INTRODUCTION

Recently a new theoretical framework has been developed to describe the fractional quantum Hall effect (FQHE) in two-dimensional electron gas (2DEG) systems, based on an exact Chern-Simons gauge transformation, which maps the original interacting electron system in a high magnetic field to that of interacting Chern-Simons (CS) bosons under an (on average) zero magnetic field [1,2]. To put it simply, this approach treats an electron plus

$2k+1$  flux quanta as a new composite (Chern-Simon) “particle” which can be shown to obey Bose statistics. For the primary FQHE states  $\nu = 1/(2k+1)$ , it is easy to show that the CS bosons on average do not see a net magnetic field. At the mean-field level, one then argues that these CS bosons condense into a superfluid state at low enough temperatures, and the (dissipationless) quantum Hall effect is equivalent to the superfluidity (or superconductivity) of the charged CS bosons, which play a similar role as the Cooper pairs in the problem of superconductivity. It can be shown that if one starts from the mean-field theory of these superfluid CS bosons, and then include the effect of quantum fluctuations calculated to (quadratic) Gaussian order, one can reproduce exactly the original Laughlin wavefunction for the primary fractional quantum Hall state  $\nu = 1/(2k+1)$  [2]. Thus this CS boson theory of FQHE is precisely equivalent to the Laughlin variational approach [3]. What this approach offers in addition to the standard Laughlin variational approach is that to a large extent, the phenomenon of fractional quantum Hall effect can be mapped onto the phenomena of superfluidity and superconductivity (for the Chern-Simons bosons), which are more familiar conceptually to condensed matter physicists. Thus the relationship between the CS gauge theory and the Laughlin wavefunction theory for FQHE is quite analogous to that between the Ginzburg-Landau formalism and the BCS variational wavefunction approach in the theory of superconductivity.

In this paper we continue to explore the similarities between the FQHE and superconductivity by considering the FQH equivalents of the Josephson Effect and the Little-Parks experiment. By testing the analogy between the two systems in this manner we find that it holds imperfectly beyond mean field order. Using this analogy we can make predictions about the existence of Little-Parks oscillations but find that gaussian fluctuations destroy the Josephson current predicted in the mean-field approximation. Thus we see the utility and danger of the analogy between FQHE and superconductivity.

## II. THE JOSEPHSON EFFECT

### A. Formulation of the problem and the mean-field solution

We envision our weak-link 2DEG system to consist of two sheets of electron gas (with equal dimensions  $L_x \times L_y$ ), which are coupled weakly at  $x = 0$  (see Fig. 1). We assume for simplicity that the junction itself has zero area, so that the “diffraction” type reduction of the Josephson current by the magnetic flux through the junction area can be neglected. In theory, such a weak-link geometry can be achieved by growing (using MBE) a GaAs/AlGaAs heterostructure on top of a disorder-free substrate which contains an atomically sharp step, as we depict in Fig. 1. Since the single electron wavefunction is confined to a short distance  $\lambda$  ( $\lambda \sim 70\text{\AA}$ ) in the vertical  $z$ -direction, an appropriate choice of the step size  $d > \lambda$  would result in a weak coupling between the two 2DEG subsystems (hereafter we label them 1 and 2). The task of the following sections is to use the Chern-Simons gauge theory to calculate the Josephson current for the system just proposed.

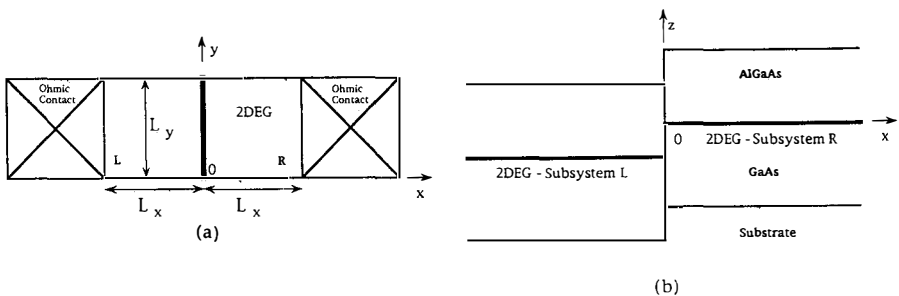


FIG. 1. The geometry of the weak-link 2DEG system under study. We assume that a high mobility GaAs/AlGaAs heterostructure system is grown on top of a disorder-free substrate which contains an atomically sharp step of height  $d$  at  $x = 0$ . (a) Top view of the device; (b) side view of the device. The two 2DEG subsystems are assumed to have the same dimensions  $L_x$  and  $L_y$ .

We confine our calculation to the primary fractional Hall states which have filling factors  $\nu = 1/(2k + 1)$ , with  $k = 0, 1, 2, \dots$ . The Hamiltonian for this weak-link FQHE system in terms of the original electron (fermion) field operators  $\psi_L(\vec{r})$  and  $\psi_R(\vec{r})$  in subsystems L (for left) and R (for right) consists of three contributions:

$$H = H_L + H_R + H_T. \quad (1)$$

The Hamiltonian for each subsystem L ( $x < 0$ ) and R ( $x > 0$ ) takes the usual form

$$H_L = \frac{1}{2m^*} \int_{x < 0} d^2x \psi_L^\dagger(\vec{x}) \left( \frac{\hbar}{i} \vec{\nabla} + \frac{e}{c} \vec{A}(\vec{x}) \right)^2 \psi_L(\vec{x}) + \frac{1}{2} \int_{x < 0} d^2x d^2y \delta \rho_L(\vec{x}) V(\vec{x} - \vec{y}) \delta \rho_L(\vec{y}), \quad (2)$$

where  $\nabla \times \vec{A}(\vec{x}) = B\hat{z}$  is the uniform external magnetic field,  $\vec{x} = (x, y)$  are the spatial coordinates,  $V(\vec{x})$  is the (Coulomb) interaction potential among electrons, and  $\delta \rho_L(\vec{x}) \equiv \rho_L(\vec{x}) - \bar{\rho}$ , where  $\rho_L(\vec{r}) = \psi_L^\dagger(\vec{r})\psi_L(\vec{r})$  is the electron density operator, and  $\bar{\rho} = \nu B/\phi_0$  is the average electron density which we assume to be the same in both subsystems L and R.

$H_R$  can be obtained from Eq. (2) by substituting  $L \rightarrow R$ , and the integrations are over the region  $x > 0$  in this case.

The tunneling Hamiltonian  $H_T$  in Eq. (1) can be written in terms of the original electron operators:

$$H_T = E_0 \sum_{\vec{k}} (T a_{\vec{k}}^\dagger b_{\vec{k}} + h.c.) \quad (3)$$

where  $a_{\vec{k}}^\dagger$  is the electron creation operator in the left (L) region ( $x < 0$ ) for momentum mode  $\vec{k}$ , and  $b_{\vec{k}}^\dagger$  is that in the right (R) region. We have here assumed implicitly that the tunnel junction between the two 2DEG subsystems is perfectly flat (in the  $y$ -direction), so that the transverse momentum of the tunneling electron is conserved upon tunneling from one side of the barrier to the other. Since the tunneling process also conserves energy, the longitudinal component of electron's momentum must also be conserved. Therefore, only the same (vector) momentum states are coupled through our tunneling Hamiltonian Eq. (3).

We take here  $E_0$  as some characteristic energy scale for the step perturbation potential at the junction, which should be of the order of the cyclotron energy  $\hbar\omega_c$ , and  $T \sim e^{-d/\lambda} \ll 1$  is a dimensionless overlap integral (amplitude transmittance) of the  $z$ -directional wavefunction from the two subsystems separated by a sharp step (see Fig. 1), or is due to some other type of tunnel barrier between the two 2DEG subsystems.

Using the relation

$$\psi_L(\vec{x}) = \frac{1}{\sqrt{A}} \sum_{\vec{k}} e^{i\vec{k}\cdot\vec{x}} a_{\vec{k}},$$

for  $x < 0$  with  $A = L_x L_y$ , etc., we can rewrite  $H_T$  as

$$H_T = E_0 T \int_{x < 0} d^2x \psi_L^\dagger(\vec{x}) \psi_R(\vec{x} + L\hat{x}) + h.c. \quad (4)$$

We see clearly that the tunneling Hamiltonian for a flat (i.e. disorder free) tunnel barrier gives rise a coupling between any given point  $\vec{x}$  in the *bulk* of the left subsystem and the corresponding point  $\vec{x} + L\hat{x}$  in the right subsystem, and vice versa. Thus it is our opinion that for the problem of coherent tunneling between the two 2DEG subsystems, the relevant physics is that of the bulk rather than the edge. The edge states are important for the dissipative (or incoherent) tunneling channel between the two subsystems, as discussed recently by Fisher and Kane [4].

We can now perform the (exact) Chern-Simons gauge transformation in subsystems L and R separately. In subsystem L, we introduce the CS boson field operator as

$$\phi_L(\vec{x}) = e^{i\theta^{CS}(\vec{x})} \psi_L(\vec{x}), \quad (5)$$

with

$$\theta^{CS}(\vec{x}) \equiv m \int_{x < 0} d^2y \alpha(\vec{x} - \vec{y}) \rho_L(\vec{y}).$$

being the Chern-Simons phase angle. Here  $m = 2k + 1$  is the odd integer corresponding to the primary filling factor  $\nu = 1/(2k + 1)$ ,  $\alpha(\vec{x} - \vec{y})$  is the azimuthal angle subtended by the vector  $\vec{x} - \vec{y}$ , and  $\phi_0 = hc/e$ . It is easy to verify that the new field operator  $\phi_L(\vec{x})$  satisfies Bose statistics:

$$[\phi_L(\vec{x}), \phi_L^\dagger(\vec{y})] = \delta(\vec{x} - \vec{y}).$$

The physical meaning of the Chern-Simons transformation is to tie  $2k + 1$  flux quanta to each electron dynamically, such that a given electron at position  $\vec{x}$  “feels” the Aharonov-Bohm phase factor from the flux quanta tied to all the other electrons. Since we tie an odd number of flux quanta to each electron at filling factor  $\nu = 1/(2k + 1)$ , an exchange operation between two electrons introduce an additional statistical factor  $(-1)^{2k+1}$  in addition to the usual Fermi exchange factor  $(-1)$ , thus making the  $\phi$  operator a bosonic one [5].

The Hamiltonian  $H_L$  in terms of the new CS boson field operators takes the form

$$H_L = \frac{1}{2m^*} \int_{x < 0} d^2x \phi_L^\dagger(\vec{x}) \left( \frac{\hbar}{i} \vec{\nabla} + \frac{e}{c} \vec{A}(\vec{x}) - \vec{a}_L(\vec{x}) \right)^2 \phi_L(\vec{x}) + \frac{1}{2} \int_{x < 0} d^2x d^2y \delta\rho_L(\vec{x}) V(\vec{x} - \vec{y}) \delta\rho_L(\vec{y}), \quad (6)$$

where  $\vec{a}_L(\vec{x})$  satisfies the CS constraint relation (corresponding to the physical requirement that each electron is tied to  $2k + 1$  flux quanta):

$$b_L(\vec{x}) \equiv (\nabla \times \vec{a}_L)_z = (2k + 1) \phi_0 \rho_L(\vec{x}). \quad (7)$$

Here, we can write  $\rho_L(\vec{x}) = \phi_L^\dagger(\vec{x}) \phi_L(\vec{x})$  in the new CS representation.

It is clear that the CS bosons in the L region feel an effective “magnetic field” given by

$$\delta b_L \equiv b_L - B = (\nabla \times \delta \vec{a}_L)_z = (2k + 1) \phi_0 \delta \rho_L(\vec{x}), \quad (8)$$

where  $\delta \rho_L(\vec{x}) = \rho_L(\vec{x}) - \bar{\rho}$ , at primary filling factor  $\nu = 1/(2k + 1)$ . Thus we see explicitly that upon averaging over the sample area, the effective magnetic field felt by the CS bosons  $\delta \bar{b}_L = 0$ . As we shall see, however, that quantum fluctuations in  $\delta b_L$  have important consequences, one of which is the severe suppression of the Josephson effect which would be present if the system were to be describable by the mean field theory.

We can perform the Chern-Simons transformation for subsystem R identically as above, with the notational change  $L \rightarrow R$ .

We now consider how the tunneling Hamiltonian is modified under the CS transformation. It now takes the form

$$H_T = E_0 \int_{x<0} d^2x \left\{ T \phi_L^\dagger(\vec{x}) \exp[i\theta_L^{CS}(\vec{x})] \times \phi_2(\vec{x} + L\hat{x}) \exp[-i\theta_R^{CS}(\vec{x} + L\hat{x})] + h.c. \right\}. \quad (9)$$

It is important to notice that in addition to the boson field operators, we have the additional Chern-Simons phase factors which we shall show lead to severe suppression of the Josephson current amplitude.

The operator form of the Josephson current at zero temperature can be derived from

$$\begin{aligned} I_J &= \dot{Q}_L = e \frac{d}{dt} \int_{x<0} d^2x \rho_L(\vec{x}) \\ &= \frac{e}{i\hbar} \int d^2x [\phi_L^\dagger(\vec{x}) \phi_L(\vec{x}), H] = \frac{e}{i\hbar} \int d^2x [\phi_L^\dagger(\vec{x}) \phi_L(\vec{x}), H_T] \\ &= \frac{2eE_0}{\hbar} \int_{x<0} d^2x \text{Im} \left\{ T \phi_L(\vec{x}) \exp[i\theta_L^{CS}(\vec{x})] \times \phi_R^\dagger(\vec{x} + L\hat{x}) \exp[-i\theta_R^{CS}(\vec{x} + L\hat{x})] \right\}. \quad (10) \end{aligned}$$

Within the mean-field (MF) theory, we make the approximation  $b_{L(R)}(\vec{x}) \rightarrow \bar{b} = B$ . Thus we may take the average CS bosonic fields (order parameters of the quantum Hall liquid) to be simply  $C$ -numbers, in the form of  $\bar{\phi}_L = \sqrt{\bar{\rho}} e^{i\bar{\theta}_L}$ , and  $\bar{\phi}_R = \sqrt{\bar{\rho}} e^{i\bar{\theta}_R}$ , where  $\bar{\theta}_L$  and  $\bar{\theta}_R$  are two mean field phases, the difference of which drives a coherent Josephson current across the tunnel barrier. Since we assume the two subsystems to be identical in shape, we also have the relation  $\bar{\theta}_L^{CS}(\vec{x}) = \bar{\theta}_R^{CS}(\vec{x} + L\hat{x})$  at the mean field level. Thus the messy CS phase factors in Eq. (10) simply drops out in the mean field theory of the Josephson effect. This immediately leads to the first Josephson relation in mean-field theory as (assuming for simplicity that the overlap integral  $T$  is a real number):

$$I_J^{MF} = I_0^{MF} \sin(\bar{\theta}_L - \bar{\theta}_R), \quad (11)$$

where the Josephson current amplitude in the mean-field theory is given by

$$I_0^{MF} = \frac{2eTE_0\bar{\rho}A}{\hbar}. \quad (12)$$

In the next subsection, we shall see how quantum fluctuations of the  $\theta^{CS}$  angular variables in the ground state (Laughlin) wavefunction suppress severely the above mean-field result for the Josephson current, which makes it essentially impossible to observe the coherent channel of quantum tunneling between two weakly coupled quantum Hall liquids.

### B. Suppression of Josephson current amplitude by quantum fluctuations

It is crucial to see how quantum fluctuations suppress the mean-field result from the previous section. i.e. we need to calculate

$$I_J = \frac{2eE_0T}{\hbar} \int_{x<0} d^2x \text{Im} \left\{ \langle \phi_L(\vec{x}) \exp[i\theta_L^{CS}(\vec{x})] \rangle_{H_L} \langle \phi_R^\dagger(\vec{x} + L\hat{x}) \exp[-i\theta_R^{CS}(\vec{x} + L\hat{x})] \rangle_{H_R} \right\}, \quad (13)$$

where  $\langle \rangle_{H_L}$  denotes the quantum expectation value ( $T = 0$ ) over the ground state (Laughlin) wavefunction for subsystem L, which is the ground state eigenfunction of  $H_L$  to Gaussian approximation (similarly for subsystem R). Introducing fluctuational variables  $\delta\rho(\vec{x})$  and  $\delta\theta(\vec{x})$  (omitting the subscript L or R from now on as it is clear from context):

$$\phi(\vec{x}) = \sqrt{\bar{\rho} + \delta\rho(\vec{x})} e^{i[\theta_1 + \delta\theta(\vec{x})]},$$

we expand  $H_L$  up to quadratic order in  $\delta\rho(\vec{x})$  and  $\delta\theta(\vec{x})$ , and perform Fourier transforms  $\delta\rho(\vec{x}) = \frac{1}{A} \sum_{\vec{q}} e^{i\vec{q}\cdot\vec{x}} \delta\rho_{\vec{q}}$ , etc., while working in the transverse gauge  $\nabla \cdot \delta\vec{a}(\vec{x}) = 0$ . We then arrive at the following simple expression for  $H_L$  [2]:

$$H_L = \text{Const.} + \frac{\hbar^2 \bar{\rho}}{2m^* A} \sum_{\vec{q}} \left\{ \left( \frac{[2\pi(2k+1)]^2}{q^2} + \frac{m^* V_{\vec{q}}}{\hbar^2 \bar{\rho}} + \frac{q^2}{\bar{\rho}^2} \right) \delta\rho_{\vec{q}} \delta\rho_{-\vec{q}} + q^2 \delta\theta_{\vec{q}} \delta\theta_{-\vec{q}} \right\}, \quad (14)$$

where  $\delta\rho_{\vec{q}}$  and  $\delta\theta_{\vec{q}}$  obey canonical commutation relation  $[\delta\rho_{\vec{q}}, \delta\theta_{\vec{p}}] = iA\delta_{\vec{q},-\vec{p}}$ . Thus for each  $\vec{q}$  mode (with  $q_x \geq 0$ ), the quantum fluctuational Hamiltonian takes the simple form of two independent harmonic oscillators, up to quadratic (Gaussian) approximation which we have made here.

After some straightforward but tedious algebra, we can identify the dominant fluctuations in the quantity of interest,  $\langle \phi_L(\vec{x}) \exp[i\theta_L^{CS}(\vec{x})] \rangle_{H_L}$ , to be from the  $\delta\theta_L(\vec{x})$  variables and the  $\delta\theta_L^{CS}(\vec{x})$  variables. Thus we may write

$$\langle \phi_L(\vec{x}) \exp[i\theta_L^{CS}(\vec{x})] \rangle_{H_L} = \sqrt{\bar{\rho}} e^{i\bar{\theta}_L} \times \exp \left\{ -\frac{1}{2} \langle \delta\theta_L(\vec{x}) \delta\theta_L(\vec{x}) \rangle - \frac{1}{2} \langle \delta\theta_L^{CS}(\vec{x}) \delta\theta_L^{CS}(\vec{x}) \rangle \right\}. \quad (15)$$

The fluctuations in the phase of the order parameter, can be readily evaluated, using the harmonic oscillator Hamiltonian in Eq. (14), yielding for a square sample of length  $L$ ,

$\frac{1}{2}(\delta\theta\delta\theta) \approx \frac{2k+1}{4} \ln(L/l_0)$ . In the last expression  $l_0 = \sqrt{\frac{\nu}{2\pi\rho}}$  is the magnetic length which we use as a cutoff length scale for the (continuum) CS gauge theory. Thus the fluctuations in  $\delta\theta$  in the order parameter will only lead to *power law* reduction factors of the Josephson current amplitude, which is not too bad.

The more severe quantum fluctuations come from the factor  $\frac{1}{2}(\delta\theta_L^{CS}(\vec{x})\delta\theta_L^{CS}(\vec{x}))$ . This quantity is a bit more complicated to evaluate, due to the presence of the azimuthal angular variable  $\alpha(\vec{x}-\vec{y})$ . We let  $l_0$  be the cutoff length of the continuum. After some tedious algebra, we find the following as a lower bound on the CS phase fluctuations

$$\langle[\delta\theta^{CS}(0)]^2\rangle \geq \frac{m}{16\pi} \left(2\frac{L}{l_0} + 16\pi \ln\left[\frac{L}{l_0}\right]\right) \quad (16)$$

Thus we see that the Josephson current amplitude  $I_0$  is severely suppressed by quantum fluctuations of the CS phase angle  $\theta^{CS}$ , with the final magnitude of order

$$I_0 \approx \frac{2eT E_0 \bar{\rho} A}{\hbar} \times \exp\left(-\frac{2k+1}{4\pi} L/l_0\right) \quad (17)$$

### III. THE LITTLE-PARKS EXPERIMENT

In this section, we propose a direct test of the Chern-Simons picture for FQHE, by considering conductance oscillations in an inhomogeneous fractional Hall system with an external capacitive gate applied to an isolated region in the center of the device. This work by two of us has just been published [6].

Our starting point is the same CSLG Hamiltonian for the FQHE as used in calculating the Josephson current in the last section. To illustrate our idea of gate voltage induced Little-Parks oscillations due to the CS gauge field, let us consider a high mobility 2DEG sample where a capacitive gate of mesoscopic dimension (e.g. with an area of order  $A \sim 10^{-10} \text{cm}^2$ ) is coupled to an isolated region of the sample. Assume the external magnetic field is such that  $\nu = 1/(2k+1)$ . Suppose we now turn on a gate voltage  $V_g$  which is coupled capacitively to the central ‘‘hole’’ region. The application of this voltage leads to a change in the local

density  $\delta\rho(x) = \rho(x) - \bar{\rho}$ , which in term results in a net magnetic field  $\delta b(x) = B - b(x)$  localized inside the hole region. However, the net flux inside a multiply connected superfluid system  $\Phi$  is not arbitrary, but quantized in units of  $\phi_0 = hc/e$ , chosen in such a way as to minimized the “kinetic” energy

$$E(\Phi) = (\Phi - \Phi_g)^2/2L \quad (18)$$

Here  $\Phi_g = (2k + 1)CV_g\phi_0/e$  is the flux induced by the gate voltage and can be changed continuously,  $C$  is the capacitance of the hole region with respect to the gate, and  $L$  is a parameter which can be related to the quasi-particle creation energy. The quantization condition is accurate as long as the sample width is large compared with the magnetic length. For  $\Phi_g = N\phi_0$ ,  $E(\Phi)$  is depicted in Fig. 2(a). In this case we obtain  $\Phi = N\phi_0$ , and we see that there is a gap to adding one more flux quantum to the system,  $\Delta E = \phi_0^2/2L$ . Integrating

$$b(\vec{x}) = \nabla \times \vec{a}(\vec{x}) = \phi_0 m \rho(\vec{x}), \quad (19)$$

over two dimensional space we obtain  $\Phi = (2k + 1)\phi_0 Q/e$ , where  $Q$  is the induced charge on the hole. Thus adding one unit of flux is equivalent to adding  $Q = e/(2k + 1)$  unit of fractional charge, and this energy can therefore be identified with the creation energy of a Laughlin quasi-particle, or the incompressibility gap. Denoting this gap by  $\Delta(2k + 1)$ , this allows us to identify the parameter  $L$  through  $\phi_0^2/2L = \Delta(2k + 1)$ . However, when  $\Phi_g = (N + 1/2)\phi_0$ ,  $E(\Phi)$  is shown in Fig. 2(b), and we see that  $\Phi = (N + 1)\phi_0$  is degenerate with  $\Phi = N\phi_0$ . The incompressibility gap vanishes and dissipation could occur in this case! Equations (19) and (18) therefore lead to a highly nonlinear, in fact stepwise dependence of the screening charge  $Q$  on the applied gate voltage [7], as shown in Fig. 2(c). Whenever  $\Phi_g = (N + 1/2)\phi_0$ ,  $Q$  changes by  $e/(2k + 1)$ . At this value of  $\Phi_g$ , there is no gap to add a fluxon to the hole region, and the change in  $Q$ , or equivalently  $\Phi$ , is accomplished by the spontaneous creation of a quasi-particle and quasi-hole pair (equivalent to a fluxon anti-fluxon pair) in the bulk followed by a tunneling process in which the quasi-hole goes

to the center hole region and the quasi-particle goes to the edge of the sample. Since the tunneling motion of fluxons across the superfluid region is associated with a longitudinal voltage drop (due to the Faraday effect), one should observe a resistance peak at this value of  $\Phi_g$ . The fundamental periodicity in  $\Phi_g$  is  $\phi_0$ . This implies a voltage periodicity of  $\Delta V_g = \frac{e}{(2k+1)C}$ , i.e. proportional to  $\nu = 1/(2k+1)$ . These resistance oscillations are similar to the Little-Parks resistance oscillations of a superconductor in an applied magnetic field, where resistance peaks at  $\phi = (N + 1/2)\phi_0/2$ , the factor of 2 difference with our case comes from the charge  $2e$  of the Cooper pairs. The resistance in between the peaks should vanish exponentially as temperature approaches zero. We suggest that in addition to measuring the resistance oscillations at a given temperature, one also measures the activation gap from the temperature dependence, to verify that it vanishes at  $\Phi_g = (N + 1/2)\phi_0$ .

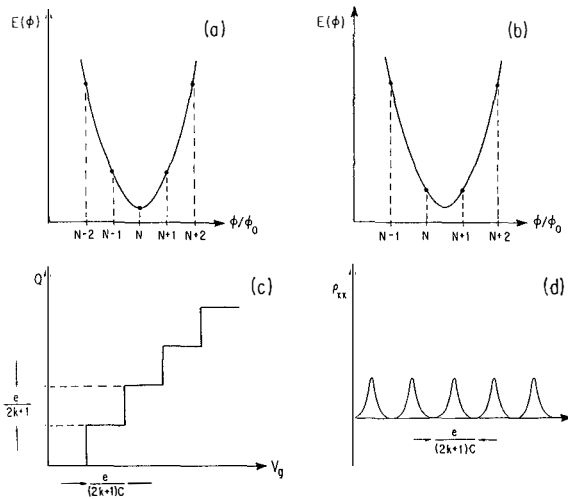


FIG. 2. For  $\nu = 1/(2k+1)$ : (a) Energy as a function of  $\Phi$  for  $\Phi_g = N\phi_0$ . (b) Energy as a function of  $\Phi$  for  $\Phi_g = (N + 1/2)\phi_0$ . (c) Induced charge  $Q$  on a capacitive gate as a function of gate voltage,  $Q$  jumps by  $e/(2k+1)$  whenever  $\Phi_g = (N + 1/2)\phi_0$ . (d) Oscillations of the longitudinal resistance as a function of gate voltage. Resistance peaks at  $\Phi_g = (N + 1/2)\phi_0$ , similar to the peaks in the Little-Parks experiment of a superconductor. Note the period in the gate voltage is proportional to  $\nu = 1/(2k+1)$ .

However, it has been argued by Thouless and Gefan [8] that at zero temperature the process of quasi-particle and quasi-hole tunneling proceeds with a rate that depends exponentially on the width of the Hall bar. Therefore, the gate potential has to be varied at a rate slower compared to the quasi-particle quasi-hole tunneling rate in order to observe the above mentioned voltage periodicity. A much faster rate is the tunneling of a real electron from the center hole region to the edge, since the tunneling barrier for this process is that between the 2D electron gas and the surrounding reservoir. If the rate for varying the gate potential is faster than the quasi-particle quasi-hole tunneling rate but slower than the tunneling rate of real electrons, then the resistance oscillation with a voltage periodicity of  $\Delta V_g = e/C$  is expected. This periodicity does not contain any information about the fractional charge.

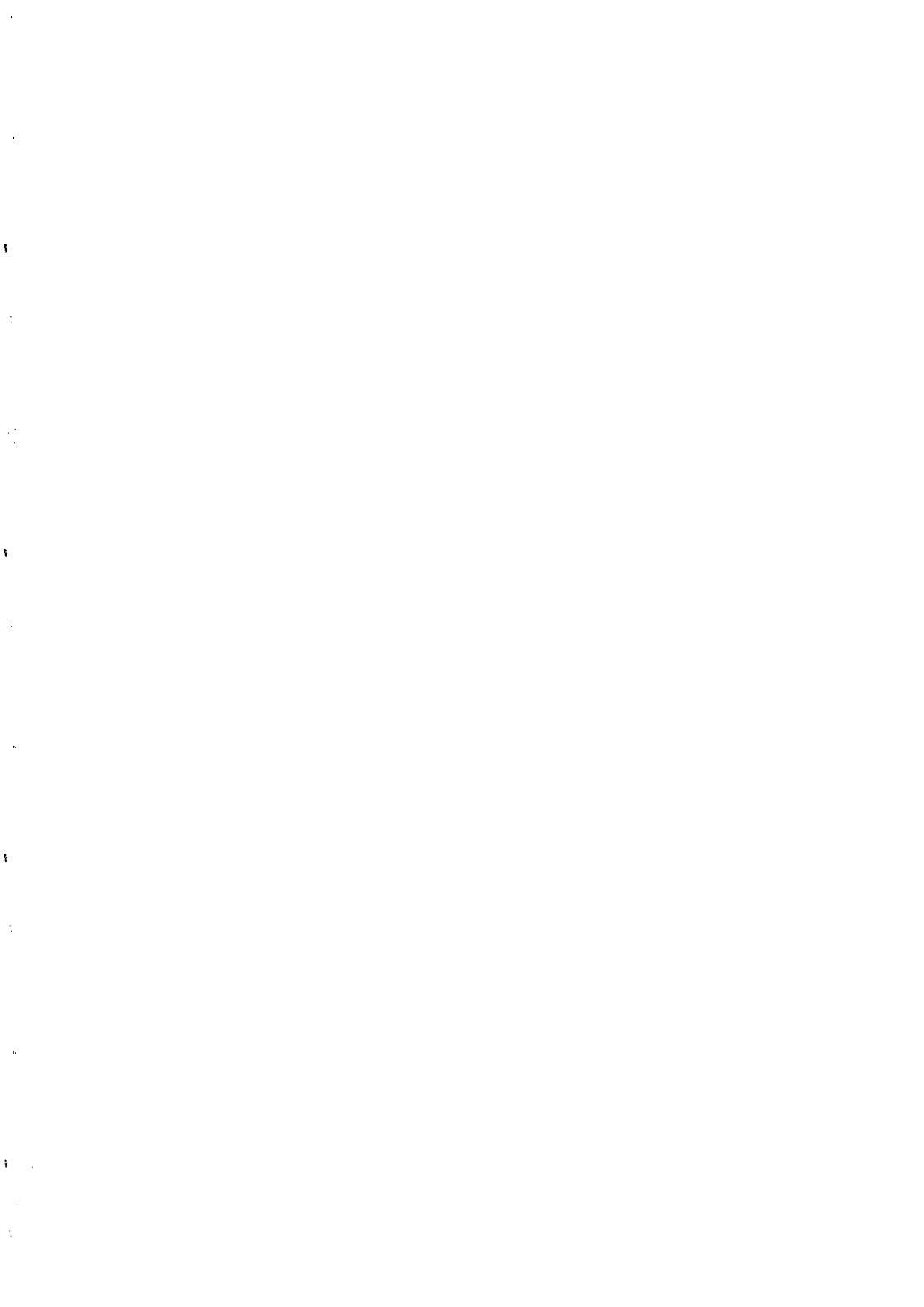
In a series of experiments by Simmons et al. [9], the conductance fluctuation is measured by both varying the external magnetic field and the uniform backgate voltage. The observed periodicity in backgate voltage is the same for  $\nu = 1$  and  $\nu = 1/3$ . This experiment is originally interpreted in terms of the theory by Kivelson and Pokrovsky [10], in which a magnetic flux period of  $hc/(e^*)$  is assumed. This observed period is different from the prediction we made above, in which the voltage periodicity of  $\Delta V_g = e^*/C$  is expected. We have two general comments concerning this point. First of all, this experiment is performed with a variation of the backgate voltage that acts on all electrons, unlike the case discussed here where a local potential is varied. The local potential in our case can be changed continuously in a controlled way, whereas the impurity potential from the donors arise from quantized positive charge, which preferably attracts integral numbers of electrons. Second, even in the case where the local potential can be varied continuously, one has to be sure that the rate of the variation is slow compared with the tunneling rate of the quasi-particles, as discussed above.

## ACKNOWLEDGMENTS

I also thank R. Bruinsma, X.-G. Wen, S. Chakravarty, S. Kivelson, D. Arovas, L. Pryadko, P. A. Lee and B. I. Halperin for useful discussions. This work is supported by the ONR under grant number N00014-92-J-4004, and the DOE under grant number DE-FG03-88ER45378.

## REFERENCES

- [1] S. C. Zhang, H. Hansson and S. Kivelson, *Phys. Rev. Letts*, 62, 82 (1989).
- [2] S. C. Zhang, *Int. J. of Modern Physics, B* 6, 25 (1992); A. Karlhede, S. A. Kivelson, and S. L. Sonhi, to appear in proceedings of the *9th Jerusalem Winter School on Theoretical Physics*.
- [3] R. B. Laughlin, *Phys. Rev. Lett.* 50, 1395 (1983).
- [4] C.L. Kane and M.P.A. Fisher, *Phys. Rev. Lett.* 68, 1220 (1992); C.L. Kane and M.P.A. Fisher, *Phys. Rev. B* 46, 7268 (1992); 46, 15233 (1992); K. Moon, H. Yi, C.L. Kane, S. Girvin, and M.P.A. Fisher, *Phys. Rev. Lett.* 71, 4381 (1993).
- [5] E. Fradkin *Field Theories of Condensed Matter Systems*, (Addison-Wesley 1991).
- [6] S. Feng and S. C. Zhang, *Phys. Rev. Lett.* 71, 3533 (1994).
- [7] D. Arovas and J. Jain, *Bull. Am. Phys. Soc*, 38, 135 (1993).
- [8] D. Thouless and Y. Gefan, *Phys. Rev. Lett.* 66, 806 (1991).
- [9] J. Simmons et al, *Phys. Rev. Lett.* 63, 1731 (1989); *Phys. Rev. B* 44, 12933 (1991); S. Hwang et al, *Sur. Sci.* 263, 72 (1992).
- [10] S. Kivelson and V. Pokrovsky, *Phys. Rev. B* 40, 1373 (1989).



## TIME-RESOLVED TUNNELING OF SINGLE ELECTRONS BETWEEN CONFINED QUANTUM HALL STATES

N.C. van der Vaart, M.P. de Ruyter van Steveninck, L.P. Kouwenhoven<sup>(a)</sup>, A.T. Johnson<sup>(b)</sup>, Y.V. Nazarov, A. van der Enden and C.J.P.M. Harmans.  
*Department of Applied Physics, Delft University of Technology  
P.O.Box 5046, 2600 GA Delft, The Netherlands*

C.T. Foxon<sup>(c)</sup>

*Philips Research Laboratories, Redhill, Surrey RH15HA, United Kingdom*

We have observed time-resolved tunneling of single electrons between two quantum Hall states in a quantum dot. The tunneling of a single electron between two Landau levels *within* the dot switches the conductance *through* the dot from on- to off-resonance. The tunnel barrier between the Landau levels is formed by an incompressible quantum Hall liquid. This barrier increases with magnetic field. Upon increasing the field we find that the time between two tunnel events reaches macroscopic values on the order of 100 s.

In the quantum Hall regime, electrons can travel over distances as long as a millimeter with only a small chance of being scattered into an adjacent edge channel<sup>1, 2</sup>. Only recently, it has become appreciated that the self-consistent arrangement of charge is important for understanding the properties of the electron states at the sample edge<sup>3-5</sup>. The emerging picture is that near the sample edge the quantum Hall states separate in alternating strips of incompressible and compressible states. This picture is still valid when the quantum Hall states are confined in a quantum dot<sup>4</sup>. Scattering between the confined quantum Hall states involves the movement of a single electron in space. At present, little is known about the dynamics of such a scattering event. In this article, we present a method, based on the Coulomb blockade of tunneling<sup>6</sup>, that enables us to control and measure single electron scattering events. We find that the time between two tunnel events can be tuned from less than 10 ms to more than 200 s, which allows a time-resolved measurement of single-electron tunneling between confined quantum Hall states.

Fig. 1 shows the geometry of our quantum dot<sup>7</sup>. The hatched parts are metallic gates fabricated on top of a GaAs / AlGaAs heterostructure with a two dimensional electron gas (2DEG) 100 nm below the surface. The ungated 2DEG has a mobility

of  $2.3 \cdot 10^6 \text{ cm}^2 / \text{Vs}$  and an electron density of  $1.8 \cdot 10^{15} \text{ m}^{-2}$  at 4.2 K. Applying a negative voltage to gates F, C, 1 and 2 depletes the electron gas underneath them, and forms a quantum dot with a diameter of about 600 nm containing roughly 300 electrons. Electron transport occurs via the tunnel barriers induced by gates 1-F, and 2-F, which couple the dot to the two wide 2DEG reservoirs. We set the conductances of the tunnel barriers at about  $0.1 \cdot e^2/h$ . The number of electrons in the dot can be varied with the voltage  $V_C$  applied to the center gate C. The experiments are performed in a dilution refrigerator with a base temperature of 10 mK using a small dc-bias voltage of  $6 \mu\text{V}$ . We work in the magnetic field regime where only the two spin-resolved states ( $LL_1$  and  $LL_2$ ) of the lowest Landau level are occupied.

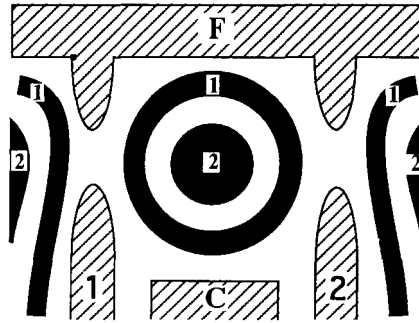


Fig. 1. Schematic of the gate geometry defining a dot with lithographic dimensions of  $0.8 \mu\text{m}$  by  $1 \mu\text{m}$ : F denotes the finger gate, 1 and 2 the quantum point contact gates, and C the center gate. The location of the compressible parts of  $LL_1$  and  $LL_2$  are denoted by the dark parts.

At zero magnetic field, we observed equally spaced Coulomb oscillations as a function of gate voltage, where each period corresponds to a change of one electron in the dot. Fig. 2 shows the conductance through the dot versus center gate voltage at a magnetic field of 4.3 T. A striking feature is that the trace shows a *split* oscillation alternated by three regular Coulomb oscillations.

The origin of the split-peaks becomes clear at higher fields. Fig. 3a shows two split-peaks and a regular Coulomb peak versus gate voltage at 5.2 T. A split-peak consists of two regular Coulomb peaks. We have added two dashed lines to each split-peak as a guide for the eye. At some gate voltages, the conductance switches discontinuously between the two branches of a split-peak. This behavior is further illustrated by Fig. 3b where we have fixed the gate voltage at the value denoted by the arrow in Fig. 3a. Here, the conductance is measured versus time and shows

switching between two discrete levels. The high value corresponds to the left branch and the low value to the right branch of the split-peak in Fig. 3a. The typical time between two switches is on the order of ten seconds. We found that at 6 T this time increases to about 200 seconds. On the other hand, in the lower magnetic field range of Fig. 2 the typical time between two switches is too short to be resolved by our measurement set-up. This smears out the switching between the two branches and gives rise to a continuous split-peak.

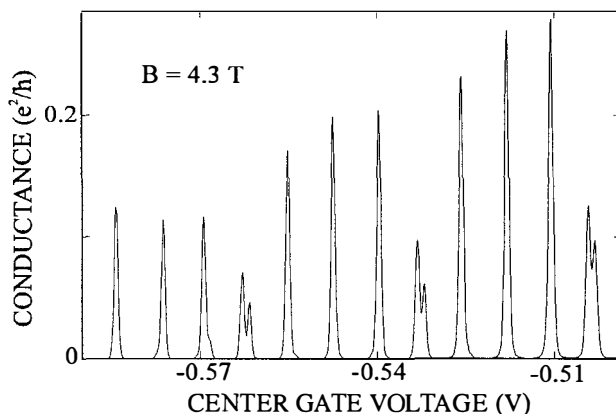


Fig. 2. Conductance through the dot versus center gate voltage at 4.3 T.

We will now discuss that a switch in the conductance in Fig. 3b is a time-resolved measurement of a tunnel event by a single electron between the two Landau levels in the dot<sup>8</sup>. McEuen et al.<sup>4</sup> have pointed out that the phase separation of quantum Hall states in a quantum dot leads to the picture of Fig. 1. Self-consistent arrangement of the charge in a high magnetic field causes LL<sub>2</sub> to form a compressible core in the center of the dot. LL<sub>1</sub> is compressible only in the ring region around the core. The ring and the core are spatially separated by an incompressible quantum Hall fluid which acts as a tunnel barrier. Transport from one 2DEG reservoir via the dot to the other reservoir primarily occurs via the ring, since the core is separated from the reservoirs over a much larger distance.

Adding an electron to a small isolated region costs a finite charging energy. At zero magnetic field, only one charging energy is important. However, in a high magnetic field with only LL<sub>1</sub> and LL<sub>2</sub> occupied, three charging energies are relevant. The total number of electrons  $N = N_1 + N_2$  is divided between  $N_1$  electrons in LL<sub>1</sub> and  $N_2$  electrons in LL<sub>2</sub>. Adding an electron to LL<sub>1</sub> increases the

electrochemical potential  $\mu_1$  of LL<sub>1</sub> with an amount  $E_1$  and also increases the electrochemical potential  $\mu_2$  with an interaction energy  $E_{12}$ . Similarly, adding an electron to LL<sub>2</sub> increases  $\mu_2$  with  $E_2$  and  $\mu_1$  by  $E_{12}$ . Single electron tunneling *within* the dot keeps the total number  $N$  constant. However, removing an electron from LL<sub>2</sub> and putting it in LL<sub>1</sub> increases  $\mu_1$  by  $E_1 - E_{12}$  and decreases  $\mu_2$  by  $E_2 - E_{12}$ . The same energies accompany the opposite process. We call these processes *internal charging*.

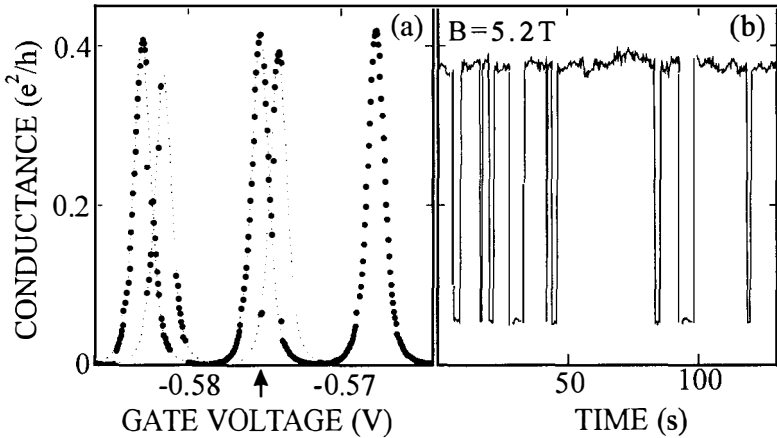


Fig. 3. (a) Conductance through the dot as function of center gate voltage at a field of 5.2 T using a time constant of 150 ms. The dashed lines are added as a guide for the eye. (b) Conductance versus time with the gate voltage fixed at the value denoted by the arrow in (a).

The concept of internal charging provides a qualitative understanding of the observed two-level switching. A peak in the conductance occurs when  $\mu_1$  is on-resonance with the reservoirs:  $\mu_1 = \mu_{res}$ . However, a tunnel event of a single electron between the Landau levels changes  $\mu_1$  which switches the conductance from *on-* to *off-resonance*. The conductance through LL<sub>1</sub> can therefore be used as a time-resolved probe to detect a tunnel event between two quantum Hall states. This type of time-resolved experiment resembles the electrometer-box configuration employed by Fulton et al.<sup>9</sup> and Lafarge et al.<sup>10</sup> to measure single electron hopping events in the superconducting and normal state of Aluminium tunnel junctions.

The values of the charging energies can be determined from the three peak spacing of the oscillations in Fig. 2. Using this, we found<sup>8</sup>:  $E_1 = 800 \mu\text{V}$ ,  $E_2 = 1175 \mu\text{V}$  and  $E_{12} = 650 \mu\text{V}$ .

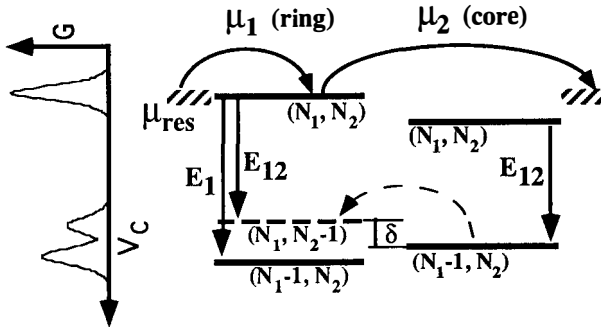


Fig. 4. Energy diagram showing the electro-chemical potentials  $\mu_{\text{res}}$  of the reservoirs,  $\mu_1$  of LL<sub>1</sub> and  $\mu_2$  of LL<sub>2</sub> for different numbers of electrons  $N_i$  in LL<sub>*i*</sub>. The width of the thick dashed line represents the applied bias voltage across the dot. The left hand side shows schematically the conductance when the gate voltage  $V_C$  is varied.

The role of the internal charging energies is illustrated in the energy diagram of Fig. 4. The electro-chemical potentials  $\mu_1$  and  $\mu_2$  denote the minimum energy for having a certain number of electrons in the ring (LL<sub>1</sub>) and the core (LL<sub>2</sub>). The left hand side shows schematically the conductance through the dot versus  $V_C$ . The topmost conductance peak occurs when  $\mu_{\text{res}}$  lines up with  $\mu_1(N_1, N_2)$  (solid arrows). By decreasing  $V_C$ , one electron is permanently removed from LL<sub>1</sub> and transport is blocked. The dot is now in the charge state  $(N_1 - 1, N_2)$ . When  $V_C$  is decreased further,  $\mu_{\text{res}}$  lines up with  $\mu_1(N_1, N_2 - 1)$  (dashed line). Transport via this state is possible only after an electron has tunneled from LL<sub>2</sub> to LL<sub>1</sub> (dashed arrow) which switches the conductance from *off-* to *on-resonance*. The conductance is switched back from *on-* to *off-resonance* when an electron tunnels back to LL<sub>2</sub>. Depending on the alignment of  $\mu_1(N_1, N_2 - 1)$  relative to  $\mu_2(N_1 - 1, N_2)$ , these processes may require thermal assistance. Another change in gate voltage aligns  $\mu_{\text{res}}$  with  $\mu_1(N_1 - 1, N_2)$ . Similar arguments show that in this case a tunnel event from LL<sub>2</sub> to LL<sub>1</sub> switches the conductance from *on-* to *off-resonance*. When the switching is too fast to be resolved, the conductance shows a continuous split-peak.

We have shown that the gate voltage and the magnetic field allow an experimental tuning of the two-level switching. Theoretically it is possible to describe the internal charging energies in terms of a capacitance model<sup>11, 12</sup>, with which we have been able to calculate the split-peaks and the regular pattern of Fig. 2. However, the dynamics of scattering between the Landau levels is still unknown. The large time scales may be explained by the large width of the incompressible strip. This width

increases with magnetic field<sup>5</sup> which will result in longer time scales. However, we would like to emphasize that scattering between the quantum Hall states involves a rearrangement of the charge distribution in the dot. The macroscopic time scale between two tunnel events is presumably related to such a kind of many-body rearrangement<sup>13</sup>. We expect that a study of the temperature dependence and the characteristics of the switching will further clarify the dynamics of scattering between confined quantum Hall states.

We would like to thank C. Dekker, L.J. Geerligs, P.L. McEuen, and J.E. Mooij for stimulating discussions, and W. Kool for contributions to the device fabrication, and the Delft Institute for MicroElectronics and Submicron technology for the use of their facilities. Financial support from FOM is gratefully acknowledged. LPK acknowledges support from the Royal Netherlands Academy of Arts and Sciences.

- (a) Present address: Lawrence Berkeley Laboratories, Mail stop 2-200, Berkeley CA 94720, USA.
- (b) Present address: Department of physics, University of Pennsylvania, David Rittenhouse Laboratory, Philadelphia PA 19014, U.S.A.
- (c) Present address: Department of Physics, University of Nottingham, Nottingham NG72RD, United Kingdom.

1. B.J. van Wees *et al.*, Phys. Rev. B **39**, 806 (1989).
2. S. Komiyama *et al.*, Phys. Rev. B **40**, 12566 (1989); B.W. Alphenaar *et al.*, Phys. Rev. Lett. **64**, 677 (1990).
3. A.M. Chang, Solid State Commun. **74**, 271 (1990); C.W.J. Beenakker, Phys. Rev. Lett. **64**, 216 (1990).
4. P.L. McEuen *et al.*, Phys. Rev. B. **45**, 11419 (1992).
5. D.B. Chklovski, B.I. Shklovskii and L.I. Glazman, Phys. Rev. B **46**, 4026 (1992).
6. For a review see: *Single Charge tunneling* eds. Grabert, H. & Devoret, M.H. (Plenum, New York, 1991).
7. L.P. Kouwenhoven *et al.*, Z. Phys. B **85**, 367 (1991).
8. N.C. van der Vaart *et al.*, submitted to Phys. Rev. Lett.
9. T.A. Fulton, P.L. Gammel and L.N. Dunkleberger, Phys. Rev. Lett. **67**, 3148 (1991).
10. P. Lafarge *et al.*, C. R. Acad. Sci. Paris **314**, 883 (1992). P. Lafarge *et al.*, Z. Phys. B. **85**, 327 (1991).
11. J.M. Kinaret and N.S. Wingreen, Phys. Rev. B **48**, 11113 (1993).
12. A.K. Evans, L.I. Glazman and B.I. Shklovskii, Phys. Rev. B **48**, 11120 (1993).
13. Y.V. Nazarov and A.V. Khaetskii, Phys. Rev. B. **49**, 5077 (1994).

## WIGNER MOLECULE ON THE TOP OF A QUANTUM DOT

Yuli V. Nazarov and A. V. Khaetskii  
*Faculteit der Technische Natuurkunde, Technische Universiteit Delft,  
 Lorentzweg 1, 2628 CJ Delft, the Netherlands*

Quantum dots in GaAs heterostructures display a complex inner structure in high magnetic field. Distribution of electrons over different Landau levels results in the formation of alternating compressible and incompressible regions.<sup>1</sup>

We investigate theoretically the situation when only a few electrons are confined to the uppermost Landau level. We show that these extra electrons form "Wigner molecule". Magnetic field controls the number of electrons in the molecule, thus creating a new possibility to manipulate few electron objects. Moreover, in this way one can manipulate *fractional* charges. We discuss briefly the stability of the molecule in the presence of a fluctuating donor potential and the slow charge dynamics which is intrinsic for the system under consideration.

It is known that for a *homogeneous* 2D electron gas the energy density as a function of electron density  $n$  shows a cusp at

$$n = \frac{p}{q} \frac{H}{\phi_0}, \quad (1)$$

$p, q$  being integer numbers,  $\phi_0 = 2\pi\hbar c/e$ . This indicates that the electron gas is *incompressible* at this point being compressible elsewhere<sup>2</sup>. The charged excitations are separated by an energy gap,  $E_g$ , from the ground incompressible state. This is why the incompressible state may be thought as an insulator, whereas the compressible one is a conventional metal. The gap drops quickly with increasing denominator  $q$ , so that only few incompressible states can actually be observed. Those with  $q = 1$  correspond to completely filled Landau levels of non-interacting electrons and give rise to the integer quantum Hall effect. Those with  $q \neq 1$  are Laughlin liquids and manifest themselves in the fractional quantum Hall effect. This picture seems to be correct in a wide range of electron-electron interaction strength.

In recent years, a set of works has appeared giving an insight into the physics of the *inhomogeneous* 2D electron gas.<sup>1,3,4</sup> The resulting picture can be summarized as follows. In the first approximation the density profile of the 2D gas is defined by the system of gate electrodes. The potential to be compensated by the gates is of the order of volts, which is much larger than the energy scale of the inner electron motion,  $\hbar\omega_c, E_g$ . Therefore the applied magnetic field can not change the density profile much. The major effect of a magnetic field is formation of a narrow strip of incompressible phase near the point where the density satisfies the magic relation (1). These insulating strips separate compressible, metallic regions. The

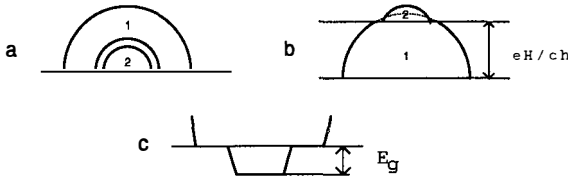


Figure 1: Quantum dot in Quantum Hall regime ( $n_{max} > eH/ch > n_{max}/2$ ). A half of the top view (a), the density profile (b) and the potential energy profile are shown. The electrons occupy two spin-split Landau levels forming two compressible regions 1, 2 and the separating incompressible strip. The unperturbed density profile is shown as a dotted line.

strip width was shown<sup>3</sup> to be much smaller than the geometric size of the system defined by gates but, at least for the widest strips, much larger than the magnetic length. The width decreases quickly with increasing  $q$ . The picture becomes irrelevant if the width is of the order of magnetic length. Hence, incompressible states with large  $q$  do not occur.

To illustrate this picture further, let us consider a quantum dot with a certain density profile,  $n_{max}$  being the electron density on the top (see Fig. 1). In addition, following<sup>1</sup>, let us assume that there are no incompressible states occurring with  $q > 1$  so that we can make use of a simple Landau level picture. If the magnetic field exceeds  $H_c = n_{max}\phi_0$ , all the electrons are in the first Landau level. If  $H_c > H > H_c/2$ , the electrons in the second Landau level are confined near the top of the quantum dot, as shown in Fig. 1. The density profile remains almost the same, the potential is flat within two metallic regions and drops by a value of  $E_g/e$  inside the insulating region. It is important to note that the wave functions of the electrons in the second Landau level have almost no overlap with the wave functions of empty states in the first Landau level. That implies that the number of electrons in each Landau level is integer. It is worth to spell out what are the limits of validity of this approach. In fact, the only requirement is that the radius of the dot  $R$  is larger than "microscopic" lengths such as Bohr radius  $a_B$ , magnetic length  $l_H$ , "interaction" length  $l_g = \epsilon(E_g/e^2)l_H^2$  and screening length. For quantum dots in the quantum Hall regime, the electron concentration is of the order of  $l_H^{-2}$ , so that the radius  $R \simeq l_H\sqrt{N}$ ,  $N$  being the number of confined electrons. Thus, the theory holds if  $N$  is big enough, say,  $N > 100$ . Starting this number, the plain electrostatics determines electron distribution in the dot and the effects of kinetic energy and magnetic field can be considered as small perturbations.

Below we present a simple extension of the theory taking into account the discreteness of electrons. This allows us to understand what happens near  $H_c$  where only few electrons in the second Landau level are confined near the top of the quantum dot. Let us first outline the results. As it was stressed above, at  $H > H_c$  all electrons in the dot are in first Landau level forming a compressible state. If  $H$  is far below  $H_c$ , there are two compressible regions corresponding to electrons in the first and in the second Landau level. The scenario of the formation of the second compressible region appears to be rather complex consisting of four stages. (see Fig. 2)

First stage: When  $H$  becomes smaller than  $H_c$ , the electrons of the first Landau level form

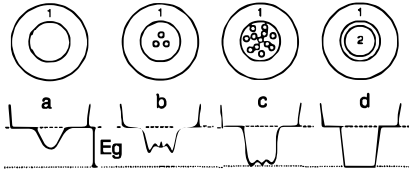


Figure 2: Four stages (a,b,c,d) the dot passes with decreasing magnetic field. The top views and potential energy profiles are shown. Small circles correspond to the electrons on the second Landau level.

an incompressible flat on the top of the dot, since the density of the first Landau level cannot exceed  $H/\phi_0 < n_{max}$ . In the flat, the density is exactly  $H/\phi_0$ . The density distortion creates a potential well. No electron can come yet to the second Landau level, since the depth of the well is smaller than  $E_g$ . The radius of the flat and the well depth increase with decreasing the magnetic field.

Second stage: At  $H = H_{c1} < H_c$  the well depth approaches  $E_g$  and the first electron appears on the second Landau level near the center of the dot. The electrostatic repulsion of the electrons prevents the second electron to enter the flat at the same field. This will happen only at a lower field  $H_{c2}$ , when the well becomes deeper. The stable configuration of two electrons on the flat is such that the distance between electrons is much smaller than the radius  $a$  of the flat but much larger than the magnetic length. The configuration is then completely determined by the interplay of the Coulomb repulsion between the electrons in the second Landau level and the confining potential of the well. Thus, a what we will call "Wigner molecule" is formed near the top of the dot. With further lowering of the field, more electrons join the molecule. The size of the molecule increases whereas the average distance between electrons gets smaller.

Third stage: For a certain number of electrons, the size of the molecule becomes comparable with the radius of the flat. Now only a narrow strip of the incompressible phase separates the compressible phase of the electrons in the first Landau level and the Wigner molecule which becomes similar to a piece of Wigner crystal. Such a formation is not yet a good metal since the distance between extra electrons exceeds the magnetic length and their wave functions do not overlap much.

Fourth stage: The concentration of electrons in the second Landau level grows, and at some field they begin to overlap in the central part of the structure thus forming a true metallic state.

Quantitative treatment implies a solution of 3D electrostatic problem in the manner of Chklovskii et al.<sup>3</sup> For concreteness, we can use a simple model of a quantum dot density profile<sup>5</sup>, which corresponds to a parabolic confining potential. In this case,  $n(r) = n_{max}\sqrt{1 - (r/R)^2}$ , and we obtain for the first critical field and the radius  $a$  of the incompress-

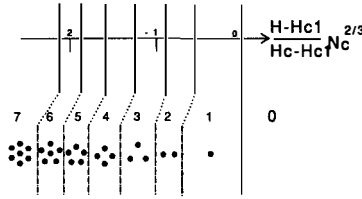


Figure 3: Configurations of the Wigner molecule versus magnetic field. Solid lines separate the domains where a certain configuration corresponds to the energy minimum. Dashed-dotted lines indicate where this configuration becomes unstable with respect to one-electron tunneling.

ible flat

$$\frac{H_c - H_{c1}}{H_c} = 1.228(l_g/R)^{2/3}, \tag{2}$$

$$a(H_{c1}) = 1.919R(l_g/R)^{1/3}. \tag{3}$$

This shows clearly that  $H_c - H_{c1} \ll H_c$  and  $l_H \ll a \ll R$  justifying the perturbation approach we made use of. Another important parameter is the lack of electrons in the flat  $N_c$  in comparison with the unperturbed density profile,  $N_c \equiv 0.565(Rl_g^2/l_H^3)^{2/3} \gg 1$ . We note that if the number of electrons in the second Landau level is much smaller than  $N_c$ , the confining potential well  $\phi(r)$  is not perturbed much. The extra electrons drop to the bottom of the well which then can be treated as a parabolic one. Let us treat the electrons as classical particles. To determine the equilibrium configuration, we shall minimize the energy of the form

$$E_N = (E_g - e\phi(0))N - \frac{e\phi''(0)}{2} \sum_i r_i^2 + \frac{1}{2} \sum_{i,j} \frac{e^2}{\epsilon|r_i - r_j|}. \tag{4}$$

Here  $N$  is the number of extra electrons,  $r_i$  are their coordinates. The problem closely resembles the model of atom proposed by J. J. Thompson. It has been also treated quantum mechanically in this century<sup>6</sup>. The paper mentioned deals with a relatively strong confinement potential where the electron wave functions overlap and quantum effects are important. Comparing the classical and quantum results, it is important to note the axial symmetry of the problem. The classical configurations can be rotated without energy change and are degenerate from the formal point of view. This degeneracy is lifted in quantum mechanics and the ground state is an eigenfunction of the angular momentum operator with all the electrons spread over a circle. In reality, the axial symmetry is approximate. We assume that either small ellipticity of the dot or small fluctuations of donor potential restore the uniqueness of the classical configuration.

We shall emphasize the interesting possibility to change the number of electrons in the molecule by changing magnetic field. Indeed, magnetic field changes  $a$  increasing the well depth  $\phi(0)$ . As a result, we obtain a series of magnetic fields at which the number of extra electrons changes from  $N - 1$  to  $N$ :

$$H_{cn} = H_{c1} + \beta_n \frac{H_c - H_{c1}}{N_c^{2/3}}, \tag{5}$$

$\beta_n$  being numerical factors. The corresponding magnetic fields are plotted for several  $n$  in Fig. 3. The average distance between the extra electrons  $r_a$  is of the order of  $(\epsilon\phi''(0)/e)^{-1/3} \simeq (a^2 l_H^2 / l_g)^{1/3} \simeq l_H (R^4 / l_H^2 l_g)^{1/9}$ . We see that  $a \gg r_a \gg l_H$ . This justifies our initial assumptions and our classical approach.

These transition magnetic fields can be measured experimentally<sup>1</sup> if one studies the transport properties of the dot. Due to Coulomb effects, conductance of the dot displays a sequence of peaks, each peak corresponds to addition of one electron to the dot. External charges may shift the potential of the conducting part of the dot changing the condition for such addition and thus influencing the conductivity. Thus the dot works as a very sensitive electrometer<sup>7</sup>: the change of number of the electrons in the molecule will shift the potential of the conducting island with respect to the leads. This gives rise to a change of conductance at transition magnetic field. The series of the transition fields given by  $\beta_n$  is a signature of the Wigner molecule. One could then extract  $H_c - H_{c1}$  and  $N_c$  from the measurements. This gives a possibility to determine  $E_g$  experimentally.

At further decreasing of the magnetic field, the number of extra electrons becomes of the order of  $N_c$ . This occurs at  $H_{c1} - H \simeq (H_c - H_{c1})$  indicating the third stage of the crossover we mentioned. Still at this magnetic field the electron wave functions do not overlap and the resulting state resembles Wigner lattice. The crossover to the true metallic state is expected to occur when the density of extra electrons corresponds to the filling factor  $0.2 - 0.15^2$ . This corresponds to  $H \approx 0.8H_{c1}$ .

We have discussed in detail the case when the incompressible state on the top of the dot corresponds to  $p = q = 1$ . The approach can be trivially generalized to the case of arbitrary  $p, q$ . The changes to be made are to substitute  $l_H \rightarrow l_H \sqrt{q/p}$  into the equations and to use  $E_g q$  of the corresponding incompressible state. The interesting detail is that the Wigner molecule can be formed by quasiparticles with *fractional* charge if  $q \neq 1$ .<sup>8</sup>

We address below two additional questions: what might be the dynamical properties of the system and how stable is the molecule with respect to the fluctuations of the donor potential.

There are three reasons to expect very slow rates of transitions which change the number of electrons in the molecule. The transition has to consist of an electron transfer from the center of the dot to the compressible region and a simultaneous flipping the spin. Similiar spin flip processes have been considered in<sup>9</sup> to explain the equilibration of edge channel populations, which inevitably involve spin-orbit or spin-spin interactions. These interactions are believed to be small in GaAs, which is the first reason for the rate to be slow.

The second reason is an exponentially small overlap between the wave functions of an electron in the flat and in the compressible region. If we just estimate this overlap for experimentally relevant parameters, we could obtain astronomical relaxation times. This forces us to think of more exotic tunneling mechanisms which could include, for example, subsequent tunneling.

The third reason is intrinsic to tunneling to and from Wigner arrays<sup>10</sup> and is related to many-body effects. If *all* the electrons in the molecule have to be shifted during the transition (compare different configurations in Fig. 3), the tunneling rate is proportional to the overlap between their wave functions in the initial and final positions. This gives an important extra suppression to the rate. However, this suppression can be relaxed far from the position

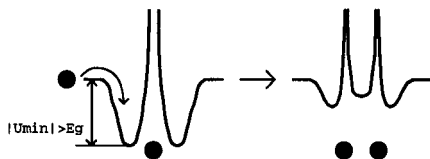


Figure 4: The potential energy profile for  $N = 1$  and  $N = 2$ . One-electron tunneling may occur only if the potential energy minimum is lower than  $-E_g$ .

of equilibrium transition where the energy difference between the initial and final states becomes larger. To illustrate this, let us consider the transition between  $N = 1$  and  $N = 2$ . Right below  $H_{\mathcal{Q}}$ , the process is possible only if accompanied by shifting the electron in the center of the flat. Lowering the field, we can reach the point  $H_{\mathcal{Q}}^*$  where such shift is not necessary. It is the field at which the bottom of the effective potential (which is the sum of the confining potential and the potential created by the extra electron in the center) reaches the value of  $E_g$ . (see Fig. 4) Below this point, the transition rate increases tremendously. We have calculated these threshold fields for  $N=1 \dots 7$  and plot them also in Fig. 3. They are of the same scale as  $H_{cn}$  and indicate the stability domains of possible metastable states.

For practical purposes, it is important to be sure of the stability of the molecule with respect to the fluctuations of the donor potential. Naively, one could expect that the fluctuations are strong enough to trap the electrons at random positions and hence destroy the molecule. Fortunately, the situation is not so bad for two reasons. First, the molecule is formed not far from the compressible region which screens the fluctuations. Second, if the fluctuations are strong but smooth, the molecule can be trapped as a whole keeping its own structure.

We are indebted to G.E.W. Bauer, A. Groshev, and especially to N. C. van der Vaart for valuable discussions.

<sup>1</sup> P. L. McEuen, E. B. Foxman, Jari Kinaret, U. Meirav, M. A. Kastner, N. S. Wingreen and S. J. Wind Phys. Rev. B **45**, 11419 (1992).

<sup>2</sup> T. Chakraborty and P. Pietiläinen, *The fractional quantum Hall effect*, Springer-Verlag, Berlin Heidelberg 1988.

<sup>3</sup> D. B. Chklovskii, B. I. Shklovskii, and L. I. Glazman Phys. Rev. B **46**, 4026; D. B. Chklovskii, K. A. Matveev and B. I. Shklovskii Phys. Rev. B **47**, 12605 (1993).

<sup>4</sup> I. K. Marmorosk and C. W. J. Beenakker, Phys. Rev. B **46**, 15562 (1992).

<sup>5</sup> V. Shikin, S. Nazin, D. Heitmann, and T. Demel Phys. Rev. B **43**, 11903 (1991)

<sup>6</sup> P. A. Maksym and T. Chakraborty Phys. Rev. Lett. **65**, 108 (1990).

<sup>7</sup> N. C. van der Vaart et al., these proceedings.

<sup>8</sup> To our knowledge, the idea of fractional charges forming a Wigner lattice was first put forward by L. P. Kowenhoven.

<sup>9</sup> A. V. Khaetskii Phys. Rev. B **45**, 13777 (1992)

<sup>10</sup> D. V. Averin and Yu. V. Nazarov Phys. Rev. B. **47**, 9944 (1993).

## THRESHOLD VOLTAGE FOR THE TRANSMISSION OF LOW FILLING FACTOR EDGE CHANNELS

C.Pasquier<sup>\*a)</sup>, D.C.Glatli<sup>a)</sup>, Y.Jin<sup>b)</sup>, B.Etienne<sup>b)</sup>

<sup>a)</sup>*Laboratoire de la Matière Condensée Quantique*

*DRECAM/SPEC CEA Saclay F-91191 Gif sur Yvette Cedex France*

<sup>b)</sup>*Laboratoire de Microstructures et Microélectronique CNRS*

*196 Av. H. Ravera, 92220 Bagneux, France*

**Abstract :** In a high mobility 2D electron gas, we observe non linearities in the transmission through a quantum point contact in high magnetic field when the filling factor is less than 0.3. A threshold voltage for conduction is observed and a vanishing conductance is found for filling factor between  $2/9$  and  $1/5$  and below  $1/5$ . These non linearities disappear below 400mK. This observation suggest the formation of a magnetically induced solid like in macroscopic samples.

In this paper we present experimental results on the transmission through a quantum point contact in high magnetic fields. We show that the transmission enters a new regime where transport non linearities and vanishing conductance appear out of the tunnel regime. These observations can be relevant for the understanding of the Quantum Hall Effect ground state at low filling factor.

Many experiments have demonstrated the presence of an insulating phase for high mobility 2D electron gas (2DEG), in high magnetic fields. This phase appears for filling factor less than  $1/5$  and a reentrant phase exists between  $2/9$  and  $1/5$ . The experiments were performed using radiofrequency<sup>1)</sup> or transport measurements<sup>2)</sup>. This phase has been attributed to the formation of a solid which is characterized by an activation energy and a threshold voltage for conduction. This solid melts for a critical temperature which is at most 400mK for usual 2DEG densities.

Although quantum transport through a Quantum Point Contact (QPC)<sup>3)</sup> has been extensively studied, no experiments have studied the electronic transport through a QPC in the low filling factor regime below  $\approx 2/9$ . At zero magnetic field, it is known that the conductance is quantized as  $\sigma = N \times (2e^2/h)$ ,  $N$  is the number of fully transmitted 1D subbands of the QPC constriction. In high magnetic field, for the Integral Quantum Hall Effect (IQHE), the confining potential of the QPC lowers the number  $\nu$  of filled Landau levels (LLs) in the leads to a value  $\nu_g < \nu$  at the constriction. A conductance quantization  $\nu_g e^2/h$  occurs when  $\nu_g$  (integer) edge channels are fully transmitted. At low temperatures, electronic correlations leads to the fractional quantum Hall effect (FQHE). A QPC conductance quantization is also observed<sup>4,5)</sup> and predicted<sup>6)</sup> for  $\nu_g$  a special odd denominator fraction of FQHE.

Here, we investigate the regime  $\nu_g \leq 2/9$ . We observe a vanishing QPC conductance and transport non linearities similar to those observed in macroscopic samples. These features seem to be consistent with the formation of crystallized edge states in the constriction as proposed in ref.7.

Two samples are used. They are obtained from the same GaAs/Ga(Al)As heterojunction with Si  $\delta$  doping layer at  $800\text{\AA}$  from the electron plane and  $200\text{\AA}$  from the surface. Both samples have  $3 \times 10^6 \text{cm}^2 \text{V}^{-1} \text{s}^{-1}$  mobility and electron density  $n_s = 1.11 - 1.17 \cdot 10^{11} \text{cm}^{-2}$ . The same pattern is defined on each sample. At the centre of a  $6\mu\text{m}$  wide Hall bar mesa, three pairs of Schottky gates are deposited using electron beam lithography. Two of them define two QPCs of lithographic width  $2800\text{\AA}$ , but only one will be used. Four point resistance measurements are made using  $1\text{M}\Omega$  or  $10\text{M}\Omega$  current sources (sample #1). A two terminal configuration is used for sample #2 (note that a  $R_s = 8.8 \text{k}\Omega$  resistance in series with the sample and the voltage across the sample  $V - R_s I$  is slightly less than the applied voltage  $V$ ).  $V/2$  is added to gate voltages for symmetrization. Differential conductance characteristics (DIDVC) are obtained using a  $117\text{Hz}$  square wave  $13\mu\text{V}$  amplitude ac voltage added to the bias voltage. The quality of the samples is shown in Fig.1 by the well pronounced zero-field conductance plateaux when sweeping  $V_g$  for sample#2. The pinch-off value is  $\approx -670\text{mV}$  and  $\approx -650\text{mV}$  for sample#1.

Both samples display pronounced Hall plateaux with  $B$ , including the main FQHE fractions. This resistance quantization is useful to check the sample quality but also to establish a relation between the QPC gate voltage  $V_g$  and the density  $n_g$  at the center of the constriction. Fig.2 shows the QPC resistance versus  $V_g$ . The data correspond to filling factors  $\nu = 8, 6, 4, 2$  (upper traces) and to  $2/3$  and  $1/2$  (lower traces). As expected, even in the FQHE regime, well defined quantized resistance plateaux ( $7, 6, 5, 4, 3, 2, 1, 2/3, 2/5, 1/3$ ) are observed from which the filling factor  $\nu_g$  is deduced. From the whole series of curves, we remark that all plateaux with the same

ratio  $v_G / v$  correspond to the same gate voltage (even for FQHE). From this, we can assert that QPC electron density  $n_G = n_s v_G / v$  is independent of the magnetic field and a capacitive relation between  $n_G$  and  $V_G$  is satisfied. This is in agreement with a Thomas-Fermi picture of quantum transport in IQHE or FQHE. As first mentioned by Halperin<sup>8)</sup>, the filling of each LL correspond to large compressible strips with fixed electrochemical potential pinned to the Fermi energy. The small regions in between are incompressible and correspond to the quantized density of an integral number of filled LLs. Recently, Chklovskii et al.<sup>9)</sup> have shown that, like in the non interacting picture, a resistance quantization occurs and is directly connected to the density at the constriction's center :  $v_G = (n_G / n_s)v$ . Because the incompressible strips are much smaller than the compressible strips, they found that the capacitive relation  $n_G(V_G)$  which holds for zero fields is only weakly affected by orders of  $a_{\text{Bohr}} / l \approx 0.05$  in the QHE ( $l \approx 2000 \text{ \AA}$  is the scale of the confining potential).

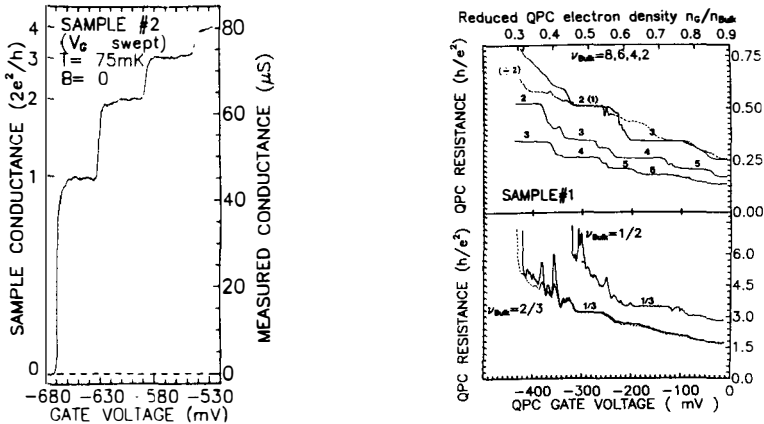


Fig. 1 (left) : Zero-field conductance plateaux for sample#2.

Fig. 2 (right) : QPC diagonal resistance versus gate voltage for different bulk filling factor.

Now we study the low filling factor regime. We use the capacitive relation between  $n_G$  and  $V_G$  to determine  $v_G$ . The traces for  $\nu = 2/3$  or  $1/2$  display a striking resistance divergence for the same  $\nu_G$ , just below  $2/9$  ( $\nu_G \leq 0.32 \times 2/3 = 0.21$  and  $0.44 \times 1/2 = 0.22$  respectively). Another feature is the resistance non linearity revealed for  $\nu_G \leq 0.3$  by comparing the dashed and solid line traces taken at  $\nu = 2/3$  and applied current 200 and 20 pA respectively. These non linearities are also observed for  $\nu_G \leq 0.3$ , in sample#2 but are better studied using conductance measurements. The same method as for sample#1 is used to determine  $n_G(V_G)$ . Here, we present experimental results for  $V_G = -560, -570$  and  $-580 \text{ mV}$  ( $n_G = 6.3 - 6.4, 6.0 - 6.1, 5.7 - 5.8 \cdot 10^{10} \text{ cm}^{-2}$  respectively). The features of the nonlinearities are the following :

1) Their magnetic field dependence at fixed  $V_G$  and  $T=60\text{mK}$  is shown in fig.3. For  $V_G = -570\text{mV}$  and  $B \geq 13.6\text{T}$ , the conductance is zero as shown for the traces taken at  $13.85\text{T} (v_G \approx 0.185)^{(10)}$ ,  $14.5\text{T} (v_G \approx 0.177)$  and  $15.9\text{T} (v_G \approx 0.161)$ . Around  $1/5$ , the conductance becomes finite ( $B=13.05\text{T}, v_G \approx 0.196$ ). Then, the conductance goes back to zero for  $1/5 < v_G < 2/9$ , (see the  $11.8\text{T}, v_G \approx 0.228$  trace) and is finite for  $v_G \approx 2/9$  ( $B=11.5\text{T}$ ). From  $11.1\text{T} (v_G \approx 0.215)$  to  $7.2\text{T}$ , the zero bias conductance shows oscillations around a finite value which increases. Finally, the DIDVC for  $B=7.2\text{T} (v_G \approx 1/3)$  is flat.

For gate voltage  $V_G = -560\text{mV}$ , the non linearities are as well pronounced. The conductance is zero for high fields and is finite only for  $B=13\text{T} (v_G \approx 1/5)$ .

The same features are observed for  $V_G = -580\text{mV}$ . For the six curves displayed, a finite conductance  $\cong 0.22\mu\text{S}$  is observed only for  $12\text{T} (v_G \approx 0.196 - 0.2)$ . At  $B=11\text{T} (v_G \cong 214 - 218)$ , the conductance is zero.

*These results strongly indicate that vanishing conductance appears for  $2/9 > v_G > 1/5$  and  $v_G < 1/5$  and is independent of the filling factor  $\nu$  of the leads.*

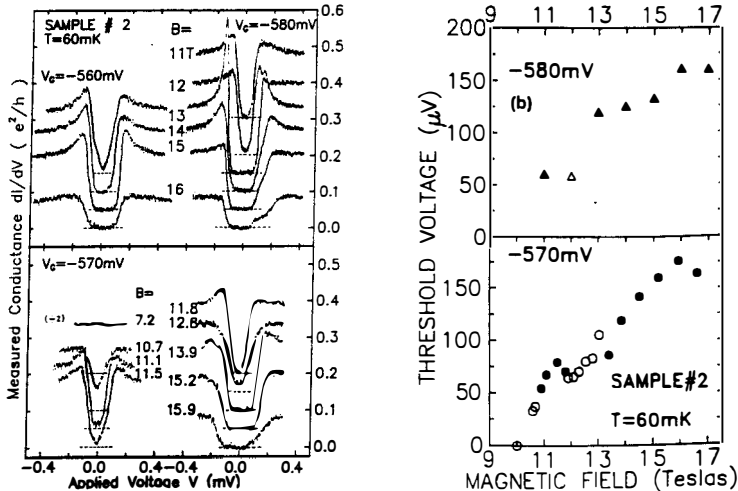


Fig.3 : DIDVC at different magnetic fields and three different gate voltages

Fig.4 : Threshold voltage for conduction versus magnetic field for  $V_G = -570\text{mV}$  and  $-580\text{mV}$ . A distinction is made between traces showing zero (dark symbols) and non zero (open symbols) conductance.

2) *Another feature of the conduction is the few hundred  $\mu\text{V}$  threshold voltage  $V_t$  for conduction* observed in the DIDVCs. Fig 4 shows its variation with  $B$  for  $V_G = -570$  and  $-580\text{mV}$ . The experimental protocol is to take  $V_t$  at half of the  $dI/dV$  peak value. Closed (opened) symbols are for DIDVCs showing zero (non zero) conductance. Both plots show the same feature :  $V_t$  decreases when  $v_G$  approaches

1/5, then slightly increases for  $\nu_0$  just above 1/5 then decreases and vanishes for some field (10 Teslas for -570mV).

3) *The asymptotic differential conductance  $\sigma_\infty$  is closed to  $\nu_0 e^2/h$ .* This can be easily verified in the 12-15 Teslas range where the mesa filling factor  $\nu \approx 1/3$ , so the longitudinal mesa resistance is roughly B independent. One finds (after  $R_s$  subtraction) for  $V_G = -580\text{mV}$ ,  $B=15\text{-}12\text{T}$  :  $e^2/(h\sigma_\infty) = 6.52, 6.1, 5.63, 5.22$  which differs from  $\nu_0^{-1} = 6.3, 5.8, 5.46, 5.04$  by the same quantity. The relation  $\sigma_\infty = \nu_0 e^2/h$  is well verified if we subtract a  $\approx 0.2h/e^2 = 5\text{k}\Omega$  mesa resistance which is the value measured at  $V_G = 0$  and  $\nu \approx 1/3$ .

4) *The variation of a DIDVC with temperature* is shown in Fig.5a. ( $V_G = -580\text{ mV}$  but with a QPC density 1% smaller due to irreversible depletion effects). The sharp onset of the conduction smoothens and the conductance minimum increases with T. Fig.5b shows, for four applied voltages, that the differential conductance (corrected for  $R_s$ ) follows a thermally activated law at low temperature. In inset, the deduced activated energy  $\Delta(V)$  is represented versus dc voltage V. Above  $\approx 250\text{ mK}$ , a simple activated law is not found and at 400mK, the DIDVC, not shown, is flat although a  $\Delta(0) \approx 0.92\text{K}$  activation energy is found at low T.  $\Delta(0)/e \approx 85\mu\text{V}$  is lower than the threshold voltage  $V_t = 110\mu\text{V}$ . Finally, the asymptotic conductance  $\sigma_\infty \approx 0.16 e^2/h \approx \nu_0 e^2/h$  is not temperature dependent.

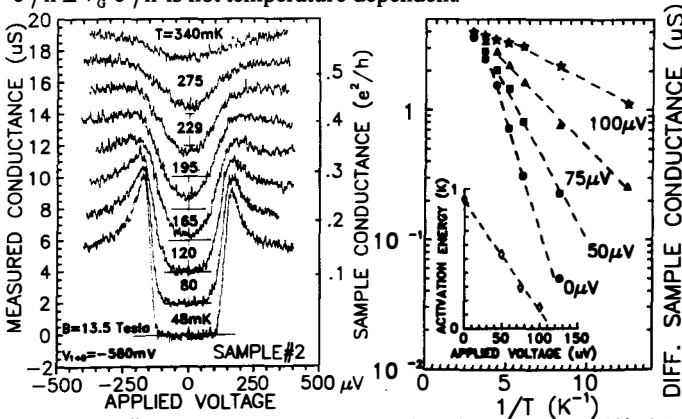


Fig.5 : (a) DIDVC at different temperatures. For clarity, the curves are shifted by  $2\mu\text{S}$ . (b) Conductance versus  $1/T$  for four applied voltages. thermal activation is found at low temperature. In the inset, the activation energy is plotted as a function of the applied voltage.

5) *The height of the  $dI/dV$  peak can exceed the Hall conductance* : this is clearly seen on the figure 3,  $B=13\text{T}$ ,  $V_G = -580\text{ mV}$  DIDVC. The height of the highest peak  $\approx 0.48 e^2/h$  is well above the Hall conductance  $\approx 0.33e^2/h$ . This is observed also for different QPC gate voltages, but only for filling factor  $\nu \approx 1/3$ .

Points 1) and 4) are consistent with the filling factor and temperature range for a solid formation in macroscopic samples, but localisation effects can also show nonmonotonic behaviour with  $\nu_g$  and depend on the energy gap of the fractional edge states. The variation of  $V_t$  with  $\nu_g$  is also similar to that observed with  $\nu$  in macroscopic samples as well as the thermal activation of the zero bias conductance. The activation energy is not in favor to a localized state schema. For resonant tunneling through localized states, an activation energy  $\Delta(0) = 0.9K$  would correspond to a length scale  $\cong 1\mu m$  much larger than expected ( $.1-2\mu m$ ) because of Coulomb effects. The relation  $\Delta(0) = eV_t$  should be verified and we do not expect that  $\Delta$  vanishes at 400mK. However, in the simplest crystallized edge state model,  $\Delta(V)$  would represent the pinning energy. In a one dimensional solid model<sup>11)</sup> :  $\Delta(0) = eV_t < n_g > a_0 w / \pi \neq eV_t$ ,  $< n_g > = n_g \pi / 4$  is the density at the center of the constriction averaged over the transverse direction,  $w$  is the constriction width and  $a_0$  is the translation period of the crystal in the transmission direction.  $\Delta(0)$  should vanish at the melting temperature because the elastic restoring force of the crystal vanishes. Using Fig.5 parameters, a reasonable  $a_0 \cong 600\text{\AA}$  slightly larger than  $(n_g)^{-1/2}$  is found. Finally, that differential conductance can exceed the Hall conductance implies that we have to consider the non linear conduction as a transmission problem in the frame of coherent adiabatic edge channel transport. Non adiabaticity would imply addition of the Hall mesa resistance to the QPC differential resistance. This picture suggests to write  $dI/dV = T(V)e^2/h$  with  $T(V) = 0$  for  $V < V_t$  and  $T(V) = \nu_g$  for  $V \gg V_t$  (note that  $I/V \leq \nu e^2/h$ , the Hall conductance of the leads).

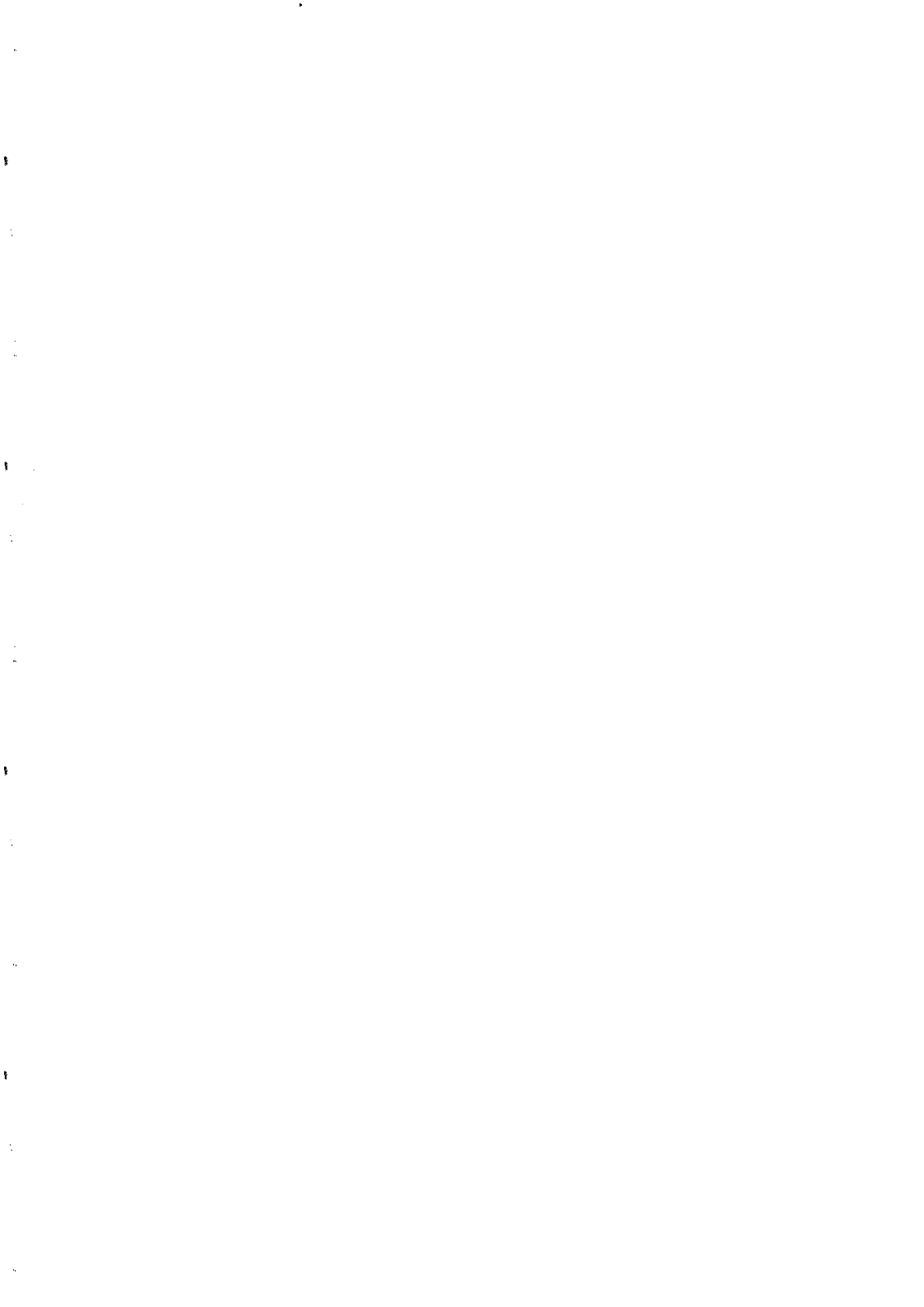
The authors acknowledge fruitful discussions with F.I.B.Williams and F.Perruchot and the technical help of C.Chaleil.

### References :

\* Present adress : Laboratoire de Physique des solides, URA02 CNRS, F-91405 Orsay, France

- 1) E.Y.Andrei et al., Phys.Rev.Lett. **60**, 2765 (1988)
- 2) H.W.Jiang et al., Phys.Rev.Lett. **65**, 633 (1990); V.J.Goldman et al., ibid. **65**, 2188 (1990); F.I.B.Williams et al., ibid. **66**,3285 (1991)
- 3) for a review : C.W.J. Beenakker&H.Van Houten, Solid State Physics **44**, 1 (1991), Plenum Press
- 4) A.M.Chang, J.E.Cunningham, Solid State Commun. **72**, 651 (1990)
- 5) L.P.Kouwenhoven et al, Phys.Rev.Lett. **64**, 685 (1990)
- 6) C.W.J. Beenakker, Phys.Rev.Lett. **64**, 216 (1990); A.M.Chang, Solid State Commun. **74**, 871 (1990); A.H.MacDonald Phys.Rev.Lett. **64**, 220 (1990)
- 7) H.A.Fertig, S.Das Sarma, Surf.Science **263**, 60 (1992); H.A.Fertig, R.Coté, A.H.MacDonald, S.Das Sarma, Phys.Rev.Lett. **69**, 816 (1992)
- 8) B.I.Halperin, Phys.Rev.B **25**,2185 (1992)
- 9) D.B.Chklovskii, K.A.Matveev, B.I.Shklovskii, ibid. **47**, 12065 (1993);
- 10) For gate voltage above  $\cong -600mV$ , we can hope  $\nu_g$  has still a meaning as the channel width  $w \geq 800\text{\AA}$ , from  $B=0$  estimation, is large :  $\geq 10(h/eB)^{1/2}$  for  $B > 11T$ .
- 11) for a review : G.Gruner, A.Zettl, Phys. Rep. **119**, 117 (1985)

## QUANTUM WIRES



## SEMI-BALLISTIC WAVE PROPAGATION IN DISORDERED CAVITIES

Th.M. Nieuwenhuizen

*Van der Waals-Zeeman Laboratorium*

*Valckenierstraat 65, 1018 XE Amsterdam, The Netherlands*

**Abstract.** — Wave transport in a waveguide with moderate disorder may be diffusive in the longitudinal direction but still ballistic in the transversal directions. This is called semi-ballistic transport. It is discussed for disordered waveguides, quantum wires, films, Fabry-Pérot interferometers and double barrier quantum wells.

### I. Introduction

Propagation of sunlight in a clear sky is a long understood phenomenon. When waves freely propagate in a confined geometry, such as a waveguide, only certain ‘cavity modes’ can occur. In a semi-classical picture this can be interpreted as ‘bouncing’ against the walls, and is therefore termed ‘ballistic’ transport.

The opposite regime is a cloudy sky, in which the sunlight diffuses. Diffusive wave transport has many applications, such as light propagation through fog, white paint, milky liquids, human tissues, propagation of acoustic waves, and propagation of electrons in dirty metals at low temperatures.

There is also a less known intermediate regime, where transport is partly diffusive and partly ballistic<sup>1)</sup>. Think of propagation of electromagnetic waves through a disordered waveguide or a dirty Fabry-Pérot interferometer, or propagation of electrons through a long but narrow channel or through a disordered double barrier quantum well. When in these systems a modest amount of disorder is present, the transversal cavity modes are still well defined. However, when the system is long in the other direction(s), it may have diffusive behavior as well. This combination of ballistic and diffusive transport has been called ‘semi-ballistic’ transport.

We discuss here results presented in ref. <sup>1)</sup> and to be presented in ref. <sup>2)</sup>.

### II. Transmission of a waveguide and a quantum wire

We consider an infinitely long waveguide confined by four conducting plates at  $x = 0$ ,  $x = d_1$ ,  $y = 0$  and  $y = d_2$ . In the section  $0 \leq z \leq d_3$  a small density of isotropic, elastic point

scatterers is present. We assume that the scattering mean free path,  $\ell$ , is much larger than the transverse sizes  $d_1$ ,  $d_2$ , so that the cavity modes are hardly influenced. On the other hand, we assume that the system is optically thick, that is to say, we assume that  $d_3 \gg \ell$ , which implies diffusive transport in the  $z$ -direction. In the scalar wave approximation the system is described by

$$\{-\nabla^2 - u \sum_i \delta(\mathbf{r} - \mathbf{R}_i)\} \psi(\mathbf{r}) = k_0^2 \psi(\mathbf{r}) \quad (1)$$

Here  $u$  is the bare scattering length and  $\mathbf{R}_i$  are the random positions of the scatterers, distributed according to a density  $n(\mathbf{r}) = n(x, y)$  for  $0 < z < d_3$  while  $n(\mathbf{r}) = 0$  elsewhere. The guide has discrete transversal eigenmodes  $\Psi_{\mathbf{p}}(\rho)$ , where  $\rho \equiv (x, y)$ ,

$$\Psi_{\mathbf{p}}(\rho) = \sqrt{2/d_1} \sin(p_1 x) \sqrt{2/d_2} \sin(p_2 y) \quad (2)$$

where  $p_{1,2} = m_{1,2}\pi/d_{1,2}$  with positive integer  $m_{1,2}$ . These modes have a Green's function

$$G_{\mathbf{p}}(q) = \frac{1}{\mathbf{p}^2 + q^2 - k_0^2 - \Sigma_{\mathbf{p}}} \quad (3)$$

where  $q$  is the momentum in the  $z$ -direction and where  $\Sigma$  is the self-energy.

### Second order Born approximation: beyond or not beyond?

For electronic systems it is customary to consider isotropic scattering in the second order Born approximation. The reason is that scattering is weak and dominated by  $s$ -wave scattering. Instead of point scatterers one often assumes an uncorrelated Gaussian disorder potential. This is an equivalent approach. In cavities it is at forehand not clear whether for realistic multiple scattering the presence of the walls is compatible with weak enough scattering.

In the second order Born approximation one approximates the self-energy by

$$\Sigma_{\mathbf{p}} \approx i\Gamma_{\mathbf{p}} \quad (4)$$

where the width satisfies the self-consistent equation

$$\Gamma_{\mathbf{p}} = \Gamma_{\mathbf{p}}^D \equiv \sum_{\mathbf{p}'} U_{\mathbf{p}\mathbf{p}'} \nu_{\mathbf{p}'} \quad (5)$$

$$\nu_{\mathbf{p}}(k_0) \equiv \text{Re} \frac{1}{2\sqrt{k_0^2 - \mathbf{p}^2 + i\Gamma_{\mathbf{p}}}}; \quad U_{\mathbf{p}\mathbf{p}'} = u^2 \int d^2\rho n(\rho) \Psi_{\mathbf{p}}^2(\rho) \Psi_{\mathbf{p}'}^2(\rho) \quad (6)$$

$\nu_{\mathbf{p}}$  is the density of states in the mode,  $U$  is a mode-mode coupling matrix. From this equation it is seen that when a new mode  $\mathbf{p}'$  opens ( $\nu_{\mathbf{p}'} \gg 1/k_0$ ), the width of all other modes increases.

Physically it stands for scattering back into the old mode  $\mathbf{p}$  of waves that entered the new mode  $\mathbf{p}'$ . As this mainly happens in a destructive way, the width of the already open modes will increase.

Let  $T_{ab}$  denote the average transmission coefficient for transport from incoming mode  $a$  (with wavevector  $\mathbf{p}_a$ ) into outgoing mode  $b$  (with wavevector  $\mathbf{p}_b$ ). It can be solved from the Bethe-Salpeter equation. For an optically thick system this leads to

$$T_{\mathbf{a}\mathbf{b}} = \frac{C_{\mathbf{a}}C_{\mathbf{b}}}{4(d_3 + 2z_0)q_{\mathbf{b}}^2} \sum_{\mathbf{p}} \Gamma_{\mathbf{p}} \ell_{\mathbf{p}}^2 \nu_{\mathbf{p}} \quad (7)$$

Here the "injection depth"  $z_0$  is a small shift,  $C_{\mathbf{p}}$  are certain coefficients that satisfy the sum rule  $\sum_{\mathbf{p}} C_{\mathbf{p}} \nu_{\mathbf{p}} = 2$  and  $\ell_{\mathbf{p}}$  is the mean free path of mode  $\mathbf{p}$ .

From  $T_{\mathbf{a}\mathbf{b}}$  we get the average conductance of a quantum wire via the Landauer formula. Due to the  $1/d_3$  dependence in eq. (7), the average conductivity is well defined and reads

$$\sigma = \frac{8e^2}{hd_1d_2} \sum_{\mathbf{p}} \Gamma_{\mathbf{p}} \ell_{\mathbf{p}}^2 \nu_{\mathbf{p}} \quad (8)$$

Let us consider the  $1D$  constriction of a  $2D$  electron gas. We are interested in the behavior of the average conductivity when new modes are opened. This may happen when one enlarges the width  $d_1$ . As is seen from figure 1, the behavior is far from monotonic. This is due to the line broadening discussed above. In this figure we also present this behavior for a film of which the number of open modes its  $z$ -direction is varied. Here there is a universal behavior for weak scattering:

$$\sigma = \sigma_B \left\{ \frac{3N}{2N+1} - \frac{N(N+1)}{2x^2} \right\} \quad x = \frac{d_1 k_F}{\pi} \quad N = \text{int}(x) \quad (9)$$

Here  $N$  is the number of open transverse modes of the film and  $\sigma_B = 2e^2 k_F^2 \ell / 3\pi\hbar$  is the Boltzmann conductivity of the bulk system. This represents *universal drops in the conductivity of disordered films*, as opposed to the *universal steps in the conductance of clean quantum wires*.

### Beyond second order Born

In optical systems scatterer sizes are often of the order of the wavelength so that one must go beyond the second order Born approximation. For electron scattering in narrow cavities one has to do the same if the scatterers are not very weak.

For an isotropic point scatterer it is simple to sum the full Born series. The  $t$ -matrix reads

$$t(\mathbf{r}) = t(\rho) = \frac{u}{1 - uG(\mathbf{r}, \mathbf{r})} \quad (10)$$

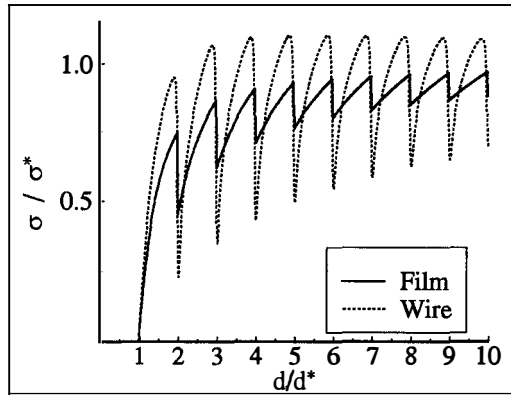


**Figure 1.** Conductivity of semi-ballistic devices with very low disorder. Solid line: a disordered film of width  $d$  as it goes through multiples of the resonant width  $d^*$ . Dashed line: a 1D constriction of a 2D electron gas of function of its width.

However, for  $D \geq 2$  the real part of the return Greens function diverges. A simple regularization was proposed in ref.<sup>3)</sup>. Here it is more appropriate<sup>2)</sup> to use a momentum cutoff factor  $\Lambda^2/(\mathbf{p}^2 + q^2 + \Lambda^2)$ , where  $\Lambda$  can be seen as the inverse radius of the scatterer. In this approach an attractive scatterer in a waveguide will always have a bound state before the opening of the cavity modes<sup>2)</sup>. The self-energy now reads

$$\Sigma_{\mathbf{p}} = \int d^2\rho |\Psi_{\mathbf{p}}(\rho)|^2 n(\rho) t(\rho) \tag{11}$$

Since in eq. (10) the return Green's function depends on  $\Sigma_{\mathbf{p}}$ , this is a self-consistent equation. The vertex is now

$$U_{\mathbf{p}\mathbf{p}'} \equiv \int d^2\rho \Psi_{\mathbf{p}}^2(\rho) \Psi_{\mathbf{p}'}^2(\rho) n(\rho) t(\rho) t^*(\rho) \tag{12}$$

With these modifications eqs. (7) and (8) remain true. Numerical simulations for a lattice model with  $1500 \times 11$  sites with 5% attractive impurities having  $u = 1$  have been performed by C. Barnes. His result for the average conductivity have been reproduced in figure 2. They are in good agreement with the full curve. The latter shows equation (8), adapted to the lattice model and evaluated beyond second order Born. No adjustable parameter occurs.

It can be seen from figure 2 that the average conductivity is quite large in the second and higher subbands. This arises because of a phenomenon called subband bottom transparency<sup>5), 6)</sup>.

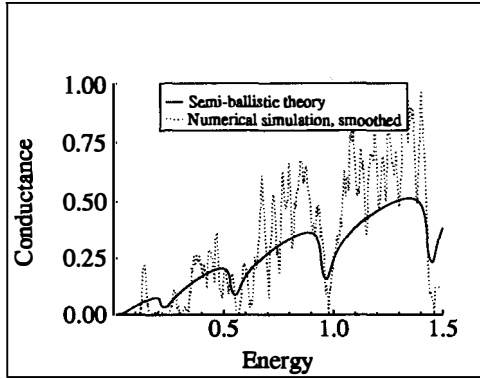


**Figure 2.** Conductivity of a semi-ballistic 11x500 quantum wire with 5 % attractive scatterers. Data points, obtained for one realization of disorder, have been smoothed over 13 neighboring points. Full line: Eqn. (8)

When at least one mode is already open, the new mode causes a small  $t$ -matrix because the return Green's function has a square-root divergency due to the 1D character of the problem. It is a *resonance effect* that leads to *less (!) scattering*. It is not contained in the second-order Born approximation.

### III. Fabry-Pérot interferometer with dust

Another problem of interest is the *transversal* transport through a system with semi-ballistic transport. An example is a Fabry-Pérot interferometer. Its mirrors acts as penetrable barriers. In a practical situation disorder may be caused by dust on the mirrors. The multiple scattering problem in the second order Born approximation, for the case of one open mode away from resonance, was considered in ref. <sup>4)</sup>. We present here a more general result.

We assume that waves coming from  $x = -\infty$  can tunnel through the mirrors at  $x = 0$  and  $x = d_1$ . The average transmission coefficient from incoming mode  $a$  to outgoing mode  $b$  is

$$T_{\mathbf{a}\mathbf{b}} = \frac{2(p_1^a)^2}{d_1 d_3} \frac{T_L^a \Gamma_{\mathbf{a}} |G_{\mathbf{a}}|^2 T_R^b \Gamma_{\mathbf{b}} |G_{\mathbf{b}}|^2}{\Sigma_{\mathbf{p}} (T_L^{p_1} + T_R^{p_1} + A_L^{p_1} + A_R^{p_1}) p_1 \nu_{\mathbf{p}}} \quad (13)$$

Here  $T_{L,R}^{p_1}$  and  $A_{L,R}^{p_1}$  are the transmission and absorption coefficients of the mirrors at  $x = 0$  and  $x = d_1$ , respectively. The Green's functions  $G_{\mathbf{a},\mathbf{b}}$  are given in eq. (3). Their selfenergy is  $\Sigma_{\mathbf{p}} = \Sigma_{\mathbf{p}}^D + \Sigma_{\mathbf{p}}^W$ , where  $\Sigma_{\mathbf{p}}^D$  is given in (11) and where  $\Sigma_{\mathbf{p}}^W \approx ip_1(T_L^{p_1} + T_R^{p_1} + A_L^{p_1} + A_R^{p_1})/2d_1$  describes transmission through and absorption by the mirrors.

From this formula, we see scattering occurring into all free cavity modes  $\mathbf{b}$ , with resonance line shapes  $|G_{\mathbf{b}}|^2$ . For an incoming plane wave, scattering inside the barrier region causes an equal distribution over all directions. Therefore, the transmitted intensity does not depend on the angle of incidence in the  $(y, z)$  plane. It does depend on the angle with respect to the  $x$ -axis, as the mode quantization implies that only certain angles are transmitted. This causes the well known appearance of fringes in the transmission pattern.

#### IV. Conductivity of a disordered double barrier quantum well

The conductivity of a double barrier quantum well can be obtained from previous transmission coefficients. For symmetric barriers one finds

$$\sigma = \frac{2e^2}{hd_2} \sum_{\mathbf{p}} T_L^{p_1} p_1 \nu_{\mathbf{p}} \quad (14)$$

The influence of disorder is strongly felt in the onset of the resonance lines. Far from resonance eq. (14) is the same as without scattering. Indeed, the flux entering the barrier is hardly altered by the presence of scatterers; due to symmetry, half of this flux should be transmitted, no matter how it was distributed over the modes. However, when the barriers are not symmetric and when more than one mode is resonant, there is a *disorder enhanced conductivity*.

In ref. <sup>1)</sup> the above result was used to explain the large resonance lineshape of GaAs-AlGaAs double barrier quantum wells observed by Guéret et al. <sup>7)</sup>. In that situation multiple scattering is caused by irregularities of the barrier interfaces. It causes a large increase of the line width.

#### Acknowledgements

The author thanks Allard Mosk and Crispin Barnes for allowing presentation of common results. This research was made possible by the Royal Netherlands Academy of Arts and Sciences (KNAW). It was also supported by NATO (Grant nr. CRG 921399).

#### References

1. Th. M. Nieuwenhuizen, Europhys. Lett, **24** (1993) 269
2. A. Mosk, Th.M. Nieuwenhuizen, and C. P. Barnes, to appear
3. Th.M. Nieuwenhuizen, A. Lagendijk, and B.A. van Tiggelen, Phys. Lett. A **169** (1992) 191
4. R. Berkovits and S. Feng, Phys. Rev. B **45** (1992) 97
5. C.S. Chu and R.S. Sorbello, Phys. Rev. B **40** (1989) 5941
6. P.F. Bagwell, Phys. Rev. B **41** (1990) 10354
7. P. Guéret, C. Rossel, E. Marclay, and H. Meier, J. Appl. Phys. **66** (1989) 278

# QUANTUM CONDUCTANCE FLUCTUATIONS IN 3D BALLISTIC ADIABATIC WIRES

Vladimir I. Fal'ko<sup>a,b)</sup> and G.B. Lesovik<sup>b)</sup>

<sup>a)</sup> *Max-Planck-Institut für Festkörperforschung, Stuttgart, Germany*

<sup>b)</sup> *Institute of Solid State Physics, Chernogolovka, 142432 Russia*

During recent years the transport properties of ballistic adiabatic conductors were extensively studied. The most of the interest in this field has been attracted by the 2D semiconductor devices, so that the features of a quantum transport in a ballistic adiabatic wire prepared of a bulk metal or semimetal has not been discussed. In the present paper we study the quantum conductance of three dimensional ballistic wires with ideally flat boundaries and show that it obeys fluctuations with the properties quite distinguishable from those of the universal conductance fluctuations (UCF, [1]): both the fluctuations amplitude and the sensitivity of the conductance to the magnetic field flux  $\Phi = HS$  penetrated into the sample cross-sectional area  $S$  are different and depend on details of the shape of a wire. When the wire has the cross section with the shape of an integrable billiard, conductance fluctuations have the enlarged amplitude  $\delta G \sim [(e^2/h)^3 G]^{1/4}$  and the universal correlation magnetic field  $H_c \sim \Phi_0/S$ . When the cross-sectional shape of a wire is non-integrable, the irregular part of a conductance has the  $e^2/h$  scale whereas the correlation field is reduced to the value of  $H_S \sim (\lambda_F/\sqrt{S})^{1/2}(\Phi_0/S)$  and the correlation voltage of the nonlinear conductance fluctuations has the scale of  $eV_c \sim \hbar^2/mS \sim E_F/(S/\lambda_F)$ , where  $\lambda_F = 1/p_F$  is the Fermi wavelength.

The following analysis is based on the application of the Landauer-Buttiker approach. That is, the two-terminal conductance  $G$  can be written as  $G = \frac{e^2}{h} \text{Tr}(\hat{t}\hat{t}^+)$ , where  $\hat{t}$  is the scattering matrix [2]. In the limit of a ballistic transport in long wires,  $t_{nm} = \delta_{nm} \times (0 \text{ or } 1)$  and the separation of variables of the electron motion along and across wire axis reduces the conductance formula to the form [3]

$$G = \frac{e^2}{h} N(E_F)$$

which includes now the number of reflectionless quasi-one-dimensional channels  $N(E_F)$ . The latter quantity is equal to the number of size-quantized energy levels in a 2D box (with the shape of a wire cross section) below the Fermi level in the system. The main contribution to  $N(E_F)$  is determined by the average density of states and depends only on the area  $S$  independently of the shape:  $N_0(E_F) \sim E_F/(2\pi\hbar^2/2mS)$ . Next, one can distinguish the term which manifests the features of the boundary conditions of the electron wave function along the surcomference  $L \sim \sqrt{S}$  of the wire surface. When those are  $\psi = 0$ , a strip  $L \times \lambda_F$  should be excluded from the cross-sectional area of a sample and, which reduces  $N_0$  by the number  $N_1 = \theta(E_F/(\hbar^2/2mL^2))^{1/2}$  [4]. These two terms give us the waveguide analogue to the Sharvin resistance formula [5]. Finally, the exact number of states  $N(E_F)$  depends on the Fermi energy irregularly, and its deviation,  $\delta N(E_F)$ , from the best smoothed approximation gives a subject for a statistical consideration. Altogether, these three contributions can be combined into the conductance

$$G = \langle G \rangle + \delta G = \frac{e^2}{h} \left[ \frac{S}{2\pi\lambda_F^2} - \frac{L}{\lambda_F} \right] + \frac{e^2}{h} \delta N(E_F). \quad (1)$$

A randomly varying part of a conductance,  $\delta G$  will be subject of the following analysis. In Ref. [6] these fluctuations have been called **geometrical conductance fluctuations** in order to distinguish them from the UCF [1].

As we know from the quantum billiards theory, the statistics of fluctuations  $\delta N(E_F)$  depend on the integrability of the particle motion in a quantum box. According to [7, 8], the fluctuations of the number of states below the Fermi level are the strongest in integrable quantum systems: the systems which possess an additional integral of motion besides the energy. The following reasoning gives a handwaving estimation of this effect. The spectrum  $\epsilon(I, n)$  of a particle confined in the integrable box can be imagined as a set of independent level series marked by different values of a quantum number  $I$ , so that at energies  $E \gg \hbar^2/mS$  higher than the mean level spacing the total spectrum is locally composed of uncorrelated contributions from different rigid staircases of levels derived from separate one-dimensional Hamiltonians (each corresponding to some value of  $I$ ). This means that at the short energy range  $\epsilon$  the spectra of integrable systems obey the Poisson type of statistics,  $\langle (\delta[N(E + \epsilon) - N(E)])^2 \rangle \approx \frac{1}{15} \langle N(E + \epsilon) - N(E) \rangle$  [8], while the width of a spectral interval  $\epsilon$  is small enough to consider all levels  $\epsilon(I, n)$  inside as taken independently from different series  $I$ . Otherwise, the mean square  $\langle (\delta[N(E + \epsilon) - N(E)])^2 \rangle$  is restricted by the number  $I_{max}$  of independent level series contributing to the spectrum formation, since each of them has a strong internal rigidity. In the case of a free

particle moving in a 2D box,  $\epsilon(I, n) \propto (I^2, n^2)$ , so that the above-mentioned Poisson law is applicable only if  $\epsilon < \epsilon_{max} \sim E_F/\sqrt{S/\lambda_F^2}$ . Beyond this scale, the amplitude of spectral fluctuations is saturated, what can be estimated as  $\langle (\delta[N(E_F + \epsilon) - N(E_F)])^2 \rangle = \langle \delta N(E_F)^2 \rangle \sim N(E_F)^{1/2}$ . It is amusing to note that the problem of calculation of  $\delta N(E_F)$  in rectangular billiards is familiar to the number-theory as a problem of an accuracy of the best smoothed series approximation of a number of square lattice vortices inside an ellipse. One of the best number-theory results [9] has predicted  $\langle \delta N^2 \rangle \propto \langle N(E) \rangle^\theta$ , where  $0.6416 \geq \theta \geq 1/2$ , which agrees with the above qualitative reasoning.

All this gives an estimation of the mean square value of the conductance fluctuations  $\delta G$  in the wire with an integrable cross sectional shape,

$$\langle \delta G^2 \rangle = \beta \alpha \left[ \left( \frac{e^2}{h} \right)^3 G \right]^{\frac{1}{2}}. \quad (2)$$

The scale of these fluctuations can exceed the quantum  $\frac{e^2}{h}$ . Here,  $\alpha$  is a specific geometrical factor (for instance,  $\alpha = 0.095$  in a rectangle with practically equal sides) and  $\beta$  accounts for the symmetry induced degeneracy of states.

The spectra of non-integrable systems are much more rigid, and the fluctuations in them are rather weak. In terms of the interaction of levels, this results from the repulsion between all of them (not only within each spectral series, as in the case of integrable billiards). The limiting case of shuc levels statistics is given by that of chaotic billiards [8], i.e., the quantity  $\delta N(E_F)$  obeys some kind of a saturated Wigner-Dyson law [10]. Therefore, the amplitude of geometrical conductance fluctuations in wires of an arbitrary shape can be estimated as

$$\langle \delta G^2 \rangle = \beta \left( \frac{e^2}{\pi h} \right)^2 \ln \left( \ln \frac{Gh}{e^2} \right). \quad (3)$$

**Fluctuations of nonlinear conductance.** Since neither the shape nor the Fermi level can be easily varied in 3D metallic wires, the most natural possibility to observe the spectral fluctuations of the transverse motion in an adiabatic wire consists in the studies of its diferential (nolinear) conductance  $dI(V)/dV$ . In the adiabatic regime, this quantity can be expressed in terms of a number of transmitted waveguide modes [11] as

$$\frac{dI(V)}{dV} = \frac{e^2}{2h} \left[ N \left( E_F + \frac{eV}{2} \right) + N \left( E_F - \frac{eV}{2} \right) \right].$$

One can see from this equation that the voltage dependence of  $dI(V)/dV$  just follows the local (in energy) fluctuations of the number of size-quantized states in the interval  $eV$  near the Fermi level. In a constriction with the cross section

presenting completely integrable billiard, this value undergoes fluctuations with the Poisson statistics at low voltages  $V < V_c = \epsilon_{max}/e$ . When  $V \geq V_c$ , the amplitude of fluctuations saturates at the value described by Eq. (2) and then  $V_c$  plays the role of the correlation voltage of these fluctuations. Therefore, in the adiabatic contact with an integrable cross-sectional shape

$$\left\langle \left[ \frac{dI(V)}{dV} - G \right]^2 \right\rangle = \begin{cases} \frac{1}{15} \left( \frac{eV}{E_F} \right) \frac{e^2}{h} G, & eV < \epsilon_{max} \\ \gamma \sqrt{\left( \frac{e^2}{h} \right)^3 G}, & eV > \epsilon_{max} \end{cases} \quad (4)$$

In *non-integrable* (i.e., chaotic) systems the spectral fluctuations are weaker [8, 10],

$$\left\langle \left[ \frac{dI(V)}{dV} - G \right]^2 \right\rangle = 3\beta \left( \frac{e^2}{\pi h} \right)^2 \begin{cases} \ln \left( \frac{VGh}{eE_F} \right), & eV < \epsilon'_{max} \\ \ln \left( \ln \left( \frac{Gh}{e^2} \right) \right), & eV > \epsilon'_{max} \end{cases} \quad (5)$$

The correlation voltage which one could assign to these fluctuations is determined by the mean level spacing  $\hbar^2/mS$  and has the form

$$V_c = \frac{1}{e} \frac{E_F}{S/\lambda_F^2}. \quad (6)$$

It is interesting to note that this result differs from the time-of-flight estimation which one could get after replacing the mean free path by the sample length in the formulae valid for diffusive conductors [12].

**Magnetoconductance fluctuations.** Another possibility to observe the geometrical conductance fluctuation consists in an application of a magnetic field oriented along the axis of a wire. In what follows, we distinguish three cases of different cross-sectional shapes of a wire.

Let us first consider the *system which is integrable and retains this property also in an applied magnetic field* (the disk obviously belongs to this class). The external magnetic field shifts series of levels marked by different value of the angular momentum  $I$ , one with respect to another. When this shift,  $\frac{\hbar e}{mc} HI \sim H \frac{\hbar e}{mc} \sqrt{E_F/(\hbar^2/2mS)}$ , becomes comparable to the mean intra-series level spacing,  $\sqrt{E_F \hbar^2/2mS}$ , the statistical configuration of the Poisson distribution of levels is renewed, which produces a random magnetoconductance variation of the order of what is represented in Eq. (2) ( $\beta = 1$ ). The characteristic scale of a sufficient magnetic field is determined by the flux quantum penetrated through the sample cross-sectional area,  $H_c S \sim hc/e$ , which means that the important physical quantity - the correlation magnetic field of fluctuations [1] - is similar to that in UCF. The visual difference between

UCF and geometrical fluctuations is only in their amplitudes. The geometrical fluctuations are enlarged parametrically in thick cylindrical wires, what has been observed in [13] in numerical simulations. On the other hand, these fluctuations can be viewed (even inside the correlation field  $H_c$ ) as a series of randomly distributed  $e^2/h$  conductance steps with the characteristic spacing of

$$\Phi_S \sim \frac{\Phi_0/\sqrt{\alpha}}{\sqrt[4]{N(E_F)}} \sim \Phi_0 \left[ \frac{2e^2/h}{\alpha^2 G} \right]^{\frac{1}{4}}.$$

Of course, one should realize that the wires with the cross-sectional shape which is integrable at any magnetic field gives us an exclusive example. *Magnetoconductance fluctuations in wires with a non-integrable cross-sectional shape* (see Eq. (3)) have a much lower amplitude what makes them more similar to the UCF. Nevertheless, they still possess one feature specific to the ballistic adiabatic system. That is, the non-integrable quantum box spectrum is much more sensitive to the magnetic field variation that it takes place in open diffusive conductors, and the penetration of a flux

$$\Phi_S = \sqrt{\frac{\lambda_F}{\sqrt{S}}} \frac{hc}{e} \ll \Phi_0 \quad (7)$$

is already enough for renewing the realization of the levels configuration [14]. In a chaotic billard, all the classical electron trajectories are infinitely long and cover the whole fixed-energy torus in the phase space. In semiclassics, the length of such trajectories is limited, since two point of the phase space which reach into the same unit volume  $dp_i dx_i \sim h$  are indistinguishable. Therefore, the length of a semiclassical trajectory in a box of characteristic dimensions  $L \sim \sqrt{S}$  should be cut when the inverse time of flight along it,  $h\sqrt{S}/v_F$  will be comparable with the mean level spacing  $\Delta \sim \hbar^2/mS$  and characteristic traces in the real space contain  $\sim \sqrt{S}/\lambda_F$  closed loops each encircling an area  $\sim S$  of a random sign. The oriented encircled area of a chaotic trajectory can be estimated as  $S^{3/2}/\lambda_F$  which produces the characteristic correlation magnetic field  $H_c \sim \Phi_S/S$ . It would be interesting to note in this connection that the features of the conductance fluctuations found in ballistic silver micro-contacts [15] are quite similar to those of wires with a non-integrable shape described by Eqs. (6,7), though the observed amplitudes were much smaller than  $e^2/h$  scale.

Finally, there exists a class of *systems which are integrable* (or partly integrable [8]) *at  $H = 0$  and loose this property after an application of a magnetic field*. For instance, we can mention the structures with a rectangular cross-sectional shape where the first penetrated flux quantum drastically changes the level statistics: from the Poisson type at  $\Phi = HS < \Phi_0$  to the Wigner-Dyson type at higher fields. This should induce a low-field magnetoconductance of a random sign with the amplitude estimated by Eq. (2), whereas the following

increase of  $\Phi$  produces fluctuations with the amplitude  $\frac{e^2}{h}$  and at the scale of  $\Phi_S$  (instead of  $\Phi_0$  observed in the UCF). The monocrystalline microwires with perfect facets (whiskers) grown of the semimetallic material would be the best candidates to show this kind of behavior.

We are grateful to P. Wyder and A. Jansen for helpful discussions.

## References

- [1] B.L. Altshuler, JETP Lett. **41**, 648 (1985); B.L. Altshuler and D.E. Khmel'nitskii, *ibid.* **42**, 359 (1985); P.A. Lee and A.D. Stone, Phys. Rev. Lett. **55**, 1622 (1985); A.D. Stone, *ibid.* **54**, 2692 (1985)
- [2] M. Buttiker et al, Phys. Rev. B **31**, 6207 (1985)
- [3] B.J. van Wees et al, Phys Rev Lett **60**, 848 (1988)
- [4] H. Weyl, "Gruppentheorie in Quantenmechanik", Hirzel, Leipzig 1931
- [5] Yu. V. Sharvin, Sov Phys JETP **21**, 655, (1965)
- [6] V.I. Fal'ko and G.B. Lesovik, Solid State Commun. **84**, 835 (1992)
- [7] O. Bohigas et al, Phys. Rev. Lett. **52**, 1 (1984); G. Casati et al, *ibid.* **54**, 1350 (1985)
- [8] M. Berry, Proc. Roy. Soc. Lond. A **400**, 229 (1985); M. Gutzwiller, "Chaos in Classical and Quantum Mechanics", Springer-Verlag, Berlin 1990
- [9] V. Vinogradov, Bull. Ac. Sci. USSR Ser. VIII **3**, 313 (1932); H.P. Baltes and E.R. Hilf, "Spectra of Finite Systems", B.I.-Wissenschaftsverlag, Mannheim 1976
- [10] E.P. Wigner, SIAM Review **9**, (1967), 1; M.L. Mehta, "Random Matrices", Academic Press, NY 1967
- [11] L.I. Glazman and A.V. Khaetskii, JETP Lett **48**, 591 (1988)
- [12] D.E Khmel'nitskii and A.I. Larkin, Phys. Scr. T **14**, 4 (1986);
- [13] E.N. Bogachek et al, Phys. Rev. B **47**, 16635 (1993)
- [14] K.B. Efetov, Adv. Phys. **32**, 53 (1983); R. Jalabert et al, Phys. Rev. Lett. **65**, 2442 (1990); A. Szafer and B.L. Altshuler, *ibid.* **70**, 587 (1993)
- [15] P.A. Holweg et al, Phys. Rev. Lett. **67**, 2549 (1991); P.A. Holweg et al, Phys. Rev. B **48**, 2479 (1993)

# Spontaneous Spin Polarization in Quantum Wires

Gerhard Fasol\*

Institute of Industrial Science, University of Tokyo,  
and

‘Structure and Functional Property’-Group, ‘Sakigake 21’-PRESTO,  
Research Development Corporation of Japan (JRDC),  
7-22-1 Roppongi, Minato-ku, Tokyo 106, Japan

**Abstract.** Electron-electron pair scattering shows strong dependence on the electron spin: in two dimensions (2D) electron pair scattering is stronger for pairs of electrons in opposite spin subbands, than for pairs of electrons in the same subband. More dramatically, in one dimensional (1D) quantum wires, electron-electron scattering only exists for pairs of electrons in opposite spin subbands. In general, the spin subbands are expected to show a wave vector dependent splitting with terms proportional to  $k^3$  in the absence of inversion symmetry. We show that the wave vector dependent spin splitting gives rise to a strong asymmetry of the electron-electron pair scattering rates with respect to the spin subbands. One consequence of this asymmetry is a new physical effect: ‘Spontaneous Spin Polarization’ due to electron-electron pair scattering.

## 1 Introduction

Intense effort is presently being spent by several groups to fabricate high quality 1D quantum wires. Among the motivations for this work are the prediction of reduced remote impurity scattering,<sup>1)</sup> the prediction of quantum wire lasers with favorable properties,<sup>2)</sup> and the question about the many-body ground state of electrons in 1D. The present work adds a further motivation: the prediction of spontaneous spin polarization effects in quantum wires. In particular, the construction of an electron spin polarizer based on a quantum wire is predicted.

Dempsey et al.<sup>3)</sup> stated recently for the case of the Quantum Hall effect: ‘... *most theoretical studies have developed a noninteracting picture of (Quantum Hall Effect) edge states, attention has recently shifted to the effects of electron-electron interactions on edge-state properties. Electron spin has played little role in theories of edge-states ...*’. A similar statement could be made for the fields of mesoscopic devices and quantum wires. Most previous work in the area of mesoscopic devices and quantum wire transport used the model of free, non-interacting, spin-less electrons.<sup>4)</sup>

Recent work started to include spin and electron interaction effects in the picture of transport in quantum wires, and lead to the simultaneous theoretical discovery of spontaneous spin polarization effects due to electron-electron interactions in the one-dimensional Quantum Hall edge states by Halperin’s group<sup>3)</sup> and in single mode quantum wires.<sup>5)</sup> A related

---

\*work in collaboration with Hiroyuki Sakaki, Research Center for Advanced Science and Technology (RCAST), University of Tokyo, 4-6-1 Komaba, Meguro-ku, Tokyo 153, Japan.

magneto-electric spin polarization effect for the case of 2D electrons has been reported earlier by Edelstein.<sup>6)</sup>

In our present work, following Hu et al.,<sup>7)</sup> we assume electrons that are well described by a conventional Fermi liquid picture.

## 2 Spin Dependence of Electron Pair Scattering in 2D

In pioneering work, Quinn and Ferrell<sup>8)</sup> and Ritchie<sup>9)</sup> calculated electron pair scattering times for the three-dimensional (3D) electron gas. Several calculations for the two-dimensional (2D) electron gas<sup>10)-12)</sup> and multiple-layer 2D electron gas<sup>13)</sup> have been performed. However previous calculations are for the ideal case of an infinitely thin electron gas,<sup>11)</sup> or obtain results for strictly zero temperature,<sup>10), 12), 13)</sup> and do not include electron spin or exchange effects.

In the course of the present work we have shown, that electron-electron scattering in 2D depends strongly on temperature, electron excess energy, electron gas width, exchange correlation effects and in particular on electron spin.<sup>14), 15)</sup> Fig. 1 demonstrates that we find much higher electron-electron pair scattering rates for pairs with electrons in opposite spin subbands as compared to pairs with electrons in the same spin subbands. We have calculated the pair scattering rates for a large range of temperatures, electron density, electron gas width, and for different exchange correlation terms.<sup>14), 15)</sup> We include electron spin, electron gas width, and an exchange term in the Coulomb matrix element. Screening is included via a wave vector and frequency dependent dielectric function in random phase approximation (RPA). An exchange term is included beyond RPA.<sup>15)</sup>

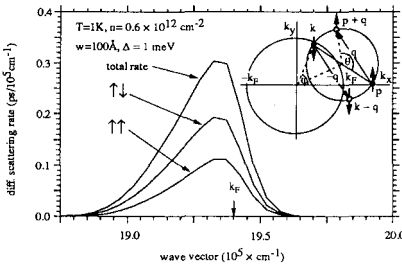


Figure 1: *Differential electron-electron pair scattering probability<sup>14)</sup> for 2D is lower for pairs of electrons with parallel spin. Insert shows schematic of electron pair scattering process in 2D.<sup>15)</sup>*

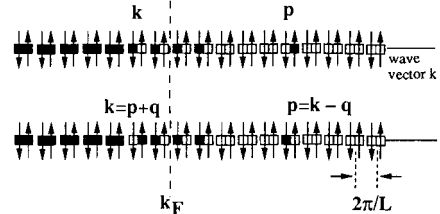


Figure 2: *Electron-electron pair scattering process in 1D, introduced by Fasol and Sakaki.<sup>5)</sup> This process has similarity with a spin flip process.*

## 3 The Electron-Electron Scattering Process in 1D

The fundamental electron-electron pair scattering process for electrons *with spin* in a 1D quantum wire has been introduced by Fasol and Sakaki<sup>5)</sup> and is demonstrated in Fig. 2. This process is very similar to a spin-flip process. After each scattering event shown in Fig. 2 propagation of an electron of similar energy will continue in the opposite spin subband.

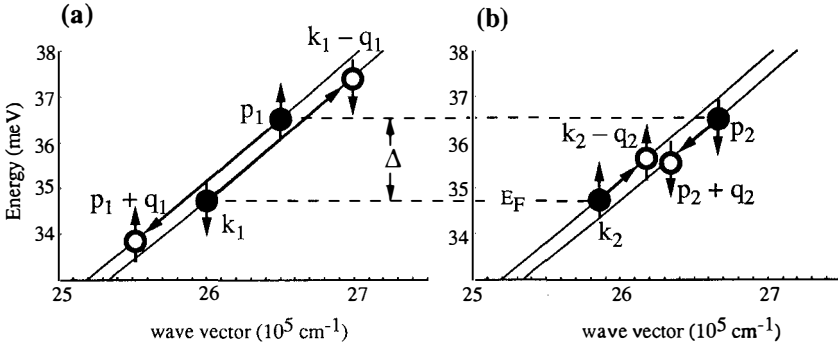


Figure 3: *Electron-electron pair scattering rates in quantum wires can be dramatically different for the different spin subbands: (a) An electron in the ‘spin-up’ band with wave vector  $p_1$  has lower scattering rate since the destination state at  $p_1 + q_1$  has high thermal probability to be filled. (b) Scattering rate for electron  $p_2$  in the ‘spin-down’ band is much higher, since the final state  $k_2 - q_2$  has lower thermal occupation probability than the destination state in (a) at  $p_1 + q_1$ . (Intra-subband pair scattering in 1D is only allowed with a partner electron of opposite spin.)*

## 4 Spontaneous Spin Polarization in 1D Quantum Wires

The ‘Spontaneous Spin Polarization’ effect is caused by the spin subband dependence of the electron-electron pair scattering rates. There are two keys to understand this new effect. The first key is the introduction of the fundamental electron-electron pair scattering process for quantum wires<sup>9</sup> discussed above. The second key is the wavevector dependence of the spin-splitting of the electron bands: in a ‘single mode’ 1D quantum wire the conduction band has two spin subbands. The spin splitting is expected to have bulk terms cubic in wave vector  $k$  (there are also weaker terms linear in  $k$ ), and in lower dimensions also additional terms due to the confinement and in-built electric fields.<sup>22), 23)</sup>

Spin-splitting of electron bands in semiconductors lacking inversion symmetry is well known in the bulk<sup>19)–21)</sup> and for 2D systems.<sup>22), 23)</sup> It has been measured in the bulk<sup>24)</sup> and for 2D systems<sup>25)–27)</sup>—similar splitting is of course also expected in quantum wires. Intrinsic spin splitting is on the order of 1meV at the Fermi edge under typical conditions.<sup>21), 25)</sup>

The basic principle of spin subband dependent pair scattering rates is demonstrated in Fig. 3. In Fig. 3(a) we look at pair scattering of an electron with wave vector  $p_1$  in the ‘spin-up’ band and in Fig. 3(b) of an electron at  $p_2$  in the spin-down band. For each case we show a typical pair scattering process with a partner electron near the Fermi surface. Once the electron at  $p_1$  or  $p_2$  and the partner electron at  $k_1$  and  $k_2$  have been chosen, energy and momentum conservation together with the band dispersion fix the final states. (Fig. 3 has been calculated using ‘Mathematica’ and a realistic dispersion relation for GaAs derived from a  $k \cdot p$  calculation, which includes  $k^3$  spin splitting terms and non-parabolicity). Note that there is a fundamental asymmetry of the electron-electron pair scattering with respect to the spin subbands: in the case of a test electron in the spin-up band the final states lie outside the energy range of the initial states, while for the case of a test electron in the spin-down band the final states lie within the energy range of the initial states. This asymmetry is a direct consequence of the wave vector dependent spin-splitting.

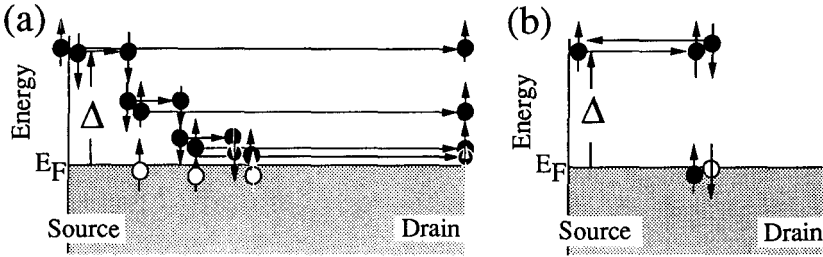


Figure 4: *Spontaneous Spin Polarization in a 1D Quantum Wire: (a) Spin-up electrons pass a 1D wire without scattering; spin-down electrons undergo strong scattering, leading to rapid thermalization and the emission of additional spin-up electrons, which emerge. (b) Scattering with partner electrons at the opposite end of the Fermi sea is expected to have a weak influence.*

The scattering process shown in Fig. 3(b) has much higher probability than the process in Fig. 3(a), since the Fermi population factors will be much more favorable for scattering. Thus  $\mathbf{p}_1 + \mathbf{q}_1$  in Fig. 3(a) has a high probability of being occupied, reducing the scattering probability of the process in Fig. 3(a) dramatically compared to Fig. 3(b).

The spin subband dependence of the scattering rates can be used to polarize a ballistic electron beam, as demonstrated in Fig. 4. An electron injected into the 'spin-up' subband with an excess energy  $\Delta$  in Fig. 4(a) passes the quantum wire with low scattering probability. An electron injected into the 'spin-down' subband on the other hand, has an increased scattering probability as demonstrated in Fig. 3(b). The 'spin-down' electron will thermalize rapidly, as shown in Fig. 4(a) and will emit a series of spin-up electrons during the thermalization process. The emitted spin-up electrons will have low scattering probability, and therefore will emerge from the quantum wire spin polarized at the drain. Thus this structure acts as an active spin polarizer, converting ballistic spin-down electrons into ballistic spin-up electrons, while spin-down electrons are rapidly thermalized. Spin dependence of scattering rates also exists for scattering with partners at the opposite,  $-\mathbf{k}_F$ , end of the Fermi surface, but the effect is weaker. The effect of this type of scattering on the polarizer is shown in Fig. 4(b).

## 5 Calculated Scattering Rates in 1D

To demonstrate the spin subband dependence of pair scattering we have calculated the differential pair scattering rates as a function of wave vector  $\mathbf{k}$  of the partner electron, and as a function of excess electronic energy  $\Delta$ .

Our calculations<sup>5), 14), 15)</sup> are based on Fermi's Golden Rule. The total scattering rate for an electron at wavevector  $\mathbf{p}$  and in spin subband  $\sigma$  is expressed as:

$$\frac{1}{\tau_{\text{ee}}|\mathbf{p}, \sigma} = \frac{2\pi}{\hbar} \sum_{\mathbf{k}, \mathbf{q}, \sigma'} f_{\mathbf{k}, \sigma'} (1 - f_{\mathbf{k}-\mathbf{q}, \sigma'}) (1 - f_{\mathbf{p}+\mathbf{q}, \sigma}) \times \left| \frac{\langle \mathbf{k} - \mathbf{p}, \mathbf{p} + \mathbf{q} | V | \mathbf{k}, \mathbf{p} \rangle}{\epsilon(\mathbf{q}, (E_{\mathbf{p}} - E_{\mathbf{p}+\mathbf{q}})/\hbar)} \right|^2 \delta(E_{\mathbf{p}+\mathbf{q}, \sigma} + E_{\mathbf{k}-\mathbf{q}, \sigma'} - E_{\mathbf{p}, \sigma} - E_{\mathbf{k}, \sigma'}), \quad (1)$$

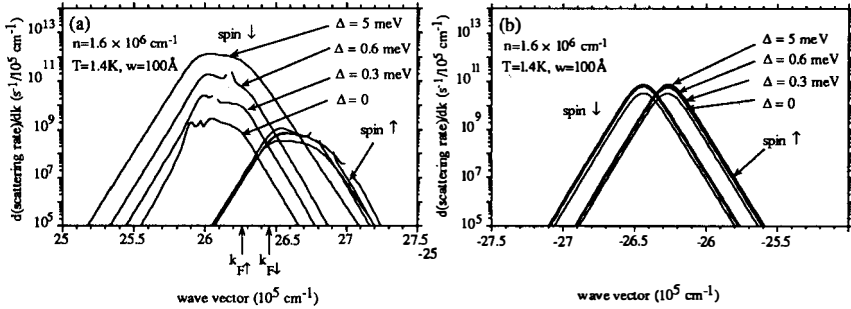


Figure 5: Calculated electron pair scattering rates for 1D: (a) For electrons above the Fermi energy ( $\Delta > 0$ ), electron pair scattering rates may be many orders of magnitude larger for one particular spin orientation (here spin-down) than for the other. (Irregularities and divergences in the curves occur for scattering vectors extremely close to  $q = 0$  and are partially eliminated from the Figure, they are not eliminated for the final integrations of total scattering rates however.) (b) Spin dependence for scattering with partners on the 'far-side' of the Fermi surface is much weaker.

where  $f_{k,\sigma'}(1 - f_{k-q,\sigma'})$  ( $1 - f_{p+q,\sigma}$ ) are the Fermi occupation factors and  $\langle k - p, p + q | V | k, p \rangle$  is the appropriate Coulomb interaction matrix element. In the actual calculation, we use a Coulomb matrix element which takes account of spin, an exchange correlation term, and the width of the electron gas. For the dielectric function  $\epsilon(q, (E_p - E_{p+q})/\hbar)$ , we use an RPA expression, which includes the finite temperature, the spin-split subband structure, and an exchange term. The  $\delta$ -function on the right expresses the conservation of energy. Details of the calculations can be found in Fasol and Sakaki.<sup>15</sup>

Fig. 5 shows typical results of the calculation, and demonstrates that the pair scattering rates can be many orders of magnitude different for the two spin subbands. The total scattering rates are the balance of scattering with partner electrons at the 'near side' (Fig. 3 and Fig. 5(a)) and the 'far side' (Fig. 5(b)) of the Fermi surface. The spin subband dependence is expected to be strongest for hot electrons, i.e. for electrons with an energy  $\Delta$  on the order of 1...5meV above the Fermi energy.

Using Fig. 4 a quantum wire spin polarizer can be constructed.<sup>5</sup> The actual orientation of 'spin-up' and 'spin-down' is given by the orientation of the crystal structure, and also by the microscopic details of the quantum wire. In a real quantum wire 'spin-up' and 'spin-down' states will be mixed.

Acoustic phonon scattering is expected to be weaker than electron scattering effects up to at least 100K, while we expect that optical phonon scattering will destroy this effect above approximately 100K. Sufficiently high mobility is required, so that impurity and roughness scattering are lower than electron-electron scattering. Since in-built microscopic electric fields affect the spin-splitting of the quantum wire, and since interface roughness can affect microscopic electric fields, it could also negatively affect the spin polarization phenomena. Plasmon emission is a possible loss mechanism and when present, is expected to destroy the spin polarization effects. Fortunately there is a threshold excess energy for emission of plasmons: an electron can only emit a plasmon, if the electron's excess energy  $\Delta$  is greater than a certain threshold energy. This threshold excess energy is much larger for typical 1D systems than for corresponding 2D systems, and is on the order of 50 to 200 meV for typical conditions in

1D.<sup>15)</sup> Therefore, plasmon emission leaves a sufficient working range for our proposed electron spin polarization device.

So far we have assumed that the background electron gas in the wire is sufficiently coupled to the environment, so that its distribution is not disturbed by the injected electron beam. The opposite limit is the case of weak coupling of the background electrons in a section of the wire to the surroundings. In this case the injected electron beam will flip background electrons between spin subbands with unequal probability, leading to unequal spin populations and a steady state spin polarization of the background electrons. This induced spin polarization effect is similar to the 2D magneto-electric effect predicted by Edelstein.<sup>6)</sup>

A further point to note is, that the spin orientation of the spin-split bands is inverted, when  $\mathbf{k}$  is inverted, i.e. if for example the 'spin-up' subband is at higher energies for  $\langle 1, 1, 0 \rangle$ , then it will be at lower energies for  $\langle -1, -1, 0 \rangle$ . This means, if a quantum wire spin polarizer device is constructed along a particular direction to produce 'spin-up' electrons, the same device, will produce 'spin-down' electrons, if the ballistic electron current is passed in the opposite direction.

## 6 Summary

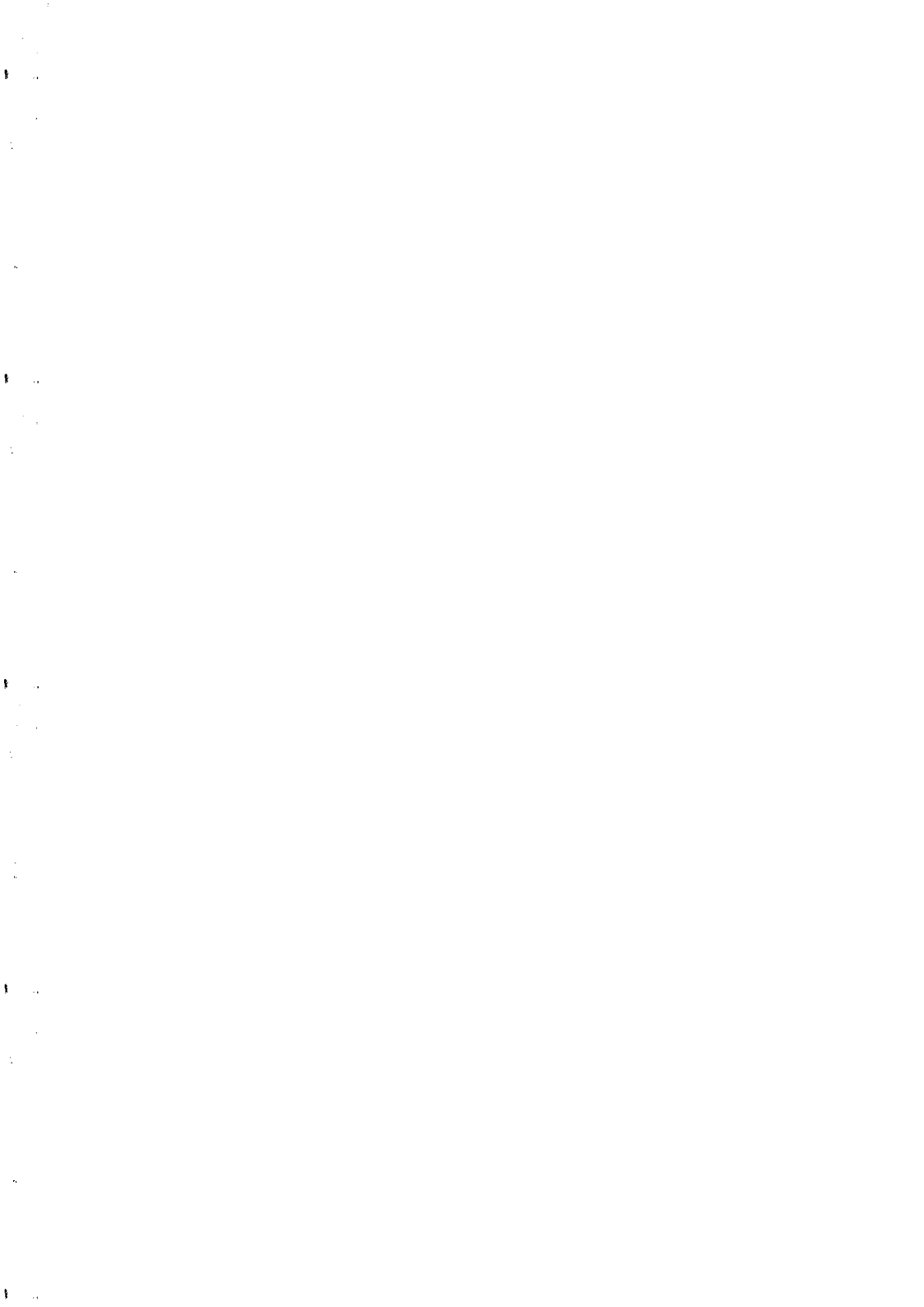
The fundamental electron-electron pair scattering process for quantum wires has been introduced. It has similarity with spin flip processes. We have shown that the naturally occurring wave vector dependence of the spin splitting of the electron bands in quantum wires can lead to an asymmetry of the electron-electron pair scattering rates with respect to the spin subbands. Electron-electron pair scattering rates in the different spin subbands can differ by many orders of magnitude. This effect can lead to 'spontaneous spin polarization effects' when ballistic electrons propagate through a quantum wire. No external magnetic field is needed for this effect.

**Acknowledgements.** One of the authors (GF) gratefully acknowledges support for part of this work by the NTT Telecommunications Endowed Chair at the Research Center for Advanced Science and Technology (RCAST) of the University of Tokyo and by the JRDC-Sakaki Quantum Wave Project and stimulating discussions with T. Noda, T. Matsusue, J. Motohisa, Y. Nagamune, Y. Arakawa and B. Jusserand.

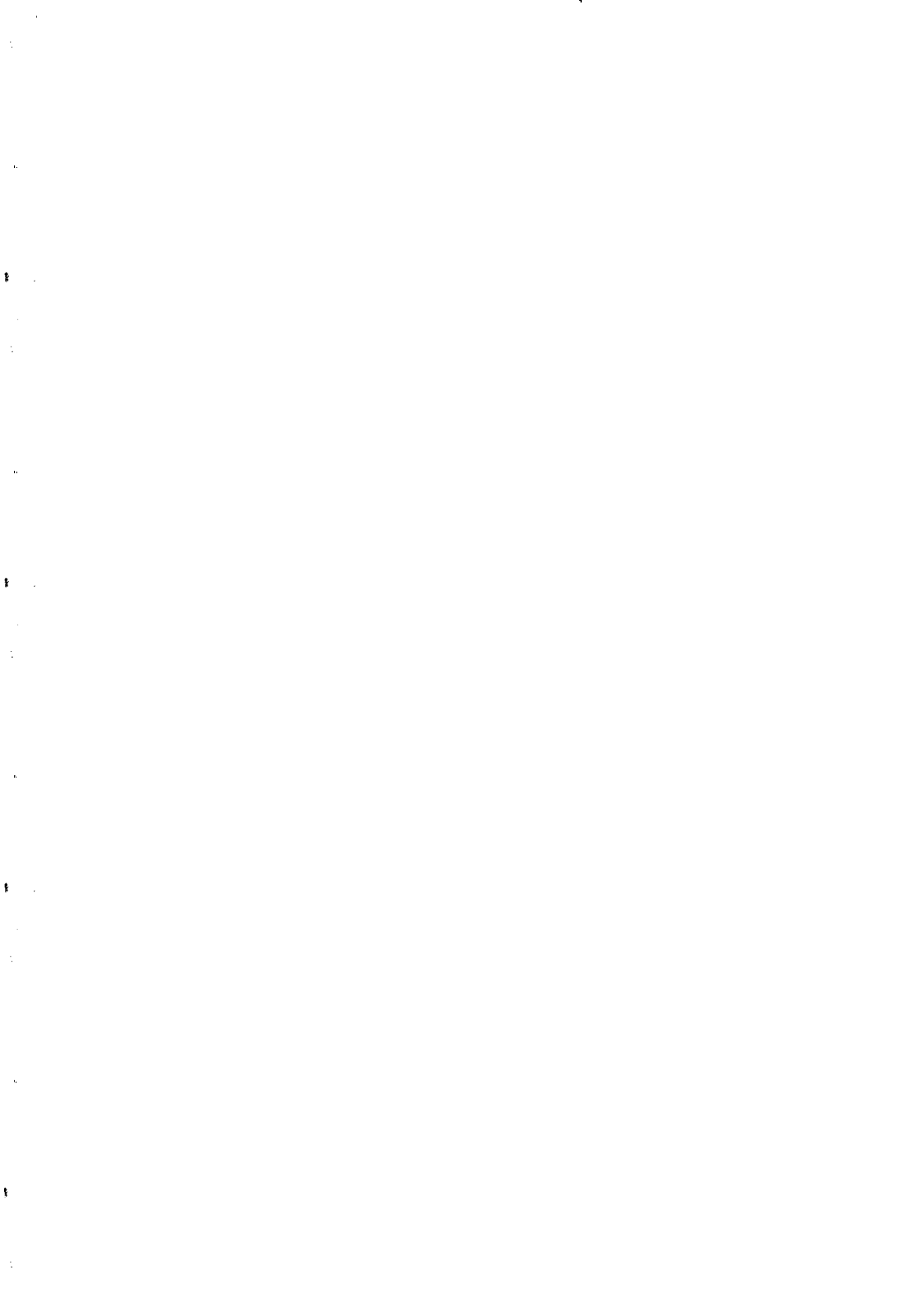
## References

- [1] H. Sakaki, Jpn. J. Appl. Physics **19**, L735 (1980), and Inst. of Physics Conf. Ser. **63**, 251 (1981).
- [2] Y. Arakawa and H. Sakaki, Appl. Phys. Lett. **40**, 939 (1982).
- [3] J. Dempsey, B. Y. Gelfand, B. I. Halperin, Phys. Rev. Lett. **70**, 3639 (1993).
- [4] C. W. Beenakker and H. van Houten, Solid State Physics, ed. by H. Ehrenreich and D. Turnbull, Academic Press (San Diego) **44**, 1 (1991).
- [5] G. Fasol and H. Sakaki, Phys. Rev. Lett. **70**, 3643 (1993); Appl. Phys. Lett. **62**, 2230 (1993).
- [6] V. M. Edelstein, Solid State Commun. **73**, 233 (1990).
- [7] Ben Yu-Kuang Hu and S. Das Sarma, Appl. Phys. Lett. **61**, 1208 (1992); Phys. Rev. Lett. **68**, 1750 (1992).

- [8] J. J. Quinn and R. A. Ferell, Phys. Rev. **112**, 812 (1958).
- [9] R. H. Ritchie, Phys. Rev. **114**, 644 (1959).
- [10] A. V. Chaplik, Zh. Eksp. Teor. Fiz. **60**, 1845 (1971) [Sov. Phys. JETP **33**, 997 (1971)].
- [11] G. F. Giuliani and J. J. Quinn, Phys. Rev. B **26**, 4421 (1982).
- [12] R. Jalabert and S. Das Sarma, Surface Science **229**, 405 (1990), Phys. Rev. B **39**, 5542 (1989), Phys. Rev. B **40**, 9723 (1989).
- [13] P. Hawrylak, G. Eliasson, and J. J. Quinn **37**, 10187 (1988); P. Hawrylak, Phys. Rev. Lett. **59**, 485 (1987).
- [14] G. Fasol and H. Sakaki, Solid State Commun. **84**, 77 (1992); G. Fasol, Proc. 21st Int. Conf. on The Physics of Semiconductors, edited by Ping Jiang and Hou-Zhi Zheng, World Scientific, Singapore (1992) page 1411.
- [15] G. Fasol and H. Sakaki, submitted to Phys. Rev. B.
- [16] D. Pines and P. Nozières, The Theory of Quantum Liquids, Addison-Wesley Publ. Co., Advanced book classics series, Redwood City, (1988).
- [17] G. Fasol, Appl. Phys. Lett. **61**, 831 (1992).
- [18] G. Fasol, Appl. Phys. Lett. **59**, 2430 (1991).
- [19] G. Dresselhaus: Phys. Rev. **186** (1958) 824.
- [20] E. O. Kane, in *Semiconductors and Semimetals*, eds. R. K. Willardson and A. C. Beer (Academic Press, New York, 1966), Vol. 1.
- [21] M. Cardona, N. E. Christensen, and G. Fasol, Phys. Rev. Lett. **56**, 2831 (1986), and Phys. Rev. B **38**, 1806 (1988).
- [22] G. Lommer, F. Malcher, and U. Rössler, Phys. Rev. Lett. **60**, 728 (1988).
- [23] G. Bastard, 'Wave Mechanics Applied to Semiconductor Heterostructures', Les Editions de Physiques, Les Ulis, (1990).
- [24] H. Riechert, S. F. Alvarado, A. N. Titkov and V. I. Safarov, Phys. Rev. Lett. **52** (1984) 2297.
- [25] B. Jusserand, D. Richards, H. Peric, and B. Etienne, Phys. Rev. Lett. **69**, 848 (1992).
- [26] B. Das, D. C. Miller, S. Datta, R. Reifenberger, W. P. Hong, P. K. Bhattacharya, J. Singh, and M. Jaffe, Phys. Rev. B **39** 1411 (1989).
- [27] P. D. Dresselhaus, C. M. A. Papavassiliou, R. G. Wheeler, and R. N. Sacks, Phys. Rev. Lett. **68**, 106 (1992).



## SHOT NOISE AND A.C. QUANTUM TRANSPORT



## EQUILIBRIUM AND SHOT NOISE IN MESOSCOPIC SYSTEMS

Thierry Martin, *Theory Division, CNLS, Los Alamos National Laboratory*

## I. INTRODUCTION

Within the last decade, there has been a resurgence of interest in the study of noise in Mesoscopic devices, both experimentally and theoretically<sup>1-27</sup>). Noise in solid state devices can have different origins: there is  $1/f$  noise<sup>28</sup>), which is believed to arise from fluctuations in the resistance of the sample due to the motion of impurities<sup>29</sup>). On top of this contribution is a frequency independent component associated with the stochastic nature of electron transport, which will be the focus of this paper.

If the sample considered is small enough that dephasing and inelastic effects can be neglected, equilibrium (thermal) and excess noise can be completely described in terms of the elastic scattering properties of the sample. As mentioned above, noise arises as a consequence of random processes governing the transport of electrons. Here, there are two sources randomness: first, electrons incident on the sample occupy a given energy state with a probability given by the Fermi-Dirac distribution function. Secondly, electrons can be transmitted across the sample or reflected in the same reservoir where they came from with a probability given by the quantum mechanical transmission/ reflection coefficients. Equilibrium noise refers to the case where no bias voltage is applied between the leads connected to the sample, where thermal agitation alone allows the electrons close to the Fermi level to tunnel through the sample<sup>23</sup>). In general, equilibrium noise is related to the conductance of the sample via the Johnson-Nyquist formula<sup>30</sup>). In the presence of a bias, in the classical regime, we expect to recover the full shot noise  $< \Delta^2 I > = 2I\Delta\mu$  as was observed a long time ago in vacuum diodes<sup>31</sup>). In the Mesoscopic regime, however, excess noise is reduced below the shot noise level, as will be explained below.

If the sample is to be described quantum mechanically, a calculation of the noise should include the Pauli principle: an electron which is successfully transmitted cannot occupy the same state as another electron incident from the opposite side, which is reflected by the potential barrier. The importance of the statistics of the charge carriers is somehow a novelty in Mesoscopic physics. After all, many experiments in Mesoscopic physics can have a direct analog if we interchange the carriers with bosonic particles. The conductance steps experiment<sup>32</sup>) which

shows the transverse quantization of the electron wave function is an example: this experiment has been successfully completed with photons<sup>33</sup>). The measurement of universal conductance fluctuations in Mesoscopic wires and rings<sup>34,35</sup>) also has an analog when one shines a laser in white paint and studies the speckle pattern generated in this way<sup>36</sup>). The Aharonov–Bohm effect was successfully observed for electrons in disordered rings<sup>35</sup>): nothing tells us that we could not repeat the experiment for bosonic particles. In contrast to these examples, a noise measurement makes a distinction between electrons and photons if we look and the correlations between two detectors collecting the carriers.

Several approaches have been proposed to calculate noise. Some are quasi-classical, as they rely on the concept of trajectory. Others use a formulation of non equilibrium thermodynamics which is based on the concept of reservoirs, introduced for the conductance formula<sup>37</sup>). The reservoir picture can be cast in a systematic way to calculate the current current correlations in time for a multi-terminal conductor<sup>38</sup>). Below we will refer to this treatment as the “poor man’s” Keldysh<sup>39</sup>) approach. In contrast to this point of view, we will introduce a more intuitive picture<sup>4,14,15</sup>), where the current passing through the device is a superposition of pulses, or electrons wave packets, which can be transmitted or reflected.

## II. HISTORY

I will start with an historical overview: the list which appears below is by no means exhaustive, and I apologize for the contributions which have been left out.

In 1984, came the first printed suspicion that excess noise could be reduced below shot noise by quantum mechanical effects<sup>1</sup>). It was observed that by varying the voltage bias applied on a point contact, coherent stimulated phonon emission processes reduce the excess noise contribution in a point contact. A theoretical confirmation of this experiment followed soon after<sup>2</sup>). The noise is reduced by a factor  $d/l$ , where  $d$  is the diameter of the point contact and  $l$  is the mean free path associated with the phonons ( $d \ll l$ ). The second derivative of the noise with respect to the bias can be related to the electron phonon interaction function. Noise in normal metal–metal and metal–superconducting junctions was analyzed using a semiclassical Keldysh approach<sup>3</sup>), with an identification of the thermal and non–equilibrium contributions. For a junction between normal metal and superconductor, an additional contribution to noise comes from Andreev reflection processes<sup>40</sup>). In 1989, the wave packet approach was introduced to calculate thermal equilibrium noise<sup>4</sup>): the calculation was done for a sample connected to two leads each carrying one channel. Around the same time, the noise in the presence of a bias was calculated using the “poor man’s” Keldysh approach<sup>5</sup>), for an adiabatic point contact (no mixing between the different transverse modes). Momentum noise was investigated in single and multiple barrier geometries<sup>6</sup>). Two experiments measuring low frequency noise were performed by the Princeton group. The first one considered a point contact<sup>7</sup>), as in the conductance step experiment<sup>32</sup>) and measured the noise as a function of the gate voltage of the contact, and the second used a resonant tunneling geometry<sup>8</sup>); The noise was measured

at a frequency of the order of  $10\text{KHz}$ , which is sufficiently low that the  $1/f$  contribution to the noise still has to be subtracted out to determine the white noise contribution we are interested in. Both experiments showed qualitatively that in the case of poor transmission, the noise level corresponds to full shot noise, while highly transmissive samples give a level which is lower than shot noise. In the point contact experiment, a new channel is opened up by varying the gate voltage, while for the resonant tunneling experiment, the transmission of electrons depends on the proximity of the incident energy to the quasi level in the center region. The result of Ref. 5 was then generalized to samples connected to an arbitrary number of leads<sup>9</sup>, where the noise was expressed directly in terms of the general S-matrix describing the scattering properties of the sample, in analogy with the earlier work on multi-probe current measurements<sup>38</sup>. Noise was measured in the quantum Hall regime<sup>10,11</sup>: noise arises when electrons are backscattered from one edge of the sample to the other. Noise plateaus were detected<sup>10</sup> at the same location as the resistance plateaus associated with the (fractional) quantum Hall regime. A semiclassical approach to the calculation of noise which used phase space trajectories<sup>12</sup> showed once again that the noise vanishes for ideal transmission. The wave packet approach introduced for thermal equilibrium in Ref. 4 was extended to treat the non-equilibrium situation<sup>14</sup>, and then generalized to the case of multi-channel, multi-terminal samples to discuss noise correlations<sup>15</sup>. The probability distribution for charge transfer in a Mesoscopic sample was found to be close to a binomial distribution<sup>16</sup>, suggesting that the current is indeed emitted in "bursts". It was pointed out<sup>17</sup> that in a four terminal geometry, noise correlations can yield flux sensitive information. Recently, an interference effect similar to that of Ref. 17 was pointed out for a two terminal geometry<sup>26</sup>, where there the sample is bent in the form of a loop and an alternating flux passes through the loop. Frequency dependent noise has been studied by several authors<sup>3,5,18</sup>. Noise was proposed<sup>19</sup> as a diagnostic of tunneling mechanism: in a resonant tunneling geometry, the noise power exhibits sharp variations where a current measurement fails to give similar information. The effect of dephasing and dissipation on the quantum noise has been analyzed<sup>20</sup> with the conclusion that dephasing alone is not sufficient to recover the macroscopic regime. Electron-electron interactions were included for a geometry where two ideal leads are connected by a central interacting region<sup>22</sup>. Electron correlations were also considered recently in the fractional quantum Hall regime<sup>27</sup>. Sample averaging was introduced<sup>13</sup> to study the suppression of shot noise in diffusive conductors, and later on in a study of the Mesoscopic fluctuations in the shot noise power of metals<sup>25</sup>. Shot noise was computed in the semiclassical regime for a metallic conductor<sup>23</sup>, and it was found to be reduced by a factor equal to the ratio of the mean free path divided by the sample length.

### III. THE WAVE PACKET APPROACH

We consider first a one dimensional sample connected to a source and a drain. The quantity we wish to calculate is the time correlation in the current:

$$C(t) = \frac{1}{T} \int dt' \langle I(t+t')I(t') \rangle \quad (1)$$

The spectral density of noise  $W(\omega)$  is related to the above quantity by a simple Fourier transform. The measurement frequencies which we consider here are low enough compared to the inverse of the time associated with the transfer of an electron from source to drain<sup>41)</sup> and allow to neglect the self inductance of the sample. Using the Fourier representation for the current, this yields:

$$W(\omega) = \lim_{T \rightarrow \infty} \left( \frac{2}{T} \langle |I(\omega)|^2 \rangle \right) \quad (2)$$

where the angular brackets denote some kind of average over electrons occupation factors. In the “poor man’s” Keldysh approach, this is equivalent to taking a thermodynamic average with a generalized grand canonical weight  $\exp(-\beta(H - \sum_i \mu_i N_i))$ , where  $N_i$  is the number operator counting the scattering states incident from a given lead  $i$ . The nonequilibrium situation is met when all chemical potentials  $\mu_i$  are not equal. A justification of this choice of thermal weight has been provided in Ref. 42. If we assume the different reservoirs to be disconnected at a time  $t = -\infty$ , and adiabatically turn on the coupling between the reservoirs to its full value at  $t = 0$ , the Lipman-Schwinger equation “transforms” the creation/annihilation operators for each reservoir into operators describing scattering states. As long as the difference between chemical potentials is sufficiently small so that we can neglect the charge pileup in the sample connecting the reservoirs, this approach provides useful answers, and constitutes a systematic way to calculate current current correlations from the S-matrix.

The wave packet approach views the current passing across the sample as a superposition of clocked pulses<sup>4,14,14)</sup>:

$$I(t) = \sum_n j(t - n\tau) g_n \quad (3)$$

In this expression  $j(t)$  is the current associated with a given pulse and  $g_n$  is an occupation factor which takes a value 1 if an electron has been transferred from the left hand side to the right hand side of the sample,  $-1$  if the electron was transferred from right to left, and 0 when no electron is transferred at all. The quantum mechanics necessary to calculate the noise is hidden in  $g_n$ . The wave packets representing the electrons are separated in time, but can overlap in space. This view of electron transport is somewhat supported in Ref. 16, where the probability distribution of charge transfer is found to be close to a binomial Bernoulli distribution with an average number of attempts in the time  $t$  equal to  $2eV/h\tau$ . An example of wave packet construction can be obtained if we consider states limited to a small energy interval  $\Delta E$ :

$$\psi^{(n)}(z, t) = \int_{E-\Delta E}^{E+\Delta E} \frac{dE'}{\Delta E} \left[ \frac{1}{2\pi} \frac{dk}{dE'} \right]^{1/2} e^{ik(E')z - iE'(t+n\tau)/\hbar}, \quad (4)$$

by choosing  $\tau = \hbar/\Delta E$ , we insure that successive pulses are orthogonal to each other. With the above definitions, the calculation of the noise contribution coming from the frequency interval  $[\nu, \nu + \delta\nu]$  and the energy interval  $[E - \Delta E/2, E + \Delta E/2]$  reduces to the calculation of the fluctuation in the occupation factors:

$$\langle \Delta I^2 \rangle_{\omega} = \frac{2\delta\nu\Delta E e^2}{\pi\hbar} \langle g^2 - \langle g \rangle^2 \rangle. \quad (5)$$

where we have dropped the index  $n$  in  $g_n$  because all pulses contribute to the noise in the same fashion. Also, note that we have subtracted the average current in order to describe the effect of the applied bias on the sample. The calculation of the spectral density of noise is thus directly related to the statistics of the current pulses.

To obtain the correlator  $\langle g^2 - \langle g \rangle^2 \rangle$ , we consider all possible pulse histories: first consider the case where two electrons are incident on the sample from opposite sides. In this situation  $g = 0$ , because there will be no current if both electrons are reflected or transmitted, and the situation where one electron is reflected and the other is transmitted is forbidden by the Pauli principle; two electrons (with the same spin) cannot occupy the same wave packet state. Secondly, there is the straightforward situation where both incident states are empty, with  $g = 0$ . The other possibilities where  $g = 0$  follow if an electron is reflected from one side, when no electron was incident from the other side. In fact the only possibilities where a current passes through the sample are when an electron incident from the right (left) is transmitted while no electron was present on the other side, giving the result  $g = 1$  ( $g = -1$ ) with respective weight  $f_1(1 - f_2)T$  ( $f_2(1 - f_1)T$ ).  $f_1$  ( $f_2$ ) is the Fermi-Dirac distribution associated with the left (right) reservoir, and  $T$  is the transmission probability. We therefore obtain:

$$\langle g^2 - \langle g \rangle^2 \rangle = T(f_1 + f_2 - 2f_1f_2) - (f_1 - f_2)^2 T^2 \quad (6)$$

Summing now over all energy intervals, we thus obtain the total excess noise:

$$\begin{aligned} \langle \Delta I^2 \rangle_{\omega} &= \frac{4e^2\delta\nu}{\pi\hbar} \int dE T(E) f_2(1 - f_1) \\ &\quad + \frac{2e^2\delta\nu}{\pi\hbar} \int dE T(E) (f_1 - f_2) [1 - T(E)(f_1 - f_2)]. \end{aligned} \quad (7)$$

In the absence of bias or at high temperatures ( $|\mu_1 - \mu_2| \ll k_B\Theta$ ), the first term on the right hand side dominates, and we recover the Johnson Nyquist<sup>30)</sup> formula for thermal equilibrium noise<sup>4)</sup>:

$$\langle \Delta I^2 \rangle_{\omega} = \frac{4e^2\delta\nu}{\pi\hbar} k_B\Theta T. \quad (8)$$

In the opposite limit,  $|\mu_1 - \mu_2| \gg k_B\Theta$ , we get a contribution which looks like shot noise, except that it is reduced by a factor  $1 - T$ :

$$\langle \Delta I^2 \rangle_{\omega} = 2e\delta\nu \langle I \rangle (1 - T). \quad (9)$$

The reduced shot noise is also called partition noise. In the limit of poor transmission,  $T \ll 1$ , and we recover the full shot noise. For highly transmissive channels,  $T \sim 1$ , and we can think of the deduction of shot noise as being the noise contribution associated with the poor transmission of holes across the sample. Because of the Pauli principle, a full stream of electrons which is transmitted with unit probability does not contribute to noise. Note that this is the effect seen qualitatively in the Princeton experiment<sup>10,11</sup>. In the intermediate regime  $|\mu_1 - \mu_2| \simeq k_B\Theta$ , there is no clear separation between the thermal and the reduced shot noise contribution.

## IV. GENERALIZATION TO MULTI-CHANNEL CASE

We now turn to the more complex situation where each lead connected to the sample has several channels. Our concern in this case is the role of channel mixing: a receiving channel on the right hand side collects electrons from all incoming channels transmitted from the left and all reflected channels on the right. We therefore expect that wave packets from these different incoming channels will interfere with each other. To avoid the issue of interference between channels and treat the system as a superposition of one dimensional contributions, we must find a wave packet representation where the mixing between channels is absent.

This representation is obtained by using a decomposition of the  $S$ -matrix describing the sample<sup>43</sup>. Let us assume for simplicity that both leads have the same number of channels  $M$ . The  $S$ -matrix is then a block matrix containing four  $M$  by  $M$  submatrices describing the reflection from the right (left) hand side,  $s_{22}$  ( $s_{11}$ ), and the transmission from left to right (right to left),  $s_{12}$  ( $s_{21}$ ):

$$S = \begin{pmatrix} s_{11} & s_{12} \\ s_{21} & s_{22} \end{pmatrix} \quad (10)$$

From the unitarity of the  $S$ -matrix, which follows from current conservation, it is possible to write the submatrices in terms of two diagonal matrices and four unitary matrices, as long as  $s_{11}^\dagger$  has no eigenvalue equal to 0 or 1:

$$s_{11} = -i\mathbf{V}_1\mathbf{R}^{1/2}\mathbf{U}_1^\dagger \quad (11a)$$

$$s_{12} = \mathbf{V}_1\mathbf{T}^{1/2}\mathbf{U}_2^\dagger \quad (11b)$$

$$s_{21} = \mathbf{V}_2\mathbf{T}^{1/2}\mathbf{U}_1^\dagger \quad (11c)$$

$$s_{22} = -i\mathbf{V}_2\mathbf{R}^{1/2}\mathbf{U}_2^\dagger \quad (11d)$$

where  $\mathbf{R}^{1/2}$  and  $\mathbf{T}^{1/2}$  are real diagonal matrices with diagonal elements  $R_i^{1/2}$  and  $T_i^{1/2}$  such that their square  $R_i$  and  $T_i$  are the eigenvalues of the matrices  $s_{11}^\dagger s_{11}$  and  $s_{21}^\dagger s_{21}$ .  $T_i$  and  $R_i$  satisfy the identity  $T_i + R_i = 1$ , and  $\mathbf{U}_1$ ,  $\mathbf{U}_2$ ,  $\mathbf{V}_1$ ,  $\mathbf{V}_2$  are unitary transformations. This decomposition of the  $S$ -matrix has been implicitly pointed out<sup>44</sup> in the context of random matrix theory, where the transfer matrix is in general the quantity of interest.

Using the unitary transformations, we can now choose a new basis of incoming and outgoing states on the left and the right side of the sample:  $\mathbf{U}_1$  ( $\mathbf{V}_1$ ) is the unitary transformation used to represent the incoming (outgoing) states on the left side, while  $\mathbf{U}_2$  ( $\mathbf{V}_2$ ) is the unitary transformation used to represent the incoming (outgoing) states on the right side of the sample. The effective  $S$ -matrix thus obtained in this new basis is a block matrix of four diagonal matrices:

$$\tilde{S} = \begin{pmatrix} -iR_1^{1/2} & \dots & 0 & T_1^{1/2} & \dots & 0 \\ \vdots & \ddots & \vdots & \vdots & \ddots & \vdots \\ 0 & \dots & -iR_M^{1/2} & 0 & \dots & T_M^{1/2} \\ T_1^{1/2} & \dots & 0 & -iR_1^{1/2} & \dots & 0 \\ \vdots & \ddots & \vdots & \vdots & \ddots & \vdots \\ 0 & \dots & T_M^{1/2} & 0 & \dots & -iR_M^{1/2} \end{pmatrix}, \quad (12)$$

Note that  $\tilde{S}$  corresponds to a situation where no mixing between channels occurs, effectively a superposition of one dimensional ( $2 \times 2$ ) S-matrices which are totally decoupled (see Fig. 1).

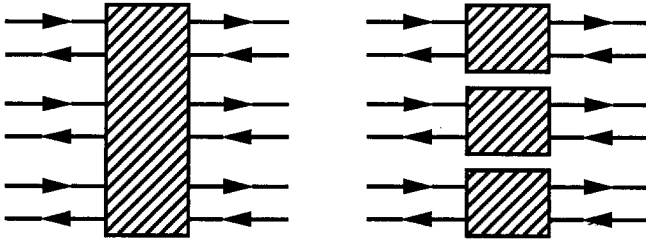


Fig. 1

In fact this is precisely the form which was assumed by Lesovik<sup>5)</sup> for the adiabatic point contact. The absence of correlations between the different incoming and outgoing wave packets allows us to write the noise as a superposition of  $M$  one dimensional contributions:

$$\begin{aligned} \langle \Delta I^2 \rangle_{\omega} &= \frac{4e^2 \delta \nu}{\pi \hbar} \int dE \sum_{i=1}^N T_i(E) f_2 (1 - f_1) \\ &\quad + \frac{2e^2 \delta \nu}{\pi \hbar} \int dE \sum_{i=1}^N T_i(E) (f_1 - f_2) [1 - T_i(E) (f_1 - f_2)]. \end{aligned} \quad (13)$$

This expression can be cast in terms of the block elements of the initial S-matrix using the properties of the trace,  $\sum_i T_i^n = \text{Tr}[(\mathbf{s}_{21}^\dagger \mathbf{s}_{21})^n]$ .

The above decomposition was based on the fact that none of the  $T_i$ 's are 0 or 1. We can escape these pathological cases by arguing that we can choose  $T_i \neq 0, 1$  but arbitrarily close to these values. But this is not even necessary; a decomposition similar to Eq. (11d) can still be found such that the effective S-matrix still has the four diagonal block structure. The case where the number of channels on each side is different can be handled in a similar manner: we can simply add a number of passive channels which are totally reflected on the side with fewer channels in order to come back to the case where there are  $M$  channels on both sides. Because

they correspond to states which are totally reflected, passive channels do not contribute to noise.

We make the following remarks: First, a number of experiments have studied the effect of backscattering in the Integer Quantum hall regime in a confined geometry where the electrons propagate along the edges the sample, a reminiscence of the classical skipping orbits<sup>45</sup>). In a typical experiment on a GaAs heterostructure, the backscattering of electrons from one edge to the other can be controlled by varying the voltage on a metallic gate placed across the Hall bar<sup>46</sup>). As the gate voltage depletes the electrons underneath, the innermost edge state is the first to experience backscattering, while the other ones are fully transmitted. In the theorist mind, assuming that there are no irregularities in the lateral confinement potential, and in the absence of impurities, neighboring edge states do not mix<sup>47</sup>), and the S-matrix associated with this situation has precisely the four diagonal structure discussed above. That is to say, there is some grain of physical reality in the decomposition of the S-matrix. Secondly, we note that in the presence of time reversal symmetry, we get additional constraints on the unitary transformations, the transformation used to describe the incident states on a given side of the sample must coincide with the transformation associated with the outgoing states on the same side:  $U_1 = V_1^*$  and  $U_2 = V_2^*$ . In the presence of a magnetic field  $B$ ,  $U_1(B) = V_1^*(-B)$  and  $U_2(B) = V_2^*(-B)$ . Similar constraints appear if the sample is a Mesoscopic ring: a ring can be viewed as a black box with incoming and outgoing states connected on two opposite sides of the box. To form a ring, an incoming lead on one side has to be connected to an outgoing lead on the other side. This imposes the constraint  $U_1 = V_2$  and  $U_2 = V_1$ . In general, the unitary transformations determine which universality class, in the random matrix theory language<sup>44</sup>), the sample belongs to.

## V. MULTITERMINAL CASE AND NOISE CORRELATIONS

The case where the sample is connected to several leads provides another challenge for the wave packet approach. Here, we will not get into the details of this situation, but rather give the essential ingredients of the approach<sup>15</sup>). Also, the discussion is restricted to the zero temperature ( $\Theta = 0$ ) case.

We consider a multiterminal sample connected to  $p$  leads, and propose to calculate the noise in a given lead  $\alpha$ . To each lead we associate a chemical potential, and we label each lead with decreasing chemical potential,  $\mu_1 > \dots > \mu_\alpha > \dots > \mu_p$ . For  $i < \alpha$ , in the energy range  $[\mu_i + 1, \mu_i]$ , reservoirs 1 to  $i$  are injecting electrons in lead  $\alpha$ . For  $i > \alpha$ , reservoirs  $i + 1$  to  $p$  inject holes in  $\alpha$ . In both cases, it is straightforward to determine the transmission matrix associated with each energy interval. In turn, the transmission matrix associated with these intervals yields the eigenvalues (the  $T_i$ 's) which enter the noise formula. Note that the basic idea of this approach is to reduce the discussion to the two lead case, which we know how to handle. The calculation of the noise in lead  $\alpha$  therefore sums up the contribution of each energy interval, and the final result can be expressed in terms of a trace on the block elements of the

S-matrix:

$$\langle \Delta I_\alpha^2 \rangle_{\delta\nu} = \frac{2e^2 \delta\nu}{\pi \hbar} \sum_{\eta < \delta} (\mu_\delta - \mu_\eta) \text{Tr}[s_{\alpha\delta} s_{\alpha\delta}^\dagger s_{\alpha\eta} s_{\alpha\eta}^\dagger]. \quad (14)$$

To calculate the noise correlations between two leads  $\alpha$  and  $\beta$ , we consider a fictitious lead  $(\alpha + \beta)$ . We then proceed as in the previous paragraph to calculate the noise in  $(\alpha + \beta)$ . The noise in this lead is equal to the noise in  $\alpha$ , the noise in  $\beta$ , plus the interference term which represents the correlations between  $\alpha$  and  $\beta$ :  $2 \langle \Delta I_\alpha \Delta I_\beta \rangle_{\delta\nu}$ . We then obtain, at zero temperature:

$$\langle \Delta I_\alpha \Delta I_\beta \rangle_{\delta\nu} = -\frac{2e^2 \delta\nu}{\pi \hbar} \sum_{\eta > \delta} (\mu_\delta - \mu_\eta) \text{Tr}[s_{\alpha\eta} s_{\beta\eta}^\dagger s_{\beta\delta} s_{\alpha\delta}^\dagger] \quad (15)$$

Admittedly, the generalization of the wave packet approach to multiprobe, multiterminal samples requires some thinking, and is so far limited to  $\Theta = 0$ . For  $\Theta \neq 0$ , Ref. 21 finds it convenient to decompose the noise into equilibrium-like and transport fluctuations: the transport fluctuations bear a negative (positive) sign as in Eq. 15 when the carrier obey the Fermi (Bose) statistics.

## VI. NOISE CORRELATIONS IN A Y-SHAPED STRUCTURE

In 1953, Hanbury-Brown and Twiss performed an experiment<sup>48)</sup> where two detectors at different locations collected photons emitted from an incoherent light source. The correlations between the two detectors were measured as a function of the distance separating the detectors, and were found to be always positive. This measurement can be viewed as a check that photons are indistinguishable particles which obey Bose-Einstein statistics. Nevertheless, it can also be fully understood in terms of classical electromagnetism<sup>49)</sup>: the photon bunching effect is a consequence of the superposition principle for light applied to noisy sources.

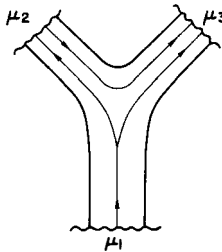


Fig. 2

It has been suggested<sup>15,50)</sup> that a similar experiment be performed for fermions. A natural “battle field” for this experiment would be to study the noise correlations for electrons injected

in a Mesoscopic device from one lead, and collected by two other leads: a Y shaped device etched in a GaAs/AlGaAs heterostructure, for example (Fig. 2). We associate the injecting lead with a chemical potential  $\mu_1$ , and fix the chemical potential in lead 2 and 3 at an equal value  $\mu_2 < \mu_1$ . For simplicity, we also assume  $\Theta \ll |\mu_1 - \mu_2|$  so as to ignore thermal effects. Using the results of the previous section, the noise correlations between the collecting leads 2 and 3 is given by:

$$\langle \Delta I_2 \Delta I_3 \rangle_{\omega} = -\frac{2e^2 \delta \omega}{\pi \hbar} [(\mu_1 - \mu_2) \text{Tr}[s_{21}^\dagger s_{21} s_{31}^\dagger s_{31}]] , \quad (16)$$

which shows that the correlations are always negative, a direct consequence of the fact that electrons obey Fermi statistics. Ref. 21 also proved that the reverse is true if the carriers are bosons. As the noise correlations measure the likelihood to detect an electron at a time  $t + t'$  in lead 3 knowing that an electron was detected in 2 at time  $t$ , we therefore have a direct analog of the Hanbury–Brown experiment for electrons. In the simplest case, where only one channel propagates in each lead, the effect will be maximal (compared to the noise contributions in each receiving lead) if we construct the Mesoscopic sample so as to minimize the backscattering of the electrons coming from the injecting lead.

#### VII. EXCHANGE INTERFERENCE IN A FOUR TERMINAL GEOMETRY

An interesting application of the result for the noise correlations in multiprobe geometries has been pointed out by Büttiker<sup>17)</sup>. For a sample connected to four (or more) probes, Eq. (15) contains products of the block elements of the S-matrix which *cannot* be written as a matrix multiplied by its hermitian conjugate. Büttiker suggested that this opens the possibility for observing interference effects in a four terminal geometry despite the fact that no coherence exist between different reservoirs.

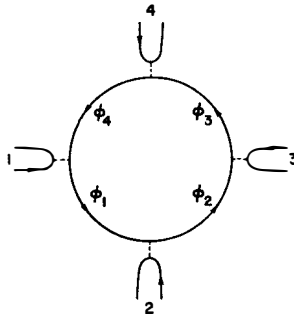


Fig. 3

Büttiker<sup>21)</sup> proposes a gedanken experiment in the integer quantum Hall regime where four leads, each containing one edge state, communicate with each other via a quantum dot which

in this case is a circulating edge state. The leads are labeled from 1 to 4 as one goes around the central island (Fig. 3, taken from Ref. 21). Attention is focused on the noise correlation between leads 2 and 4. In a first step (a) electrons are injected from lead 1:  $\mu = \mu_1$  and  $\mu_0 = \mu_2 = \mu_3 = \mu_4$  ( $\mu_0 < \mu$ ), in a second step (b) electrons are injected from lead 3:  $\mu = \mu_3$  and  $\mu_0 = \mu_1 = \mu_2 = \mu_4$ , and finally (c) electrons are injected from both 1 and 3:  $\mu = \mu_1 = \mu_3$  and  $\mu_2 = \mu_4$ . Evaluating the noise correlations in these three cases, Buttiker finds the relation:

$$\begin{aligned} \langle \Delta I_2 \Delta I_4 \rangle_c = & \langle \Delta I_2 \Delta I_4 \rangle_a + \langle \Delta I_2 \Delta I_4 \rangle_b \\ & - 2\delta\nu(e^2/h) \int dE (f - f_0) [Tr(\mathbf{s}_{21}^\dagger \mathbf{s}_{23} \mathbf{s}_{43}^\dagger \mathbf{s}_{41}) + Tr(\mathbf{s}_{23}^\dagger \mathbf{s}_{21} \mathbf{s}_{41}^\dagger \mathbf{s}_{43})], \end{aligned} \quad (17)$$

where  $\langle \Delta I_2 \Delta I_4 \rangle_{a,b}$  are the noise correlations associated with steps (a) and (b), which do not contain any phase information, and  $f(f_0)$  is the Fermi factor associated with the chemical potential  $\mu$  ( $\mu_0$ ). In contrast to the two first contributions, the last term in Eq. (17) can carry phase information. This is seen by determining the S-matrix associated with this geometry in terms of the transmission/reflection probabilities and the phase shifts associated with the transfer from one reservoir to another. The end result is that:

$$Tr(\mathbf{s}_{21}^\dagger \mathbf{s}_{23} \mathbf{s}_{43}^\dagger \mathbf{s}_{41}) \propto \exp(i\chi), \quad (18)$$

where  $\chi$  is the total phase accumulated in one cycle around the central island. It would then be possible to observe Aharonov-Bohm type oscillations when measuring noise correlations in the appropriate way. This is quite a surprising result, because unlike in the traditional Aharonov-Bohm effect, here there is no single electron trajectory which traps a magnetic flux. Büttiker<sup>17,21)</sup> argues that the interference predicted from the noise correlation experiment represents a new type of interference, which arises from exchange effects. In the (different) context of particle physics, a similar phenomenon was pointed out<sup>51)</sup> 30 years ago: the intensity cross correlation between two detectors analyzing the scattering of particles off a target illuminated by two incoherent sources can yield phase information. Indeed, the wave function associated with a system of two particles has to be written as an antisymmetrized product of single particle wave functions. As a consequence, the probability density contains terms which are sensitive to an external flux.

### VIII. NON STATIONARY AHARONOV-BOHM EFFECT

A somehow similar effect has been predicted by Lesovik and Levitov<sup>26)</sup> for a simple, two lead geometry. The sample is bent in the shape of a loop, but the source and drain do not touch each other, so that there is no single electron trajectory which can trap flux. An alternating flux  $\phi(t) = \phi_a \sin(\Omega t)$  is imposed through the loop. The frequency  $\Omega$  is assumed to be small compared to the traversal time of an electron in the sample, and the Fermi energy is assumed to be much larger than the applied bias, as well as the quantum  $\hbar\Omega$ .

If the field is weak, the essential role played by the magnetic field is to give a phase  $\oint \mathbf{A} \cdot d\mathbf{l}$  to an electron transmitted from the source to the drain. The current predicted in this situation is constant, and has no dependence on flux.

The central point of this gedanken experiment is that it is possible to observe an oscillatory behavior in the low frequency noise. The derivative of the noise with respect to the applied bias  $\partial S/\partial V$  is found to have a staircase-like structure:

$$\frac{\partial S}{\partial V} = \frac{2e^2}{\pi} \sum_n \lambda_n \Theta(eV - n\hbar\Omega) \quad (19)$$

where  $\Theta(x)$  is here the Heavyside function, and the height of the steps is given by

$$\lambda_n = T(1 - T)J_n^2(\phi_a/\phi_0) \quad (20)$$

where  $T$  is the transmission probability,  $\phi_0$  is the flux quantum, and  $J_n$  is the Bessel function of order  $n$ . By varying the amplitude of the oscillatory flux, the height of the steps oscillates, and decays for large amplitudes. The noise power measurement yields phase information where a simple current measurement fails to do so. The non-stationary Aharonov-Bohm effect is believed to arise from exchange interference between states incident on the sample from the source and the drain, which energies shifted by an amount  $\hbar n\Omega$ : the presence of the alternating flux allows these states to “communicate”.

#### IX. NOISE IN CORRELATED ELECTRONS SYSTEMS

A calculation of noise in the presence of Coulomb repulsion has been proposed by Hershfield<sup>22</sup>). In this work, the Mesoscopic sample consists of two ideal leads (non interacting electrons) connected by a central island where interactions are taken into account. Later on, the central region is taken to be an Anderson impurity site. Also, it is assumed that the tunneling rates on each side of the island are independent of the energy. The calculation is performed using the Keldysh approach, and the lowest order vertex corrections are computed in perturbation theory, using the Hartree approximation. By comparison with the non-interacting case, Hershfield identifies the different contributions. A first term resembles the non interacting result. A second term arises because the electron distribution function at the impurity site is modified by the interaction. A third term is associated with inelastic scattering processes. Finally, the last contribution cannot be identified with corrections to the noninteracting case, and is believed to contain memory effects associated with the interaction: in general, the resulting noise power at low frequencies cannot be written in terms of an effective transmission probability.

Another specific situation allows an effective treatment of the correlations between electrons. Such is the case of Ref. 27, which deals with the non equilibrium noise in the fractional quantum Hall regime for a constriction. The constriction renders the problem one dimensional, and one can then make use of the bosonization methods developed for one dimensional interacting electron systems<sup>52</sup>) In a constricted quantum Hall geometry, transport is believed to occur primarily at the edges. For a fractional filling factor  $\nu = 1/m$ , the edge excitations form a single channel chiral Luttinger liquid<sup>53</sup>) [53], characterized by a dimensionless conductance  $g = 1/m$ . Kane and Fisher<sup>27</sup>) The noise in this situation arises from the backscattering of Laughlin quasi particles<sup>54</sup>, which are composed of a fraction  $g$  of an electron bound to one

vortex. As a consequence of this binding, current and voltage fluctuations are locked together at low temperatures.

In the limit of strong backscattering, Fisher and Kane find that the noise reduces to the classical (Poissonian) case. The noise is due to uncorrelated tunneling of electrons through the constriction from source to drain:

$$S = e \coth\left(\frac{eV_{sd}}{2k_B\Theta}\right) \quad (21)$$

with  $V_{sd}$  the source to drain voltage.

In the opposite limit of weak backscattering, noise arises from the tunneling of Laughlin quasiparticles from one edge to the other. Since the transmission at the constriction is good, this tunneling can also be considered as a Poissonian process. This time, the *voltage* fluctuations satisfy a classical shot noise form, where the charge of the electron is replaced by the charge of a Laughlin particle  $ge$ . Relating the voltage fluctuations to the current fluctuations yields a shot noise formula:

$$S = ge\langle I_{max} - \langle I \rangle \rangle \quad (22)$$

with  $I_{max} = g(e^2/h)V_{sd}$  the current associated with perfect transmission. Because of the prefactor  $ge$  in Eq. (22), a noise experiment in this regime would yield a direct observation of fractional charge! In the case of a resonance, where two constrictions isolate a central region<sup>27)</sup> it is possible to suppress the contribution from single quasiparticle tunneling. The dominant process is then the tunneling of pairs of quasiparticles, so that the noise contribution of Eq. (22) has to be multiplied by 2.

## X. CONCLUSION

This contribution has attempted to review the work on noise in the last decade, focusing on a few specific topics which were chosen because of their importance in the author's opinion, and/or because they represent a nontrivial generalization of the elastic case. Among the first category is the reduction of shot noise for highly transmissive samples. While this effect has been qualitatively seen in several experiments, it would be useful to repeat these experiments in order to obtain more quantitative results. The role of the statistics of the charge carriers has been emphasized throughout the paper. Noise correlations in a Y-shaped structure and the "new" exchange interference effect were discussed mainly with the goal of motivating an experimental effort in this direction.

The inclusion of interactions<sup>22,27)</sup> has opened a new direction of research, which will hopefully lead to a better understanding of the constraints imposed by the Coulomb repulsion on the transport of electrons. At this point, it is not clear whether the Coulomb interaction between electrons will further reduce the shot noise power below the level obtained for the single electron result. Our intuition leads us to the belief that this will be the case, simply because in a narrow sample with few transverse channels, the Coulomb interaction will restrict the flow of electrons further than the constraints imposed by the Pauli principle.

We have omitted a discussion of the calculation of noise at finite frequencies, although there has been some effort in this direction in recent years<sup>18)</sup>. Frankly, we are somewhat uncomfortable with these results because they do not treat the electrons in a self consistent manner. Ideally, when discussing frequency dependent phenomena, one should take into account self inductance effects arising due to the magnetic field created by current flow, as well as capacitive effects<sup>55)</sup> associated with the electric fields in the circuitry. Capacitive effects are understood to be at the origin of the Coulomb blockade<sup>56)</sup>, [?], but have been vastly neglected in theories of quantum transport at finite frequencies. To be fair, a self consistent treatment of current current correlations at finite frequencies has been proposed recently<sup>24)</sup> but in our opinion, it fails to describe the self consistent screening of electrons at the *microscopic* level. In conclusion, there are still many issues in this field which need more attention, and the field clearly suffers from a low experiment to theory ratio; this will hopefully change in the near future.

#### ACKNOWLEDGMENTS

The viewpoint chosen in this contribution reflects to a large extent a collaboration with R. Landauer, whom I am grateful for stimulating my interest in this topic.

- 1 I.K. Yanson, A.I. Akimenko and A.B. Verkin, *Solid State Commun.* **43**, 765 (1982); A.I. Akimenko, A.V. Verkin and I.K. Yanson, *J. Low Temp. phys.* **54**, 247 (1984).
- 2 I.O. Kulik and A.N. Omel'yanchuk, *Sov. J. Low Temp. Phys.* **10**, 158 (1984) (*Fiz. Nizk. Temp.* **10**, 305 (1984)).
- 3 V. A. Klus, *Sov. phys. JETP* **66** 1243 (1987) (*Zh. EKsp. Teor. Fiz.* **93**, 2179 (1987)).
- 4 R. Landauer, *Physica* **D38**, 226 (1987).
- 5 G. B. Lesovik, *JETP Lett.* **49**, 594 (1989).
- 6 B. Yurke and G. P. Kochlanski, *Phys. Rev.* **B41**, 8141 (1990).
- 7 Y. P. Li, A. Zaslavsky, D. C. Tsui, M. Santos and M. Shayegan, *Phys. Rev. B* **41**, 8388 (1990); *Resonant Tunneling in Semiconductors: Physics and Applications*, edited by L. L. Chang, E. E. Mendez and C. Tejedor (Plenum, New York 1991).
- 8 Y. P. Li, D. C. Tsui, J. J. Heremans, J. A. Simmons and G. W. Weimann, *Appl. Phys. Lett.* **57**, 774 (1990).
- 9 M. Büttiker, *Phys. Rev. Lett.* **65**, 2901 (1990).
- 10 S. Washburn, R. J. Haug, K. Y. Lee and J. M. Hong, *Phys. Rev. B* **44**, 3875 (1991).
- 11 A. J. Kil, R. J. J. Zijlstra, M. F. H. Schuurmans and J. P. Andre, *Phys. Rev.* **B41**, 5169 (1990).
- 12 C. W. J. Beenakker and H. van Houten, *Phys. Rev. B* **43**, 12066 (1991).
- 13 C.W.J. Beenakker and M. Büttiker, *Phys. Rev. B* **43**, 12066 (1991).
- 14 R. Landauer and Th. Martin, *Physica B* **175**, 167 (1991); **182**, 288 (1992).
- 15 Th. Martin and R. Landauer, *Phys. Rev. B* **45**, 1742 (1992).

- 16 G.B. Lesovik and L.S. Levitov, JETP Lett. **58**, 230 (1992).
- 17 M. Büttiker, Phys. Rev. Lett. **68** 843 (1992).
- 18 M. Büttiker, Phys. Rev. B **45**, 3807 (1992); L.Y. Chen and C.S. Ting Phys. Rev. B **43**, 4534 (1991); S.R. Eric Yang, Solid State Commun. **81**, 375 (1992).
- 19 J.W. Wilkins *et al.*, Physica Scripta T**42**, 115 (1992).
- 20 A. Shimizu and M. Ueda, Phys. Rev. Lett. **69**, 1403 (1992).
- 21 M. Büttiker, Phys. Rev. B **46**, 12485 (1992).
- 22 S. Hershfield, Phys. Rev. B **46**, 7061 (1992).
- 23 R. Landauer, Phys. Rev. B **47**, 16427 (1993).
- 24 M. Büttiker, A. Prêtre and H. Thomas, Phys. Rev. Lett. **70**, 4114 (1993).
- 25 M.J.M. de Jong and C.W.J. Beenakker, preprint (1993).
- 26 G. Lesovik and L.S. Levitov, Phys. Rev. Lett. **72**, 538 (1994).
- 27 C.L. Kane and M.P.A. Fisher, Phys. Rev. Lett. **72**, 724 (1994).
- 28 P. Dutta and P. M. Horn, Rev. Mod. Phys. **53**, 497 (1981); M. B. Weissman, Rev. Mod. Phys. **60**, 537 (1988).
- 29 S. Feng, P. A. Lee and A. D. Stone, Phys. Rev. Lett. **56**, 1960 (1986).
- 30 J. B. Johnson, Phys. Rev. B **29**, 367 (1927); H. Nyquist, Phys. Rev. **32**, 110 (1928).
- 31 J. R. Pierce, Bell Syst. Tech. J. **27**, 15 (1948).
- 32 Van Wees B. J. van Wees *et al.* Phys. Rev. Lett. **60**, 848 (1988).
- 33 E.A. Montie *et al.*, Nature **350**, 594 (1991); Physica B **175**, 149 (1991).
- 34 J.C. Licini *et al.*, Phys. Rev. Lett. **55**, 2987 (1985); W.J. Skocpol *et al.* Phys. Rev. Lett. **56**, 2865 (1986).
- 35 S. Washburn and R. Webb, Adv. Phys. **35**, 375 (1986).
- 36 M.P. van Albada, J.F. de Boer and A. Lagendijk, Phys. Rev. Lett. **64**, 2787 (1990); J.F. de Boer, M.P. van Albada and A. Lagendijk, Physica B **175**, 17 (1991).
- 37 R. Landauer, Z. Phys. B **68**, 217 (1987); M. Büttiker, Y. Imry, R. Landauer and S. Pinhas, Phys. Rev. B **31**, 6207 (1985).
- 38 M. Büttiker, Phys. Rev. Lett. **57**, 1761 (1986); M. Büttiker, Phys. Rev. B **38**, 9375 (1988).
- 39 L. V. Keldysh, Sov. Phys. JETP **20**, 1018 (1965).
- 40 A. F. Andreev, Sov. Phys. JETP **19**, 1228 (1964) (Zh. Eksp. Teor. Fiz. **46**, 1823 (1964)).
- 41 M. Büttiker and R. Landauer, Phys. Rev. Lett. **49**, 1739 (1982).
- 42 S. Hershfield, Phys. Rev. Lett. **70**, 2134 (1993).
- 43 M. Büttiker and Th. Martin, unpublished (1991).
- 44 P. A. Mello, P. Peyreya and N. Kumar, Ann. Phys. **181**, 290 (1988); P. A. Mello and J. L. Pichard, J. Phys. I **1**, 493 (1991).

- 45 J. K. Jain and S. A. Kivelson, *Phys. Rev. Lett.* **60**, 1542 (1988), and *Phys. Rev. B* **37**, 4276 (1988); P. Streda, J. Kucera and A. H. MacDonald, *Phys. Rev. Lett.* **59**, 1973 (1987).
- 46 S. Washburn, A. B. Fowler, H. Schmid and D. Kern, *Phys. Rev. Lett.* **61**, 2801 (1988); R. J. Haug, A. H. MacDonald, P. Streda and K. v. Klitzing, *Phys. Rev. Lett.* **61**, 2797 (1988).
- 47 Th. Martin and S. Feng, *Phys. Rev. Lett.* **64**, 1971 (1990).
- 48 R. Hanbury Brown and R. Q. Twiss, *Nature* **177**, 27 (1956); R. Hanbury Brown and R. Q. Twiss, *Proc. Royal Soc. London Ser. A* **242**, 300 (1957); *ibid.* **243**, 291 (1957).
- 49 E.M. Purcell, *Nature* **178**, 1449 (1956).
- 50 S. Murphy, private communication.
- 51 M. I. Goldberger, H.W. Lewis, and K.M. Watson, *Phys. Rev.* **132**, 2764 (1963).
- 52 V. J. Emery, in *Highly Conducting One Dimensional Solids*, J. T. Devreese, R. P. Evrard and V. E. van Doren eds. (Plenum, New York, 1979), p.327; J. Solyom, *Adv. Phys.* **28**, 201 (1979).
- 53 X.G. Wen, *Phys. Rev. B* **43**, 11025 (1991); *Phys. Rev. Lett.* **64**, 2206 (1990).
- 54 R.B. Laughlin, *Phys. Rev. Lett.* **50**, 1395 (1983).
- 55 R. Landauer, *Physica Scripta T* **42**, 100 (1992).
- 56 see for example: C.W.J. Beenakker and H. van Houten, in *Single Charge Tunneling* (eds. H. Grabert and M.H. Devoret), Plenum, New York (1991).

# DYNAMIC ADMITTANCE OF A MESOSCOPIC CAPACITOR

A. Prêtre, H. Thomas

*Institut für Physik, Universität Basel, Klingelbergstr. 82, CH-4056 Basel, Switzerland*

M. Büttiker

*IBM T. J. Watson Research Center, P. O. Box 218, Yorktown Heights, N. Y. 10598*

We study a mesoscopic capacitor with plates connected via leads to electron reservoirs, and investigate the current response under time-oscillating electro-chemical potentials in the reservoirs [1]. In our model the piled-up charges and induced electrostatic potentials on the two plates are related by a conventional electrostatic capacitance  $C_e$  which takes the Coulomb coupling into account. Each arm is treated as a one-lead system with a corresponding scattering matrix.

Because of the small number of accessible states at a mesoscopic plate it is important to distinguish carefully between the electrostatic potential difference and the electro-chemical potential difference. We find that the experimentally relevant capacitance  $C_\mu$ , which governs the leading order of the frequency-dependent admittance, may strongly deviate from  $C_e$ : it formally looks like the electrostatic capacitance  $C_e$  in series with two capacitances represented by the plate densities of states at the Fermi energies in units of  $e^{-2}$ ; only in the limit where the latter are much larger than  $C_e$  would the difference between  $C_\mu$  and  $C_e$  disappear. In quadratic order in frequency, the resistance factor is given by a charge relaxation resistance  $R_q$ . This novel resistance differs from the dc-resistance which one would measure if the lead instead of being connected to the capacitor plate at one side would be connected to another electron reservoir.

We briefly allude to extensions of the theory which treat the microscopic potential landscape [2].

## I. INTRODUCTION

The experimental devices studied at nanoscale usually consist of several metallic regions and doping layers, let us call them conductors, separated by insulators: some of them are designed to “form the sample of interest”, others (gates) to “define its characteristics”; all of them are coupled by long-range Coulomb forces.

Capacitance spectroscopy has already raised the question of how far the standard description of a capacitor holds in mesoscopics [3]. What is the analogon to the conventional electrostatic capacitances  $C_{mn} = dQ_m/dV_n$  relating charges and voltages? Let us consider a mesoscopic assembly of conductors, each connected to a contact, i.e., to an electron reservoir whose electro-chemical potential can be experimentally controlled (see Fig. 1a). In contrast to the macroscopic case, here the electro-chemical contact potential cannot be identified with the effective potential on the corresponding mesoscopic conductor. We will calculate the change of charge on conductor  $m$  under electro-chemical potential variation at reservoir  $n$ ,  $C_{mn} = edQ_m/d\mu_n$ .

The system exhibits no dc-transport between the conductors since we exclude any cross-tunnelling. Under time-oscillating electro-chemical potentials ac-transport can take place: we discuss the frequency-dependent admittance  $g_{mn}(\omega) = edI_m(\omega)/d\mu_n(\omega)$ , where  $I_m$  is the current flowing from reservoir  $m$  to conductor  $m$ . The capacitances are determined by the leading order in  $\omega$ ,  $g_{mn} = ed\dot{Q}_m/d\mu_n = -i\omega C_{mn} + O(\omega^2)$ .

In previous work the contact-lead currents in a multi-probe sample have been calculated in response to perturbations which act only on the carriers in the leads [4,5]. In this first step

the electrons are treated as non-interacting. At finite frequencies charge accumulates in the sample and the leads. As a consequence the current is not conserved. In contrast for interacting electrons the total current (particle plus displacement current) is conserved. Therefore, it is crucial to include the long-range Coulomb interaction. In a second step, we thus evaluate the potential generated by the unscreened charges and include its effect on the current response. We treat this second step in a number of different ways: i) In a discrete potential model we assign to the sample an effective capacitance  $C^{env}$  with respect to its environment, associating an induced potential to the charge piled up in the sample [5], and obtain the response self-consistently by requiring invariance under an overall-shift of the contact potentials and of the effective sample potential (which is an alternative way to state the current-conservation law). ii) Alternatively, restricted to the case of overall charge neutrality on the conducting sample (cp. with  $C^{env} = 0$  above), we calculate the spatial landscape of the induced potential in a Thomas-Fermi approximation appropriate for metals [6]. iii) For semiconductors both short-range screening and long-range screening is important. A discussion based on a microscopic potential landscape is given in Ref. [2].

Our purpose here is to deal with the long-range Coulomb interactions: Our system includes all conductors on which charge is mutually induced. We consider a volume with a surface  $S$  which intersects the macroscopic reservoirs connected to the conductors at such large distance that there are no unbalanced charges in its interior, and we calculate the currents on the cross sections defined by the cuts of  $S$  with the reservoirs (see Fig. 1). The current response is expressed as a sum of an external response to the bare external *chemical* potentials, which is typical of non-interacting carriers; and an internal response to the internally induced effective potential, which requires additional specifications in the material description of the conductors. To find the internal response it is crucial to assume that  $S$  contains zero total charge.

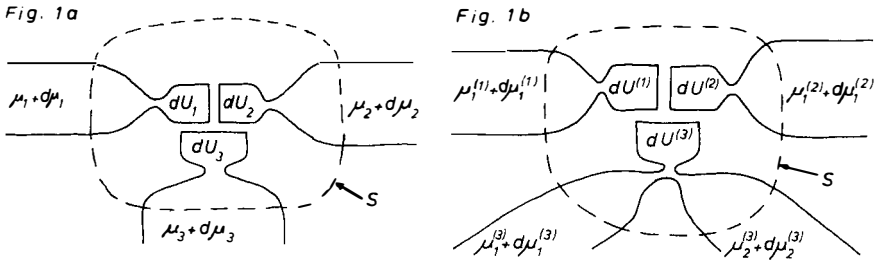


Fig. 1. Assembly of conductors interacting via long-range Coulomb forces; inside the surface  $S$  the total charge vanishes. The configuration of Fig. 1a permits no dc-transport, whereas the configuration of Fig. 1b does.

## II. THE TWO-PLATE CAPACITANCE: MESOSCOPIC VERSUS MACROSCOPIC

The two-plate capacitor is sketched in Fig. 2a. We want to discuss the voltage distribution on the capacitor plates, the leads and the reservoirs as function of the chemical potentials of the reservoirs. If the reservoir potentials  $\mu_\alpha$  deviate from an equilibrium reference potential  $\mu_\alpha^{ref}$ ,  $\mu_\alpha = \mu_\alpha^{ref} + d\mu_\alpha$ , the potential landscape changes (see Fig. 2b). Away from the capacitor plates the bottom of the electron conduction band changes by an amount  $edU_\alpha = d\mu_\alpha$  to maintain the conductor in a locally charge-neutral state. On the capacitor plates the potential landscape changes to accommodate the charge induced by Coulomb coupling between the two

conductors. On a macroscopic conductor the change in potential landscape is entirely confined to the surface of the conductor. The conduction band bottom follows the chemical potential except near a small region of the surface of the conductor, where the induced charge changes the way in which the conduction band rises. In a mesoscopic conductor the induced charge cannot be accommodated by a change in the confinement potential alone. Instead near the capacitor plates the induced charge will cause the conduction band bottom to rise (or fall). On the capacitor plates  $edU_\alpha$  generally deviates from  $d\mu_\alpha$ . To avoid unnecessary complexity we assume that the entire effect of the potential change on the capacitor plate can be described by a change in the bottom of the conduction band  $edU_\alpha$ . Indicating by  $dN_\alpha/dE$  the density of states of plate  $\alpha$  which can be accessed by carriers injected by reservoir  $\alpha$ , we can express the total charge on the capacitor plate  $\alpha$  as

$$dQ_\alpha = e(dN_\alpha/dE)(d\mu_\alpha - edU_\alpha). \quad (1)$$

As a consequence of the Coulomb coupling, a charge  $dQ_\alpha$  on one plate induces a countercharge  $-dQ_\alpha$  on the other plate. We assume the dependence of the mutually induced charge on the electrostatic potential difference between the two conductors to be linear, determined by an electrostatic-like capacitance  $C_e$ . The very notion of this concept may be questioned in the case of nanostructures where electric field lines can considerably penetrate into the sample instead of ending near the surface. However, here  $C_e$  should be understood as a phenomenological parameter which, under quite general assumptions, is mainly sensitive to the geometry. The induced charge is thus given by

$$dQ_\alpha = C_e(dU_\alpha - dU_\beta). \quad (2)$$

Fig. 2a

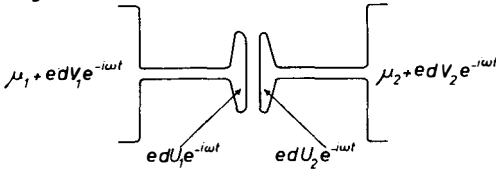


Fig. 2c

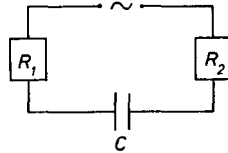


Fig. 2b

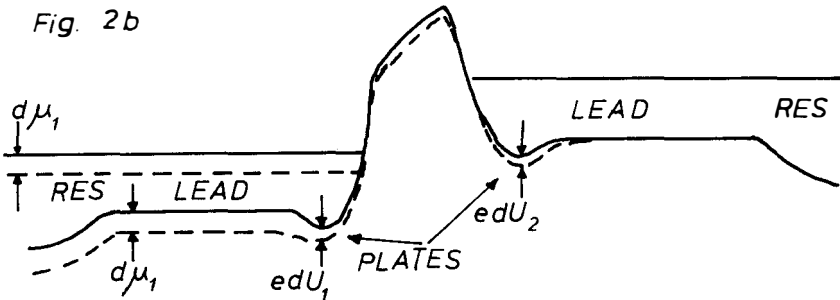


Fig. 2a. Nanostructured two-plate capacitor. Fig. 2b. Bottom of the conduction band and electro-chemical potentials for the reference applied voltage (solid lines) and for an additional infinitesimal applied voltage. Fig. 2c. Macroscopic two-plate capacitor.

Equalizing the RHS of Eqs. (1) and (2), for  $\alpha = 1, 2$ , gives two coupled linear equations, from which we find the potentials  $dU_1$  and  $dU_2$ . Then the charges are expressed as  $dQ_\alpha = C_\mu(d\mu_\alpha - d\mu_\beta)$ , where the electro-chemical capacitance  $C_\mu$  turns out to be a series connection of the electrostatic capacitance  $C_e$  and two quantum capacitances determined by the injected density of states on the plates:

$$\frac{1}{C_\mu} = \frac{d\mu}{e dQ} = \frac{1}{C_e} + \frac{1}{e^2} \left( \frac{1}{dN_1/dE} + \frac{1}{dN_2/dE} \right). \quad (3)$$

Note that  $dN_1/dE$  and  $dN_2/dE$  are not exactly intrinsic features of the plates, but depend on the scattering properties of the whole reservoir-to-plate arm, thermodynamically averaged at the reservoir, as can be seen from Eq. (8) below. The distinction of electrostatic capacitance and electro-chemical capacitance becomes irrelevant if both densities of states to the left and to the right are large compared to  $C_e$ .

### III. DYNAMIC ADMITTANCE WITH COULOMB INTERACTION

Here we present a discrete potential approach to get the admittance of an assembly of conductors (labelled by Roman superscripts). Each conductor may be connected to several reservoirs (labelled by greek subscripts) thus allowing for dc transport. Each conductor  $m$  is characterized by a non-interacting admittance matrix  $g_{\alpha\beta}^{est(m)}(\omega)$  calculated in Ref. [4], and it is assumed that no tunnelling occurs between different conductors. In our formulation the Coulomb interaction enters solely via the long-range part between conductor pairs: it is taken into account by introduction of a discrete set of internal potentials  $dU^{(m)}$  and of electrostatic capacitances  $C_{mn}$ , which relate the charges to the *internal potentials*:

$$dQ_m = \sum_n C_{mn} dU_n, \quad \text{with} \quad C_{mn} = C_{nm} \quad \text{and} \quad \sum_n C_{mn} = 0. \quad (4)$$

The above sum rule for  $C$  is a consequence of charge conservation inside the considered surface  $S$ . To proceed we must find the relationship between the internal potentials and the electro-chemical potentials.

The current at contact  $\alpha$  in conductor  $m$  is the sum of the response of non-interacting carriers to the oscillating external potentials  $d\mu_\beta^{(m)}(\omega) \equiv e dV_\beta^{(m)}(\omega)$  and to the oscillating internal potential  $dU^{(m)}$ ,

$$\begin{aligned} I_\alpha^{(m)}(\omega) &= \sum_\beta g_{\alpha\beta}^{est(m)}(\omega) dV_\beta^{(m)}(\omega) + g_\alpha^{int(m)}(\omega) dU^{(m)}(\omega) \\ &= \sum_\beta g_{\alpha\beta}^{est(m)}(\omega) \left( dV_\beta^{(m)}(\omega) - dU^{(m)}(\omega) \right). \end{aligned} \quad (5)$$

The last step in Eq. (5) is a key step: the current response of an interacting system is invariant under an overall potential shift. We emphasize that this invariance holds actually *separately* in each single conductor, since the wave functions of carriers of one conductor vanish in all other conductors and do not feel any effect of the potential beyond their own conductor. Note that at this stage the current  $I_\alpha^{(m)}$  only sees the potentials on its own conductor  $m$ . However  $dU^{(m)}$  depends via Coulomb long-range forces on the external potentials at the other conductors. The self-consistent condition for it is given by the time derivative of Eq. (4)

$$\sum_\alpha dI_\alpha^{(m)} = -i\omega \sum_{n \neq m} C_{mn} \left( dU^{(n)}(\omega) - dU^{(m)}(\omega) \right). \quad (6)$$

Substituting Eq. (5) into each of the Eqs. (6) we obtain an inhomogeneous linear system with a dimension equal to the number of conductors, which supplies  $\{dU^{(m)}\}$  in terms of  $\{dV^{(n)}\}$ . From Eq. (5) we then find the individual currents in the form  $dI_\alpha^{(m)}(\omega) = \sum_{n\beta} g_{\alpha\beta}^{I(mn)}(\omega)dV_\beta^{(n)}(\omega)$ , where  $g_{\alpha\beta}^{I(mn)}$  is the admittance matrix of the interacting system.

If the system under consideration does not permit dc transport as in Fig. 1a, then the first order of the conductances yields the mesoscopic capacitances,  $g^{I(mn)}(\omega) = -i\omega C_{\mu,mn} + O(\omega^2)$ .

Next we give explicitly the result for the two-plate mesoscopic capacitor. How would things look in the macroscopic regime? The classical analogon (see Fig. 2c) consists of a capacitor characterized by a capacitance  $C$ , and of two pieces of wire characterized by resistances  $R_1$  and  $R_2$ , which connect the capacitor to a battery. Under ac bias the current response is  $dI = \{-iC\omega + RC^2\omega^2 + O(\omega^3)\}dV$ , with  $R = R_1 + R_2$ , where the three parameters,  $C$ ,  $R_1$  and  $R_2$ , express features which are specific to the separate constituents of the macroscopic system. In this respect, the situation for a nanostructured device is very different.

For non-interacting carriers the current at arm  $m$  in response to an oscillating external potential  $edV_m(\omega) \equiv d\mu_m(\omega)$  [4], when properly expanded at  $kT$  fixed [1], is

$$g_{mm}^{ext}(\omega) = -ie^2 \frac{dN_m}{dE} \omega + e^4 \left( \frac{dN_m}{dE} \right)^2 R_{qm} \omega^2 + O(\omega^3). \quad (7)$$

Here  $(dN_m/dE)$  is the reservoir-to-plate injected density of states

$$\frac{dN_m}{dE} = \frac{1}{2\pi i} \int dE \left( -\frac{df}{dE} \right) \text{Tr} \left[ s^{t(m)}(E) \frac{\partial s^{(m)}(E)}{\partial E} \right], \quad (8)$$

and  $R_{qm}$  has the dimension of a resistance,

$$R_{qm} = \frac{\hbar}{2e^2} \frac{\int dE (-df_m/dE) \text{Tr} [s^{t(m)}(E) \partial s^{(m)}(E) / \partial E]^2}{\{dN_m/dE\}^2}. \quad (9)$$

The scattering matrix  $s^{(m)}(E)$  relates the incoming to the outgoing current amplitudes in arm  $m$ .

Then the solution of Eqs. (5 and 6) for the two-plate capacitor yields, for the interacting admittance,

$$g^I(\omega) = -iC_\mu\omega + R_q C_\mu^2 \omega^2 + O(\omega^3), \quad R_q = R_{q1} + R_{q2}, \quad (10)$$

where  $dI_1 = -dI_2 = g^I(dV_1 - dV_2)$ .

The thermodynamic character of  $g^I$  is evident from Eqs.(3, 8 and 9): statistical averages over the grand-canonical reservoir ensembles are present in both  $C_\mu$  and  $R_q$ .

Let us try to give a meaning to the charge relaxation resistance  $R_q$ . The first factor in  $R_q$  is half the resistance quantum, the Sharvin-Imry [7] lead-reservoir interface resistance of a single quantum channel. This resistance is multiplied by the ratio  $\langle \tau_D^2 \rangle / \langle \tau_D \rangle^2$ , where  $\tau_D$  is the time carriers incident from the leads dwell [8] on the capacitor plates,

$$R_{qm} = \frac{\hbar}{2e^2} \frac{\langle \tau_D^2 \rangle}{\langle \tau_D \rangle^2} = \frac{\hbar}{2e^2} \frac{(\sum_n (d\phi_n^{(m)}/dE)^2)_m}{\{(\sum_n (d\phi_n^{(m)}/dE))_m\}^2}.$$

The brackets  $\langle \rangle$  denote both a quantum-mechanical average and a statistical average.  $R_{qm}$  can be directly expressed in terms of energy derivatives of the eigenvalues  $s_n^{(m)} = \exp(i\phi_n^{(m)})$ . The

presence of such a ratio in the current response is the hallmark of a non-self-averaging system. For a small number of channels  $M_m$  the resistance  $R_{qm}$  scales usually as  $1/M_m$ . For large  $M_m$ , on the other hand, Pendry et al. [9] have shown that in the diffusive regime the probability distribution of the conductance makes extreme excursions, or "maximal fluctuations". We might expect this non-self-averaging system to react to an energy change with maximal changes of the phase  $\phi$  for a minimum number of eigenchannels, whereas in the other eigenchannels no phase changes take place. Thus a non-self-averaging system is likely to exhibit a larger charge relaxation resistance than a usual system. The charge distribution of localized states in the insulator between the capacitor plates is likely to be another important source of mesoscopic fluctuations [10]. To study this effect an approach is required which treats the microscopic potential landscape.

#### IV. FROM THE DISCRETE-PARAMETER MODEL TO SPATIAL DEPENDENCE

For a system as in Fig. 1a, capacitances  $C_{kl}$  can be more accurately found by means of space-dependent induced potentials: this requires the tools of the spatially resolved response, like the characteristic potential functions  $u_l(\vec{r})$  and the Lindhard response functions  $\Pi_k(\vec{r}, \vec{r}')$  appearing in the table below. In principle, however, the derivation proceeds in full analogy to the scheme of Sect. 2. Crucial are the roles of the surface  $S$  and of the invariance under an overall potential shift (OPS) of the electro-chemical and the induced potentials. The following table compares the differing approaches:

<i>Discrete-parameter model</i>	<i>Microscopic model</i>
$edU_k = \sum_l \tilde{u}_{kl} d\mu_l$	$edU([\mu_l], \vec{r}) = \sum_l u_l(\vec{r}) d\mu_l$
$\xrightarrow{\text{OPS}} \sum_l \tilde{u}_{kl} = 1$	$\xrightarrow{\text{OPS}} \sum_l u_l(\vec{r}) = 1$
$dQ_k = \sum_l C_{kl} dU_l$	$-\nabla^2 dU(\vec{r}) = 4\pi e \sum_l dn_k(\vec{r})$
$dQ_k = e(dN_k/dE)d\mu_k - \tilde{\Pi}_k edU_k$	$dn_k(\vec{r}) = (dn(\vec{r}, k)/dE)d\mu_k + dn_{ind,k}(\vec{r}) =$ $= (dn(\vec{r}, k)/dE)d\mu_k - \int d^3r' \Pi_k(\vec{r}, \vec{r}') edU(\vec{r}')$
$\xrightarrow{\text{OPS}} \tilde{\Pi}_k = edN_k/dE$	$\xrightarrow{\text{OPS}} \int d^3r' \Pi_k(\vec{r}, \vec{r}') = dn(\vec{r}, k)/dE$

#### V. CONCLUSION

A mesoscopic capacitance has been introduced for systems interacting via long-range Coulomb forces and the calculation of the dynamic admittance has been outlined.

Focussing on a simple system for the results, we find that the "capacitance" and "resistance" governing the ac admittance of a nanostructured capacitor exhibit mesoscopic signatures: they are quantities which reflect the behavior of the system as a whole indivisible unit. In fact the charge relaxation resistance in each arm and the corrections to the standard classical capacitance are determined by the scattering properties along either side of the capacitor averaged over the grand-canonical ensemble of the corresponding reservoir.

- |   |   |
|---|---|
| [1] M. Büttiker, H. Thomas, and A. Prêtre, <i>Phys. Lett. A</i> <b>180</b> , 364 (1993)   | [5] M. Büttiker, A. Prêtre, and H. Thomas, <i>Phys. Rev. Lett.</i> <b>70</b> , 4114 (1993)  |
| [2] M. Büttiker, <i>J. Phys. Condensed Matter</i> <b>5</b> , 9361 (1993)  | [6] M. Büttiker, H. Thomas, and A. Prêtre, <i>Z. Phys.</i> <b>B94</b> , 133 (1994)  |
| [3] T.P. Smith III, W.J. Wang, and P.J. Stiles, <i>Phys. Rev. B</i> <b>34</b> , 2995 (1986); L. Lambe and R.C. Jaklevic, <i>Phys. Rev. Lett.</i> <b>22</b> , 1371 (1969)                          | [7] U. Sivan and Y. Imry, <i>Phys. Rev. B</i> <b>33</b> , 551 (1986)  |
| [4] M. Büttiker and H. Thomas, in: <i>Quantum-Effect Physics, Electronics and Applications</i> , ed K. Ismail et al., (Institute of Physics Conference Series Number 127, Bristol), p. 19. (1992) | [8] C. R. Leavens and G. C. Acers, <i>Phys. Rev. B</i> <b>39</b> , 1202 (1989)  |
|   | [9] J.B. Pendry, <i>IBM J. Res. Develop.</i> <b>32</b> , 137 (1988); J.B. Pendry, A. MacKinnon, and A. Prêtre, <i>Phys. Lett. A</i> <b>168</b> , 400 (1990) |
|   | [10] B. L. Shklovskii, Private communication.   |

## SUB-POISSONIAN SHOT NOISE IN A DIFFUSIVE CONDUCTOR

M. J. M. de Jong<sup>a,b</sup> and C. W. J. Beenakker<sup>b</sup>*(a) Philips Research Laboratories, 5656 AA Eindhoven, The Netherlands**(b) Instituut-Lorentz, University of Leiden, 2300 RA Leiden, The Netherlands*

**Abstract.** — A review is given of the shot-noise properties of metallic, diffusive conductors. The shot noise is one third of the Poisson noise, due to the bimodal distribution of transmission eigenvalues. The same result can be obtained from a semiclassical calculation. Starting from Oseledec's theorem it is shown that the bimodal distribution is required by Ohm's law.

**I. Introduction**

Time-dependent fluctuations in the electrical current caused by the discreteness of the charge carriers are known as shot noise. These fluctuations are characterized by a white noise spectrum and persist down to zero temperature. The noise spectral density  $P$  (per unit frequency bandwidth) is a measure for the magnitude of these fluctuations. A well-known example is a saturated vacuum diode, for which Schottky found that  $P = 2eI \equiv P_{\text{Poisson}}$ , with  $I$  the average current.<sup>1)</sup> This indicates that the electrons traverse the conductor as uncorrelated current pulses, i.e. are transmitted in time according to Poisson statistics. It is also known that a metal wire, of macroscopic length  $L$ , does not exhibit shot noise, because inelastic scattering reduces  $P$  by a factor  $l_i/L$ , which is much smaller than 1 in a macroscopic conductor ( $l_i$  is the inelastic scattering length). In the last decade, the investigation of transport on smaller length scales has become accessible through the progress in microfabrication techniques. The physics on this mesoscopic scale displays a wealth of new phenomena.<sup>2,3)</sup> Theoretical analysis<sup>4-7)</sup> shows that the shot noise in mesoscopic conductors may be suppressed below  $P_{\text{Poisson}}$ , due to correlated electron transmission as a consequence of the Pauli principle. This raises the question how large  $P$  is in a *metallic, diffusive* conductor of length  $L < l_i$ , but still longer than the elastic mean free path  $\ell$ . It has been predicted theoretically<sup>8-10)</sup> that  $P = \frac{1}{3}P_{\text{Poisson}}$ . This suppression of the

shot noise by a factor one third is *universal*, in the sense that it does not depend on the specific geometry nor on any intrinsic material parameter (such as  $\ell$ ). The purpose of this paper is to discuss the origin of the one-third suppression. First, we review the fully quantum-mechanical calculation, where the suppression originates from the bimodal distribution of transmission eigenvalues. Then, a semiclassical calculation is presented, which surprisingly yields the same suppression by one third. One might therefore ask whether there exists a semiclassical explanation for the bimodal eigenvalue distribution. Indeed, we find that this distribution is required by Ohm's law. We conclude with a brief discussion of an experimental observation of suppressed shot noise in a disordered wire, which has recently been reported.<sup>11)</sup>

## II. Quantum-mechanical theory

A scattering formula for the shot noise in a phase-coherent conductor has been derived by Büttiker.<sup>7)</sup> It relates the zero-temperature, zero-frequency shot-noise power  $P$  of a spin-degenerate, two-probe conductor to the transmission matrix  $\mathbf{t}$ :

$$P = P_0 \text{Tr} [\mathbf{t}^\dagger (1 - \mathbf{t} \mathbf{t}^\dagger)] = P_0 \sum_{n=1}^N T_n (1 - T_n). \quad (1)$$

Here  $P_0 \equiv 2eV(2e^2/h)$ , with  $V$  the applied voltage,  $T_n$  denotes an eigenvalue of  $\mathbf{t} \mathbf{t}^\dagger$ , and  $N$  is the number of transverse modes at the Fermi energy  $E_F$ . It follows from current conservation that the transmission eigenvalues  $T_n \in [0, 1]$ . Equation (1) is the multi-channel generalization of single-channel formulas found earlier.<sup>4-6)</sup> Levitov and Lesovik have shown<sup>12)</sup> that Eq. (1) follows from the fact that the electrons in each separate scattering channel are transmitted in time according to a binomial (Bernoulli) distribution (depending on  $T_n$ ). The Poisson noise is then just a result of the limiting distribution for small  $T_n$ . Using the Landauer formula for the conductance

$$G = G_0 \text{Tr} \mathbf{t} \mathbf{t}^\dagger = G_0 \sum_{n=1}^N T_n, \quad (2)$$

with  $G_0 \equiv 2e^2/h$ , one finds from Eq. (1) that indeed  $P = 2eVG = 2eI = P_{\text{Poisson}}$  if  $T_n \ll 1$  for all  $n$ . However, if the transmission eigenvalues are not much smaller than 1, the shot noise is suppressed below  $P_{\text{Poisson}}$ . As mentioned above, this suppression is a consequence of the electrons being fermions. In a scattering channel with  $T_n \ll 1$  the electrons are transmitted in time in uncorrelated fashion. As  $T_n$  increases the electron transmission becomes more correlated because of the Pauli principle. In a scattering channel with  $T_n = 1$  a constant current is flowing, so that its contribution to the shot noise is zero.

Let us now turn to transport through a diffusive conductor ( $L \gg \ell$ ), in the metallic regime ( $L \ll$  localization length). To compute the ensemble averages  $\langle \dots \rangle$  of Eqs. (1) and (2) we need the density of transmission eigenvalues  $p(T) = \langle \sum_n \delta(T - T_n) \rangle$ . The first moment of  $p(T)$  determines the conductance,

$$\langle G \rangle = G_0 \int_0^1 dT p(T) T, \quad (3)$$

whereas the shot-noise power contains also the second moment

$$\langle P \rangle = P_0 \int_0^1 dT p(T) T(1 - T). \quad (4)$$

In the metallic regime, Ohm's law for the conductance holds to a good approximation, which implies that  $\langle G \rangle \propto 1/L$ , up to small corrections of order  $e^2/h$  (due to weak localization). The Drude formula gives

$$\langle G \rangle = G_0 \frac{N\bar{\ell}}{L}, \quad (5)$$

where  $\bar{\ell}$  equals the mean free path  $\ell$  times a numerical coefficient.<sup>13)</sup> From Eqs. (3) and (5) one might surmise that for a diffusive conductor all the transmission eigenvalues are of order  $\bar{\ell}/L$ , and hence much smaller than 1. This would imply the shot-noise power  $P = P_{\text{Poisson}}$  of a Poisson process.

However, the surmise  $T_n \approx \bar{\ell}/L$  for all  $n$  is completely incorrect for a metallic, diffusive conductor. This was first pointed out by Dorokhov,<sup>14)</sup> and later by Imry<sup>15)</sup> and by Pendry *et al.*<sup>16)</sup> In reality, a fraction  $\bar{\ell}/L$  of the transmission eigenvalues is of order unity (open channels), the others being exponentially small (closed channels). The full distribution function is

$$p(T) = \frac{N\bar{\ell}}{2L} \frac{1}{T\sqrt{1-T}} \Theta(T - T_0), \quad (6)$$

where  $T_0 \simeq 4 \exp(-2L/\bar{\ell}) \ll 1$  is a cutoff at small  $T$  such that  $\int_0^1 dT p(T) = N$  (the function  $\Theta(x)$  is the unit step function). One easily checks that Eq. (6) leads to the Drude conductance (5). The function  $p(T)$  is plotted in Fig. 1. It is *bimodal* with peaks near unit and zero transmission. The distribution (6) follows from a scaling equation, which describes the evolution of  $p(T)$  on increasing  $L$ .<sup>17-19)</sup> A microscopic derivation of Eq. (6) has recently been given by Nazarov.<sup>20)</sup>

The bimodal distribution (6) implies for the shot-noise power (4) the unexpected result<sup>8)</sup>

$$\langle P \rangle = \frac{1}{3} P_0 \frac{N\bar{\ell}}{L} = \frac{1}{3} P_{\text{Poisson}}. \quad (7)$$

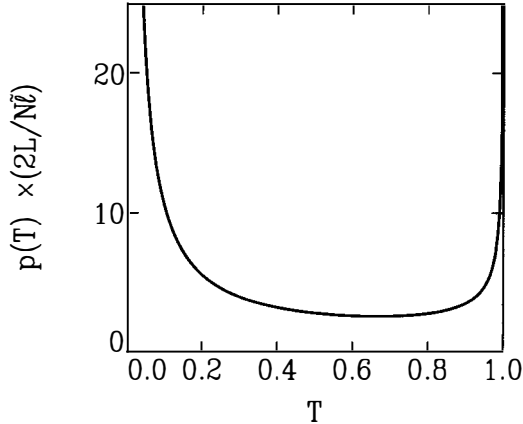


**Figure 1.** The bimodal distribution of transmission eigenvalues according to Eq. (6). The cutoff for  $T \lesssim 4 \exp(-2L/\bar{\ell})$  is not shown.

Corrections to Eq. (7) due to weak localization have also been computed,<sup>10)</sup> and are smaller by a factor  $L/N\bar{\ell}$  (which is  $\ll 1$  in the metallic regime).

### III. Semiclassical calculation

Since the Drude conductance (5) can be obtained semiclassically (without taking quantum-interference effects into account), one may wonder whether the sub-Poissonian shot noise (7) — which follows from the same  $p(T)$  — might also be obtained from a semiclassical calculation. Such a calculation was presented by Nagaev,<sup>9)</sup> who independently from Refs. 8, 10 arrived at the result (7). Nagaev uses a Boltzmann-Langevin approach,<sup>21,22)</sup> which is a classical kinetic theory for the non-equilibrium fluctuations in a degenerate electron gas. We refer to this method as semiclassical, because the motion of the electrons is treated classically — without quantum-interference effects — whereas the Pauli principle is accounted for, through the use of Fermi-Dirac statistics. Nagaev's approach does not yield a formula with the same generality as Büttiker's formula (1), but is only applicable for diffusive transport.

To put the quantum-mechanical and the semiclassical theories of shot noise on equal terms, we have recently derived a scattering formula for  $P$  from the Boltzmann-Langevin approach. This formula is valid from the ballistic to the diffusive transport regime. A detailed description will be the subject of a forthcoming publication. Here, we merely present the result. For simplicity, we consider a two-dimensional wire (length  $L$  and width  $W$ ), with a circular Fermi

surface. The geometry is shown in Fig. 2 (inset). The scattering formula relates  $P$  to the classical transmission probabilities  $T(\mathbf{r}, \varphi)$ , which denote the probability that an electron at position  $\mathbf{r} \equiv (x, y)$  with velocity  $\mathbf{v} \equiv v_F(\cos \varphi, \sin \varphi)$  (with  $v_F$  the Fermi velocity) is transmitted into lead number 2. The result is

$$P = \frac{NP_0}{4\pi W v_F} \int_0^L dx \int_0^W dy \int_0^{2\pi} d\varphi \int_0^{2\pi} d\varphi' W_{\varphi\varphi'}(\mathbf{r}) [T(\mathbf{r}, \varphi) - T(\mathbf{r}, \varphi')]^2 \bar{T}(\mathbf{r}, \varphi) [1 - \bar{T}(\mathbf{r}, \varphi')], \quad (8)$$

where the number of channels  $N = W m v_F / \hbar \pi$ , and  $W_{\varphi\varphi'}(\mathbf{r})$  is the transition rate for (elastic) impurity-scattering from  $\varphi$  to  $\varphi'$ , which may in principle depend also on  $\mathbf{r}$ . The time-reversed probability  $\bar{T}(\mathbf{r}, \varphi)$  gives the probability that an electron at  $(\mathbf{r}, \varphi)$  has originated from lead 2. From now on we assume time-reversal symmetry (zero magnetic field), so that  $\bar{T}(\mathbf{r}, \varphi) = T(\mathbf{r}, \varphi + \pi)$ . Equation (8) corrects a previous result.<sup>23</sup> In this notation, the conductance is given by

$$G = \frac{NG_0}{2W} \int_0^W dy \int_0^{2\pi} d\varphi \cos \varphi T(\mathbf{r}, \varphi). \quad (9)$$

Eq. (9) is independent of  $x$  because of current conservation. The transmission probabilities obey a Boltzmann type of equation<sup>24</sup>)

$$\mathbf{v} \cdot \nabla T(\mathbf{r}, \varphi) = \int_0^{2\pi} \frac{d\varphi'}{2\pi} W_{\varphi\varphi'}(\mathbf{r}) [T(\mathbf{r}, \varphi) - T(\mathbf{r}, \varphi')], \quad (10)$$

where  $\nabla \equiv (\partial/\partial x, \partial/\partial y)$ .

We now apply Eq. (8) to the case  $W_{\varphi\varphi'}(\mathbf{r}) = v_F/\ell$  of isotropic impurity scattering. Since the scattering is modeled by one parameter, the resulting  $P$  is the ensemble average. We assume specular boundary scattering, so that the transverse coordinate ( $y$ ) becomes irrelevant. Let us first show that in the diffusive limit ( $\ell \ll L$ ) the result of Nagaev<sup>9</sup>) is recovered. For a diffusive wire the solution of Eq. (10) can be approximated by

$$T(\mathbf{r}, \varphi) = \frac{x + \ell \cos \varphi}{L}. \quad (11)$$

Substitution into Eq. (9) yields the Drude conductance  $\langle G \rangle = NG_0 \pi \ell / 2L$  in accordance with Eq. (5). For the shot-noise power one obtains, neglecting terms of order  $(\ell/L)^2$ ,

$$\langle P \rangle = NP_0 \frac{\pi \ell}{L} \int_0^L \frac{dx}{L} \frac{x}{L} \left(1 - \frac{x}{L}\right) = \frac{1}{3} P_{\text{Poisson}}, \quad (12)$$

in agreement with Eq. (7).

We can go beyond Ref. 9 and apply our method to quasi-ballistic wires, for which  $\ell$  and  $L$  become comparable. In Ref. 24 it is shown how in this case the probabilities  $T(\mathbf{r}, \varphi)$  can be

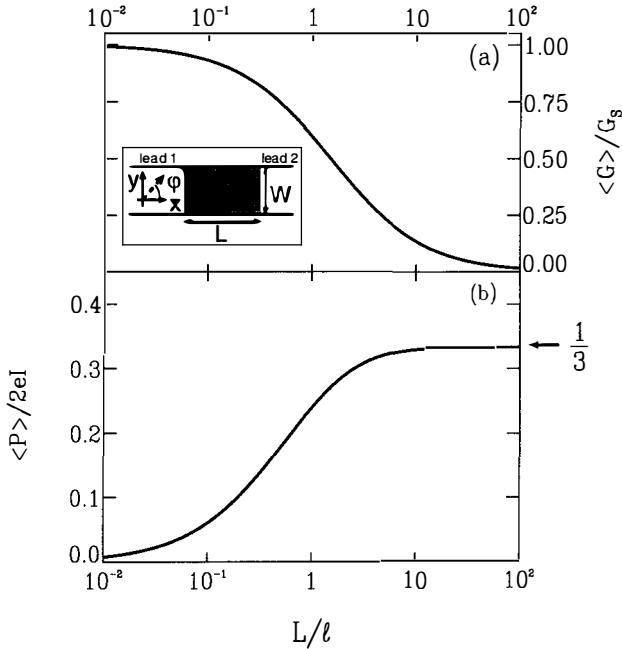


**Figure 2.** (a) The conductance (normalized by the Sharvin conductance  $G_S \equiv NG_0$ ) and (b) the shot-noise power (in units of  $P_{\text{Poisson}} \equiv 2eI$ ), as a function of the ratio  $L/\ell$ , computed from Eqs. (8) and (9) for isotropic impurity scattering. The inset shows schematically the wire and its coordinates.

calculated numerically by solving Eq. (10) through Milne's equation. In Fig. 2 we show the result for both the conductance and the shot-noise power. The conductance crosses over from the Sharvin conductance ( $G_S \equiv NG_0$ ) to the Drude conductance with increasing wire length.<sup>24</sup> This crossover is accompanied by a rise in the shot noise, from zero to  $\frac{1}{3}P_{\text{Poisson}}$ .

#### IV. Bimodal eigenvalue distribution from Ohm's law

Now that it is established that the quantum-mechanical calculation (Sec. II) and the semiclassical approach (Sec. III) yield the one-third suppression of the shot noise, we would like to close the circle by showing how the bimodal distribution (6) of the transmission eigenvalues can be obtained semiclassically.

It is convenient to work with the parametrization

$$T_n = \frac{1}{\cosh^2(\alpha_n L)}, \quad n = 1, 2, \dots, N, \quad (13)$$

which relates the eigenvalues  $T_n$  of  $\mathbf{t}\mathbf{t}^\dagger$  to the eigenvalues  $\exp(\pm 2\alpha_n L)$  of  $\mathbf{M}\mathbf{M}^\dagger$ . Here  $\mathbf{t}$  is the  $N \times N$  transmission matrix,  $\mathbf{M}$  is the  $2N \times 2N$  transfer matrix of the conductor, and  $\alpha_n \in [0, \infty)$  for all  $n$ . The eigenvalues of  $\mathbf{M}\mathbf{M}^\dagger$  come in inverse pairs as a result of current conservation.<sup>19)</sup> The  $\alpha_n$ 's are known as the inverse localization lengths of the conductor. Scattering channels for which the localization length is longer than the sample length ( $\alpha_n L \ll 1$ ) are open, if the sample length exceeds the localization length ( $\alpha_n L \gg 1$ ) the scattering channel is closed, as is clear from Eq. (13). The bimodal distribution (6) of the transmission eigenvalues is equivalent to a *uniform* distribution of the inverse localization lengths,

$$\rho(\alpha) = N\tilde{\ell}\Theta(\alpha - 1/\tilde{\ell}), \quad (14)$$

where  $\rho(\alpha) \equiv \langle \sum_n \delta(\alpha - \alpha_n) \rangle$ . Furthermore, the distribution of the  $\alpha$ 's implied by Eq. (14) is *independent* of the sample length  $L$ . We will argue that these two properties,  $L$ -independence and uniformity, of  $\rho(\alpha)$  follow from Oseledec's theorem<sup>25)</sup> and Ohm's law, respectively.

We recall<sup>19)</sup> that the transfer matrix has the multiplicative property that if two pieces of wire with matrices  $\mathbf{M}_1$  and  $\mathbf{M}_2$  are connected in series, the transfer matrix of the combined system is simply the product  $\mathbf{M}_1\mathbf{M}_2$ . In this way the transfer matrix of a disordered wire can be constructed from the product of  $N_L$  individual transfer matrices  $\mathbf{m}_i$ ,

$$\mathbf{M} = \prod_{i=1}^{N_L} \mathbf{m}_i, \quad (15)$$

where  $N_L \equiv L/\lambda$  is a large number proportional to  $L$ . The  $\mathbf{m}_i$ 's are assumed to be independently and identically distributed random matrices, each representing transport through a slice of conductor of small, but still macroscopic, length  $\lambda$ . In the theory of random matrix products,<sup>26)</sup> the limits  $\lim_{L \rightarrow \infty} \alpha_n$  are known as the Lyapunov exponents. Oseledec's theorem<sup>25)</sup> is the statement that this limit exists. Numerical simulations<sup>19)</sup> indicate that the large- $L$  limit is essentially reached for  $L \gg \ell$ , and does not require  $L \gg N\ell$ . This explains the  $L$ -independence of the distribution of the inverse localization lengths in the metallic, diffusive regime ( $\ell \ll L \ll N\ell$ ).

Oseledec's theorem tells us that  $\rho(\alpha)$  is independent of  $L$ , but it does not tell us how it depends on  $\alpha$ . To deduce the uniformity of  $\rho(\alpha)$  we invoke Ohm's law,  $\langle G \rangle \propto 1/L$ . This requires

$$L \int_0^\infty d\alpha \rho(\alpha) \frac{1}{\cosh^2(\alpha L)} = C, \quad (16)$$

where  $C$  is independent of  $L$ . It is clear that Eq. (16) implies the uniform distribution  $\rho(\alpha) = C$ . A cutoff at large  $\alpha$  is allowed, since  $1/\cosh^2(\alpha L)$  vanishes anyway for  $\alpha L \gg 1$ . From Drude's formula (4) we deduce  $C = N\bar{\ell}$ , and normalization then implies a cutoff at  $\alpha \gtrsim 1/\bar{\ell}$ , in accordance with Eq. (14).

## V. Conclusion

In summary, we have discussed the equivalence of the fully quantum-mechanical and the semiclassical theories of sub-Poissonian shot noise in a metallic, diffusive conductor. Both approaches yield a one-third suppression of  $P$  relative to  $P_{\text{Poisson}}$ . The bimodal distribution, which is at the heart of the quantum-mechanical explanation, can be understood semiclassically as a consequence of a mathematical theorem on eigenvalues (Oseledec) and a law of classical physics (Ohm's law).

The fact that phase coherence is not essential for the one-third suppression of  $P$  suggests that this phenomenon is more robust than other mesoscopic phenomena, such as universal conductance fluctuations. This might explain the success of the recent attempt to measure the shot-noise suppression due to open scattering channels in a disordered wire defined in a 2D electron gas.<sup>11)</sup> In this experiment a rather large current was necessary to obtain a measurable shot noise, and it seems unlikely that phase coherence was maintained under such conditions.

In both the quantum-mechanical and semiclassical theories discussed in this review, the effects of electron-electron interactions have been ignored. The Coulomb repulsion is known to have a strong effect on the noise in confined geometries with a small capacitance.<sup>27)</sup> We would expect the interaction effects to be less important in open conductors.<sup>28)</sup> While a fully quantum-mechanical theory of shot noise with electron-electron interactions seems difficult, the semiclassical Boltzmann-Langevin approach discussed here might well be extended to include electron-electron scattering and screening effects.

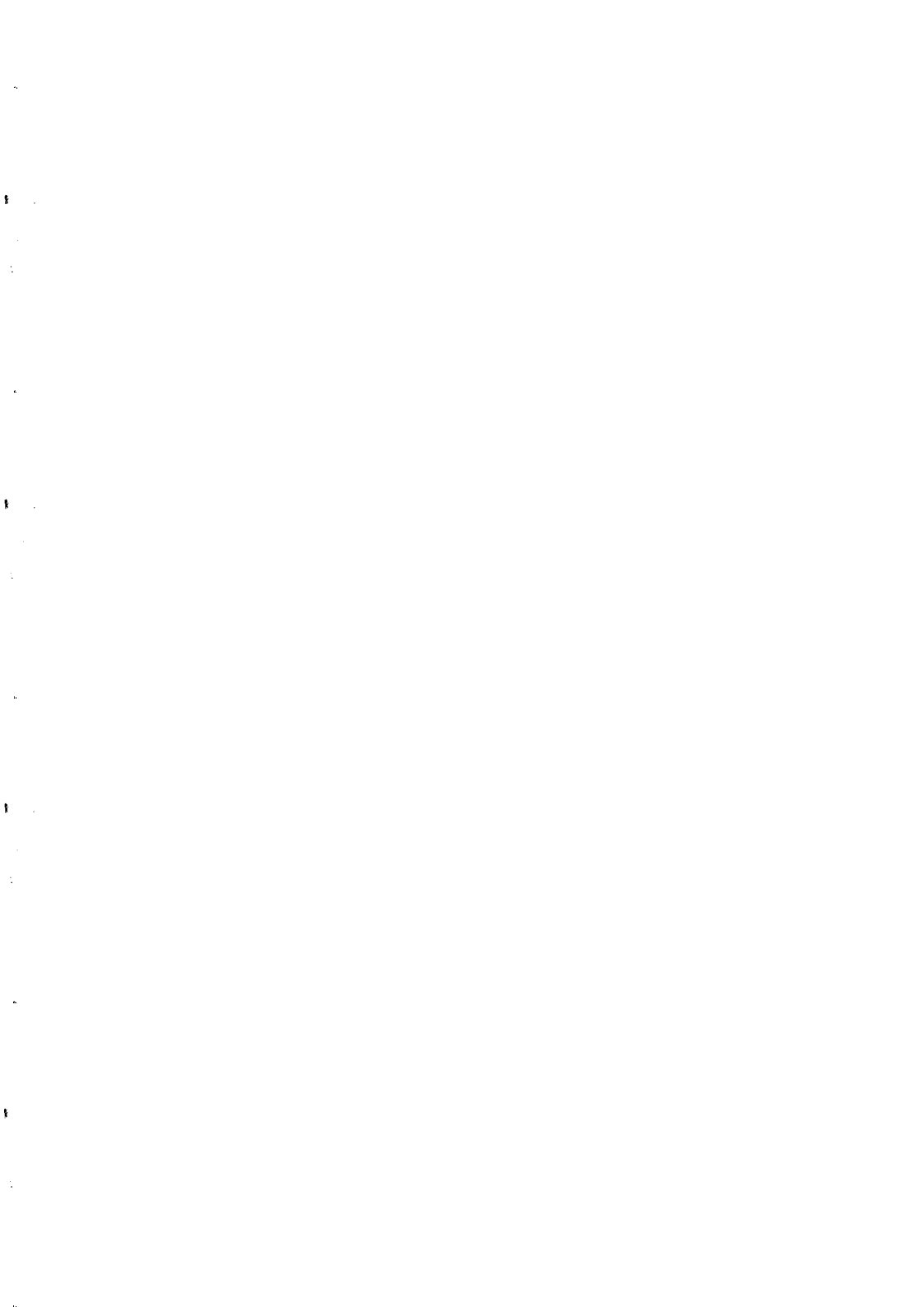
## Acknowledgements

The authors would like to thank H. van Houten, R. Landauer, and L. W. Molenkamp for valuable discussions. This research was supported by the "Nederlandse organisatie voor Wetenschappelijk Onderzoek" (NWO) and by the "Stichting voor Fundamenteel Onderzoek der Materie" (FOM).

## References

1. W. Schottky, *Ann. Phys. (Leipzig)* **57**, 541 (1918).

2. C. W. J. Beenakker and H. van Houten, *Solid State Phys.* **44**, 1 (1991).
3. *Mesoscopic Phenomena in Solids*, edited by B. L. Al'tshuler, P. A. Lee, and R. A. Webb (North-Holland, Amsterdam, 1991).
4. V. A. Khlus, *Zh. Eksp. Teor. Fiz.* **93**, 2179 (1987) [*Sov. Phys. JETP* **66**, 1243 (1987)].
5. G. B. Lesovik, *Pis'ma Zh. Eksp. Teor. Fiz.* **49**, 513 (1989) [*JETP Lett.* **49**, 592 (1989)].
6. B. Yurke and G. P. Kochanski, *Phys. Rev. B* **41**, 8184 (1990).
7. M. Büttiker, *Phys. Rev. Lett.* **65**, 2901 (1990).
8. C. W. J. Beenakker and M. Büttiker, *Phys. Rev. B* **46**, 1889 (1992).
9. K. E. Nagaev, *Phys. Lett. A* **169**, 103 (1992).
10. M. J. M. de Jong and C. W. J. Beenakker, *Phys. Rev. B* **46**, 13400 (1992).
11. F. Liefink, J. I. Dijkhuis, M. J. M. de Jong, L. W. Molenkamp, and H. van Houten (preprint).
12. L. S. Levitov and G. B. Lesovik, *Pis'ma Zh. Eksp. Teor. Fiz.* **58**, 225 (1993) [*JETP Lett.* **58**, 230 (1993)].
13. The precise relationship between  $\ell$  and  $\bar{\ell}$  depends on the dimensionality of the Fermi surface and on the specific kind of scattering. For isotropic impurity scattering with mean free path  $\ell$  one has  $\bar{\ell} = \pi\ell/2$  in 2D (Fermi circle) and  $\bar{\ell} = 4\ell/3$  in 3D (Fermi sphere).
14. O. N. Dorokhov, *Solid State Comm.* **51**, 381 (1984).
15. Y. Imry, *Europhys. Lett.* **1**, 249 (1986).
16. J. B. Pendry, A. MacKinnon, and P. J. Roberts, *Proc. R. Soc. London Ser. A* **437**, 67 (1992).
17. O. N. Dorokhov, *Pis'ma Zh. Eksp. Teor. Fiz.* **36**, 259 (1982) [*JETP Lett.* **36**, 318 (1982)].
18. P. A. Mello, P. Pereyra, and N. Kumar, *Ann. Phys. (New York)* **181**, 290 (1988).
19. A. D. Stone, P. A. Mello, K. A. Muttalib, and J.-L. Pichard, in Ref. 3.
20. Yu. V. Nazarov (preprint).
21. B. B. Kadomtsev, *Zh. Eksp. Teor. Fiz.* **32**, 943 (1957) [*Sov. Phys. JETP* **5**, 771 (1957)].
22. Sh. M. Kogan and A. Ya. Shul'man, *Zh. Eksp. Teor. Fiz.* **56**, 862 (1969) [*Sov. Phys. JETP* **29**, 467 (1969)].
23. C. W. J. Beenakker and H. van Houten, *Phys. Rev. B* **43**, 12066 (1991).
24. M. J. M. de Jong, *Phys. Rev. B* (March 15, 1994).
25. V. I. Oseledec, *Trans. Moscow Math. Soc.* **19**, 197 (1968).
26. A. Crisanti, G. Paladin, and A. Vulpiani, *Products of Random Matrices in Statistical Physics* (Springer, Berlin, 1993).
27. See e.g., S. Hershfield, J. H. Davies, P. Hyldgaard, C. J. Stanton, and J. W. Wilkins, *Phys. Rev. B* **47**, 1967 (1993).
28. M. Büttiker, in: *Noise in Physical Systems and 1/f Fluctuations*, edited by P. H. Handel and A. L. Chung (American Institute of Physics Conference 285, New York, 1993).



## LIST OF PARTICIPANTS

Alexander Altland  
 Univ. Köln  
 Institut für Theoretische Physik  
 50937 Köln  
 Germany

Eugene Altshuler  
 Weizmann Institute  
 Condensed Matter Department  
 76100 Rehovot  
 Israel

Ray Ashoori  
 MIT  
 Dept. of Physics  
 MA 02139 Cambridge  
 USA

Dmitri Averin  
 SUNY  
 Department of Physics  
 NY 11794 Stony Brook  
 USA

Crispin Barnes  
 RIKEN  
 Frontier Research Program  
 Wako-Shi  
 351-01 Saitama  
 Japan

Carlo Beenakker  
 Univ. of Leiden  
 Instituut-Lorentz  
 P.O. Box 9506  
 2300 RA Leiden  
 The Netherlands

Alain Benoit  
 CNRS-CRTBT  
 CNRS  
 25 Ave des Martyrs bp 166  
 38042 Grenoble  
 France

Gerd Bergmann  
 USC  
 Physics Department  
 CA 90089-0484 Los Angeles  
 USA

Harry Bernas  
 Ultimatch-CNRS  
 CSNSM  
 Bat 108  
 F-91405 Orsay  
 France

Hélène Bouchiat  
 Univ. Paris-Sud  
 Lab. de Physique des Solides Bât. 510  
 F-91400 Orsay Cedex  
 France

Daniel Braun  
 Univ. Paris-Sud  
 Lab. de Physique des Solides  
 Bat 510  
 F-91400 Orsay  
 France

John Chalker  
 Univ. of Oxford  
 Theoretical Physics  
 1, Keble Road  
 OX1 3NP Oxford  
 U.K.

Avraham Cohen  
 PTB  
 Bundesallee 100  
 38116 Braunschweig  
 Germany

Hervé Courtois  
 CNRS-CRTBT  
 CNRS  
 25 Ave des Martyrs BP166  
 38042 Grenoble cedex 9  
 France

Marc De Jong  
 Philips Research Lab.  
 Prof. Holstlaan 4  
 5656AA Eindhoven  
 The Netherlands

Jerome Dubois  
 Univ. of Nijmegen

Toenooiveld  
 6525 ED Nijmegen  
 The Netherlands

Louis Dumoulin  
Univ. Paris-Sud  
CSNSM-CNRS  
Bat 108  
F-91405 Orsay  
France

Laurence Eaves  
Univ. of Nottingham  
Dept. of Physics  
NG72RD Nottingham  
U.K.

Wiveka Elion  
Delt Univ. of Tech.  
Department of Ap. Physics  
P.O. Box 5046  
NL-2600GA Delft  
The Netherlands

Mikio Eto  
Keio University  
Dep. of Physics, Fac. S.&T.  
3-14-1 Hiyoshi, Kohoku-ku  
223 Yokohama  
Japan

Giancarlo Faini  
L2M - CNRS  
196 Av. Henri Barbusse  
92220 Bagneux  
France

Vladimir Falko  
Max-Planck-Institut  
Heisenbergstrasse, 1  
D-70569 Stuttgart  
Germany

Gerhard Fasol  
Univ. of Tokyo  
Inst. of Industrial Science  
7-22-1 Roppongi-Minato-Ku  
106 Tokyo  
Japan

Rosario Fazio  
Facolta di Ingegneria  
Istituto di Fisica  
Viale A. Doria 6  
95129 Catania  
Italy

Shechao Feng  
UCLA  
Dept. of Physics  
UCLA 154705  
CA-90024-1547 Los Angeles  
USA

Karsten Flensberg  
Mikro Elektr. Center  
DTH  
Bldg.344  
DK-2800 Lyngby  
Denmark

J.R. Gao  
Univ. of Groningen  
Department of Applied Physics  
Nijenborh 4-13  
9747 PB Groningen  
The Netherlands

Yuval Gefen  
Weizmann Institute  
Condensed Matter Department  
76100 Rehovot  
Israel

Michael Gershenson  
Russian Acad. Sciences  
Inst. of Radio Engin. & Electr.  
11 Mokhovaya Str.  
103907 Moscow  
Russia

Lut Gielen  
Katholieke Univ.  
Lab. voor v.-s.-physica en mag.  
Celestynenlaan 200D  
B-3001 Leuven  
Belgium

Christian Glattli  
C.E.N. Saclay  
SPEC  
F-91191 Gif s/Yvette Cedex  
France

Michael Gunn  
Univ. of Birmingham  
School of Physics  
B-15 2TT Birmingham  
U.K.

Yuichi Harada  
Chalmers  
Physics Dept.  
AVD4  
S-412 96 Göteborg  
Sweden

Klaus Hasselbach  
CNRS-CRTBT  
CNRS  
25 ave des Martyrs BP166  
38042 Grenoble  
France

Thomas Heinzl  
LMU  
Sektion Physik der LMU  
Geschwister-Scholl-Platz  
80539 München  
Germany

Frank Hekking  
I.T.F.  
Engesserstrasse 7  
76128 Karlsruhe  
Germany

Rodolfo Jalabert  
Univ. Paris-Sud  
Inst. de Physique Nucléaire  
Div. de Physique Théorique  
91406 Orsay  
France

Mats Jonson  
Chalmers  
Dept. of Applied Physics  
S-41296 Göteborg  
Sweden

Philippe Joyez  
C.E.N. Saclay  
SPEC  
F-91191 Gif-sur-Yvette  
France

Jari Kinaret  
NORDITA  
Blegdamsvej 17  
DK-2100 Copenhagen  
Denmark

Anders Kristensen  
Univ. Copenhagen  
Niels Bohr Institute  
Universitetsparken 5  
DK-2100 Copenhagen  
Denmark

Arvind Kumar  
Massachusetts Inst.  
Dept. of Electrical Engin.  
Room 39-415  
MA 02139 Cambridge  
USA

Denis L'hôte  
C.E.N. Saclay  
SPEC  
F-91191 Gif s/Yvette cedex  
France

Rolf Landauer  
IBM Research Div.  
T. J. Watson Res. Center  
P.O. Box 218  
10598 Yorktown Heights  
NY USA

Patricio Lebœuf  
Univ. Paris-Sud  
Inst. de Physique Nucléaire  
Dept. Physique Théorique  
F-91406 Orsay  
France

K.-M. H. Lenssen  
Delt Univ. of Tech.  
Dept. of Applied Physics  
P.O. Box 5046  
NL 2600 GA Delft  
The Netherlands

Igor Lerner  
Univ. of Birmingham  
School of Physics  
B-15 2TT Birmingham  
U.K.

Gordei Lesovik  
Univ. Köln  
Institute for Theoretical Physics  
Zulpicher Strasse 77  
D-50937 Köln  
Germany

Jérôme Lesueur  
 Univ. Paris-Sud  
 CSNSM-CNRS  
 Bat 108  
 F-91405 Orsay  
 France

Poul Erik Lindelof  
 Univ. Copenhagen  
 Niels Bohr Institute  
 Universitetsparken 5  
 DK-2100 Copenhagen  
 Denmark

Dominique Maillly  
 L2M CNRS  
 196, av. Henri Barbusse  
 92 220 Bagneux  
 France

Thierry Martin  
 Los Alamos Nat. Lab.  
 CNLS - MS B 258  
 NM 87545 Los Alamos  
 USA

Ygal Meir  
 Univ. of California  
 Physics Department  
 CA-93106 Santa Barbara  
 USA

Ana Celia Mota  
 ETH Hönggerberg  
 Lab. für Festkörperphysik  
 CH-8093 Zürich  
 Switzerland

Jochen Müller  
 MPI Heidelberg  
 Postfach 103980  
 69029 Heidelberg  
 Germany

Kazuo Nakazato  
 Hitachi Cambridge Lab.  
 Cavendish Lab.  
 Madingley Road  
 CB3 0HE Cambridge  
 U.K.

Yuli Nazarov  
 D.U.T.  
 Technische Universiteit Delft  
 Lorentzweg 1  
 2628CJ Delft  
 The Netherlands

Theo Nieuwenhuizen  
 Univ. of Amsterdam  
 Van der walls-Zeeman lab.  
 Valckenierstraat 65  
 1018-XE Amsterdam  
 The Netherlands

Stephane Ouvry  
 Univ. Paris-Sud  
 Inst. de Physique Nucléaire.  
 Dept. de Physique Theorique  
 F-91406 Orsay  
 France

Zvi Ovadyahu  
 The Hebrew Univ.  
 Racah Institute of Physics  
 91904 Jerusalem  
 Israel

Bernard Pannetier  
 CNRS-CRTBT  
 CNRS  
 25 Av. des Martyrs  
 F-38042 Grenoble  
 France

Claude Pasquier  
 C.E.N. Saclay  
 SPEC  
 F-91191 Gif-sur-Yvette Cedex  
 France

Magnus Persson  
 Chalmers  
 Dept. of Physics  
 S-41296 Göteborg  
 Sweden

Jean-Louis Pichard  
 C.E.N. Saclay  
 SPEC  
 F-91191 Gif-sur-Yvette cedex  
 France

Hugues Pothier  
 C.E.N. Saclay  
 SPEC  
 F-91191 Gif-sur-Yvette Cedex  
 France

Uri Sivan  
 Technion  
 Solid State Institute  
 32000 Haifa  
 Israel

Anna Pretre  
 University of Basel  
 Institute for Physics  
 Klingelbergstr. 82  
 CH-4056 Basel  
 Switzerland

Nijs Van der Vaart  
 Delt Univ. of Tech.  
 Faculty of applied Physics  
 P.O. Box 5046  
 2600GA Delft  
 The Netherlands

Mikhail Raikh  
 University of Utah  
 Department of Physics  
 201JFB  
 Utah 84112 Salt Lake City  
 USA

Piero Visani  
 ETH Hönggerberg  
 Laboratorium für Festkörperphysik  
 8093 Zürich  
 Switzerland

Barbara Sanborn  
 NIST  
 Semiconductor Electronics Div.  
 MD20899 Gaithersburg  
 USA

Felix Von Oppen  
 MPI Heidelberg  
 Saupfercheckweg 1  
 69117 Heidelberg  
 Germany

Marc Sanquer  
 C.E.N. Saclay  
 SPEC  
 F-91191 Gif-sur-Yvette cedex  
 France

David Wharam  
 LMU  
 Sektion Physik der LMU  
 Geschwister-Scholl-Platz 1  
 80539 München  
 Germany

Peter Scheuzger  
 Université Neuchâtel  
 Institut de Physique  
 Rue A.-L. Breguet 1  
 ch-2000 Neuchâtel  
 Switzerland

Tito Williams  
 C.E.N. Saclay  
 SPEC  
 F-91191 Gif-sur-Yvette Cedex  
 France

Valeri Shikin  
 Inst. of Solid States Ph.  
 Tchernogolovka  
 142432 Moscow  
 Russia

David Williams  
 Hitachi Cambridge Lab.  
 Cavendish Lab.  
 Madingley Road  
 CB3 0HE Cambridge  
 U.K.

Ben Simons  
 Massachusetts Inst.  
 Dept. of Physics - Rm 12-105  
 77, Massachusetts Avenue  
 MA02139 Cambridge  
 USA

